$m' = m$. The following rules are applied to the UEs that monitor PDCCH candidates while supporting carrier aggregation [5]:

- The UE monitors one common search space at each of the aggregation levels 4 and 8 on the primary cell.
- A UE, which is not configured with a CIF, monitors one UE-specific search space at each of the aggregation levels 1, 2, 4, and 8 on each activated serving cell.
- A UE configured with a CIF monitors one or more UE-specific search spaces at each of the aggregation levels 1, 2, 4, and 8 on one or more activated serving cells configured through higher layer signaling.
- The common and UE-specific search spaces on the primary cell may overlap.
- A UE that is configured with the CIF associated with monitoring a PDCCH on serving cell monitors the PDCCH whose CRC may have been scrambled with C-RNTI in the UE-specific search space of the serving cell.
- A UE configured with the CIF associated with monitoring the PDCCH on the primary cell monitors the PDCCH whose CRC may have been scrambled with SPS C-RNTI in the UE-specific search space of the primary cell.
- The UE monitors the common search space for the PDCCH without CIF.
- For the serving cell on which the PDCCH is monitored, if the UE is not configured with a carrier aggregation, then it is required to monitor the UE-specific search space for the PDCCH without CIF; otherwise, the UE is required to monitor the UE-specific search space for the PDCCH with CIF.
- A UE is not expected to monitor the PDCCH of a secondary cell, if it is configured to monitor the PDCCH with CIF corresponding to that secondary cell in another serving cell. For the serving cell on which the PDCCH is monitored, the UE monitors PDCCH candidates at least for the same serving cell.
- A UE configured to monitor PDCCH candidates whose CRCs are scrambled with C-RNTI or SPS C-RNTI, with a common payload size and with the same first CCE index n_{CCE}, but with different sets of DCI information fields in the common and UE-specific search spaces on the primary cell, is required to assume that only the PDCCH in the common search space is transmitted by the primary cell.
- A UE configured to monitor PDCCH candidates in a given serving cell with a given DCI format size with CIF, and CRC scrambled with C- RNTI, where the PDCCH candidates may have one or more possible values of CIF for the given DCI format size, can assume that a PDCCH candidate with the given DCI format size may be transmitted in the given serving cell in any UE-specific search space corresponding to any of the possible values of CIF for the given DCI format size.

The aggregation levels defining the search spaces are listed in Table 9.24. The DCI formats that the UE is expected to monitor depend on the configured transmission mode in each serving cell. For the common search spaces, Y_k is set to 0 for the two aggregation levels $L = 4$ and $L = 8$.

Petitioners' Exhibit 1021
Nokia of America Corp., et al. v. KT Corporation, et al.
Case No. IPR2025-00036; U.S. Patent No. 11,627,631
Page 605 of 1122

9.12.5 Enhanced PDCCH

In LTE Rel-8 downlink control channel design, the PDCCH capacity is constrained by the number of available CCEs and the aggregation level associated with each scheduled PDCCH. Since the size of the time-division-multiplexed control region in each subframe is limited to three OFDM symbols, there might be some scenarios where the eNB exhausts the resources for PDCCH transmission. With the increased use of DM-RS, DCI format 2C will be more often used. DCI format 2C should use at least two CCEs for most UEs, since using only one CCE results in high coding rates (e.g., 0.81 for a 10 MHz FDD system). Moreover, for the UEs at the cell-edge configured for the CoMP mode, a large number of CCEs is needed for the PDCCH to maintain coverage, because the PDCCH cannot use CoMP to improve cell-edge performance. Furthermore, LTE Rel-11 downlink MIMO enhancement for heterogeneous network deployments requires increased PDCCH capacity and the use of virtual cell identities to overcome the limitation of the existing LTE technology in new deployment scenarios related to CoMP, HetNet, etc., where several low-power nodes or subsets of a macro-cell may share the same physical cell identity with the macro-cell.

Sharing the same cell identity by the neighboring nodes would increase intra-cell interference and degrade the channel estimation performance and coherent detection of data and control channels, as well as limit the use of advanced closed-loop SU-MIMO/MU-MIMO techniques. Also, the use of the same identifier by subordinate nodes would prevent transmission/reception node identification and switching. An example case is a non-uniform network deployment comprising a macro-node with several low-power RRHs using the same physical cell identifier as the macro-node. In such a case, there is one common PDCCH for the macro eNB and all RRHs, thus the capacity of the current control region might be too small for sending all PDCCHs without collision.

The use of different scrambling sequences initialized with unique cell identifiers would achieve interference randomization and help the UE to separate data and control channels transmitted by different transmission nodes. Since the reference signals (e.g., CRS, DM-RS, CSI-RS) are also scrambled with cell-specific sequences to allow the UE to conduct various channel estimations and mobility measurements on different transmission nodes, the use of unique identifiers would facilitate these functions, as well as node selection and switching in homogeneous and heterogeneous networks.

Several justifications for the design of a new downlink control structure were discussed in LTE Rel-11 contributions that are summarized below [149–155]:

- Limited PDCCH capacity: The existing PDCCH structure was designed to provide control signaling and resource assignments for UEs in a single transmission point per macro-cell deployment. Under CoMP scenario 4 (see Chapter 12), several RRHs having the same cell identity are deployed in a single macro-cell. In such a scenario, the assignments corresponding to all RRHs may have to be simultaneously transmitted. This can cause a significant

Petitioners' Exhibit 1021
Nokia of America Corp., et al. v. KT Corporation, et al.
Case No. IPR2025-00036; U.S. Patent No. 11,627,631
Page 606 of 1122

increase in the number of resource assignments and shortage of CCEs per subframe. In CoMP scenario 3, each RRH has a different cell identity relative to the associated macro-cell; however, all nodes share the same time/frequency resources, which may result in significant intra-cell interference. Therefore, the detection performance of the PDCCH in subframes with strong interference may be unsatisfactory. Although the almost-blank subframe concept is supported in LTE Rel-10, it requires the network node to reduce the activity (e.g., transmission power) in the almost-blank subframe, leading to inefficient spectral utilization. Hence, the PDCCH enhancements were necessary for this scenario, as well.

- Increased resource assignment payload size: Since the initial Rel-8 PDCCH design, several improvements have been made to the standard. In particular, new transmission modes, based on UE-specific reference signals, with support for MU-MIMO were designed. It is anticipated that transmission mode 9 will be widely used in future deployments. One of the DCI formats used with transmission mode 9 is DCI format 2C. With its large payload size, the use of DCI format 2C may result in fewer resource assignments (i.e., fewer CCEs per subframe) based on the existing PDCCH structure.
- Interference avoidance/coordination on the control channels: The enhancement of MIMO performance through improved CSI feedback for certain deployment scenarios, especially the case of four transmit antennas in a cross-polarized downlink configuration, in both homogeneous and heterogeneous cases, was of special interest in LTE Rel-11. In such environments, neighboring transmission nodes may interfere with each other. The existing mechanisms in earlier releases of LTE may not be sufficient for robust transmission of control channels in dense and diverse deployments. In that case, it might be beneficial to be able to perform interference avoidance/coordination by orthogonalizing the users in neighboring cells.
- Higher user throughput: Due to capacity limits of the PDCCH, some data resources may not be allocated in a timely manner. One reason for the limitation is the use of the hashing function to map CCEs in the control region. The hashing function (in some cases) may cause two candidate sets to collide, especially when an aggregation level higher than one is chosen for each UE. As a result, the number of assignments that can be transmitted on the PDCCH will be limited, reducing the overall user throughput and increasing transmission latency.
- Use of soft frequency partitioning and fractional frequency reuse with PDCCH: The time-division-multiplexed structure of PDCCH was designed based on a single-frequency partition in each slot/subframe and assuming a frequency reuse factor of one. While hard frequency partitioning is very undesirable from a network deployment and frequency planning perspective, the soft frequency partitioning combined with fractional-frequency reuse techniques has been shown to provide more robustness and reliability for transmission of control signaling and data, due to improved interference mitigation. The use of frequency-division-multiplexing of data and control regions would allow separate power control for each channel type.

Petitioners' Exhibit 1021
Nokia of America Corp., et al. v. KT Corporation, et al.
Case No. IPR2025-00036; U.S. Patent No. 11,627,631
Page 607 of 1122

- MU-MIMO and beamforming of control channels: The existing structure of the PDCCH relies on CRS for channel estimation and coherent detection. It is shown that CRS has more overhead and is less effective when using closed-loop precoding techniques, beamforming, and MU-MIMO. The beamforming of the control channels can significantly improve the performance of the cell-edge users. The use of DM-RS instead of CRS would facilitate the use of beamforming for the control channels.
- Control overhead reduction: The resource allocation granularity is one OFDM symbol for the PDCCH, thus it amounts to approximately 7% overhead per OFDM symbol. In the frequency-domain, the control channel overhead can be significantly lower if the granularity is defined as one PRB. For instance, in a 10 MHz system, the resource allocation granularity (L1/L2 overhead per PRB) is 2% and 1% in a 20 MHz system. Therefore, the design of the ePDCCH can result in more efficient resource utilization for the control channel.

To overcome the above limitations, an enhanced physical downlink control channel (ePDCCH) was introduced in 3GPP LTE Rel-11. In LTE Rel-11, the ePDCCH can be used to convey scheduling assignments. The ePDCCH is transmitted by aggregating one or several eCCEs. Each eCCE consists of multiple enhanced REGs (eREGs). In an FDD system, the number of eREGs per eCCE $N_{\text{eCCE}}^{\text{eREG}}$ is four for subframes with normal cyclic prefix, and eight for subframes with an extended cyclic prefix. In a TDD system, there are four eREGs per eCCE for subframes with a normal cyclic prefix and special subframe configurations 3, 4, and 5. In addition, there are eight eREGs per eCCE in TDD systems with an extended cyclic prefix and special subframe configurations 1, 2, 3, 5, and 6 [3]. The eCCEs that construct ePDCCHs are numbered from 0 to $N_{\text{ePDCCH}}^{\text{eCCE}} - 1$, where the number of eCCEs per ePDCCH $N_{\text{ePDCCH}}^{\text{eCCE}}$ depends on the ePDCCH format as given in Table 9.25.

The eREGs are used to define the mapping of enhanced control channels to resource elements. There are 16 eREGs in each PRB pair. The eREG indexing is obtained by numbering all resource elements within a PRB pair cyclically from 0 to 15 in an increasing order of first frequency then time, skipping the resource elements designated to DM-RS for antenna ports $p = \{107, 108, 109, 110\}$ for a normal cyclic prefix or $p = \{107, 108\}$ for an extended cyclic prefix. All resource elements with number i in that PRB pair constitute eREG_i (see Figure 9.99).

As shown in Figure 9.100, the mapping of the ePDCCH to resource elements within resource block pairs can be performed in a localized or distributed manner, where the mapping defines how the eCCEs are associated with eREGs and PRB pairs. It must be noted that multiplexing of ePDCCH and PDSCH within a PRB pair is not permitted. If a UE is configured to monitor multiple ePDCCHs, then there are one or two sets of PRB pairs, which the UE is required to monitor. All ePDCCH candidates in ePDCCH set S_{m} exclusively use localized or distributed mapping which is configured by higher layers. Within ePDCCH set S_{m} in subframe i, the eCCEs available for transmission of ePDCCHs are numbered from 0 to $N_{\text{eCCE}}(m, i) - 1$, where eCCE index n corresponds to eREGs numbered $(n \bmod N_{\text{RB}}^{\text{eCCE}}) + \text{j}N_{\text{RB}}^{\text{eCCE}}$ in PRB index $\lfloor n/N_{\text{RB}}^{\text{eCCE}} \rfloor$ for localized mapping, or

Table 9.25 ePDCCH Formats [3]

ePDCCH Format	Number of eCCEs per ePDCCH ($N_{\text{ePDCCH}}^{\text{eCCE}}$)			
	Regular TDD/FDD Subframes and TDD Special Subframe Configurations 3, 4, 8 with Normal Cyclic Prefix (DCI Formats 2/2A/2B/2C/2D and $N_{\text{RB}}^{\text{DL}} \geq 25$ or Any DCI Format and $N_{\text{ePDCCH}} < 104$)		All Other Cases	
	Localized Transmission	Distributed Transmission	Localized Transmission	Distributed Transmission
0	2	2	1	1
1	4	4	2	2
2	8	8	4	4
3	16	16	8	8
4	–	32	–	16

it corresponds to eREGs numbered $\lfloor n/N_{\text{RB}}^{S_{\text{m}}} \rfloor + \text{j}N_{\text{RB}}^{\text{eCCE}}$ in PRB indices $(n + \text{jmax}[1, N_{\text{RB}}^{S_{\text{m}}}/N_{\text{eCCE}}^{\text{eREG}}])\text{mod}\, N_{\text{RB}}^{S_{\text{m}}}$ for distributed mapping. The parameter $j = 0, 1, \ldots, N_{\text{eCCE}}^{\text{eREG}} - 1$, $N_{\text{eCCE}}^{\text{eREG}}$ is the number of eREGs per eCCE, and $N_{\text{RB}}^{\text{eCCE}} = 16/N_{\text{eCCE}}^{\text{eREG}}$ is the number of eCCEs per resource block pair (see Figure 9.99). The PRB pairs that form ePDCCH set S_{m} are numbered in ascending order from 0 to $N_{\text{RB}}^{S_{\text{m}}} - 1$ [3].

The physical layer processing of the ePDCCH can be described as follows. The block of bits $(b_0, b_1, \ldots, b_{N_{\text{bit}}-1})$ that is going to be transmitted on an ePDCCH in a subframe is scrambled, resulting in a block of scrambled bits $(\tilde{b}_0, \tilde{b}_1, \ldots, \tilde{b}_{N_{\text{bit}}-1})$ in which $\tilde{b}_i = [b_i + c(i)]\text{mod}\, 2$. The UE-specific scrambling sequence $c(i)$ defined in previous sections is initialized with $c_{\text{init}} = \lfloor n_{\text{s}}/2 \rfloor 2^9 + N_{\text{ID}}^{\text{ePDCCH}(i)}$, where index i is the ePDCCH set number, and $N_{\text{ID}}^{\text{ePDCCH}(i)}$ is provided by higher layers. The block of scrambled bits $(\tilde{b}_0, \tilde{b}_1, \ldots, \tilde{b}_{N_{\text{bit}}-1})$ is modulated using QPSK modulation, resulting in a block of complex-valued modulation symbols $(d_0, d_1, \ldots, d_{N_{\text{s}}-1})$. The block of complex-valued modulated symbols is mapped to a single layer and precoded according to $y_i = d_i|_{i=0,1,\ldots,N_{\text{s}}-1}$. The precoded block of symbols can be mapped to physical resource elements using localized or distributed mapping.

The block of complex-valued symbols $(y_0, y_1, \ldots, y_{N_{\text{s}}-1})$ is sequentially mapped to resource elements (k, l) starting with y_0 to the associated antenna port, provided that those physical resources are part of the eREGs assigned for transmission and are not part of a physical resource-block pair used for transmission of PBCH or synchronization signals, and are not used for CRSs, CSI-RSs for the

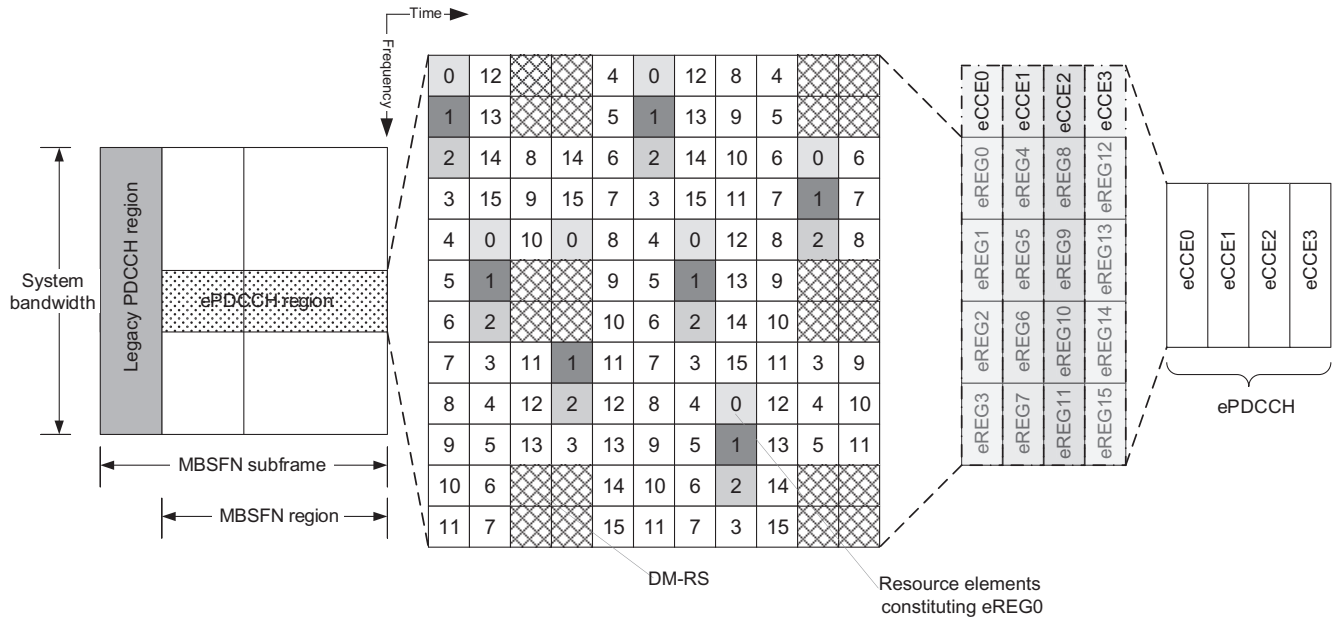


FIGURE 9.99

Structure and formation of an example ePDCCH, eCCE, and eREG [3].

Petitioners' Exhibit 1021
Nokia of America Corp., et al. v. KT Corporation, et al.
Case No. IPR2025-00036; U.S. Patent No. 11,627,631
Page 610 of 1122

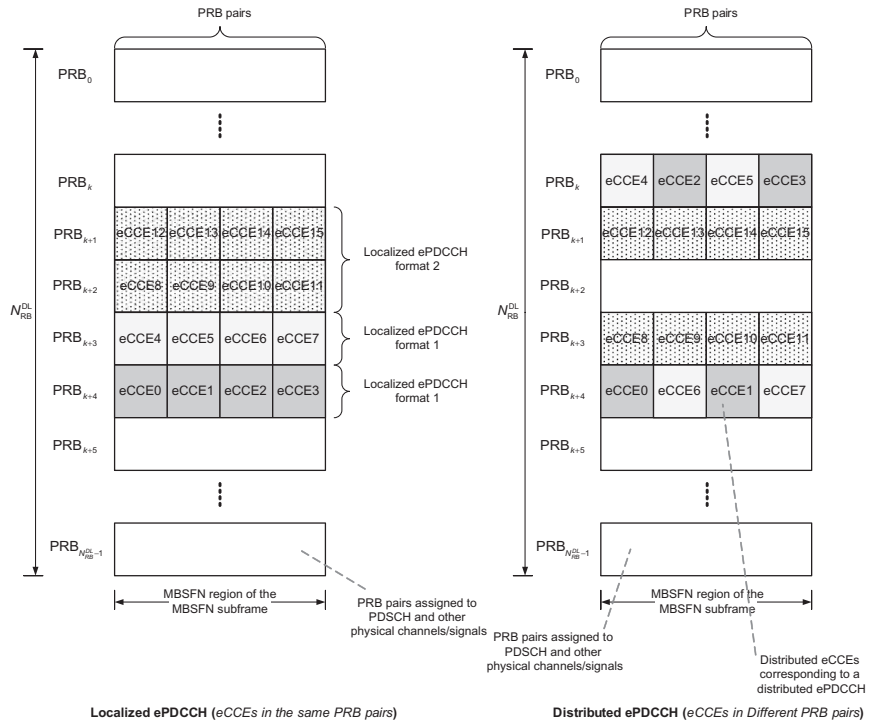


FIGURE 9.100

Structure and formation of localized and distributed ePDCCH and eCCEs [3].

specific UE; and further the index l in the first slot in a subframe stratifies the condition $l \geq l_{\text{ePDCCH}_{\text{start}}}$. The mapping to resource elements (k, l) on antenna port p is performed in increasing order of first the index k and then the index l, starting with the first slot and ending with the second slot in a subframe. For localized transmission, the single antenna port p to use for ePDCCH transmission is parameterized with parameter $n_{\text{ap}} = n_{\text{eCCE}_{\text{L}}} \bmod N_{\text{RB}}^{\text{eCCE}} + n_{\text{RNTI}} \bmod \min(N_{\text{ePDCCH}}^{\text{eCCE}}, N_{\text{RB}}^{\text{eCCE}})$, where $n_{\text{eCCE}_{\text{L}}}$ denotes the lowest eCCE index used by the referenced ePDCCH transmission in the ePDCCH set, n_{RNTI} corresponds to the RNTI associated with the ePDCCH transmission, and $N_{\text{ePDCCH}}^{\text{eCCE}}$ is the number of eCCEs per referenced ePDCCH. For FDD/TDD subframes with a normal cyclic prefix and TDD special subframe configurations 3, 4, and 8, depending on the value of parameter n_{ap} the following antenna port assignments are made [3]:

$$
\begin{aligned}
n_{\text{ap}} = 0 \quad &\rightarrow \quad p = 107 \\
n_{\text{ap}} = 1 \quad &\rightarrow \quad p = 108 \\
n_{\text{ap}} = 2 \quad &\rightarrow \quad p = 109 \\
n_{\text{ap}} = 3 \quad &\rightarrow \quad p = 110
\end{aligned}
$$

Petitioners' Exhibit 1021
Nokia of America Corp., et al. v. KT Corporation, et al.
Case No. IPR2025-00036; U.S. Patent No. 11,627,631
Page 611 of 1122

For distributed transmission, each resource element in an eREG is associated with one out of two antenna ports in an alternating manner, where $p \in \{107, 109\}$ for a normal cyclic prefix and $p \in \{107, 108\}$ for an extended cyclic prefix.

For each serving cell, higher layer signaling can configure a UE with one or multiple ePDCCH-PRB sets for ePDCCH monitoring. Each ePDCCH-PRB set consists of a set of eCCEs indexed from 0 to $N_{\text{eCCE}}(p,k) - 1$, where $N_{\text{eCCE}}(p,k)$ denotes the number of eCCEs in ePDCCH-PRB set p in subframe k. Each ePDCCH-PRB set can be configured for either localized or distributed ePDCCH transmission. The UE is required to monitor a set of ePDCCH candidates on one or more activated serving cells configured via higher-layer signaling for control information, where monitoring implies attempting to blindly decode each of the ePDCCHs in the set according to the monitored DCI formats.

The set of ePDCCH candidates that the UE is expected to monitor are defined in terms of ePDCCH UE-specific search spaces. For each serving cell, the subframes in which the UE monitors ePDCCH UE-specific search spaces are configured via higher-layer signaling. In TDD systems using a normal cyclic prefix in downlink subframes, the UE is not expected to monitor the ePDCCH in special subframe configurations 0 and 5. A UE is not expected to monitor an ePDCCH candidate whose eCCE(s) is mapped to a PRB pair that overlaps in frequency with a transmission of either PBCH or primary/secondary synchronization signals in the same subframe.

The UE is required to monitor one common search space in every non-DRX subframe at aggregation levels 4 and 8 on the primary cell. If a UE is not configured for ePDCCH monitoring, and if it is not configured with a CIF, then it is required to monitor one PDCCH UE-specific search space at aggregation levels 1, 2, 4, 8 on each activated serving cell in every non-DRX subframe. In another case where a UE is not configured to monitor ePDCCH, but it is configured with a CIF, then it is required to monitor one or more UE-specific search spaces at aggregation levels 1, 2, 4, 8 on one or more activated serving cells that are configured through higher-layer signaling in every non-DRX subframe. Furthermore, if a UE is configured for ePDCCH monitoring on an activated serving cell, but it is not configured with CIF, then it is required to monitor one PDCCH UE-specific search space at aggregation levels 1, 2, 4, 8 on the serving cell in all non-DRX subframes where ePDCCH is not monitored on that serving cell. If a UE is configured for ePDCCH monitoring on a serving cell, and if that serving cell is activated, and if the UE is configured with a CIF, then the UE is required to monitor one or more PDCCH UE-specific search spaces at each of the aggregation levels 1, 2, 4, and 8 on that serving cell as configured by higher layer signaling in all non-DRX subframes where ePDCCH is not monitored on that serving cell. The common and PDCCH UE-specific search spaces on the primary cell may overlap. It can be concluded that in each subframe on an activated serving cell, the UE either monitors ePDCCH or PDCCH and not both of them, in order to simplify the UE search mechanism.

Petitioners' Exhibit 1021
Nokia of America Corp., et al. v. KT Corporation, et al.
Case No. IPR2025-00036; U.S. Patent No. 11,627,631
Page 612 of 1122

9.12.6 Physical downlink shared channel

The physical downlink shared channel is a downlink channel that is used for transmission of all user data, paging messages, and part of the system information which is not carried in the PBCH. The data is transmitted on the PDSCH in units of transport blocks that correspond to the MAC sub-layer PDUs. The transport blocks are received from the MAC sub-layer in each TTI where the default TTI value in LTE/LTE-Advanced is 1 ms, corresponding to one subframe duration. The maximum number of transport blocks that can be transmitted per UE per subframe is limited to two, depending on the transmission mode selected for the PDSCH for each UE. The transmission mode defines the multi-antenna configuration that is used for data transmission over the PDSCH. There are 10 transmission modes specified for LTE Rel-11 that are summarized in Table 9.26. Note that transmission mode 10 was included as part of Rel-11 enhancements to support coordinated multi-point transmission/reception; especially with multiple CSI processes configured, TM10 can be seen as enhanced TM9 with well-defined UE behavior in interference measurement via CSI interference measurement configuration [3,5].

With the exception of transmission modes 7, 8, 9, and 10, the phase reference for coherent demodulation of PDSCH is obtained from CRSs and the number of eNB antenna ports used for transmission of PDSCH is the same as the number of antenna ports used in the cell for PBCH transmission. In transmission modes 7, 8, 9, and 10, the UE-specific reference signals provide the phase reference for coherent demodulation of the PDSCH. The configured transmission mode further controls the formats of the associated downlink control signaling messages as given in Table 9.26, and the type of channel quality feedback from the UE.

The coded transport block is scrambled with a binary scrambling sequence. The sequence is based on cell identity and RNTI to make it cell- and UE-specific. The binary scrambled bits are modulated using a suitable modulation scheme considering the channel conditions and required data rate. The permissible modulation schemes for PDSCH are QPSK (2 bits/symbol), 16QAM (4 bits/symbol), or 64QAM (6 bits/symbol). Support of 64QAM is mandatory for all LTE/LTE-Advanced UE categories. The selection of modulation scheme is based on CQI feedback from the UE. The resulting codewords after modulation are mapped to spatial layers. Spatial multiplexing uses one to eight layers less than or equal to the number of antenna ports. For transmit diversity, the number of layers is equal to the number of antenna ports. The precoding matrix applies antenna weighting (phase and amplitude) for each data stream, and maps the stream to different antenna ports. In resource blocks in which UE-specific reference signals are not transmitted, PDSCH is transmitted on the same set of antenna ports used for PBCH.

All downlink resource elements are available for the PDSCH except those reserved for special purposes, such cell-specific, positioning, MBSFN, CSI, and UE-specific reference signals, synchronization signals, and control signaling. Therefore, when the UE is informed through control signaling of a resource allocation within a pair of resource blocks in a subframe, it is only the available resource elements within those resource block pairs which actually carry PDSCH

Petitioners' Exhibit 1021
Nokia of America Corp., et al. v. KT Corporation, et al.
Case No. IPR2025-00036; U.S. Patent No. 11,627,631
Page 613 of 1122

Table 9.26 Summary of PDSCH Transmission Modes in LTE/LTE-Advanced when using C-RNTI [5,13]

Release	Mode	PDSCH Transmission Scheme	DCI Format	Search Space	Channel State Information Feedback
8	1	Single-antenna transmission on antenna port 0	1	UE-specific	CQI
			1A	Common and UE-specific	
	2	Transmit diversity	1	UE-specific	CQI
			1A	Common and UE-specific	
	3	Transmit diversity	1A	Common and UE-specific	CQI and RI
		Open-loop spatial multiplexing or transmit diversity	2A	UE-specific	
	4	Transmit diversity	1A	Common and UE-specific	CQI, RI, and PMI
		Closed-loop spatial multiplexing or transmit diversity	2	UE-specific	
	5	Transmit diversity	1A	Common and UE-specific	CQI and PMI
		MU-MIMO	1D	UE-specific	
	6	Transmit diversity	1A	Common and UE-specific	CQI and PMI
		Closed-loop spatial multiplexing using single-layer transmission (closed-loop rank-1 precoding)	1B	UE-specific	
	7	Single-antenna transmission on antenna port 5 (transmission using UE-specific reference signals with a single layer)	1	UE-specific	CQI
		Single-antenna transmission using antenna port 0 or transmit diversity	1A	Common and UE-specific	

(*Continued*)

Petitioners' Exhibit 1021
Nokia of America Corp., et al. v. KT Corporation, et al.
Case No. IPR2025-00036; U.S. Patent No. 11,627,631
Page 614 of 1122

Table 9.26 (Continued)

Release	Mode	PDSCH Transmission Scheme	DCI Format	Search Space	Channel State Information Feedback
9	8	Single-antenna transmission using antenna port 0 or transmit diversity	1A	Common and UE-specific	CQI (PMI/RI if configured by eNB)
		Dual-layer transmission on antenna ports 7 and 8 or single-antenna transmission on antenna port 7 or 8 (transmission using UE-specific reference signals with up to two layers)	1B	UE-specific	
10	9	Single-antenna transmission on antenna port 0 or transmit diversity	1A	Common and UE-specific	CQI (PMI/RI if configured by eNB)
		Spatial multiplexing up to eight layers on antenna ports 7−14 (transmission using UE-specific reference signals with up to eight layers)	2C	UE-specific	
11	10	Coordinated multi-point transmission and reception (support CoMP operation and configure Rel-11 non-zero-power CSI-RS resources and interference measurement resources)	1A/2D	UE-specific	CQI (PMI/RI if configured by eNB)

Petitioners' Exhibit 1021
Nokia of America Corp., et al. v. KT Corporation, et al.
Case No. IPR2025-00036; U.S. Patent No. 11,627,631
Page 615 of 1122

data. The allocation of resource block pairs to PDSCH transmission for a particular UE is signaled to the UE by means of dynamic control signaling transmitted at the start of the relevant subframe using ePDCCH/PDCCH. The mapping of PDSCH resource elements in a subframe is illustrated in Figure 9.101. The modulation symbols are mapped to resource elements (k, l) in the allocated resource blocks. The mapping is performed first along frequency and then along symbols in time. The modulation symbols are mapped by incrementing the sub-carrier index k first along the allocated resource blocks. When the final resource block is reached, the symbol index l is incremented. After mapping, the OFDM modulation is performed across all sub-carriers on a symbol-by-symbol basis.

The paging control channel (PCCH) is a logical channel that is mapped to the paging channel (PCH) which is a transport channel. The PCH is transmitted via PDSCH similar to other data transmissions. When PCH is transmitted, a unique 16-bit identifier known as P-RNTI with a value of 0xFFFE is used to signal paging messages in the PDCCH. Multiple UEs may be paged simultaneously using a single paging allocation with the UE identity indicated within the paging message itself (Figure 9.102).

A UE is required to decode the corresponding PDSCH allocation in the same subframe (considering the restriction on the number of transport blocks signaled through RRC messages) upon detection of an ePDCCH/PDCCH of a serving cell with DCI format 1/1A/1B/1C/1D or 2/2A/2B/2C/2D intended for the UE in that subframe [5]. The UE may assume that PRSs are not present in resource blocks in which it is required to decode PDSCH when a PDCCH whose CRC is scrambled with SI-RNTI or P-RNTI with DCI format 1A or 1C is successfully detected. If the UE is configured with the CIF for a given serving cell, it must assume that the CIF is not present in any PDCCH of the serving cell in the common search space; otherwise, the UE must assume that for the given serving cell, the CIF is present in the ePDCCH/PDCCH located in the UE-specific search space, when the ePDCCH/PDCCH CRC is scrambled with C-RNTI or SPS C-RNTI.

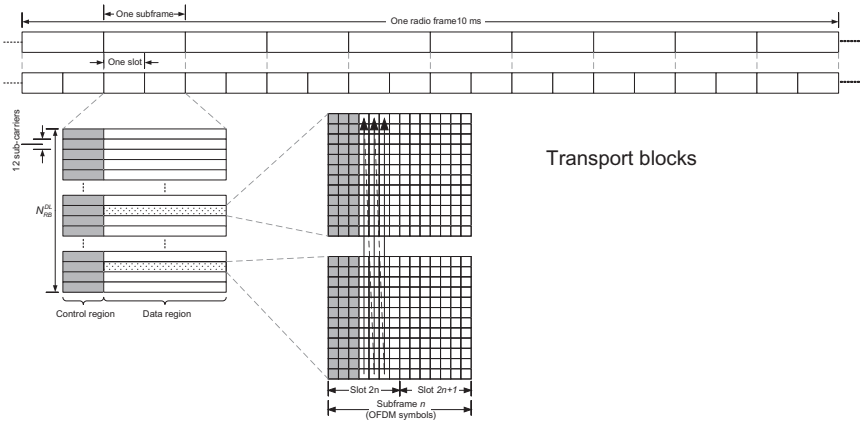


FIGURE 9.101

Illustration of PDSCH resource element mapping.

Petitioners' Exhibit 1021
Nokia of America Corp., et al. v. KT Corporation, et al.
Case No. IPR2025-00036; U.S. Patent No. 11,627,631
Page 616 of 1122

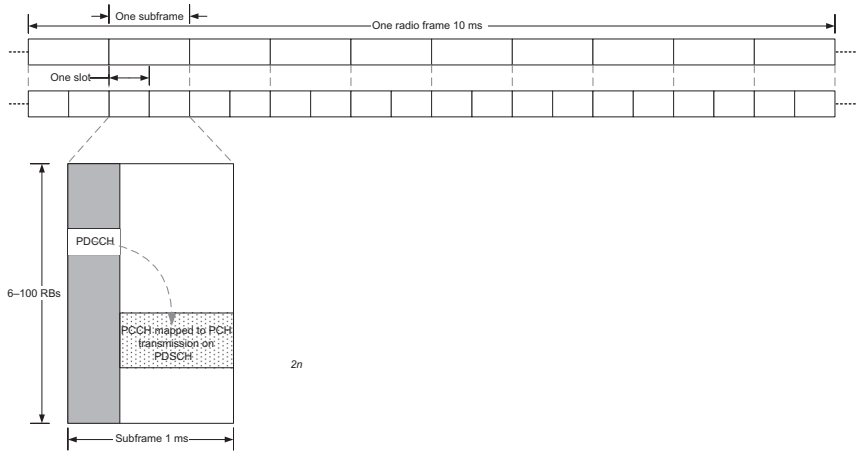


FIGURE 9.102

PCH transmission on PDSCH.

If a UE is configured by higher layers to decode the PDCCH with its CRC scrambled with SI-RNTI, the UE is required to decode PDCCH and the corresponding PDSCH according to any of the permissible combinations of DCI formats and multi-antenna schemes. The PDSCH corresponding to these PDCCHs is also scrambled with SI-RNTI. Similarly, if a UE is configured to monitor PDCCHs whose CRCs are scrambled with P-RNTI, C-RNTI, SPS C-RNTI, or RA-RNTI, the UE is required to decode the PDCCH and the corresponding PDSCH according to any of the permissible combinations of DCI formats and multi-antenna schemes. An example is given in Table 9.26 for C-RNTI [5]. Note that if the CRC of PDCCH is scrambled with broadcast identifiers such as SI-RNTI, P-RNTI, and RA-RNTI, the UE only monitors the common search space and decodes the PDSCH accordingly. For multi-user MIMO transmission of PDSCH, the UE may assume that the eNB transmission on PDSCH is on one layer. An additional power offset of $\delta_{\text{power-offset}} = -3$ dB may be applied if the downlink power offset field signaled on PDCCH with DCI format 1D is zero.

9.13 Principles of multi-antenna transmission

Design of mobile broadband wireless communication systems capable of data transmission rates in excess of 1 Gbps has been of practical interest in the past decade to enable the new generations of cellular systems and IMT-Advanced. The use of multiple antennas at the transmitter and/or receiver commonly known as the MIMO system has become a pragmatic and cost-effective approach that offers substantial gain in making 1 Gbps wireless links a reality. This section provides an

Petitioners' Exhibit 1021
Nokia of America Corp., et al. v. KT Corporation, et al.
Case No. IPR2025-00036; U.S. Patent No. 11,627,631
Page 617 of 1122

overview of the MIMO wireless technology including channel models, performance limits, coding, and transceiver design. MIMO techniques can increase system throughput and transmission reliability without increasing the required bandwidth. While most communication systems suffer in multi-path channels, a MIMO system benefits from propagation over different paths through which the signals arrive at the receiver. A MIMO system typically performs better in an indoor environment while it may not properly perform in LoS environments.

The performance improvements resulting from the use of multi-antenna systems are mainly due to array gain, diversity gain, spatial multiplexing gain, and interference reduction that may be achieved through appropriate MIMO configurations. The main advantages of the multi-antenna techniques can be summarized as follows [20]:

- Array gain can be achieved through signal processing at the transmitter and/or the receiver, and results in an increase in average SINR at the receiver due to coherent combining effect. The increased SINR further results in improved coverage and user throughput. Transmit or receive array gain requires channel knowledge in the transmitter and receiver, respectively, and further depends on the number of transmit and receive antennas. The channel knowledge in the receiver is typically available (through channel estimation based on downlink reference signals), whereas CSI in the transmitter is in general more difficult to attain.
- The signal power is faded randomly in a wireless communication channel. Diversity is an effective technique to mitigate fading in a wireless channel. The diversity schemes rely on transmitting the signal over multiple and ideally independent fading channels in time, frequency, and/or space. Spatial diversity is preferred over time or frequency diversity as it does not consume additional transmission time or bandwidth. If the $N_{RX} \times N_{TX}$ links forming the MIMO channel fade independently and the transmitted signal is properly constructed, the receiver can combine the arriving signals such that the resulting signal exhibits considerably reduced amplitude variability relative to a single-input single-output (SISO) link, and a diversity gain on the order of $N_{RX} \times N_{TX}$ can be achieved. Spatial diversity gain in the absence of channel knowledge at the transmitter can be achieved using suitably designed transmit signal which is known as space−time coding.
- MIMO channels provide a linear increase in capacity as a function of $\min(N_{RX}, N_{TX})$ without requiring additional power or transmission bandwidth. This gain, referred to as spatial multiplexing gain, is realized by transmitting independent data streams from individual transmit antennas. Note that the number of independent data streams is limited to $\min(N_{RX}, N_{TX})$. Under good channel conditions and sufficiently high SINR values, the receiver can detect different data streams, yielding a linear increase in capacity.
- Co-channel interference is generated due to frequency reuse in wireless channels. When multiple antennas are used, the differentiation between the spatial signatures of the desired signal and co-channel signals can be utilized to reduce interference. While interference cancelation requires proper knowledge of the desired signal's channel, exact knowledge of the interferers'

Petitioners' Exhibit 1021
Nokia of America Corp., et al. v. KT Corporation, et al.
Case No. IPR2025-00036; U.S. Patent No. 11,627,631
Page 618 of 1122

channels may not be necessary. The interference avoidance schemes can also be implemented at the transmitter where the goal is to minimize the interference energy sent toward the co-channel users while delivering the signal to the desired user. Interference reduction allows aggressive frequency reuse, and thereby increases multi-cell capacity. It must be noted that not all advantages of MIMO schemes can be simultaneously achieved due to conflicting demands on the spatial degrees of freedom or the number of transmit and/or receive antennas. The degree to which these conflicts can be resolved depends on the signaling scheme and transceiver design.

9.13.1 Capacity of MIMO channels

As shown in Figure 9.103, a generic MIMO system consists of a MIMO transmitter with N_{TX} transmit antennas, a MIMO receiver with N_{RX} receive antennas, and $N_{RX} \times N_{TX}$ paths or channels between transmit and receive antennas. Let $x_k(t)$ denote the transmitted signal from the kth transmit antenna at time t, then the received signal at the lth antenna can be expressed as follows:

$$y_l(t) = \sum_{k=1}^{N_{TX}} h_{lk}(t)^* x_k(t) + n_l(t) \tag{9.54}$$

where $h_{lk}(t)$ and $n_l(t)$ are the channel impulse response between the kth transmit antenna, the lth receive antenna, and the additive noise at the lth receive antenna port, respectively. The above equation can be written in the frequency-domain as:

$$Y_l(\omega) = H_{lk}(\omega)X_k(\omega) + N_l(\omega) \tag{9.55}$$

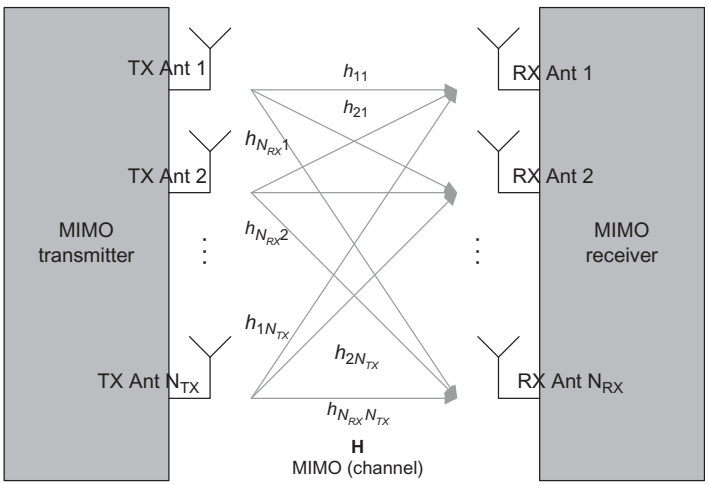


FIGURE 9.103

Illustration of the general principle of a MIMO system.

Petitioners' Exhibit 1021
Nokia of America Corp., et al. v. KT Corporation, et al.
Case No. IPR2025-00036; U.S. Patent No. 11,627,631
Page 619 of 1122

If $\mathbf{x}(\omega) = (X_1(\omega), X_2(\omega), \ldots, X_{N_{TX}}(\omega))^{\mathrm{T}}$, $\mathbf{y}(\omega) = (Y_1(\omega),\ Y_2(\omega), \ldots, Y_{N_{RX}}(\omega))^{\mathrm{T}}$, and $\mathbf{n}(\omega) = (N_1(\omega), N_2(\omega), \ldots, N_{N_{RX}}(\omega))^{\mathrm{T}}$ denote the Fourier transform vectors of $\mathbf{x}_k(t)$, $\mathbf{y}_l(t)$, and $\mathbf{n}_l(t)$, respectively, then $\mathbf{y}(\omega) = \mathbf{H}(\omega)\,\mathbf{x}(\omega) + \mathbf{n}(\omega)$, where $\mathbf{H}(\omega)$ is an $N_{\mathrm{RX}} \times N_{\mathrm{TX}}$ channel matrix with $H_{lk}(\omega)|_{k=1,2,\ldots,N_{TX};l=1,2,\ldots,N_{\mathrm{RX}}}$ entries.

Assuming a linear time-invariant MIMO channel, the channel input−output relationship can be further described in the discrete time-domain as follows:

$$y_l(nT) = \sum_{k=1}^{N_{\mathrm{TX}}} \sum_{m=0}^{M-1} h_{lk}(mT) x_k[(n-m)T] + n_l(nT) \quad 0 \le n \le M-1;\ 1 \le l \le N_{\mathrm{RX}} \tag{9.56}$$

where $x_k(n)|_{k=1,2,\ldots,N_{\mathrm{TX}}}$ and $y_l(n)|_{l=1,2,\ldots,N_{\mathrm{RX}}}$ represent the channel input and output time-domain signals, respectively. In the case of time-varying channels, Eq. (9.54) can be written as $y_l(t) = \sum_{k=0}^{N_{\mathrm{TX}}-1} h_{lk}(t,\tau) x_k(\tau) + n_l(t)$, where $h_{lk}(t,\tau)$ denotes the time-varying impulse response of the lkth channel. The matrix form of Eq. (9.55) in the frequency-domain sampled at a single frequency ω_m can be written as follows:

$$\mathbf{y}(\omega_m) = \mathbf{H}(\omega_m)\mathbf{x}(\omega_m) + \mathbf{n}(\omega_m) \tag{9.57}$$

In an OFDM system, the signal processing is inherently performed in the frequency-domain. Furthermore, OFDM transforms a frequency-selective fading channel to a flat-fading channel when considering narrowband orthogonal sub-carriers. In such a system, the MIMO signal processing can be performed at each sub-carrier. This is the main reason for the suitability of MIMO extension to an OFDM system. When MIMO processing is done at each sub-carrier, the MIMO channel input−output relationship can be demonstrated as $\mathbf{y} = \mathbf{H}\mathbf{x} + \mathbf{n}$, where the channel between the transmitter and the receiver is typically modeled as a finite impulse response (FIR) filter. In this case, each tap is typically a complex-valued Gaussian random variable with exponentially decaying magnitudes. The tap delays correspond to the RMS delay spread and the channel type (e.g., low delay spread or flat fading, high delay spread or frequency selective fading). There is a new realization of the channel at every transmitted packet, if the channel remains invariant for the duration of the packet; otherwise, the variation of the channel is explicitly modeled in the signal detection. As mentioned earlier, there are $N_{\mathrm{RX}} \times N_{\mathrm{TX}}$ paths between the transmitter and the receiver where each channel is the sum of several FIR filters with different delay spreads. The channels may or may not be correlated. The MIMO schemes can be used with non-OFDM systems when the channel is modeled as flat fading such that:

$$y_l(nT) = \sum_{k=1}^{N_{TX}} h_{lk} x_k(nT) + n(nT) \tag{9.58}$$

An important question is to what extent MIMO techniques can increase the throughput and improve the reliability of the wireless communication systems.

Petitioners' Exhibit 1021
Nokia of America Corp., et al. v. KT Corporation, et al.
Case No. IPR2025-00036; U.S. Patent No. 11,627,631
Page 620 of 1122

This question can be answered by calculating the information theoretic capacity of a SISO channel, and comparing it with that of single-input multiple-output (SIMO), multiple-input single-output (MISO), and MIMO channels. For a memory-less SISO channel (i.e., one transmit and one receive antenna), the channel capacity is given by:

$$C_{\text{SISO}} = \log_2(1 + \gamma|h|^2) \tag{9.59}$$

where h is the normalized complex-valued gain/attenuation of a fixed wireless channel or that of a particular realization of a random channel, and $\gamma = E_s/N_0$ denotes the SNR at the receive antenna port. As the number of receive antennas increases, the statistics of channel capacity improve. Using N_{RX} receive antennas and one transmit antenna, a SIMO system is formed with a capacity given by (when the channel is unknown to the transmitter):

$$C_{\text{SIMO}} = \log_2(1 + \gamma \sum_{i=1}^{N_{\text{RX}}} |h_i|^2) \tag{9.60}$$

where h_i is the gain of the ith channel corresponding to the ith receive antenna. Note that increasing the value of N_{RX} results in a logarithmic increase in average channel capacity. It can be shown that knowledge of the channel at the transmitter in SIMO cases does not provide any capacity benefit. In the case of MISO or transmit diversity, where the transmitter does not typically have knowledge of the channel, the capacity is given by:

$$C_{\text{MISO}} = \log_2(1 + \frac{\gamma}{N_{\text{TX}}} \sum_{i=1}^{N_{\text{TX}}} |h_i|^2) \tag{9.61}$$

It is noted from the above equation that when the channel information is not available at the transmitter, $C_{\text{MISO}} < C_{\text{SIMO}}$. The power normalization factor N_{TX} ensures that the total transmit power is uniformly distributed among the transmit antennas. Furthermore, one notes the absence of an array gain in this case (MISO) compared to that of the receive diversity scenario where the energy of the multipath channels can be coherently combined. In addition, the MISO capacity has a logarithmic relationship with N_{TX} similar to that of a SIMO scheme. When the channel information is available at the transmitter, the capacity of a MISO system can approach that of a SIMO system [20].

The use of diversity at both transmitter and receiver sides gives rise to a MIMO system. The capacity of a MIMO system with N_{TX} transmit antennas and N_{RX} receive antennas is expressed as follows:

$$C_{\text{MIMO}} = \log_2\left(\det\left[\mathbf{I} + \frac{\gamma}{N_{\text{TX}}}\mathbf{H}\mathbf{H}^{\text{H}}\right]\right) \tag{9.62}$$

where $\mathbf{I}$ is an $N_{\text{RX}} \times N_{\text{RX}}$ identity matrix and $\mathbf{H}$ is the $N_{\text{RX}} \times N_{\text{TX}}$ channel matrix. Note that both MISO and MIMO channel capacities are based on equal power

Petitioners' Exhibit 1021
Nokia of America Corp., et al. v. KT Corporation, et al.
Case No. IPR2025-00036; U.S. Patent No. 11,627,631
Page 621 of 1122

and uncorrelated sources. It is demonstrated in the literature that the capacity of the MIMO channel increases linearly with $\min(N_{RX}, N_{TX})$ rather than logarithmically as in the case of MISO or SIMO channel capacity, since the determinant operator yields the product of non-zero eigenvalues of its channel-dependent matrix argument, each eigenvalue characterizing the SNR over a SISO eigen-channel. It will be shown later that the overall MIMO channel capacity is the sum of capacities of each of these SISO eigen-channels. The increase in capacity is dependent on properties of the channel eigenvalues. If the channel eigenvalues decay rapidly, then linear growth in capacity will not occur. However, the eigenvalues have a known limiting distribution and tend to be spaced out along the range of this distribution. Hence, it is unlikely that most eigenvalues are very small and the linear growth is indeed achieved [20].

Figures 9.104 and 9.105 show the impulse responses and the frequency responses of a large delay-spread MIMO channel (two transmit and two receive antennas) measured over the extent of a subframe. It is noted that channel characteristics vary from one path (between one transmit and one receive antenna) to another, and across time from one symbol to another. The information theoretic capacities of some MIMO channels with a different number of transmit and receive antennas are compared in Figure 9.106.

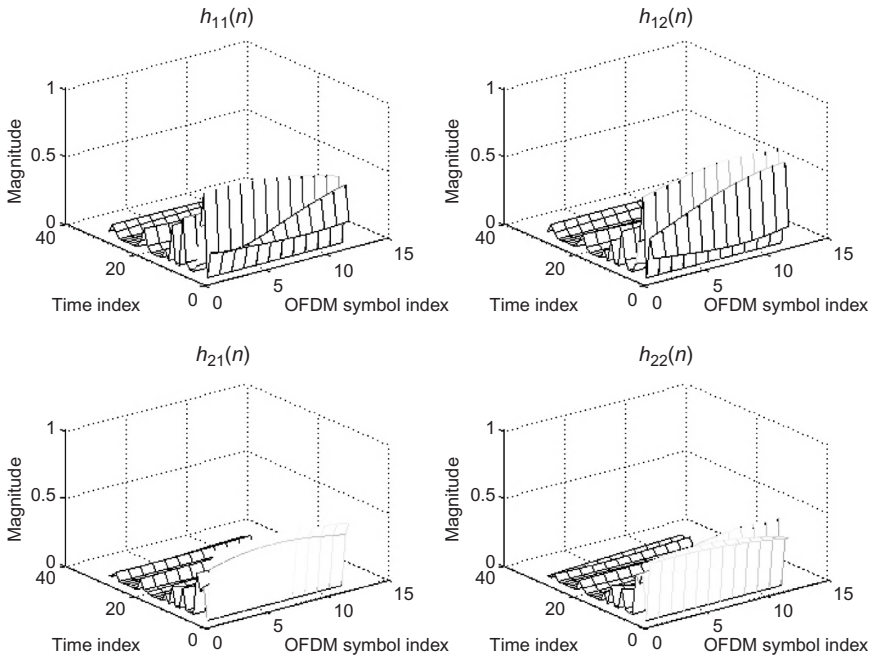


FIGURE 9.104

Example of multipath impulse responses of $N_{TX} = 2$, $N_{RX} = 2$ MIMO channel [141].

Petitioners' Exhibit 1021
Nokia of America Corp., et al. v. KT Corporation, et al.
Case No. IPR2025-00036; U.S. Patent No. 11,627,631
Page 622 of 1122

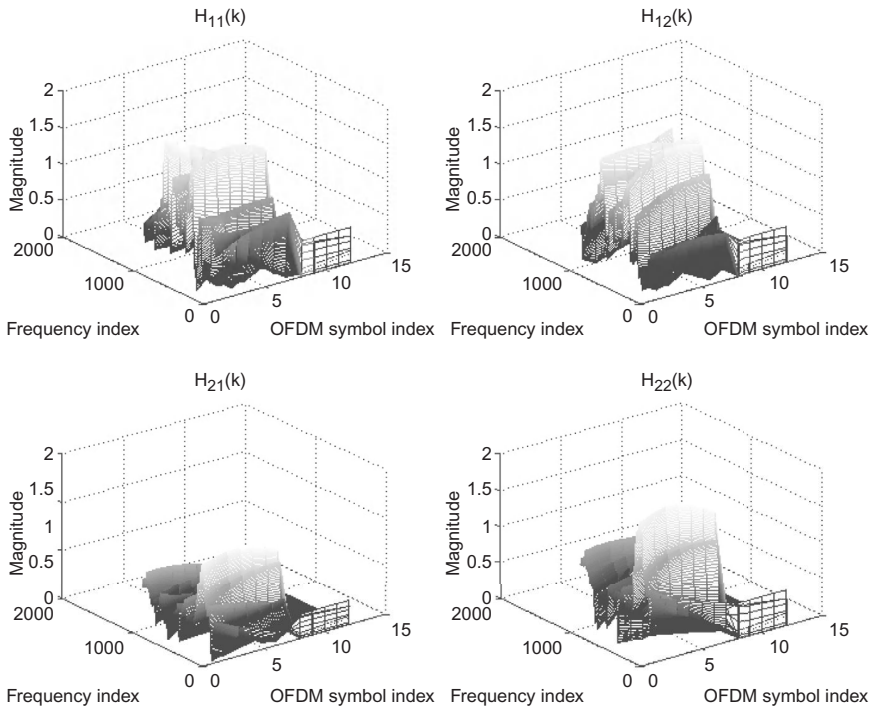


FIGURE 9.105

Example of multipath frequency responses of $N_{TX} = 2$, $N_{RX} = 2$ MIMO channel [141].

The capacity of the MIMO channel can be calculated under various conditions and different assumptions. Depending on whether the receiver has perfect channel knowledge, or whether the channel is flat fading or frequency-selective fading, different expressions for the channel capacity can be obtained. The MIMO channel capacity in Eq. (9.62) can be analyzed under two different assumptions: (1) the transmitter has no channel knowledge; and (2) the transmitter has perfect channel knowledge through feedback from the receiver or reciprocity of the downlink and uplink channels. Let us denote by $\boldsymbol{\Xi}$ the $N_{TX} \times N_{TX}$ covariance matrix of the channel input vector $\mathbf{x}$, and further assume that the channel is unknown to the transmitter, then it can be shown that the MIMO channel capacity can be written as [20]:

$$C_{MIMO} = \log_2(\det[\mathbf{I} + \mathbf{H}\boldsymbol{\Xi}\mathbf{H}^H]) \tag{9.63}$$

where $\text{trace}(\boldsymbol{\Xi}) \leq \gamma$ ensures that the total signal power does not exceed a certain limit. It can be shown that for equal transmit power and uncorrelated sources $\boldsymbol{\Xi} = (\gamma/N_{TX})\mathbf{I}$, Eq. (9.63) becomes identical to Eq. (9.62). This is true when the channel matrix is unknown to the transmitter and the input signal is Gaussian-distributed, maximizing the mutual information. If the receiver measures and

Petitioners' Exhibit 1021
Nokia of America Corp., et al. v. KT Corporation, et al.
Case No. IPR2025-00036; U.S. Patent No. 11,627,631
Page 623 of 1122

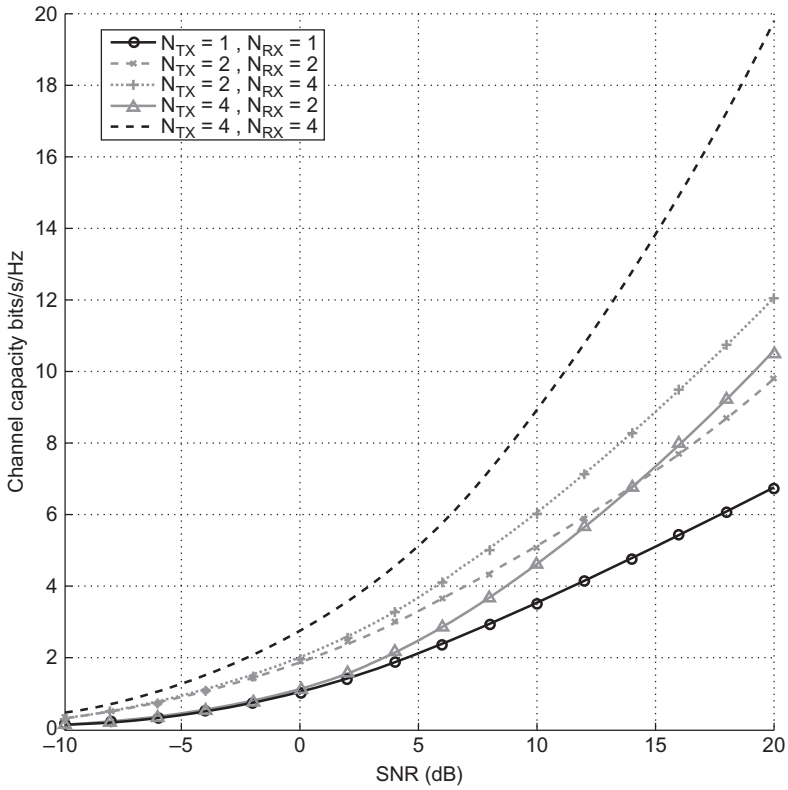


FIGURE 9.106

Comparison of the information theoretic capacity of some MIMO channels [141].

sends channel quality feedback or CSI to the transmitter, the covariance matrix $\boldsymbol{\Xi}$ is not proportional to the identity matrix, rather it is constructed from a water-filling algorithm. If one compares the capacity achieved assuming equal transmit-power and unknown channel with that of perfect channel estimation through feedback, then the capacity gain due to use of feedback is obtained. For the independent identically distributed Rayleigh fading scenario, the linear capacity growth discussed earlier will be observed. It is shown that Eq. (9.62) can be written as follows:

$$C_{\text{MIMO}} = \sum_{i=1}^{\min(N_{\text{TX}},N_{\text{RX}})} \log_2\left(1 + \frac{\gamma\lambda_i^2}{N_{\text{TX}}}\right) \tag{9.64}$$

where $\lambda_i, i = 1, 2, \ldots,$ and $\min(N_{\text{TX}}, N_{\text{RX}})$ are the non-zero eigenvalues of $\mathbf{HH}^{\text{H}}$. We can decompose the MIMO channel into $K \leq \min(N_{\text{TX}}, N_{\text{RX}})$ equivalent

Petitioners' Exhibit 1021
Nokia of America Corp., et al. v. KT Corporation, et al.
Case No. IPR2025-00036; U.S. Patent No. 11,627,631
Page 624 of 1122

parallel SISO channels using the singular value decomposition (SVD) theorem[21] [28,29]. Let $\mathbf{y} = \mathbf{Hx} + \mathbf{n}$ describe the input−output relationship of the MIMO channel where $\mathbf{y}$ is the output vector with N_{RX} components, $\mathbf{x}$ is the input vector with N_{TX} components, $\mathbf{n}$ is the additive noise vector with N_{RX} components, and $\mathbf{H}$ is the $N_{RX} \times N_{TX}$ channel matrix. Using the SVD theorem, we can show $\mathbf{H} = \mathbf{U\Sigma V}^{H}$. Let $\widehat{\mathbf{x}} = \mathbf{V}^{H}\mathbf{x}, \widehat{\mathbf{y}} = \mathbf{U}^{H}\mathbf{y}$, and $\widehat{\mathbf{n}} = \mathbf{U}^{H}\mathbf{n}$ denote the unitary transformation of the channel input and output and noise vectors, then it can be shown that $\widehat{\mathbf{y}} = \mathbf{\Sigma}\,\widehat{\mathbf{x}} + \widehat{\mathbf{n}}$. Since $\mathbf{U}$ and $\mathbf{V}$ are unitary matrices and $\mathbf{\Sigma} = \mathbf{diag}(\lambda_1, \lambda_2, \ldots, \lambda_{\min(N_{RX},N_{TX})}, 0, 0, \ldots, 0)$, it is clear that the capacity of this model is the same as the capacity of the model $\mathbf{y} = \mathbf{Hx} + \mathbf{n}$. However, $\mathbf{\Sigma}$ is a diagonal matrix with K non-zero elements on the main diagonal, thus $\widehat{y}_1 = \lambda_1\widehat{x}_1 + \widehat{n}_1, \ldots, \widehat{y}_K = \lambda_K\widehat{x}_K + \widehat{n}_K, \widehat{y}_{K+1} = \widehat{n}_{K+1}$. The latter equations are conceptually equivalent to K parallel SISO eigen-channels, each with signal power of $\lambda_i^2, i = 1, 2, \ldots, \min(N_{TX}, N_{RX})$. Hence, the MIMO channel capacity can be rewritten in terms of the eigenvalues of the input signal covariance matrix $\mathbf{\Xi}$.

When the channel knowledge is available at the transmitter and receiver, then $\mathbf{H}$ is known and we can optimize the capacity over $\mathbf{\Xi}$ subject to the power constraint $\text{trace}(\mathbf{\Xi}) \leq \gamma$. It is shown in the literature that the optimal $\mathbf{\Xi}$ in this case exists and is known as the water-filling solution. The channel capacity in this case is given by [20,26]:

$$\begin{aligned} C &= \sum_{k=1}^{K} \log_2(\eta\lambda_i^2)^+ \\ \gamma &= \sum_{k=1}^{K} (\eta - \lambda_i^{-2})^+ \end{aligned} \tag{9.65}$$

where $(x)^+ = x \forall x \geq 0, (x)^+ = 0 \forall x < 0$ and η is a non-linear function of eigenvalues of the channel input covariance matrix. The effect of various channel conditions on the channel capacity has been extensively studied in the literature. For example, increasing the LoS signal strength at fixed SNR reduces capacity in Rician channels [20]. This can be explained in terms of the channel matrix rank

[21]The concept of decomposition of an $N \times N$ Hermitian matrix in terms of quadratic product of $N \times N$ unitary matrix composed of eigenvectors and $N \times N$ diagonal matrix of eigenvalues can be generalized to $M \times N$ complex-valued matrices of rank K. If $\mathbf{A}$ is an $M \times N$ where $(M > N)$ complex-valued matrix of rank K, then $\mathbf{A} = \mathbf{U\Sigma V}^{H}$ denotes the singular value decomposition of $\mathbf{A}$. The $M \times M$ unitary matrix $\mathbf{U}$ is composed of the eigenvectors of $\mathbf{AA}^{H}$, i.e., $\mathbf{U} = (\mathbf{u_1}, \mathbf{u_2}, \ldots, \mathbf{u_m})$, where $\mathbf{AA}^{H}\mathbf{u}_i = \sigma_i^2\mathbf{u}_i$. The $N \times N$ unitary matrix $\mathbf{V}$ is composed of eigenvectors of $\mathbf{A}^{H}\mathbf{A}$, i.e., $\mathbf{V} = (\mathbf{v_1}, \mathbf{v_2}, \ldots, \mathbf{v_n})$, where $\mathbf{A}^{H}\mathbf{Av}_i = \sigma_i^2\mathbf{v}_i$. The elements of the $M \times N$ matrix $\mathbf{\Sigma} = \begin{pmatrix} \mathbf{\Lambda} & \mathbf{0} \\ \mathbf{0} & \mathbf{0} \end{pmatrix}$, $\mathbf{\Lambda} = \mathbf{diag}(\sigma_1, \sigma_2, \ldots, \sigma_K)$ are the square roots of the eigenvalues of matrix $\mathbf{A}^{H}\mathbf{A}$ which are referred to as the singular values of matrix $\mathbf{A}$. Therefore, matrix $\mathbf{A}$ may be written as $\mathbf{A} = \sum_{i=1}^{K} \sigma_i\mathbf{u}_i\mathbf{v}_i^{H}$. The number of non-zero singular values of matrix $\mathbf{A}$ is the rank of $\mathbf{A}$. The singular values of matrix $\mathbf{A}$ are positive real numbers which satisfy $\sigma_1 \geq \sigma_2 \geq \ldots \geq \sigma_K > 0$ [29].

Petitioners' Exhibit 1021
Nokia of America Corp., et al. v. KT Corporation, et al.
Case No. IPR2025-00036; U.S. Patent No. 11,627,631
Page 625 of 1122

or through various eigenvalue properties. The issue of correlated fading is of considerable importance for implementations where the antennas are required to be closely spaced. The optimal water-filling allocation strategy is obtained when the power allocated to each spatial sub-channel is non-negative. Figure 9.107 illustrates an example where the water-filling algorithm is applied to an OFDM system assuming the number of sub-channels = 16, total power = −20 dBm, N_0 = −80 dBm, and bandwidth = 1 MHz. It can be observed that depending on the inverse C/N of each sub-channel, the amount of power allocated to each sub-channel differs, provided that the sum of sub-channel powers does not exceed the total available power. The power allocated to each sub-channel corresponds to parameters λ_i^2.

9.13.2 Instantaneous capacity, ergodic capacity, and outage capacity of MIMO systems

In the design of wireless communication systems, the main objective is to exploit the transmission schemes whose performance can approach the channel capacity

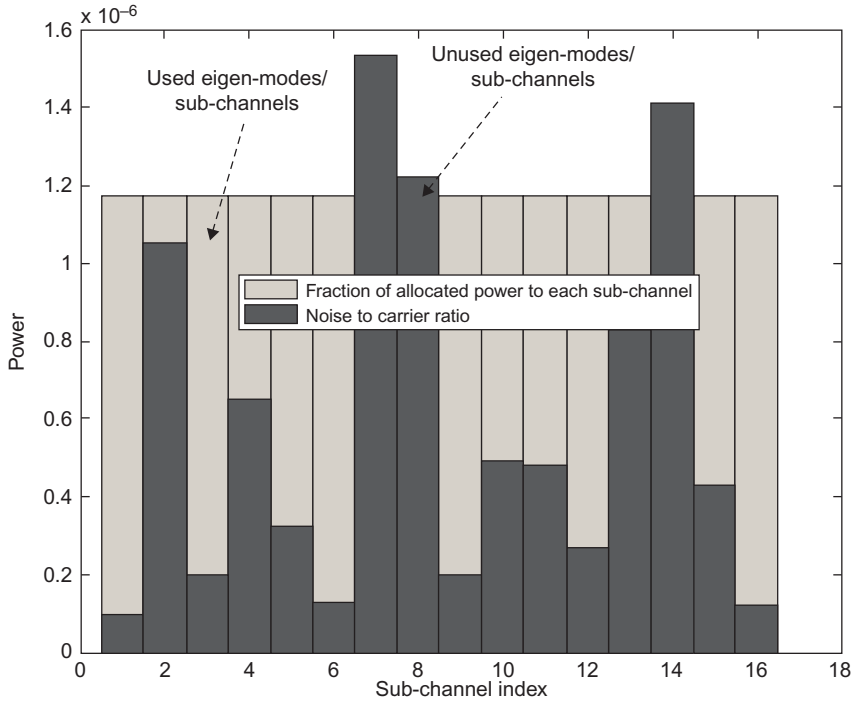


FIGURE 9.107

Example illustration of a water-filling algorithm in an OFDM system [141].

Petitioners' Exhibit 1021
Nokia of America Corp., et al. v. KT Corporation, et al.
Case No. IPR2025-00036; U.S. Patent No. 11,627,631
Page 626 of 1122

as much as possible. Therefore, it is important to understand the underlying concepts and various information theoretical definitions of channel capacity and what can be pragmatically achieved under realistic channel conditions and transceiver implementations.

Let us begin our concise study with the most generic definition of channel capacity. We denote the input and output of a memory-less SISO wireless channel with the random variables X and Y, respectively, the channel capacity is defined as [39]:

$$C = \max_{p(x)} I(X;Y) \tag{9.66}$$

where $I(X;Y)$ represents the mutual information between X and Y. Shannon's theorem [33] gives an operational meaning to the definition of the instantaneous capacity as the maximum number of bits we can transmit reliably over the channel with vanishing probability of error. The mutual information in Eq. (9.66) is maximized with respect to all possible transmit signal statistical distributions $p(x)$. Mutual information is a measure of the amount of information that one random variable contains about another variable. The mutual information between X and Y can also be written as $I(X;Y) = H(Y) - H(Y|X)$, where $H(Y|X)$ represents the conditional entropy between the random variables X and Y. The entropy of a random variable can be described as the measure of uncertainty in the random variable or the amount of information required on the average to describe the random variable. Thus, the mutual information representation of channel capacity can be described as the reduction in the uncertainty of one random variable due to the knowledge of the other. Note that the mutual information between X and Y depends on the properties of the channel through a channel matrix $\mathbf{H}$, and the properties of X through the probability distribution of X [166].

Throughout this section, it is assumed that the channel matrix $\mathbf{H}$ is random and that the receiver has perfect channel knowledge. It is also assumed that the channel is memory-less, i.e., for each use of the channel an independent realization of $\mathbf{H}$ is drawn. This means that the capacity can be computed as the maximum of the mutual information as defined earlier. The results are also valid when $\mathbf{H}$ is generated by an ergodic process, because as long as the receiver observes the $\mathbf{H}$ process, only the first order statistics are needed to determine the channel capacity.

The ergodic (mean) capacity of a random channel with $N_{RX} = N_{TX} = 1$ and an average transmit power constraint P_T can be expressed as:

$$C_{\text{ergodic}} = \mathscr{E}_{\mathbf{H}}\{\max_{p(x):P \le P_T} I(X;Y)\} \tag{9.67}$$

where P is the average power of a single codeword, transmitted over the channel, and $\mathscr{E}_{\mathbf{H}}\{.\}$ denotes the expectation over all channel realizations. Compared to the generic definition, the capacity of the channel is now defined as the maximum of the mutual information between the input and the output over all statistical

Petitioners' Exhibit 1021
Nokia of America Corp., et al. v. KT Corporation, et al.
Case No. IPR2025-00036; U.S. Patent No. 11,627,631
Page 627 of 1122

distributions on the input that satisfy the power constraint. In general, the capacity of a random MIMO channel with power constraint P_T can be expressed as [20]:

$$C_{\text{ergodic}} = \mathscr{E}_{\mathbf{H}}\{\max_{p(\mathbf{x}):\text{trace}(\mathbf{\Phi}) \le P_T} I(\mathbf{x};\mathbf{y})\} \tag{9.68}$$

where $\mathbf{\Phi} = \mathscr{E}[\mathbf{x}\mathbf{x}^H]$ is the covariance matrix of the transmit signal vector $\mathbf{x}$. The total transmit power is limited to P_T irrespective of the number of transmit antennas. For a fading channel, the channel matrix $\mathbf{H}$ is a stochastic process, and hence the associated channel capacity $C(\mathbf{H})$ is also a random variable. In this case, the ergodic channel capacity is defined as the average of instantaneous channel capacity over the distribution of $\mathbf{H}$. The ergodic channel capacity of the MIMO transmission scheme is given by:

$$C_{\text{ergodic}} = \mathscr{E}\left\{\max_{\text{trace}(\mathbf{\Phi}) = N_{TX}} \log_2\left(\det\left[\mathbf{I} + \frac{\gamma}{N_{TX}}\mathbf{H}\mathbf{\Phi}\mathbf{H}^H\right]\right)\right\} \tag{9.69}$$

where $\mathbf{\Phi}$ denotes the $N_{TX} \times N_{TX}$ covariance matrix of the channel input vector $\mathbf{x}$. According to information theoretic concepts, this capacity cannot be achieved unless channel coding is employed across an infinite number of independently fading blocks. Let us focus on the case of perfect CSI at the receiver side and no CSI at the transmitter side. Obviously, this implies that the maximization of the latter equation is now more restricted than in the previous case. Nevertheless, it has been shown in the literature that the optimal signal covariance matrix has to be chosen according to $\mathbf{\Phi} = \mathbf{I}$. This means that the antennas should transmit uncorrelated streams with the same average power. With this result, the ergodic MIMO channel capacity reduces to [20,24]:

$$C_{\text{ergodic}} = \mathscr{E}\left\{\log_2\left(\det\left[\mathbf{I} + \frac{\gamma}{N_{TX}}\mathbf{H}\mathbf{H}^H\right]\right)\right\} \tag{9.70}$$

Clearly, this is not the Shannon capacity in a true sense, since as mentioned before and with perfect channel knowledge at the transmitter one can choose a signal covariance matrix that outperforms $\mathbf{\Phi} = \mathbf{I}$ case. Nevertheless, we refer to the expression in Eq. (9.70) as the ergodic channel capacity with CSI at the receiver and no CSI at the transmitter.

The capacity under channel ergodicity was defined as the average of the maximal value of the mutual information between the transmitted and the received signals, where the maximization was carried out with respect to all possible transmit signal statistical distributions. Another measure of channel capacity that is frequently used is outage capacity. With outage capacity, the channel capacity is associated to an outage probability. Capacity is treated as a random variable which depends on the channel instantaneous response and remains constant during the transmission of a finite-length coded block of information. If the channel capacity falls below the outage capacity, there is no possibility that the transmitted block of information can be decoded with no errors, no matter which coding scheme is employed. The probability that the capacity is less than the outage

Petitioners' Exhibit 1021
Nokia of America Corp., et al. v. KT Corporation, et al.
Case No. IPR2025-00036; U.S. Patent No. 11,627,631
Page 628 of 1122

capacity denoted by C_{outage} is ρ. This can be expressed in mathematical terms by $p(C < C_{\text{outage}}) = \rho$. In this case, the latter expression represents an upper bound since there is a finite probability ρ that the channel capacity is less than the outage capacity. It can also be written as a lower bound, representing the case where there is a finite probability $(1 - \rho)$ that the channel capacity is higher than C_{outage}, which means $p(C > C_{\text{outage}}) = 1 - \rho$. In other words, since the MIMO instantaneous channel capacity is a random variable, it is meaningful to consider its statistical distribution. A useful measure of its statistical behavior is the outage capacity. Outage analysis quantifies the level of performance (in this case capacity) that is guaranteed with a certain level of reliability. The ρ% outage capacity $C_{\text{outage}}(\rho)$ is defined as the information rate that is guaranteed for $(100 - \rho)$% of the channel realizations ($p(C < C_{\text{outage}}) = \rho$). The outage capacity is often a more relevant measure than the ergodic channel capacity, because it describes in some way the quality of the channel. This is due to the fact that the outage capacity measures how the instantaneous rate supported by the channel is distributed, in terms of probability. Thus, if the rate supported by the channel is spread over a wide range, the outage capacity for a fixed probability level may become small, whereas the ergodic channel capacity may be high [166].

9.13.3 Spatial multiplexing and diversity

The main objective of space−time coding schemes is to exploit the inherent spatial (multipath) diversity in MIMO channels through properly designed space−time codes. In this section, two transmit diversity schemes, namely the Alamouti scheme and CDD, are described where both realize full spatial diversity of the channel without requiring channel knowledge at the transmitter. In the Alamouti scheme, we consider a MIMO channel with two transmit antennas and any number of receive antennas. The Alamouti scheme can be described as follows. Two different complex-valued data symbols s_1 and s_2 are transmitted simultaneously from antenna ports 1 and 2, respectively, during the first symbol period. In the second symbol period, symbols $-s_2^*$ and s_1^* are sent from antenna ports 1 and 2, respectively. It must be noted that the rate equals one in the Alamouti scheme since two independent data symbols are transmitted over two symbol periods. Let us consider the following case with two transmit antennas and one receive antenna, thereby we have two channels H_1 and H_2. The received signal at the first and second symbol period can be expressed as follows [58]:

$$\begin{aligned} y_1 &= H_1 s_1 + H_2 s_2 + n_1 \\ y_2 &= -H_1 s_2^* + H_2 s_1^* + n_2 \end{aligned} \tag{9.71}$$

Let $\mathbf{r} = (y_1, y_2^*)^{\text{H}}, \mathbf{s} = (s_1, s_2)^{\text{H}}$, $\mathbf{n} = (n_1, n_2)^{\text{H}}$, and $\mathbf{H} = \begin{bmatrix} H_1 & H_2 \\ H_2^* & -H_1^* \end{bmatrix}$, the relationship between the output and the input of the channel can be written as $\mathbf{r} = \mathbf{Hs} + \mathbf{n}$ where multiplying both sides of the latter equation by $\mathbf{H}^{\text{H}}$ yields

Petitioners' Exhibit 1021
Nokia of America Corp., et al. v. KT Corporation, et al.
Case No. IPR2025-00036; U.S. Patent No. 11,627,631
Page 629 of 1122

$\tilde{\mathbf{r}} = \mathbf{H}^{\mathrm{H}}\mathbf{H}\mathbf{s} + \tilde{\mathbf{n}}$. Since $\mathbf{H}$ is orthogonal, i.e., $\mathbf{H}^{\mathrm{H}}\mathbf{H} = \alpha\mathbf{I}$ where $\alpha = |H_1|^2 + |H_2|^2$; dividing both sides of the equation by α yields [58]:

$$\begin{aligned}\frac{\tilde{r}_1}{|H_1|^2 + |H_2|^2} &= s_1 + \frac{H_1^* n_1}{|H_1|^2 + |H_2|^2} + \frac{H_2 n_2}{|H_1|^2 + |H_2|^2} \\ \frac{\tilde{r}_2}{|H_1|^2 + |H_2|^2} &= s_2 + \frac{H_2^* n_1}{|H_1|^2 + |H_2|^2} + \frac{-H_1 n_2}{|H_1|^2 + |H_2|^2}\end{aligned} \tag{9.72}$$

It is assumed that the channels are independent and identically distributed with frequency-flat fading and remain constant over (at least) two consecutive symbol periods. Appropriate processing at the receiver, as shown in Eqs. (9.71) and (9.72), collapses the vector channel into a scalar channel for either of the transmitted data symbols, where $\tilde{\mathbf{r}}$ is the processed received signal corresponding to transmitted symbol $\mathbf{s}$, and $\tilde{\mathbf{n}}$ is the processed noise. Even though the CSI knowledge is not available at the transmitter, the Alamouti scheme achieves $2N_{\mathrm{RX}}$ order diversity. We note that array gain is realized only at the receiver since the transmitter does not have the CSI. The Alamouti scheme may be extended to channels with more than two transmit antennas through orthogonal space−time block coding. The link-level performance of the Alamouti scheme is compared to the SISO and SIMO cases in Figure 9.108 assuming BPSK-modulated input symbols and Rayleigh fading channel.

Delay diversity is an alternative method in which the same symbol is transmitted at different time instances such that each symbol experiences different fading. The delay diversity converts spatial diversity to frequency diversity by transmitting the data signal from the first antenna port and a delayed replica of the signal from the second antenna port. Assuming two transmit antennas and one receive antenna and that the delay induced by the second antenna equals one symbol period, the effective channel seen by the data signal is a frequency-selective fading SISO channel with impulse response $h(k) = h_1\delta(k) + h_2\delta(k-1)$, where h_1 and h_2 are complex-valued flat-fading channels. We note that the effective channel resembles a two-path SISO channel with independent fading paths and equal average path energy. An ML detector will realize full second-order diversity at the receiver. If the same signal is transmitted from two or more transmit antennas, a beamforming effect is created where in some directions the signal is attenuated, while in other directions it may be amplified. The CDD scheme mitigates this problem by transmitting cyclically shifted signals from the transmit antennas. Let us consider an OFDM symbol with constellation d_k at the kth frequency index, the time-domain signal corresponding to this symbol which is transmitted from antenna port 1 can be expressed as follows:

$$s_1(t) = \mathrm{Re}\left\{ \mathrm{e}^{\mathrm{j}\omega_c t} \sum_{k=-(N_{\mathrm{FFT}}-1)/2}^{(N_{\mathrm{FFT}}-1)/2} d_k \, \mathrm{e}^{\mathrm{j}2\pi k(t-t_g)/T_u} \right\} \quad mT_u \le t \le (m+1)T_u \tag{9.73}$$

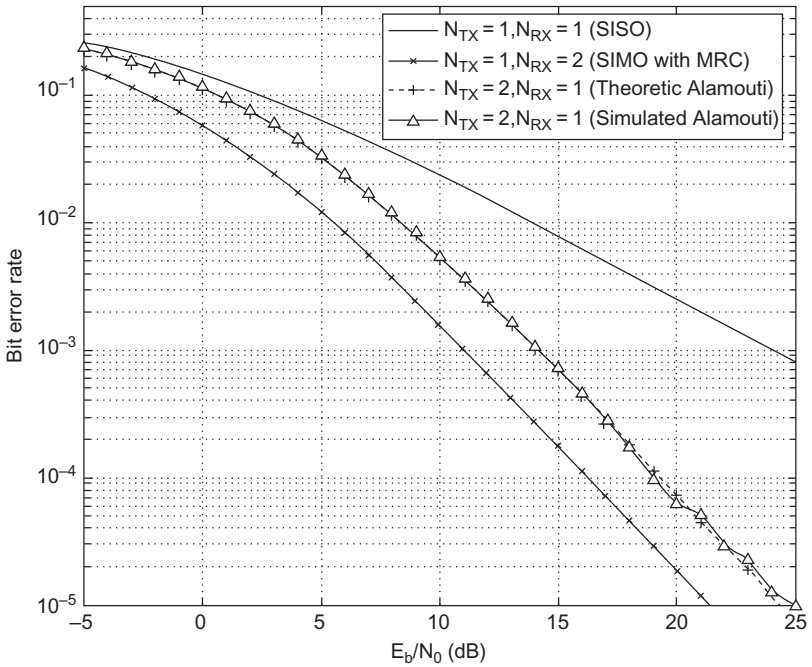


FIGURE 9.108

Performance of the Alamouti scheme [141].

Using the CDD scheme, the transmitted signal from the second antenna port is given by:

$$s_2(t) = \mathrm{Re}\left\{ e^{j\omega_c t} \sum_{k=-(N_{\mathrm{FFT}}-1)/2}^{(N_{\mathrm{FFT}}-1)/2} d_k \, e^{j2\pi k(t-t_g-T_{CDD})/T_u} \right\} \quad mT_u \le t \le (m+1)T_u \quad (9.74)$$

This is equivalent to a cyclic rotation of the signal in the time-domain. The implementation of the CDD scheme is simplified, if the cyclic shift T_{CDD} is an integer multiple of the sampling time. At the receiver, the effect of CDD at the kth index is of receiving through the channel $H_1(k) + \exp(j2\pi k T_{\mathrm{CDD}}/T_u)H_2(k)$. The advantage over the case of $H_1(k) + H_2(k)$, which is the result of transmission of the same signal over the two channels, is the prevention of the beamforming effect, i.e., directed transmission in one direction and undesired emission in the other directions.

The main objective of spatial multiplexing, as opposed to space−time diversity coding, is to maximize transmission data rate. Therefore, $\min(N_{\mathrm{TX}}, N_{\mathrm{RX}})$ independent data symbols are transmitted per symbol period such that the spatial rate is $\min(N_{\mathrm{TX}}, N_{\mathrm{RX}})$. There are several encoding options that can be used in

conjunction with spatial multiplexing to achieve the increased data rate. Single codeword and multi-codeword transmission are the prominent encoding options that are typically used in wireless communication systems. In a multi-codeword scheme, the bit stream to be transmitted is de-multiplexed into separate data streams where each stream is processed through the transmission chain, i.e., independent temporal encoding, symbol mapping, and interleaving, and is then transmitted from the corresponding antennas. The antenna to stream mapping remains static over time. The spatial rate is $\min(N_{\mathrm{TX}}, N_{\mathrm{RX}})$ and the overall signaling rate is $n_{\text{modulation-order}} r_{\mathrm{b}} \min(N_{\mathrm{TX}}, N_{\mathrm{RX}})$, where r_{b} denotes the channel coder input bit rate and $n_{\text{modulation-order}}$ denotes the QAM modulation order. The multi-codeword scheme can at most achieve N_{RX} order diversity, since any given information bit is transmitted from only one transmit antenna and received by N_{RX} receive antennas. While this is a source of sub-optimality of the multi-codeword architecture, it does simplify receiver design. The coding gain achieved by the multi-codeword scheme depends on the coding gain of the temporal code. Furthermore, a maximum array gain of N_{RX} can be realized using the multi-codeword scheme.

In the single-codeword architecture, the bit stream undergoes temporal encoding, symbol mapping, and interleaving after which it is de-multiplexed into $\min(N_{\mathrm{TX}}, N_{\mathrm{RX}})$ streams transmitted from the individual antennas. This form of encoding can achieve full $N_{\mathrm{TX}} \times N_{\mathrm{RX}}$ order diversity, provided that the temporal code is designed properly, since each information bit can be spread across all the transmit antennas. Nevertheless, the single-codeword scheme requires joint decoding of the sub-streams, which increases receiver implementation complexity compared to the multi-codeword scheme where the individual data streams can be decoded separately. The spatial rate of the single-codeword is $\min(N_{\mathrm{TX}}, N_{\mathrm{RX}})$, and the overall signaling rate is $n_{\text{modulation-order}} r_{\mathrm{b}} \min(N_{\mathrm{TX}}, N_{\mathrm{RX}})$. The coding gain achieved by the single-codeword scheme will depend on the temporal channel coding characteristic and a maximum array gain of N_{RX} can be achieved [24].

Space-frequency block coding is the frequency-domain version of the space–time block codes (STBC). This family of codes is designed to achieve diversity gain by transmitting orthogonal streams which yields optimal SNR with a linear receiver. Since, in the OFDM systems, the number of OFDM symbols in a subframe may often be an odd number, while STBC (e.g., Alamouti code) operates on pairs of adjacent symbols in the time-domain, the application of STBC would not be straightforward. For SFBC transmission, the adjacent sub-carriers on each OFDM symbol are paired, encoded, and transmitted from two base station antenna ports where the encoding is defined as follows:

$$\mathbf{W} = \begin{bmatrix} x_k & x_{k+1} \\ -x_{k+1}^{*} & x_k^{*} \end{bmatrix} \tag{9.75}$$

where $(x_k, -x_{k+1}^{*})$ and (x_{k+1}, x_k^{*}) are transmitted from antenna ports 1 and 2, respectively. Note that the spatial rate of the SFBC codes in this case is one.

Petitioners' Exhibit 1021
Nokia of America Corp., et al. v. KT Corporation, et al.
Case No. IPR2025-00036; U.S. Patent No. 11,627,631
Page 632 of 1122

9.13.4 MIMO receivers

An orthogonal space–time block coding scheme transforms a vector-detection problem into a number of scalar-detection problems. Similar concepts can be applied to frequency-selective fading MIMO channels, inspiring receiver design techniques such as zero-forcing (ZF), MMSE estimation, and (optimal) ML sequence detection [20]. The use of transmit diversity techniques such as CDD or frequency-offset diversity transforms a MISO channel into a number of SISO channels, and allows the application of SISO receiver architectures. For a general space–time trellis code, a vector Viterbi decoder can be employed. The space–time trellis coding in general provides improved performance over orthogonal space–time block coding at the expense of receiver complexity. The problem encountered by a receiver for spatial multiplexing is the presence of multi-stream interference, since the signals sent from different transmit antennas interfere with each other. Note that in spatial multiplexing, different data streams are transmitted in the same channel and occupy the same resources in time and frequency. For the sake of simplicity, we restrict our attention to the case where $N_{RX} \geq N_{TX}$.

9.13.4.1 Maximum likelihood receiver

The optimal detection for spatially multiplexed signals is to use maximum likelihood criterion. The ML receiver performs vector decoding and is optimal in the sense of minimizing the error probability. Assuming equally likely, temporally uncoded vector symbols, the ML receiver generates an estimate of the transmitted signal vector as follows:

$$\hat{\mathbf{s}} = \arg\min_{\mathbf{s}} \left\| \mathbf{y} - \sqrt{\frac{E_s}{N_{TX}}}\mathbf{H}\mathbf{s} \right\|^2 \tag{9.76}$$

where the minimization is performed over all possible transmit vector symbols $\mathbf{s}$. Let Z denote the alphabet size of the scalar constellation transmitted from each antenna, a complete implementation requires an exhaustive search over a total of $Z^{N_{TX}}$ vector symbols or hypotheses, making the decoding complexity of this receiver exponentially grow with the number of transmit antennas. Recent development of fast ML detection algorithms reduces the computational complexity of the ML decoder. The ML receiver realizes N_{RX} diversity order for the multi-codeword scheme and $N_{RX} \times N_{TX}$ diversity order for the single-codeword scheme [20,25].

9.13.4.2 Successive interference cancelation receiver

An alternative non-linear approach to detection of spatially multiplexed signals is successive interference cancelation (SIC) assuming that the spatially multiplexed signals are separately coded (i.e., multi-codeword transmission). As shown in Figure 9.109, in an SIC receiver, one of the spatially multiplexed signals is initially demodulated and decoded. Upon successful decoding, the data is

Petitioners' Exhibit 1021
Nokia of America Corp., et al. v. KT Corporation, et al.
Case No. IPR2025-00036; U.S. Patent No. 11,627,631
Page 633 of 1122

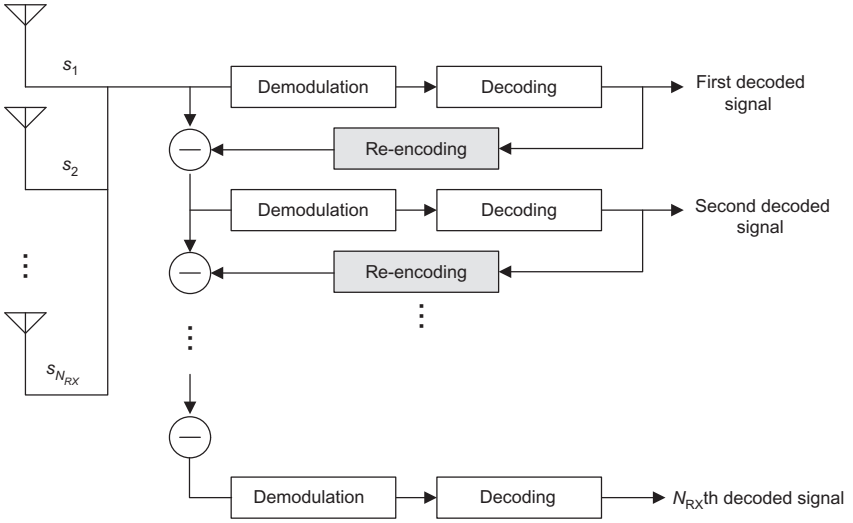


FIGURE 9.109

Structure of a successive interference cancelation MIMO receiver.

re-encoded and subtracted from the received signals. The second spatially multiplexed signal can then be demodulated and decoded in the absence of interference from the first detected signal. The subtraction would ideally improve the signal-to-interference ratio. The procedure is iterated until all spatially multiplexed signals are demodulated and decoded. It is noted that the first signals to be decoded using this approach are subject to higher interference levels compared to those that are decoded later in the process. Therefore, the ith signal to be decoded must be more robustly coded than the $(i+1)$th signal. This can be achieved in multi-codeword transmission by applying different modulation and coding schemes to different spatially multiplexed signals. The latter scheme is often referred to as per-antenna rate control (PARC) [20,25,42].

9.13.4.3 Zero-forcing receiver

The decoding complexity of the ML receiver can be reduced using a linear filter to separate the transmitted data streams and then independently decode each stream. The ZF and MMSE linear detectors are examples of such receivers. The ZF weighting matrix (filter) that decomposes the received signal into its component streams is given by the following equation [20,42]:

$$\mathbf{G}_{\mathrm{ZF}} = \sqrt{\frac{N_{\mathrm{TX}}}{E_{\mathrm{s}}}}\mathbf{H}^{\dagger} = \sqrt{\frac{N_{\mathrm{TX}}}{E_{\mathrm{s}}}}(\mathbf{H}^{\mathrm{H}}\mathbf{H})^{-1}\mathbf{H}^{\mathrm{H}} \tag{9.77}$$

where $\mathbf{G}_{ZF}$ is an $N_{TX} \times N_{RX}$ matrix that inverts the channel matrix and $\mathbf{H}^{\dagger}$ denotes the Moore–Penrose inverse[22] of the channel matrix $\mathbf{H}$. The output of the ZF receiver is obtained as follows:

$$\mathbf{y} = \mathbf{s} + \sqrt{\frac{N_{TX}}{E_s}}\mathbf{H}^{\dagger}\mathbf{n} \tag{9.78}$$

which shows that the ZF receiver decomposes the channel matrix into parallel scalar channels with additive spatially colored noise. Each scalar channel is then decoded independently irrespective of noise correlation across the processed streams. The ZF receiver transforms the joint decoding problem into single stream decoding problems, thereby significantly reducing receiver complexity. This complexity reduction is achieved at the expense of noise enhancement, which in general results in a significant performance degradation (compared to the ML decoder). The diversity order achieved by each of the individual data streams equals $N_{RX} - N_{TX} + 1$. Figure 9.110 illustrates the link-level performance of a 2×2 MIMO system with a ZF receiver. It is shown that the performance is close to that of a SISO system, since the diversity order is one.

9.13.4.4 Minimum mean square error receiver

The MMSE receiver balances multi-stream interference mitigation and noise enhancement effect, and minimizes the total error. The MMSE weighting matrix (filter) is given by the following expression [20,42]:

$$\mathbf{G}_{MMSE} = \arg\min_{\mathbf{G}} \mathscr{E}\left\{ ||\mathbf{G}\mathbf{y} - \mathbf{s}||^2 \right\} = \sqrt{\frac{N_{TX}}{E_s}}\left(\mathbf{H}^{H}\mathbf{H} + \frac{N_{TX}N_0}{E_s}\mathbf{I}\right)^{-1}\mathbf{H}^{H} \tag{9.79}$$

where $\mathbf{I}$ is an $N_{RX} \times N_{RX}$ identity matrix. In low signal-to-interference plus noise ratios (i.e., SINR < 0 dB), the performance of the MMSE receiver approaches that of a matched-filter receiver, outperforming the ZF detector which tends to enhance noise. In high signal-to-interference plus noise ratios, however, the performance of the MMSE receiver approaches that of a ZF receiver and therefore realizes $N_{RX} - N_{TX} + 1$ order diversity for each data stream.

---

[22] Given a matrix $\mathbf{A}$ and vector $\mathbf{b}$ and equation $\mathbf{Ax} = \mathbf{b}$, we find the vector $\mathbf{x}$ that minimizes $\|\mathbf{Ax} - \mathbf{b}\|$. Using the orthogonality principle, the error is taken perpendicular to estimation vector such that $\mathbf{x}^{H}\mathbf{A}^{H}(\mathbf{Ax} - \mathbf{b}) = 0$ which implies that $\mathbf{A}^{H}\mathbf{Ax} = \mathbf{A}^{H}\mathbf{b}$ (since $\mathbf{x} \neq 0$), or $\mathbf{x} = (\mathbf{A}^{H}\mathbf{A})^{-1}\mathbf{A}^{H}\mathbf{b}$. One should note that $\mathbf{Ax} = \mathbf{A}(\mathbf{A}^{H}\mathbf{A})^{-1}\mathbf{A}^{H}\mathbf{b}$. The matrix $\mathbf{A}^{\dagger} = (\mathbf{A}^{H}\mathbf{A})^{-1}\mathbf{A}^{H}$ is defined as the Moore–Penrose inverse of the matrix $\mathbf{A}$. If $\mathbf{A}^{H}\mathbf{A}$ is not invertible, the SVD algorithm is used to calculate the matrix pseudo-inverse. In that case, we may write $\mathbf{A} = \mathbf{V}_K\mathbf{\Sigma}_K\mathbf{U}_K^{H}$ and seek $\mathbf{x}$ such that $||\mathbf{V}_K\mathbf{\Sigma}_K\mathbf{U}_K^{H}\mathbf{x} - \mathbf{b}||$ is minimized. Using the orthogonality principle, we have $\mathbf{x}^{H}\mathbf{U}_K\mathbf{\Sigma}_K\mathbf{V}_K^{H}(\mathbf{V}_K\mathbf{\Sigma}_K\mathbf{U}_K^{H}\mathbf{x} - \mathbf{b})$ or (assuming $\mathbf{x} \neq 0$) $\mathbf{U}_K\mathbf{\Sigma}_K^2\mathbf{U}_K^{H}\mathbf{x} - \mathbf{U}_K\mathbf{\Sigma}_K\mathbf{V}_K^{H}\mathbf{b} = 0$ such that $\mathbf{\Sigma}_K^2\mathbf{U}_K^{H}\mathbf{x} - \mathbf{\Sigma}_K\mathbf{V}_K^{H}\mathbf{b} = 0$, multiplying both sides by $\mathbf{\Sigma}_K^{-2}$, yields $\mathbf{U}_K^{H}\mathbf{x} - \mathbf{\Sigma}_K^{-1}\mathbf{V}_K^{H}\mathbf{b} = 0$. The latter is true when $\mathbf{x} = \mathbf{\Sigma}_{i=1}^{K}\left(\frac{1}{\sigma_i}\mathbf{v}_i^{H}\mathbf{b}\right)\mathbf{u}_i$; therefore $\mathbf{x} = \mathbf{U}_K\mathbf{\Sigma}_K^{-1}\mathbf{V}_K^{H}\mathbf{b}$ [29].

Petitioners' Exhibit 1021
Nokia of America Corp., et al. v. KT Corporation, et al.
Case No. IPR2025-00036; U.S. Patent No. 11,627,631
Page 635 of 1122

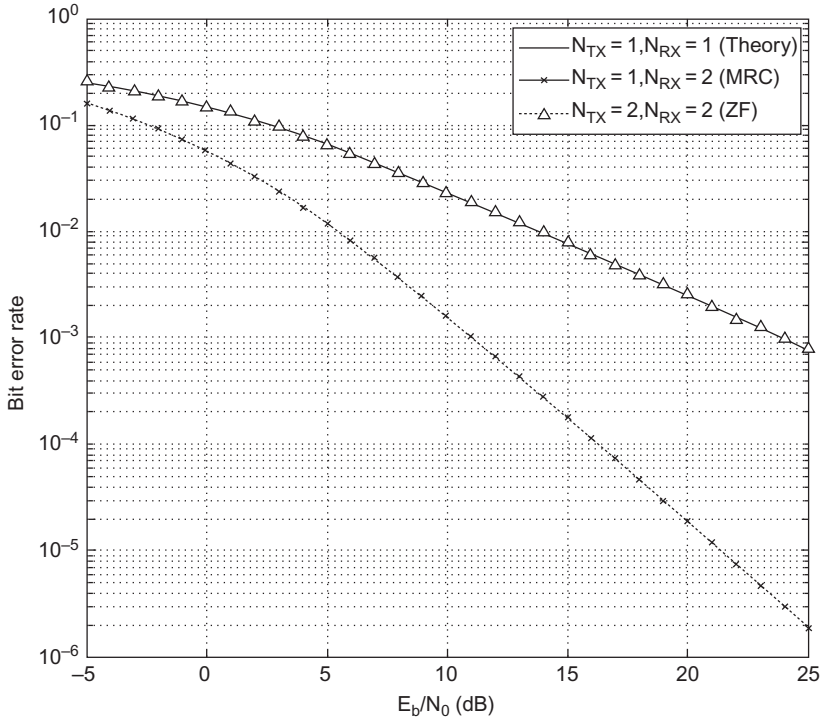


FIGURE 9.110

Link-level performance of 2×2 MIMO system with ZF equalizer (Rayleigh channel and BPSK modulation).

9.13.4.5 Maximal ratio combining receiver

In maximal ratio combining (MRC), the output is a weighted sum of all receiver branches, thus the coefficients $\alpha_i, i = 1, 2, \ldots,$ and N_{RX} are all non-zero. The signals are co-phased and $\alpha_i = \beta_i \, \mathrm{e}^{-\mathrm{j}\theta_i}, i = 1, 2, \ldots, N_{\mathrm{RX}}$ where θ_i is the phase of the received signal on the ith branch (Figure 9.111). The magnitude of the combined output can be written as $y = \sum_{i=1}^{N_{\mathrm{RX}}} \beta_i r_i$. Let us assume that the noise power spectral density is $N_0/2$ in each branch, which yields the combined noise at the output $n = \sum_{i=1}^{N_{\mathrm{RX}}} \beta_i^2 N_0/2$. The SNR at the output of the combiner is given as:

$$\gamma = \frac{1}{N_0} \frac{\left(\sum_{i=1}^{N_{\mathrm{RX}}} \beta_i r_i\right)^2}{\sum_{i=1}^{N_{\mathrm{RX}}} \beta_i^2} \tag{9.80}$$

The objective is to find $\alpha_i, i = 1, 2, \ldots, N_{\mathrm{RX}}$ which maximize the output SNR. It can be understood that branches with higher SNR are weighted more than those

Petitioners' Exhibit 1021
Nokia of America Corp., et al. v. KT Corporation, et al.
Case No. IPR2025-00036; U.S. Patent No. 11,627,631
Page 636 of 1122

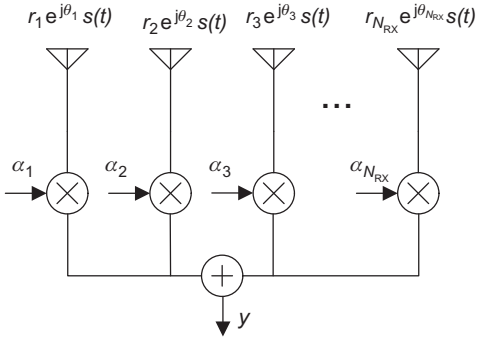


FIGURE 9.111

A generic linear combining receiver.

with lower SNR; therefore, the coefficients $\alpha_i, i = 1, 2, \ldots,$ and N_{RX} are proportional to the branch SNRs. The coefficients are found by taking partial derivatives of the output SNR expression and solving the resulting equations for the optimal weights which yields $\alpha_i = r_i^2/N_0, i = 1, 2, \ldots, N_{\mathrm{RX}}$ and the output SNR will be the sum of the SNRs of the receiving branches. Therefore, the output SNR and the corresponding array gain increase linearly with the number of the diversity branches (i.e., the number of receive antennas).

9.13.4.6 MMSE-interference rejection combining receiver

The interference rejection combining (IRC) receiver is an effective method for improving the cell-edge user throughput, since it attempts to suppress the inter-cell interference. The IRC receiver is typically based on the minimum mean square error criteria, which requires channel estimation and covariance matrix estimation including the inter-cell interference with high accuracy. The gain from the IRC receiver is tied to the estimation of the interference signal, i.e., the covariance matrix, in terms of the downlink user throughput performance in a multi-cell environment. We define the $N_{\mathrm{RX}} \times 1$ received signal vector $\mathbf{y}(k, l)$ corresponding to the kth sub-carrier and the lth OFDM symbol as follows: $\mathbf{y}(k, l) = \sum_{i=0}^{N_{cell}-1} \mathbf{H}_i(k, l)\mathbf{W}_{\mathrm{TX}}^i(k, l)\mathbf{s}_i(k, l) + \mathbf{n}(k, l)$, where $\mathbf{H}_i(k, l)$ represents the $N_{\mathrm{RX}} \times N_{\mathrm{TX}}$ channel matrix between the ith cell and the UE, $\mathbf{W}_{\mathrm{TX}}^i(k, l)$ represents the $N_{\mathrm{TX}} \times N_l$ precoding matrix of the ith cell, $\mathbf{s}_i(k, l)$ denotes the $N_l \times 1$ signal vector of the ith cell, and $\mathbf{n}(k, l)$ is the $N_{\mathrm{RX}} \times 1$ noise vector with variance σ^2. In this context, $N_{\mathrm{TX}}, N_{\mathrm{RX}}, N_l,$ and N_{cell} are the number of transmit antennas of each cell, the number of receive antennas at the UE, the number of transmission layers for the UE, i.e., transmission ranks and total number of cells in the model, respectively. The zeroth cell is assumed to be the serving cell for the UE.

Petitioners' Exhibit 1021
Nokia of America Corp., et al. v. KT Corporation, et al.
Case No. IPR2025-00036; U.S. Patent No. 11,627,631
Page 637 of 1122

The received signal vector at the UE denoted by $\hat{\mathbf{s}}_0(k,l)$ is detected using a $N_l \times N_{\mathrm{RX}}$ weighting matrix $\mathbf{W}_{\mathrm{RX}}^0(k,l)$ expressed as $\hat{\mathbf{s}}_0(k,l) = \mathbf{W}_{\mathrm{RX}}^0(k,l)\mathbf{y}(k,l)$. Based on MMSE criterion, the weighting matrix $\mathbf{W}_{\mathrm{RX}}^0(k,l)$ is obtained by $\mathbf{W}_{\mathrm{RX}}^0(k,l) = P_0\overline{\mathbf{G}}_0^H(k,l)\overline{\mathbf{R}}_{yy}^{-1}$ and $\overline{\mathbf{G}}_0(k,l) = \overline{\mathbf{H}}_0(k,l)\mathbf{W}_{\mathrm{TX}}^0$ where P_0, $\overline{\mathbf{G}}_0$, $\overline{\mathbf{H}}_0$, and $\overline{\mathbf{R}}_{yy}$ denote the transmission power of the serving cell, the composite channel from the serving cell, the $N_{\mathrm{RX}} \times N_{\mathrm{TX}}$ channel matrix of the serving cell, and the covariance matrix of the received signal, respectively [180].

The baseline MMSE receiver is defined as a receiver that only suppresses the inter-layer interference, i.e., separates multiple data streams that achieve the maximum SINR for each data stream within a cell. The inter-cell interference is assumed to be AWGN at each receive antenna, making the covariance matrix a diagonal matrix. In the special case of rank-1 transmission, the MMSE receiver is equivalent to the MRC receiver. When a composite channel from the serving cell is obtained, the covariance matrix without the inter-cell interference can be represented by the composite channel from the serving cell, and the interference power from other cells and noise power. Therefore, the respective MMSE weighting matrices with ideal and realistic channel estimation are obtained as follows [180]:

$$\begin{aligned}
\mathbf{W}_{\mathrm{MMSE}}^{\mathrm{Ideal}}(k,l) &= P_0\mathbf{G}_0^H(k,l)[P_0\mathbf{G}_0(k,l)\mathbf{G}_0^H(k,l) + \boldsymbol{\Omega} + \sigma_N^2\mathbf{I}]^{-1} \\
\boldsymbol{\Omega} &= diag(\sigma_{I_0}^2, \sigma_{I_1}^2, \ldots, \sigma_{I_{N_{\mathrm{RX}}}}^2) \\
\mathbf{W}_{\mathrm{MMSE}}^{\mathrm{Realistic}}(k,l) &= P_0\hat{\mathbf{G}}_0^H(k,l)(P_0\hat{\mathbf{G}}_0(k,l)\hat{\mathbf{G}}_0^H(k,l) + \boldsymbol{\Omega} + \sigma_N^2\mathbf{I})^{-1}
\end{aligned} \tag{9.81}$$

where $\mathbf{G}_0(k,l)$, $\hat{\mathbf{G}}_0(k,l)$, $\sigma_{I_j}^2$, and σ_{N}^2 denote the ideal composite channel matrix, the estimated composite channel matrix based on the DM-RSs, which are precoded in the same manner as the data signals, the interference power from other cells at the jth receive antenna, and the noise power, respectively [180].

The MMSE-IRC receiver can suppress not only the inter-layer interference, but also the inter-cell interference when the degrees of freedom at the receiver are high, i.e., the number of receive antennas is higher than that of the desired transmission rank. If the composite channels from N_{cell} cells are perfectly known at the receiver, the ideal IRC weighting matrix is obtained as follows:

$$\mathbf{W}_{\mathrm{IRC}}^{\mathrm{Ideal}}(k,l) = P_0\mathbf{G}_0^H(k,l)\left(\sum_{i=0}^{N_{\mathrm{cell}}-1} P_i\mathbf{G}_i(k,l)\mathbf{G}_i^H(k,l) + \sigma_{\mathrm{N}}^2\mathbf{I}\right)^{-1} \tag{9.82}$$

However, it is assumed that the composite channel matrices from other $N_{\mathrm{cell}} - 1$ cells cannot be estimated at the receiver; therefore, the covariance matrix including the inter-cell interference is obtained by statistical averaging of the receiver signal, yielding:

$$\mathbf{R}_{yy} = \mathscr{E}[\mathbf{y}(k,l)\mathbf{y}^{\mathrm{H}}(k,l)] \tag{9.83}$$

Petitioners' Exhibit 1021
Nokia of America Corp., et al. v. KT Corporation, et al.
Case No. IPR2025-00036; U.S. Patent No. 11,627,631
Page 638 of 1122

The resulting IRC weighting matrices in the case of ideal and realistic channel estimations can be obtained as follows:

$$\begin{aligned}\mathbf{W}_{\text{IRC}}^{\text{Ideal}}(k,l) &= P_0\mathbf{G}_0^H(k,l)(\mathscr{E}[\mathbf{y}(k,l)\mathbf{y}^{\text{H}}(k,l)])^{-1}\\ \mathbf{W}_{\text{IRC}}^{\text{Realistic}}(k,l) &= P_0\hat{\mathbf{G}}_0^H(k,l)(\mathscr{E}[\mathbf{y}(k,l)\mathbf{y}^{\text{H}}(k,l)])^{-1}\end{aligned} \tag{9.84}$$

The accuracy of the IRC weighting depends on the accuracy of the channel estimation and covariance matrix. Therefore, in order to obtain an accurate covariance matrix, the covariance matrix must be averaged using the received samples which have gone through the same precoding matrix at the transmitter side and the same channel matrix with high correlation. More specifically, in order to ensure the use of the same precoding matrix, one can assume that the covariance matrix is averaged over one resource block using all samples except for the control signaling, the CRSs, and the CSI-RSs. Note that LTE Rel-10 allows the use of different precoding matrices for different resource blocks. Furthermore, it must be noted that some signals, such as control signaling, CRSs, and CSI-RSs, are transmitted without precoding [180].

The time-domain averaging is given more priority over frequency-domain averaging within a resource block because the channel variation within a subframe is smaller than that within a resource block in the frequency-domain. Two averaging methods, i.e., time-domain only, and time- and frequency-domain averaging are performed where the resulting covariance matrices are calculated as follows [180]:

$$\begin{aligned}\mathbf{R}_{yy}^{\text{time}} &= \frac{1}{N_{\text{time}}}\sum_{l}\mathbf{y}(k,l)\mathbf{y}^{\text{H}}(k,l)\\ \mathbf{R}_{yy}^{\text{time-frequency}} &= \frac{1}{N_{\text{time-frequency}}}\sum_{k}\sum_{l}\mathbf{y}(k,l)\mathbf{y}^{\text{H}}(k,l)\end{aligned} \tag{9.85}$$

where N_{time} and $N_{\text{time-frequency}}$ denote the average number of samples for the time-domain and time- and frequency-domain averaging, respectively [180].

9.13.4.7 Sphere decoding

In its search for the ML solution, the sphere decoder (SD) evaluates all transmit signal vectors $\mathbf{x}$ fulfilling the following criterion: $||\mathbf{y}-\mathbf{H}\mathbf{x}||^2 < R^2$, where R is the search radius of a hyper-sphere. It is obvious that the selection of R is a critical issue largely influencing the complexity of any SD algorithm. Choosing R too large would lead to a sphere containing a large number of hypotheses (also referred to as candidates), leading to high detection complexity. On the other hand, choosing R too small would result in an empty sphere and the search having to be restarted with an increased radius, eventually leading to similar problems. The search for candidates fulfilling the above inequality is done by back-substitution algorithms.

Petitioners' Exhibit 1021
Nokia of America Corp., et al. v. KT Corporation, et al.
Case No. IPR2025-00036; U.S. Patent No. 11,627,631
Page 639 of 1122

Toward this goal, the Cholesky[23] or QR[24] decompositions of the channel matrix $\mathbf{H}$ may be equivalently used. Note that using a Cholesky decomposition may be advantageous in systems with more transmit than receive antennas, since the size of the upper triangular matrix $\mathbf{R}$ is limited by $\min(N_{\mathrm{RX}}, N_{\mathrm{TX}})$, which for $N_{\mathrm{RX}} < N_{\mathrm{TX}}$ leads to an under-determined problem for the QR implementation of the SD [181].

In the following, we focus on the symmetric case, i.e., $N_{\mathrm{RX}} = N_{\mathrm{TX}}$, and use a QR decomposition of $\mathbf{H}$, for practicality of implementation. With $\mathbf{H} = \mathbf{QR}$, where $\mathbf{R}$ is upper-triangular and $\mathbf{Q}$ is unitary, the above inequality may be rewritten as follows:

$$||\mathbf{y}-\mathbf{Hx}||^2 < R^2 \Rightarrow ||\mathbf{Q}^{\mathrm{H}}\mathbf{y}-\mathbf{Rx}||^2 < R^2 \Rightarrow ||\mathbf{y}'-\mathbf{Rx}||^2 < R^2 \tag{9.86}$$

The above expression can be written as follows:

$$\sum_{i=l}^{N_{\mathrm{TX}}} \left| y_i^{'} - \sum_{j=i}^{N_{\mathrm{TX}}} r_{ij} x_j \right|^2 < R^2 \quad l = 1, 2, \ldots, N_{\mathrm{TX}} \tag{9.87}$$

The detection process starts with the last layer $l = N_{\mathrm{TX}}$, for which the latter expression reduces to $|y_{N_{\mathrm{TX}}}^{'} - r_{N_{\mathrm{TX}}N_{\mathrm{TX}}} x_{N_{\mathrm{TX}}}|^2 < R^2$ and continues until the first layer is detected. This process is quite similar to SIC techniques, i.e., the signals from previously detected layers are subtracted from the received signal before detection within the current layer is performed. However, in SD, detection at the ith layer essentially takes on the following form:

$$|c_{ki} - x_i|^2 < \frac{R_{ki}^2}{r_{ii}^2} \tag{9.88}$$

where c_{ki} is the search center and R_{ki} is the remainder search radius for the currently considered (incomplete) candidate c. Both SIC and SD methods depend on the estimates for previously detected layers, and hence vary from one candidate to another. The above inequality implies that not only a single, but several constellation points may be selected. The SD receiver hence performs its search in a tree like structure, which motivates the search for appropriate enumeration

[23]Given a symmetric positive-definite matrix $\mathbf{H}$, the Cholesky decomposition is an upper triangular matrix $\mathbf{U}$ with strictly positive diagonal entries such that $\mathbf{H} = \mathbf{U}^{\mathrm{H}}\mathbf{U}$ [28,29]. Alternatively, if $\mathbf{H}$ has real entries and is symmetric (or more generally, has complex-valued entries and is Hermitian) and positive-definite, then $\mathbf{H}$ can be decomposed as $\mathbf{H} = \mathbf{LL}^{\mathrm{H}}$, where $\mathbf{L}$ is a lower triangular matrix with strictly positive diagonal entries and $\mathbf{L}^{\mathrm{H}}$denotes the conjugate transpose of $\mathbf{L}$. The Cholesky decomposition is unique, i.e., given a Hermitian, positive-definite matrix $\mathbf{H}$, there is only one lower triangular matrix $\mathbf{L}$ with strictly positive diagonal entries such that $\mathbf{H} = \mathbf{LL}^{\mathrm{H}}$. In the special case that $\mathbf{H}$ is a symmetric positive-definite matrix with real entries, then $\mathbf{L}$ has real entries as well [28,29].

[24]Given a matrix $\mathbf{H}$, its QR decomposition is a matrix decomposition of the form $\mathbf{H} = \mathbf{QR}$ where $\mathbf{R}$ is an upper triangular matrix and $\mathbf{Q}$ is a unitary matrix, i.e., one satisfying $\mathbf{Q}^{\mathrm{T}}\mathbf{Q} = \mathbf{I}$ where $\mathbf{Q}^{\mathrm{T}}$ is the transpose of $\mathbf{Q}$ and $\mathbf{I}$ is the identity matrix [28,29].

Petitioners' Exhibit 1021
Nokia of America Corp., et al. v. KT Corporation, et al.
Case No. IPR2025-00036; U.S. Patent No. 11,627,631
Page 640 of 1122

strategies. Since we eventually consider coded transmission where extracting good quality soft outputs require finding a predefined minimum number of candidates $N_{c_{min}}$, we take a different approach toward this problem. Our interest lies in ensuring a certain minimum number of entries N_c at the bottom of the search tree. With the entries of $\mathbf{H}$ and the noise $\mathbf{n}$ at the receiver being random variables, N_c is obviously a random variable, as well. If we allow for all hypotheses fulfilling the original inequality to be tested, we obtain an upper bound on the expected complexity. Note that whenever an empty sphere is declared, the search must be restarted with an increased radius. Since the overall detection complexity is the sum of all attempts to find the ML point, it is unfavorable to choose a small initial search radius and then increase it stepwise until $N_{c_{min}}$ candidates are found.

For our symmetric $N_{RX} = N_{TX}$ MIMO system, the initial value for R reduces to $R^2 = 2\sigma^2 K N_{RX}$. Since in our system we normalize $2\sigma^2 = 1$ and then scale the transmitter signal constellation, this is further reduced to $R^2 = K N_{RX}$ where the critical point lies in the selection of K. It was found empirically that it would be beneficial to use a small initial search radius at low SNR that is subsequently increased with increasing SNR. The results of evaluations provided in the literature suggest that using $K = \frac{1}{60} L R_c \sqrt{\frac{E_b}{N_0}}$, where L is the number of bits per symbol and R_c is the code rate, provides a good choice that minimizes detection complexity in a wide SNR range. The middle factor ensures that the scaling of the transmitter signal set is taken into account and the last term derives from the notion that in the high SNR region, finding too many candidates becomes less probable and that the number of events with an empty sphere should be minimized. The radius can be increased by a factor of 1.5, whenever an empty sphere is declared [181].

9.13.4.8 CSI feedback

The reciprocity principle in wireless communication indicates that the channel from an antenna A to another antenna B is identical to the transpose of the channel from antenna B to antenna A, provided that the two channels are measured at the same time, the same frequency, and the same antenna locations. This principle further suggests that the transmitter can obtain information of the downlink (A to B) channel from the uplink (B to A) channel measurements, which the receiver at A can conduct. This information can involve the instantaneous channel or other channel parameters, including the channel statistics. In real full-duplex communications, however, the downlink and uplink channels cannot use identical frequency, time, and spatial instances. The reciprocity principle may still hold approximately, if the difference in any of these dimensions is relatively small compared to the channel variation across the referenced dimension.

Let us consider a scenario in which the base station measures the uplink channel during reception and uses this measurement for the CSIT of the next transmission in the downlink. In voice communications, the downlink and uplink channels to and from all the users operate in consecutive time slots. Therefore, uplink

Petitioners' Exhibit 1021
Nokia of America Corp., et al. v. KT Corporation, et al.
Case No. IPR2025-00036; U.S. Patent No. 11,627,631
Page 641 of 1122

channel measurements can be made regularly using reference signals. These measurements periodically refresh the CSIT. In data communications, the downlink and uplink channels may not operate continuously; hence, specially scheduled uplink transmissions for channel measurements, known as channel sounding, are used. A subset of the users, for whom CSIT is required, is scheduled to send sounding signals. The sounding signals are orthogonal among simultaneously scheduled users, using orthogonal sub-carriers in OFDM or orthogonal codes in CDMA systems. Sounding is an effective channel measurement technique for systems with multiple transmit antennas at the base station.

One complication in using reciprocity methods is that the principle only applies to the radio channel between the antennas, while in practice the channel is measured and used at the baseband processor. Different transmit and receive RF hardware chains; therefore, become part of the downlink and uplink channels. Since these chains have different frequency transfer characteristics, reciprocity requires transmit−receive chain calibration to equalize the effects of the two chains. Calibration is expensive and has made open-loop methods less attractive in practice.

Another method of obtaining CSIT is using feedback from the UE. The channel information is measured at the receiver at B during the downlink (A to B) transmission and then sent to the transmitter at A on the uplink. In practice, the downlink transmission from a base station includes reference signals, received by all active users. These users, when instructed by the serving base station, can measure their respective channels. The users then periodically or aperiodically send their measured channel information in the uplink channel to the base station to be used in calculation of their CSIT.

The feedback transmission can either be scheduled separately or piggybacked on ongoing transmissions. In data communications, CSIT may be needed for only a subset of users, who are then scheduled to transmit their channel information. Feedback is not limited by the reciprocity requirements. However, it imposes additional system overhead by consuming radio resources. Techniques to reduce the amount of feedback have been a subject of intense study, e.g., designing vector codebooks, quantizing channel information, or selecting only the important information. Furthermore, feedback information is susceptible to channel variation due to the delay in the feedback loop. The effectiveness of feedback depends on this delay and the channel Doppler spread. For a fast time-varying channel in mobile communications, feedback techniques are usually effective up to a certain mobile speed, depending on the carrier frequency, the transmission frame length, and the round trip time. The effects of feedback delay and error have been analyzed for various precoding techniques in LTE/LTE-Advanced, revealing potentially severe performance degradation. Therefore, the optimal use of feedback must account for the information quality.

The trade-off among transmission rate, error rate, and SINR for the scenarios where the transmitter has no channel knowledge and the receiver has perfect knowledge of CSI has been studied in the literature. If the MIMO channel is

Petitioners' Exhibit 1021
Nokia of America Corp., et al. v. KT Corporation, et al.
Case No. IPR2025-00036; U.S. Patent No. 11,627,631
Page 642 of 1122

assumed to be block fading, the length of the transmitted codewords is less than or equal to the channel block length, and if the channel was perfectly known to the transmitter, we could choose a signaling rate equal to or less than channel capacity and achieve error-free transmission. The coding scheme to achieve capacity consists of performing modal decomposition which decouples the MIMO channel into parallel SISO channels and then using ideal SISO channel coding. In practice, turbo codes can achieve near MIMO channel capacity performance. If the channel is unknown to the transmitter, modal decomposition is not possible. Since the channel is selected randomly according to a given fading distribution, there will always be a non-zero probability that a given transmission rate is not supported by the channel. We assume that the transmitted codeword is decoded successfully if the rate is at or below the mutual information, assuming a spatially white transmit covariance matrix, associated with the given channel realization. A decoding error is declared if the rate exceeds the mutual information. Therefore, if the transmitter does not have any knowledge of the channel, the PER would be equal to the outage probability associated with the transmission rate. We define the diversity order for a given transmission rate as [78]:

$$d(R) = -\lim_{\gamma \to \infty} \frac{\log[P_e(R,\gamma)]}{\log(\gamma)} \tag{9.89}$$

where $P_e(R,\gamma)$ is the PER corresponding to transmission rate R and SNR γ. Thus, the diversity order is the magnitude of the slope of the PER plotted as a function of the SNR on the logarithmic scale [78].

The differential feedback is a different approach to the enhancement of feedback accuracy. The differential feedback exploits the correlation between precoding matrices adjacent in time or frequencies. It only feeds back the difference between the current and the previous beamforming matrices. If the channel variation between two feedbacks is small, quantization codewords are concentrated in a small region on Grassmannian manifold[25] and not uniformly distributed over the entire beamforming space. For low-mobility users, the differential feedback may improve the feedback accuracy without increasing the number of feedback bits. The feedback starts initially and restarts periodically by sending a single feedback that fully describes the precoder. Differential feedbacks follow the start and restart feedbacks. The start and restart feedbacks employ a codebook that is

[25]A Grassmann manifold is a certain collection of vector subspaces of a vector space. In particular, $g_{n,k}$ is the Grassmann manifold of k-dimensional subspaces of the vector space $\mathbb{R}^n$. It has a natural manifold structure as an orbit space of the Stiefel manifold $v_{n,k}$ of orthonormal k-frames in G^n. One of the main features of Grassmann manifolds is that they are classifying spaces for vector bundles. A manifold is a topological space that is locally Euclidean (i.e., around every point, there is a neighborhood that is topologically the same as the open unit ball in $\mathbb{R}^n$). The Grassmannian $Gr(n,k)$ is the set of k-dimensional subspaces in an n-dimensional vector space. For example, the set of lines $Gr(n,k)$ is projective space. The real Grassmannian (as well as the complex Grassmannian) are examples of manifolds [31,32].

Petitioners' Exhibit 1021
Nokia of America Corp., et al. v. KT Corporation, et al.
Case No. IPR2025-00036; U.S. Patent No. 11,627,631
Page 643 of 1122

self-contained, e.g., the base codebook. Figure 9.112 illustrates the operation of differential feedback across time [83].

An example of differential feedback is a transformation-based differential codebook. Let t, $\mathbf{D}(t)$, and $\mathbf{V}(t)$ denote the feedback index, the corresponding feedback matrix, and the corresponding precoder, respectively. The sequential index is reset to 0 at $T_{\max}+1$. The index for the start and restart feedbacks are 0. Let $\mathbf{U}$ be a vector or a matrix and $\mathbf{Q}_{\mathbf{U}}$ be a rotation matrix determined by $\mathbf{U}$. The precoders of the subsequent differential feedbacks are denoted as $\mathbf{D}(t)$ for $t=1,2,\ldots,T_{\max}$ and the corresponding precoders are given as follows:

$$\begin{aligned}\mathbf{V}(t) &= \mathbf{Q}_{\mathbf{V}(t-1)}\mathbf{D}(t)\\ \mathbf{D}(t) &= \mathbf{Q}^{H}_{\mathbf{V}(t-1)}\mathbf{V}(t)\end{aligned} \qquad t=0,1,2,\ldots,T_{\max} \tag{9.90}$$

where the rotation matrix $\mathbf{Q}_{\mathbf{V}(t-1)}$ is an $N_{\mathrm{TX}}\times N_{\mathrm{TX}}$ unitary matrix derived from the previous precoder matrix $\mathbf{V}(t-1)$, and N_{TX} denotes the number of transmit antennas. The dimension of the feedback matrix $\mathbf{D}(t)$ is $N_{\mathrm{TX}}\times N_l$, where N_l denotes the number of spatial streams. The feedback matrix $\mathbf{D}(t)$ can be viewed as a description of time/frequency correlation properties which does not change over the entire frequency band and a long period of time, and $\mathbf{Q}_{\mathbf{V}(t-1)}$ can be viewed as a description of narrowband and short-term channel properties which correspond to a specific sub-band and subframe. Due to correlation between beamforming matrices across time and frequency, feedback overhead can be reduced, if the correlation property can be efficiently exploited. Let us take the time-domain correlation as an example to explain the differential feedback scheme. The hypothetical operations at the UE and at the eNB can be described as follows [18]:

1. Derivation of the differential codeword matrix at the UE, $\mathbf{D}=\hat{\mathbf{Q}}^{\mathrm{H}}_{\mathbf{V}(t-1)}\mathbf{V}(t)=[\hat{\mathbf{V}}(t-1),\hat{\mathbf{V}}^{\perp}(t-1)]^{\mathrm{H}}\mathbf{V}(t)$.
2. Quantization of the differential codeword matrix at the UE, $\hat{\mathbf{D}}=\arg\max_{\mathbf{D}_i\in\boldsymbol{\Omega}}||\mathbf{D}^{\mathrm{H}}\mathbf{D}_i||_F$ where $||\mathbf{D}^{\mathrm{H}}\mathbf{D}_i||_F$ denotes the Chordal distance between

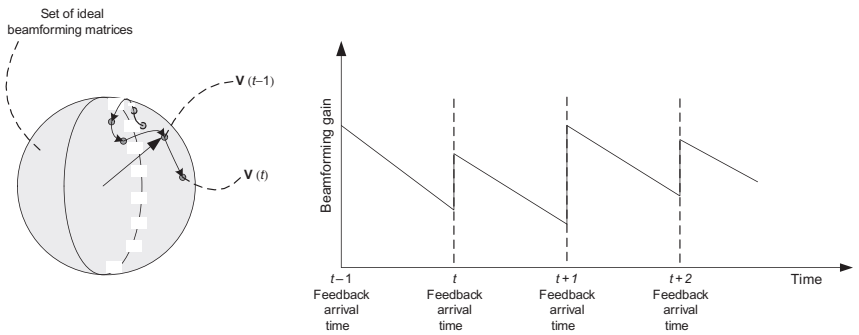


FIGURE 9.112

Example illustration of differential feedback and effect on beamforming gain.

Petitioners' Exhibit 1021
Nokia of America Corp., et al. v. KT Corporation, et al.
Case No. IPR2025-00036; U.S. Patent No. 11,627,631
Page 644 of 1122

the two codeword matrices $\mathbf{D}$ and $\mathbf{D}_i$. Therefore, the optimal codebook is selected based on the maximum distance between $\mathbf{D}$ and the codeword matrices contained in the codebook $\mathbf{\Omega}$.

3. Beamforming matrix reconstruction at the eNB, $\hat{\mathbf{V}}(t) = \hat{\mathbf{Q}}_{\mathbf{V}}(t-1)\hat{\mathbf{D}} = [\hat{\mathbf{V}}(t-1), \hat{\mathbf{V}}^{\perp}(t-1)]\hat{\mathbf{D}}$.
4. Beamforming at the eNB, $\mathbf{y} = \mathbf{H}\hat{\mathbf{V}}(t)\mathbf{s} + \mathbf{n}$.

In the above equations, $\mathbf{V}(t)$ and $\hat{\mathbf{V}}(t)$ denote the ideal and quantized $N_{\mathrm{TX}} \times N_l$ beamforming matrices at time instant t, respectively, the columns of $\hat{\mathbf{V}}^{\perp}(t-1)$ have unit norm and are orthogonal to $\hat{\mathbf{V}}(t-1)$ where $\hat{\mathbf{V}}^{\perp}(t-1)$ can be calculated from $\hat{\mathbf{V}}(t-1)$ by a Householder transformation,[26] $\mathbf{D}_i$ is the codeword matrix of the differential codebook denoted by $\mathbf{\Omega}$. The quantization criterion maximizes the received signal power. Other criteria such as channel capacity or mean squared error can also be used. If $N_l = 1$, $\mathbf{V}(t-1)$ would be a vector (with unit norm) and the rotation matrix is given by $\mathbf{Q}_{\mathbf{V}(t-1)} = \mathbf{I} - 2\varphi\varphi^{\mathrm{H}}; ||\varphi|| > 0$ wherein $\varphi = \exp(-\mathrm{j}\theta)\mathbf{V}(t-1) - \varepsilon$ and θ is the phase of the first entry of $\mathbf{V}(t-1)$ and $\varepsilon = (1, 0, 0, \ldots, 0)^{\mathrm{T}}$.

9.13.5 Precoding and beamforming

Multiple antennas at the transmitter and receiver can be used to achieve array and diversity gain instead of capacity gain. In this case, the same symbol weighted by a complex-valued scale factor is sent from each transmit antenna so that the input covariance matrix has unit rank. This scheme is referred to as beamforming. It must be noted that there are two conceptually and practically different classes of beamforming: (1) direction-of-arrival beamforming (i.e., adjustment of transmit or receive antenna directivity); and (2) eigen-beamforming (i.e., a mathematical approach to maximize signal power at the receive antenna based on certain criterion). In this section, we only consider eigen-beamforming schemes.

A classic eigen-beamforming scheme usually performs linear, single-layer, complex-valued weighting on the transmitted symbols such that the same signal is transmitted from each transmit antenna using appropriate weighting factors. In this scheme, the objective is to maximize the signal power at the receiver output. When the receiver has multiple antennas, the single-layer beamforming cannot

[26] In linear algebra, Householder transformation is defined as a linear transformation that describes a reflection about a plane or hyper-plane containing the origin. The Householder transformations are widely used in linear algebra to perform QR decompositions. This is a linear transformation given by the Householder matrix $\mathbf{Q} = \mathbf{I} - 2\mathbf{u}\mathbf{u}^{\mathrm{H}}$ where $\mathbf{I}$ denotes the identity matrix and $\mathbf{u}$ is given as a column unit vector. The Householder matrix has the following properties: (1) it is hermitian, i.e., $\mathbf{Q} = \mathbf{Q}^{\mathrm{H}}$; and (2) it is unitary, i.e., $\mathbf{Q}^{-1} = \mathbf{Q}^{\mathrm{H}}$ [31,32].

Petitioners' Exhibit 1021
Nokia of America Corp., et al. v. KT Corporation, et al.
Case No. IPR2025-00036; U.S. Patent No. 11,627,631
Page 645 of 1122

simultaneously maximize the signal power at every receive antennas, hence, precoding is used for multi-layer beamforming in order to maximize the throughput of a multi-antenna system. Precoding is a generalized beamforming scheme to support multi-layer transmission in a MIMO system. Using precoding, multiple streams are transmitted from the transmit antennas with independent and appropriate weighting per each antenna such that the throughput is maximized at the receiver output.

Let us begin our concise study of eigen-beamforming and MIMO precoding using a simplified model. In a single-user MIMO (SU-MIMO) system, identity matrix precoding (for open-loop) and SVD precoding (for closed-loop) can be used to achieve link-level MIMO channel capacity. In addition, random unitary precoding can achieve the open-loop MIMO channel capacity with no signaling overhead in the uplink. The SVD precoding, on the other hand, has been shown to achieve the MIMO channel capacity when CSI is signaled to the transmitter. In a precoded SU-MIMO system with N_{TX} transmit antennas and N_{RX} receive antennas, the input−output relationship can be described as $\mathbf{y} = \mathbf{HWs} + \mathbf{n}$ where $\mathbf{s} = (s_1, s_2 \ldots, s_{\mathrm{M}})^{\mathrm{T}}$ is an $M \times 1$ vector of normalized complex-valued modulated symbols, $\mathbf{y} = (y_1, y_2, \ldots, y_{N_{\mathrm{RX}}})^{\mathrm{T}}$ and $\mathbf{n} = (n_1, n_2, \ldots, n_{N_{\mathrm{RX}}})^{\mathrm{T}}$ are the $N_{\mathrm{RX}} \times 1$ vectors of received signal and noise, respectively, $\mathbf{H}$ is the $N_{\mathrm{RX}} \times N_{\mathrm{TX}}$ complex-valued channel matrix, and $\mathbf{W}$ is the $N_{\mathrm{TX}} \times M$ linear precoding matrix. The superscript "T" denotes the transpose operator.

In the receiver, a hard-decoded symbol vector $\hat{\mathbf{s}}$ is obtained by decoding the received vector $\mathbf{y}$ using a vector decoder, assuming perfect knowledge of the channel and the precoding matrices. We assume that the entries of $\mathbf{H}$ are independent and identically distributed according to $\mathbb{Z}(0, 1)$, and the entries of noise vector $\mathbf{n}$ are independent and identically distributed according to $\mathbb{Z}(0, N_0)$. The input vector $\mathbf{s}$ is assumed to be normalized, thus $\mathrm{E}[\mathbf{ss}^{\mathrm{H}}] = \mathbf{I}$ where $\mathbf{I}$ is an identity matrix. Let us further assume that precoding matrix $\mathbf{W}$ is unitary, thus $\mathbf{WW}^{\mathrm{H}} = \mathbf{I}$. The receiver selects a precoding matrix $\mathbf{W}_i, i = 1, 2, \ldots, N_{\mathrm{codebook}}$ from a finite set of quantized precoding matrices $\Omega = \{\mathbf{W}_1, \mathbf{W}_2, \ldots, \mathbf{W}_{N_{\mathrm{codebook}}}\}$ and sends the index of the chosen precoding matrix back to the transmitter over a low-delay feedback channel. There are two important issues concerning the above precoding scheme: (1) optimal selection criterion for choosing a precoding matrix from set $\mathbf{\Omega}$; and (2) design of codebook $\mathbf{\Omega}$. The matrix $\mathbf{W}_i, i = 1, 2, \ldots, N_{\mathrm{codebook}}$ can be selected from $\mathbf{\Omega}$ by using either of the following optimization criteria [82]: (1) minimizing the trace of the mean squared error (MMSE-trace selection); (2) minimizing the determinant of the mean squared error (MMSE-determinant selection); (3) maximizing the minimum singular value of $\mathbf{HW}$ (singular value selection); (4) maximizing the instantaneous capacity (capacity selection); or (5) maximizing the minimum received symbol vector distance (minimum distance selection). The above selection criteria may be evaluated at the receiver using a full search over all matrices in $\mathbf{\Omega}$. Using distortion functions based on the selection criteria, it can be shown that the codebook $\mathbf{\Omega}$ is designed using Grassmannian subspace packing [82]. If MMSE-trace, singular value, or minimum distance selection is used, the codebook

Petitioners' Exhibit 1021
Nokia of America Corp., et al. v. KT Corporation, et al.
Case No. IPR2025-00036; U.S. Patent No. 11,627,631
Page 646 of 1122

is designed such that $\varepsilon = \min_{\mathbf{W_i} \neq \mathbf{W_j}} ||\mathbf{W}_i \mathbf{W}_i^{\mathrm{H}} - \mathbf{W}_j \mathbf{W}_j^{\mathrm{H}}||_2$[27] is maximized. If the MMSE-determinant or capacity selection optimization method is used, the codebook is designed such that $\varepsilon = \min_{\mathbf{W_i} \neq \mathbf{W_j}} \arccos|\det(\mathbf{W}_i^{\mathrm{H}} \mathbf{W}_j)|$ is maximized [82].

The MIMO codebooks are designed based on a trade-off between performance and complexity. The following are some desirable properties of the codebooks:

1. Low-complexity codebooks can be designed by choosing the elements of each constituent matrix or vector from a small binary set, e.g., a four alphabet ($\pm 1, \pm j$) set, which eliminates the need for matrix or vector multiplication. In addition, the nested property of the codebooks can further reduce the complexity of CQI calculation when rank adaptation is performed.
2. The base station may perform rank overriding which results in significant CQI mismatch, if the codebook structure cannot adapt to it. A nested property with respect to rank overriding can be exploited to mitigate the mismatch effects.
3. Power amplifier balance is taken into consideration when designing codebooks with constant modulus property, which may eliminate unnecessary increase in PAPR.
4. Good performance for a wide range of propagation scenarios, e.g., uncorrelated, correlated, and dual-polarized antennas, is expected from the codebook design algorithms. A DFT-based codebook is optimal for linear array with small antenna spacing since the vectors match with the structure of the transmit array response. Additionally, with an optimal selection of the matrices and the entries of the codebook (rotated block diagonal structure), significant gains can be obtained in dual-polarized scenarios.
5. Low feedback and signaling overhead are desirable from an operation and performance perspective.
6. Low memory requirement is another design consideration for the MIMO codebooks.

An alternative approach to codebook-based precoding is to use differential codebook precoding, in which the transmitter computes the precoding matrix by using a differential codebook precoding matrix specified by the receiver and the previous precoding matrix used in the transmitter, thus $\mathbf{W}_k = \mathbf{C}_{m_{\mathrm{opt}}} \mathbf{W}_{k-1}$ where each differential codebook precoding matrix $\mathbf{C}_m, m = 1, 2, \ldots, N'_{\mathrm{codebook}}$ is an $N_{\mathrm{TX}} \times N_{\mathrm{TX}}$ matrix. The receiver selects the optimum differential precoding matrix which maximizes the instantaneous capacity as follows [83]:

$$\mathrm{Optimum-codebook-index}: m_{\mathrm{opt}} = \arg \max_{\mathrm{m}} \log_2 \det\left(\mathbf{I} + \frac{\gamma}{N_{\mathrm{TX}}} \mathbf{H}_k \mathbf{W} \mathbf{C}'_m{}^{\mathrm{H}} \mathbf{H}_k^{\mathrm{H}}\right) \tag{9.91}$$

[27]The Euclidean norm of square matrix $\mathbf{A}$ is defined as $||\mathbf{A}||_2 = \sup_{||\mathbf{x}||=1} ||\mathbf{A}\mathbf{x}||_2$. The spectral norm of matrix $\mathbf{A}$ is the largest singular value of $\mathbf{A}$ or the square root of the largest eigenvalue of the positive-semi-definite matrix $\mathbf{A}^{\mathrm{H}}\mathbf{A}$; i.e., $||\mathbf{A}||_2 = \sqrt{\lambda_{\max}(\mathbf{A}^{\mathrm{H}}\mathbf{A})}$ where $\mathbf{A}^{\mathrm{H}}$ denotes the conjugate transpose of $\mathbf{A}$ [44].

Petitioners' Exhibit 1021
Nokia of America Corp., et al. v. KT Corporation, et al.
Case No. IPR2025-00036; U.S. Patent No. 11,627,631
Page 647 of 1122

where $\{\mathbf{C}'_1,\mathbf{C}'_2,\ldots,\mathbf{C}'_{N'_{\text{codebook}}}\} = \{\mathbf{C}_1\mathbf{W}_{k-1},\mathbf{C}_2\mathbf{W}_{k-1},\ldots,\mathbf{C}_{N'_{\text{codebook}}}\mathbf{W}_{k-1}\}$ and γ is the signal-to-noise ratio. The initial precoding matrix can be set as the first M columns of the $N_{\text{TX}} \times N_{\text{TX}}$ identity matrix. One advantage of the differential precoding scheme is that the candidate precoding matrices $\{\mathbf{C}'_1,\mathbf{C}'_2,\ldots,\mathbf{C}'_{N'_{\text{codebook}}}\}$ are refined in each precoding update instance, which virtually increases the codebook size to realize finer quantization of the channel [83]. Since the differential precoding schemes compute the precoding matrix by using the previous precoding matrix, different criteria should be used to generate precoding matrices. In a slow fading environment where precoding is more effective, the channel variation during the precoding matrix update interval is relatively small. In this case, the ideal codebook matrix which is multiplied by the previous precoding matrix should be close to the identity matrix. Thus, the codebook design strategy is to optimize the codebook such that the codebook includes quasi-diagonal matrices. More specifically, codebook matrices are computed from two unitary matrices as $\mathbf{C}_{\text{m}} = \mathbf{G}^{\text{H}}(t)\mathbf{G}(t+\Delta t)$, where $\mathbf{G}(t) \in \mathbb{C}^{N_{\text{TX}} \times N_{\text{TX}}}$ is a random unitary matrix. Note that since both $\mathbf{G}(t)$ and $\mathbf{G}(t+\Delta t)$ are unitary matrices, each codebook matrix $\mathbf{C}_{\text{m}} \in \mathbb{C}^{N_{\text{TX}} \times N_{\text{TX}}}$ also has unitary properties, and small perturbation Δt produces quasi-diagonal matrices whose diagonal entries are more dominant than other entries. A set of codebooks $\{\mathbf{C}_1,\mathbf{C}_2,\ldots,\mathbf{C}_{N'_{\text{codebook}}}\}$ are generated by using various Δt values where the codebook is optimized by capacity maximization criterion.

In SVD precoding, assuming the perfect knowledge of the CSI, the channel matrix is decomposed as $\mathbf{H} = \mathbf{U}\boldsymbol{\Sigma}\mathbf{V}^{\text{H}}$, where $\mathbf{U}$ and $\mathbf{V}$ are unitary matrices (i.e., $\mathbf{U}^{\text{H}}\mathbf{U} = \mathbf{I}, \mathbf{V}^{\text{H}}\mathbf{V} = \mathbf{I}$) and $\boldsymbol{\Sigma}$ is a diagonal matrix containing eigenvalues of the channel matrix. If the relationship between the output and input of the channel is described as $\mathbf{y} = \mathbf{H}\mathbf{s} + \mathbf{n}$, then by replacing the channel matrix with its SVD form and multiplying both sides by $\mathbf{U}^{\text{H}}$, one can write $\mathbf{U}^{\text{H}}\mathbf{y} = \mathbf{U}^{\text{H}}\mathbf{U}\boldsymbol{\Sigma}\mathbf{V}^{\text{H}}\mathbf{s} + \mathbf{U}^{\text{H}}\mathbf{n}$. Further simplification of the latter equation would yield $\tilde{\mathbf{y}} = \boldsymbol{\Sigma}\mathbf{x} + \tilde{\mathbf{n}}$, if the input signal is precoded with $\mathbf{x} = \mathbf{V}^{\text{H}}\mathbf{s}$. Using SVD precoding, the channel matrix is diagonalized and the spatial interference is removed without any matrix inversion or non-linear processing. Since $\mathbf{U}$ is unitary, $\mathbf{U}^{\text{H}}\mathbf{n}$ still has the same variance as $\mathbf{n}$, thus, the SVD precoding does not result in noise enhancement. Due to substantial feedback and complexity of singular value decomposition of the channel matrix, the SVD precoding is not considered a viable precoding scheme. This procedure is illustrated in Figure 9.113.

In general, the precoding algorithms for multi-user MIMO (MU-MIMO) can be classified into linear and non-linear classes. Linear precoding schemes can achieve reasonable performance with lower complexity compared to non-linear precoding techniques. Linear precoding includes unitary and zero-forcing precoding schemes. Non-linear precoding can achieve near optimal capacity at the expense of increased complexity. Non-linear precoding is designed based on the concept of dirty paper coding (DPC), where any known interference at the transmitter can be canceled if the optimal precoding scheme is applied to the transmit signal.

Unitary precoding includes unitary and semi-unitary precoding, both of which are a simple extension of SVD precoding in SU-MIMO with the addition of the SDMA-based user scheduling technique. The SDMA-based opportunistic user

Petitioners' Exhibit 1021
Nokia of America Corp., et al. v. KT Corporation, et al.
Case No. IPR2025-00036; U.S. Patent No. 11,627,631
Page 648 of 1122

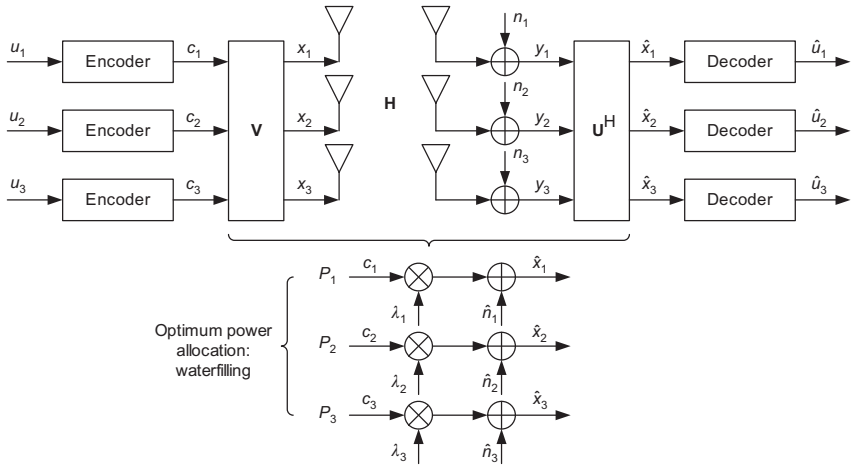


FIGURE 9.113

Illustration of the SVD concept [46].

scheduling technique groups near orthogonal users to avoid intra-group interferences at the cost of additional signaling overhead, which results in higher performance relative to the SU-MIMO. For example, it can increase diversity order to approximately the number of transmit antennas even with simple linear decoding at the receiver.

The zero-forcing precoding consists of zero-forcing and regularized zero-forcing precoding. If the transmitter has perfect knowledge of the downlink CSI, the ZF-based precoding can achieve near channel capacity performance when the number of users is large. With limited CSI at the transmitter, ZF-precoding requires increased feedback to achieve the full multiplexing gain. Hence, inaccurate CSI at the transmitter may result in significant loss of performance due to residual interference among transmit streams.

DPC is a coding technique that cancels known interference without power penalty provided that the transmitter has perfect knowledge of the interfering signals regardless of whether the receiver has knowledge of CSI. This category includes Costa precoding [89], Tomlinson-Harashima precoding [80], and the vector perturbation technique [80]. Vector perturbation uses modulo operation at the transmitter to perturb the transmitted signal vector to avoid the transmit power enhancement incurred by zero-forcing methods. The optimal perturbation method is found by solving a minimum distance problem, and thus can be implemented using sphere decoding or full search-based algorithms [73–80].

Now let us consider MU-MIMO systems and briefly study how precoding is applied in those scenarios. In the downlink direction of a precoded MU-MIMO system (alternatively known as broadcast channel in the literature) with N_{TX} transmit antennas at the base station and one receive antenna at the kth mobile station, the input–output relationship can be written as $y_k = \mathbf{h}_k^H \mathbf{x} + n_k, k = 1, 2, \ldots, N_{user}$, where

Petitioners' Exhibit 1021
Nokia of America Corp., et al. v. KT Corporation, et al.
Case No. IPR2025-00036; U.S. Patent No. 11,627,631
Page 649 of 1122

$\mathbf{x} = \sum_{i=1}^{N_{\text{user}}} s_i \mathbf{w}_i$ is the $N_{\text{TX}} \times 1$ vector of weighted transmitted symbols s_i, y_k and n_k are the received signal and noise, respectively, $\mathbf{h}_k$ is the kth $N_{\text{TX}} \times 1$ channel vector, where matrix $\mathbf{H} = (\mathbf{h}_1, \mathbf{h}_2, \ldots, \mathbf{h}_{N_{\text{user}}})^{\text{T}}$ is the $N_{\text{user}} \times N_{\text{TX}}$ complex-valued downlink channel matrix, and $\mathbf{w}_k$ is the kth $N_{\text{TX}} \times 1$ normalized linear precoding vector.

The mathematical relationship for the input and output of a precoded MU-MIMO system in the uplink (alternatively known as multiple access channel in the literature) with N_{RX} receive antennas at the base station and one transmit antenna at each user's terminal can be written as $\mathbf{y} = \sum_{k=1}^{N_{\text{user}}} s_k v_k \mathbf{h}_k + \mathbf{n}$ where $s_k v_k$ is the weighted complex-valued modulated symbol from the kth user, $\mathbf{y} = (y_1, y_2, \ldots, y_{N_{\text{RX}}})^{\text{T}}$ and $\mathbf{n} = (n_1, n_2, \ldots, n_{N_{\text{RX}}})^{\text{T}}$ are the $N_{\text{RX}} \times 1$ vectors of received signal and noise, respectively, $\mathbf{h}_k$ is the kth $N_{\text{RX}} \times 1$ channel vector, where matrix $\mathbf{H} = (\mathbf{h}_1, \mathbf{h}_2, \ldots, \mathbf{h}_{N_{\text{user}}})^{\text{T}}$ is the $N_{\text{RX}} \times N_{\text{user}}$ complex-valued uplink channel matrix. As mentioned earlier, perfect knowledge of the CSI is necessary at the transmitter in order to achieve the capacity of a MU-MIMO channel. However, in practical systems, the receiver only provides partial CSI through uplink feedback channels to the transmitter, i.e., the MU-MIMO precoding with limited feedback.

The received signal in the downlink of a MU-MIMO system with limited feedback precoding is mathematically expressed as: $y_k = \mathbf{h}_k^{\text{H}} \sum_{i=1}^{N_{\text{user}}} s_i \hat{\mathbf{w}}_i + n_k, k = 1, 2, \ldots, N_{\text{user}}$. The transmit vector for limited feedback precoding is modeled as $\hat{\mathbf{w}}_i = \mathbf{w}_i + \varepsilon_i$ where ε_i is the error vector generated as a result of the limited feedback and vector quantization, and the expression for the received signal can be rewritten as:

$$y_k = \mathbf{h}_k^{\text{H}} \sum_{i=1}^{N_{\text{user}}} s_i \mathbf{w}_i + \mathbf{h}_k^{H} \sum_{i=1}^{N_{\text{user}}} s_i \varepsilon_i + n_k, \quad k = 1, 2, \ldots, N_{\text{user}} \tag{9.92}$$

where $\mathbf{h}_k^{\text{H}} \sum_{i=1}^{N_{\text{user}}} s_i \varepsilon_i$ is the residual interference due to the limited-feedback precoding. To reduce the residual interference term, one should use more accurate CSI feedback which results in the use of more uplink resources for the feedback. It is shown in the literature that the number of feedback bits per user N_{feedback} must be increased linearly with the SNR γ_{dB} (in decibels) at the rate of $N_{\text{feedback}} = (N_{\text{TX}} - 1)\log_2 \gamma = \gamma_{\text{dB}}(N_{\text{TX}} - 1)/3$ in order to achieve the full multiplexing gain of N_{TX}. In addition, the scaling of N_{feedback} guarantees that the throughput loss relative to zero-forcing precoding with perfect CSI knowledge at the transmitter is upper-bounded by N_{TX} bps/Hz, which corresponds to approximately 3 dB power offset [78]. The throughput of a feedback-based zero-forcing system is bounded, if the SNR approaches infinity and the number of feedback bits per user is fixed. Reducing the number of feedback bits according to $N_{\text{feedback}} = \alpha \log_2 \gamma$ for any $\alpha < N_{\text{TX}} - 1$ results in a strictly inferior multiplexing gain of $N_{\text{TX}}[\alpha/(N_{\text{TX}} - 1)]$ where N_{TX} is the number of transmit antennas and γ is the SNR of the downlink channel. In order to calculate the amount of feedback required to maintain certain

Petitioners' Exhibit 1021
Nokia of America Corp., et al. v. KT Corporation, et al.
Case No. IPR2025-00036; U.S. Patent No. 11,627,631
Page 650 of 1122

throughput, the difference between the feedback rates of zero-forcing precoding with perfect feedback $R_{PF-ZF}(\gamma)$ and with limited feedback $R_{LF-ZF}(\gamma)$ is required to satisfy the following constraint $\Delta R(\gamma) = R_{PF-ZF}(\gamma) - R_{LF-ZF}(\gamma) \leq \log_2 b$. In order to maintain a rate offset less than $\log_2 b$ (per user) between zero-forcing with perfect CSI and with finite-rate feedback (i.e., $\Delta R(\gamma) \leq \log_2 b, \forall \gamma$), it is sufficient to scale the number of feedback bits per user according to $N_{feedback} = \gamma_{dB}(N_{TX} - 1)/3 - (N_{TX} - 1)\log_2(b - 1)$. The rate offset of $\log_2 b$ (per user) is translated into a power offset, which is a more useful metric from the design perspective. Since a multiplexing gain of N_{TX} is achieved with zero-forcing, the zero-forcing curve has a slope of N_{TX} bps/Hz/3 dB at asymptotically high SNR. Therefore, a rate offset of $\log_2 b$ bps/Hz per user corresponds to a power offset of $3\log_2 b$ decibels. To feedback $N_{feedback}$ bits through the uplink channel, the throughput of the uplink feedback channel should be larger than or equal to $N_{feedback}$, i.e., $w_{FB} \log_2(1 + \gamma_{FB}) \geq N_{feedback}$ where γ_{FB} denotes the SNR of the feedback channel. Thus, the required feedback resource to satisfy the constraint $\Delta R(\gamma) \leq \log_2 b$ can be shown to be given as follows $w_{FB} \geq [\gamma_{dB}(N_{TX} - 1)/3 - (N_{TX} - 1)\log_2(b - 1)]/\log_2(1 + \gamma_{FB})$, i.e., the required feedback resource is a function of both downlink and uplink channel conditions [78].

We defined precoding as adaptive or non-adaptive weighting of the spatial streams prior to transmission from each antenna port (in a multi-antenna configuration) using a precoding matrix for the purpose of improving the reception or separation of the spatial streams at the receiver. Both feed-back and feed-forward precoder matrix selection schemes can be used in order to select the optimal weights. Feed-back precoding matrix selection techniques do not rely on channel reciprocity, rather they use feedback channels provided that the feedback latency is less than the channel coherence time. In feed-forward approaches, the necessary CSI can be theoretically obtained through direct feedback, where the CSI is explicitly signaled to the transmitter by the receiver, or sounding reference signals. The direct channel feedback methods preclude the channel reciprocity requirement, whereas channel sounding methods rely on channel reciprocity. Therefore, explicit control signaling is required for the PMI-based (feedback) schemes. However, in reciprocity-based schemes, the sounding signals in the uplink and precoded pilots in the downlink are used to assist the transmitter and receiver to appropriately select the precoding matrix. The reciprocity-based schemes have the additional advantage of not being constrained to a finite set of codebooks. Beamforming relies on long-term statistics of the radio channel and unlike reciprocity-based techniques, does not require short-term correlation between the uplink and downlink in order to properly function.

9.13.6 SU-MIMO and MU-MIMO

Single-user MIMO techniques are point-to-point schemes that improve channel capacity and reliability through the use of space−time/space−frequency codes (transmit/receive diversity) in conjunction with spatial multiplexing schemes. In a

Petitioners' Exhibit 1021
Nokia of America Corp., et al. v. KT Corporation, et al.
Case No. IPR2025-00036; U.S. Patent No. 11,627,631
Page 651 of 1122

SU-MIMO transmission, the advantage of MIMO processing is obtained from the coordination of processing among all the transmitters or receivers. In the multi-user channel, on the other hand, it is usually assumed that there is no coordination among the users. As a result of the lack of coordination among users, uplink and downlink MU-MIMO channels are different. In the uplink scenario, users transmit to the base station over the same channel. The challenge for the base station is to separate the signals transmitted by the users, using array processing or multi-user detection methods. Since the users are not able to coordinate with each other, there is not much that can be done to optimize the transmitted signals with respect to each other. If some channel feedback is allowed from the transmitter back to the users, some coordination may be possible, but it may require that each user knows all the other users' channels rather than only its own. Otherwise, the challenge in the uplink is mainly in the processing done by the base station to separate the users. In the downlink channel, where the base station simultaneously transmits to a group of users over the same channel, there is some inter-user interference for each user which is generated by the signals transmitted to other users. Using multi-user detection techniques, it may be possible for a given user to overcome the multiple access interference, but such techniques are often extremely complicated for use at the receivers. Ideally, one would like to mitigate the interference at the transmitter by carefully designing the transmitted signal. If CSI is available at the transmitter, it is aware of what interference is being created for user i by the signal it is transmitting to user j, and vice versa. The inter-user interference can be mitigated by beamforming or the use of dirty paper codes.

In general, SU-MIMO and MU-MIMO schemes are compared as follows [60−64]:

- SU-MIMO is a point-to-point link with predictable link capacity, whereas a MU-MIMO channel is a broadcast channel in the downlink direction and a multiple access channel in the uplink direction whose link-level data rates are characterized in terms of capacity regions.
- Multi-layer SU-MIMO schemes offer layer/stream diversity in the sense that if one stream has a poor SNR, the system will not necessarily experience an outage, whereas in the same situation, a MU-MIMO system will be in outage. This is due to the fact that in MU-MIMO schemes, users have typically an equal target data rate and symbol error rate on their respective links, while in SU-MIMO systems, only the sum rate of the overall link is considered, since all streams are delivered to same user.
- The MU-MIMO schemes suffer from a near-far problem due to significant differences between the path losses experienced by each user, resulting in a large deviation in the SINR of the corresponding user links. This would benefit the users with better channel conditions, while there is no near-far problem in SU-MIMO systems. The near-far problem in MU-MIMO systems may be alleviated via appropriate grouping of the users with similar channel conditions.

Petitioners' Exhibit 1021
Nokia of America Corp., et al. v. KT Corporation, et al.
Case No. IPR2025-00036; U.S. Patent No. 11,627,631
Page 652 of 1122

- The use of cooperative collocated transmit antennas in SU-MIMO schemes can facilitate the encoding at the transmitter and decoding at the receiver. In contrast, the users in a MU-MIMO scheme can cooperate in encoding at the base station in the downlink and decoding in the uplink; however, the users cannot cooperate in decoding in the downlink or encoding in the uplink directions.
- The capacity of the downlink and uplink are theoretically identical in the downlink and uplink for the SU-MIMO systems (given the same transmit power and perfect channel knowledge in the transmitter and the receiver); however, the capacity of the MU-MIMO broadcast channel and multiple access channel are not identical.
- The capacity of the SU-MIMO schemes is less impacted by lack of CSI at the transmitter, whereas the capacity of the MU-MIMO broadcast channel significantly suffers from lack of CSI at the transmitter.
- SU-MIMO suffers from limited exploitation of multi-user diversity. The number of spatial dimensions is limited by the number of antennas at the UE. There is a potential that spatial dimensions are wasted, if the UEs have fewer antennas compared to the base station.
- MU-MIMO more efficiently exploits the multi-user diversity since all spatial dimensions which are supported by the base station can be exploited. It will achieve capacity gain, if UEs have fewer antennas relative to the base station. Stronger spatial dimensions are exploited, particularly in the case of a low rank channel. The utilized spatial dimensions may be weak in the case of a low rank channel due to spatial correlation.

The advantages/disadvantages of SU-MIMO and MU-MIMO schemes are summarized in Table 9.27.

An important metric for measuring the performance of any communication channel is the information theoretic capacity. In a SU-MIMO channel, the capacity is the maximum amount of information that can be transmitted as a function of available bandwidth given a constraint on transmitted power. In SU-MIMO channels, it is common to assume that the total power distributed among all

Table 9.27 Comparison of SU-MIMO and MU-MIMO Schemes [46]

	SU-MIMO	MU-MIMO
Advantages	High user throughput High peak data rates	High system capacity Full exploitation of multi-user diversity
Disadvantages	Multiple transmit antennas at the base station are not fully exploited Multi-user diversity is not fully exploited	Degradation of peak data rates due to inter-user interference (ZF may not work perfectly due to imperfect CSIT)

Petitioners' Exhibit 1021
Nokia of America Corp., et al. v. KT Corporation, et al.
Case No. IPR2025-00036; U.S. Patent No. 11,627,631
Page 653 of 1122

transmit antennas is limited. For the MU-MIMO channel, the problem is somewhat more complex. Given the constraint on the total transmit power, it is possible to allocate varying fractions of that power to different users in the network, thus for any value of total power, different information rates are obtained. The result is a capacity region shown in Figure 9.114 for a two-user MU-MIMO channel. The maximum capacity for user 1 is achieved when 100% of the power is allocated to user 1, and for user 2, the maximum capacity is also obtained when it is allocated the full power. For every possible power distribution, there is an achievable information rate, which results in the capacity regions depicted in the figure. Two regions are shown in Figure 9.114, the larger one for the case where both users have roughly the same maximum capacity (similar channel conditions), and the other region for a case where one of the users has a much better channel condition than the other user. For N_{user} users, the capacity region is characterized by an N_{user}-dimensional hyper-region.

Let us use a simple MU-MIMO system model to demonstrate how the sum rate of the system is calculated. The simplified model of MU-MIMO broadcast channel is shown in Figure 9.115. Based on this model, the transmit vector $\mathbf{x}$ can be expressed as the weighted sum (precoded) of the input data symbols $s_k|_{k=1,2,\ldots,N_{\text{user}}}$ as follows: $\mathbf{x} = \sum_k \mathbf{p}_k s_k = \mathbf{Ps}$ where $N_{\text{user}} \times 1$ dimensional vector $\mathbf{s} = (s_1, s_2, \ldots, s_{N_{\text{user}}})^{\text{T}}$ denotes the data symbols from N_{user} users, and $\mathbf{P} = (\mathbf{p}_1, \mathbf{p}_2, \ldots, \mathbf{p}_{N_{\text{user}}})$ is the precoding matrix comprising N_{user} precoding vectors. It is assumed that the finite transmit power at the transmitter can be calculated as $P_{\text{TX}} = E\{\mathbf{x}^{\text{H}}\mathbf{x}\}$. The kth complex-valued output of the system can be written as

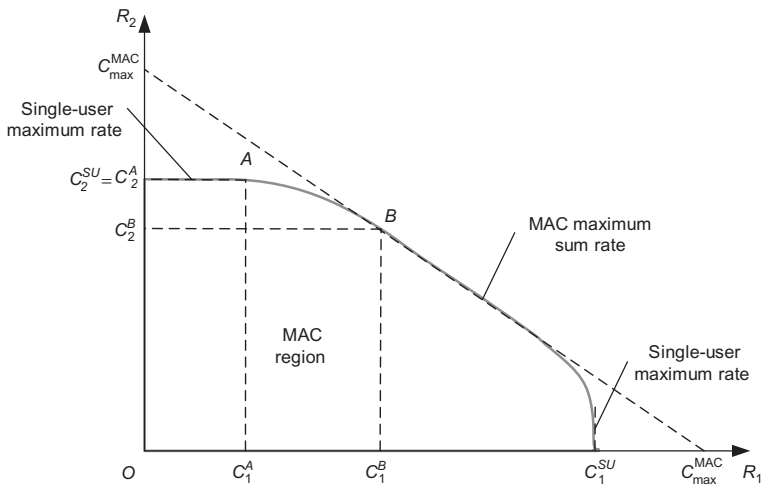


FIGURE 9.114

Capacity region of MU-MIMO multiple access channel (MAC) with two users compared to SU-MIMO [46].

Petitioners' Exhibit 1021
Nokia of America Corp., et al. v. KT Corporation, et al.
Case No. IPR2025-00036; U.S. Patent No. 11,627,631
Page 654 of 1122

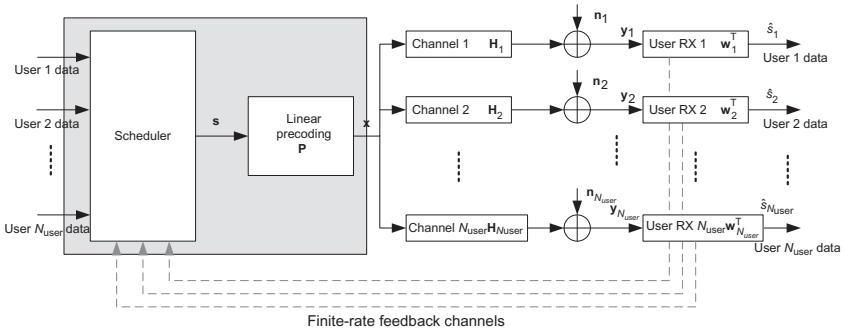


FIGURE 9.115

MU-MIMO broadcast channel model [46]

$\mathbf{y}_k = \mathbf{H}_k\mathbf{x}_k + \mathbf{n}_k \in \mathbb{C}^N$ where N denotes the dimension of vector $\mathbf{y}$. The kth branch user data can be detected using a linear MMSE receiver as $\hat{s}_k = \mathbf{w}_k^{\mathrm{T}}\mathbf{x}_k \in \mathbb{C}$ in which the MMSE weighting matrix is given by [46]:

$$\mathbf{w}_k = \left(\mathbf{H}_k^{*}\mathbf{P}^{*}\mathbf{P}^{\mathrm{T}}\mathbf{H}_k^{\mathrm{T}} + \frac{N_{user}}{P_{\mathrm{TX}}}\mathbf{I}_N\right)^{-1}\mathbf{H}_k^{*}\mathbf{p}_k^{*} \tag{9.93}$$

It can be further shown that the SINR at the kth output is given by:

$$\gamma_k = \frac{|\mathbf{w}_k^{\mathrm{T}}\mathbf{H}_k\mathbf{p}_k|^2}{||\mathbf{w}_k||_2^2\frac{N_{user}}{P_{\mathrm{TX}}} + \sum_{i(i\neq k)}|\mathbf{w}_k^{\mathrm{T}}\mathbf{H}_k\mathbf{p}_i|^2} \tag{9.94}$$

The sum rate of the system is given as $R_{\mathrm{sum}} = \sum_k \log_2(1+\gamma_k)$ [46].

Figure 9.116 illustrates a generic MU-MIMO scenario where N_{user} users, each having N_{TX_i} transmit antennas, transmit simultaneously to the eNB in the uplink. The maximum achievable throughput of the system is determined by the point on the N_{user}-dimensional hyper-region that maximizes the sum of all of the users' information rates, and is referred to as the sum capacity of the channel (Figure 9.117). In the case of a near-far problem where one user has a more strongly attenuated channel than other users, or some users are closer to the eNB than others, obtaining the sum capacity would cause the user with the worst channel to achieve a lower rate.

As shown in Figure 9.116, in the uplink of a MU-MIMO system, the received signal at the eNB can be written as $\mathbf{y} = \sum_{k=1}^{N_{\mathrm{user}}}\mathbf{H}_k^{\mathrm{H}}\mathbf{x}_k + \mathbf{n}$ where $\mathbf{x}_k$ is the $N_{\mathrm{TX}_k} \times 1$ transmitted signal vector of the kth UE with N_{TX_k} transmit antennas, $\mathbf{H}_k \in \mathbb{C}^{N_{\mathrm{TX}_k} \times N_{\mathrm{RX}}}$ denotes the flat-fading channel matrix from the kth user to the eNB, and $\mathbf{n} = (n_1, n_2, \ldots, n_{N_{\mathrm{RX}}}), n_k \sim \mathbb{N}(0,1)$ is an independent and identically

Petitioners' Exhibit 1021
Nokia of America Corp., et al. v. KT Corporation, et al.
Case No. IPR2025-00036; U.S. Patent No. 11,627,631
Page 655 of 1122

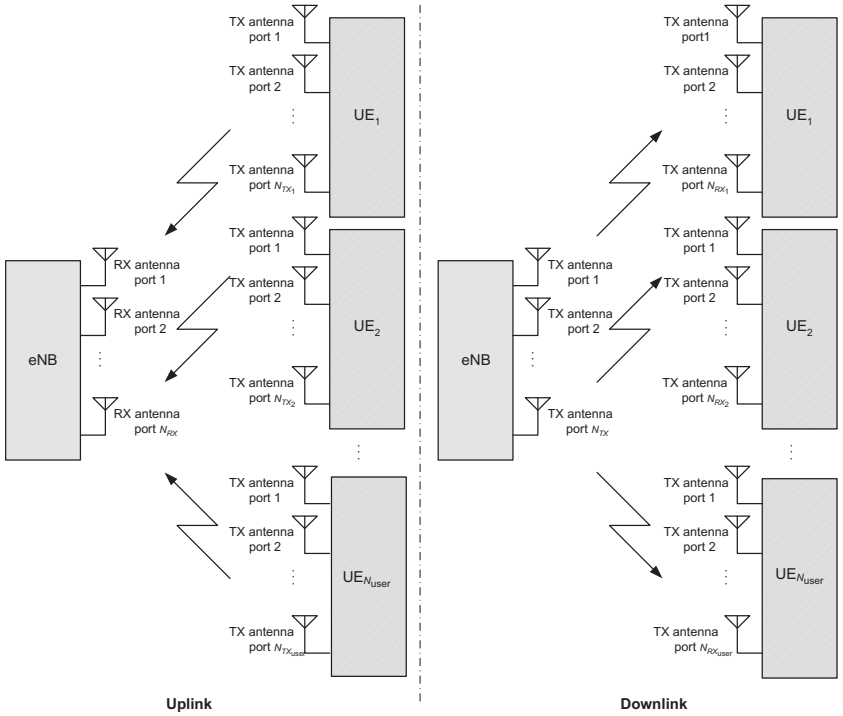


FIGURE 9.116

A generic multi-user MIMO transmission model [18].

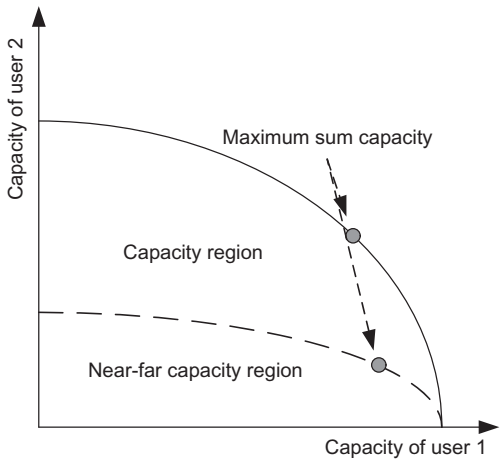


FIGURE 9.117

An example illustration of capacity region.

Petitioners' Exhibit 1021
Nokia of America Corp., et al. v. KT Corporation, et al.
Case No. IPR2025-00036; U.S. Patent No. 11,627,631
Page 656 of 1122

distributed additive white Gaussian noise vector at the eNB. We assume that the receiver k has perfect and instantaneous knowledge of the channel matrix $\mathbf{H}_k$. Note that the eNB is equipped with N_{TX} transmit and N_{RX} receive antennas.

In the downlink as illustrated in Figure 9.116, the received signal at the kth receiver can be written as $\mathbf{y}_k = \mathbf{H}_k\mathbf{x} + \mathbf{n}_k \forall k = 1, 2, \ldots, N_{\text{user}}$ where $\mathbf{H}_k \in \mathbb{C}^{N_{\text{RX}_k} \times N_{\text{TX}}}$ is the downlink channel and $\mathbf{n}_k \in \mathbb{C}^{N_{\text{RX}_k} \times 1}$ is the complex-valued additive Gaussian noise vector at the kth receiver. We assume that each receiver also has perfect and instantaneous knowledge of its own channel matrix $\mathbf{H}_k$. The transmitted signal $\mathbf{x}$ is a function of multiple users' information data, i.e., $\mathbf{x} = \sum_{k=1}^{N_{\text{user}}} \mathbf{x}_k$ where $\mathbf{x}_k$ is the signal carrying the kth user's message with covariance matrix $\mathbf{\Omega}_k = E\{\mathbf{x}_k\mathbf{x}_k^{\text{H}}\}$. The power allocated to the kth user is given by $\rho_k = \text{trace}(\mathbf{\Omega}_k)$. Under a sum power constraint at the eNB, the power allocation needs to maintain $\sum_{k=1}^{N_{\text{user}}} \rho_k \leq P_{\text{total}}$. Assuming a unit variance for the noise, it is now known that the capacity region for a given matrix channel realization can be written as [80]:

$$C_{\text{DL}} = \bigcup_{(\rho_1,\rho_2,\ldots,\rho_{N_{\text{user}}} | \sum \rho_k \leq P_{\text{total}})} (R_1, R_2, \ldots, R_{N_{\text{user}}}) \in \mathbb{R}^{+N_{\text{user}}}, R_l \leq \log_2 \frac{\det\left[\mathbf{I} + \mathbf{H}_i\left(\sum_{j \geq i} \mathbf{\Omega}_j\right)\mathbf{H}_i^{\text{H}}\right]}{\det\left[\mathbf{I} + \mathbf{H}_i\left(\sum_{j > i} \mathbf{\Omega}_j\right)\mathbf{H}_i^{\text{H}}\right]} \Bigg\} \tag{9.95}$$

where $\mathbb{R}^{+N_{\text{user}}}$ is the N_{user}-dimensional set of positive real numbers. The above equation may be optimized over each possible user ordering. Although difficult to realize in practice, the computation of the capacity region can be simplified using the assumption that the downlink capacity region can be calculated through the union of regions of the dual multiple access channel with all uplink power allocation vectors meeting the sum power constraint. The fundamental effect of the use of multiple antennas at either the eNB or the user terminals in increasing the channel capacity is best comprehended by examining how the sum capacity, i.e., the point obtained by the maximum $\sum_{k=1}^{N_{\text{user}}} R_k$ in the capacity region, scales with the number of active users.

The capacity region in the uplink of a MU-MIMO system can be calculated for two different cases: (1) joint decoding, i.e., the signals from a group of users are decoded in a cooperative manner; and (2) independent decoding where the signals from users are independently decoded in parallel.

The capacity of the MU-MIMO channels can be calculated using DPC techniques. The method was inspired by interference cancelation schemes. It is shown that the capacity of a channel where the transmitter has knowledge of interference is the same as if there were no interference. The DPC concept can be better

Petitioners' Exhibit 1021
Nokia of America Corp., et al. v. KT Corporation, et al.
Case No. IPR2025-00036; U.S. Patent No. 11,627,631
Page 657 of 1122

comprehended by comparing the scheme to writing on a dirty paper with a properly selected ink color so that the scripts have high contrast and are clearly readable. It can be shown that the capacity of the MU-MIMO multiple-access channel in the above cases is given as follows [75]:

$$R_i \leq \log_2\left[\frac{\det(\mathbf{R}_\mathbf{y})}{\det(\mathbf{R}_\mathbf{y} - E_{s_i}\mathbf{h}_i\mathbf{h}_i^{\mathrm{H}})}\right], \quad i = 1, 2, \ldots, N_{\text{user}} \quad \text{(independent decoding)}$$

$$\sum_{k\in\mathfrak{R}} R_k \leq \log_2 \det\left(\mathbf{I}_{N_{\text{RX}}} + \frac{1}{N_0}\mathbf{H}_{\mathfrak{R}}\mathbf{R}_{\mathbf{s}_{\mathfrak{R}}}\mathbf{H}_{\mathfrak{R}}^{\mathrm{H}}\right) \quad \text{(joint decoding)} \tag{9.96}$$

In the above equations N_{RX} denotes the number of receive antennas at the base station, N_{user} is the number of users each with only one transmit antenna, $\mathfrak{R}$ is a subset of users whose signals are jointly decoded, $\mathbf{H}_{\mathfrak{R}}$ is the $N_{\text{RX}} \times N_{\mathfrak{R}}$ complex-valued channel matrix where $N_{\mathfrak{R}}$ is the cardinality of the set $\mathfrak{R}$, $\mathbf{R}_{\mathbf{s}_{\mathfrak{R}}}$ denotes the covariance matrix of the signals transmitted by the users contained in the set $\mathfrak{R}$, $\mathbf{I}_{N_{\text{RX}}}$ is an $N_{\text{RX}} \times N_{\text{RX}}$ identity matrix, R_k is the rate that can be reliably achieved by user k, s_i is the complex-valued symbol transmitted by user $i, i = 1, 2, \ldots, N_{\text{user}}$, E_{s_i} is the average energy of the signal from the ith user which differs from one user to another, $\mathbf{R}_\mathbf{y}$ is the covariance matrix of the received signal at the base station, and $\mathbf{H} = [\mathbf{h}_1, \mathbf{h}_2, \ldots, \mathbf{h}_{N_{\text{user}}}]$ is the normalized $N_{\text{RX}} \times N_{\text{user}}$ complex-valued channel matrix composed of individual user complex-valued channel vectors $\mathbf{h}_i$.

An efficient UE pairing scheme is required at the eNB to choose the correct pair of UEs for MU-MIMO transmission in MU-MIMO systems. This pairing scheme is required to maintain minimal interference among scheduled UEs in MU-MIMO transmission. A proper pairing scheme can be designed by maximizing the Chordal distance[28] between the feedback precoding matrices of the UEs. The Chordal distance between two matrices is given in [31,32] and represented by $d_c(\mathbf{p}_i, \mathbf{p}_j) = (1/\sqrt{2})||\mathbf{p}_i\mathbf{p}_i^{\mathrm{H}} - \mathbf{p}_j\mathbf{p}_j^{\mathrm{H}}||_F$ where $||.||_{\mathrm{F}}$ denotes the Frobenius norm of the matrix. The Chordal distance generalizes the distance between two points on the unit sphere through an isometric embedding from complex Grassmann manifold $Gr(N_{\text{TX}}, N_l)$ to the unit sphere. Assuming an infinite number of UEs served by the current eNB, the kth UE with reported precoding matrix $\mathbf{p}_k$ will be paired with the mth UE, where the mth UE reports precoding matrix $\mathbf{p}_m$ and the Chordal distance between precoding matrices is maximized. With the maximized Chordal

[28]The asymptotic performance of a coding scheme is dominated by the shortest distance between any pair of codewords. The relevant distance measure between two codewords (vectors) $\mathbf{x}_1$ and $\mathbf{x}_2$ of an orthogonal code (of size M) for a non-coherent MIMO system is the Chordal distance defined as $d^2(\mathbf{x}_1, \mathbf{x}_2) = M - \left\|\mathbf{x}_1\mathbf{x}_2^{\mathrm{H}}\right\|_{\mathrm{F}}^2$ [31,32].

Petitioners' Exhibit 1021
Nokia of America Corp., et al. v. KT Corporation, et al.
Case No. IPR2025-00036; U.S. Patent No. 11,627,631
Page 658 of 1122

distance criterion, $\mathbf{p}_m$ stays in the anti-polar position of $\mathbf{p}_k$, hence $||\mathbf{H}_k\mathbf{p}_m||^2$ is minimized, yielding the minimized inter-UE interference. Consequently, the UE pairing scheme for MU-MIMO transmission in practical systems is designed to find the best match between two UEs (e.g., the mth UE and the kth UE) based on the reported precoding matrices and the following criterion $\mathbf{p}_m = \arg \max_{\forall \mathbf{p}_i \in \mathbf{P}_{\mathrm{UE}}} \mathrm{d_c}(\mathbf{p}_i, \mathbf{p}_k)$ with $\mathbf{P}_{\mathrm{UE}}$ representing the set containing all reported precoding matrices at a certain eNB.

If the conventional AWGN channel were modified to include an additive interference term that is known at the transmitter, and the received signal were expressed as the sum of the transmitted signal + interference + noise, one could set the transmitted signal equal to the desired data minus the interference term; however, such an approach requires increased power and perfect knowledge of interference. It is shown in the literature that the capacity in such a scenario is the same as if the interference were not present; no additional power is required to cancel the interference than is used in a nominal additive white Gaussian noise channel. Therefore, writing on dirty paper, from an information theoretic perspective, is equivalent to writing on clean paper when one knows in advance where the dirt is located. This concept has been used to characterize the sum-capacity and capacity region of the multi-antenna multi-user channels. A DPC technique for the downlink of a MU-MIMO system uses the QR decomposition[29] of the channel matrix as the product of a lower triangular matrix $\mathbf{R}$ with a unitary matrix $\mathbf{Q}$ such that $\mathbf{H} = \mathbf{QR}$. The signal to be transmitted is precoded with the $\mathbf{Q}^{\mathrm{H}}$ matrix, resulting in the effective channel $\mathbf{R}$. The first user of this equivalent system sees no interference from other users, i.e., the signal may be chosen irrespective of other users. The second user sees interference only from the first user; this interference is known and thus may be canceled using DPC. The other users are dealt with in a similar manner. Alternative approaches apply dirty paper techniques directly, rather than for individual users. An important difference between the MU-MIMO channel and the interference channels for which dirty paper techniques are applied is that the interference depends on the signal being designed [80].

Block diagonalization (BD) is a linear precoding technique for the downlink of MU-MIMO systems. It decomposes a MU-MIMO downlink channel into multiple parallel orthogonal SU-MIMO channels. The signal of each user is pre-processed at the transmitter using a modulation matrix that lies in the null space of all other users' channel matrices; thereby the multi-user interference in the system is effectively zero. The block diagonalization scheme is restricted

[29]In linear algebra, the QR decomposition of a matrix is defined as decomposition of a matrix into an orthogonal matrix and an upper triangular matrix. The QR decomposition is often used to solve the linear least squares problems. The QR decomposition of a real square matrix $\mathbf{A}$ is $\mathbf{A} = \mathbf{QR}$ where $\mathbf{Q}$ is an orthogonal matrix, i.e., $\mathbf{Q}^{\mathrm{H}}\mathbf{Q} = \mathbf{I}$ and $\mathbf{R}$ is an upper triangular matrix. This can be generalized to a complex-valued square matrix $\mathbf{A}$ and a unitary matrix $\mathbf{Q}$. If $\mathbf{A}$ is non-singular, then this factorization is unique if one requires that the diagonal elements of $\mathbf{R}$ are positive-valued [29].

Petitioners' Exhibit 1021
Nokia of America Corp., et al. v. KT Corporation, et al.
Case No. IPR2025-00036; U.S. Patent No. 11,627,631
Page 659 of 1122

to channels where the number of transmit antennas N_{TX} is greater or equal to the total number of receive antennas in the network N_{RX}. Let us define the precoder matrices as $\mathbf{F} = [\mathbf{F}_1, \mathbf{F}_2, \ldots, \mathbf{F}_{N_{user}}] \in \mathbb{C}^{N_{RX} \times N_l}$ where $\mathbf{F}_i \in \mathbb{C}^{N_{RX} \times N_{l_i}}$ is the ith user precoder matrix. We assume that $N_l \leq N_{RX}$ is the total number of the transmitted data streams, while $N_{l_i} \leq N_{RX_i}$ is the number of data streams transmitted to the ith user. We can find the optimal precoding matrix $\mathbf{F}$ such that multi-user interference is zero by choosing a precoding matrix $\mathbf{F}_i$ that lies in the null space of the other users' channel matrices. Thereby, an MU-MIMO downlink channel is decomposed into multiple parallel independent SU-MIMO channels [80].

Minimum mean-squared-error beamforming improves the system performance by allowing a certain amount of interference especially for users equipped with a single antenna. However, it suffers from performance loss when it attempts to mitigate the interference between two closely spaced antennas, a situation that usually occurs when the user terminal is equipped with more than one receive antenna. Successive MMSE (SMMSE), which is an improved version of the MMSE precoding algorithm, was developed to mitigate this problem by successively calculating the columns of the precoding matrix for each of the receive antennas separately. Linear equalization suffers from noise enhancement, and hence has poor power efficiency in some cases. The same drawback is experienced by linear precoding, which alleviates noise by boosting the transmit power [76].

The Tomlinson−Harashima precoding (THP) algorithm is a non-linear precoding technique originally developed for multipath SISO channels. The THP algorithm is performed by moving the feedback part of the decision-feedback equalizer to the transmitter. It has also been applied for the pre-equalization of multi-user interference in MU-MIMO systems; hence, no error propagation occurs and the precoding can be performed for the interference-free channel. The MMSE precoding in combination with THP is another approach to balance the multi-user interference in order to reduce the performance loss that occurs with zero interference techniques while THP is used to reduce the multi-user interference and to improve the diversity [46].

Space-division multiple access (SDMA) is a special case of MU-MIMO where several users share the same time−frequency physical resource block due to their spatial separation. SDMA uses antenna beam direction or angle (using directional antennas) as another dimension in signal space which can be channelized and assigned to different users (Figure 9.118). Orthogonal channels can be assigned only if the angular separation between users exceeds the angular resolution of the directional antenna. In practice, SDMA is often implemented using sectorized antenna arrays. The 360° angular space is divided into a number of sectors and in each sector a highly directional antenna array is used to minimize the inter-user interference. The users within each sector can be served using multiple access schemes such as OFDMA and CDMA. The SDMA system adapts to the mobility of the users by beam-steering or assigning a user to a new channel when the user changes its geographical location [25].

Petitioners' Exhibit 1021
Nokia of America Corp., et al. v. KT Corporation, et al.
Case No. IPR2025-00036; U.S. Patent No. 11,627,631
Page 660 of 1122

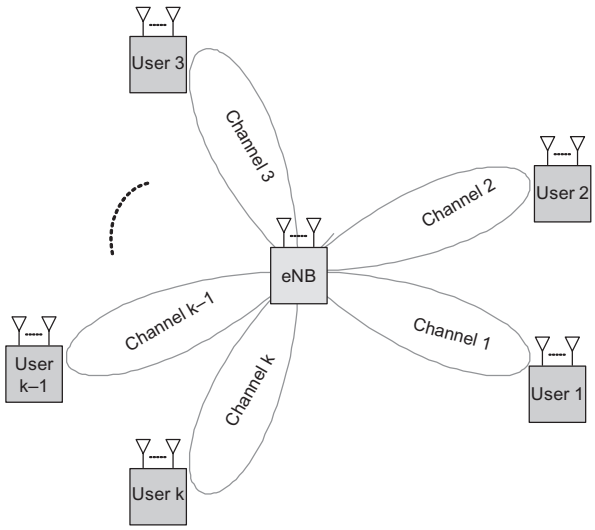


FIGURE 9.118

Illustration of the SDMA concept.

9.13.7 Collaborative MIMO and collaborative spatial multiplexing

Collaborative spatial multiplexing is a virtual MIMO technique where users transmit over the same time−frequency resource unit in the uplink. This type of spatial multiplexing improves the sector throughput without requiring multiple transmit antennas at the mobile station. The received signals from the simultaneous uplink transmission of the users are processed in the base station using maximum likelihood detection techniques. The base station's scheduler groups the users with similar channel conditions and assigns their uplink transmissions to the same time−frequency region. The operation of a collaborative spatial multiplexing scheme is conceptually similar to the regular spatial multiplexing scheme using transmit antennas that are located at different locations (user terminals are geographically apart). The throughput of collaborative spatial multiplexing theoretically increases by the number of users which are scheduled to simultaneously transmit over the same physical resource units.

The collaborative MIMO (Co-MIMO) is an extension of conventional single eNB-based MIMO techniques. It allows multiple base stations to serve one or multiple mobile stations simultaneously over the same radio resource through coordination among the participating base stations. The Co-MIMO is characterized by the following three features:

1. In Co-MIMO, each UE is jointly served by multiple base stations, which is different from conventional MIMO techniques where each UE is only served by a single eNB. Through inter-eNB coordination, the inter-cell interference among these coordinated base stations can be significantly reduced when using low-frequency reuse factors.

Petitioners' Exhibit 1021
Nokia of America Corp., et al. v. KT Corporation, et al.
Case No. IPR2025-00036; U.S. Patent No. 11,627,631
Page 661 of 1122

2. In Co-MIMO, each eNB can also simultaneously serve multiple mobile stations using the same radio resource in order to increase the system throughput. The co-channel interference among these mobile stations can be minimized through use of SDMA techniques such as beamforming or MU-MIMO schemes.
3. In Co-MIMO, SDMA processing is implemented independently within individual coordinated base stations based on the CSI between the eNB and the mobile stations that are served by the eNB. Therefore, the Co-MIMO limits the amount of information exchange between base stations, which is different from other eNB coordination approaches requiring considerable information exchange.

A central scheduler, that is a logical functional module in the network, is responsible for coordinating a group of base stations, collecting information from the participating base stations, and determining the serving relationship between base stations and mobile stations. The overall complexity of the network operation increases with increasing number of coordinated base stations in Co-MIMO scheme. The Co-MIMO scheme has the advantage of inter-cell interference reduction and spectral efficiency improvement. The inter-cell interference mitigation is realized by turning interference from neighboring cells into useful signals and separating signals for different users via MU-MIMO or SDMA techniques. The spectral efficiency improvement is achieved via interference mitigation and the number of users supported over the same time−frequency resource region. Moreover, the Co-MIMO provides a simple approach to implementation of eNB coordination and a reasonable trade-off between the performance gain and the stringent requirement on the core network traffic and implementation complexity. In practice, the user data delivery to multiple coordinated base stations in a Co-MIMO scheme can be realized in the same manner as the multicast over backhaul is done in the multicast and broadcast services. There is no additional computational complexity in base stations supporting Co-MIMO compared to the base stations which support MU-MIMO techniques [138].

In order to demonstrate the advantages of Co-MIMO, an example system-level simulation was conducted where the collaborative zone is defined over three neighboring sectors belonging to different eNBs as shown in Figure 9.119. Given that the inter-cell interference is more severe in the cell-edge, the evaluation of Co-MIMO performance is performed in the cell-edge area. The cell-edge area is characterized by the cell-edge length in the simulation, as shown in Figure 9.119. We assume a 19-cell collaborative-zone configuration in the simulation as depicted in Figure 9.119. The users are randomly dropped with a uniform distribution in the cell-edge area, one user per sector. The system performance with different sizes of cell-edge area is evaluated by setting the cell-edge length to 150, 100, and 50 m. In each collaborative region, three coordinated base stations communicate with three mobile stations located in their cell-edge areas allocating the same time and frequency resource. Each UE in the cell-edge area will be served by two coordinated base stations, and each eNB serves two mobile stations

Petitioners' Exhibit 1021
Nokia of America Corp., et al. v. KT Corporation, et al.
Case No. IPR2025-00036; U.S. Patent No. 11,627,631
Page 662 of 1122

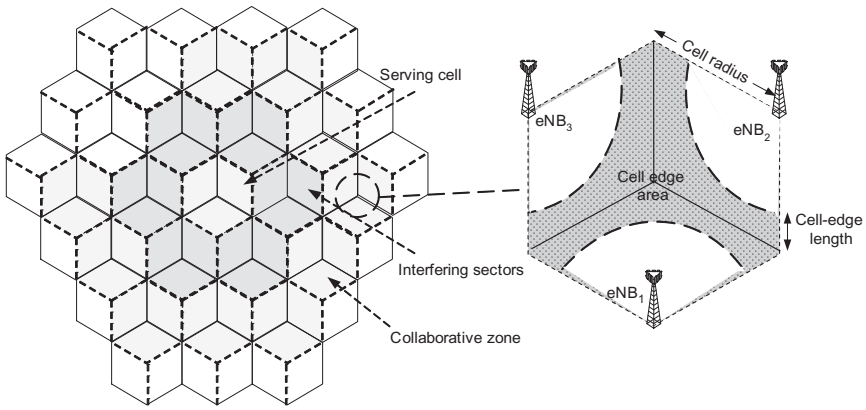


FIGURE 9.119

Example of cell configuration and cell-edge area in a collaborative zone [138].

simultaneously. The precoding matrices for the two served mobile stations are calculated independently within each single sector of a coordinated eNB. Each coordinated eNB transmits with full power and equal power allocation to the mobile stations. A single narrowband sub-carrier is assumed in the system without loss of generality. A conventional SU-MIMO scheme is used as the benchmark for comparison where three mobile stations in the cell-edge area are served independently by different base stations without any coordination in frequency reuse one deployment. As shown in Figure 9.120, even though there remains a certain amount of residual inter-cell interference, the interference power from neighboring cells within the collaborative zone is considerably reduced. If the interference from cells outside of the collaborative zone is taken into consideration, the reduction in overall interference level is less noticeable, and can be further improved by extending the collaborative zone to contain more coordinated base stations. The cumulative distribution function of the cell-edge users within the cell-edge area as a function of cell-edge length for SU-MIMO and Co-MIMO are compared and shown in Figure 9.120. It is shown that the interference power increases with increasing cell-edge length (see Figure 9.119). There is a considerable reduction in the interference power from cells within the Co-MIMO zone when using Co-MIMO techniques compared to the conventional SU-MIMO schemes. The performance gain decreases when comparing the overall interference [138].

9.13.8 Non-linear precoding and dirty-paper coding

In this section, we discuss some advanced non-linear multi-antenna transmission techniques that are not supported in current releases of LTE/LTE-Advanced, but may be considered as viable improvements in future releases of LTE standards. While the following techniques are theoretically proven to achieve higher

Petitioners' Exhibit 1021
Nokia of America Corp., et al. v. KT Corporation, et al.
Case No. IPR2025-00036; U.S. Patent No. 11,627,631
Page 663 of 1122

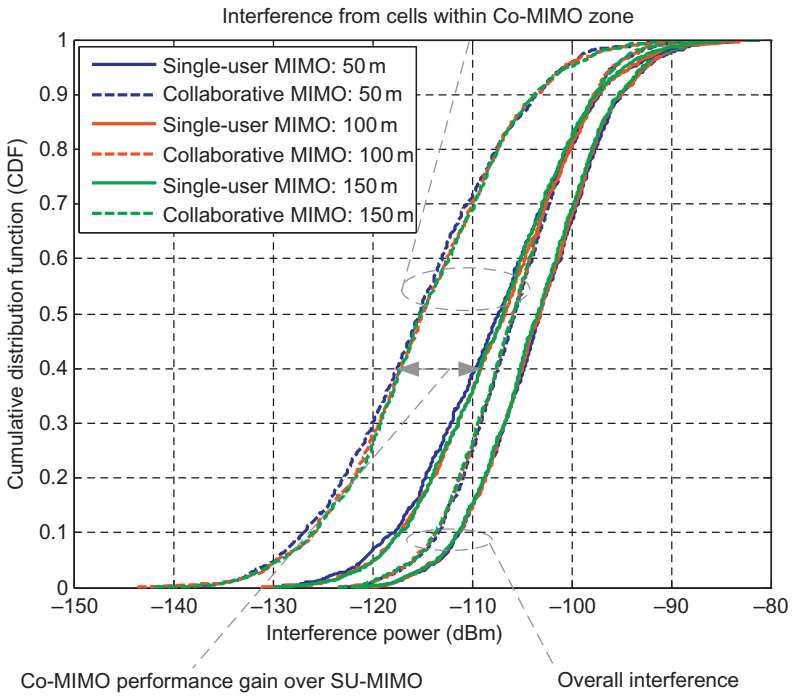


FIGURE 9.120

CDF of interference power of the cell-edge users as a function of cell-edge length [138].

capacities and user throughputs, their implementation complexities have prevented their application in real-life scenarios.

When the channel is frequency-selective, the precoder can also exploit the frequency selectivity and become frequency dependent. For single-carrier systems, non-linear precoding techniques using spatial extensions of the Tomlinson–Harashima precoder can be employed [46]. For multi-carrier systems such as OFDM, frequency-flat precoding techniques can be applied on a per sub-carrier basis. To reduce feedback overhead in OFDM, the CSIT feedback is sampled and interpolated in the frequency-domain. Exploiting the OFDM structure and sub-carrier correlation results in precoders with frequency-dependent eigen-beam directions and frequency-beam-dependent power allocation. In multi-user scenarios, partial CSIT is also highly relevant, since the channel time variation makes it impractical to attain perfect CSIT for all users. The studies have shown that the loss of degrees of freedom due to no CSIT reduces the capacity region of an isotropic vector broadcast channel to that of a scalar one. Imperfect CSIT also severely reduces the growth of the sum-rate broadcast capacity at high SNRs. Some techniques such as opportunistic scheduling, which require only an SNR feedback, can

Petitioners' Exhibit 1021
Nokia of America Corp., et al. v. KT Corporation, et al.
Case No. IPR2025-00036; U.S. Patent No. 11,627,631
Page 664 of 1122

achieve an optimal throughput growth rate in broadcast channels with a large number of users. With finite-rate feedback, however, the feedback rate needs to be increased with the SNR to achieve the full multiplexing gain. Figure 9.121 illustrates two hypothetical linear and non-linear precoding schemes in a MU-MIMO scenario where $\mathbf{x} = (x_1, x_2, \ldots, x_{N_{\text{user}}})^{\text{T}}$ and the precoding matrix $\mathbf{V}$ is given as follows [46]:

$$\mathbf{V} = (\mathbf{v}_1, \mathbf{v}_2, \ldots, \mathbf{v}_{N_{\text{user}}})^{\text{T}} = \begin{bmatrix} v_{11} & v_{12} & \cdots & v_{1N_{\text{user}}} \\ v_{21} & v_{22} & \cdots & v_{2N_{\text{user}}} \\ \vdots & \vdots & \ddots & \vdots \\ v_{N_{\text{TX}}1} & v_{N_{\text{TX}}2} & \cdots & v_{N_{\text{TX}}N_{\text{user}}} \end{bmatrix} \tag{9.97}$$

In the non-linear scheme, it is assumed that the interference is known to the transmitter and is mitigated via DPC techniques, as discussed later in this section.

Let us consider a scenario where we have a downlink channel with one base station equipped with N_{TX} transmit antennas and N_{user} users each with one antenna as the simplest form of MU-MIMO Gaussian broadcast channel. A time sample of this channel is characterized by $\mathbf{y} = \mathbf{Hx} + \mathbf{n}$ where $\mathbf{x}$ is the signal vector transmitted in parallel by N_{TX} transmit antennas, $\mathbf{y} = (y_0, y_1, \ldots, y_{N_{\text{user}}-1})^{\text{T}}$ is the vector of signals individually received by N_{user} users, and $\mathbf{n} \sim \mathbb{Z}(0,\mathbf{I})$ is an independent and identically distributed Gaussian noise vector. The channel matrix $\mathbf{H} = (\mathbf{h}_1, \mathbf{h}_2, \ldots, \mathbf{h}_{N_{\text{user}}-1})^{\text{H}}$ contains the channel coefficients from the N_{TX} transmit antennas to the N_{user} users, where the row vector $\mathbf{h}_i$ is the channel as seen by the ith user. The input signal power is constrained such that $\text{trace}[\mathscr{E}(\mathbf{xx}^{\text{H}})] \leq P$ where P denotes the total downlink transmitted power or the energy per channel use. Let us further assume that perfect CSI is available at the transmitter and ideal coherent receivers are utilized at the user terminals.

Under the above assumptions, a linear precoding scheme can be defined as a scheme where the transmit signal $\mathbf{x}$ is given by $\mathbf{x} = \boldsymbol{\Theta}\mathbf{u}$ where $\boldsymbol{\Theta} \in \mathbb{C}^{N_{\text{TX}} \times N_{\text{user}}}$ and the vector $\mathbf{u} = (u_1, u_2, \ldots, u_{N_{\text{user}}-1})^{\text{T}}$ contains the user coded symbols. The symbols u_i are independently generated by channel encoders for the users. Without loss of generality, we assume that $E(\mathbf{uu}^{\text{H}}) = \mathbf{I}$ (i.e., normalized signal power), the power constraint implies that $\text{trace}(\boldsymbol{\Theta}\boldsymbol{\Theta}^{\text{H}}) \leq P$. The kth user SINR under linear precoding is given as follows:

$$\text{SINR}_k = \frac{\varphi_{kk} p_k}{1 + \sum_{i \neq k} \varphi_{ki} p_i} \tag{9.98}$$

where $\boldsymbol{\Phi} = [\varphi_{ij}]|_{i=0,1,\ldots,N_{\text{user}}-1; j=0,1,\ldots,N_{\text{TX}}-1}$ denotes a matrix whose entries are defined as $\varphi_{ij} = |\mathbf{h}_i \mathbf{w}_j^{\text{H}}|^2$, $\mathbf{w}_j = \boldsymbol{\theta}_j / \sqrt{p_j}$ is the precoding vector, $\boldsymbol{\theta}_j$ denotes the jth column of $\boldsymbol{\Theta}$, and $p_j = |\boldsymbol{\theta}_j|^2$. It can be shown that assuming Gaussian codes and minimum distance decoding at the receivers, the user rates $R_k = \log_2(1 + \text{SINR}_k)$ are achievable. The transmit matrix $\boldsymbol{\Theta}$ can be designed in several ways. The

Petitioners' Exhibit 1021
Nokia of America Corp., et al. v. KT Corporation, et al.
Case No. IPR2025-00036; U.S. Patent No. 11,627,631
Page 665 of 1122

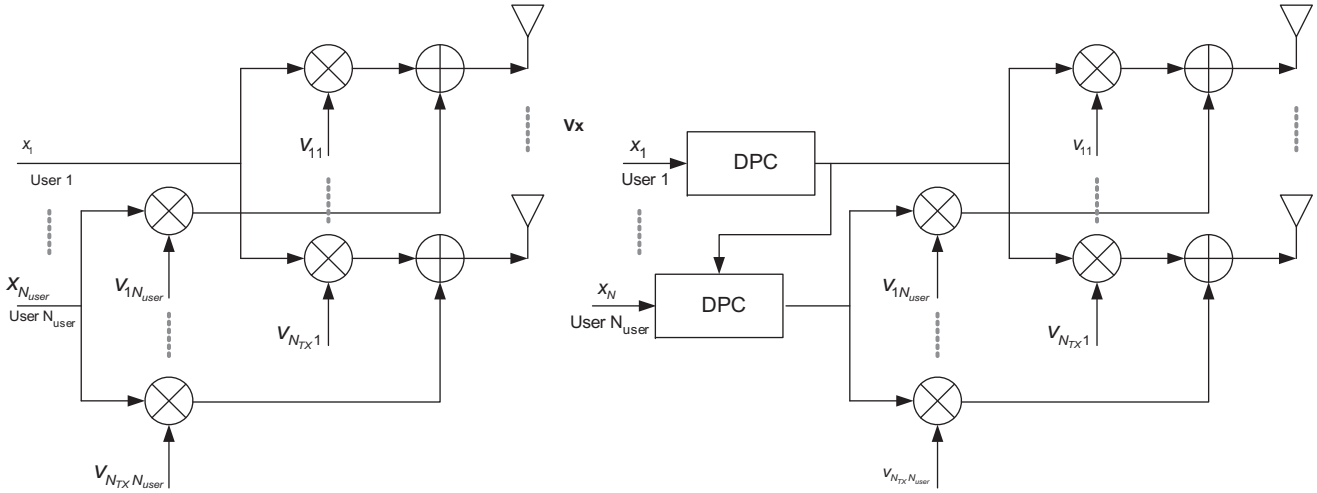


FIGURE 9.121

Illustration of linear and non-linear precoding concept [46].

Petitioners' Exhibit 1021
Nokia of America Corp., et al. v. KT Corporation, et al.
Case No. IPR2025-00036; U.S. Patent No. 11,627,631
Page 666 of 1122

throughput optimization criterion $\max_{\Theta} \sum_k R_k$ is a non-convex optimization problem that yields a maximal sum rate in a MU-MIMO scenario. The constrained maximization with respect to $\boldsymbol{\Theta}$ can be replaced by an unconstrained maximization with respect to $\hat{\boldsymbol{\Theta}}$, where the transmit signal is given by the following expression:

$$\mathbf{x} = \sqrt{\frac{P}{\text{trace}(\hat{\boldsymbol{\Theta}}\hat{\boldsymbol{\Theta}}^H)}}\hat{\boldsymbol{\Theta}}\mathbf{u} \tag{9.99}$$

The input constraint is automatically satisfied with equality for any arbitrary $\hat{\boldsymbol{\Theta}}$ [182].

A non-linear precoder, on the other hand, produces the transmitted signal $\mathbf{x}$ in the form of $\mathbf{x} = \gamma\boldsymbol{\Theta}[\mathbf{u} + \boldsymbol{\delta} - \boldsymbol{\lambda}(\mathbf{u}, \boldsymbol{\delta})]$ where $\boldsymbol{\Theta}$ is a transmit matrix such that $\text{trace}(\boldsymbol{\Theta}\boldsymbol{\Theta}^{\text{H}}) \leq P$, $\boldsymbol{\delta}$ is a random dithering signal assumed to be known at the transmitter side, and $\boldsymbol{\lambda}$ is a data-dependent lattice point, i.e., $\boldsymbol{\lambda}$ is a function of $\mathbf{u}$ and $\boldsymbol{\delta}$. The normalization coefficient γ is defined as follows:

$$\gamma^2 = \frac{P}{\text{trace}(\boldsymbol{\Theta}^{\text{H}}\boldsymbol{\Theta}\mathscr{E}\{(\mathbf{u} + \boldsymbol{\delta} - \boldsymbol{\lambda})(\mathbf{u} + \boldsymbol{\delta} - \boldsymbol{\lambda})^{\text{H}}\})} \tag{9.100}$$

where the expectation operator corresponds to the data vectors $\mathbf{u}$ and $\boldsymbol{\delta}$ [182].

The capacity of the additive white Gaussian noise channel with interference known at the transmitter was determined by Costa [89]. In his model, as shown in Figure 9.122, the channel input vector $\mathbf{x} = (x_1, x_2, \ldots, x_K)^{\text{T}}$ consisting of K real-valued components is modified by two additive memory-less Gaussian noise and interference sources. The interference source produces the vector $\mathbf{s} = (s_1, s_2, \ldots, s_K)^{\text{T}}$ with normally distributed components $s_i \sim \mathbb{N}(0, \sigma_I^2)$. The interference vector is observed by the encoder before the transmission process starts. The encoder produces the code vector $\mathbf{x} = f(w, \mathbf{s})$. Here $w \in \{1, 2, \ldots, M\}$ is the index of the message that must be conveyed. All messages are equally likely, which means that $\Pr(W = w) = 1/M \quad \forall w$. All code vectors $\mathbf{x}$ should satisfy a power constraint, i.e., $P_{\mathbf{x}} = \mathscr{E}[||\mathbf{x}||^2] \leq P_{\text{T}}$ where P_{T} denotes the total transmit power. The channel noise vector $\mathbf{z} = (z_1, z_2, \ldots, z_K)^{\text{T}}$ has normally distributed components

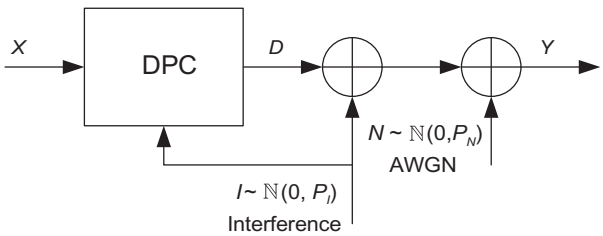


FIGURE 9.122

Costa's dirty paper coding model [89].

Petitioners' Exhibit 1021
Nokia of America Corp., et al. v. KT Corporation, et al.
Case No. IPR2025-00036; U.S. Patent No. 11,627,631
Page 667 of 1122

$z_i \sim \mathbb{N}(0, \sigma_z^2)$. The channel output vector $\mathbf{y} = (y_1, y_2, \ldots, y_K)^{\mathrm{T}} = \mathbf{x} + \mathbf{s} + \mathbf{z}$ is processed by the decoder and results in the message estimate $\hat{w} = D(\mathbf{y})$. The system has two parameters that determine its performance. For a given total transmit power $\mathrm{P_T}$, and interference and noise variances σ_I^2 and σ_z^2, the information rate $R \sim \log_2 M$ should be as large as possible, while on the other hand the expected error probability $P_e = Pr(\hat{w} \neq w)$ should be as small as possible. The largest rate that is achievable with arbitrarily small expected error probability is called the channel capacity. Costa showed that this capacity is determined only by the transmitter power P_{T} and the variance of the channel noise σ_z^2, i.e., the noise that is unknown to the transmitter. It appears that the channel capacity in this case is determined as $C = 0.5 \log_2(1 + P_{\mathrm{T}}/\sigma_z^2)$ bits/transmission. Since the interference is known to the transmitter a priori, this signaling method is known as writing on dirty paper [89]. Interference which is known to the transmitter does not cause any loss in terms of capacity.

The above concept can be generalized to the case of MU-MIMO when the interference vector is known to the transmitter a priori. Without loss of generality, let us consider the transmission model shown in Figure 9.123, in which a hypothetical base station is precoding and transmitting signals to three mobile stations each equipped with one receive antenna. Let $\mathbf{h}_k = (h_k^1, h_k^2, \ldots, h_k^{N_{\mathrm{TX}}})^{\mathrm{T}}$ denote the channel vector as seen by the kth mobile station. The corresponding precoding vector at the transmitter is represented by $\mathbf{v}_k = (v_1^k, v_2^k, \ldots, v_{N_{\mathrm{TX}}}^k)^{\mathrm{T}}$. The precoding vector $\mathbf{v}_k$ is designed such that it is orthogonal to all $\mathbf{v}_j : j < k$ by subtracting a linear combination of all previous $\mathbf{v}_j$ from $\mathbf{h}_k^*$ (Gram−Schmidt orthogonalization procedure[30]), i.e., $\mathbf{v}_k = \frac{\mathbf{P}_k \mathbf{h}_k^*}{\|\mathbf{P}_k \mathbf{h}_k^*\|}$ where $\mathbf{P}_1 = \mathbf{I}_{N_{TX}}$ and $\mathbf{P}_{k+1} = \mathbf{P}_k(\mathbf{I}_{N_{\mathrm{TX}}} - \mathbf{v}_k \mathbf{v}_k^{\mathrm{H}})$. The objective is to achieve the following $\mathbf{v}_l^{\mathrm{H}} \mathbf{v}_k = 0 \forall l < k, \mathbf{v}_k^{\mathrm{H}} \mathbf{v}_k = 1$, and $\mathbf{h}_k^H \mathbf{v}_j = 0 \ \forall k < j$. The latter criteria are meant to minimize the interference toward a particular mobile station from downlink transmissions to other mobile stations by appropriately selecting the precoding vectors at the transmitter. As a result, the received signal at the kth mobile station is given as follows [46]:

$$y_k = \underbrace{\sum_{i=1}^{k-1} \mathbf{h}_k^{\mathrm{T}} \mathbf{v}_i \mathbf{x}_i}_{\text{eliminated by DPC}} + \underbrace{\mathbf{h}_k^{\mathrm{T}} \mathbf{v}_k \mathbf{x}_k}_{\text{desired signal}} + \underbrace{\sum_{i=k+1}^{N_{user}} \mathbf{h}_k^{\mathrm{T}} \mathbf{v}_i \mathbf{x}_i}_{\text{eliminated by ZF}} + n_k \tag{9.101}$$

[30] In linear algebra, the Gram−Schmidt orthogonalization procedure is defined as a method for orthonormalizing a set of vectors in an inner product space (e.g., the Euclidean space $\mathbb{R}^n$). The Gram−Schmidt procedure takes a finite set of linearly-independent vectors $S = \{\mathbf{v}_1, \mathbf{v}_2, \ldots, \mathbf{v}_k\} \forall k \leq n$ and generates an orthonormal set of vectors. $S' = \{\mathbf{u}_1, \mathbf{u}_2, \ldots, \mathbf{u}_k\}$ that spans the same k-dimensional subspace of $\mathbb{R}^n$ as the original set. We define the projection operator by $\mathrm{proj}_{\mathbf{u}}(\mathbf{v}) = \frac{\langle \mathbf{u}, \mathbf{v} \rangle}{\langle \mathbf{u}, \mathbf{u} \rangle} \mathbf{u}$ where $\langle \mathbf{u}, \mathbf{v} \rangle$ denotes the inner product of the vectors $\mathbf{u}$ and $\mathbf{v}$. This operator projects the vector $\mathbf{v}$ orthogonally onto the line spanned by vector $\mathbf{u}$. The Gram−Schmidt procedure then continues as follows to generate the remaining vectors in the orthonormal set S' [44]: $\mathbf{u}_1 = \mathbf{v}_1$ and $\mathbf{u}_k = \mathbf{v}_k - \sum_{i=1}^{k-1} \mathrm{proj}_{\mathbf{u}_i}(\mathbf{v}_k)$

Petitioners' Exhibit 1021
Nokia of America Corp., et al. v. KT Corporation, et al.
Case No. IPR2025-00036; U.S. Patent No. 11,627,631
Page 668 of 1122

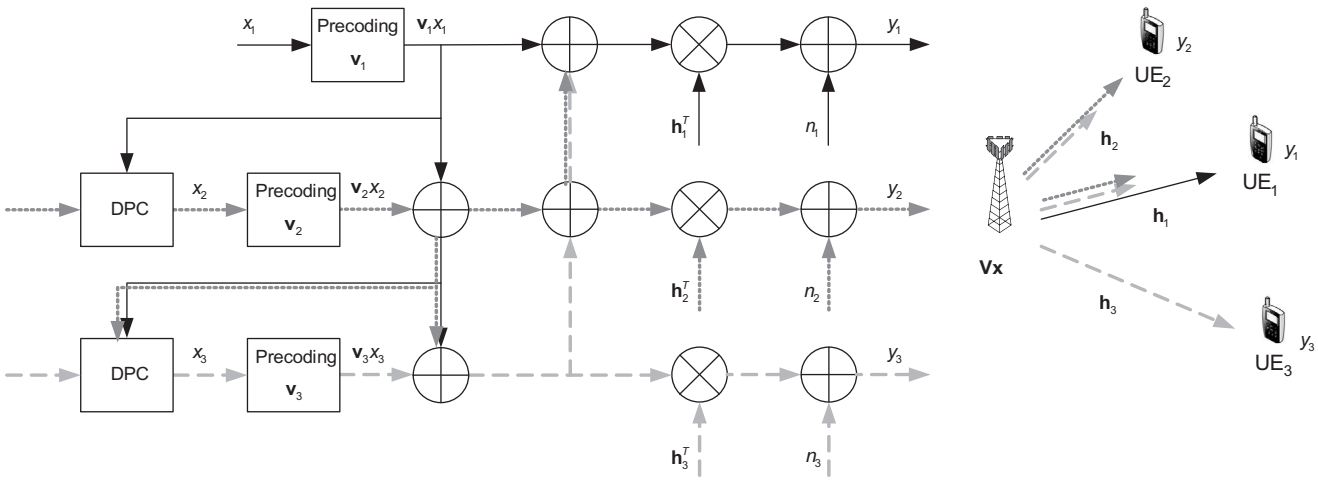


FIGURE 9.123

Sequential encoding with dirty paper coding (DPC) and ZF [46].

The sequential generation of the precoding vectors $\mathbf{v}_k$ through the Gram−Schmidt orthogonalization procedure allows optimized ordering of the users and scheduling of the users even when $N_{\text{user}} > N_{\text{TX}}$ [46]. Note that when $N_{\text{user}} > N_{\text{TX}}$, only N_{TX} users can be scheduled assuming each user has only one receive antenna. The scheduling rule in this case can be summarized as follows:

At each step $k = 1, 2, \ldots, N_{\text{TX}}$:

1. Compute precoding vector $\mathbf{v}_l$ for all users that have not been served yet.
2. For each user l, determine the effective channel $\mathbf{h}_l^{\text{T}}\mathbf{v}_l$ and the resulting sum capacity increment which would be achieved, if user l were scheduled at step k.
3. Allocate the respective resource units to the user who achieves the highest sum capacity increment, considering $C_{\text{sum-capacity}} = \sum_{k=1}^{N_{\text{user}}} C_k$, where C_k is the capacity/rate of the kth user.

9.14 LTE/LTE-Advanced downlink multi-antenna transmission schemes

Having discussed the underlying theory of multi-antenna operation, we now focus on the multi-antenna transmission techniques that have been used in LTE/LTE-Advanced. There are some practical constraints which impact the real-life performance of the theoretical MIMO systems that include limitations in practical cell deployment and antenna configurations, propagation conditions, channel characterization, measurement inaccuracies and latencies, hardware imperfections and implementation margins, and inherent implementation complexity of the multi-antenna schemes in practice. These aspects are often crucial for assessing the performance of a particular multi-antenna transmission scheme in a given propagation channel and configuration, and have been of great importance in the selection of MIMO schemes for LTE/LTE-Advanced.

The advantages of MIMO, i.e., array gain, diversity gain, and multiplexing gain, observed through link-level and system-level simulations assume ideally uncorrelated antennas and full-rank MIMO channel matrices. In this regard, the propagation environment and the antenna design (e.g., the spacing and polarization) play a significant role. If the antenna separation at the eNB and the UE is small relative to the operating wavelength, strong correlation will be observed between the spatial signatures especially in an LoS scenario, limiting the usefulness of spatial multiplexing schemes. However, this can to some extent be circumvented by means of dual-polarized antennas, which provide orthogonality even in LoS environments. Aside from use of such antennas, the condition of spatial signature independence with SU-MIMO can only be satisfied using a rich random multipath propagation environment. In diversity-based schemes, the invertibility of the channel matrix is not required, yet the entries of the channel

Petitioners' Exhibit 1021
Nokia of America Corp., et al. v. KT Corporation, et al.
Case No. IPR2025-00036; U.S. Patent No. 11,627,631
Page 670 of 1122

matrix should be statistically uncorrelated. Although a greater LoS to non-LoS power ratio will tend to correlate the fading coefficients on the various antennas, this effect will be counteracted by the reduction in fading measured through the LoS component.

Another source of inconsistency between theoretical MIMO gains and practically achieved performance lies in the inability of the receiver and/or the transmitter to acquire reliable knowledge of the propagation channel. At the receiver, channel estimation is typically performed over finite samples of reference signals. In the case of beamforming and MIMO precoding, the transmitter must acquire the CSI from the receiver usually through a limited feedback channel, which causes further degradation to the available CSIT. The potential advantages of MU-MIMO over SU-MIMO include robustness with respect to the propagation environment and the preservation of spatial multiplexing gain, even in the case of UEs with a small number of antennas. However, these advantages rely on the ability of the base station to compute the required beamforming coefficients, which requires accurate CSIT; if no CSIT is available and the fading statistics are identical for all the UEs, the MU-MIMO gains disappear and the SU-MIMO becomes more advantageous. Consequently, one of the challenges in making MU-MIMO practical for cellular applications, and particularly for an FDD system, is developing efficient feedback mechanisms that allow accurate CSI to be estimated at the base station. This requires the use of appropriate codebooks for quantization.

Another issue which arises in the practical implementation of MIMO schemes is the interaction between the physical layer and the scheduling protocol. As noted earlier, in both uplink and downlink cases, the number of UEs which can be scheduled using MU-MIMO is typically limited to the number of the transmit antennas at the base station. Often one may even decide to limit the number of scheduled users to a value strictly less than the number of transmit antennas at the eNB to preserve some degrees of freedom for per-user diversity. As the number of active users typically exceeds the number of scheduled users, a sophisticated selection algorithm must be implemented to identify which set of users will be scheduled for simultaneous transmission over a particular time−frequency resource. This algorithm is not included in the specification, and various approaches are possible where a combination of rate maximization and QoS constraints will typically be considered. It is important to note that the choice of UEs that will maximize the sum rate (the sum over the individual rates for a given subframe) is one that favors UEs exhibiting not only good instantaneous SINR, but also spatial separability among their spatial signatures [14].

A 2×2 antenna configuration for MIMO is assumed as the baseline in the LTE downlink, i.e., two transmit antennas at the base station and two receive antennas at the terminal side [1,2]. Configurations with up to eight transmit or receive antennas are also supported in the specification. Different downlink MIMO modes are supported in LTE/LTE-Advanced, which can be adapted based on channel and traffic conditions, QoS requirements, and UE capability. These include transmit diversity, open-loop spatial multiplexing, codebook-based and

Petitioners' Exhibit 1021
Nokia of America Corp., et al. v. KT Corporation, et al.
Case No. IPR2025-00036; U.S. Patent No. 11,627,631
Page 671 of 1122

non-codebook-based closed-loop spatial multiplexing, SU-MIMO and MU-MIMO, and precoding. The maximum number of codewords is two irrespective of the number of antennas with fixed mapping between codewords to layers. There is a semi-static switching between SU-MIMO and MU-MIMO per UE.

The objective of dynamic SU-MIMO/MU-MIMO switching is to improve system performance by allowing the network to serve a UE using either SU-MIMO or MU-MIMO. The SU/MU-MIMO switching aspect is important because, depending on the channel and traffic conditions, some UEs may be best served with SU-MIMO, while others benefit from MU-MIMO operation. As channel and traffic conditions may vary from one subframe to another, the dynamic switching aspect is important to optimize system performance. Important factors that influence the suitability of SU-MIMO versus MU-MIMO include the spatial characteristics of the MIMO channel (e.g., potential rank deficiency that could be relaxed by performing MU-MIMO), as well as the UE's typical signal-to-interference-plus-noise ratio conditions. In addition, channel and traffic variations are important factors (e.g., UE mobility or the characteristics of user traffic). MU-MIMO is more suitable when UE mobility is low and traffic conditions are stable as this improves the ability to find a suitable grouping of UEs for MU-MIMO operation.

In spatial multiplexing, up to two codewords can be mapped to different layers (i.e., up to eight layers). One codeword represents the output from one channel coder. The number of spatial layers available for transmission is equal to the rank of the channel matrix.[31] Precoding in the transmitter side is used to support spatial multiplexing. This is achieved by multiplying the signal with a precoding matrix prior to transmission. The optimum precoding matrix is selected from a predefined codebook which is known to both the eNB and UE. The optimum precoding matrix is the one which maximizes the capacity. The UE estimates the channel and selects the optimum precoding matrix. This feedback is provided to the eNB. Depending on the available bandwidth, this information is made available per resource block or group of resource blocks, since the optimum precoding matrix may vary between resource blocks. The network may configure a subset of the codebooks that the UE is able to select from. In the case of UEs with high velocity, the quality of the feedback may deteriorate. Thus, an open-loop spatial

[31]The column rank of matrix $\mathbf{P}$ is the maximum number of linearly independent column vectors of $\mathbf{P}$. The row rank of matrix $\mathbf{P}$ is the maximum number of linearly independent row vectors of $\mathbf{P}$. Equivalently, the column rank of $\mathbf{P}$ is the dimension of the column space of $\mathbf{P}$, whereas the row rank of $\mathbf{P}$ is the dimension of the row space of $\mathbf{P}$. An important property in linear algebra is that for any matrix, the column rank and the row rank are always equal. Therefore, the number of linearly independent rows or columns is simply referred to as the rank of matrix $\mathbf{P}$. It can be easily verified that the rank of $\mathbf{P}$ and $\mathbf{P}^T$ are equal. The rank is also defined as the dimension of the image of the linear transformation $\mathbf{y} = \mathbf{Px}$. If a linear operator on a vector space with infinite-dimension has finite-dimensional range (i.e., a finite-rank operator), then the rank of the operator is defined as the dimension of the range. The rank of an $M \times N$ matrix is always less than or equal to min (M, N). A matrix is said to be full rank, if its rank is equal to min (M, N); otherwise, the matrix is rank deficient [29].

Petitioners' Exhibit 1021
Nokia of America Corp., et al. v. KT Corporation, et al.
Case No. IPR2025-00036; U.S. Patent No. 11,627,631
Page 672 of 1122

multiplexing mode is also supported which is based on predefined settings for spatial multiplexing and precoding. In the case of four antenna ports, different precoders are assigned cyclically to the resource elements. The eNB will select the optimum MIMO mode and the precoding configuration. The information is conveyed to the UE as part of the downlink control information on the PDCCH.

LTE Rel-8 supports spatial multiplexing with a maximum of four layers in SU-MIMO. In LTE-Advanced, the maximum number of layers for SU-MIMO was extended to eight in order to increase the peak spectral efficiency. Aside from the increased number of spatial layers, the SU-MIMO in Rel-8 and Rel-10 differ in the use of beamforming or closed-loop precoding. The SU-MIMO in Rel-8 was developed under the codebook-based precoding framework where transmit precoding vectors/matrices at the eNB are restricted within a finite set. This is because the demodulation is based on the cell-specific reference signals that are not precoded. Therefore, the precoding matrix at the eNB has to be explicitly signaled to the UE in the physical downlink control channel to enable MIMO decoding. It is obvious that codebook-based precoding limits the eNB's precoding flexibility, which is particularly important for MU-MIMO that relies on beamforming to mitigate the inter-user interference. The latter inflexibility motivated design of non-codebook-based precoding schemes in LTE-Advanced through the introduction of multi-layer demodulation reference signals. Because the demodulation reference signals are precoded with the same precoding vector/matrix as the user data/control information, the effective composite channel after precoding can be readily measured with demodulation reference signals, obviating the need to explicitly signal the transmit precoder to the UE. Furthermore, the eNB may choose arbitrary precoding vectors/matrices and achieve greatly improved precoding flexibility for both SU-MIMO and MU-MIMO schemes. Although non-codebook-based precoding has a small performance difference relative to codebook-based precoding for SU-MIMO, it is proven to be the key enabling feature for MU-MIMO in LTE-Advanced. The CSI feedback in LTE is based on implicit feedback where the UE reports a set of recommended MIMO transmission metrics (RI/PMI/CQI). The same feedback scheme is applied in LTE-Advanced for both SU-MIMO and MU-MIMO.

The CSI feedback allows downlink transmission to be adapted based on the instantaneous channel conditions. In LTE Rel-8, the CSI measurement is based on cell-specific reference signals, which is also used for data demodulation. In contrast, the CSI measurement in LTE-Advanced is based on a set of newly designed CSI-RS signals, which are low duty-cycle and low-density, and further allow a higher reuse factor compared to cell-specific reference signals. The feedback mechanisms of LTE Rel-8 and LTE Rel-10 are both based on the implicit feedback framework that has been established and tested since early 3GPP releases. The UE measures the downlink channel quality through reference signals and feeds back the CSI in the form of recommended transmission formats, which includes RI, PMI, and CQI metrics. In LTE, the CQI is defined as a set of transport block sizes, each of which translates to a maximum code rate and modulation

Petitioners' Exhibit 1021
Nokia of America Corp., et al. v. KT Corporation, et al.
Case No. IPR2025-00036; U.S. Patent No. 11,627,631
Page 673 of 1122

order that can be received by the UE at a certain block error rate. As a criterion for testing the CQI report accuracy, when the reported code rate and modulation order is used for actual data transmission, the UE must be able to decode the data with a BLER of less than 0.01.

In order to support MIMO operation, the UE can be configured to report PMI and RI, in addition to CQI reports. In the case of codebook-based spatial multiplexing, precoding at the eNB is applied relative to the phase of the cell-specific reference signals for each antenna port. As a result, if the UE knows the precoding matrices that could be applicable (as defined in the configured codebook), and if it knows the transfer function of the channels from the transmit antenna ports, it can determine which codebook is the most suitable under the current channel conditions and signals this to the eNB. The preferred codebook, whose index constitutes the PMI report, is the precoder that maximizes the aggregate number of data bits which could be received across all layers. The number of resource blocks used to calculate each PMI depends on the feedback mode configured by the eNB as follows (Figure 9.124):

- Wideband PMI: The UE reports a single PMI corresponding to the preferred precoder assuming transmission over the entire system bandwidth. This is applicable for PMI feedback that is configured to be sent periodically on PUCCH, and also for PMI feedback that is sent aperiodically in conjunction with UE-selected sub-band CQI reports on PUSCH.
- Sub-band PMI: The UE reports one PMI for each sub-band over the system bandwidth, where the sub-band size is between 4 and 6 resource blocks depending on the system bandwidth (Table 9.28). This is used in scenarios where PMI feedback is sent aperiodically on PUSCH in addition to a wideband CQI report. If the eNB intends to schedule a wideband data

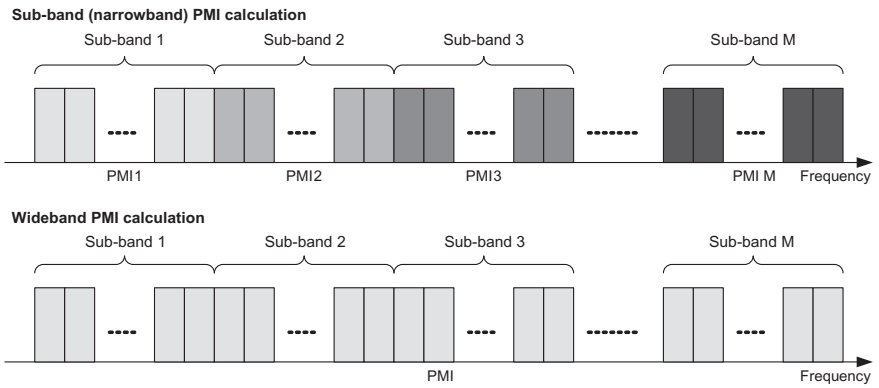


FIGURE 9.124

Illustration of wideband and sub-band PMI concept.

Petitioners' Exhibit 1021
Nokia of America Corp., et al. v. KT Corporation, et al.
Case No. IPR2025-00036; U.S. Patent No. 11,627,631
Page 674 of 1122

Table 9.28 Sub-band Sizes as a Function of System Bandwidth Applicable to the Best-M Method [5]

System Bandwidth (Number of Resource Blocks)	Sub-band Size *k* (Number of Resource Blocks)	Number of Preferred Sub-bands *M*
6–7	N/A	N/A
8–10	2	1
11–26	2	3
27–63	3	5
64–110	4	6

transmission to a UE in a frequency-selective channel, the precoder used by the eNB can change from one sub-band to another within one transport block.

- UE-selected sub-band PMI (Best-M): The UE selects a set of M preferred sub-bands, each consists of k resource blocks, and reports a single PMI corresponding to the preferred precoder assuming transmission over all of the M selected sub-bands. This is applicable in conjunction with UE-selected sub-band CQI reports on PUSCH. The eNB is not obligated to use the precoder requested by the UE; however, if the eNB selects another precoder, then it has to adjust the transmission format according to the inconsistency with the reported CQI. The eNB may also restrict the set of precoders which the UE may evaluate and report. This is known as codebook subset restriction. It enables the eNB to prevent the UE from reporting precoders which may not be useable, e.g., in some eNB antenna configurations or in correlated fading scenarios. In the case of open-loop spatial multiplexing, codebook subset restriction is equivalent to a restriction on the rank which the UE may report.

9.14.1 Transmit diversity

In LTE/LTE-Advanced, transmit diversity is only defined for two and four transmit antennas and one codeword. In order to maximize diversity gain, the antennas typically need to be uncorrelated, so they need to be sufficiently separated relative to the operating wavelength or have different polarizations. Transmit diversity is useful in a number of scenarios where the SNR is low, or for applications with low delay tolerance. Diversity schemes are also suitable for channels for which no uplink feedback is available (e.g., multimedia broadcast multicast services, physical broadcast channel, and synchronization signals), or when the feedback is not sufficiently accurate such as high-speed scenarios. Transmit diversity is also used as a fallback scheme in LTE/LTE-Advanced when other multi-antenna schemes fail. In LTE/LTE-Advanced, the multi-antenna schemes are independently configured for the physical control channels and the traffic channels, and in the case of traffic channels, it is configured independently per UE. In this

Petitioners' Exhibit 1021
Nokia of America Corp., et al. v. KT Corporation, et al.
Case No. IPR2025-00036; U.S. Patent No. 11,627,631
Page 675 of 1122

section, we discuss space–frequency block codes and frequency-switched transmit diversity (FSTD) diversity schemes. Transmit diversity may be utilized for transmission of PBCH, PDCCH, and for PDSCH, if the transmit diversity mode is configured for a UE. Another transmit diversity technique which is commonly associated with OFDM is CDD. The CDD is not used in LTE as a diversity scheme, but rather as a precoding scheme for spatial multiplexing on the PDSCH.

LTE Rel-8 supports downlink transmissions on one, two, or four cell-specific antenna ports, each corresponding to one, two, or four cell-specific reference signals, where each reference signal corresponds to one antenna port. An additional antenna port associated with one UE-specific reference signal is available, as well. This antenna port can be used for conventional beamforming, especially in the case of TDD operation. The number of downlink spatial layers was increased to eight through addition of demodulation reference signals and CSI reference signals in LTE-Advanced. Transmit diversity with rank-1 is supported through Alamouti-based space–time codes in the frequency-domain. The encoding operation is performed over space and frequency dimensions so the output block $\mathbf{X}_n$ from the precoder is limited to consecutive data resource elements over a single OFDM symbol. If single-codeword transmission is assumed, the modulated symbols of a single codeword are mapped to all layers. The transmit-diversity schemes for two and four cell-specific antenna ports are also supported. Note that these transmit-diversity schemes can be used for PBCH, PDCCH, and PCFICH. Furthermore, the number of cell-specific antenna ports used to encode the PBCH is the same as the total number of configured cell-specific antenna ports, and those antenna ports are also used for other control channels. Thus, all UEs must support up to four cell-specific antenna ports and the corresponding transmit-diversity schemes. For the case of two antenna ports, the output from the precoder is given as follows:

$$\begin{matrix}\text{Antenna Port } 0\rightarrow \\ \text{Antenna Port } 1\rightarrow\end{matrix} \mathbf{X}_n = \begin{bmatrix} s_{n1} & s_{n2} \\ -s_{n2}^{*} & s_{n1}^{*} \end{bmatrix} \tag{9.102}$$

where the rows correspond to the antenna ports and the columns to consecutive data resource elements over the same OFDM symbol. When four antenna ports are utilized, a combination of SFBC and FSTD is used to provide robustness against the correlation between channels from different transmit antennas and for less-complex UE receiver implementation. The output from the precoder is given as follows:

$$\begin{matrix}\text{Antenna Port } 0\rightarrow \\ \text{Antenna Port } 1\rightarrow \\ \text{Antenna Port } 2\rightarrow \\ \text{Antenna Port } 3\rightarrow\end{matrix} \mathbf{X}_n = \begin{bmatrix} s_{n0} & s_{n1} & 0 & 0 \\ 0 & 0 & s_{n2} & s_{n3} \\ -s_{n1}^{*} & s_{n0}^{*} & 0 & 0 \\ 0 & 0 & -s_{n3}^{*} & s_{n2}^{*} \end{bmatrix} \tag{9.103}$$

The precoder in Eq. (9.103) consists of two SFBC codes which are transmitted on antenna ports 0, 2, and 1, 3, respectively. The reason for distributing a single SFBC code in such an interlaced manner on every other antenna port instead of

Petitioners' Exhibit 1021
Nokia of America Corp., et al. v. KT Corporation, et al.
Case No. IPR2025-00036; U.S. Patent No. 11,627,631
Page 676 of 1122

consecutive antenna ports is related to the fact that the first two cell-specific antenna ports have a higher reference signal density than the other reference signals; therefore, the channel estimation accuracy may be lower on the third and fourth antenna ports. The above transmit-diversity scheme can be used for all downlink channels other than PHICH. For the latter case, four different ACK/NACK bits are multiplexed using orthogonal codes with a spreading factor of four over a group of four sub-carriers, and the resulting group is repeated three times in the frequency-domain to achieve frequency-diversity gain. To maintain the orthogonality between different codes in each repetition of four sub-carriers, antenna switching is not applied within each repetition. Instead, the set of antennas changes across different repetitions.

9.14.2 Spatial multiplexing

Let us review a few terms before turning our focus on spatial multiplexing schemes in LTE/LTE-Advanced. As mentioned earlier, a spatial layer refers to one of the streams generated by spatial multiplexing, or alternatively a mapping of symbols to the transmit antenna ports. Each layer is identified by a precoding vector of size equal to the number of transmit antenna ports. The rank is defined as the number of transmission layers. A codeword represents an independently encoded data block corresponding to a single transport block delivered to the physical layer by the MAC sub-layer in the transmitter and protected with a CRC. For ranks greater than one, two codewords may be transmitted (as shown in Figure 9.125). Note that the number of codewords is always less than or equal to the number of layers, which in turn is always less than or equal to the number of antenna ports.

In principle, an SU-MIMO spatial multiplexing scheme can either use a single codeword mapped to all the available layers or multiple codewords mapped to one or more spatial layers. The advantage of using one codeword is the obvious reduction in the amount of control signaling required for CQI reporting where only a single value would be needed for all layers, and for HARQ ACK/NACK

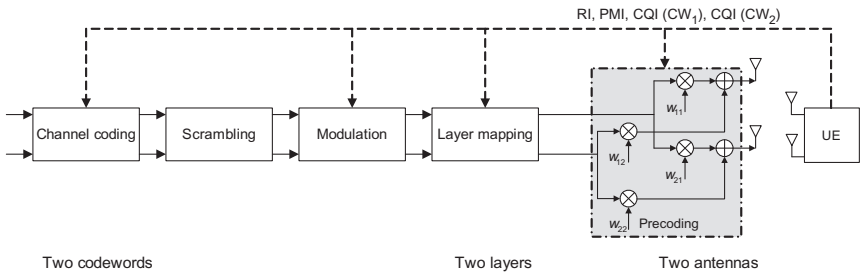


FIGURE 9.125

Example of closed-loop spatial multiplexing with precoding rank = 2 [46].

where only one ACK or NACK would be signaled per subframe per UE. In that case, the MLD receiver is optimal in terms of minimizing the BLER. At the opposite extreme, a separate codeword could be mapped to each of the layers. The advantage of such mapping is that significant gains can be achieved using an SIC receiver at the expense of additional control signaling. An MMSE-SIC receiver is shown to approach the Shannon capacity. Note that an MMSE receiver is more practical for both transmitter structures (i.e., single-codeword and multi-codeword). For LTE/LTE-Advanced, at most two codewords are used even though four layers may be transmitted. The codeword-to-layer mapping is static, since only minimal gains were shown for a dynamic mapping method. Note that in LTE/LTE-Advanced, all resource blocks associated with the same codeword use the same modulation and coding scheme (MCS), even if a codeword is mapped to multiple layers.

The PDSCH transmission modes for open-loop and closed-loop spatial multiplexing use precoding vectors derived from a predefined codebook to form the transmit layers. Each codebook consists of a set of predefined precoding matrices. In the case of closed-loop spatial multiplexing, the UE sends the index of the most desirable entry from a predefined codebook as feedback to the eNB. The preferred precoder is the weighting matrix which would maximize the capacity based on the receiver capabilities. In a single-cell and interference-free environment, the UE will typically indicate the precoder that would result in a transmission with an effective SNR that most closely follow the largest singular value of its estimated channel matrix. An example algorithm by which a UE selects the codebook which is the best fit to the propagation channel at a specific time is as follows [158]:

1. Calculate metric $\zeta(i) = \mathbf{W}_i(\mathbf{H}^{\mathrm{H}}\mathbf{H})\mathbf{W}_i^{\mathrm{H}}$ for every element in the codebook, where $\mathbf{H}$ is the channel matrix and $\mathbf{W}_i$ is the ith precoding matrix/vector.
2. Select the codebook element which minimizes the above metric $\mathrm{PMI} = \arg\min_i(\zeta(i))$.
3. Report the index of the selected codebook element (PMI) to the eNB.

Some important properties of the codebooks utilized in the precoding are as follows [14,15]:

- The LTE/LTE-Advanced precoders only perform phase corrections and no amplitude changes. This is to ensure that the power amplifiers connected to each antenna are uniformly loaded. One exception is the use of the identity matrix as the precoder. Although the identity matrix precoder may completely switch off one antenna on one layer, since each layer is still connected to one antenna at constant power, the effect across the layers is still constant modulus toward the power amplifier.
- The LTE/LTE-Advanced precoders were designed to exploit the nested property. The nested property is a method of organizing the codebooks of different ranks so that the lower rank codebook is formed by a subset of the

Petitioners' Exhibit 1021
Nokia of America Corp., et al. v. KT Corporation, et al.
Case No. IPR2025-00036; U.S. Patent No. 11,627,631
Page 678 of 1122

higher rank codebook vectors. This property simplifies the CQI calculation across different ranks. It ensures that the precoded transmission for a lower rank is a subset of the precoded transmission for a higher rank, thereby reducing the number of calculations required for the UE to generate the feedback. For example, if a specific index in the codebook corresponds to columns 1, 2, and 3 from the precoder $\mathbf{W}$ in the case of a rank-3 transmission, then the same index in the case of rank-2 transmission consists of either columns 1 and 2, or columns 1 and 3 from $\mathbf{W}$.

- The LTE/LTE-Advanced precoders were designed to minimize complex computations. The codebook associated with dual antenna transmission consists of ± 1 and $\pm j$, which eliminates the need for any complex multiplications. The four transmit antenna codebook contains ± 1 and $\pm j$ along with magnitude scaling to enhance the performance.

Figures 9.126 and 9.127 illustrate effect of precoding on the antenna radiation pattern using precoding matrices $\mathbf{W}_0$ and $\mathbf{W}_1$ (closed-loop spatial multiplexing

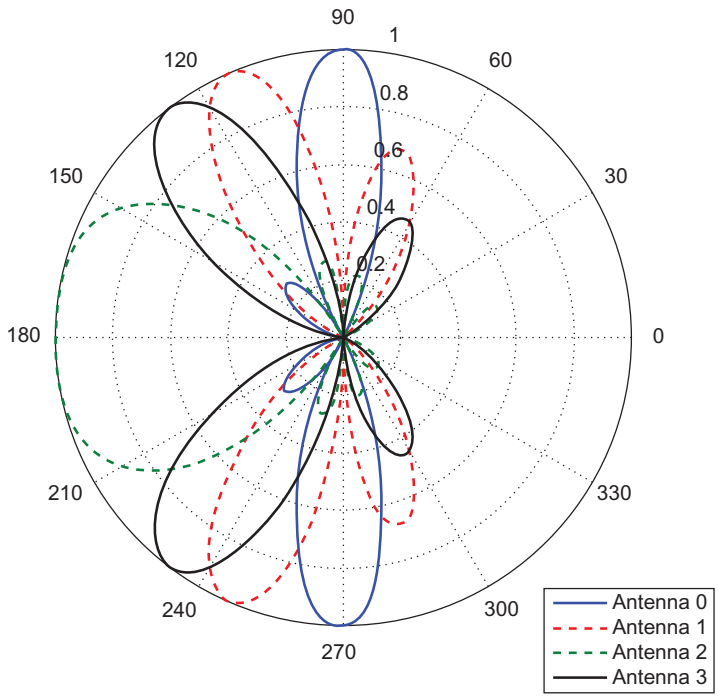


FIGURE 9.126

Effect of precoding on the antenna radiation pattern using precoding matrix $\mathbf{W}_0$ (closed-loop spatial multiplexing with four transmit antennas and rank-4 transmission).

with four transmit antennas and rank-4 transmission), respectively. The precoding matrices are defined as follows:

$$\mathbf{W}_0 = \begin{pmatrix} 0.5 & 0.5 & 0.5 & 0.5 \\ 0.5 & 0.5 & -0.5 & -0.5 \\ 0.5 & -0.5 & 0.5 & -0.5 \\ 0.5 & -0.5 & -0.5 & 0.5 \end{pmatrix}$$

and

$$\mathbf{W}_1 = \begin{pmatrix} 0.5 & -0.5\text{j} & -0.5 & 0.5\text{j} \\ 0.5\text{j} & 0.5 & 0.5\text{j} & 0.5 \\ -0.5 & -0.5\text{j} & 0.5 & 0.5\text{j} \\ -0.5\text{j} & 0.5 & -0.5\text{j} & 0.5 \end{pmatrix}$$

It can be seen that the eigen-beamforming changes the radiation pattern of the transmit antennas to direct the transmit power in a certain direction consistent with instantaneous propagation channel conditions in order to maximize the signal-to-noise ratio at the UE receiver.

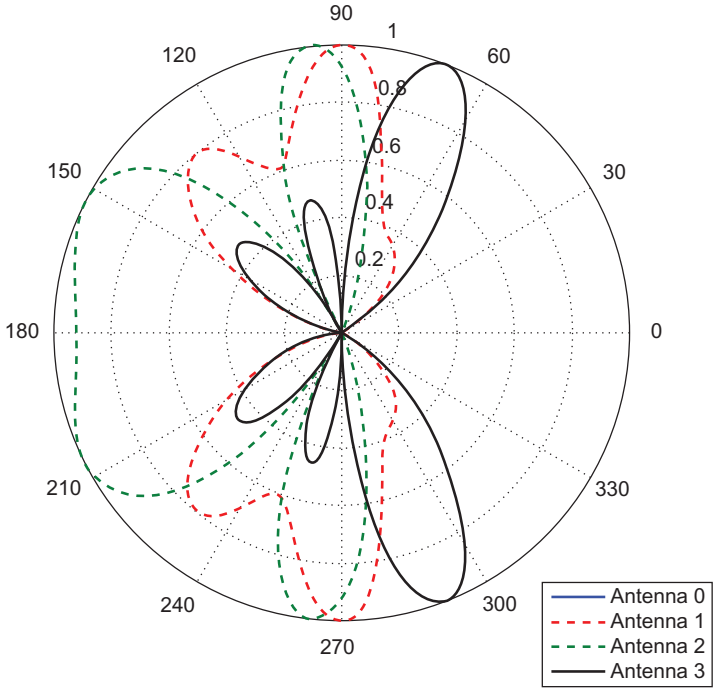


FIGURE 9.127

Effect of precoding on the antenna radiation pattern using precoding matrix $\mathbf{W}_1$ (closed-loop spatial multiplexing with four transmit antennas and rank-4 transmission).

Petitioners' Exhibit 1021
Nokia of America Corp., et al. v. KT Corporation, et al.
Case No. IPR2025-00036; U.S. Patent No. 11,627,631
Page 680 of 1122

9.14.3 Cyclic delay diversity

In the case of open-loop spatial multiplexing, the UE does not feedback PMI; rather, it sends the rank of the channel. In this mode, if the rank used for PDSCH transmission is greater than one, LTE uses a CDD scheme where the same set of OFDM symbols on the same set of sub-carriers are transmitted from multiple transmit antennas with different delays applied to each antenna. The delay is applied before the cyclic prefix is added, thereby guaranteeing that the delay is cyclic over the FFT size. Adding a time delay is equivalent to applying a phase shift in the frequency-domain. As the same time delay is applied to all sub-carriers, it corresponds to a linear phase shift across the sub-carriers. Each sub-carrier experiences a different beamforming pattern as the non-delayed sub-carrier from one antenna interferes constructively or destructively with the delayed version from another antenna. The diversity effect of CDD originates from the fact that linearly phase-shifted sub-carriers are affected differently in a multipath channel, thus artificially increasing the frequency-selectivity of the channel. Although this approach does not optimally exploit the channel in the way that ideal precoding would be matching the precoding matrix to the eigenvectors of the channel, it does help to ensure that any destructive fading is constrained to individual sub-carriers rather than affecting the entire transport block. This can be particularly beneficial if the channel information at the transmitter is unreliable, e.g., due to the limited feedback or high UE mobility. The fact that the delay is added before the cyclic prefix insertion suggests that any delay value can be used without increasing the overall delay spread of the channel. In contrast, if the delay were added after the addition of the cyclic prefix, then the range of applicable delays would be limited in order to ensure that the delay spread of the delayed symbol is not more than the maximum delay spread of the channel. The equivalence of time-delay and phase-shift implies that the CDD operation can be implemented as a frequency-domain precoder for the affected antennas, where the precoder phase is changed per sub-carrier basis according to a fixed linear function.

In LTE Rel-8, precoding for spatial multiplexing using antenna ports with cell-specific reference signals is only used in combination with layer mapping for spatial multiplexing. Spatial multiplexing supports two or four antenna ports and the set of antenna ports used is $p = 0$, 1 or $p = 0$, 1, 2, 3, respectively with p denoting the antenna port number. The precoding for spatial multiplexing without CDD is defined as $(y_i^0, y_i^1, \ldots, y_i^{N_p-1})^{\mathrm{T}} = \mathbf{W}_i(x_i^0, x_i^1, \ldots, x_i^{N_l-1})^{\mathrm{T}}$ where $\mathbf{W}_i$ is the $N_p \times N_l$ precoding matrix, N_p is the number of antenna ports, N_l denotes the number of layers, $i = 0, 1, \ldots, N_s^p - 1$, and $N_s^p = N_s^l$. For spatial multiplexing, the value of $\mathbf{W}_i$ is selected among the precoder elements in the codebook configured in the eNB and the UE. The eNB can further confine the precoder selection in the UE to a subset of the elements in the codebook using codebook subset restrictions [3].

For large-delay CDD, precoding for spatial multiplexing is defined as $(y_i^0, y_i^1, \ldots, y_i^{N_p-1})^{\mathrm{T}} = \mathbf{W}_i\mathbf{D}_i\mathbf{U}(x_i^0, x_i^1, \ldots, x_i^{N_l-1})^{\mathrm{T}}$ (Figure 9.128), where $\mathbf{D}_\mathrm{i}$ and $\mathbf{U}$ are $N_l \times N_l$ matrices supporting CDD as given in Table 9.29 for different numbers

Petitioners' Exhibit 1021
Nokia of America Corp., et al. v. KT Corporation, et al.
Case No. IPR2025-00036; U.S. Patent No. 11,627,631
Page 681 of 1122

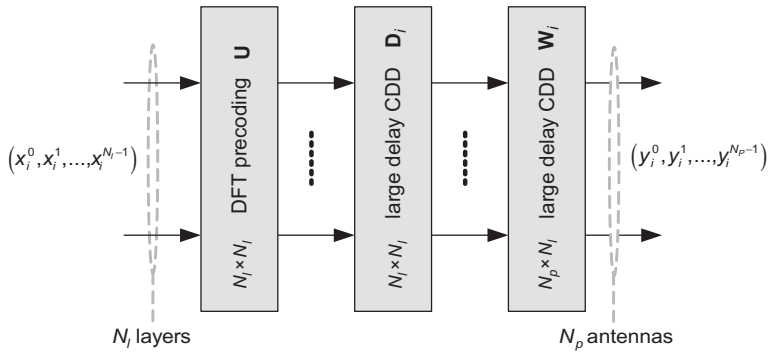


FIGURE 9.128

Open-loop spatial multiplexing with N_p antenna ports and N_l transmission layers [3].

Table 9.29 Large-Delay Cyclic Delay Diversity [3]

Number of Layers N_l	U	D_i
2	$\frac{1}{\sqrt{2}}\begin{bmatrix}1 & 1\\ 1 & e^{-j2\pi/2}\end{bmatrix}$	$\begin{bmatrix}1 & 0\\ 0 & e^{-j2\pi i/2}\end{bmatrix}$
3	$\frac{1}{\sqrt{3}}\begin{bmatrix}1 & 1 & 1\\ 1 & e^{-j2\pi/3} & e^{-j4\pi/3}\\ 1 & e^{-j4\pi/3} & e^{-j8\pi/3}\end{bmatrix}$	$\begin{bmatrix}1 & 0 & 0\\ 0 & e^{-j2\pi i/3} & 0\\ 0 & 0 & e^{-j4\pi i/3}\end{bmatrix}$
4	$\frac{1}{2}\begin{bmatrix}1 & 1 & 1 & 1\\ 1 & e^{-j2\pi/4} & e^{-j4\pi/4} & e^{-j6\pi/4}\\ 1 & e^{-j4\pi/4} & e^{-j8\pi/4} & e^{-j12\pi/4}\\ 1 & e^{-j6\pi/4} & e^{-j12\pi/4} & e^{-j18\pi/4}\end{bmatrix}$	$\begin{bmatrix}1 & 0 & 0 & 0\\ 0 & e^{-j2\pi i/4} & 0 & 0\\ 0 & 0 & e^{-j4\pi i/4} & 0\\ 0 & 0 & 0 & e^{-j6\pi i/4}\end{bmatrix}$

of layers. For two antenna ports, the precoder is selected according to $\mathbf{W}_i = \mathbf{C}_1$ where $\mathbf{C}_1$ denotes the precoding matrix corresponding to precoder index zero in Table 9.30. For four antenna ports, the UE may assume that the eNB cyclically assigns different precoders to different vectors $(x_i^0, x_i^1, \ldots, x_i^{N_l-1})^{\mathrm{T}}$ on the physical downlink shared channel. A different precoder is used every N_l vectors, where N_l denotes the number of transmission layers in the case of spatial multiplexing. In particular, the precoder is selected according to $\mathbf{W}_i = \mathbf{C}_k$, where k is the precoder index given by $k = \left(\lfloor i/N_l \rfloor \bmod 4\right) + 1 \in \{1, 2, 3, 4\}$, and $\mathbf{C_1}$, $\mathbf{C_2}$, $\mathbf{C_3}$, $\mathbf{C_4}$ denote precoder matrices. When two antenna ports are configured, the number of codewords is equal to the transmission rank, and codeword n is mapped to layer n.

Petitioners' Exhibit 1021
Nokia of America Corp., et al. v. KT Corporation, et al.
Case No. IPR2025-00036; U.S. Patent No. 11,627,631
Page 682 of 1122

Table 9.30 Codebook for Transmission on Antenna Ports 0 and 1 [3]

	Number of Layers N_l	
Codebook Index	**1**	**2**
0	$\frac{1}{\sqrt{2}}\begin{bmatrix}1\\1\end{bmatrix}$	$\frac{1}{\sqrt{2}}\begin{bmatrix}1 & 0\\0 & 1\end{bmatrix}$
1	$\frac{1}{\sqrt{2}}\begin{bmatrix}1\\-1\end{bmatrix}$	$\frac{1}{2}\begin{bmatrix}1 & 1\\1 & -1\end{bmatrix}$
2	$\frac{1}{\sqrt{2}}\begin{bmatrix}1\\j\end{bmatrix}$	$\frac{1}{2}\begin{bmatrix}1 & 1\\j & -j\end{bmatrix}$
3	$\frac{1}{\sqrt{2}}\begin{bmatrix}1\\-j\end{bmatrix}$	–

For transmission on two antenna ports ($p = 0,1$), the precoding matrix $\mathbf{W}_i$ is selected from Table 9.30 or a subset of it. The open-loop spatial multiplexing may be used when reliable PMI feedback is not available at the eNB, e.g., when the UE moves fast or when the feedback overhead on the uplink is extremely high. The open-loop spatial multiplexing with N_l layers and N_p antenna ports ($N_p \geq N_l$) is illustrated in Figure 9.128. The feedback consists of the RI and the CQI in open-loop spatial multiplexing. In contrast to the closed-loop spatial multiplexing, the eNB only determines the transmission rank, and a fixed set of precoding matrices are applied cyclically across all the scheduled sub-carriers in the frequency-domain. It is noted that in the open-loop spatial multiplexing mode, the transmit diversity scheme is applied when the transmission rank is set to one [3].

9.14.4 Beamforming and MU-MIMO

In LTE/LTE-Advanced, two beamforming techniques are supported for the PDSCH transmission: (1) closed-loop rank-1 precoding; and (2) beamforming with UE-specific reference signals. In closed-loop rank-1 precoding, only a single layer is transmitted, and it can also be seen as a special case of the SU-MIMO spatial multiplexing using codebook-based precoding. In this mode, the UE sends CSI feedback (PMI) to the eNB to indicate suitable precoding to apply for the beamforming. In a beamforming scheme using UE-specific reference signals, the precoding is not restricted to a predefined codebook, thus the UE will rely on DM-RS as opposed to cell-specific reference signals for PDSCH demodulation. Rel-8 of LTE only supported single-layer beamforming and the scheme was extended to support dual-layer beamforming in Rel-9. These transmission modes are used to extend cell coverage by concentrating the eNB power in the directions in which the radio channels provide the strongest paths to the UE. They are typically implemented with an array of closely spaced antenna elements

Petitioners' Exhibit 1021
Nokia of America Corp., et al. v. KT Corporation, et al.
Case No. IPR2025-00036; U.S. Patent No. 11,627,631
Page 683 of 1122

(or pairs of cross-polarized elements) for creating directional transmissions (Figures 9.129 and 9.130).

The geometric design of the antenna array significantly affects the radiation characteristics. This is discussed here using the example of conventional base

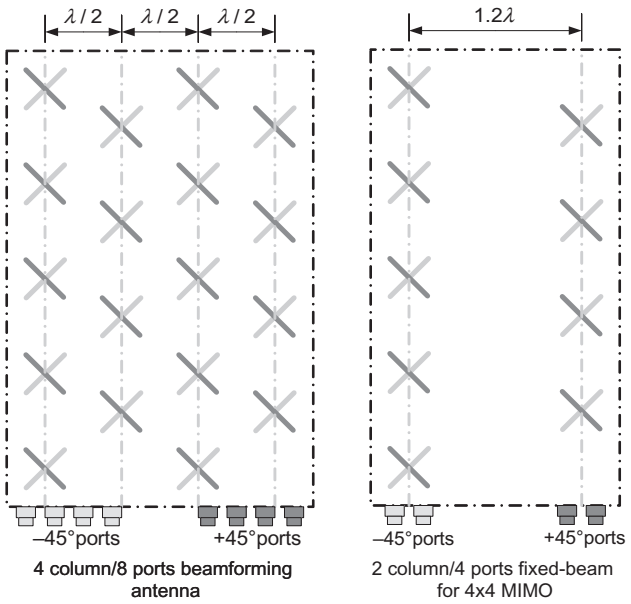


FIGURE 9.129

Practical configuration of beamforming and fixed-beam quad-port cross-polarized physical antenna elements [146].

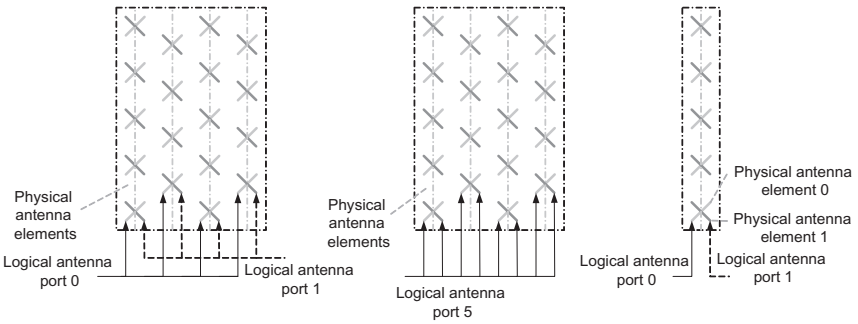


FIGURE 9.130

Example mapping of one/two antenna ports to multiple cross-polarized physical antenna elements [13].

Petitioners' Exhibit 1021
Nokia of America Corp., et al. v. KT Corporation, et al.
Case No. IPR2025-00036; U.S. Patent No. 11,627,631
Page 684 of 1122

station antennas. At present, conventional passive base station antennas are typically made up of multiple cross-polarized elements. In the *y*-axis, multiple elements are combined in order to satisfy the cell coverage requirements. All elements that have the same polarity radiate the same signal (see Figures 9.127 and 9.128). Particularly relevant for MIMO and beamforming is the arrangement of the cross-polarized elements and the columns in the *x*-axis. In Figure 9.129, the antenna at the left consists of two elements arranged at 90° relative to each other (cross-polarized). Each polarization column represents an antenna element that can transmit a different signal. This makes it possible to transmit four signals with a compact antenna arrangement, such as in 4×4 MIMO or transmit diversity. Analogously, the antenna shown in the figure can radiate four independent signals ($4 \times N$ MIMO), while the antenna at the right can radiate eight independent signals ($2 \times N$ MIMO). The antennas shown in Figure 9.129 can be used for beamforming. Beamforming requires correlated channels, i.e., elements with the same polarization ($+45°$ or $-45°$) must be used. Also, the distance between the columns should be small relative to the wavelength. Beamforming can be carried out with two antenna elements (columns with the same polarization) in the antenna array shown in the left side of Figure 9.129, or with four antenna elements in the layout on the right side. Base station antenna designs are constantly evolving. Active antennas are an important trend that allow seamless integration of beamforming concepts, e.g., by implementing dedicated transceivers for the required number of antenna elements [164].

The mapping of the (logical) antenna ports to physical antenna elements of the eNB may be realized in different ways depending on the multi-antenna scheme that is used. Figure 9.130 shows three example cases where one or two antenna ports are mapped to an array of cross-polarized physical antenna elements. As shown in the figure, the array of physical antennas radiates one signal corresponding to antenna port 5 or two signals corresponding to antenna ports 0 and 1. In the case of dual antenna port transmission, the UE sees two downlink transmissions, one associated with antenna port 0 and another one associated with antenna port 1. The physical antenna mapping and arrangement are transparent to the UE. The composite radiation pattern of the eNB transmit antennas are determined based on the combination of individual antenna radiation pattern, array antenna radiation pattern, and the precoding weights (vectors) that are applied for eigen-beamforming. Two example composite radiation patterns are shown in Figures 9.126 and 9.127.

In the case where UE-specific reference signals are used, due to the fact that no precoding codebook is used (non-codebook-based transmission), an arbitrary number of transmit antennas is theoretically supported; in practical deployments up to eight antennas are typically used (e.g., an array of four cross-polarized pairs). The signals from the correlated antenna elements are phased appropriately so that they add up constructively at the location of the UE. The UE is not aware that it is receiving a precoded directional transmission as opposed to a cell-wide transmission, except that the UE is instructed to use UE-specific reference signals as the phase reference for demodulation. To the UE, the phased array of antennas

Petitioners' Exhibit 1021
Nokia of America Corp., et al. v. KT Corporation, et al.
Case No. IPR2025-00036; U.S. Patent No. 11,627,631
Page 685 of 1122

appears as one antenna port. In LTE Rel-8, only a single UE-specific antenna port and associated reference signal is defined. As a consequence the beamformed PDSCH can only be transmitted with a single spatial layer. The support of two UE-specific antenna ports was introduced in Rel-9, thus enabling beamforming with two spatial layers with direct one-to-one mapping between the layers and antenna ports.

The UE-specific reference signals in LTE Rel-9 were designed to be orthogonal in order to facilitate separation of the spatial layers at the receiver. The two associated PDSCH layers can then be transmitted to a single user (SU-MIMO) in good channel conditions to increase the individual data rate, or to multiple users (MU-MIMO) to increase the system capacity. The LTE Rel-10 further extended the support for beamforming with an increased number of UE-specific reference signals and spatial layers. When two layers are transmitted over multiple spatial streams, they share the available transmit power of the eNB, thus the increase in data rate comes at the expense of a reduction of coverage. This makes rank adaptation, which is used in the codebook-based spatial multiplexing transmission mode, an important mechanism for the dual-layer beamforming. In this case, the UE is configured to feedback RI in conjunction with the PMI. It should be noted that beamforming in LTE can only be applied to PDSCH and not to the downlink control channels, although the coverage of a traffic channel can be extended through beamforming, the overall cell coverage may still be limited by the control channels. Similar to any other precoding technique, the beamforming schemes in LTE require reliable CSIT, which can ideally be obtained either via UE feedback or based on estimation of the uplink channel condition.

In the single-layer beamforming mode of Rel-8, the UE does not feed back any precoding-related information, and the eNB extracts this information from the uplink, e.g., using DoA estimations.[32] It is worth noting that in this case

[32]If the position of the UE is known, the beamforming weights can be adapted accordingly to optimize transmission for the UE. Therefore, signal classification algorithms such as multiple signal classification (MUSIC) can be used in the base station to determine the DoA for the UE signal and thus determine its location. A uniform linear array (ULA) antenna array is typically used, where the distance d between the individual antennas is the same and $d \leq \lambda/2$. This type of array can be seen as a spatial filtering and sampling in the signal space. Just as the Nyquist criterion applies to sampling a signal over time, the distance here must be $d \leq \lambda/2$ in order to determine the DoA [164].
The MUSIC algorithm estimates the frequency content of a signal or autocorrelation matrix using an eigen-space method. This method assumes that a signal $x(n)$ consists of L complex exponentials in the presence of additive white Gaussian noise. Given an $M \times M$ autocorrelation matrix $\mathbf{R}_{\mathbf{x}}$, if the eigenvalues are sorted in decreasing order, the eigenvectors corresponding to the L largest eigenvalues span the signal subspace. Note that for $M = L + 1$, the result from MUSIC algorithm is identical to that of Pisarenko's method. The general idea is to use averaging to improve the performance of the Pisarenko's estimator. The frequency estimation function for MUSIC is given by $\hat{P}_{\mathrm{MU}}(e^{j\omega}) = \left(\sum_{i=L+1}^{M} \left|\mathbf{e}^{\mathrm{H}}\mathbf{v}_i\right|^2\right)^{-1}$ where $\mathbf{v}_i$'s are the noise eigenvectors and vector $\mathbf{e} = (1, e^{j\omega}, e^{j2\omega}, \ldots, e^{j(M-1)\omega})^{\mathrm{T}}$. The locations of the L largest peaks of the estimation function give the frequency estimates for the L signal components [28].

Petitioners' Exhibit 1021
Nokia of America Corp., et al. v. KT Corporation, et al.
Case No. IPR2025-00036; U.S. Patent No. 11,627,631
Page 686 of 1122

calibration of the eNB RF paths may be necessary. The dual-layer beamforming mode of LTE Rel-9 provides the possibility for the UE to help the eNB to derive the beamforming precoding weights by sending PMI feedback in the same way as for codebook-based closed-loop spatial multiplexing. For beamforming, this is particularly suitable for FDD deployments where channel reciprocity cannot be exploited as effectively as in the case of TDD. Nevertheless, this PMI feedback can only provide partial CSIT, since it is based on measurements of the cell-specific reference signals which, in beamforming deployments, are usually transmitted from multiple antenna elements with broad radiation patterns; furthermore, the PMI feedback uses the same codebook as for closed-loop spatial multiplexing; therefore it is constrained by quantization granularity. For CQI feedback, the eNB must take into account the fact that in the beamforming modes the channel quality experienced by the UE on the beam-formed PDSCH resources will typically be different than on the cell-specific reference signals based on which the CQI is calculated. The UE-specific reference signals cannot be used for CQI estimation because they are only in existence in the resource blocks assigned to a specific user. It must be noted that beamforming also reduces the interference to neighboring cells. In addition, the beamforming may be coordinated among neighboring eNBs to take advantage of the spatial interference created by beamforming in multiple cells [14,15].

Other algorithms may be used in which the optimum beamforming precoder is determined by channel estimation. In a TDD system, uplink and downlink are on the same frequency, thus the channel characteristics are the same based on the reciprocity principle. That is why a feedback is not needed from the UE when a suitable uplink signal is present that the base station can use to estimate the channel. In the case of LTE TDD, the uplink sounding reference signal can be used.

In LTE Rel-8, a UE configured in MU-MIMO mode assumes that an eNB transmission on the PDSCH would be performed on one layer using one of the rank-1 codebook entries defined for two or four antenna ports. Therefore, the MU-MIMO transmission is limited to a single layer and single codeword per scheduled UE, and the RI and PMI feedback are similar to a SU-MIMO rank-1 transmission. The eNB can simultaneously schedule multiple UEs on the same resource blocks, typically by pairing UEs that report orthogonal PMIs. The eNB can therefore signal to those UEs (using one bit in the DCI format 1D message on PDCCH) that the PDSCH power is reduced by 3 dB relative to the cell-specific reference signals. This assumes that the transmission power of the eNB is equally divided between the two codewords and implies that in practice a maximum of two UEs may be concurrently scheduled in Rel-8 MU-MIMO mode. The CQI reporting for MU-MIMO in Rel-8 does not take into account any interference from transmissions to jointly scheduled users. The CQI values reported are equivalent to those that would be reported for a rank-1 SU-MIMO transmission. In LTE Rel-9, the support for MU-MIMO is enhanced by the introduction of dual-layer beamforming in conjunction with precoded UE-specific reference signals. This eliminates the constraint on the use of the feedback for precoding and

Petitioners' Exhibit 1021
Nokia of America Corp., et al. v. KT Corporation, et al.
Case No. IPR2025-00036; U.S. Patent No. 11,627,631
Page 687 of 1122

provides more flexibility to utilize other approaches to MU-MIMO user separation, e.g., according to a zero-forcing beamforming criterion. Note that with an increasing number of UEs, zero-forcing beamforming converges to unitary precoding. The use of precoded DM-RSs eliminates the need for explicitly signaling the precoder to the UEs. Instead, the UEs estimate the effective channel, i.e., the combination of the precoding matrix and physical channel. The DM-RS design in Rel-9 allows for up to four UEs to be scheduled for MU-MIMO transmissions [14].

9.15 PDSCH transmission modes

Each PDSCH transmission mode defines a specific set of physical layer procedures and configurations based on which the transport blocks are processed and the complex-valued baseband signals for transmission on the antenna ports are generated. There are 10 transmission modes that have been defined for LTE/LTE-Advanced of which transmission modes 1−7 apply to LTE Rel-8, transmission mode 8 was defined for LTE Rel-9, transmission mode 9 was developed in Rel-10, and transmission mode 10 was introduced in LTE Rel-11. The transmission modes in LTE/LTE-Advanced can be explained as follows [5,14,15]:

- *Transmission mode 1* uses only one transmit antenna and is a SISO or SIMO mode.
- *Transmission mode 2* utilizes transmit diversity and is the default MIMO mode in LTE. It sends the same information via various antennas, whereby each antenna stream uses different space−time coding and different frequency resources. This improves the signal-to-noise ratio and makes transmission more robust. In LTE, transmit diversity is used as a fallback option for some transmission modes, such as when spatial multiplexing cannot be used. Control channels, such as PBCH and PDCCH, are also transmitted using transmit diversity. For two antennas, a frequency-based version of the Alamouti code [58] or SFBC is used, while for four antennas, a combination of SFBC and FSTD is used.
- *Transmission mode 3* supports spatial multiplexing of two to four layers that are multiplexed to two to four antennas, respectively, in order to achieve higher data rates. It requires less UE feedback on the channel condition, i.e., no precoding matrix indicator is included and is used when channel information is missing or when the channel rapidly changes, e.g., for UEs moving at high velocity. In addition to the precoding, the signal is fed to each antenna with a specific delay (CDD), thus artificially creating frequency diversity. For two transmit antennas, a fixed precoding (codebook index 0 is used), while for four antennas, the precoders are cyclically switched.
- *Transmission mode 4* supports spatial multiplexing with up to four layers that are multiplexed to up to four antennas, respectively, in order to achieve higher data rates. To allow channel estimation at the receiver, the base station

Petitioners' Exhibit 1021
Nokia of America Corp., et al. v. KT Corporation, et al.
Case No. IPR2025-00036; U.S. Patent No. 11,627,631
Page 688 of 1122

transmits cell-specific reference signals, distributed over various resource elements and over various time slots. The UE sends a response regarding the channel condition, which includes information about which precoding is preferred from a predefined codebook. This is accomplished using an index (PMI) to the codebook, which is a table with possible precoding matrices that is known to both sides.

- *Transmission mode 5* is similar to mode 4. It uses codebook-based closed-loop spatial multiplexing; however, one layer is dedicated for each UE.
- *Transmission mode 6* is a special type of closed-loop spatial multiplexing in mode 4. In contrast to mode 4, only one layer is used (rank-1). The UE estimates the channel and sends the index of the most suitable precoding matrix back to the base station. The base station sends the precoded signal via all antenna ports. The precoding in the baseband changes the magnitude and phase of the signals to different antennas and results in beamforming effect. With four transmit antennas, there are 16 different beamforming diagrams. This implicit beamforming effect is distinguished from classical beamforming used in transmission modes 7 and 8, that are aiming at achieving a direct impact on the antenna pattern, e.g., for covering particular areas of a cell.
- *Transmission mode 7* uses UE-specific reference signals. Both data and reference signals are transmitted using the same antenna precoding. Because the UE requires only the UE-specific reference signal for demodulation of the PDSCH, the data transmission for the UE appears to have been received from only one transmit antenna, and the UE does not see the actual number of transmit antennas. Therefore, this transmission mode is also called single antenna port (port 5). The transmission appears to be originated from a single virtual antenna port 5. The LTE standard does not specify any methods for determining the beamforming parameters. Other methods such as beam-switching are also possible. The number of antennas and the antenna architecture are not specified and are implementation specific.
- *Transmission mode 8* specifies dual-layer beamforming which allows the base station to weight two layers individually at the antennas so that beamforming can be combined with spatial multiplexing for one or more UEs. As in mode 7, UE-specific reference signals are used in this mode. Since the same resource elements are used, the reference signals must be coded differently so that the UE can distinguish between them. Because two layers are used, both layers can be assigned to one UE (SU-MIMO), or the two layers can be assigned to two separate UEs (MU-MIMO).
- *Transmission mode 9* was introduced in Rel-10 and uses non-codebook-based precoding which supports up to eight layers using UE-specific reference signals.
- *Transmission mode 10* was introduced in Rel-11 to support CoMP operation and to configure Rel-11 non-zero-power CSI-RS resources and interference measurement resources. This new transmission mode was defined to provide Rel-11 UEs capable of operating on new carrier types, which do not carry CRS, to conduct the CSI measurement and feedback necessary for CoMP

Petitioners' Exhibit 1021
Nokia of America Corp., et al. v. KT Corporation, et al.
Case No. IPR2025-00036; U.S. Patent No. 11,627,631
Page 689 of 1122

essential functions. More specifically, transmission mode 10 is used for all channel measurements on Rel-11 CSI-RS resources, all interference measurements on Rel-11 interference measurement resources, and PDSCH demodulation based on UE-specific reference signals.

The performance of LTE Rel-8 transmission modes in terms of BLER and throughput as a function of SNR for a number of antenna configurations have been simulated and are shown in Figures 9.131 and 9.132. In these figures, OLSM and CLSM refer to open-loop and closed-loop spatial multiplexing,

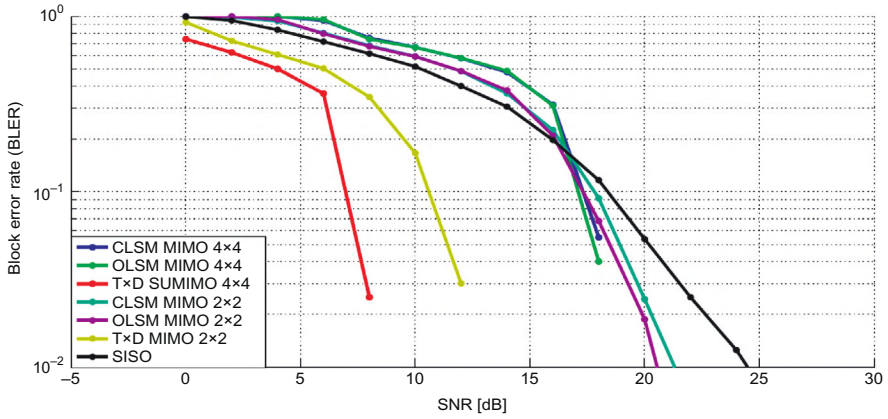


FIGURE 9.131

BLER of LTE transmission modes (modified ITU-VehA 120 km/h,CQI9,800 Subframes) [141,142].

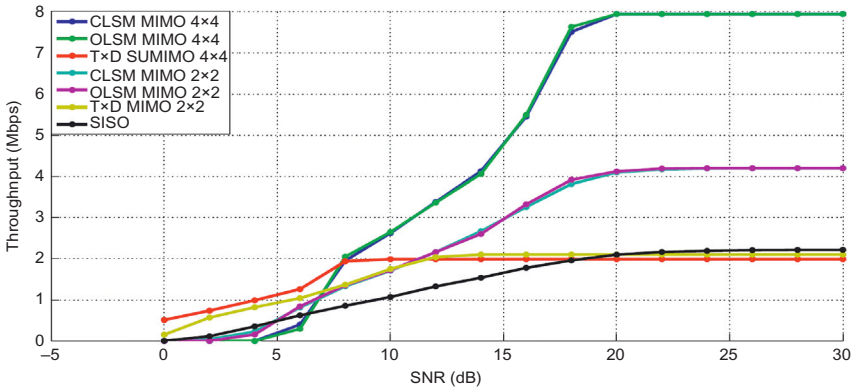


FIGURE 9.132

Throughput of LTE transmission modes (modified ITU-VehA 120 km/h) [141,142].

respectively (transmission modes 3 and 4), and TxD denotes transmit diversity (transmission mode 2) [141,142].

When a UE is configured to decode PDCCH with CRC that has been scrambled by C-RNTI, the UE is required to decode PDCCH and the corresponding PDSCH according to combinations defined in Table 9.31. Note that PDSCH transmission corresponding to these PDCCHs is scrambled by C-RNTI. Similar PDSCH transmission specifications when configured with other UE identifiers such as SPS C-RNTI are given in 3GPP TS 36.213 [5].

The UE can be semi-statically configured via higher layer signaling to receive PDSCH data transmissions signaled via ePDCCH according to one of the transmission modes 1−10. In transmission mode 10, a UE can be configured with scrambling identities $n_{\mathrm{ID}}^{\mathrm{DM\text{-}RS_i}}|_{i=0,1}$ for UE-specific reference signal generation to decode PDSCH according to a detected PDCCH/ePDCCH with CRC scrambled by the C-RNTI with DCI format 2D intended for the UE [5].

A UE in transmission mode 10 can be configured with one or more CSI processes per serving cell by higher layers. Each CSI process is associated with a CSI-RS resource and a CSI-interference measurement (CSI-IM) resource. In transmission mode 10, PUSCH PMI feedback/CQI feedback modes 1-2, 2-2, and 3-1 are supported, if the UE is configured by the eNB to report PMI/RI and the number of CSI-RS ports is greater than one; otherwise, PUSCH PMI feedback/CQI feedback modes $2-0$, and $3-0$ are supported, if the UE is configured without PMI/RI reporting or the number of CSI-RS ports is equal to one. A UE in transmission mode 10 can be configured by higher layers for multiple periodic CSI reports corresponding to one or more CSI processes per serving cell on PUCCH.

In LTE Rel-11 the concept of quasi-collocated antenna ports was introduced in order to support distributed antenna systems. Two antenna ports are quasi-collocated, if the large-scale properties of the channel over which a symbol on one antenna port is conveyed can be inferred from the channel over which a symbol on the other antenna port is conveyed. The large-scale properties include one or more of delay spread, Doppler spread, Doppler shift, average gain, and average delay. The UE does not assume that two antenna ports are quasi-collocated unless specified otherwise.

As a result, when a Rel-11 UE is configured in transmission mode 10 on a given serving cell, it can be configured with up to 4 parameter sets by higher layer signaling in order to decode PDSCH according to a detected PDCCH/ePDCCH with DCI format 2D which is intended for the UE and the given serving cell. The UE then uses the parameter set according to the value of the PDSCH Resource Element Mapping and Quasi-Collocation indicator field in the detected PDCCH/ePDCCH with DCI format 2D for determining the PDSCH resource element mapping and antenna port quasi-collocation, provided that the UE is configured with Type B quasi-collocation. For PDSCH without a corresponding PDCCH/ePDCCH, the UE uses the parameter set indicated in the PDCCH/ePDCCH with DCI format 2D corresponding to the associated semi-persistent scheduling activation for determining the PDSCH resource element mapping and antenna port quasi-collocation [5].

Petitioners' Exhibit 1021
Nokia of America Corp., et al. v. KT Corporation, et al.
Case No. IPR2025-00036; U.S. Patent No. 11,627,631
Page 691 of 1122

Table 9.31 Characteristics of PDSCH Modes when Configured with C-RNTI [5]

Transmission Mode	Release	DCI Format	PDCCH Search Space	Transmission Format of PDSCH	Number of Codewords	CSI Feedback from UE	Number of Layers	Number of Antenna Ports	Type of Reference Signals
1	8	1A	Common and UE-specific	Single-antenna port	1	CQI	1	1 (AP0)	Cell-specific
		1	UE-specific	Single-antenna port			1	1 (AP0)	Cell-specific
2	8	1A	Common and UE-specific	Transmit diversity	1	CQI	2,4	2,4	Cell-specific
		1	UE-specific	Transmit diversity			2,4	2,4	Cell-specific
3	8	1A	Common and UE-specific	Transmit diversity	1	CQI,RI	2,4	2,4	Cell-specific
		2A	UE-specific	Large delay CDD or transmit diversity	2		2,4	2,4	Cell-specific
4	8	1A	Common and UE-specific	Transmit diversity	1	CQI,RI,PMI	2,4	2,4	Cell-specific
		2	UE-specific	Closed-loop spatial multiplexing or transmit diversity	2		2,4	2,4	Cell-specific
5	8	1A	Common and UE-specific	Transmit diversity	1	CQI,PMI	2	2	Cell-specific
		1D	UE-specific	Multi-user MIMO	1		2	2	Cell-specific
6	8	1A	Common and UE-specific	Transmit diversity	1	CQI,PMI	2	2	Cell-specific
		1B	UE-specific	Closed-loop spatial multiplexing using a single transmission layer	1		1	1	UE-specific

(*Continued*)

Petitioners' Exhibit 1021
Nokia of America Corp., et al. v. KT Corporation, et al.
Case No. IPR2025-00036; U.S. Patent No. 11,627,631
Page 692 of 1122

Table 9.31 (Continued)

Transmission Mode	Release	DCI Format	PDCCH Search Space	Transmission Format of PDSCH	Number of Codewords	CSI Feedback from UE	Number of Layers	Number of Antenna Ports	Type of Reference Signals
7	8	1A	Common and UE-specific	If the number of PBCH antenna ports is one, single-antenna on AP0; otherwise, transmit diversity	1	CQI	1,2,4	1 (AP0) or 2,4	Cell-specific
		1	UE-specific	Single-antenna	1		1	1 (AP5)	UE-specific
8	9	1A	Common and UE-specific	If the number of PBCH antenna ports is one, single-antenna on AP0; otherwise, transmit diversity	1,2	CQI	1,2,4	1 (AP0) or 2,4	UE-specific
		2B	UE-specific	Dual layer transmission on AP7 and AP8 or single-antenna on AP7 or AP8	1,2		1,2	1 (AP7 or AP8) 2 (AP7 and AP8)	UE-specific
9	10	1A	Common and UE-specific	Non-MBSFN subframe: if the number of PBCH antenna ports is one, single-antenna on AP0; otherwise, transmit diversity MBSFN subframe: single-antenna on AP7	1,2	CQI (PTI, PMI, and RI if configured by the eNB)	Non-MBSFN: 1,2,4 MBSFN: 1	Non-MBSFN: 1 (AP0),2,4 MBSFN: 1 (AP7)	UE-specific

Petitioners' Exhibit 1021
Nokia of America Corp., et al. v. KT Corporation, et al.
Case No. IPR2025-00036; U.S. Patent No. 11,627,631
Page 693 of 1122

		2C	UE-specific	Up to eight layer transmission on AP7-14 or single-antenna on AP7 or AP8	1,2		Up to 8	Up to 8 (AP7-AP14) 1 (AP7 or AP8)	UE-specific
10	11	1A	Common and UE-specific	Non-MBSFN subframe: if the number of PBCH antenna ports is one, single-antenna on AP0; otherwise, transmit diversity MBSFN subframe: single-antenna on AP7	1,2	CQI (PTI, PMI, and RI if configured by the eNB)	Non-MBSFN: 1,2,4 MBSFN: 1	Non-MBSFN: 1 (AP0),2,4 MBSFN: 1 (AP7)	UE-specific
		2D	UE-specific	Up to eight layer transmission on AP7-14 or single-antenna on AP7 or AP8	1,2		Up to 8	Up to 8 (AP7-AP14) 1 (AP7 or AP8)	UE-specific

9.16 OFDM signal generation

The continuous time-domain signal $s_l^p(t)$ on antenna port p in OFDM symbol l in a downlink slot (assuming 12 sub-carriers per resource block) is defined as follows [3]:

$$s_l^p(t) = \sum_{k=-\lfloor 6N_{\mathrm{RB}}^{\mathrm{DL}} \rfloor}^{-1} a_{k^-}^p(l) \mathrm{e}^{\mathrm{j}2\pi k \Delta f (t - N_{CP}(l) T_s)} + \sum_{k=1}^{\lceil 6N_{\mathrm{RB}}^{\mathrm{DL}} \rceil} a_{k^+}^p(l) \mathrm{e}^{\mathrm{j}2\pi k \Delta f (t - N_{\mathrm{CP}}(l) T)} \quad (9.104)$$

where $0 \le t < (N_{\mathrm{CP}} + N_{\mathrm{FFT}})T_{\mathrm{s}}$, $k^- = k + \lfloor 12N_{\mathrm{RB}}^{\mathrm{DL}} \rfloor$, $k^+ = k + \lfloor 6N_{\mathrm{RB}}^{\mathrm{DL}} \rfloor - 1$, and the parameter $N_{\mathrm{FFT}} = 2048$ for $\Delta f = 15$ kHz sub-carrier spacing. The OFDM symbols in a slot are transmitted in increasing order of index l starting at $l = 0$, where OFDM symbol $l > 0$ starts at time $\sum_{l'=0}^{l-1} [N_{\mathrm{CP}}(l') + N_{\mathrm{FFT}}]T_{\mathrm{s}}$ within the slot. In the case where the first OFDM symbol(s) in a slot use a normal cyclic prefix and the remaining OFDM symbols use an extended cyclic prefix (e.g., MBSFN subframes), the starting position of the OFDM symbols with an extended cyclic prefix are identical to those in a slot where all OFDM symbols use an extended cyclic prefix. Therefore, there will be a part of the time slot between the two cyclic prefix regions where the transmitted signal is not specified.

9.17 Timing advance

In LTE/LTE-Advanced, when a UE attempts to establish a RRC connection with the eNB, it transmits a random access preamble from which the eNB estimates the transmission time (Figure 9.133). Then the eNB transmits a random access response which includes a timing advance command, based on which the UE adjusts the uplink frame transmit timing. Transmission of the uplink radio frame number k from the UE starts $(N_{\mathrm{TA}} + N_{\mathrm{TA}}^{\mathrm{offset}})T_{\mathrm{s}}$ seconds before the start of the corresponding downlink radio frame at the UE where $0 \le N_{\mathrm{TA}} \le 20,512$ (samples) and $N_{\mathrm{TA}}^{\mathrm{offset}} = 0$ for frame structure type 1, and $N_{\mathrm{TA}}^{\mathrm{offset}} = 624$ (samples) for frame structure type 2. Note that there may be no transmission in some slots in a radio frame. Upon reception of a timing advance command, the UE is required to adjust its uplink transmission timing for the PUCCH, PUSCH, and SRS of the primary cell. The timing advance command indicates the change of the uplink timing

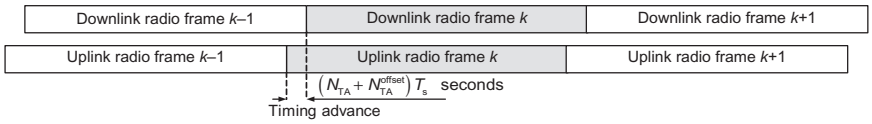


FIGURE 9.133

Relative timing of uplink and downlink radio frames [3,5].

relative to the current uplink timing in multiples of $16T_s$ (samples). The start timing of the random access preamble is discussed in Chapter 10. In LTE Rel-10, the uplink transmission timing for the PUSCH and SRS of a secondary cell is the same as the primary cell.

In the case of random access response, an 11-bit timing advance command parameter $T_A = 0, 1, 2, ..., 1282$ indicates the N_{TA} values where the amount of the timing alignment is given by $N_{TA} = 16T_A$. In other cases, a 6-bit timing advance command parameter $T_A = 0, 1, 2, ..., 63$ indicates the adjustment of the current N_{TA} value where the updated N_{TA} value is given by $N_{TA}^{New} = N_{TA}^{Old} + 16(T_A - 31)$. Note that the adjustment of N_{TA} value by a positive or a negative offset indicates advancing or deferring the uplink transmission time by a given amount, respectively. For a timing advance command received in subframe n, the timing adjustment is applied from subframe $n + 6$ onward. When the UE's uplink PUCCH, PUSCH, and SRS transmissions in subframe n and subframe $n + 1$ are overlapping due to the timing adjustment, the UE transmits the entire subframe n and does not transmit the overlapped portion of subframe $n + 1$. If the received downlink timing changes and the uplink−downlink offset is not compensated or is only partially compensated by the uplink timing adjustment without timing advance command, the UE is expected to change N_{TA} accordingly [3]

After initial uplink synchronization via the random access channel, the UE maintains its uplink frame timing alignment using the timing advance control element sent as part of a MAC PDU on PDSCH that allows the eNB to periodically send timing commands to the UE. The network may also send timing commands as part of a random access response message. The timing advance is a 6-bit number that adjusts timing (advances or delays) relative to the current UE timing, when sent as a MAC control element. The timing advance for random access response is an 11-bit quantity that specifies absolute uplink frame timing relative to the downlink frame. The eNB calculates the desired timing advance based on uplink transmissions from the UE. The eNB also configures the UE's timing alignment timer. If the UE does not receive a timing advance MAC control element before the timing alignment timer expires, it is no longer considered to be uplink-synchronized with the serving cell. When this timer expires, the UE must flush HARQ buffers and reinitialize the HARQ processes. The UE must further release all PUCCH and SRS resources. If any uplink transmission is required, the UE must perform a contention-based random access procedure in order to obtain timing alignment and an uplink grant before it can transmit in the uplink [5].

After the UE has been synchronized to the downlink transmissions from the eNB, the initial timing advance is set by means of the random access procedure in order to establish uplink synchronization. This requires the UE to transmit a random access preamble from which the eNB estimates the uplink timing and responds with an 11-bit initial timing advance command contained in the random access response message. This allows the timing advance to be configured by the eNB with a granularity of 0.52 μs from 0 up to a maximum of 0.67 ms corresponding to a cell radius of 100 km. A cell range of 100 km is sufficient for most

practical rural deployment scenarios. The granularity of 0.52 μs enables the uplink transmission timing to be set with an accuracy within the length of the uplink SC-FDMA symbol cyclic prefix. This granularity is also significantly finer than the length of a cyclic shift of the uplink reference signals. Studies have shown that timing misalignment of up to 1 μs does not cause any significant degradation in system performance due to increased intra-cell interference. Thus the granularity of 0.52 μs is sufficiently fine to allow for additional timing errors arising from the uplink timing estimation in the eNB and the accuracy with which the UE sets its initial transmission timing.

Following the initial timing advance establishment for each UE in the cell, it will then need to periodically update the uplink timing in order to counter changes in the arrival time of the uplink signals at the eNB. Such changes may arise from different causes including the movement of a UE (causing the propagation delay to change at a rate dependent on the relative velocity of the UE and the eNB), sudden changes in propagation delay due to changing multipath profile (such changes typically occur most frequently in dense urban environments as the UEs move around the corners of buildings), oscillator frequency drifts in the UE, and Doppler frequency shift arising from the movement of the UE especially in LoS propagation, resulting in an additional frequency offset of the uplink signals received at the eNB [14].

The update of the timing advance to mitigate the aforementioned effects is performed by a closed-loop mechanism whereby the eNB measures the received uplink timing and issues timing advance update commands to instruct the UE to adjust its transmission timing accordingly relative to its current transmission timing. In deriving the timing advance update commands, the eNB may measure any uplink signal including sounding reference signals, demodulation reference signals, channel quality indicators, HARQ feedback, or uplink data transmissions. In general, wideband uplink signals enable more accurate timing estimation. The advantage of accurate timing estimation has to be traded off with the uplink overhead caused by use of wideband reference signals. In addition, cell-edge UEs are typically power-limited, and thus are bandwidth-limited for a given uplink SINR. The timing estimation accuracy of narrowband uplink signals can be improved through averaging multiple measurements over time and interpolating the resulting power delay profile.

The eNB must balance the overhead of sending regular timing advance update commands to all the UEs in the cell against the UE's ability to transmit as soon as data becomes available in its transmit buffer. The eNB thus configures a timer for each UE, which the UE restarts each time a timing advance update command is received; if the UE does not receive another timing advance update command before the timer expires, it must then consider its uplink to have lost synchronization. In that case, in order to avoid the risk of generating interference to uplink transmissions from other UEs, the UE is not permitted to make another uplink transmission without first transmitting a random access preamble to reinitialize the uplink timing adjustment. One further use of timing advance is to create a

Petitioners' Exhibit 1021
Nokia of America Corp., et al. v. KT Corporation, et al.
Case No. IPR2025-00036; U.S. Patent No. 11,627,631
Page 697 of 1122

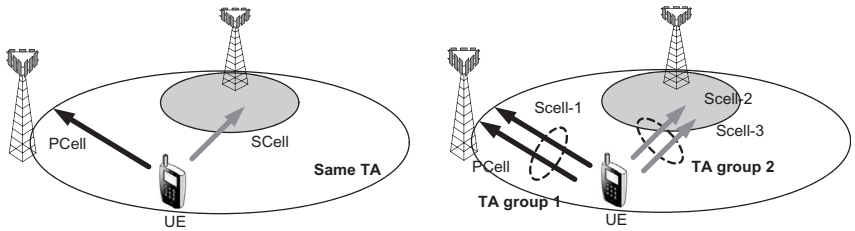


FIGURE 9.134

Illustration of single and multiple timing advance concepts [165].

switching time between uplink reception at the eNB and downlink transmission for TDD and H-FDD operation. This switching time can be generated by applying an additional timing advance offset to the uplink transmissions, to increase the amount of timing advance beyond what is required to compensate for the round-trip propagation delay [14].

Heterogeneous networks (HetNet) comprising macro-cells and small-cell base stations are considered as a key enabler for performance improvement in future cellular networks. LTE Rel-11 has specified carrier aggregation with multiple uplink timing advances and other enhancements to support non-collocated cells, e.g., multiple uplink power control instances or improved sounding reference signals. One of the scenarios of interest in HetNet is the use of remote radio heads (or geographically separated RF transceivers) connected via fiber-optic to a central baseband processing unit. A variation of this scenario, shown in Figure 9.134, would involve macro-cells which overlay small cells where both simultaneously use the same component carriers, requiring inter-cell interference coordination for proper operation (e.g., using an LTE Rel-10 feature known as enhanced inter-cell interference coordination (eICIC) which utilizes almost blank subframes (ABS)). In these scenarios, multiple timing advances are required to support non-collocated cells with carrier aggregation. Assuming synchronization to the macro-cell's PCell is already obtained, the UE has to subsequently synchronize to the SCell of the other site. Therefore, the PCell eNB will request a RACH on the SCell immediately after SCell activation (see Figure 9.134). The RACH request is sent via PDCCH signaling from the PCell. Enhanced MAC control elements are used to signal multiple timing advance values using previously reserved fields in the header.

In the case where several RF carriers require the same timing advance, these carriers will be grouped in what is known as a timing advance group (TAG).[33] The TAGs will be configured by eNB RRC signaling. This will reduce the overall

[33]A timing advance group is a group of serving cells that is configured by RRC signaling and uses the same timing reference cell and the same timing advance value. Primary timing advance group (pTAG) is the timing advance group containing the PCell. Secondary timing advance group (sTAG) is the timing advance group not containing the PCell [7].

Petitioners' Exhibit 1021
Nokia of America Corp., et al. v. KT Corporation, et al.
Case No. IPR2025-00036; U.S. Patent No. 11,627,631
Page 698 of 1122

complexity and signaling overhead for multiple TAs in case carrier aggregation is being used at each transmission point. For each TAG, a reference carrier for synchronization will be configured as a timing reference.

In carrier aggregation scenarios where two or more component carriers are aggregated to provide wider transmission bandwidths, a UE may simultaneously receive or transmit on one or multiple cells depending on its capabilities. A UE with single timing advance capability for carrier aggregation can simultaneously receive and/or transmit on multiple RF carriers corresponding to multiple serving cells sharing the same timing advance (multiple serving cells grouped in one TAG). A UE with multiple timing advance capability for carrier aggregation can simultaneously receive and/or transmit on multiple RF carriers corresponding to multiple serving cells with different timing advances (multiple serving cells grouped in multiple TAGs). It must be noted that each TAG contains at least one serving cell with configured uplink where the mapping of each serving cell to a TAG is configured by RRC signaling. A UE which does not support carrier aggregation can transmit/receive on a single RF carrier corresponding to one serving cell (one serving cell in one TAG).

LTE-Advanced supports contiguous and non-contiguous aggregation of component carriers where each RF carrier is limited to a maximum of 110 resource blocks in the frequency-domain using the LTE Rel-8/9 OFDM parameters. It is possible to configure a UE to aggregate a different number of RF carriers originating from the same eNB and of possibly different bandwidths in the uplink and the downlink. The number of TAGs that can be configured depends on the TAG capability of the UEs.

The UE is required to adjust uplink transmission timing for PUCCH/PUSCH/SRS of the primary cell based on the received timing advance command for a TAG containing the primary cell. The uplink transmission timing for PUSCH/SRS of a secondary cell is the same as the primary cell, if the secondary cell and the primary cell belong to the same TAG. In the case where a carrier-aggregation-enabled UE receives a timing advance command for a TAG that does not contain the primary cell, then it is required to adjust its uplink transmission timing for PUSCH/SRS of all the secondary cells in the TAG based on the received timing advance command.

9.18 Power control and link adaptation

Power control is a mechanism where the transmit power of the downlink or uplink control or traffic channels are adjusted at the base station or at mobile stations, based on instructions from the serving base station such that with minimal impact on the reliability of the downlink/uplink transmissions and throughput, the inter-user/inter-cell interference among users and base stations are reduced. Therefore, power control can be considered as a link adaptation

Petitioners' Exhibit 1021
Nokia of America Corp., et al. v. KT Corporation, et al.
Case No. IPR2025-00036; U.S. Patent No. 11,627,631
Page 699 of 1122

mechanism that is utilized for interference mitigation in cellular systems. While increasing the transmit power over a communication link has certain advantages such as higher SNR at the receiver, which reduces the bit error rate and allows higher data rate and results in greater spectral efficiency as well as more protection against signal attenuation over fading channels, a higher transmit power; however, it has several drawbacks including increased power consumption of the transmitting device, reducing the UE battery life, and increased interference to other users in the same or adjacent frequency bands. The following sections describe the power control algorithms that are incorporated in LTE/LTE-Advanced.

9.18.1 Basic concepts

LTE/LTE-Advanced provide uplink power control mechanisms to compensate the effects of path loss, shadowing, fast fading, and implementation loss. The uplink power control is further used to mitigate inter-cell and intra-cell interference, thereby enhancing the overall throughput and reducing the effective UE power consumption. The uplink power control includes open-loop and closed-loop power control. The base station transmits necessary power control information through transmission of power control messages. The parameters of the power control algorithm are optimized on a system-wide basis by the eNB, and are broadcast periodically or trigged by events. The UE provides the necessary information through higher-layer control messages to the serving eNB in order to enable uplink power control. The eNB can exchange necessary information with neighboring base stations through backhaul to support uplink power control to facilitate the handover process.

The power control scheme may not be effective in high mobility scenarios for compensating the effects of a fast fading channel due to variation of the channel impulse response. As a result, the power control is used to mitigate the distance-dependent path loss, shadowing, and implementation loss. The uplink power control takes into consideration the MIMO transmission mode and whether a single user or multiple users are supported on the same resource at the same time. The open-loop power control compensates the channel variations and implementation loss without requiring frequent interactions with the serving eNB. The UE can determine the transmit power based on the transmission parameters sent by the eNB, uplink channel quality, downlink CSI, or the interference knowledge obtained from downlink transmissions. The open-loop power control provides a coarse initial transmit power setting for the mobile station before establishing connection with the base station.

It is perceived that rate control is more efficient than power control under certain conditions [15]. Rate control in principle implies that the power amplifier is always transmitting at full power and therefore is efficiently utilized. On the other hand, power control often results in inefficient utilization of the power amplifier because the transmission power is often less than its maximum. In practice, the

Petitioners' Exhibit 1021
Nokia of America Corp., et al. v. KT Corporation, et al.
Case No. IPR2025-00036; U.S. Patent No. 11,627,631
Page 700 of 1122

radio-link data rate is controlled by adjusting the modulation scheme and/or the channel coding rate. In good channel conditions, the value of E_b/N_0 at the receiver is high, and the main limitation of the data rate is the bandwidth of the radio link. In such conditions, use of higher-order modulation, e.g., 16QAM or 64QAM, together with a high coding rate, is more appropriate for link adaptation. Similarly, in the case of poor channel conditions, the use of QPSK and low-rate coding is preferred. Link adaptation by means of rate control is referred to as adaptive modulation and coding (AMC).

A power control mechanism takes into consideration the serving eNB target link SINR and/or interference level to other cells/sectors for mitigating inter-cell interference. In order to achieve the target SINR, the serving eNB path loss can be fully or partially compensated based on a trade-off between overall system throughput and cell-edge performance. The mobile station's transmit power is adjusted in order to ensure the level of interference is less than the permissible interference level. The closed-loop power control, on the other hand, compensates channel variations through periodic power-control commands from the serving eNB. The base station measures the uplink CSI and interference level using uplink data and/or control channel transmissions, and sends power control commands to the mobile stations. Upon receiving the power control command from the eNB, the UE adjusts its uplink transmit power. The closed-loop power control is active during data and control channel transmissions.

A UE is expected to maintain the transmit power density (i.e., total transmit power normalized by transmission bandwidth) for each data and control channel below a certain level that is determined by the maximum permissible power level for the UE, emission mask, and other regulatory constraints. In other words, when the number of active logical resource units assigned to a particular user is reduced, the total transmitted power must be reduced proportionally by the UE in the absence of any additional change of power control parameters. When the number of resource blocks is increased, the total transmitted power must be proportionally increased such that the transmitted power level does not exceed the permissible power levels specified by 3GPP and the regulatory specifications [1]. For interference level control, the information about the current interface level of each eNB may be shared among the base stations via backhaul.

The (uplink) transmit power control (TPC) in mobile communication systems is meant to balance the transmitted energy per bit in order to maintain the link quality corresponding to the minimum QoS requirements, to minimize interference to other users in the system, and to minimize the power consumption of the mobile terminal. In achieving these goals, the power control has to adapt to the characteristics of the propagation channel, including path loss, shadowing, and fast fading, as well as overcoming interference from other users both within the same cell and in neighboring cells.

The requirements for uplink interference management in LTE are different from the operational requirements in the uplink of the CDMA systems. In CDMA

Petitioners' Exhibit 1021
Nokia of America Corp., et al. v. KT Corporation, et al.
Case No. IPR2025-00036; U.S. Patent No. 11,627,631
Page 701 of 1122

systems, the uplink is not orthogonal and the primary source of interference which has to be managed is intra-cell interference among different intra-cell users. The uplink users in a CDMA system share the same time–frequency resources and they all contribute to a rise in interference above thermal noise level at the base station receiver; a phenomenon typically known as rise over thermal (RoT),[34] that ought to be carefully controlled and shared among users. The primary mechanism for increasing the uplink data rate for a given user is to reduce the spreading factor and increase the transmission power accordingly, consuming a larger proportion of the total available RoT in the cell. In contrast, in LTE, the uplink is theoretically orthogonal and intra-cell interference management is consequently less critical than that of a CDMA system.

The main mechanisms for adapting the uplink data rate in LTE are varying the transmit bandwidth and varying the MCS, while the transmit power spectral density (PSD) could typically remain approximately constant for a given MCS. Moreover, in a CDMA system, the power control was primarily designed with continuous transmission in mind for circuit-switched services, while in LTE, different UEs are scheduled at 1 ms transmission time intervals. This is reflected in the fact that power control in CDMA is periodic, while LTE allows for larger power steps which do not have to be periodic, with a minimum loop delay of about 5 ms. With the above considerations in mind, the power control scheme provided in LTE employs a combination of open-loop and closed-loop control, which theoretically requires less feedback than a closed-loop scheme, because the closed-loop feedback is only needed to compensate for cases when the UE's own estimate of the required power setting is not adequate.

A typical mode of operation for power control in LTE involves setting a coarse operating point for the transmit PSD based on path loss estimation. This would provide a suitable PSD setting for reference MCS in the prevailing path loss and shadowing conditions. Faster adaptation can then be applied around the open-loop operating point by closed-loop power control. This can control the interference level and adapt the transmit power setting according to the channel conditions including fast fading. However, due to the orthogonal nature of the LTE uplink, the LTE closed-loop power control does not need to be as fast as in CDMA systems. In fact, the fastest and most frequent adaptation of the uplink transmissions is by means of the uplink scheduling grants, which vary the transmission bandwidth and accordingly the total transmit power, together with setting the MCS, in order to attain the desired uplink data rate. With this combination,

[34]In CDMA systems, the rise over thermal (RoT) indicates the ratio between the total power received from wireless sources at a base station and the thermal noise. In order to decode the data at the base station, a minimum SINR at the receiver must be guaranteed. RoT metric is a measure of the uplink loading. By increasing the number of transmitting UEs and their transmit power, the level of interference in the uplink increases. This interference is perceived by the base station as noise adversely affecting the SINR. The base station controls the interference level by adjusting the UE uplink assignments and transmit-power [40].

Petitioners' Exhibit 1021
Nokia of America Corp., et al. v. KT Corporation, et al.
Case No. IPR2025-00036; U.S. Patent No. 11,627,631
Page 702 of 1122

the power control scheme in LTE in practice provides support for more than one mode of operation [14].

The initial open-loop operating point for the transmit power per resource block depends on a number of factors including the inter-cell interference and cell loading. It can be further divided into two components: (1) a semi-static base-level value comprising a nominal power level that is common for all UEs in the cell (measured in dBm per resource block) and a UE-specific offset; and (2) an open-loop path loss compensation component. Different base levels can be configured for PUSCH data transmissions depending on the scheduling mode (i.e., dynamic or semi-persistent scheduling), which in principle allows different BLER operating points to be used for each scheduling mode. One possible use for different BLER operating points is to achieve a lower probability of retransmission when using semi-persistent scheduling. The UE-specific offset component of the base level enables the eNB to correct the systematic offsets of the UE's transmission power setting. The path loss compensation component is based on the UE's estimate of the downlink path loss, which can be derived from the UE's measurement of RSRP and the known transmit power of the downlink reference signals, which is broadcast by the eNB.

In order to obtain a reasonable indication of the uplink path loss, the UE should filter the downlink path loss estimate with a suitable time window to remove the effect of fast fading but not shadowing. Typical filter lengths are between 100 and 500 ms [14]. For PUSCH and SRS, the degree to which the uplink PSD is adapted to compensate for the path loss can be set by the eNB, on a scale from "no compensation" to "full compensation." This is an important feature of power control in LTE and is known as fractional power control; it is configured by means of a fractional path loss compensation factor, referred to as α. In principle, the combination of the base level and the path loss compensation component allow the eNB to configure the degree to which the UE responds to the path loss. At one extreme, the eNB could configure the base level to the lowest level (−126 dBm) and rely entirely on the UE's path loss measurement to raise the power toward the cell-edge; alternatively, the eNB can set the base level to a higher value, possibly in conjunction with only partial path loss compensation. Disregarding the UE-specific offset, the range of the base level for PUSCH (−126 to +23 dBm per RB) is intended to cover the full range of target SINR values for different degrees of path loss compensation, transmission bandwidths, and interference levels. For example, the highest value of the base level corresponds to the maximum permissible transmission power of an LTE UE and would typically only be used, if path loss compensation was not used. The lowest value of base level for PUSCH −126 dBm is relevant to a case when full path loss compensation is used and the uplink transmission and reception conditions are optimal. In general, the maximum path loss that can be compensated depends on the required SINR and the transmission bandwidth. Note that this assumes full path loss compensation and ignores the dynamic offset [14]. In other

Petitioners' Exhibit 1021
Nokia of America Corp., et al. v. KT Corporation, et al.
Case No. IPR2025-00036; U.S. Patent No. 11,627,631
Page 703 of 1122

words, LTE defines the setting of the UE transmit power for PUSCH by the following equation [5]:

$$P_{\text{PUSCH}} = \min[P_{T_{\max}}, 10\log_{10} M + P_0 + \alpha P_{\text{L}} + \delta_{\text{MCS}} + f(\Delta_i)]\ [\text{dBm}] \quad (9.105)$$

where

- $P_{T_{\max}}$ is the maximum allowed transmit power that depends on the UE power class (i.e., UE maximum output power which is typically + 23 dBm for a power class 3 UE).
- M denotes the number of physical resource blocks assigned for uplink transmission.
- P_0 is a cell/UE-specific base level parameter that is signaled through higher-layer signaling.
- α represents the path loss compensation factor, which is a 3-bit cell-specific parameter in the range of [0 1] which is signaled through higher-layer signaling, where $\alpha = 0$ corresponds to "no compensation" and $\alpha = 1$ corresponds to "full compensation."
- P_{L} is the downlink path loss estimate, which is calculated by the UE based on RSRP measurement.
- δ_{MCS} is cell/UE-specific MCS defined in 3GPP specifications for LTE.
- $f(\Delta_i)$ is a UE-specific function which indicates the use of accumulated or absolute correction value and Δ_i is the closed-loop correction value. The UE-specific TPC commands can operate in two different modes: (1) accumulative TPC commands that are available for PUSCH, PUCCH, and SRS; and (2) absolute TPC commands that are available for PUSCH only. In the case of PUSCH, the switch between these two modes is configured semi-statically for each UE by RRC signaling, i.e., the mode cannot be changed dynamically. With the accumulative TPC commands, each TPC command signals a power step relative to the previous level. This is the default mode and is particularly suitable for fine-tuning of the transmission power, and for situations where a UE receives power control commands in groups of successive subframes. This mode is similar to the closed-loop power control in CDMA systems.

In the above equation $P_0 = \alpha(\text{SNR}_0 + P_{\text{N}}) + (1 - \alpha)(P_{T_{\max}} - 10\log_{10} M_0)$ [dBm] where:

- SNR_0 is the open-loop SNR target.
- P_{N} is the noise power per resource block.
- M_0 defines the number of resource blocks for which the SNR target is set with full-power.

Some of the parameters in the above equations are broadcast by the eNB, i.e., the same value for all the users in the cell. The UE sets its initial transmission power based on received parameters from the eNB and path loss calculated by the UE per se. It is worthwhile to note that Δ_i is signaled by the eNB

Petitioners' Exhibit 1021
Nokia of America Corp., et al. v. KT Corporation, et al.
Case No. IPR2025-00036; U.S. Patent No. 11,627,631
Page 704 of 1122

to any UE after it sets its initial transmit power, i.e., Δ_i has no contribution in the initial setting of the UE transmit power. The expression, based on which a UE sets its initial power, can be obtained from the above equations by ignoring δ_{MCS} and the closed-loop correction factor, thus $P_{PUSCH} = 10\log_{10} M + P_0 + \alpha P_L$ [dBm] where the parameter M denotes the total number of resource blocks scheduled by the eNB. The power assignment for transmission at the UE is performed on the basis of per resource block, and each resource block contains an equal amount of power. Therefore, by neglecting M, the expression used by the UE to assign power to each resource block is given by $PSD_{TX} = P_0 + \alpha P_L$ [dBm/RB].

The above equation represents the transmit SPD of a resource block expressed in dBm/RB. Note that each resource block corresponds to the 180 kHz subchannel. The parameter PSD_{TX} is a helpful means to explain the basic difference between conventional and fractional power control schemes. Setting the path loss compensation factor α to one (full compensation of path loss) leads to conventional power control, whereas the use of values $0 < \alpha < 1$ (fractional compensation of path loss) leads to fractional power control. Note that $\alpha = 0$ (no compensation of path loss) leads to no power control, i.e., all users will use the maximum allowed transmission power.

When $\alpha = 1$, it can be shown that $P_0 = SNR_0 + P_N$ [dBm], thus $PSD_{TX} = P_0 + P_L$ [dBm/RB], taking into account the path loss, the received PSD at the eNB is given by $PSD_{RX} = P_0$ [dBm/RB]. It is important to note that the received PSD at the eNB is equal to P_0; therefore, a conventional power control scheme leads all users to equal SPD. This scheme is widely used in cellular systems which are not using an orthogonal transmission scheme in the uplink, such as CDMA-based systems. One of the advantages of this power control scheme is that it removes the near-far problem which is typical of CDMA systems, since it equalizes the power level of the UEs before receiving at the base station. It can be shown that under these conditions, the received PSD is the same for all users independent of their path loss for a given target SNR.

The fractional power control scheme allows the user terminals' transmissions to be received with variable PSD depending on their path loss, i.e., the user with good channel conditions will be received with high PSD. Using $0 < \alpha < 1$, the PSD is given by $PSD_{TX} = P_0 + \alpha P_L = \alpha(SNR_0 + P_N) + (1 - \alpha)P_{max} + \alpha P_L$ [dBm/RB]. In contrast to conventional power control, which allows full compensation of path loss, fractional power control compensates for a fraction of the path loss and this is the reason for the term "fractional power control." The received PSD can be obtained by taking path loss into account and is given by $PSD_{RX} = P_0 + (\alpha - 1)P_L$ [dBm/RB]. The received PSD in the case of a conventional power control scheme results in P_0, whereas the case of a fractional power control scheme has an additional term, where both P_0 and $(\alpha - 1)P_L$ are cell-specific and broadcast to the UEs by the eNB, which means that they are the same for all the UEs. Thus, P_L is the key factor that allows users to be received with different power spectral densities [15].

Petitioners' Exhibit 1021
Nokia of America Corp., et al. v. KT Corporation, et al.
Case No. IPR2025-00036; U.S. Patent No. 11,627,631
Page 705 of 1122

The fractional path loss compensation factor α can be seen as a tool to trade off the fairness of the uplink scheduling against the total cell capacity. Full path loss compensation maximizes fairness for cell-edge UEs. However, when considering multiple cells together as a system, the use of partial path loss compensation can increase the total system capacity in the uplink, as fewer resources are consumed, ensuring the success of transmissions from cell-edge UEs and less inter-cell interference is caused to neighboring cells. Path loss compensation factors around 0.7−0.8 typically give a close-to-maximal uplink system capacity (typically around 15−25% greater than can be achieved with full path loss compensation) without causing significant degradation to the cell-edge data rate. The target received PSD for a given MCS is reduced as the path loss increases, so that cell-edge UEs cause less inter-cell interference. Inter-cell interference is of particular concern for UEs located near the edge of a cell, as they may disrupt the uplink transmissions in the neighboring cells [14].

Open-loop power control is the ability of the UE transmitter to set its uplink transmit power to a specified value suitable for the eNB receiver. The uplink transmit power is given as $P_{\mathrm{OL}} = \min[P_{\max}, 10\log_{10} M + P_0 + \alpha P_{\mathrm{L}}]$ [dBm], which is set by open-loop power control. The choice of α depends on whether a conventional or fractional power control scheme is used. Using $\alpha = 1$ leads to conventional open-loop power control, while $0 < \alpha < 1$ leads to fractional open-loop power control. The estimate of the path loss is obtained after measuring the RSRP and then the calculation for transmission power is performed based on the above equation.

Closed-loop power control is the ability of the UE to adapt the uplink transmit-power according to the closed-loop correction values received from the eNB, also known as TPC commands. The TPC commands are transmitted by the eNB to the UE, based on the closed-loop target signal-to-interference and noise ratio and the measured received SINR. In a closed-loop power control mechanism, the uplink receiver at the eNB estimates the SINR of the received signal and compares it with the target SINR value. When the received SINR value is below the target SINR, a TPC command is transmitted to the UE to instruct the UE to increase the transmitter power. Otherwise, the TPC command will cause the UE transmitter power to decrease. The LTE closed-loop power control mechanism operates around the open-loop operation point. The UE adjusts its uplink transmission power based on the TPC commands it receives from the eNB when the uplink power setting is performed at the UE using open-loop power control.

For the low-rate PUCCH (carrying HARQ ACK/NACK and CQI reports), full path loss compensation is always applied, because PUCCH transmissions from different UEs are code-division-multiplexed. Full path loss compensation facilitates good control of the interference among different users, and thereby helps to maximize the number of users which can be accommodated simultaneously on PUCCH. A different base level value P_0 is also provided for PUCCH compared to that used for PUSCH, assuming a reference PUCCH format. For SRS, an

Petitioners' Exhibit 1021
Nokia of America Corp., et al. v. KT Corporation, et al.
Case No. IPR2025-00036; U.S. Patent No. 11,627,631
Page 706 of 1122

additional semi-static offset relative to the PUSCH power operating point may be configured through RRC signaling.

Downlink power control determines the energy per resource element (EPRE) which implies the energy prior to cyclic prefix insertion. The term resource element energy also implies the average energy taken over all constellation points for the modulation scheme in use. Uplink power control determines the average power over a SC-FDMA symbol, on which the physical channel is transmitted.

9.18.2 Downlink power allocation

The cell-specific reference signals are embedded into the overall system bandwidth at certain resource elements. In the frequency-domain, every sixth sub-carrier carries a reference signal. The reference signal pattern is a pseudo-random sequence, whose generation depends on the cell identity and the cyclic prefix. Furthermore, a frequency shift is applied that is based on a modulo-6 operation. The mapping of the pattern is therefore cell-specific, but the spacing is always six sub-carriers. In the time-domain, every fourth OFDM symbol carries reference symbols. Due to their importance, reference signals are the highest powered components within the downlink signal. The power level for the reference signals is signaled within system information to the device. The reference signal power level is cell-specific and is in the range of -60 to $+50$ dBm per 15 kHz. It is a requirement that the LTE base station transmits all reference signals with constant power over the entire bandwidth. The power of all other signal components (synchronization signals, PBCH, PCFICH, PDCCH, PDSCH, and PHICH) is set relative to this value. As mentioned above, there are OFDM symbols that contain reference signals and there are OFDM symbols that do not contain reference signals.

The relative PDSCH power for these symbols is given by two different parameters ρ_A and ρ_B (see Figure 9.135). For the majority of cases, ρ_A corresponds to the parameter P_A that is signaled via higher layers. Only for some special cases such as transmit diversity with four antennas or MU-MIMO, ρ_A is computed differently. Parameter P_A is device specific, is obtained as part of the *RRCConnectionSetup* message, and can take one out of eight different values. In Figure 9.135, it is assumed that P_A is -4.77 dB. Parameter P_B is related to the cell-specific reference signal power and cannot be changed dynamically. It can take one out of four integer values. Depending on the number of transmit antennas (1, 2, or 4), each value corresponds to a certain ratio and thus a power offset. LTE Rel-8/9 networks that are currently deployed worldwide are supporting a 2×2 MIMO baseline configuration. Let us assume $P_B = 3$, in that case, the resource element carrying data in that OFDM symbol where reference signals are present is transmitted with an additional offset of 3 dB compared to

Petitioners' Exhibit 1021
Nokia of America Corp., et al. v. KT Corporation, et al.
Case No. IPR2025-00036; U.S. Patent No. 11,627,631
Page 707 of 1122

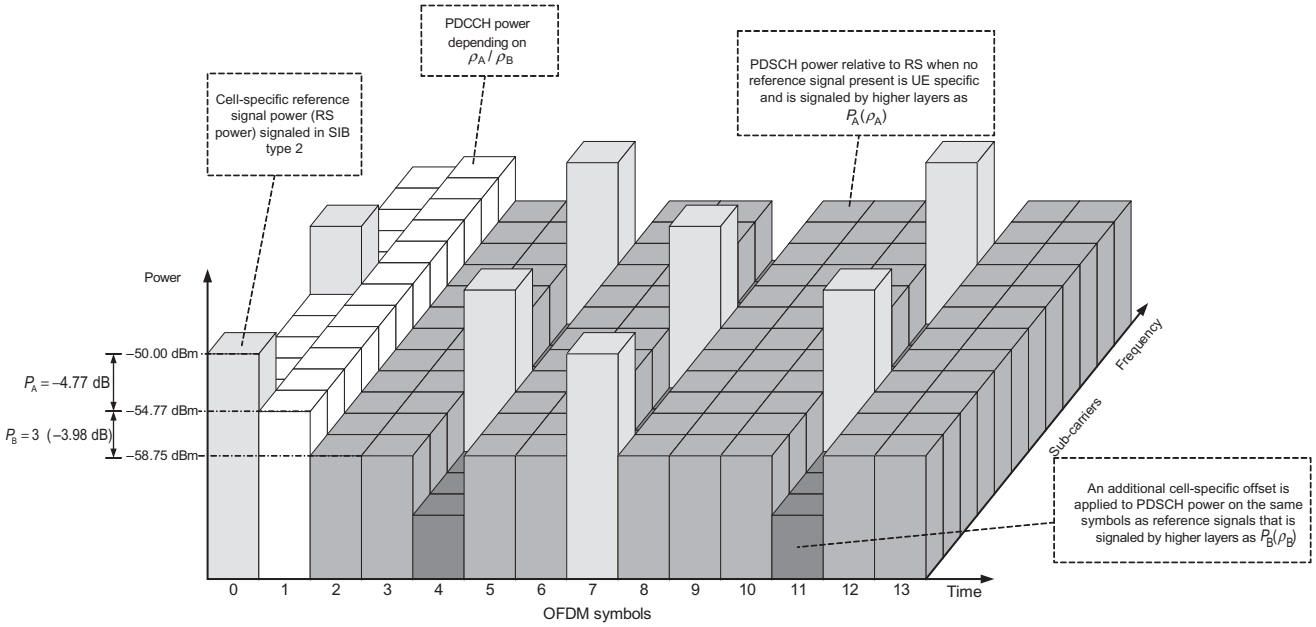


FIGURE 9.135

Example of LTE Rel-8 downlink power allocation [134].

symbols without reference signals. For only one transmit antenna (SISO), $P_B = 3$ translates to -3.98 dB as shown in Figure 9.135. The overall goal is to have a constant power for all OFDM symbols to avoid power variations at the UE receiver. With less PDSCH power given by P_B, the boost of reference signals is compensated, compared to OFDM symbols that do not contain reference signals. The PDSCH power always depends on the resource allocation, i.e., the number of allocated resource blocks. Resource allocation can change from one subframe to another subframe, thus P_A can also change on a subframe-by-subframe basis. While incorporating P_A and P_B, it is ensured that the overall OFDM symbol power remains constant, even when the PDSCH allocation is changed [5].

9.18.3 PUSCH power control

Starting with LTE Rel-10 and in the case of carrier aggregation, it is possible to transmit multiple PUSCH on different component carriers simultaneously, or it is possible to simultaneously transmit PUSCH and PUCCH on the same or different component carriers (this was not allowed in previous releases of LTE). In principle, each physical channel is separately and independently power controlled. However, in the case of concurrent transmission of multiple physical channels from the same terminal, the total transmit power for all physical channels may occasionally exceed the maximum terminal output power setting according to the terminal power class. The basic strategy is to ensure reliable transmission of all control signaling by allocating an appropriate amount of power to the respective physical channels. The remaining power is then assigned to the rest of the physical channels. For each uplink component carrier configured for a terminal, there is also an associated and explicitly configured maximum per-carrier transmit power, which may be different for different component carriers. This may be explained as follows. In many practical scenarios, the terminal will not be scheduled for uplink transmission on all of its configured component carriers, so the terminal should be able to transmit with its maximum output power. As will be seen in this section, the power control of each physical channel explicitly ensures that the total transmit power for a given component carrier does not exceed maximum per-carrier transmit-power; however, separate power-control algorithms do not ensure that the total transmit power for all component carriers does not exceed the maximum terminal output power. The latter limitation will be enforced by a subsequent power scaling applied to the physical channels that are concurrently transmitted. This power scaling is carried out in a way that control signaling channels have higher priority relative to traffic channels during concurrent transmission in the uplink.

If the UE does not simultaneously transmit PUSCH and PUCCH on the serving cell k, i.e., the kth component carrier because component carriers are referred

Petitioners' Exhibit 1021
Nokia of America Corp., et al. v. KT Corporation, et al.
Case No. IPR2025-00036; U.S. Patent No. 11,627,631
Page 709 of 1122

to as cells in LTE-Advanced, then the UE transmit power $P^k_{\text{PUSCH}}(i)$ for PUSCH transmission in the ith subframe is given as follows:

$$P^k_{\text{PUSCH}}(i) = \min\left\{ \underbrace{P^k_{\max}(i)}_{\substack{\text{Maximum Power per}\\ \text{Component Carrier}}}, \underbrace{10\log_{10}(M^k_{\text{PUSCH}}(i))}_{\text{Bandwidth Factor}} + \underbrace{P^k_0(j) + \alpha_k(j)P^k_L}_{\substack{\text{Basic Open-loop}\\ \text{Operating Point}}} + \underbrace{\Delta^k_{\text{TF}}(i) + f_k(\Delta_{\text{TPC}}(i))}_{\text{Dynamic Offset}} \right\} \text{[dBm]} \quad (9.106)$$

If the UE transmits PUSCH and PUCCH simultaneously on the serving cell k, then the UE transmit power $P^k_{\text{PUSCH}}(i)$ when transmitting PUSCH in the ith subframe is given as follows:

$$P^k_{\text{PUSCH}}(i) = \min\left\{ \underbrace{10\log_{10}(\hat{P}^k_{\max}(i) - \hat{P}_{\text{PUCCH}}(i))}_{\substack{\text{Maximum available power per}\\ \text{component carrier}}}, \underbrace{10\log_{10}(M^k_{\text{PUSCH}}(i))}_{\text{Bandwidth Factor}} + \underbrace{P^k_0(j) + \alpha_k(j)P^k_{\text{L}}}_{\substack{\text{Basic open-loop}\\ \text{operating point}}} + \underbrace{\Delta^k_{\text{TF}}(i) + f_k(\Delta_{\text{TPC}}(i))}_{\text{Dynamic offset}} \right\} \text{[dBm]} \quad (9.107)$$

In the above equations:

- $P^k_{\max}(i)$ is the configured UE transmit power in the ith subframe for serving cell k, implying that this channel power is calculated and set for every subframe.
- $\hat{P}_{\text{PUCCH}}(i)$ is the linear value of $P_{\text{PUCCH}}(i)$.
- $M^k_{\text{PUSCH}}(i)$ is the number of resource blocks allocated for the UE in the ith subframe and on serving cell k.
- $P^k_0(j)$ is a parameter composed of the sum of a component $P^k_{0\ NOMINAL\_PUSCH}(j)$ provided through higher-layer signaling for $j = 0,1$ and another component $P^k_{0\ UE\_PUSCH}(j)$ that is provided by higher layers for $j = 0,1$ in the kth serving cell.
- P^k_L is the downlink path loss estimated via RSRP measurements by the UE on serving cell k in dB.
- $\Delta^k_{\text{TF}}(i)$ is the MCS-dependent component, referred to as transport format in the LTE specifications, which allows the transmitted power per resource block to be adapted according to the information data rate.
- i denotes the subframe number.
- $j = 0$ or 1.
- $f_k(\Delta_{\text{TPC}}(i))$ denotes a TPC command and $f_k(.)$ represents an accumulation function in the case of accumulative TPC commands.

The above power control equation allows the UE's transmit power to be controlled with a granularity of 1 dB within the range of -40 dBm to $+23$ dBm. The maximum transmission power of a UE may be subject to additional

Petitioners' Exhibit 1021
Nokia of America Corp., et al. v. KT Corporation, et al.
Case No. IPR2025-00036; U.S. Patent No. 11,627,631
Page 710 of 1122

restrictions, such as the maximum transmission power in a cell may be restricted to a lower level by RRC signaling, or in some configurations, reductions in maximum output power may be applied in order to satisfy in-band and out-of-band emission requirements. For LTE Rel-10 UEs which support carrier aggregation in the uplink, the transmission power of an individual carrier or uplink physical channel may have to be scaled down according to certain rules in order to satisfy the total output power constraints. The UE accuracy in setting total transmission power depends on the length of time since the last uplink transmission has taken place, and the size of the required change in transmission power [15].

It was mentioned above that if the total transmit power of the UE exceeds $\hat{P}_{T_{\max}}(i)$, the UE scales down the power of PUSCH for the serving cell k in the ith subframe $\hat{P}^k_{\text{PUSCH}}(i)$ such that the condition $\sum_k a_i \hat{P}^k_{\text{PUSCH}}(i) \leq (\hat{P}_{T_{\max}}(i) - \hat{P}_{\text{PUCCH}}(i))$ is satisfied where $\hat{P}_{\text{PUCCH}}(i)$ is the linear value of $P_{\text{PUCCH}}(i)$, $\hat{P}^k_{\text{PUSCH}}(i)$ is the linear value of $P^k_{\text{PUSCH}}(i)$, $\hat{P}_{T_{\max}}(i)$ is the linear value of the UE total configured maximum output power $P_{T_{\max}}$ in the ith subframe, and $0 \leq a_i \leq 1$ is the scaling factor of $\hat{P}^k_{\text{PUSCH}}(i)$ for serving cell k. In a hypothetical scenario, when the UE is scheduled to transmit PUSCH containing UCI on the jth serving cell and transmit PUSCH without UCI in the remaining serving cells, and if the total transmit power of the UE is going to exceed $\hat{P}_{T_{\max}}(i)$, the UE is required to scale $\hat{P}^k_{\text{PUSCH}}(i)$ for the serving cells without UCI in the ith subframe such that the following condition is satisfied [5]:

$$\sum_{k \neq j} a_i \hat{P}^k_{\text{PUSCH}}(i) \leq (\hat{P}_{T\max}(i) - \hat{P}^j_{\text{PUSCH}}(i)) \tag{9.108}$$

where $\hat{P}^j_{\text{PUSCH}}(i)$ is the PUSCH transmit power for the cell with UCI and a_i is the scaling factor of $\hat{P}^k_{\text{PUSCH}}(i)$ for serving cell k containing no UCI. In this case, the power scaling is not applied to $\hat{P}^j_{\text{PUSCH}}(i)$ unless $\sum_{k \neq j} a_i \hat{P}^k_{\text{PUSCH}}(i) = 0$ and the total transmit power of the UE would still exceed $\hat{P}_{T_{\max}}(i)$. Note that values of the scaling coefficients a_i are the same across serving cells when $a_i > 0$, but for certain serving cells a_i may be set to zero. In another hypothetical scenario where the UE has simultaneous PUCCH and PUSCH transmission with UCI on the jth serving cell and PUSCH transmission without UCI in the remaining serving cells, if the total transmit power of the UE would exceed $\hat{P}_{T_{\max}}(i)$, the UE sets $\hat{P}^k_{\text{PUSCH}}(i)$ according to the following criteria [5]:

$$\hat{P}^j_{\text{PUSCH}}(i) = \min[\hat{P}^j_{\text{PUSCH}}(i), \hat{P}_{T_{\max}}(i) - \hat{P}_{\text{PUCCH}}(i)] \tag{9.109}$$

and

$$\sum_{k \neq j} a_i \hat{P}^k_{\text{PUSCH}}(i) \leq (\hat{P}_{T\max}(i) - \hat{P}_{\text{PUCCH}}(i) - \hat{P}^j_{\text{PUSCH}}(i)) \tag{9.110}$$

Petitioners' Exhibit 1021
Nokia of America Corp., et al. v. KT Corporation, et al.
Case No. IPR2025-00036; U.S. Patent No. 11,627,631
Page 711 of 1122

9.18.4 PUCCH power control

The appropriate level of the received signal power for PUCCH transmission is simply determined by the minimum power necessary to achieve a satisfactory block error rate in decoding of the uplink control signaling information transmitted on PUCCH. However, it is important to take the following considerations into account: (1) In general, decoding performance is not determined by the received signal strength, but rather by the received signal-to-interference-plus-noise ratio, i.e., an appropriate received signal power depends on the interference level at the receiver, where the interference level depends on network deployment and is time-variant since loading of the network varies across time. (2) There are different PUCCH formats which are used to carry a different types of uplink control information. The different PUCCH formats thus carry a different number of information bits per subframe and the information they carry may also have different error-rate requirements. The required received SINR may differ in different PUCCH formats, something that needs to be taken into account when setting the PUCCH transmit power in a given subframe. The power control for PUCCH can be described by the following expression [5]:

$$P_{\text{PUCCH}}(i) = \min \left[\underbrace{P^{k}_{\max}(i)}_{\substack{\text{Maximum available} \\ \text{power for PUCCH}}} \; , \; \underbrace{P_0 + P^{k}_{\text{L}}}_{\text{Basic operating point}} + \underbrace{\Delta_{\text{PUCCH-FORMAT}}}_{\substack{\text{Format-dependent} \\ \text{power adjustment} \\ \text{factor}}} + \underbrace{\delta_{\text{PUCCH}}(i)}_{\substack{\text{Dynamic adjustment} \\ \text{based on TPC} \\ \text{commands}}} \right] \tag{9.111}$$

where:

- $P^{k}_{T_{\max}}(i)$ is the configured UE transmit power in the ith subframe on serving cell k.
- $P_{\text{PUCCH}}(i)$ denotes the PUCCH transmit power in a given subframe.
- P^{k}_{L} represents the downlink path loss as estimated by the terminal based on downlink RSRP.
- P_0 is a cell-specific parameter that is broadcast as part of the system information and can be seen as the desired or target received signal power. As discussed earlier, the required received power depends on the receiver noise and uplink interference level.
- $\delta_{\text{PUCCH}}(i)$ is a UE-specific dynamic correction value, also referred to as a TPC command, included in the PDCCH with DCI format 1/1A/1B/1D/2/2A/2B/2C/2D for the primary cell or sent jointly coded with other UE-specific PUCCH correction values on a PDCCH with DCI format 3/3A whose CRC is scrambled with TPC-PUCCH-RNTI.

Petitioners' Exhibit 1021
Nokia of America Corp., et al. v. KT Corporation, et al.
Case No. IPR2025-00036; U.S. Patent No. 11,627,631
Page 712 of 1122

In practice, it is not possible to allow P_0 to vary with interference level for the following reasons: (1) the terminal does not read the system information continuously and thus it does not have access to the updated P_0 value; and (2) the uplink path loss estimate is derived from downlink measurements and is not fully accurate due to differences between the instantaneous downlink and uplink propagation conditions, as well as measurement inaccuracies. Thus, in practice, P_0 may reflect the average interference level or the relatively constant noise level.

In order to reflect different SINR requirements for various PUCCH formats, the PUCCH power control expression includes the term $\Delta_{\text{PUCCH-FORMAT}}$ which adds a format-dependent power offset to the transmit power. The power offsets are defined such that a baseline PUCCH format, i.e., the format corresponding to the transmission of a single HARQ ACK/NACK, has an offset equal to 0 dB, while the offsets for the remaining formats can be explicitly configured by the network. For example, PUCCH format 1 with QPSK modulation, carrying two simultaneous acknowledgment and used in the case of downlink spatial multiplexing, should have a power offset of 3 dB, reflecting the fact that twice as much power is needed to communicate two acknowledgment bits as opposed to one. It is possible for the network to directly adjust the PUCCH transmit power by providing the terminal with explicit power control commands that adjust the term $\delta_{\text{PUCCH}}(i)$ in the above expression. The power control commands are accumulative, i.e., each received TPC command increases or decreases the term $\delta_{\text{PUCCH}}(i)$ by a certain amount. The power control commands for PUCCH can be provided to the terminal via two different means: (1) by including a power control command in each downlink assignment (i.e., the terminal receives a TPC command every time it is scheduled on the downlink); and (2) the power control commands can also be sent using DCI format 3/3A that simultaneously provides power control commands to multiple terminals. In practice, such TPC commands are typically transmitted on a regular basis and can be used to adjust the PUCCH transmit power prior to periodic uplink channel-state reports. The power control command carried within the uplink scheduling grant consists of 2 bits, corresponding to four different update steps ($-1, 0, +1, +3$ dB). The same is true for the power control command carried on DCI format 3/3A designated for power control. On the other hand, when the PDCCH is configured to use DCI format 3, each TPC command consists of a single bit, corresponding to the update steps -1 and $+1$ dB. In the latter case, twice as many terminals can be power controlled by a single PDCCH. The reason for including a 0 dB value (no change of PUCCH transmit power) as a power-control step is that the power control command is included in every downlink scheduling assignment and sometimes it is desirable not to update the PUCCH transmit power for each assignment.

9.18.5 SRS power control

The UE sets the transmit power of the sounding reference signal in the ith subframe and the kth component carrier as follows [5]:

$$P^k_{\text{SRS}}(i) = \min[P^k_{\max}(i), P^k_{\text{SRS\_OFFSET}}(m) + 10\log_{10}(M^k_{\text{SRS}}) + P^k_0(j) + \alpha_k(j)P^k_L + f_k(i)] \text{ [dBm]} \quad (9.112)$$

Petitioners' Exhibit 1021
Nokia of America Corp., et al. v. KT Corporation, et al.
Case No. IPR2025-00036; U.S. Patent No. 11,627,631
Page 713 of 1122

where:

- $P^k_{\max}(i)$ is the configured UE transmit power in the ith subframe on serving cell k.
- $P^k_{\text{SRS\_OFFSET}}(m), m = 0, 1$ is a 4-bit parameter semi-statically configured by higher layers for the serving cell.
- M^k_{SRS} denotes the bandwidth of the SRS transmission in subframe i for serving cell k in number of resource blocks.
- $f_k(i)$ is the current PUSCH power control adjustment state for serving cell k.
- $P^k_0(j)$ and $\alpha_c(j)$ terms are the same as PUSCH power control with $j = 1$.

If the total transmit power of the UE for the sounding reference signal is going to exceed $\hat{P}^k_{\max}(i)$, i.e., the maximum allotted power for the kth component carrier, the UE scales down $\hat{P}^k_{\text{SRS}}(i)$ in subframe i such that $\sum_k a_i \hat{P}^k_{\text{SRS}}(i) \leq \hat{P}^k_{\max}(i)$ is satisfied where $\hat{P}^k_{\text{SRS}}(i)$ denotes the linear value of $P^k_{\text{SRS}}(i)$ and $\hat{P}^k_{\max}(i)$ is the linear value of $P^k_{\max}$ defined in 3GPP TS 36.211 [3] in the ith subframe, and $0 < a_i \leq 1$ are the scaling factor of $\hat{P}^k_{\text{SRS}}(i)$. Note that α_i values are the same across serving cells.

9.18.6 PRACH power control

The UE must be synchronized in the uplink before it can send signaling or data. Given that the UEs within a cell's coverage area are geographically distributed at different distances from the eNB location, each will exhibit a different propagation delay when accessing the network. Without uplink synchronization, subframes transmitted from different UEs would likely overlap and interfere with each other.

To overcome this problem, the UE performs uplink synchronization procedures on the RACH. The process is initiated by sending RACH preambles using the physical random access channel (PRACH). The random access procedure may be contention-based or contention-free. In the contention-based procedure, the UE selects a preamble from an available set of two groups. If two UEs select the same preamble in the same RACH resource, a collision can result that must be resolved before either UE can access the system. Contention-based RACH is generally used during initial access or if the UE has lost uplink synchronization. With contention-free synchronization, the UE uses a dedicated preamble and it is possible that it had already connected to the network and must resynchronize following a handover to a new cell. During the random access procedure, the preamble index, the target preamble received power (denoted by *Preamble_Received_Target_Power* parameter), the corresponding RA-RNTI, and the PRACH resource are signaled by the higher layers. The preamble transmission power P_{PRACH} is determined by $P_{\text{PRACH}} = \min[P^k_{\max}(i),\ Preamble\_Received\_Target\_Power + P^k_L]$ [dBm] where $P^k_{\max}(i)$ is the configured UE transmit power for the ith subframe of the primary cell, and P^k_{L} is the downlink path loss estimate calculated by the UE for the primary cell.

Petitioners' Exhibit 1021
Nokia of America Corp., et al. v. KT Corporation, et al.
Case No. IPR2025-00036; U.S. Patent No. 11,627,631
Page 714 of 1122

During the RACH procedure, the UE transmits a preamble randomly selected from 64 possible preamble sequences divided into two groups. The group from which the UE selects the preamble depends on the size of the message that it would like to transmit and on the calculated path loss to the eNB. Once the preamble is transmitted, the UE monitors the downlink after three subframes following the end of the preamble transmission for a duration controlled by a configurable window. If no downlink response is detected, then the preamble is retransmitted with a power that is increased by a configurable parameter. This process continues until the maximum number of preamble transmissions is reached. If the preamble is successfully detected by the eNB, then the downlink random access response (RAR) message is sent allocating resources for the UE to transmit its message or enforcing a back-off. In the final step, contention resolution must be performed for a contention-based access attempt. The UE sets its initial power level to the following value: *Preamble_Initial_Received_Target_Power* + *Delta_Preamble* (see Table 9.32 for the permissible values). The parameter *Delta_Preamble* depends on the type of preamble format. The UE selects the first available RACH resource for the transmission. If there is no response within (three subframes + *RA_Response_Window* subframes), the UE assumes that the transmission has been unsuccessful. It selects another RACH preamble and performs the back-off procedure. The power level is increased by the amount *Power_Ramp_Step*. This process can be repeated until the *Preamble_Transmission_Counter* timer expires, in that case, an access failure is declared to the upper layers.

9.18.7 Power headroom

In order to assist the eNB to schedule/allocate the uplink resources to different UEs, it is important that the UE can report its available power headroom to the eNB. The eNB can use the power headroom reports (PHRs) to determine how much uplink bandwidth per subframe the UE can use. This can help to avoid allocating uplink transmission resources to UEs which are unable to properly use them.

The UE PHR MAC control element indicates the power headroom available in the UE. The PHR is encoded in 6 bits with a reporting range from +40 to −23 dB in steps of 1 dB. Positive values indicate the difference between the maximum UE transmit power and current UE transmit power. Negative values

Table 9.32 *Delta_Preamble* Values [8]

Preamble Format	Delta_Preamble Value
0	0 dB
1	0 dB
2	−3 dB
3	−3 dB
4	8 dB

Petitioners' Exhibit 1021
Nokia of America Corp., et al. v. KT Corporation, et al.
Case No. IPR2025-00036; U.S. Patent No. 11,627,631
Page 715 of 1122

indicate the difference between the maximum UE transmit power and the calculated UE transmit power (Figure 9.136). The UE transmit power is calculated based on whether the UE were to transmit according to the current grant with allocated HARQ and RV configuration. The PHR can be configured to be sent periodically or when the downlink path loss changes by a specified amount. For periodic reporting, a report is trigged by the expiration of the *Periodic_PHR_Timer*, which can be configured with values between 10 ms and infinity. For threshold reporting, a PHR is triggered when the path loss changes by the value of *DL_PathlossChange* parameter (1, 3, 6, or infinity dB), provided that the configurable timer *Prohibit_PHR_Timer* has expired. The *Prohibit_PHR_Timer* starts when a PHR has been transmitted and can have values between 0 and 1000 ms.

A PHR can only be sent in subframes in which a UE has an uplink grant, i.e., the report is related to the subframe in which it is transmitted. Therefore, the PHR is a prediction rather than a direct measurement. The UE cannot directly measure its actual transmission power headroom for the subframe in which the report is transmitted and relies on reasonably accurate calibration of the UE's power amplifier output, especially at high output powers when information about power headroom is critical to the system performance.

There are two different types of PHRs. A Type 1 PHR report indicates the power headroom assuming PUSCH-only transmission on the component carrier, while a Type-2 PHR report assumes joint PUSCH and PUCCH transmission, which is a feature added in LTE Rel-10.

9.18.8 Link adaptation

In cellular systems, the quality of the signal received by a UE depends on the channel quality from the serving cell, the level of interference from other cells, and the noise level. To optimize system capacity and coverage for a given transmission power, the transmitter attempts to adapt (and optimize) the information rate and the transmission format, as well as the multi-antenna mode for each user

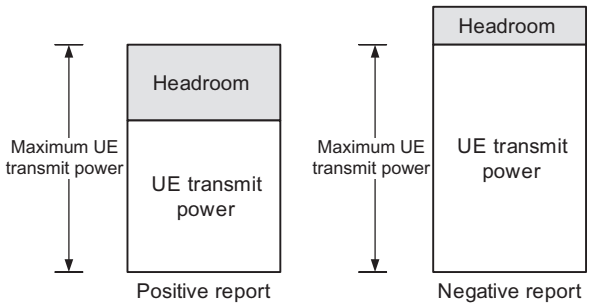


FIGURE 9.136

Power headroom interpretation.

according to the variations in received signal quality at the UE. This is commonly referred to as link adaptation and is typically based on AMC, power control, and adaptation of multi-antenna modes. Low-order modulation such as BPSK and QPSK are more robust and can tolerate higher levels of interference, but provide lower bit rates. High-order modulation such as 16QAM and 64QAM offer higher bit rates, but nonetheless are more prone to errors due to their higher sensitivity to interference, noise, and channel estimation errors; therefore, they are more useful, when the SINR is sufficiently high.

For a given modulation scheme, the code rate can be chosen depending on the channel conditions. A lower code rate can be used in poor channel conditions and a higher code rate can be used when SINR is sufficiently high. The adaptation of the code rate is achieved by applying puncturing to increase the code rate or code repetition to reduce the code rate. In LTE, the modulation and channel coding rates are constant over the allocated frequency resources for a given user, and time-domain channel-dependent scheduling and AMC are supported instead. In addition, when multiple transport blocks are transmitted to one user in a given subframe using multi-layer MIMO, each transport block can use an independent MCS. Furthermore, the UE can be configured to report CQIs to assist the eNB in selecting an appropriate MCS to use for the downlink transmissions. The CQI reports are derived from the downlink received signal quality, typically based on measurements of the downlink reference signals. It is important to note that the reported CQI is not a direct indication of SINR. Instead, the UE reports the highest MCS that it can decode with a BLER not exceeding 10%. Thus the information received by the eNB takes into account the characteristics of the UE's receiver and not just the prevailing channel quality. A UE that is designed with advanced receivers such as MLD or SIC may report a higher channel quality and depending on the characteristics of the eNB's scheduler, can receive a higher data rate [15].

A simple method by which a UE can choose an appropriate CQI value could be based on a set of BLER thresholds, as illustrated in Figure 9.137. The UE will periodically or aperiodically report the CQI value corresponding to the MCS that ensures a BLER less than 10% based on the measured received signal quality.

The CQI metric is generally used in selecting the best MCS under current channel conditions. The CQI measurement typically consists of four basic steps: measuring SINR over the bandwidth of interest (sub-band or wideband), introducing measurement error to the measured SINR, converting the SINR value to discrete CQI values, and finally reporting the CQI using PUCCH or PUSCH. The linear SINR is calculated for each set of resource blocks using the received cell-specific reference signal power and the total interference in every measurement period. The measured linear SINR value for the nth resource block is converted to logarithmic scale as follows $\mathrm{SINR}_{\mathrm{dB}}(n) = 10\log_{10}[\mathrm{SINR}_{\mathrm{linear}}(n)] + \varepsilon_{\mathrm{dB}}$ where $\varepsilon_{\mathrm{dB}}$ is a Gaussian distributed error with zero-mean and parameterized variance, which is added to the measured (ideal) SINR. The SINR values are quantized and converted to discrete CQI values $\mathrm{CQI}_{\mathrm{dB}}(n) = \Delta_Q \lfloor \mathrm{SINR}_{\mathrm{dB}}(n)/\Delta_Q + 0.5 \rfloor$. The CQI is measured at integer multiples of transmission time interval. The

Petitioners' Exhibit 1021
Nokia of America Corp., et al. v. KT Corporation, et al.
Case No. IPR2025-00036; U.S. Patent No. 11,627,631
Page 717 of 1122

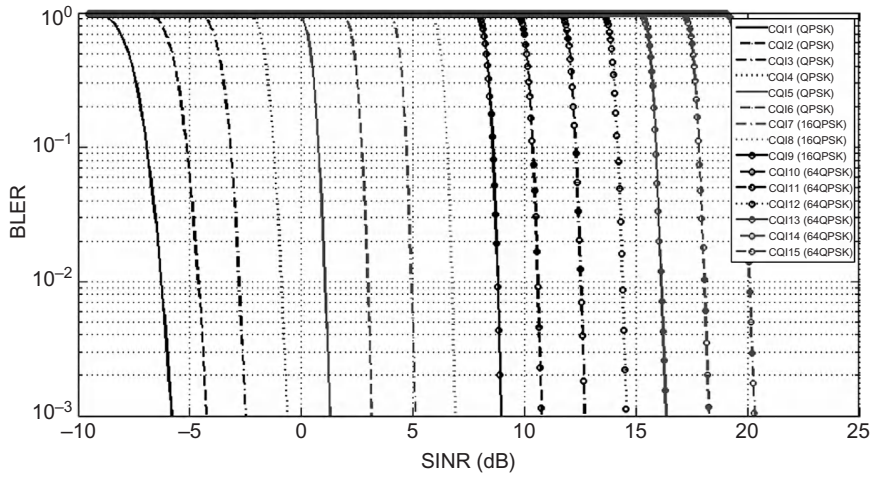


FIGURE 9.137

Link-level BLER as a function of SINR with CQI (MCS) as a parameter [142].

measured CQI values are reported with a certain delay using a specific CQI reporting scheme. It is possible to change the granularity of the basic reporting scheme by changing the number of CQI reports per TTI. Full feedback reporting is done by measuring and reporting individual CQI values for all resource blocks. The minimum granularity is achieved by wideband CQI, which is an average value calculated over all resource blocks.

The granularity of the CQI reports is determined by defining a number of sub-bands $N_{\text{sub-band}}$, each consists of $k_{\text{sub-band}}$ contiguous physical resource blocks. The value of $k_{\text{sub-band}}$ depends on the type of CQI report and is a function of the system bandwidth (see Table 9.28). In each case, the number of sub-bands spans the entire system bandwidth and is given by $N_{\text{sub-band}} = \lceil N_{\text{RB}}^{\text{DL}}/k_{\text{sub-band}} \rceil$ where $N_{\text{RB}}^{\text{DL}}$ is the number of resource blocks over the entire system bandwidth. The CQI reports can be wideband, eNB-configured sub-band, or UE-selected sub-band. In the case of multiple transmit antennas at the eNB, the CQI values may be reported for both codewords.

The eNB scheduler needs to know the number of resource blocks and MCS corresponding to each CQI value in order to properly allocate the resources for each UE. With the modulation scheme obtained from Table 9.33, one would derive a certain range of MCS that can be used for each CQI index. However, in order to obtain a specific MCS and the number of resource blocks, the code rate, given in Table 9.33, is required. Nevertheless, there is not a single formula that would give you a unique value for MCS and the number of resource blocks. Therefore, there is a set of MCS and number of resource blocks that meet the modulation scheme and code rate requirement in Table 9.33. An example is provided in Table 9.34, where the CIF is assumed to be two OFDM symbols for the

Petitioners' Exhibit 1021
Nokia of America Corp., et al. v. KT Corporation, et al.
Case No. IPR2025-00036; U.S. Patent No. 11,627,631
Page 718 of 1122

Table 9.33 CQI Values and the Corresponding Code Rates [5]

CQI Index	Modulation Scheme	Coding Rate × 1024	Information Bits per Symbol
0		Out of Range	
1	QPSK	78	0.1523
2	QPSK	120	0.2344
3	QPSK	193	0.3770
4	QPSK	308	0.6016
5	QPSK	449	0.8770
6	QPSK	602	1.1758
7	16QAM	378	1.4766
8	16QAM	490	1.9141
9	16QAM	616	2.4063
10	64QAM	466	2.7305
11	64QAM	567	3.3223
12	64QAM	666	3.9023
13	64QAM	772	4.5234
14	64QAM	873	5.1152
15	64QAM	948	5.5547

Table 9.34 Example Mapping of CQI Values to Number of Resource Blocks [158]

CQI Index	Modulation Scheme	Bits/ Symbol	REs/ PRB	N_{RB}	I_{MCS}	Transport Block Size	Code Rate
0			Out of Range				
1	QPSK	2	138	20	0	536	0.101449
2	QPSK	2	138	20	0	536	0.101449
3	QPSK	2	138	20	2	872	0.162319
4	QPSK	2	138	20	5	1736	0.318841
5	QPSK	2	138	20	7	2417	0.442210
6	QPSK	2	138	20	9	3112	0.568116
7	16QAM	4	138	20	12	4008	0.365217
8	16QAM	4	138	20	14	5160	0.469565
9	16QAM	4	138	20	16	6200	0.563768
10	64QAM	6	138	20	20	7992	0.484058
11	64QAM	6	138	20	23	9912	0.600000
12	64QAM	6	138	20	25	11448	0.692754
13	64QAM	6	138	20	27	12576	0.760870
14	64QAM	6	138	20	28	14688	0.888406
15	64QAM	6	138	20	28	14688	0.888406

Petitioners' Exhibit 1021
Nokia of America Corp., et al. v. KT Corporation, et al.
Case No. IPR2025-00036; U.S. Patent No. 11,627,631
Page 719 of 1122

control region, i.e., 138 resource elements per resource block pair in each subframe, and further it is assumed that there are 20 resource blocks assigned to the UE. The transport block size (excluding the 24-bit CRC) is then determined for various values of the CQI and modulation schemes.

As we mentioned earlier, power control dynamically adjusts the transmit power to compensate for variations in the instantaneous channel condition. The objective of these adjustments is to maintain an approximately constant E_b/N_0 at the receiver in order to successfully transmit data with an acceptable block error rate. In principle, TPC increases the power at the transmitter when the radio link experiences poor radio conditions, and vice versa. Therefore, the transmit power is in essence inversely proportional to the channel quality. This results in an approximately constant data rate, regardless of the channel variations. For services such as circuit-switched voice, this is a desirable property. Transmit-power control can be seen as one type of link adaptation, i.e., the adjustment of transmission parameters, in this case the transmit power, is adapted to differences and variations in the instantaneous channel conditions to maintain the received E_b/N_0 at a desired level. However, in mobile communication scenarios and in particular packet-data transmission, there is no desire to provide a constant data rate over a radio link at all times. In such cases, an alternative to transmit-power control is link adaptation by means of dynamic rate control. Rate control does not aim at keeping the instantaneous radio-link data rate constant, regardless of the instantaneous channel conditions. Instead, with rate control, the data rate is dynamically adjusted to compensate for the varying channel conditions, i.e., the data rate is increased when good channel conditions prevail, and vice versa. Thus, rate control maintains $E_b/N_0 \sim (P_{TX}, R)$ at the desired level, not by adjusting the transmission power P_{TX}, but rather by adjusting the data rate R. It can be shown that rate control is more efficient than power control. Rate control in principle implies that the power amplifier is always transmitting at full power and therefore is efficiently utilized. On the other hand, power control results in inefficient utilization of the power amplifier, as the transmission power is typically less than its maximum value. In practice, the link-level data rate is controlled by adjusting the modulation scheme and/or the channel coding rate. In the case of good channel conditions, the energy per bit E_b at the receiver is high and the main limitation of the data rate is going to be the bandwidth of the radio link [15].

The list of modulation schemes and code rates which can be signaled by means of a CQI value is given in Table 9.33. The AMC can exploit the UE feedback by assuming that the channel fading is sufficiently slow. This requires the channel coherence time to be greater than the CQI measurement delay (i.e., the time interval between the UE's measurement of the downlink reference signals and the subframe containing the correspondingly adapted downlink transmission on PDSCH), which is typically 7−8 ms (depending on the UE speed and the operating frequency). However, a trade-off needs to be made between the amount of CQI information reported by the UEs and the accuracy with which the link adaptation can track the prevailing channel conditions. More frequent reporting of the

Petitioners' Exhibit 1021
Nokia of America Corp., et al. v. KT Corporation, et al.
Case No. IPR2025-00036; U.S. Patent No. 11,627,631
Page 720 of 1122

CQI in the time-domain allows better tracking of the channel and interference variations, while finer resolution in the frequency-domain enables better use of frequency selective scheduling gain. However, both lead to increased feedback overhead in the uplink. Therefore, the eNB can configure both the time-domain update rate and the frequency-domain resolution of the CQI to optimize the overall performance of the system.

References

3GPP Specifications[35]

[1] 3GPP TS 36.101, Evolved Universal Terrestrial Radio Access (E-UTRA); User Equipment (UE) radio transmission and reception (Release 11), December 2012.

[2] 3GPP TS 36.104, Evolved Universal Terrestrial Radio Access (E-UTRA); Base Station (BS) radio transmission and reception (Release 11), December 2012.

[3] 3GPP TS 36.211, Evolved Universal Terrestrial Radio Access (E-UTRA), Physical Channels and Modulation (Release 11), December 2012.

[4] 3GPP TS 36.212, Evolved Universal Terrestrial Radio Access (E-UTRA) Multiplexing and Channel Coding (Release 11), December 2012.

[5] 3GPP TS 36.213, Evolved Universal Terrestrial Radio Access (E-UTRA); Physical layer procedures (Release 11), December 2012.

[6] 3GPP TS 36.214, Evolved Universal Terrestrial Radio Access (E-UTRA); Physical layer – Measurements (Release 11), December 2012.

[7] 3GPP TS 36.300, Evolved Universal Terrestrial Radio Access (E-UTRA) and Evolved Universal Terrestrial Radio Access Network (E-UTRAN) Overall description, Stage 2 (Release 11), December 2012.

[8] 3GPP TS 36.321, Evolved Universal Terrestrial Radio Access (E-UTRA); Medium Access Control (MAC) Protocol specification (Release 11), December 2012.

[9] 3GPP TS 36.331 Evolved Universal Terrestrial Radio Access (E-UTRA); Radio Resource Control (RRC); Protocol specification (Release 11), December 2012.

[10] 3GPP TR 36.912 Feasibility Study for Further Advancements for E-UTRA (LTE-Advanced) (Release 11), September 2012.

[11] 3GPP TR 36.814 Feasibility Study for Further Advancements for E-UTRA (LTE-Advanced) (Release 9), March 2010.

[12] 3GPP TR 36.819 Coordinated Multi-Point Operation for LTE Physical Layer Aspects (Release 11), December 2011.

Books

[13] C. Johnson, Long Term Evolution in Bullets, second ed., Create Space Independent Publishing Platform, 2012.

[14] S. Sesia, I. Toufik, M. Baker, LTE, the UMTS Long Term Evolution: From Theory to Practice, second ed., John Wiley & Sons, 2011.

[35] 3GPP Specifications can be found at the following URL: http://www.3gpp.org/ftp/Specs/archive/36_series/

Petitioners' Exhibit 1021
Nokia of America Corp., et al. v. KT Corporation, et al.
Case No. IPR2025-00036; U.S. Patent No. 11,627,631
Page 721 of 1122

[15] E. Dahlman, S. Parkvall, J. Skold, 4G: LTE/LTE-Advanced for Mobile Broadband, Academic Press, 2011.
[16] H. Holma, A. Toskala, LTE Advanced: 3GPP Solution for IMT-Advanced, John Wiley & Sons, 2012.
[17] H. Holma, A. Toskala, LTE for UMTS: Evolution to LTE-Advanced, John Wiley & Sons, 2011.
[18] S. Ahmadi, Mobile WiMAX: A Systems Approach to Understanding IEEE 802.16m Radio Access Technology, Academic Press, 2010.
[19] B. Sklar, Digital Communications: Fundamentals and Applications, second ed., Prentice Hall, 2001.
[20] A. Paulraj, et al., Introduction to Space−Time Wireless Communications, Cambridge University Press, 2008.
[21] W.C. Jakes, Microwave Mobile Communications, second ed., Wiley-IEEE Press, 1994.
[22] G. Savo, Glisic, Advanced Wireless Communications: 4G Cognitive and Cooperative Broadband Technology, second ed., Wiley Inter-science, 2007.
[23] D.E. Dudgeon, R.M. Mersereau, Multidimensional Digital Signal Processing, Prentice Hall, 1984.
[24] D. Tse, P. Viswanath, Fundamentals of Wireless Communication, Cambridge University Press, 2005.
[25] E. Biglieri, et al., MIMO Wireless Communications, Cambridge University Press, 2010.
[26] A. Goldsmith, Wireless Communications, Cambridge University Press, 2005.
[27] S. Lin, D.J. Costello, Error Control Coding, second ed., Prentice Hall, 2004.
[28] S.L. Marple, Digital Spectral Analysis with Applications, Prentice Hall, 1987.
[29] G.H. Golub, C.F. Van Loan, Matrix Computations, third ed., Johns Hopkins University Press, 1996.
[30] A. Papoulis, Probability, Random Variables and Stochastic Processes, fourth ed., McGraw Hill Higher Education, 2002.
[31] L. Rade, Mathematics Handbook for Science and Engineering, Springer, 2010.
[32] G.A. Korn, T.M. Korn, Mathematical Handbook for Scientists and Engineers: Definitions, Theorems, and Formulas for Reference and Review, Revised Edition, Dover Publications, 2000.
[33] C.E. Shannon, W. Weaver, The Mathematical Theory of Communication, University of Illinois Press, 1998.
[34] F. Dowla, Handbook of RF and Wireless Technologies, Newnes, 2003.
[35] G. Arfken, *Bessel functions*, Mathematical Methods for Physicists, third ed., Academic Press, 1985.
[36] W.G. Bickley, Bessel Functions and Formulae, Cambridge University Press, Cambridge, England, 1957.
[37] F. Bowman, Introduction to Bessel Functions, Dover, 2010.
[38] H.G. Myung, D. Goodman, Single Carrier FDMA: A New Air Interface for Long Term Evolution, Wiley & Sons, 2008.
[39] T.M. Cover, J.A. Thomas, Elements of Information Theory, John Wiley & Sons, 1991.
[40] J.G. Proakis, Digital Communications, fifth ed., McGraw-Hill, November 2007.
[41] N. Costa, S. Haykin, Multiple-Input Multiple-Output Channel Models: Theory and Practice, John Wiley & Sons, 2010.
[42] C. Oestges, B. Clerckx, MIMO Wireless Communications: From Real-World Propagation to Space−Time Code Design, Academic Press, 2007.

Petitioners' Exhibit 1021
Nokia of America Corp., et al. v. KT Corporation, et al.
Case No. IPR2025-00036; U.S. Patent No. 11,627,631
Page 722 of 1122

[43] A. Sibille, C. Oestges, A. Zanella, MIMO: From Theory to Implementation, Academic Press, 2010.
[44] I. Stakgold, M.J. Holst, Green's Functions and Boundary Value Problems, third ed., John Wiley & Sons, 2011.
[45] R.G. Gallager, Principles of Digital Communication, Cambridge University Press, 2008.

Articles

[46] G. Bauch, G. Dietl, MIMO for 3GPP LTE-Advanced and Beyond, Global Telecommunications Conference (GLOBECOM), 2010.
[47] C. Mehlfuhrer, et al., The vienna LTE simulators—enabling reproducibility in wireless communication research, EURASIP J. Adv. Signal Process. 2011 (1) (2011).
[48] B. Sklar, Rayleigh fading channels in mobile digital communication systems. I. Characterization, IEEE Commun. Mag. 35 (7) (1997).
[49] B. Sklar, Rayleigh fading channels in mobile digital communication systems. II. Mitigation, IEEE Commun. Mag. 35 (7) (July 1997).
[50] Y. Okumura, E. Ohmori, K. Fukuda, Field strength and its variability in VHF and UHF land mobile radio service, Rev. Electr. Commun. Lab. 16 (1968).
[51] M. Hata, Empirical formulae for propagation loss in land mobile radio services, IEEE Trans. Veh. Technol. VT-29 (3) (1980).
[52] Y. Wu, W.Y. Zou, Orthogonal frequency division multiplexing: a multi-carrier modulation scheme, IEEE Trans. Consum. Electron. 41 (3) (1995).
[53] H. Su, et. al., Analysis of tone reservation method for WiMAX system, International Symposium on Communications and Information Technologies, ISCIT'06, 2006.
[54] A. Osseiran, J.C. Guey, Hopping pilot pattern for interference mitigation in OFDM, IEEE 19th International Symposium on Personal, Indoor and Mobile Radio Communications, 2008.
[55] R. Nilsson, O. Edforst, M. Sandellt, P. Ola Borjesson, An analysis of two-dimensional pilot-symbol assisted modulation for OFDM, 1997 IEEE International Conference on Personal Wireless Communications Publication, 1997.
[56] H. Sampath, P. Stoica, A. Paulraj, Generalized linear precoder and decoder design for MIMO channels using the weighted MMSE criterion, IEEE Trans. Commun. 49 (12) (2001).
[57] Y.S. Choi, P.J. Voltz, F.A. Cassara, On channel estimation and detection for multicarrier signals in fast and selective rayleigh fading channels, IEEE Trans. Commun. 49 (8) (2001).
[58] S.M. Alamouti, A simple transmit diversity technique for wireless communications, IEEE J. Sel. Areas Commun. 16 (8) (1998).
[59] A. Nosratinia, T.E. Hunter, A. Hedayat, Cooperative communication in wireless networks, IEEE Commun. Mag. (2004).
[60] J.G. Andrews, Interference cancellation for cellular systems: a contemporary overview, IEEE Wirel. Commun. (2005).
[61] D. Gesbert, et al., From theory to practice: an overview of MIMO space−time coded wireless systems, IEEE J. Sel. Areas Commun. 21 (3) (2003).
[62] R.D. Murch, K. Ben Letaief, Antenna systems for broadband wireless access, IEEE Commun. Mag. (2002).
[63] S. Catreux, et al., Adaptive modulation and MIMO coding for broadband wireless data networks, IEEE Commun. Mag. (2002).

Petitioners' Exhibit 1021
Nokia of America Corp., et al. v. KT Corporation, et al.
Case No. IPR2025-00036; U.S. Patent No. 11,627,631
Page 723 of 1122

[64] A.J. Paulraj, D.A. Gore, R.U. Nabar, H. Bölcskei, An *overview of MIMO communications—a key to gigabit wireless*, Proc. IEEE 92 (2) (2004).
[65] M.G. Parker, K.G. Patersonyand, C. Tellambura, Golay complementary sequences, in: J.G. Proakis (Ed.), Wiley Encyclopedia of Telecommunications, John Wiley & Sons, 2003.
[66] D.J. Love, R.W. Heath Jr., Grassmannian beamforming for multiple-input multiple-output wireless systems, IEEE Trans. Inf. Theory 49 (10) (2003).
[67] V. Tarokh, H. Jafarkhani, On the computation and reduction of the peak-to-average power ratio in multicarrier communications, IEEE Trans. Commun. 48 (1) (2000).
[68] T.M. Schmid, D.C. Cox, Robust frequency and timing synchronization for OFDM, IEEE Trans. Commun. 45 (12) (1997).
[69] M. Pukkila, Channel Estimation Modeling, Postgraduate Course in Radio-communications, Fall 2000.
[70] M.S. Akram, Pilot-based channel estimation in OFDM systems, Master Thesis, 2007.
[71] Freescale Semiconductor Application Note, Channel Estimation in OFDM Systems, AN3059 Rev. 0, 2006.
[72] V. Srivastava, et al., Robust MMSE channel estimation in OFDM systems with practical timing synchronization, IEEE Wireless Communications and Networking Conference 2004.
[73] L. Zheng, D.N.C. Tse, Diversity and multiplexing: a fundamental tradeoff in multiple-antenna channels, IEEE Trans. Inf. Theory 49 (5) (2003).
[74] H. Weingarten, Y. Steinberg, S. Shamai, The capacity region of the gaussian multiple-input multiple-output broadcast channel, IEEE Trans. Inf. Theory 52 (9) (2006).
[75] F. Kaltenberger, et al., Capacity of linear multi-user MIMO precoding schemes with measured channel data, EURECOM, Sophia-Antipolis, France.
[76] V. Stankovic, M. Haardt, Multi-user MIMO downlink precoding for users with multiple antennas, in: Proceedings of the 12th Meeting of the Wireless World Research Forum (WWRF), Toronto, Canada, 2004.
[77] Q.H. Spencer, A.L. Swindlehurst, M. Haardt, Zero-Forcing methods for downlink spatial multiplexing in multiuser MIMO channels, IEEE Trans. Signal Process. 52 (2) (2004).
[78] N. Jindal, MIMO broadcast channels with finite-rate feedback, IEEE Trans. Inf. Theory 52 (11) (2006).
[79] Q.H. Spencer, C.B. Peel, A. Lee Swindlehurst, M. Haardt, An introduction to the multi-user MIMO downlink, IEEE Commun. Mag. (2004).
[80] D. Gesbert, et al., Shifting the MIMO paradigm, IEEE Signal Process. Mag. (2007).
[81] L. Wei, Capacity of Hybrid Open-Loop and Closed-Loop MIMO with Channel Uncertainty at Transmitter, Helsinki University of Technology, Espoo, 2008.
[82] D.J. Love, R.W. Heath Jr., Grassmannian precoding for spatial multiplexing systems, in: Proceedings of the Allerton Conference on Communication Control and Computing, Monticello, 2003.
[83] T. Abe, G. Bauch, Differential codebook MIMO precoding technique, 2007 IEEE Global Telecommunications Conference, 2007.
[84] B. Bandemer, M. Haardt, S. Visuri, Linear MMSE multi-user MIMO downlink precoding for users with multiple antennas, 17th Annual IEEE International Symposium on Personal, Indoor and Mobile Radio Communications (PIMRC), 2006.

Petitioners' Exhibit 1021
Nokia of America Corp., et al. v. KT Corporation, et al.
Case No. IPR2025-00036; U.S. Patent No. 11,627,631
Page 724 of 1122

[85] G. Mitchell, F.R. Kschischang, An augmented orthogonal code design for the non-coherent MIMO channel, 2008 24th Biennial Symposium on Communications, 2008.
[86] Y. Fan, P. Lundén, M. Kuusela, M. Valkama, Efficient semi-persistent scheduling for VoIP on EUTRA downlink, IEEE 68th Vehicular Technology Conference (VTC), Fall 2008.
[87] Goldsmith, et al., Capacity limits of MIMO channels, IEEE J. Sel. Areas Commun. 21 (2003).
[88] H. Weingarten, Y. Steinberg, S. Shamai, The capacity region of the gaussian MIMO broadcast channel, in: Proceedings of the Conference Information Sciences and Systems (CISS), Princeton, NJ, 2004.
[89] M. Costa, Writing on dirty paper, IEEE Trans. Inf. Theory 29 (1983).
[90] T. Svantesson, A.L. Swindlehurst, A performance bound for prediction of a multi-path MIMO channel, in: Proceedings of the 37th Asilomar Conference on Signals, Systems, and Computers, Session: Array Processing for Wireless Communications, Pacific Grove, CA, 2003.
[91] C.B. Peel, B.M. Hochwald, A.L. Swindlehurst, A vector-perturbation technique for near-capacity multi-antenna multi-user communication, IEEE Trans. Commun. (2003).
[92] M. Bengtsson, B. Ottersten, Optimal and suboptimal beamforming, in: L.C. Godara (Ed.), Handbook of Antennas in Wireless Communications, CRC Press, 2001.
[93] M. Schubert, H. Boche, Solution of the multiuser downlink beamforming problem with individual SINR constraints, IEEE Trans. Veh. Technol. 53 (2004).
[94] Q.H. Spencer, A.L. Swindlehurst, M. Haardt, Zero-forcing methods for downlink spatial multiplexing in multi-user MIMO channels, IEEE Trans. Signal Process. 52 (2004).
[95] G. Caire, S. Shamai, On the achievable throughput of a multi-antenna gaussian broadcast channel, IEEE Trans. Inf. Theory 49 (2003).
[96] U. Erez, S. Shamai, R. Zamir, Capacity and lattice strategies for cancelling known interference, in: Proceedings International Symposium Information Theory and its Applications, 2000.
[97] C. Windpassinger, R.F.H. Fischer, J.B. Huber, Lattice-reduction-aided broadcast precoding, in: Proceedings of Fifth ITG Conference Source and Channel Coding, 2004.
[98] Berrou, Glavieux, Thitimajshima, Near shannon limit error-correcting coding and decoding: turbo-codes, in: Proceedings of 1993 International Communication Conference, 1993.
[99] Q.H. Spencer, A.L. Swindlehurst, Channel allocation in multi-user MIMO wireless communications systems, in: Proceedings of 2004 International Communication Conference, 2004.
[100] Perez, Seghers, Costello, A distance spectrum interpretation of turbo codes, IEEE Trans. Inf. Theory 42 (6) (1996).
[101] J. Rothweller, Turbo codes, IEEE Potentials 18 (1) (1999).
[102] C. Berrou, A. Glavieux, P. Thitimajshima, Near Shannon limit error-correcting coding and decoding: turbo codes, in: Proceedings of 1993 International Communication Conference, 1993.
[103] C. Berrou, A. Glavieux, Near optimum error correcting coding and decoding: turbo-codes, IEEE Trans. Commun. 44 (10) (1996).

Petitioners' Exhibit 1021
Nokia of America Corp., et al. v. KT Corporation, et al.
Case No. IPR2025-00036; U.S. Patent No. 11,627,631
Page 725 of 1122

[104] C. Heegard, Stephen B. Wicker, Turbo Coding, Springer, 2010.
[105] C. Berrou, R. Pyndiah, P. Adde, C. Douillard, R. Le Bidan, An overview of turbo codes and their applications, The European Conference on Digital Wireless Technology, 2005.
[106] H. Ma, J. Wolf, On tail biting convolutional codes, IEEE Trans. Commun. COM-34 (2) (1986).
[107] C. Weiss, C. Bettstetter, S. Riedel, Code construction and decoding of parallel concatenated tail-biting codes, IEEE Trans. Inf. Theory 47 (1) (2001).
[108] Y.E. Wang, R. Ramesh, To bite or not to bite—a study of tail bits versus tail-biting, Seventh IEEE International Symposium Personal, Indoor and Mobile Radio Communications, PIMRC'96, vol. 2, 1996.
[109] B.E. Priyanto, H. Codina, Initial performance evaluation of DFT-Spread OFDM Based SC-FDMA for UTRA LTE Uplink, IEEE 65th Vehicular Technology Conference (VTC), 2007.
[110] J. Lee, J.-K. Han, J. Zhang, MIMO Technologies in 3GPP LTE and LTE-Advanced, EURASIP J. Wireless Commun. Networking (2009).
[111] S. Catreux, P.F. Driessen, L.J Greenstein, Attainable throughput of an interference-limited multiple-input multiple-output (MIMO) cellular system, IEEE Trans. Commun. 49 (8) (2001).
[112] I. Telatar, Capacity of multi-antenna Gaussian channels, AT&T Technical Memorandum, 1995.
[113] G.J. Foschini, M.J. Gans, On limits of wireless communications in a fading environment when using multiple antennas, Wireless Pers. Commun 1998.
[114] M.-S. Alouini, A. Goldsmith, Capacity of Nakagami multipath fading channels, Proceedings Vehicular Technology Conference, 1997.
[115] D. Chizhik, G.J. Foschini, R.A. Valenzuela, Capacities of multi-element transmit and receive antennas: correlations and keyholes, Electron. Lett. 36 (2000).
[116] D. Gesbert, H.B̈olcskei, D. Gore, A. Paulraj, MIMO wireless channels: capacity and performance prediction, Global Telecommunications Conference (GLOBECOM), 2000.
[117] D.A. Gore, R.U. Nabar, A. Paulraj, Selecting an optimal set of transmit antennas for a low rank matrix channel, Proc. ICASSP 2000 49 (8) (2000).
[118] S. Sandhu, R.U. Nabar, D.A. Gore, A. Paulraj, Near-optimal selection of transmit antennas for a MIMO channel based on Shannon capacity, in: Proceedings of the 34th Asilomar Conference on Signals, Systems and Computers, 2000.
[119] A.F. Molisch, M.Z. Win, J.H. Winters, A. Paulraj, Capacity of MIMO systems with antenna selection, in: Proceedings of the IEEE International Conference on Communications (ICC), 2001.
[120] Z. Shen, et al., Overview of 3GPP LTE-advanced carrier aggregation for 4G wireless communications, IEEE Commun. Mag. 50 (2) (2012).
[121] Y.-H. Nam, et al., Evolution of reference signals for LTE-advanced systems, IEEE Commun. Mag. 50 (2) (2012).
[122] L. Liu, et al., Downlink MIMO in LTE-advanced: SU-MIMO vs. MU-MIMO, IEEE Commun. Mag. 50 (2) (2012).
[123] D. Lee, et al., Coordinated multipoint transmission and reception in LTE-advanced: deployment scenarios and operational challenges, IEEE Commun. Mag. 50 (2) (2012).
[124] D. Bai, et al., LTE-Advanced modem design: challenges and perspectives, IEEE Commun. Mag. 50 (2) (2012).

Petitioners' Exhibit 1021
Nokia of America Corp., et al. v. KT Corporation, et al.
Case No. IPR2025-00036; U.S. Patent No. 11,627,631
Page 726 of 1122

[125] J. Lee, Y. Kim, et al., Coordinated multipoint transmission and reception in LTE-Advanced systems, IEEE Commun. Mag. 50 (2) (2012).
[126] Z. Shen, et al., Dynamic uplink-downlink configuration and interference management in TD-LTE, IEEE Commun. Mag. 50 (2) (2012).
[127] C.S. Park, et al., Evolution of uplink MIMO for LTE-advanced, IEEE Commun. Mag. 49 (2) (2011).
[128] R. Irmer, et al., Coordinated multipoint: concepts, performance, and field trial results, IEEE Commun. Mag. 49 (2) (2011).
[129] M. Vu, A. Paulraj, MIMO Wireless Linear Precoding, IEEE Signal Process. Mag. 24 (5) (2007).
[130] R. Gold, Optimal binary sequences for spread spectrum multiplexing, IEEE Trans. Inf. Theory 13 (4) (1967).
[131] X. Cai, G.B. Giannakis, Bounding performance and suppressing inter-carrier interference in wireless mobile OFDM, IEEE Trans. Commun. 51 (12) (2003).
[132] J. Lee, H.-L. Lou, D. Toumpakaris, J.M. Cioffi, Effect of carrier frequency offset on OFDM systems for multipath fading channels, Global Telecommunications Conference (GLOBECOM), 2004.

Miscellaneous

[133] 3G Americas, MIMO and smart antennas for 3G and 4G wireless systems. <http://www.3gamericas.org>, 2010.
[134] Rohde, Schwarz Application Notes, LTE-Advanced technology introduction, 2010.
[135] 3G Americas, 3GPP mobile broadband innovation path to 4G: Release 9, Release 10 and beyond: HSPA + , SAE/LTE and LTE-Advanced, 2010.
[136] 3G Americas, HSPA to LTE-Advanced: 3GPP broadband evolution to IMT-Advanced (4G), 2009.
[137] 3G Americas, The mobile broadband evolution: 3GPP release 8 and beyond HSPA + , SAE/LTE and LTE-Advanced, 2009.
[138] IEEE 802.16m-07/244r1, Y. Song, L. Cai, K. Wu, H. Yang, Collaborative MIMO, 2007.
[139] Agilent Technologies, 3GPP long term evolution: system overview, product development, and test challenges. <http://www.agilent.com>, 2009.
[140] IEEE C802.16m-08/153, B.-C. Ihm, J. Choi, W. Lee, Pilot related to DL-MIMO, 2008.
[141] MATLAB CENTRAL, An open exchange for the MATLAB and SIMULINK user community. <http://www.mathworks.com/matlabcentral>.
[142] Vienna University of Technology, Institute of Telecommunications, LTE link-level and system-level simulators. <http://www.nt.tuwien.ac.at/about-us/staff/josep-colom-ikuno/lte-simulators>, 2012.
[143] 3GPP R1-060385 Motorola, Cubic metric in 3GPP-LTE, 2006.
[144] The Coded Modulation Library (The Iterative Solutions Coded Modulation Library (ISCML) is an open source toolbox for simulating capacity approaching codes in Matlab). <http://www.iterativesolutions.com>.
[145] 4G Americas, 4G mobile broadband evolution: release 10, release 11 and beyond—HSPA, SAE/LTE and LTE-Advanced, 2012.
[146] 4G Americas, MIMO and smart antennas for mobile broadband networks, 2012.
[147] 4G Americas, Developing and integrating a high performance HET-NET, 2012.

Petitioners' Exhibit 1021
Nokia of America Corp., et al. v. KT Corporation, et al.
Case No. IPR2025-00036; U.S. Patent No. 11,627,631
Page 727 of 1122

[148] 4G Americas, 4G mobile broadband evolution: 3GPP release 10 and beyond—HSPA + , SAE/LTE and LTE-Advanced, 2011.
[149] 3GPP R1-113297, NTT DOCOMO, Enhanced PDCCH for DL MIMO in Rel-11, 2011.
[150] 3GPP R1-112928, Ericsson, ST-Ericsson, On enhanced PDCCH design, 2011.
[151] 3GPP R1-113175, Renesas Mobile, Link-level evaluation of E-PDCCH design aspects, 2011.
[152] 3GPP R1-113194, LG Electronics, Consideration on transmit diversity scheme for enhanced PDCCH transmission, 2011.
[153] 3GPP R1-113202, Intel Corporation, Performance analysis of enhanced downlink control signaling, 2011.
[154] 3GPP R1-113238, Research in Motion, E-PDCCH transmission with transmit diversity, 2011.
[155] 3GPP R1-114302, NTT DOCOMO, DM-RS design for E-PDCCH in Rel-11, 2011.
[156] Anritsu, Future technologies and testing for fixed mobile convergence, SAE and LTE in cellular mobile communications. <http://www.anritsu.com/search/en-US/downloadssearch.aspx>, 2008.
[157] Wireless World Initiative New Radio—WINNER + , Enabling Techniques for LTE-A and beyond, Deliverable D2.2. <http://projects.celtic-initiative.org/winner + /deliverables_winnerplus.html>, 2010.
[158] LTE System Description. <http://www.sharetechnote.com>.
[159] DSPLOG Signal Processing for Communication <http://www.dsplog.com>.
[160] 4G Evolution Lab—LTE and LTE-Advanced Toolbox and Block-set: a simulation library for the 3GPP LTE and LTE Advanced specification for the Mathworks MATLAB and Simulink. <http://www.steepestascent.com>.
[161] R. Duncan, Supporting Operators with LTE Roaming, CDG International Roaming Team, August 2012.
[162] Samsung Electronics, LTE PHY specification. <http://www.slideshare.net/alla-bout4g/lte-rel-8-physical-layer>, 2008.
[163] Motorola White Paper, TD-LTE, Exciting alternative global Momentum. <www.motorola.com>, 2010.
[164] B. Schulz, LTE Transmission modes and beamforming, Rohde & Schwarz White Paper, 2011.
[165] E. Seidel, LTE-A Carrier Aggregation Enhancements in Release 11, NOMOR Research GmbH, Munich, Germany, 2012.
[166] B. Holter, On the Capacity of the MIMO Channel- A Tutorial Introduction, Norwegian University of Science and Technology, 2001.
[167] S. Giraud, et al., Bulk acoustic wave filters synthesis and optimization for multi-standard communication terminals, IEEE Trans Ultrason Ferroelectr Freq Control 57 (1) (2010).
[168] L.A. Coldren, R. Rosenberg, Surface-acoustic-wave resonator filters, Proc. IEEE 67 (1) (1979).
[169] Return loss, from Wikipedia, < http://en.wikipedia.org/wiki/Return_loss > .
[170] Masaaki Koiwa, et al., Multiband Mobile Terminals, NTT DoCoMo Tech. J. 8 (2) (2006).
[171] Siemens White Paper, TD-SCDMA: the Solution for TDD bands, March 2004 < http://www.tdscdma-forum.org/ > .

Petitioners' Exhibit 1021
Nokia of America Corp., et al. v. KT Corporation, et al.
Case No. IPR2025-00036; U.S. Patent No. 11,627,631
Page 728 of 1122

[172] D.C. Chu, Polyphase Codes With Good Periodic Correlation Properties, IEEE Trans Inf Theory (1972).
[173] Maximum length sequence, from Wikipedia, <http://en.wikipedia.org/wiki/Maximum_length_sequence>.
[174] Jung-In Kim, et al., SSS Detection Method for Initial Cell Searchin 3GPP LTE FDD/TDD Dual Mode Receiver, Nineth International Symposium on Communication and Information Technologies, 2009.
[175] J. van de Beek, et al., Low-complex frame synchronization in OFDM systems, Fourth IEEE International Conference on Universal Personal Communications. 1995.
[176] ARTIST 4G Project, D2.2 Advanced receiver signal processing techniques – evaluation and characterization, 2011.
[177] Hidekazu Taoka, et al., MIMO and CoMP in LTE-Advanced, DoCoMo Techn. J. 12 (2) (2010).
[178] Sigen Ye, et al., Enhanced Physical Downlink Control Channel in LTE Advanced Release 11, IEEE Communications Magazine, 2013.
[180] Yusuke Ohwatari, et al., Performance of Advanced Receiver Employing Interference Rejection Combining to Suppress Inter-cell Interference in LTE-Advanced Downlink, IEEE Vehicular Technology Conference (VTC), 2011.
[181] Ernesto Zimmermann, et al., On the Complexity of Sphere Decoding, in Proceedings International Symposium on Wireless Personal Multimedia Communication, 2004.
[182] Federico Boccardi, et al., Precoding Schemes for the MIMO-GBC, Int. Zurich Seminar on Communications (IZS), 2006.

Petitioners' Exhibit 1021
Nokia of America Corp., et al. v. KT Corporation, et al.
Case No. IPR2025-00036; U.S. Patent No. 11,627,631
Page 729 of 1122

CHAPTER

Uplink Physical Layer Functions

10

CHAPTER CONTENTS

10.1 Overview of uplink physical layer processing 724
10.2 Principles of SC-FDMA 724
10.3 SC-FDMA and clustered SC-FDMA 734
10.4 Uplink frame structure 736
10.5 Physical resource structure and channel mapping 738
10.5.1 Physical resource blocks 742
10.5.2 Uplink resource allocation 743
10.5.2.1 Uplink resource allocation type 0 747
10.5.2.2 Uplink resource allocation type 1 748
10.6 Uplink reference signals and channel estimation 753
10.6.1 Uplink demodulation reference signals 754
10.6.2 Sounding reference signals 762
10.7 Uplink physical channel processing 769
10.7.1 Physical uplink control channel 774
10.7.2 PUCCH formats 778
10.7.2.1 PUCCH formats 1, 1a, 1b 780
10.7.2.2 PUCCH formats 2, 2a, 2b 785
10.7.2.3 PUCCH format 3 797
10.7.3 Physical uplink shared channel 802
10.7.4 Physical random-access channel 821
10.8 SC-FDMA signal generation 837
10.9 LTE/LTE-Advanced uplink multi-antenna transmission schemes 838
10.9.1 Transmit antenna selection 839
10.9.2 Virtual MU-MIMO (cooperative MIMO) 840
10.9.3 Closed-loop spatial multiplexing 841
10.9.4 Transmit diversity 844
10.9.5 Uplink MIMO receivers 846
10.9.5.1 LMMSE receiver 849
10.9.5.2 MRC receiver 849
10.9.5.3 MMSE-IRC receiver 849
10.9.5.4 SIC receiver 850
10.10 Uplink transmission modes 851

LTE-Advanced.

© 2014 Elsevier Inc. All rights reserved.

Petitioners' Exhibit 1021
Nokia of America Corp., et al. v. KT Corporation, et al.
Case No. IPR2025-00036; U.S. Patent No. 11,627,631
Page 730 of 1122

10.11 Uplink feedback in LTE/LTE-Advanced 852
10.12 Uplink transmitter and receiver chain 861
References 866

This chapter describes the physical layer protocols and functional processing in the LTE/LTE-Advanced uplink direction. As shown in Figure 10.1, the physical layer is the lowest protocol layer in baseband signal processing that interfaces with the physical media (in this case air-interface) through which the signal is transmitted and received. The physical layer receives MAC PDUs (transport blocks) and processes them through channel coding, interleaving, baseband modulation, layer mapping for multi-antenna transmission, eigen-precoding, resource element, and antenna mapping. The choice of the appropriate modulation and coding scheme and multi-antenna transmission mode are critical to achieve the

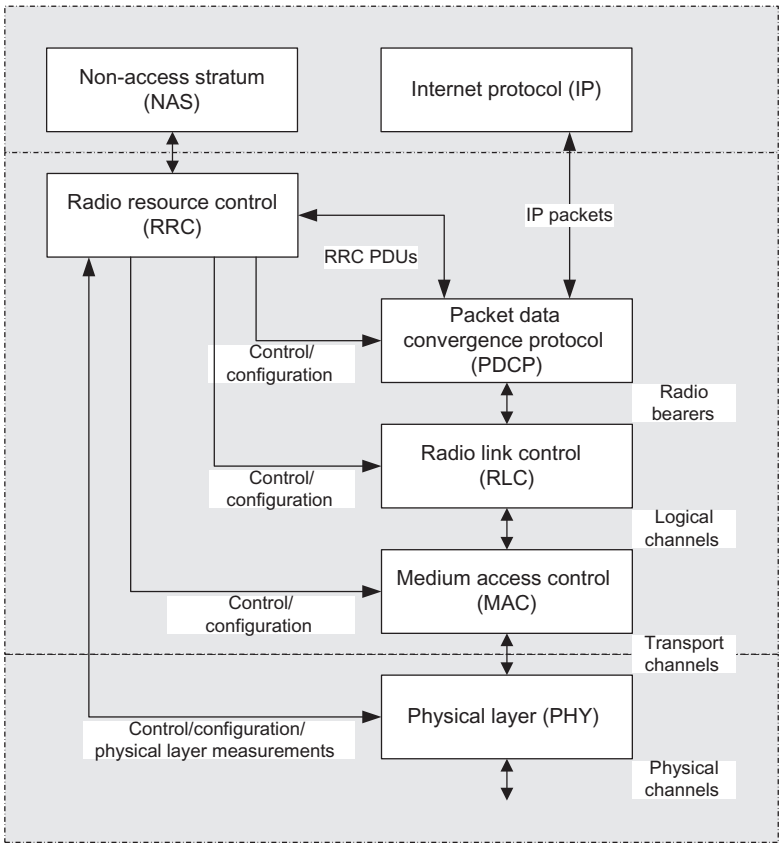


FIGURE 10.1

Overall view of LTE/LTE-Advanced physical layer.

Petitioners' Exhibit 1021
Nokia of America Corp., et al. v. KT Corporation, et al.
Case No. IPR2025-00036; U.S. Patent No. 11,627,631
Page 731 of 1122

desired reliability/robustness and system/user throughput in mobile wireless data communications. Typical mobile radio channels tend to be dispersive and time variant and exhibit severe Doppler effects, multipath delay variation, intra-cell and inter-cell interference, and fading.

A good and robust design of the physical layer ensures that the system can normally operate and overcome the above deleterious effects, and can provide the maximum throughput and lowest latency under various operating conditions. The chapters on physical layer in this book are dedicated to the systematic design of physical layer protocols and functional blocks of Rel-10/11 of LTE systems, the theoretical background on physical layer procedures, and performance evaluation of physical layer components. The theoretical background is provided to ensure that the reader understands the underlying theory governing the operation of various functional blocks and procedures. While the focus is mainly on the techniques that were incorporated in the design of the LTE/LTE-Advanced physical layer, the author has attempted to take a more generic and systematic approach to the design of physical layer for the systems beyond IMT-Advanced so that the reader can understand and apply the learnings to the design and implementation of any MIMO-OFDM-based physical layer irrespective of the radio access technology. Physical layer processes both control-plane and user-plane signals; however, due to different design requirements and reliability and performance criteria, the procedures tend to be different.

While the requirements for the design of the LTE/LTE-Advanced uplink physical layer are mainly similar to those of the downlink, there are some design attributes that are specific to the uplink physical layer including the desire for orthogonal uplink transmission by different UEs to minimize intra-cell interference and maximize the capacity, flexible data rate adaptation as a function of SINR, sufficiently low peak-to-average power ratio (PAPR) of the transmitted signal to avoid excessive cost, size, and power consumption of the UE transmit circuitry, ability to exploit the frequency diversity attainable by the wider bandwidths even when transmitting at low data rates, support for frequency-selective scheduling, and support for advanced multiple-antenna techniques in order to exploit spatial diversity and to enhance uplink capacity. The multiple-access scheme selected for the LTE uplink to satisfy the above design requirements is single-carrier frequency division multiple access (SC-FDMA). A major advantage of SC-FDMA over the direct-sequence code-division multiple access (DS-CDMA) scheme used in UMTS is that it achieves intra-cell orthogonality even in frequency-selective channels. The SC-FDMA scheme avoids strong intra-cell interference linked to DS-CDMA, which significantly reduces system capacity and limits the use of adaptive modulation. A code-division multiplexed uplink further suffers from an increased PAPR, if multi-code transmission is used from a single UE.

The use of OFDM for the LTE uplink would have been attractive given the maximal uplink/downlink functional commonality and ease of scheduling/implementation. In principle, an OFDM scheme similar to the LTE downlink could

Petitioners' Exhibit 1021
Nokia of America Corp., et al. v. KT Corporation, et al.
Case No. IPR2025-00036; U.S. Patent No. 11,627,631
Page 732 of 1122

satisfy all the uplink design criteria listed above, except the low PAPR requirement. The SC-FDMA combines the desirable characteristics of OFDM with the low PAPR of single-carrier transmission schemes. Similar to OFDM, the SC-FDMA divides the transmission bandwidth into multiple parallel sub-carriers, with the orthogonality between the sub-carriers being maintained in frequency-selective channels by the use of a cyclic prefix or guard period. The use of a cyclic prefix prevents inter-symbol interference (ISI) between SC-FDMA symbols. It transforms the linear convolution of the multipath channel into a circular convolution, enabling the receiver to equalize the channel simply by scaling each sub-carrier by a complex gain factor. However, unlike OFDM, where the data symbols directly modulate each sub-carrier independently such that the amplitude of each sub-carrier at a given time instant is set by the constellation points of the baseband modulation scheme, in SC-FDMA the signal modulated on a given sub-carrier is a linear combination of the data symbols transmitted at the same time instant. Therefore, in each symbol period, the transmitted sub-carriers of an SC-FDMA signal carry a component of each modulated data symbol. This gives SC-FDMA its crucial single-carrier property, which results in the PAPR being significantly lower than pure multi-carrier transmission schemes such as OFDM [39].

10.1 Overview of uplink physical layer processing

This section provides an overview of physical layer processing in the LTE/LTE-Advanced uplink. The processing steps and the associated control signaling are depicted in Figure 10.2. The main criteria in the design of the LTE/LTE-Advanced physical layer were to increase the application throughput and capacity, reduce access latency, support higher user mobility, minimize intra-cell and inter-cell interference, improve reliability of control and data channel coverage especially at the cell-edge, and reduce the complexity and signaling overhead. The overall performance evaluations provided in Chapter 11 suggest that the above requirements have been successfully met. In the next sections, we describe in detail the functional blocks and protocols of the uplink physical layer and their interactions based on the order the information is processed, as shown in Figure 10.2.

10.2 Principles of SC-FDMA

The LTE uplink uses SC-FDMA with a cyclic prefix in order to achieve inter-user orthogonality and to enable efficient frequency-domain equalization at the receiver. The discrete Fourier transform (DFT)-spread OFDM (DFT-S OFDM) is a form of the single-carrier transmission technique, where the signal is generated in the frequency-domain similar to OFDMA, and is illustrated in Figure 10.3.

Petitioners' Exhibit 1021
Nokia of America Corp., et al. v. KT Corporation, et al.
Case No. IPR2025-00036; U.S. Patent No. 11,627,631
Page 733 of 1122

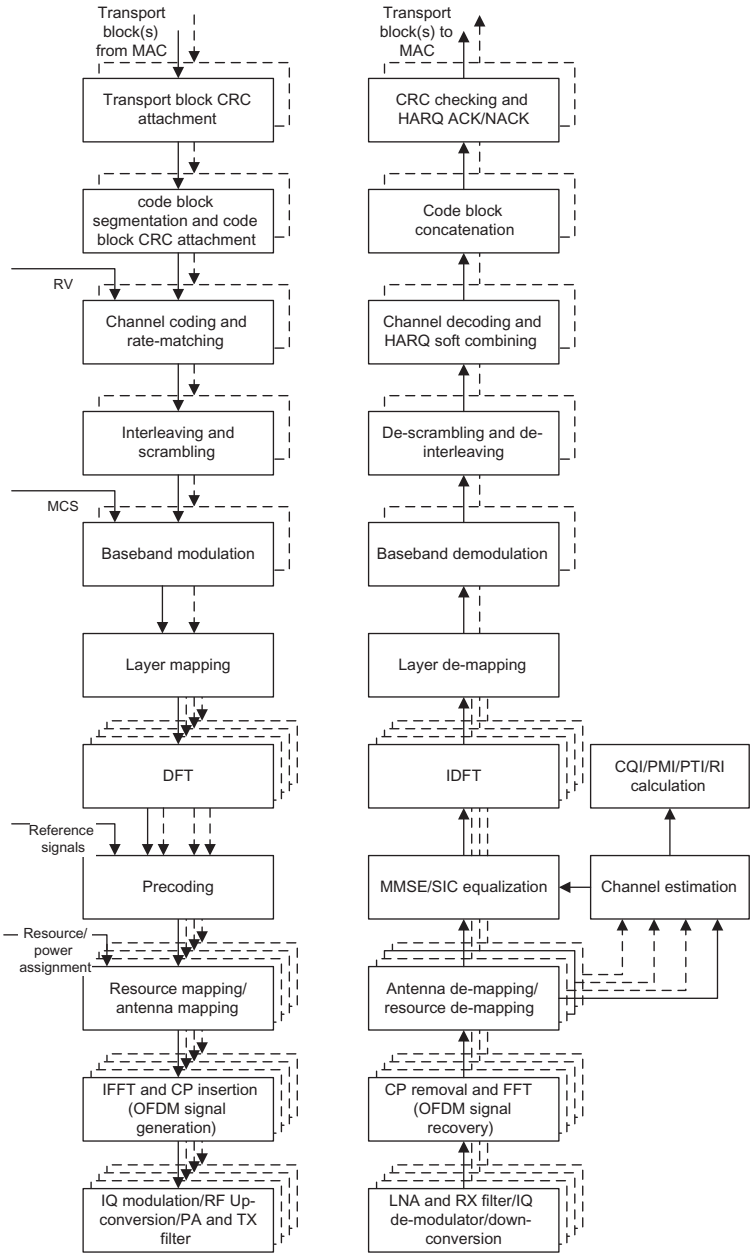


FIGURE 10.2

The LTE/LTE-Advanced uplink physical layer processing blocks [3,14,15,16].

Petitioners' Exhibit 1021
Nokia of America Corp., et al. v. KT Corporation, et al.
Case No. IPR2025-00036; U.S. Patent No. 11,627,631
Page 734 of 1122

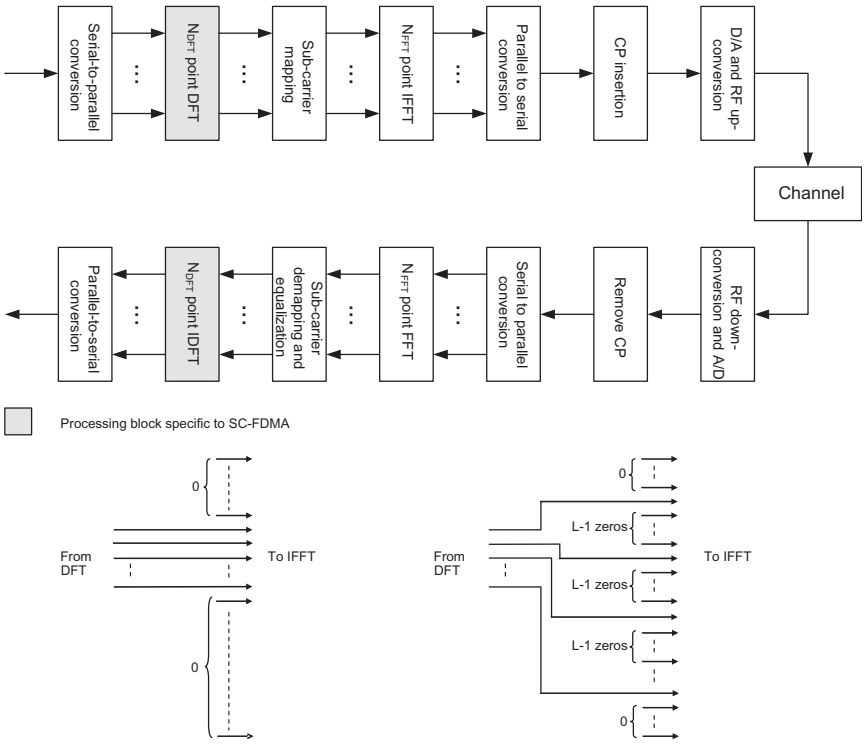


FIGURE 10.3

Transmitter/receiver structure for SC-FDMA with localized and distributed sub-carrier mapping schemes (note that $N_{DFT} < N_{FFT}$) [39].

In Figure 10.3, the common processing blocks in OFDMA and SC-FDMA are distinguished from those that are specific to SC-FDMA. This allows for a relatively high degree of commonality with the downlink OFDMA baseband processing using the same parameters, e.g., clock frequency, sub-carrier spacing, and FFT/IFFT size. The use of SC-FDMA in the uplink is mainly due to relatively inferior PAPR properties of OFDMA that result in worse uplink coverage compared to SC-FDMA. The PAPR characteristics are important for cost-effective design of a mobile station's power amplifiers (PAs).

The principles of SC-FDMA signal processing can be explained as follows. The ith transmitted symbol in an SC-FDMA system without cyclic prefix in single transmit/receive antenna case can be expressed as a vector of length N_{FFT} samples defined by $\mathbf{y} = \mathbf{F\Theta Dx}$, where $\mathbf{x} = (x_1, x_2, \ldots, x_{N_{DFT}})^T$ is an $N_{DFT} \times 1$ vector with N_{DFT} QAM-modulated symbols (the superscript "T" denotes matrix transpose operation), $\mathbf{D}$ is an $N_{DFT} \times N_{DFT}$ matrix which performs N_{DFT}-point DFT operation, $\mathbf{\Theta}$ is the $N_{FFT} \times N_{DFT}$ mapping matrix for sub-carrier assignment, and

Petitioners' Exhibit 1021
Nokia of America Corp., et al. v. KT Corporation, et al.
Case No. IPR2025-00036; U.S. Patent No. 11,627,631
Page 735 of 1122

F performs N_{FFT}-point IFFT operation. After the propagation through the multipath fading channel and addition of the additive white Gaussian noise and removing the cyclic prefix and going through the N_{FFT}-point FFT module, the received signal vector in the frequency-domain can be expressed as $\mathbf{z} = \mathbf{H\Theta Dx} + \mathbf{w}$, where **H** is the diagonal channel matrix and **w** is the receiver noise vector. Note that the maximum excess delay of the channel is assumed to be shorter than the cyclic prefix; therefore, the ISI can be mitigated by the cyclic prefix. The amplitude and phase distortion in the received signal due to the multipath channel is compensated by a frequency-domain equalizer (FDE) and the signal at the FDE output can be described as $\mathbf{v} = \mathbf{Cz}$, where $\mathbf{C} = \text{diag}(c_1, c_2, \ldots, c_{N_{\text{FFT}}})$ is the diagonal matrix of FDE coefficients. The FDE complex coefficients can be derived using minimum mean-square error (MMSE) criterion as follows:

$$c_k = \frac{H_k^*}{|H_k|^2 + \sigma_{\text{n}}^2/\sigma_{\text{s}}^2} \tag{10.1}$$

where k denotes the sub-carrier index, σ_{n}^2 denotes the variance of the additive noise, and σ_{s}^2 is the variance of the transmitted pilot symbol. Following the sub-carrier de-mapping function and IDFT de-spreading, an $N_{\text{DFT}} \times 1$ vector $\hat{\mathbf{x}}$ containing N_{DFT} QAM-modulated symbols as an estimate to the input vector **x** is obtained at the receiver. The IDFT de-spreading block in the receiver averages the noise over each sub-carrier. A particular sub-carrier may experience deep fading in a frequency-selective fading channel. The IDFT de-spreading averages and spreads the fading effect, which results in a noise enhancement to all the QAM symbols. Therefore, the IDFT de-spreading makes DFT-S OFDM more sensitive to the noise.

As shown in Figure 10.3, the modulation symbols in blocks of N_{DFT} symbols are processed through an N_{DFT}-point DFT processor, where N_{DFT} denotes the number of sub-carriers assigned to the transmission of the data/control block. The rationale for the use of DFT precoding is to reduce the cubic metric (CM) of the transmitted signal. From an implementation point of view, the DFT size should ideally be a power of 2. However, such a constraint would limit the scheduler flexibility in terms of the amount of resources that can be assigned for an uplink transmission. In LTE, the DFT size and the size of the resource allocation is limited to products of the integers 2, 3, and 5. For example, the DFT sizes of 60, 72, and 96 are allowed, but a DFT size of 42 is not allowed [16]. Therefore, the DFT can be implemented as a combination of relatively low-complex radix-2, radix-3, and radix-5 FFT processing blocks.

The sub-carrier mapping in SC-FDMA determines which part of the spectrum is used for transmission by inserting a number of zeros (i.e., null sub-carriers inserted between the data sub-carriers) in the upper and/or lower end of the frequency region, as shown in Figure 10.3. Distributed mapping can be obtained by inserting $L - 1$ zeros between each DFT output sample. A mapping with $L = 1$ (as shown in Figure 10.3) corresponds to localized transmissions, i.e., transmissions

Petitioners' Exhibit 1021
Nokia of America Corp., et al. v. KT Corporation, et al.
Case No. IPR2025-00036; U.S. Patent No. 11,627,631
Page 736 of 1122

where the DFT outputs are mapped to consecutive sub-carriers. In localized sub-carrier mapping, a group of N_{DFT} adjacent sub-carriers are allocated to a user, where $N_{DFT} < N_{FFT}$ results in zeros being appended to the output of the DFT spreading which results in an interpolated version of the original N_{DFT} QAM data symbols at the IFFT output of the OFDM modulator. The transmitted signal is similar to a narrowband single carrier with a cyclic prefix, which is equivalent to time-domain generation with a repetition factor of one ($L = 1$) and sinc($\cdot$) function pulse shaping. Distributed transmission, on the other hand, allocates N_{DFT} equally spaced sub-carriers (i.e., every Lth sub-carrier). Therefore, $L - 1$ zeros are inserted between the N_{DFT} DFT outputs and additional zeros are appended to either side of the DFT output prior to the IFFT operation. Similar to the localized case, the zeros appended on either side of the DFT output provide sinc($\cdot$) function interpolation effect, while the zeros inserted between the DFT outputs produce waveform repetition in the time-domain. This results in a transmitted signal similar to time-domain interleaved FDMA (IFDMA) with repetition factor L and pulse shaping. Unlike the standard OFDM where the each data symbol is carried by the individual sub-carriers, the SC-FDMA transmitter carries data symbols over a group of sub-carriers transmitted simultaneously. In other words, the group of sub-carriers that carry each data symbol can be viewed as one frequency band carrying data sequentially in a standard FDMA. It can be mathematically shown that the SC-FDMA baseband time-domain samples after IDFT are the original data symbol set repeated in time-domain over the symbol period (Figure 10.4).

The performance of SC-FDMA with localized and distributed sub-carrier mapping was simulated to demonstrate the potential gain that can be obtained via sub-carrier distribution across frequency, particularly in higher mobility conditions. Figure 10.5 shows the block error rate (BLER) as a function of signal-to-noise

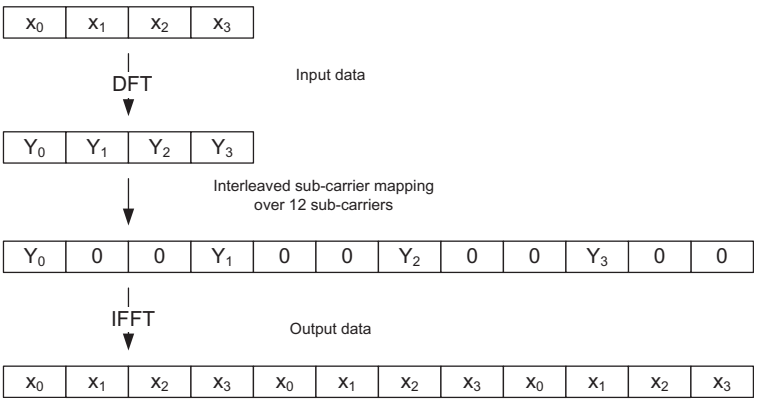


FIGURE 10.4

Time-domain representation of interleaved SC-FDMA.

Petitioners' Exhibit 1021
Nokia of America Corp., et al. v. KT Corporation, et al.
Case No. IPR2025-00036; U.S. Patent No. 11,627,631
Page 737 of 1122

ratio (SNR) for localized and distributed sub-carrier mapping. It is assumed that $N_{DFT} = 60, N_{FFT} = 512,$ and $N_{CP} = 20$ (number of samples constituting the cyclic prefix). Furthermore, the evaluation is conducted with ITU-PedA and ITU-VehA channel models, MMSE equalization at the receiver, QPSK modulation, and raised-cosine pulse shaping at the transmitter. It can be observed that the distributed sub-carrier mapping is more suited for high-mobility conditions and the gain is increased with increasing mobility.

The goal of equalization is to compensate the effects of channel distortion due to frequency-selectivity and to restore the original signal. One approach to signal equalization is in the time-domain using a linear equalizer, which consists of a linear filter with an impulse response $w(t)$ operating on the received signal. By selecting different filter impulse responses, different receiver/equalizer schemes can be implemented. For example, in DS-CDMA systems, a RAKE receiver is typically used. The RAKE receiver is an equalization method in which the filter impulse response is selected to match the channel impulse response $w(t) = h^*(-t)$. Therefore, in a RAKE receiver, the filter impulse response is selected as the complex conjugate of the time-reversed channel impulse response. Selecting the receiver filter according to the maximal ratio combining (MRC) criterion as above, i.e., a channel-matched filter, the filter maximizes the post-processing SNR. However, MRC-based filtering does not provide any compensation for any radio channel frequency selectivity and no equalization. Thus, MRC-based receiver filtering is appropriate when the received signal is mainly impaired by noise or interference from other transmissions. Another alternative is to select the receiver filter to compensate the radio channel frequency selectivity. This can be achieved by selecting the receiver filter impulse response to satisfy $w(t) * h(t) = 1$, where the

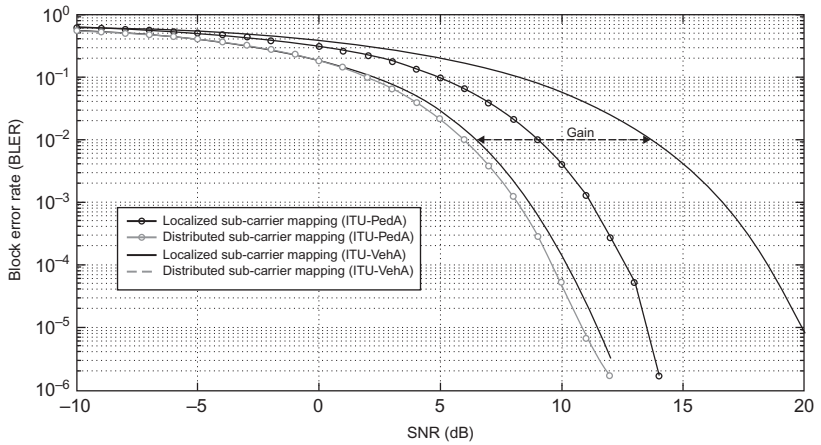


FIGURE 10.5

Comparison of localized and distributed sub-carrier mapping in SC-FDMA [136].

Petitioners' Exhibit 1021
Nokia of America Corp., et al. v. KT Corporation, et al.
Case No. IPR2025-00036; U.S. Patent No. 11,627,631
Page 738 of 1122

operator "*" denotes linear convolution. This method of filtering is known as zero-forcing (ZF) equalization, which compensates any channel frequency selectivity. However, the ZF equalization may lead to a significant increase in the noise level after equalization, degrading the overall link performance. This will be the case especially when the channel has large variations in its frequency response. Another alternative is to select a filter which provides a trade-off between signal distortion due to channel frequency selectivity and the corruption due to noise/interference, resulting in a filter impulse response that minimizes the mean-square error between the equalizer output and the transmitted signal. The linear equalizers are typically implemented as a time-discrete finite impulse response (FIR) filter with a certain number of taps. In general, the complexity of such a discrete-time equalizer increases with increasing bandwidth of the signal [16].

An alternative to time-domain equalization is frequency-domain equalization which can significantly reduce the complexity of linear equalization. In this method, the equalization is performed on a block of data. The received signal is transformed to the frequency-domain using a DFT operation. The equalization is done as a frequency-domain filtering operation, where the frequency-domain filter $W(k)$ is the DFT of the corresponding time-domain impulse response $w(n)$. The equalized frequency-domain signal is then transformed to the time-domain using an IDFT operator. For processing of each signal block of size $N = 2^m$, the frequency-domain equalization would include two N-point DFT/IDFT operations and N complex multiplications.

With the introduction of a cyclic prefix, the channel would appear as a circular convolution over a receiver processing block of size N. Therefore, there would be no need for overlap-and-discard in the receiver processing. Furthermore, the frequency-domain filter taps can now be calculated directly from an estimate of the sampled channel frequency response. Similar to the OFDM case, the drawback of using a cyclic prefix in conjunction with single-carrier transmission is the overhead in terms of extra power and bandwidth consumption. One method to reduce the relative cyclic-prefix overhead is to increase the block size N of the FDE. However, the accuracy of block equalization requires the channel to be approximately constant over a time period corresponding to the size of the processing block.

The detection procedure for an SC-FDMA signal is illustrated in Figure 10.6, and is compared with that of an OFDM waveform. The transmission through a time-dispersive or equivalently a frequency-selective channel will distort the SC-FDMA signal and an equalizer is needed to compensate for the effects of channel frequency-selectivity. However, as shown in Figure 10.6, a simple one-tap equalizer can be applied to each sub-carrier in OFDM, whereas in the case of SC-FDMA, the frequency-domain equalization function is applied to the complex-valued symbols at the output of the sub-carrier de-mapping and prior to the IDFT operation (Figure 10.7).

It must be noted that in OFDM downlink parameterization, the DC sub-carrier is unused in order to support direct conversion receiver architectures. In contrast, nulling DC sub-carrier is not possible in SC-FDMA since it affects the low

Petitioners' Exhibit 1021
Nokia of America Corp., et al. v. KT Corporation, et al.
Case No. IPR2025-00036; U.S. Patent No. 11,627,631
Page 739 of 1122

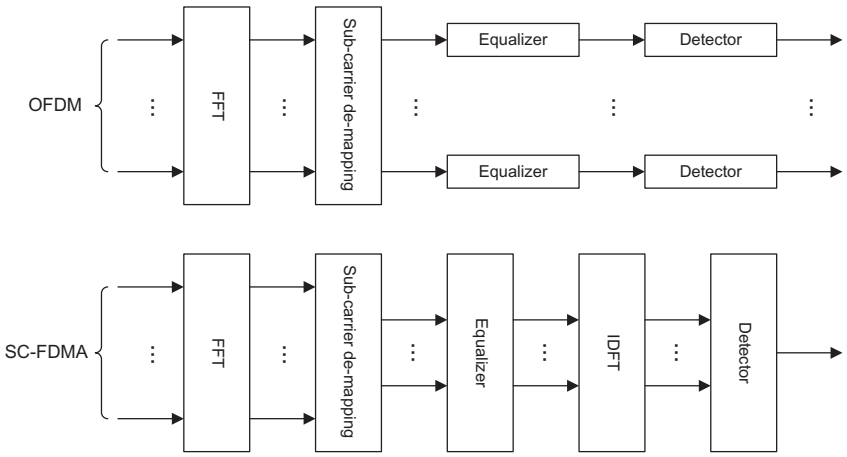


FIGURE 10.6

Illustration of different equalization/detection aspects of SC-FDMA and OFDM [39].

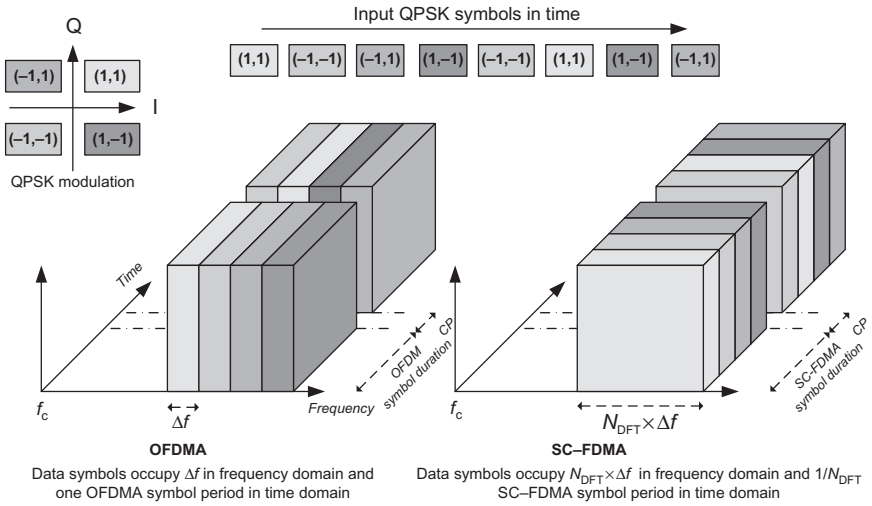


FIGURE 10.7

Comparison of OFDMA and SC-FDMA operation using QPSK modulation with $N_{DFT} = 4$ and $L = 1$. The input QPSK symbols, shown on top, are fed into the modulator from left to right [134].

Petitioners' Exhibit 1021
Nokia of America Corp., et al. v. KT Corporation, et al.
Case No. IPR2025-00036; U.S. Patent No. 11,627,631
Page 740 of 1122

CM/PAPR property of the transmit signal. Direct conversion transmitters and receivers can introduce distortion at the carrier frequency (zero frequency or DC sub-carrier in baseband) due to local oscillator leakage. In the LTE/LTE-Advanced downlink, this issue is avoided by inclusion of an unused DC sub-carrier. However, for the uplink, the same solution may adversely impact the low CM property of the transmitted signal. In order to minimize the impact of such distortion on the packet error rate and the CM/PAPR, the DC sub-carrier of the SC-FDMA signal is modulated in the same way as all the other sub-carriers but the sub-carriers are all frequency-shifted by half a sub-carrier spacing ($\Delta f/2$), resulting in an offset of 7.5 kHz relative to the DC sub-carrier. Therefore, two sub-carriers straddle the DC location; hence, the amount of distortion affecting any individual resource block is reduced by half.

In order to demonstrate the similarities and differences between OFDMA and SC-FDMA operation, let us assume that one wishes to transmit a sequence of eight QPSK symbols as shown in Figure 10.7 [134]. In the OFDMA case, assuming $N_{\text{DFT}} = 4$, four QPSK symbols would be processed in parallel, each of them modulating its own sub-carrier at the appropriate QPSK phase. After one OFDM symbol period, a guard period or cyclic prefix is inserted to mitigate the multipath effects. For SC-FDMA, each symbol is transmitted sequentially. With $N_{\text{DFT}} = 4$, there are four data symbols transmitted in one SC-FDMA symbol period. The higher-rate data symbols require four times the bandwidth, and so each data symbol occupies $N_{\text{DFT}} \times \Delta f$ Hz of the spectrum assuming a sub-carrier spacing of Δf Hz. After four data symbols, the cyclic prefix is inserted. Note the OFDMA and SC-FDMA symbol periods are the same [134].

As mentioned earlier, the PAPR of OFDM is intrinsically inferior to SC-FDMA. Figure 10.8 shows the comparison of complementary cumulative distribution functions (CCDF)[1] of OFDM and SC-FDMA PAPRs. It can be seen that the PAPR of SC-FDMA is approximately 3 dB better than that of OFDM with a probability of 0.99. In the case of 16QAM modulation, the PAPR of SC-FDMA increases relative to that of SC-FDMA with QPSK modulation, whereas in the case of OFDM, the PAPR distribution is more or less independent of the modulation scheme because the OFDM signal is the sum of a large number of independently modulated sub-carriers, thus the instantaneous power has an approximately exponential distribution, regardless of the modulation scheme applied to the different sub-carriers [16].

A new study suggests that the PAPR of an OFDM signal does not precisely predict the PA power de-rating or power capability as accurately as the CM criterion. The CM criterion has been adopted by 3GPP as a method to determine PA power de-rating because of its accuracy over a wide range of devices and signals.

[1]The CDF of the real-valued random variable X is defined as $x \rightarrow F_X(x) = P(X \leq x), \forall x \in \mathbb{R}$, where the right-hand side represents the probability that the random variable X takes on a real value less than or equal to x. The CDF of X can be defined in terms of the probability density function $f(x)$ as $F(x) = \int_{-\infty}^{x} f(x)\text{d}x$. The CCDF, on the other hand, is defined as $P(X > x) = 1 - F_X(x)$ [31–33].

Petitioners' Exhibit 1021
Nokia of America Corp., et al. v. KT Corporation, et al.
Case No. IPR2025-00036; U.S. Patent No. 11,627,631
Page 741 of 1122

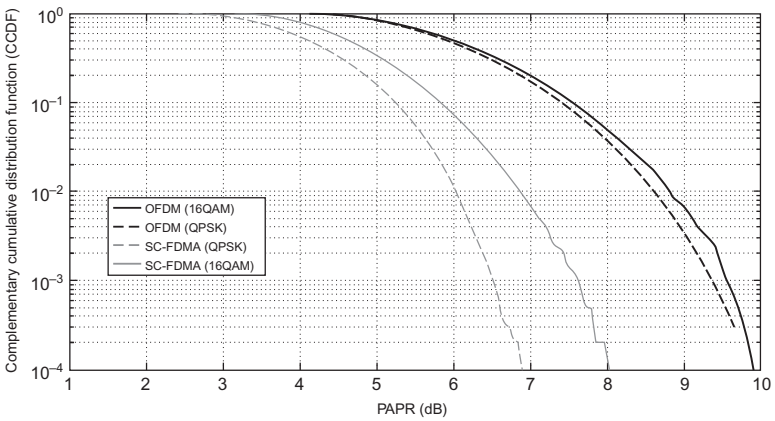


FIGURE 10.8

Comparison of OFDM and SC-FDMA PAPRs (5 MHz bandwidth) [136].

This method has proven to be more accurate for WCDMA signals compared to methods that use the statistical PAPR to predict power de-rating based on the information that has been collected from several devices for a variety of signals. The CM can be calculated using the following equation [138]:

$$\mathrm{CM} = \frac{20\log(s^3_{\mathrm{norm_{RMS}}}) - 20\log(s^3_{\mathrm{norm\text{-}reference_{RMS}}})}{K} \tag{10.2}$$

where $s_{\mathrm{norm_{RMS}}}$ denotes the root mean-square (RMS) value of the normalized voltage waveform of the input signal, and $s_{\mathrm{norm\text{-}reference_{RMS}}}$ is the RMS value of the normalized voltage waveform of the reference signal (i.e., signal generated using 12.2kbps adaptive multi-rate (AMR) speech codec [ref]). The CM is used to model the impact of nonlinearity in the PA on the adjacent-channel leakage ratio. A small value of the CM represents a small PA backoff. The CM is insensitive to the highest power values of the distribution that only have very low probabilities. Thus, methods to reduce the PAPR may not have any major impact on the CM. In practice, the value of parameter K was empirically determined to be 1.85 for a set of WCDMA signals. In other words, this equation computes the cubic power of a signal $s(t)$ and, compares it to a reference signal $s_{\mathrm{reference}}(t)$, and uses the empirical slope factor K to estimate the CM value. Although the signal vectors are shown as a function of time, the timescale is effectively removed in the RMS operation and is not a part of the computation. Thus, the raw CM result is not a function of symbol rate, or alternatively not a function of signal bandwidth. Similarly, a change in chip rate has no effect on PAPR. The bandwidth effects will be significant in this study since it includes signals with 3 dB bandwidths larger than the 3.84 MHz used for WCDMA. Table 10.1 gives the CM values corresponding to some example input signals such as OFDM, DFT-S OFDM, and

Petitioners' Exhibit 1021
Nokia of America Corp., et al. v. KT Corporation, et al.
Case No. IPR2025-00036; U.S. Patent No. 11,627,631
Page 742 of 1122

Table 10.1 Example CM Values Corresponding to Slope Factor *K* [138]

Signal					
Type	Modulation	RAW CM (dB)	*K*	Bandwidth Offset (dB)	CM (dB)
WCDMA	Voice	1.52	–	0.00	0
OFDM	16QAM	7.75	1.56	0.77	4.76
DFT-S OFDM	QPSK	3.44	1.56	0.77	2.00
DFT-S OFDM	16QAM	4.85	1.56	0.77	2.90
DFT-S OFDM	64QAM	5.18	1.56	0.77	3.11
IFDMA	QPSK	2.40	1.56	0.00	0.56
IFDMA	16QAM	4.36	1.56	0.00	1.82
IFDMA	64QAM	4.64	1.56	0.00	2.00

IFDMA which is a variant of SC-FDMA. It can be seen that DFT-S OFDM has an advantage relative to other signals shown in the table. In Table 10.1, the bandwidth offset in decibels denotes a de-rating increase of 0.77 dB from the CM regression line that can be used to estimate the actual de-rating of higher bandwidth signals. The *K* factor is empirically derived based on the measurements on various PAs.

10.3 SC-FDMA and clustered SC-FDMA

The LTE Rel-8 uplink is based on single-carrier frequency division multiple access scheme, which allocates carriers across a contiguous block of spectrum, thus limiting scheduling flexibility. LTE-Advanced introduced clustered SC-FDMA in the uplink, allowing frequency-selective scheduling of component carriers for better link-level performance. The physical uplink shared channel (PUSCH) and the physical uplink control channel (PUCCH) can be scheduled together to reduce latency. However, clustered SC-FDMA increases PAPR, leading to transmitter non-linearity issues. Furthermore, the presence of multi-carrier signals increases opportunities for co-channel and adjacent-channel interference.

LTE-Advanced enhances the uplink multiple access scheme by adopting clustered SC-FDMA. This scheme is similar to SC-FDMA but has the advantage that it allows non-contiguous (clustered) groups of sub-carriers to be allocated for transmission by a single UE, thus enabling uplink frequency-selective scheduling and improved link performance. Clustered SC-FDMA was chosen with preference to pure OFDM to avoid a significant increase in PAPR. It helps satisfy the requirement for increased uplink spectral efficiency while maintaining backward

Petitioners' Exhibit 1021
Nokia of America Corp., et al. v. KT Corporation, et al.
Case No. IPR2025-00036; U.S. Patent No. 11,627,631
Page 743 of 1122

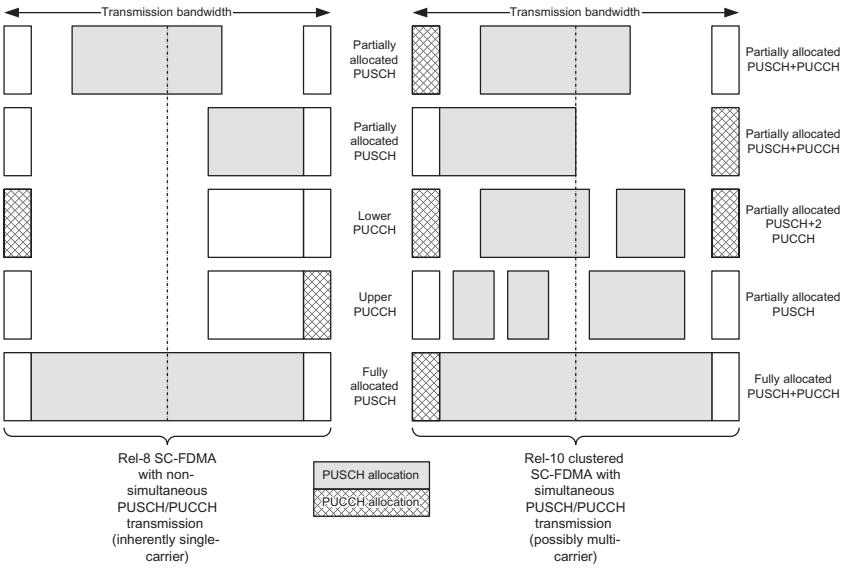


FIGURE 10.9

Comparison of LTE and LTE-Advanced uplink transmission [161].

compatibility with LTE Rel-8. There is only one transport block and one HARQ entity per scheduled component carrier. Each transport block is mapped to a single component carrier and a UE may be scheduled over multiple component carriers simultaneously using carrier aggregation.

Examples of different LTE Rel-8 and Rel-10 uplink configurations are shown in Figure 10.9. The main observation is that all LTE Rel-8 configurations are single carrier, which means that the PAPR is no greater than the underlying QPSK or 16QAM modulation format, whereas in LTE Rel-10, it is possible to transmit more than one carrier, which makes the PAPR higher than the Rel-8 cases. Note that the carriers mentioned above in the context of clustered SC-FDMA and simultaneous PUCCH/PUSCH transmission are contained within one component carrier and should not be confused with multiple component carriers and carrier aggregation. The initial specifications limit the number of SC-FDMA clusters to two, which will provide some improved spectral efficiency over a single cluster when transmitting through a frequency-selective channel with more than one distinct peak.

The clustered SC-FDMA must be distinguished from multiple SC-FDMA in the sense that clustered SC-FDMA retains a single DFT operation, but modifies the resource element mapping at the output of the DFT operation from a single cluster as used for SC-FDMA to multiple clusters which are multiplexed with $N_{\text{FFT}} - N_{\text{DFT}}$ zeros to form the input of the IFFT operation over N_{FFT} virtual subcarriers. The resulting waveform is no longer single-carrier but still has a low CM

Petitioners' Exhibit 1021
Nokia of America Corp., et al. v. KT Corporation, et al.
Case No. IPR2025-00036; U.S. Patent No. 11,627,631
Page 744 of 1122

value. On the other hand, multiple SC-FDMA consists of a number of DFT operations, where the kth DFT block is of size N_{DFT}^{k}; the output symbols are then multiplexed with $N_{\text{FFT}} - \sum_{k=1}^{N_{\text{cluster}}} N_{\text{DFT}}^{k}$ zeros to fit the N_{FFT}-point IFFT operation. This waveform is no longer single carrier and experiences worse CM compared to that of clustered SC-FDMA for the same number of clusters [16].

10.4 Uplink frame structure

The LTE frame structure for the FDD and TDD schemes was discussed in Chapter 9. The downlink and uplink frame structure parameters are the same, except that the time-domain underlying symbols in the downlink are OFDM symbols, whereas in the uplink the underlying symbols are SC-FDMA symbols due to the use of different multiple access methods in the uplink and downlink. In this chapter, some of the uplink-specific aspects of frame structure are repeated to set the ground for further uplink physical layer discussions as well as physical channel mappings. As mentioned in Chapter 9, LTE/LTE-Advanced downlink and uplink transmissions are organized into radio frames of duration 10 ms consisting of 10 equally-sized consecutive subframes of 1 ms each, consisting of a number of consecutive OFDM/SC-FDMA symbols. Each subframe is further divided into two equally sized slots of 0.5 ms. The number of OFDM/SC-FDMA symbols within one subframe is either 14 for a normal cyclic prefix or 12 for an extended cyclic prefix (Figure 10.10).

In an FDD scheme, all ten subframes within a radio frame contain either downlink or uplink subframes depending on the link direction. The uplink and downlink transmitters use separate frequency bands for transmissions; therefore, both downlink and uplink transmitters can transmit at all times and at the same time [3]. In a TDD scheme, the bandwidth is shared between uplink and downlink, with the sharing being performed by allotting different periods of time to uplink and downlink (i.e., time multiplexing). In LTE/LTE-Advanced, there are seven different patterns of uplink/downlink switching known as uplink−downlink configurations 0 through 6 that are shown in Table 10.2 [3].

As shown in Figure 10.10 and Table 10.2, the special subframe (subframe 1 in every uplink−downlink configuration and subframe 6 in uplink−downlink configurations 0, 1, 2, and 6) contains a portion of downlink transmission at the start of the subframe (downlink pilot time slot or DwPTS), a portion of unused symbols in the middle of the subframe (guard period), and a portion of uplink transmission at the end of the subframe (uplink pilot time slot or UpPTS). The lengths of DwPTS, GP, and UpPTS can take one of the ten combinations of values given in Table 10.3. The LTE standard specifies the lengths in terms of the sampling time T_s, but the lengths can be interpreted in terms of the number of OFDM/SC-FDMA symbols, as shown in Table 10.3.

Petitioners' Exhibit 1021
Nokia of America Corp., et al. v. KT Corporation, et al.
Case No. IPR2025-00036; U.S. Patent No. 11,627,631
Page 745 of 1122

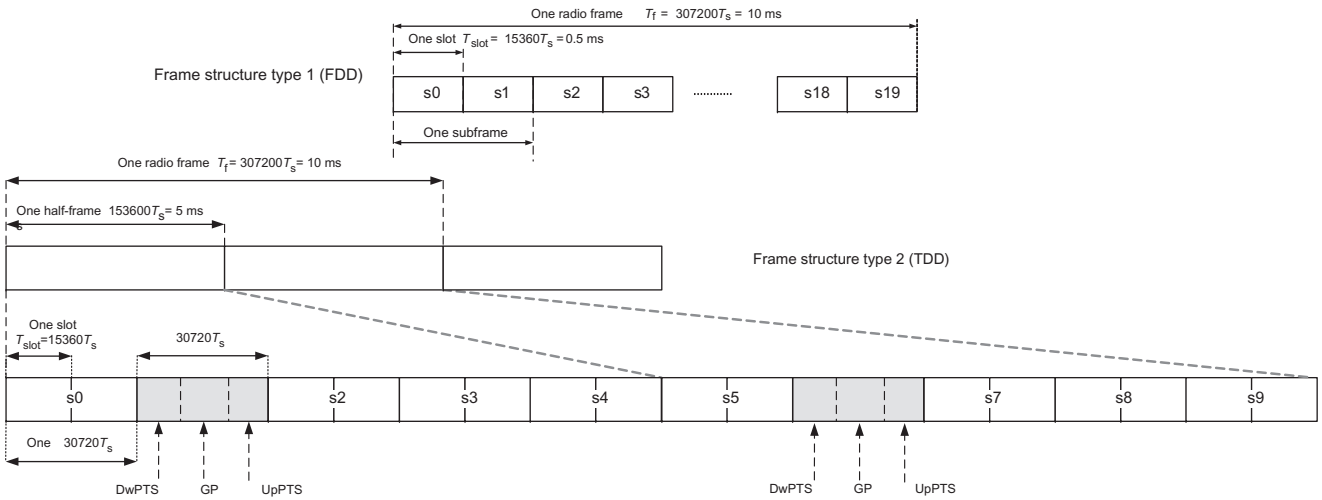


FIGURE 10.10

LTE/LTE-Advanced FDD/TDD frame structures [3].

Table 10.2 LTE/LTE-Advanced TDD Frame Configurations [3]

Uplink–Downlink Configuration	Multiplexing of Downlink, Uplink, and Special Subframes in One Radio Frame
0	DL SP UL UL UL DL SP UL UL UL
1	DL SP UL UL DL DL SP UL UL DL
2	DL SP UL DL DL DL SP UL DL DL
3	DL SP UL UL UL DL DL DL DL DL
4	DL SP UL UL DL DL DL DL DL DL
5	DL SP UL DL DL DL DL DL DL DL
6	DL SP UL UL UL DL SP UL UL DL

10.5 Physical resource structure and channel mapping

The smallest resource unit for uplink transmissions is a resource element (one sub-carrier). An uplink physical channel corresponds to a set of resource elements carrying information originating from the higher layers. The following uplink physical channels are defined:

- The physical uplink shared channel (PUSCH) carries user data and upper layer signaling as well as control information such as HARQ ACK/NACK, channel

Table 10.3 Special Subframe Configurations in TDD [3]

Special Subframe Configuration	Normal Cyclic Prefix in Downlink			Extended Cyclic Prefix in Downlink		
	DwPTS	UpPTS		DwPTS	UpPTS	
		Normal Cyclic Prefix in Uplink	Extended Cyclic Prefix in Uplink		Normal Cyclic Prefix in Uplink	Extended Cyclic Prefix in Uplink
0	3	1	1	3	1	1
1	9			8		
2	10			9		
3	11			10		
4	12			3		
5	3			8	2	2
6	9			9		
7	10	2	2	–	–	–
8	11			–	–	–
9	6			–	–	–

quality indicator (CQI), precoding matrix index (PMI), and rank indication (RI).

- The physical uplink control channel (PUCCH) carries control information such as HARQ ACK/NACK, CQI, and RI. In LTE Rel-8, the UE transmits control information on the PUCCH, when no PUSCH allocations are available to the UE. Starting from LTE Rel-10, PUCCH and PUSCH can be simultaneously transmitted by the UE. The PUCCH carries uplink control information (UCI). Each PUCCH uses one resource block in each of the two slots of the subframe. As shown in Figure 10.11, the PUCCH resource blocks are always allocated at the edge of the channel. This helps reduce out-of-band (OOB) emissions from data transmissions on inner resource blocks. Allocating the PUCCH in the center of the band would further create non-contiguous PUSCH resources, which limits contiguous resources that can be allocated to a single UE, and thus would limit the achievable peak throughput. The PUCCH resource blocks are transmitted with a hopping pattern from one edge to the other edge in each slot of the subframe. Frequency hopping provides frequency diversity for PUCCH. A maximum of four resource blocks are reserved for PUCCH in this example. The physical resources used for PUCCH depend on parameters that are provided by the higher layers. The PUCCH allocations also contain demodulation reference signals (DM-RSs) for coherent demodulation.

Petitioners' Exhibit 1021
Nokia of America Corp., et al. v. KT Corporation, et al.
Case No. IPR2025-00036; U.S. Patent No. 11,627,631
Page 748 of 1122

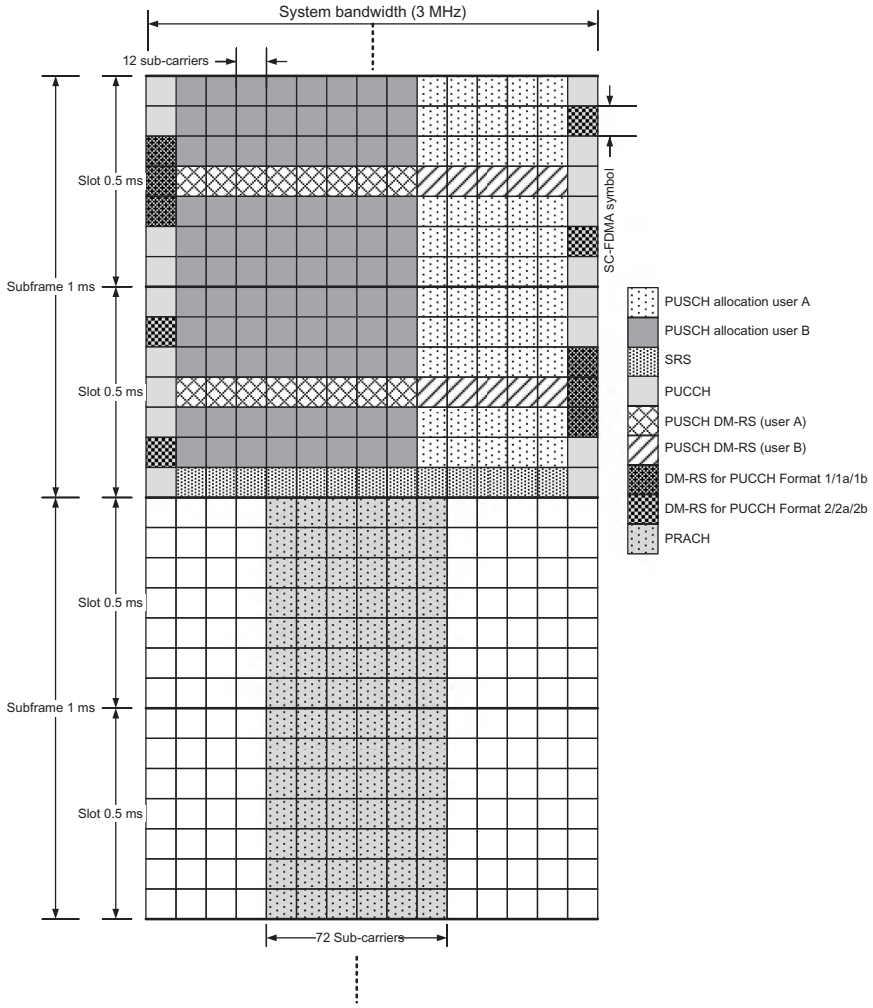


FIGURE 10.11

Example of uplink frame structure and location of the physical signals/channels.

The PUCCH allocation may contain one, two, or three DM-RS symbols. The DM-RS for each UE is generated using a cyclic shift of base Zadoff−Chu sequences. The RRC sub-layer assigns cyclic shift parameters (i.e., cyclic shift and base sequence group) to the UE during the RRC connection setup. The location of DM-RS differs based on formats and the length of the cyclic prefix.

- The physical random-access channel (PRACH) is used by non-synchronized UEs to access the network. It is further used during initial system access,

Petitioners' Exhibit 1021
Nokia of America Corp., et al. v. KT Corporation, et al.
Case No. IPR2025-00036; U.S. Patent No. 11,627,631
Page 749 of 1122

handovers, and radio link failure recovery scenarios. A preamble sequence, which may be randomly selected from a group of sequences or assigned (dedicated) by the eNB, is transmitted over PRACH. The sequences are Zadoff−Chu sequences of length 839. There are 64 different cyclic shifts generated from each root Zadoff−Chu sequence with zero correlation between them. Therefore, different cyclic shifts are essentially orthogonal to each other. The PRACH resource consists of six consecutive resource blocks. The location of PRACH is indicated by an offset parameter signaled by higher-layer signaling. There is at most one PRACH resource per subframe in FDD mode. Multiple UEs can access the PRACH resource by using different preambles. The UEs may select preambles randomly, which may result in collision. Therefore, contention resolution mechanisms are necessary. The PRACH may not be present in every subframe and every radio frame. The *PRACH configuration index* parameter indicates frame number and subframe numbers in which the PRACH resource is available. The sub-carrier spacing for PRACH transmission is different from that of other channels in the uplink. The number of sub-carriers is equal to the length of preamble, which is 839 (due to longer OFDM symbol length for PRACH). The sub-carrier spacing is 1.25 kHz, resulting in a longer symbol duration of 800 μs. The choice of sub-carrier spacing also results in additional guard bands on both sides because the entire 1.08 MHz is not used for the PRACH transmission.

In addition, there are two types of reference signals in the uplink as follows:

- The demodulation reference signal is a known signal transmitted in PUSCH and/or PUCCH whenever they are transmitted and provides a coherent demodulation reference for uplink transmissions. The DM-RS provides the reference for channel estimation and coherent demodulation of uplink transmissions from the UE on PUSCH or PUCCH. The DM-RS is transmitted only in the resource blocks transmitted from the UE for PUSCH or PUCCH. It is transmitted during a specific symbol and time-division multiplexed with the resource blocks allocated to the UE for data or control information transmission. The DM-RS signal is based on Zadoff−Chu sequences with a length of up to the maximum number of resource blocks. Thirty groups of base sequences are defined where each group contains three base sequences. Group hopping patterns and sequence hopping patterns are defined, resulting in different base sequences in different slots. The base sequences are generated differently based on whether they are more or less than three resource blocks. From these base sequences, different cyclic shifts are defined. The cyclic shifts are derived from UE-specific parameters assigned in DCI format 0 and cell identity. This creates the UE-specific cyclic shifts necessary to achieve orthogonality for MU-MIMO, where the same resource block is allocated to multiple users. The cyclic shift is also derived from the slot number, resulting in different cyclic shifts in different slots for the same UE.

Petitioners' Exhibit 1021
Nokia of America Corp., et al. v. KT Corporation, et al.
Case No. IPR2025-00036; U.S. Patent No. 11,627,631
Page 750 of 1122

- The sounding reference signal (SRS) is a wideband signal transmitted by the UE for several purposes. The eNB can use SRS transmission to select the best resource blocks to allocate to the UE (i.e., frequency-selective scheduling). It may also be used for uplink power control. If uplink MIMO is supported, it may be further used for adaptive antenna switching for uplink transmit diversity. The SRS sequences are selected from the same Zadoff−Chu root sequences used for DM-RS. The cyclic shifts are configured for each UE when SRS transmission is configured. If configured, the SRS transmission always occurs in the last SC-FDMA symbol of a subframe. The SRS transmission may not be allowed in every subframe. The periodicity of subframes containing SRS may be limited to 2, 5, 10, 20, 40, 80, 160, or 320 ms [5]. The bandwidth for SRS transmission is specified in terms of number of resource blocks and may extend from 4 to 36 resource blocks, if the maximum number of resource blocks in the uplink is in the range of 6-40. The SRS bandwidth may extend from 4 to 96 resource blocks, if the maximum number of resource blocks in the uplink is in the range of 80−110 [3]. The SRS parameters (periodicity, bandwidth, etc.) can be cell-specific and broadcast from each cell. Additionally, UE-specific parameters that override cell-specific parameters may be configured through higher-layer signaling. Frequency hopping may be defined for SRS transmission, if the SRS bandwidth is smaller than the system bandwidth.

The uplink unit of resource allocation is a resource block. A resource block is a two-dimensional array of all SC-FDMA symbols in a slot and 12 sub-carriers in the frequency-domain. There are 72 (6 symbols by 12 sub-carriers) or 84 (7 symbols by 12 sub-carriers) resource elements in a resource block corresponding to extended cyclic prefix or normal cyclic prefix, respectively. The number of resource blocks depends on the channel bandwidth. There is a minimum of six resource blocks for the 1.4 MHz channel and 100 resource blocks for the 20 MHz channel. A UE is allocated a number of contiguous or non-contiguous resource blocks. Figure 10.11 illustrates an example of mapping of uplink physical channels and signals to the physical resources within a subframe for an uplink bandwidth of 3 MHz (15 resource blocks).

10.5.1 Physical resource blocks

The signal transmitted in each slot is described by one or several resource grids of $12 \times N_{RB}^{UL}$ sub-carriers and N_s^{UL} SC-FDMA symbols. The uplink resource grid is illustrated in Figure 10.12. The parameter N_{RB}^{UL} denotes the number of uplink resource blocks, which depends on the uplink transmission bandwidth, configured in the cell whose value falls in the range of $\min(N_{RB}^{UL}) \leq N_{RB}^{UL} \leq \max(N_{RB}^{UL})$, where $\min(N_{RB}^{UL}) = 6$ and $\max(N_{RB}^{UL}) = 110$ represent the minimum and maximum uplink bandwidths, respectively. The number of SC-FDMA symbols in a slot N_s^{UL} depends on the cyclic prefix length which is configured by the higher layer signaling. Similar to the downlink, there are seven SC-FDMA symbols for the normal cyclic prefix and six SC-FDMA symbols for extended cyclic prefix in each slot.

Petitioners' Exhibit 1021
Nokia of America Corp., et al. v. KT Corporation, et al.
Case No. IPR2025-00036; U.S. Patent No. 11,627,631
Page 751 of 1122

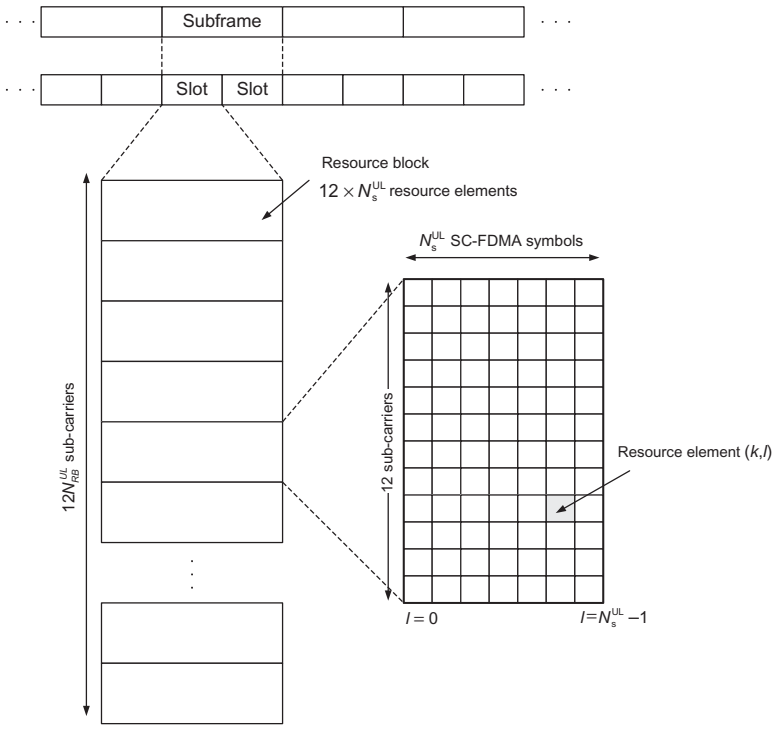


FIGURE 10.12

Uplink physical resource structure [3].

Each resource element in the resource grid within a slot is uniquely defined by the index pair (k, l), where $k = 0, 1, \ldots, 12 \times N_{\mathrm{RB}}^{\mathrm{UL}} - 1$ and $l = 0, 1, \ldots, N_{\mathrm{s}}^{\mathrm{UL}} - 1$ are the frequency and time-domain indices, respectively. The resource element (k, l) on antenna port p corresponds to the complex-valued symbol a_{kl}^{p}. A physical resource block (PRB) is defined as $N_{\mathrm{s}}^{\mathrm{UL}}$ consecutive SC-FDMA symbols in the time-domain and 12 consecutive sub-carriers in the frequency-domain. Note that the number of sub-carriers in a resource block corresponding to sub-carrier spacing 7.5 kHz is 24; however, throughout this book, we assume a 15 kHz sub-carrier spacing. A PRB in the uplink thus consists of $12 \times N_{\mathrm{s}}^{\mathrm{UL}}$ resource elements, corresponding to one slot in the time-domain and 180 kHz in the frequency-domain. The PRB number in the frequency-domain n_{PRB} and the resource element (k, l) in a slot are related as $n_{\mathrm{PRB}} = \lfloor k/12 \rfloor$.

10.5.2 Uplink resource allocation

The concept of virtual resource blocks (VRBs) or distributed resource allocation and the mapping of VRBs to PRB were discussed in Chapter 9 for downlink resource allocations. The distributed resource allocation in the downlink consists

of two separate steps that include mapping from VRB pairs to PRB pairs such that frequency-consecutive VRB pairs are not mapped to frequency-consecutive PRB pairs, as well as splitting of each resource-block pair such that the two resource blocks of the resource-block pair are transmitted with a certain frequency gap over the slots of each subframe. The latter step can be seen as frequency hopping on a slot basis. In the absence of the frequency hopping, each VRB is directly mapped to a PRB. Note that localized transmissions without use of frequency hopping can achieve some degree of frequency-selective-scheduling gain, whereas localized transmission using frequency hopping yields frequency-diversity gain as well as inter-cell interference randomization [16].

The VRB concept can also be used in the uplink, allowing use of frequency-diversity transmission in the uplink. However, in the uplink, where transmission from a terminal should always be over a set of consecutive sub-carriers in the absence of clustered SC-FDMA, distribution of resource-block pairs in the frequency-domain is not possible. Therefore, uplink distributed resource allocation is only similar to the second step of downlink distributed transmission, i.e., inserting a frequency gap between the PRBs in the first and second slots of a subframe. This is referred to as PUSCH frequency hopping in the literature. There are two types of uplink frequency hopping defined for PUSCH as follows: (1) sub-band hopping according to cell-specific hopping/mirroring patterns (as shown in Figure 10.13); and (2) hopping based on explicit hopping information contained in the scheduling grant. The uplink frequency hopping is not supported for clustered SC-FDMA transmission, since sufficient frequency diversity gain can be achieved by properly assigning the location of the clusters.

In order to support sub-band frequency hopping according to cell-specific hopping/mirroring patterns, a set of consecutive sub-bands with predetermined size are defined as illustrated in Figure 10.13. It should be noted that the sub-bands do not cover the total uplink frequency band due to the fact that a number of resource blocks at the edges of the uplink frequency band are designated for transmission of PUCCH. As an example, if the overall uplink bandwidth contains 25 resource blocks and there are a total of four sub-bands, each consisting of five resource blocks, then five resource blocks at both edges of the band are not included in the hopping bandwidth and can be used for PUCCH transmission (see Figure 10.13). In the case of sub-band hopping, the set of VRBs provided in the scheduling grant are mapped to a corresponding set of PRBs according to a cell-specific hopping pattern. The physical resources to be used for transmission are obtained by shifting the VRBs provided in the scheduling grant by a number of sub-bands according to the hopping pattern, where the hopping pattern can provide different shifts for each slot. The hopping pattern is cell specific, which implies that it is the same for all terminals within a cell; however, different terminals will transmit on non a_{kl}^{p} overlapping physical resources as long as they are assigned non a_{kl}^{p} overlapping virtual resources [16].

In addition to the hopping pattern, there is also a cell-specific mirroring pattern defined in a cell. The mirroring pattern controls, on a slot basis, if mirroring

Petitioners' Exhibit 1021
Nokia of America Corp., et al. v. KT Corporation, et al.
Case No. IPR2025-00036; U.S. Patent No. 11,627,631
Page 753 of 1122

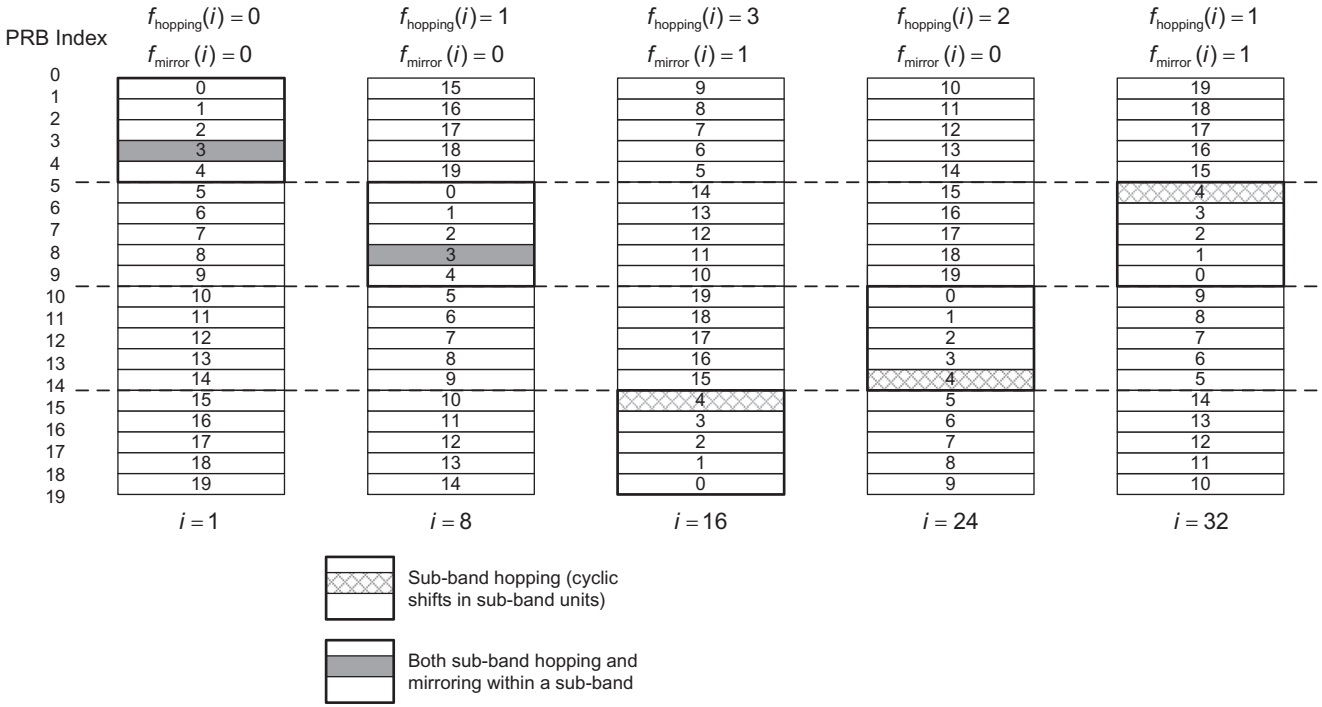


FIGURE 10.13

Illustration of an example PUSCH frequency hopping (20 resource blocks, $L_{sb} = 4$) [156].

Petitioners' Exhibit 1021
Nokia of America Corp., et al. v. KT Corporation, et al.
Case No. IPR2025-00036; U.S. Patent No. 11,627,631
Page 754 of 1122

within each sub-band should be applied to the assigned resource. In principle, mirroring suggests that the resource blocks within each sub-band are numbered right to left instead of left to right. Figure 10.13 illustrates an example of mirroring in conjunction with hopping within a sub-band. The mirroring pattern is not applied to the first slot, while mirroring is applied to the second slot. Both hopping and mirroring patterns depend on the physical layer cell identity and are typically different in neighboring cells. Furthermore, the periodicity of the hopping/mirroring patterns is one radio frame.

An alternative approach to uplink cell-specific hopping/mirroring is frequency hopping according to explicit information provided in the scheduling grant. In such cases, the scheduling grant includes information about the resource allocation for uplink transmission in the first slot and information related to the amount of offset applicable to the resource to be used for uplink transmission in the second slot relative to the resource location in the first slot. Selection between hopping according to cell-specific hopping/mirroring patterns as described above, or hopping according to explicit information in the scheduling grant, can be made dynamically. More specifically, for cell bandwidths less than 50 resource blocks, there is a flag in the scheduling grant indicating whether frequency hopping is based on cell-specific hopping/mirroring patterns or according to information in the scheduling grant. In the latter case, the hopping is always half of the hopping bandwidth. In the case of larger bandwidths in excess of 50 resource blocks, there are 2 bits in the scheduling grant. One of the combinations indicates that hopping should be according to the cell-specific hopping/mirroring patterns, while the three remaining combinations indicate hopping of 1/2, +1/4, and −1/4 of the hopping bandwidth [16].

The uplink also supports transmission time interval (TTI) bundling where four consecutive subframes are bundled together following a downlink grant. Four HARQ processes are necessary, the downlink PHICH transmissions correspond to the last subframe of the bundle, and the retransmissions are non-dynamic. The purpose of TTI bundling is to enable successful reception of the uplink transmissions in coverage-limited scenarios. The TTI bundling is configured by the RRC sub-layer.

The uplink resource allocation scheme in LTE Rel-8 is single-cluster allocation, which is contiguous resource allocation in the frequency-domain. LTE-Advanced has enabled multi-cluster uplink transmissions. The single-cluster allocations use uplink resource allocation type 0, which is identical to downlink resource allocation type 2, except that the single-bit flag indicating localized/distributed transmission is replaced by a single-bit hopping flag. The resource allocation field in the DCI provides the set of VRBs to be used for uplink transmission. The set of PRBs to use in the two slots of a subframe is controlled by the hopping flag.

The multi-cluster allocations with up to two clusters were introduced in LTE Rel-10 and use uplink resource allocation type 1. In resource allocation type 1, the starting and ending positions of two clusters of frequency-contiguous resource blocks are encoded and indicated with an index. The uplink resource allocation

Petitioners' Exhibit 1021
Nokia of America Corp., et al. v. KT Corporation, et al.
Case No. IPR2025-00036; U.S. Patent No. 11,627,631
Page 755 of 1122

type 1 does not support frequency hopping since the frequency diversity is achieved through the use of the clustered allocation. It is evident that indication of two clusters of resources requires additional signaling compared to the single-cluster case. However, the total number of bits used for resource allocation type 1 is identical to that of type 0 (see Figure 10.13). This is similar to the case of downlink allocation types 0 and 1. Since frequency hopping is not supported for allocation type 1, the bit, otherwise designated to the hopping flag, can be used for extending the resource allocation field. However, despite the extension of the resource allocation field by 1 bit, the number of bits is not sufficient to provide a single-resource-block resolution in the two clusters for all bandwidths. Instead, similar to downlink resource allocation type 0, groups of resource blocks are used and the starting and ending positions of the two clusters are given in terms of group numbers. The size of the group is proportional to the uplink bandwidth. The size of the group is one for small bandwidths and four for large system bandwidths [16]. Both DCI formats 0 and 4 support uplink resource allocation types 0 and 1. The number of allocated resource blocks is always equal to one or a multiple of 2, 3, or 5. It means that 1, 2, 3, 4, 5, 6, 8, 9, 10, 12, 15, etc., are permissible resource allocation sizes in the uplink (Figure 10.14).

10.5.2.1 Uplink resource allocation type 0

The resource allocation information contained in uplink resource allocation type 0 for a scheduled UE contains a set of contiguously allocated VRB indices denoted by n_{VRB}. A resource allocation field in the scheduling grant consists of a resource indication value (RIV) parameter corresponding to the starting resource block $\mathrm{RB}_{\mathrm{START}}$ and the length of the allocation in terms of contiguously allocated resource blocks $L \geq 1$. The RIV is defined as $\mathrm{RIV} = N_{\mathrm{RB}}^{\mathrm{UL}}(L-1) + \mathrm{RB}_{\mathrm{START}}$ if $(L-1) \leq \lfloor N_{\mathrm{RB}}^{\mathrm{UL}}/2 \rfloor$; otherwise, the RIV is given as $\mathrm{RIV} = N_{\mathrm{RB}}^{\mathrm{UL}}(N_{\mathrm{RB}}^{\mathrm{UL}} - L + 1) + (N_{\mathrm{RB}}^{\mathrm{UL}} - 1 - \mathrm{RB}_{\mathrm{START}})$. This is similar to resource allocation type 2 in the downlink. An example of uplink resource allocation using type 0 in 1.4 MHz (6 resource blocks) is shown in Figure 10.15.

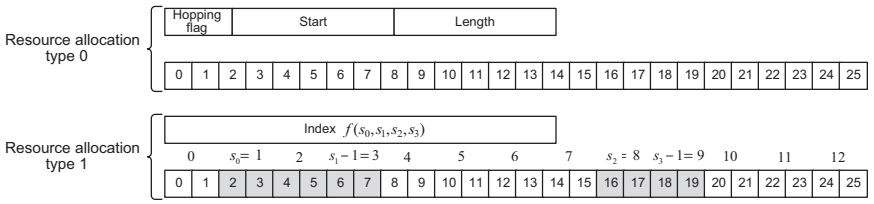


FIGURE 10.14

Illustration of uplink resource allocation types [16].

Petitioners' Exhibit 1021
Nokia of America Corp., et al. v. KT Corporation, et al.
Case No. IPR2025-00036; U.S. Patent No. 11,627,631
Page 756 of 1122

10.5.2.2 Uplink resource allocation type 1

The uplink resource allocation type 1 was introduced in LTE Rel-10 to allow allocation of non-contiguous resource-block groups (RBGs). In uplink resource allocation type 1, an indication is provided to a scheduled UE of two sets of resource blocks where each set includes one or more consecutive RBGs of size N_{RBG}, assuming a system bandwidth of $N_{\text{RB}}^{\text{UL}}$. This type of resource allocation is defined by four indices that are combined into a single combinatorial index l before being sent to the UE. A complete representation of combinatorial index l requires $\left\lceil \log_2 \left[\binom{\lceil N_{\text{RB}}^{\text{UL}}/N_{\text{RBG}} + 1 \rceil}{4} \right] \right\rceil$ bits. The bits from the resource allocation field in the scheduling grant represent index l, unless the number of bits in the resource allocation field in the scheduling grant is either smaller or larger than that required number to represent index l. If the number of bits is smaller than that required to represent l, the bits in the resource allocation field in the scheduling grant would represent the least-significant bits of l and the value of the remaining bits of l are set to zero. If the number of bits is larger than that required for representation of l, index l would be mapped to the least-significant bits of the resource allocation field in the scheduling grant. Note that resource-block allocation in this case is defined by four indices (s_0, s_1, s_2, s_3). The parameters s_0 and s_1 define the first and the last RBG within the first set of RBGs, and the parameters s_2 and s_3 define the first and the last RBG within the second set of RBGs. Therefore, the combinatorial index l corresponds to the starting and the ending index of resource-block-set 1 (s_0 and s_1), and resource-block-set 2 (s_2 and s_3), respectively, where $l = \sum_{i=0}^{M-1} \binom{N - s_i}{M - i}$, $M = 4$, and $N = \lceil N_{\text{RB}}^{\text{UL}}/N_{\text{RBG}} \rceil + 1$. If the corresponding ending RBG index is equal to the starting index, only one RBG is allocated.[2]

---

[2]The combinatorial index l is calculated based on the sorted set of M sub-band indices $\{s_i\}_{i=0,1,\ldots,M-1}$ given $1 \le s_k \le N, s_k < s_{k+1}$ as $l = \sum_{i=0}^{M-1} \binom{N - s_i}{M - i}$ where $\binom{x}{y} : x \ge y$ is the extended binomial coefficient and $l \in \left\{0, 1, \ldots, \binom{N}{M} - 1\right\}$. The uniqueness and the range of the combinatorial index are proven in the literature [162,163]. In the receiving end, the de-mapper regenerates the set of indices $\{s_i\}_{i=0,1,\ldots,M-1}$ from the received label l using the following algorithm:

$x_{\min} = 1$;
for $i = 0$ to $M - 1$
$x = x_{\min}$;
$p = \binom{N - x}{M - i}$;
while $p > l$
  $x = x + 1$;
  $p = \binom{N - x}{M - i}$;
end
$s_i = x$;
$x_{\min} = s_i + 1$;
$l = l - p$;
end

Petitioners' Exhibit 1021
Nokia of America Corp., et al. v. KT Corporation, et al.
Case No. IPR2025-00036; U.S. Patent No. 11,627,631
Page 757 of 1122

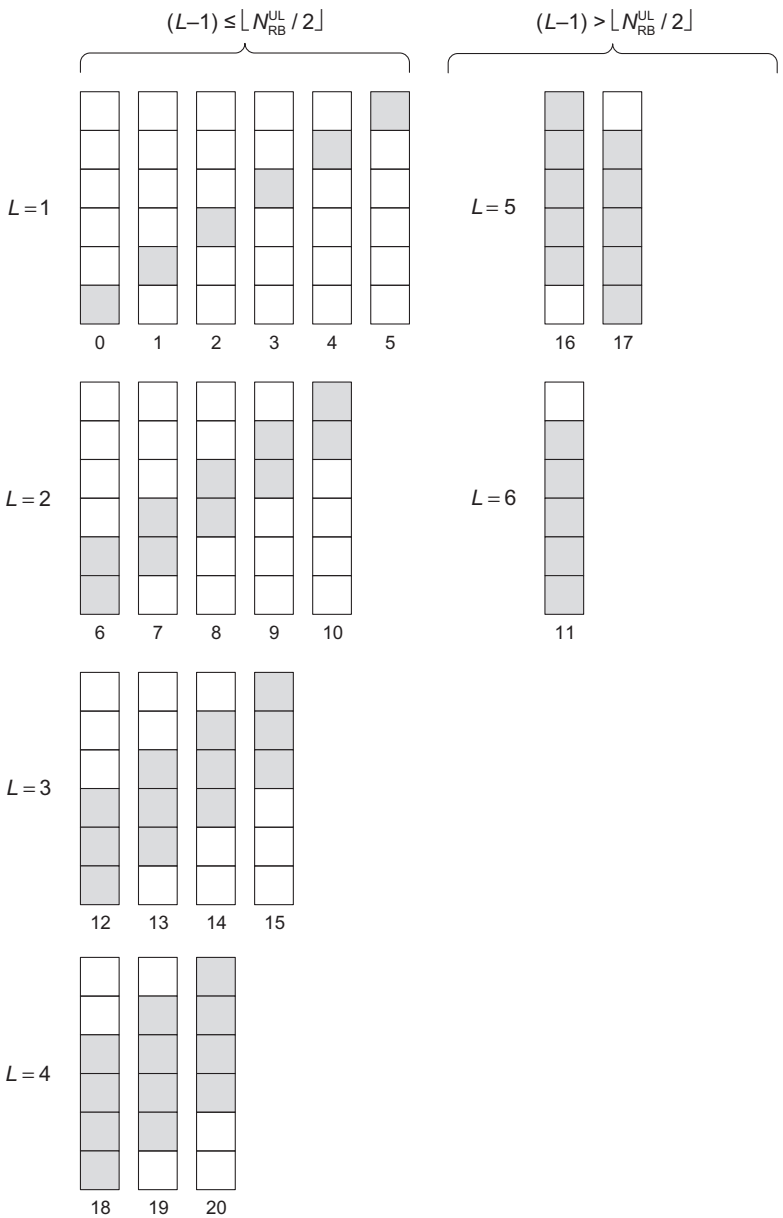


FIGURE 10.15

Illustration of an example uplink resource allocation type 0 in 1.4 MHz [14].

Petitioners' Exhibit 1021
Nokia of America Corp., et al. v. KT Corporation, et al.
Case No. IPR2025-00036; U.S. Patent No. 11,627,631
Page 758 of 1122

Table 10.4 Subframe Delay k Between PDCCH Assignment and PUSCH Transmission for TDD Mode [5]

TDD Uplink/Downlink Configuration (DL:UL)	PDCCH/PHICH Subframe Number n									
	0	1	2	3	4	5	6	7	8	9
0 (2:3)	4	6	–	–	–	4	6	–	–	–
1 (3:2)	–	6	–	–	4	–	6	–	–	4
2 (4:1)	–	–	–	4	–	–	–	–	4	–
3 (7:3)	4	–	–	–	–	–	–	–	4	4
4 (8:2)	–	–	–	–	–	–	–	–	4	4
5 (9:1)	–	–	–	–	–	–	–	–	4	–
6 (5:5)	7	7	–	–	–	7	7	–	–	5

An important consideration concerning the uplink resource allocation is the timing relevance of PDCCH uplink assignment (or PHICH transmission) and the uplink subframe in which physical resources are reserved for the UE PUSCH transmission or retransmission. In FDD mode, the uplink resource allocation using PDCCH (or PHICH transmission) for the UE in subframe n is related to PUSCH transmission/retransmission in subframe $n+4$, i.e., there is a delay of four subframes between the uplink resource assignment (or HARQ ACK/NACK) in the downlink and the corresponding uplink transmission. For TDD mode, the timing relevance of PDCCH assignment (or PHICH transmission) and PUSCH transmission/retransmission is more complicated and depends on the downlink/uplink subframe configuration. The delay (in number of subframes) between receiving an uplink resource assignment in PDCCH or HARQ ACK/NACK in PHICH in subframe n and PUSCH transmission in subframe $n+k$ (where $k \geq 4$ and is selected such that $n+k$ is an uplink subframe when the ACK/NACK can be transmitted from the UE on PUCCH or PUSCH) for TDD mode for various downlink/uplink configurations is given in Table 10.4 [5]. It can be noted that, due to certain limitations imposed by downlink/uplink subframe configuration, PUSCH transmission may be delayed by up to seven subframes.

The uplink/downlink subframe configuration 0 is a special case because the number of uplink subframes is greater than the number of downlink subframes. Due to an insufficient number of downlink subframes, the downlink portion of the special subframe is also used for downlink transmission.

Multiplexing is a method for grouping and sending several independent HARQ ACK/NACKs in the TDD mode in a single uplink subframe for the previously received transport blocks. This method allows independent retransmission of erroneous transport blocks. However, it also implies that multiple ACK/NACK bits need to be transmitted from the UE, which can potentially limit the uplink coverage. Alternatively, bundling of HARQ ACK/NACKs implies that the outcome of the decoding of downlink transport blocks from multiple downlink subframes can

Petitioners' Exhibit 1021
Nokia of America Corp., et al. v. KT Corporation, et al.
Case No. IPR2025-00036; U.S. Patent No. 11,627,631
Page 759 of 1122

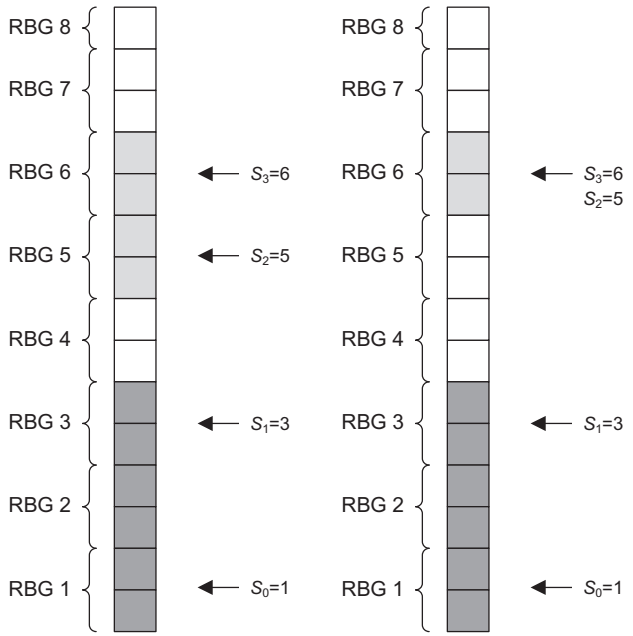


FIGURE 10.16

Example of uplink resource allocation type 1 in 3 MHz [14].

be combined into a single acknowledgement in the uplink. Combining acknowledgments related to multiple downlink transmissions into a single uplink message assumes that the terminal has not missed any of the scheduling assignments on which the ACK is based. As an example, assume that the eNB schedules the UE in two (subsequent) subframes, but the terminal misses the PDCCH transmission in the first subframe and successfully decodes the control information in the second subframe. The terminal would transmit one ACK as if it was scheduled in the second subframe only, while the eNB would interpret the ACK as if both transmissions were successfully received by the UE. To avoid such misinterpretations, the downlink assignment index (DAI) field in the scheduling assignment on the PDCCH is used. The DAI informs the terminal about the number of transmissions it should expect before generating a combined acknowledgment. If there is a mismatch between the DAI and the number of transmissions the terminal actually received, the terminal concludes that some assignments are missing. As a result, the UE does not transmit any HARQ acknowledgment [15] (Figure 10.16).

Let us consider a TDD example, downlink/uplink subframe configuration 2 includes six downlink subframes, two special subframes, and two uplink subframes. Downlink data can be transmitted within the DwPTS portion of the special subframes, which effectively results in eight downlink transmission opportunities.

Petitioners' Exhibit 1021
Nokia of America Corp., et al. v. KT Corporation, et al.
Case No. IPR2025-00036; U.S. Patent No. 11,627,631
Page 760 of 1122

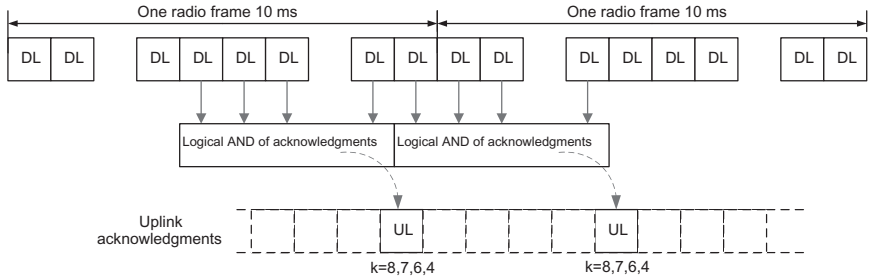


FIGURE 10.17

Illustration of HARQ acknowledgment bundling for TDD frame configuration 2 [14].

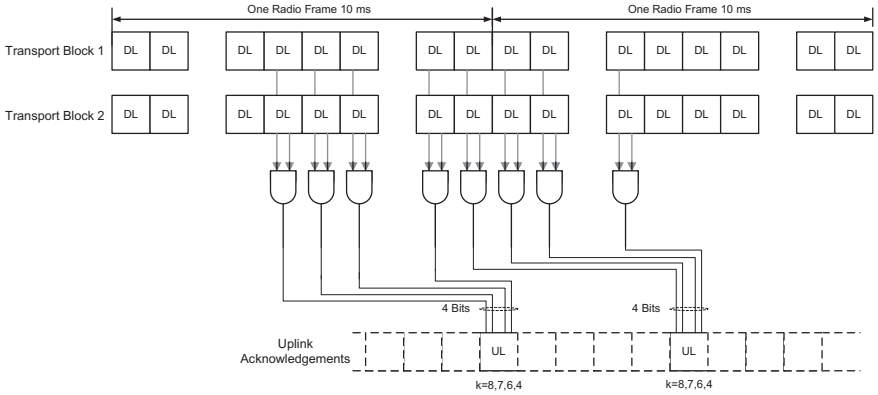


FIGURE 10.18

Illustration of HARQ ACK multiplexing for TDD frame configuration 2 [14].

If the downlink transmissions are divided into two groups and a single acknowledgment is generated from each group, each uplink subframe is required to carry a single HARQ ACK/NACK, which is called ACK/NACK bundling as depicted in Figure 10.17. On the other hand, for the same subframe configuration, 16 acknowledgments per radio frame can be reduced to eight acknowledgments using two uplink subframes. PUCCH format 1b can be used to carry four acknowledgments when channel selection is used, i.e., the PUCCH payload carries two ACKs and the selection of PUCCH resources carriers the other two ACKs, as illustrated in Figure 10.18 [14].

The use of bundled ACKs in a single uplink subframe is not limited to TDD mode. The carrier aggregation in FDD with a different number of uplink and downlink component carriers encounters the same problem. In LTE Rel-10, there is only one PUCCH that is always transmitted on the primary component carrier.

Petitioners' Exhibit 1021
Nokia of America Corp., et al. v. KT Corporation, et al.
Case No. IPR2025-00036; U.S. Patent No. 11,627,631
Page 761 of 1122

Hence, even in asymmetric carrier aggregation scenarios, the possibility to transmit more than two HARQ ACK bits in the uplink must be supported. This is performed via resource selection or by using PUCCH format 3. The ACKs in response to PUSCH transmissions are transmitted using multiple PHICHs, where the PHICH is transmitted on the same downlink component carrier as the uplink scheduling grant initiating the uplink transmission.

10.6 Uplink reference signals and channel estimation

There are two types of reference signals specified for the LTE/LTE-Advanced uplink. The uplink demodulation reference signals are used by the eNB for channel estimation and coherent demodulation of uplink physical channels (PUSCH and PUCCH). The demodulation reference signals are only transmitted in conjunction with PUSCH or PUCCH within the same bandwidth as the corresponding physical channel. Uplink demodulation reference signals are used by the eNB for channel state information (CSI) estimation, and to support uplink channel-dependent scheduling and link adaptation. The demodulation reference signals can also be used in cases when uplink transmission is needed, although there is no data to transmit. An example would be to enable the network to adjust uplink frame timing via an uplink timing alignment procedure. The uplink demodulation reference signals can also be used to estimate the downlink CSI from uplink transmission, when sufficient uplink/downlink reciprocity exists.

Since maintaining low CM value and PA efficiency for uplink transmissions is very important, the requirements for design of uplink reference signals are different compared to those in the downlink. In principle, transmitting reference signals together with other uplink transmissions from the same terminal is not efficient for the uplink. Instead, certain SC-FDMA symbols are exclusively designated for DM-RS transmission. Therefore, the reference signals are time-multiplexed with other uplink transmissions from the same terminal. The structure of the reference signal per se ensures a low CM value over the reference symbols. In the case of PUSCH transmission, a DM-RS is transmitted over the fourth SC-FDMA symbol of each uplink slot. In the case of PUCCH transmission, the number of SC-FDMA symbols used for a reference signal in a slot, as well as the exact position of these symbols, differs among different PUCCH formats [16].

In general, there is no advantage in estimating the channel outside the frequency band of the corresponding PUSCH or PUCCH transmission that is going to be coherently demodulated. The bandwidth of the reference signal corresponding to the length of the reference signal sequence is equal to the bandwidth of the corresponding PUSCH or PUCCH transmission measured in the number of subcarriers. The latter requirement suggests that, for PUSCH transmission, it should be possible to generate reference signal sequences of different length corresponding to the possible bandwidths of PUSCH transmission. However, it must be noted that the length of the reference signal sequence must be a multiple of 12

Petitioners' Exhibit 1021
Nokia of America Corp., et al. v. KT Corporation, et al.
Case No. IPR2025-00036; U.S. Patent No. 11,627,631
Page 762 of 1122

(i.e., the size of a basic PRB), since uplink resource allocations for PUSCH transmissions are always measured in terms of the number of resource blocks. The PUCCH transmission from a terminal is always carried out over a single resource block in the frequency-domain. In the case of PUCCH transmission, the length of the reference signal sequence is equal to 12. The uplink reference signals should preferably have the following properties [121]:

- Limited power variation in the frequency-domain to allow similar channel estimation quality for all frequencies, or constant amplitude in the frequency-domain for equal excitation of all the allocated sub-carriers for unbiased channel estimates.
- Low CM value, no worse than data transmissions, in the time-domain. Note that a lower CM value for reference signals relative to the data would allow power boosting of the reference signals at the cell-edge.
- Good autocorrelation property for accurate channel estimation.
- Good cross-correlation property to reduce interference among different reference signals transmitted on the same resources by neighboring cells.

We will discuss how the above requirements have been addressed in the design of the LTE/LTE-Advanced uplink reference signals.

10.6.1 Uplink demodulation reference signals

The uplink DM-RS design in LTE Rel-8 is based on extended Zadoff−Chu sequences. This choice is because of the low PAPR property of these sequences, as well as the possibility of using mechanisms for orthogonalizing multiple DM-RS sequences which are utilized in spatial multiplexing schemes. The use of different cyclic shifts of a root Zadoff−Chu sequence in the time-domain allows multiple users to transmit their (orthogonally code-division multiplexed) DM-RS to the same eNB provided that the reference signals are transmitted in the same set of resource blocks [121].

In LTE-Advanced, SU-MIMO with up to four-layer spatial multiplexing is supported in the uplink. While the uplink DM-RS corresponding to different layers can be theoretically orthogonalized via assigning different cyclic shifts to each layer, the orthogonality property of the cyclically shifted sequences may not hold in high-delay-spread scenarios. Furthermore, the orthogonality of the cyclically shifted sequences is guaranteed only when the root Zadoff−Chu sequences have identical waveform and length, which implies that the time−frequency resource allocation of MU-MIMO UEs should be identical. The uplink DM-RS in LTE-Advanced are designed to overcome these drawbacks, while maintaining backward compatibility.

In LTE/LTE-Advanced, two SC-FDMA symbols (one DM-RS per slot) are configured for DM-RS in a subframe within the allocated time−frequency resources as shown in Figure 10.19 for PUSCH transmission. Each uplink demodulation reference signal sequence $r_{uv}(k, \tau)$ associated with PUSCH transmission is defined by the time-domain cyclic shift $\tau(\lambda)$ of the base sequence $r_{uv}(k)$ according to

Petitioners' Exhibit 1021
Nokia of America Corp., et al. v. KT Corporation, et al.
Case No. IPR2025-00036; U.S. Patent No. 11,627,631
Page 763 of 1122

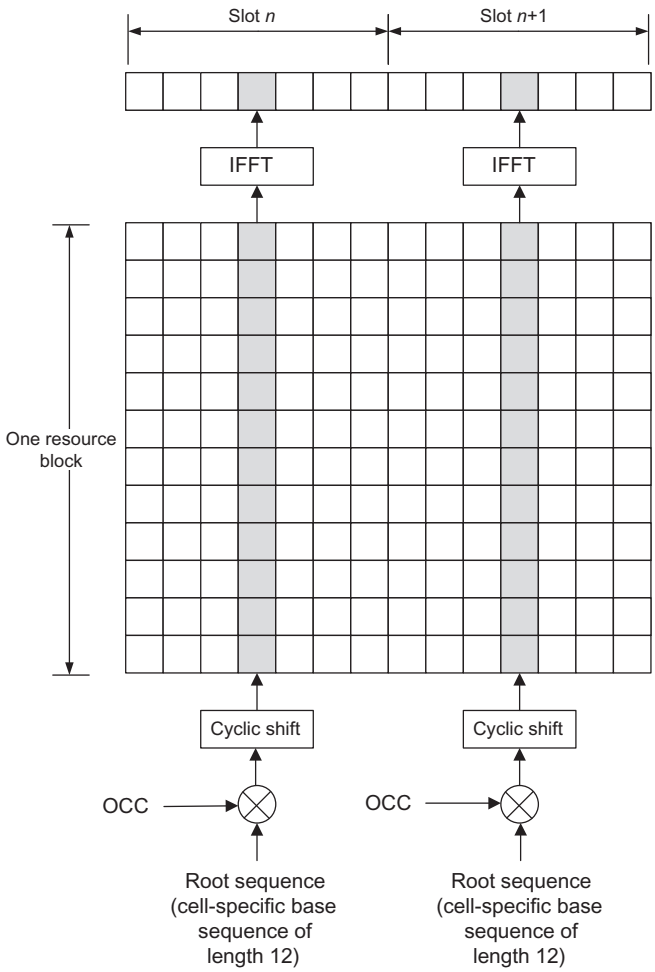


FIGURE 10.19

Uplink DM-RS generation and structure in time and frequency [121,14].

$r_{uv}(mL_{RS}+k,\tau)=w_m(\lambda)e^{j\tau(\lambda)k}\ r_{uv}(k)|0\le k<L_{RS}-1, m=0,1,$ where $L_{RS}=12m'$ (i.e., the length of the reference signal is an integer multiple of the basic resource-block size in frequency) is the length of the reference signal sequence, $1\le m'\le \max(N_{RB}^{UL})$, and $\lambda\in\{0,1,\ldots,N_l-1\}$ denotes the spatial layer index. Using the latter expression, multiple reference signal sequences can be generated from a single base sequence through different values of cyclic shift $\tau(\lambda)$ [3].

The base sequences $r_{uv}(k)$ are divided into groups where the index $u\in\{0,1,\ldots,29\}$ represents the group number and v is the base sequence number within the group, such that each group contains one base sequence $v=0$ for each

Petitioners' Exhibit 1021
Nokia of America Corp., et al. v. KT Corporation, et al.
Case No. IPR2025-00036; U.S. Patent No. 11,627,631
Page 764 of 1122

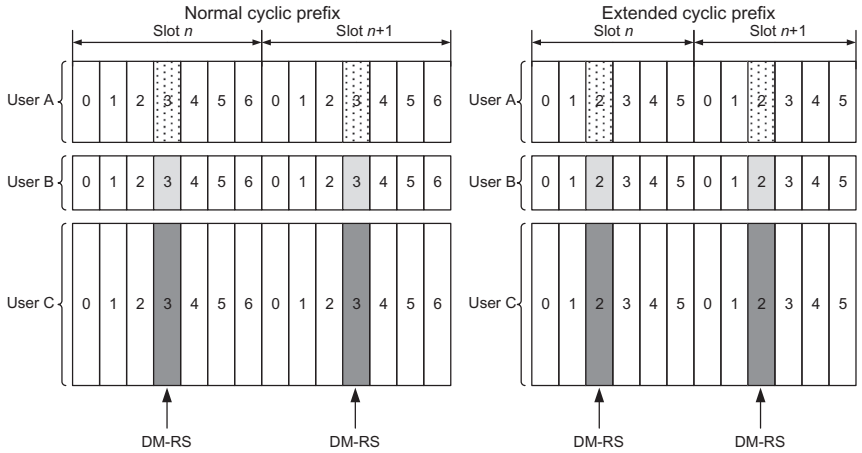


FIGURE 10.20

PUSCH DM-RS location in time and frequency [155].

length $L_{RS} = 12m' | 1 \leq m' \leq 5$ and two base sequences denoted by $v \in \{0, 1\}$ of each length $L_{RS} = 12m' | 6 \leq m' \leq \max(N_{RB}^{UL})$. The sequence-group number u and the index v within the group may vary across time. The definition of the base sequence $\{r_{uv}(0), r_{uv}(1), \ldots, r_{uv}(L_{RS} - 1)\}$ depends on the sequence length L_{RS} (Figure 10.21).

The time-domain cyclic shift (post IFFT in the OFDM modulation) can be interpreted as a phase rotation in the frequency-domain (pre-IFFT in the OFDM modulation). For frequency non-selective channels over 12 sub-carriers constituting a resource block, it is possible to achieve orthogonality among DM-RSs generated from the same base sequence, if $\tau(\lambda) = \frac{k\pi}{6}, k = 0, 1, \ldots, 11$, assuming the DM-RSs are synchronized in time. The orthogonality can be exploited to transmit DM-RS at the same time, using the same frequency resources without interference. In general, DM-RS generated from different base sequences will not be orthogonal; however, they will present low cross-correlation properties. To maximize the number of available Zadoff−Chu sequences, a prime length sequence is needed. The minimum sequence length in the uplink is 12 (i.e., the number of sub-carriers in a resource block), which is not prime number. Therefore, Zadoff−Chu sequences are not suitable by themselves; thus, there are effectively two types of base reference sequences: (1) those with a sequence length larger than 36 sub-carriers (spanning three or more resource blocks), which use a cyclic extension of Zadoff−Chu sequences; and (2) those with a sequence length less than 36 sub-carriers (spanning one or two resource blocks where the latter use a special QPSK sequence $(r_{uv}(k) = e^{j\phi(k)\pi/4}, \quad 0 \leq k \leq L_{RS} - 1)$ [3].

For sequences of length three resource blocks and larger, the base sequence is a repetition, with a cyclic offset, of a Zadoff−Chu sequence of length N_{ZC}^{RS}, where

N_{ZC}^{RS} is the largest prime number that satisfies the condition $N_{ZC}^{RS} < L_{RS}$. Therefore, the base sequence will contain one complete length N_{ZC}^{RS} Zadoff−Chu sequence plus a fractional repetition appended on the end. At the receiver, the appropriate de-repetition can be done and the zero autocorrelation property will hold across the length N_{ZC}^{RS} vector. For sequences shorter than three resource blocks, the sequences are a composition of unity modulus complex numbers derived from computer simulation, and are defined in the LTE specifications [3].

There are a total of 30 sequence groups, each containing one sequence with length shorter than 60 sub-carriers. This corresponds to transmission bandwidths of 1, 2, 3, 4, and 5 resource blocks. Additionally, there are two sequences (one for $v = 0$ or 1) with length greater than 72 sub-carriers corresponding to transmission bandwidths of six resource blocks or more. Note that not all values of m' are allowed, where m' is the number of resource blocks used for transmission of the PUSCH DM-RS. Only values which are the product of powers of 2, 3, and 5 are valid, i.e., $m' = 2^{\alpha_1}3^{\alpha_2}5^{\alpha_3}$ and $\alpha_1, \alpha_2,$ and α_3 are non-negative integers. This is due to the fact that the DFT sizes of the SC-FDMA precoding operation are limited to values which are the product of powers of 2, 3, and 5. The DFT operation can span more than one resource block. Since each resource block has 12 sub-carriers, the total number of sub-carriers fed to the DFT will be equal to $12m'$. Given that the value of $12m'$ has to be a product of powers of 2, 3, and 5, this implies that the number of resource blocks must themselves be the product of powers of 2, 3, and 5. Therefore, values of m' such as 7, 11, 14, or 19 are not valid [16].

For a given time slot, the uplink reference signal sequences to use within a cell are taken from a specific sequence group. If the same group is used for all slots, then this is known as fixed assignment. On the other hand, if the group number u varies for all slots within a cell, this is known as group hopping. The cell system information determines which method to use, and the group assignment depends on the type of physical channel (PUSCH or PUCCH). The PUSCH demodulation reference signal is mapped to the fourth SC-FDMA symbol of the slot for a normal cyclic prefix and to every third SC-FDMA slot for an extended cyclic prefix, as shown in Figure 10.20.

The LTE Rel-10 uses codebook-based precoding for uplink SU-MIMO data transmissions, and obviously the same precoding mechanism is applied to the uplink DM-RS. As such, a receiver can directly estimate the spatially precoded channel. Note that the uplink DM-RSs are distributed in the same manner as data when clustered SC-FDMA is used. An eNB can choose root Zadoff−Chu sequences for the reference signal by considering the autocorrelations and cross-correlations of the sequences that are in use among neighboring eNBs. However, such coordination is not always practically feasible for cellular operators. Hence, a root Zadoff−Chu sequence randomization mechanism, referred to as sequence hopping and sequence-group hopping, is available depending on each operator's choice, where the root Zadoff−Chu sequence varies in every slot, if sequence-group hopping is enabled. The spreading factor $w(\lambda_i) = \pm 1 | i = 0, 1, 2, 3$ is an

Petitioners' Exhibit 1021
Nokia of America Corp., et al. v. KT Corporation, et al.
Case No. IPR2025-00036; U.S. Patent No. 11,627,631
Page 766 of 1122

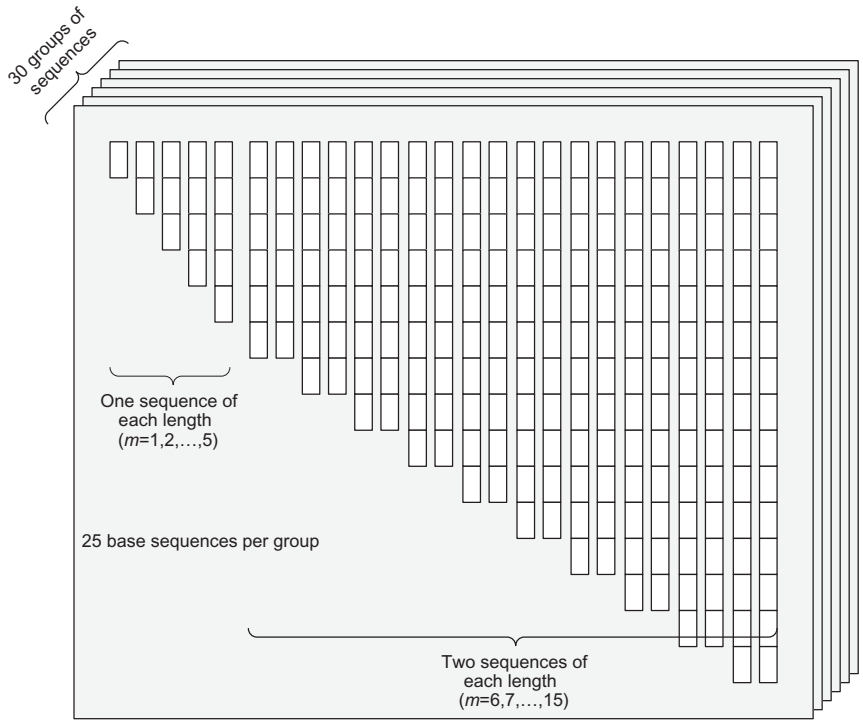


FIGURE 10.21

Illustration of base sequence grouping used for PUCCH/PUSCH DM-RS in 3 MHz [14].

orthogonal cover code (OCC), which is used to spread the reference signal sequence over two SC-FDMA symbols. The introduction of OCC was motivated in order to efficiently support SU-MIMO and MU-MIMO operation in the uplink (see Figure 10.19).

For $L_{RS} \geq 36$, the base sequence $\{r_{uv}(0), r_{uv}(1), \ldots, r_{uv}(L_{RS}-1)\}$ is given by $r_{uv}(k) = x_l(k \bmod N_{ZC}^{RS}) \mid \quad 0 \leq k < L_{RS} - 1$, where the lth-root Zadoff−Chu sequence is defined by the following expression [3]:

$$x_l(m) = -\exp\left(j\frac{\pi l m(m+1)}{N_{ZC}^{RS}}\right), \quad 0 \leq m \leq N_{ZC}^{RS}-1, \quad l = \lfloor l' + 0.5 \rfloor + (-1)^{\lfloor 2l' \rfloor} v, \quad l' = N_{ZC}^{RS}(u+1)/31 \tag{10.3}$$

The length N_{ZC}^{RS} of the Zadoff−Chu sequence is given by the largest prime number such that $N_{ZC}^{RS} < L_{RS}$. The sequence-group number u in slot n_s is defined by a group hopping pattern $f_{\text{group-hopping}}(n_s)$ and a sequence-shift pattern $f_{\text{shift-pattern}}$ according to $u = [f_{\text{group-hopping}}(n_s) + f_{\text{shift-pattern}}] \bmod 30$. There are 17 different

hopping patterns and 30 different sequence-shift patterns. Sequence-group hopping can be enabled or disabled through a cell-specific parameter signaled by higher layers (see Figure 10.20) [3].

The DM-RS group hopping pattern is defined as $f_{\text{group-hopping}}(n_s) = \left[\sum_{i=0}^{7} c(8n_s + i)2^i\right] \bmod 30$ when group hopping is enabled and is set to zero, otherwise, which is the same for PUSCH and PUCCH. The pseudo-random sequence $c(i)$ was defined in Chapter 9 and is initialized with $c_{\text{init}} = \lfloor N_{\text{ID}}^{\text{RS}}/30 \rfloor$ at the beginning of each radio frame.[3] Note that the definition of the sequence-shift pattern $f_{\text{shift-pattern}}$ is different for PUCCH and PUSCH. For PUCCH, the sequence-shift pattern is given by $f_{\text{shift-pattern}}^{\text{PUCCH}} = N_{\text{ID}}^{\text{RS}} \bmod 30$. For PUSCH, the sequence-shift pattern is given by $f_{\text{shift-pattern}}^{\text{PUSCH}} = (N_{\text{ID}}^{\text{cell}} + \Delta_{\text{ss}}) \bmod 30 \quad |\Delta_{\text{ss}} \in \{0, 1, \ldots, 29\}$ and is configured via higher-layer signaling [3], if no value for $n_{\text{ID}}^{\text{PUSCH}}$ is provided by the higher layers, or if the PUSCH transmission corresponds to a *Random Access Response* or a retransmission of the same transport block as part of the contention-based random access procedure; otherwise, it is defined as $f_{\text{ss}}^{\text{PUSCH}} = N_{\text{ID}}^{\text{RS}} \bmod 30$. The parameter Δ_{ss} is cell-specific and is broadcast in SIB2 which defines an offset between 0 and 29 that can be used to select different sequence groups for cells with the same physical cell identifier $N_{\text{ID}}^{\text{cell}}$. The concept of virtual cell identity was introduced in LTE Rel-11 to overcome the limitation of earlier releases of LTE technology in new deployment scenarios related to CoMP, HetNet, etc., where several low-power nodes or subsets of a macro-cell may share the same physical layer cell identity with the macro-cell. Sharing of the same cell identifier by the neighboring nodes would increase intra-cell interference and degrade the channel estimation performance and coherent detection of data and control channels, as well as limiting the use of advanced closed-loop SU-MIMO/MU-MIMO beamforming techniques. Also, the use of the same identifier by subordinate nodes would prevent transmission/reception node identification and switching. The use of different scrambling sequences initialized with unique cell identifiers would achieve interference randomization and help the UE to separate data and control channels transmitted by different transmission nodes. Since the reference signals (e.g., CRS, DM-RS, CSI-RS) are also scrambled with cell-specific sequences to allow the UE to conduct various channel estimations and mobility measurements on different transmission nodes, the use of unique scrambling sequences would facilitate these functions as well as node selection and switching in homogeneous and heterogeneous networks.

[3]The definition of virtual cell identity $N_{\text{ID}}^{\text{RS}}$ (a new concept in LTE Rel-11) depends on the type of uplink physical channel [3]. For transmissions on PUSCH, $N_{\text{ID}}^{\text{RS}} = N_{\text{ID}}^{\text{cell}}$, if no value for $N_{\text{ID}}^{\text{PUSCH}}$ is configured by the higher layers or if the temporary C-RNTI was used to transmit the most recent uplink-related DCI for the transport block associated with the corresponding PUSCH transmission; otherwise $N_{\text{ID}}^{\text{RS}} = N_{\text{ID}}^{\text{PUSCH}}$. For transmissions on PUCCH, the virtual cell identity $N_{\text{ID}}^{\text{RS}} = N_{\text{ID}}^{\text{cell}}$, if no value for $N_{\text{ID}}^{\text{PUCCH}}$ is configured by the higher layers; otherwise $N_{\text{ID}}^{\text{RS}} = N_{\text{ID}}^{\text{PUCCH}}$. For sounding reference signal transmission, the virtual cell identity is defined as $N_{\text{ID}}^{\text{RS}} = N_{\text{ID}}^{\text{cell}}$ [3,5].

Petitioners' Exhibit 1021
Nokia of America Corp., et al. v. KT Corporation, et al.
Case No. IPR2025-00036; U.S. Patent No. 11,627,631
Page 768 of 1122

The sequence hopping is only applied to reference signals whose length $N_{RS} \geq 72$ and the base sequence number defined as $v = c(n_s)$ within the base sequence group in slot n_s, if group hopping is disabled but sequence hopping is enabled. The pseudo-random sequence $c(i)$ was defined earlier and is initialized with $c_{init} = \lfloor N_{ID}^{RS}/30 \rfloor 2^5 + f_{shift\text{-}pattern}^{PUSCH}$ at the beginning of each radio frame. For reference signals of length $N_{RS} < 72$, the base sequence number v within the base sequence group is given by $v = 0$ [3].

The cyclic shift $\tau(\lambda)$ in slot n_s is defined as $\tau(\lambda) = \pi n_{CS}(\lambda)/6$, where $n_{CS}(\lambda) = [n_{DM\text{-}RS}^{(1)} + n_{DM\text{-}RS}^{(2)}(\lambda) + n_{PN}(n_s)] \bmod 12$. The values of parameters $n_{DM\text{-}RS}^{(1)}$ and $n_{DM\text{-}RS}^{(2)}(\lambda)$ are determined based on the value of the cyclic shift for the DM-RS field in the latest uplink grant within DCI format 0 or 4, and are given in Table 10.5. The first row of Table 10.5 can be used to obtain $n_{DM\text{-}RS}^{(2)}(0)$ and $w_m(\lambda)$, if there is no uplink-related DCI for the same transport block associated with the corresponding PUSCH transmission, and if the initial PUSCH for the same transport block is semi-persistently scheduled, or if the initial PUSCH for the same transport block is scheduled by the random-access response grant. The parameter $n_{PN}(n_s)$ is given by $n_{PN}(n_s) = \sum_{i=0}^{7} c(8N_s^{UL}n_s + i)2^i$, where the cell-specific pseudo-random sequence $c(i)$ was defined in Chapter 9. The pseudo-random sequence generator in this case is initialized with $c_{init} = \lfloor N_{ID}^{cell}/30 \rfloor 2^5 + f_{shift\text{-}pattern}^{PUSCH}$ at the beginning of each radio frame, if no value for $N_{ID}^{PUSCH\text{-}DM\text{-}RS}$ is configured by the higher layers, or if the temporary C-RNTI was used to transmit the most recent uplink-related DCI for the transport block associated with PUSCH transmission; otherwise, it is defined as $c_{init} = \left\lfloor \frac{N_{ID}^{PUSCH\text{-}DM\text{-}RS}}{30} \right\rfloor 2^5 + (N_{ID}^{PUSCH\text{-}DM\text{-}RS} \bmod 30)$ [3].

The vector of the UE-specific DM-RSs is precoded according to the following equation:

$$[\tilde{r}_{PUSCH}^{(0)}, \tilde{r}_{PUSCH}^{(1)}, \ldots, \tilde{r}_{PUSCH}^{(N_P-1)}]^T = \mathbf{W}[r_{PUSCH}^{(0)}, r_{PUSCH}^{(1)}, \ldots, r_{PUSCH}^{(N_l-1)}]^T \quad (10.4)$$

where N_P denotes the number of antenna ports used for PUSCH transmission and $\mathbf{W}$ is the precoding matrix. For PUSCH transmission using a single antenna port $N_P = 1, W = 1$, and $N_l = 1$. For spatial multiplexing $N_P = 2$ or $N_P = 4$ and the precoding matrix $\mathbf{W}$ is identical to the precoding matrix used for precoding of the PUSCH in the same subframe [3].

In uplink SU-MIMO where a UE transmits multiple spatial layers simultaneously, multiple DM-RS can be orthogonally multiplexed by assigning a different cyclic shift value for each layer. However, as mentioned earlier, the orthogonality among the sequences may not be preserved when the delay spread is high due to increased correlation among the spatial layers. To overcome this limitation, the OCCs were introduced in LTE-Advanced. As shown in Figure 10.19 and further emphasized in Table 10.5, different OCCs are applied for higher-numbered layers (i.e., $\lambda \geq 3$) and lower-numbered layers (i.e., $\lambda \geq 2$), so reference signals associated with the higher rank transmissions (i.e., $N_l \geq 3$)

Petitioners' Exhibit 1021
Nokia of America Corp., et al. v. KT Corporation, et al.
Case No. IPR2025-00036; U.S. Patent No. 11,627,631
Page 769 of 1122

Table 10.5 OCC and Cyclic Shift Parameters for Uplink DM-RS [3]

Cyclic Shift Value Carried in Uplink Grant	Layer-Dependent Cyclic Shift					Layer-Dependent Orthogonal Cover Code $(w_0(\lambda), w_1(\lambda))$			
	$n^{(1)}_{\text{DM-RS}}$	$n^{(2)}_{\text{DM-RS}}(\lambda)$							
		$\lambda = 0$	$\lambda = 1$	$\lambda = 2$	$\lambda = 3$	$\lambda = 0$	$\lambda = 1$	$\lambda = 2$	$\lambda = 3$
000	0	0	6	3	9	$[1 \quad 1]$	$[1 \quad 1]$	$[1 \quad -1]$	$[1 \quad -1]$
001	2	6	0	9	3	$[1 \quad -1]$	$[1 \quad -1]$	$[1 \quad 1]$	$[1 \quad 1]$
010	3	3	9	6	0	$[1 \quad -1]$	$[1 \quad -1]$	$[1 \quad 1]$	$[1 \quad 1]$
011	4	4	10	7	1	$[1 \quad 1]$	$[1 \quad 1]$	$[1 \quad 1]$	$[1 \quad 1]$
100	6	2	8	5	11	$[1 \quad 1]$	$[1 \quad 1]$	$[1 \quad 1]$	$[1 \quad 1]$
101	8	8	2	11	5	$[1 \quad -1]$	$[1 \quad -1]$	$[1 \quad -1]$	$[1 \quad -1]$
110	9	10	4	1	7	$[1 \quad -1]$	$[1 \quad -1]$	$[1 \quad -1]$	$[1 \quad -1]$
111	10	9	3	0	6	$[1 \quad 1]$	$[1 \quad 1]$	$[1 \quad -1]$	$[1 \quad -1]$

Petitioners' Exhibit 1021
Nokia of America Corp., et al. v. KT Corporation, et al.
Case No. IPR2025-00036; U.S. Patent No. 11,627,631
Page 770 of 1122

are still sufficiently orthogonal, even though cyclic shift separation is small. Although the orthogonality provided by the OCCs may also fall apart due to high Doppler shift, the effect is minimal because higher rank transmission is mainly used for stationary or nomadic UEs [121].

The generation of LTE Rel-8/9 DM-RS sequences (no OCC is applied) for PUSCH in each uplink slot can be summarized as follows:

1. Determine whether group hopping and sequence hopping are enabled from higher layer signaling.
2. Obtain Δ_{ss} and the cyclic shift from higher layer signaling.
3. Calculate $c_{init} = \lfloor N_{ID}^{cell}/30 \rfloor$ thus find the scrambling sequence $c(i)$.
4. Obtain $n_{DM\text{-}RS}^{(1)}, n_{DM\text{-}RS}^{(2)}(\lambda)$ from Table 10.5 given the cyclic shift value is known.
5. Calculate $f_{group\text{-}hopping}(n_s) = \left[\sum_{i=0}^{7} c(8n_s + i)2^i\right] \bmod 30$ and $v = c(n_s)$ or 0 given n_s is known.
6. Calculate $f_{shift\text{-}pattern}^{PUSCH} = (N_{ID}^{cell} + \Delta_{ss}) \bmod 30$.
7. Calculate $u = \left[f_{group\text{-}hopping}(n_s) + f_{shift\text{-}pattern}\right] \bmod 30$.
8. Calculate $n_{PN}(n_s) = \sum_{i=0}^{7} c(8N_s^{UL}n_s + i)2^i$.
9. Calculate $n_{CS}(\lambda) = \left[n_{DM\text{-}RS}^{(1)} + n_{DM\text{-}RS}^{(2)}(\lambda) + n_{PN}(n_s)\right] \bmod 12$.
10. Calculate $\tau(\lambda) = \pi n_{CS}(\lambda)/6$.
11. Calculate lth-root Zadoff−Chu sequence $x_l(m) = -\exp\left(j\frac{\pi lm(m+1)}{N_{ZC}^{RS}}\right)$ given that $0 \le m \le N_{ZC}^{RS} - 1$, $l = \lfloor l' + 0.5 \rfloor + (-1)^{\lfloor 2l' \rfloor} v, l' = N_{ZC}^{RS}(u+1)/31$ (*Note that N_{ZC}^{RS} is the largest prime number less than the size of PUSCH allocation or L_{RS}*).
12. Calculate $r_{uv}(mL_{RS} + k, \tau) = e^{j\tau(\lambda)k} r_{uv}(k) | 0 \le k < L_{RS} - 1, m = 0, 1$.

The MU-MIMO schemes can be categorized into two classes from a DM-RS orthogonality perspective, i.e., identical-band MU-MIMO and non-identical-band MU-MIMO [121]. Identical-band MU-MIMO is a scheme in which the frequency band allocations for MU-MIMO-capable UEs are identical and the DM-RS orthogonality can be achieved by assigning different cyclic shifts. Although this scheme is LTE Rel-8/9 compatible and can be used for multiplexing LTE Rel-8/9 and Rel-10 UEs, the scheduling restriction may adversely impact the uplink system throughput. Non-identical-band MU-MIMO is a scheme in which the frequency band allocations for MU-MIMO UEs are not identical. Although this improves frequency scheduling flexibility and may improve the uplink system throughput, it implies that the DM-RS root Zadoff−Chu sequences for the two slots of a subframe should be the same in order to utilize the OCCs. Therefore, the OCCs can be used to realize non-identical-band MU-MIMO [121].

10.6.2 Sounding reference signals

The SRS are physical signals transmitted in the uplink to enable the eNB to estimate the CSI over a range of frequencies. The estimation of the CSI assists the

Petitioners' Exhibit 1021
Nokia of America Corp., et al. v. KT Corporation, et al.
Case No. IPR2025-00036; U.S. Patent No. 11,627,631
Page 771 of 1122

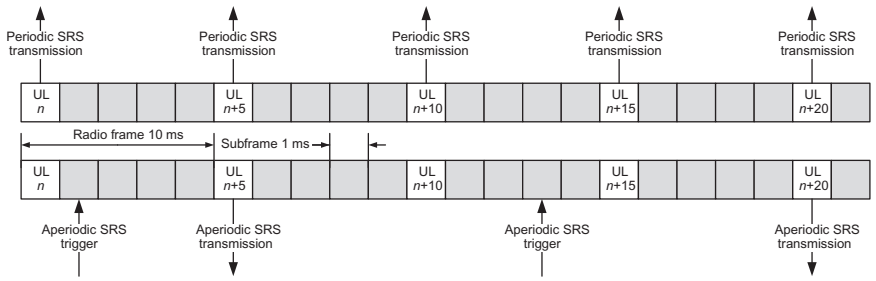


FIGURE 10.22

Illustration of periodic and aperiodic SRS transmission [121].

eNB scheduler to properly allocate radio resources to the UE, and to select different transmission parameters such as the instantaneous data rate and uplink multi-antenna transmission parameters for optimized uplink transmission (i.e., uplink channel-dependent scheduling). The SRS transmission can be further used for uplink timing estimation as well as to estimate downlink channel conditions assuming downlink/uplink channel reciprocity. When uplink/downlink channel reciprocity is assumed, SRS measurements can also be used to support downlink transmissions such as angle-of-arrival (AoA) measurements on SRS to support downlink beamforming [14]. Therefore, SRS is not necessarily transmitted together with an uplink physical channel and when transmitted in conjunction with PUSCH, the SRS may cover a different and typically larger frequency region. There are two types of SRS specified for uplink transmission, i.e., periodic and aperiodic SRS (Figure 10.22).

The subframe in which SRS is transmitted by any UE within the cell is signaled via cell-specific broadcast signaling. A 4-bit cell-specific parameter indicates 15 possible sets of subframes in which SRS may be transmitted within each radio frame. This configurability provides sufficient flexibility in adjusting the SRS overhead depending on the deployment scenario. The 16th configuration switches the SRS off in the cell, which may be appropriate for a cell serving primarily high-speed UEs. The SRS transmissions are always in the last SC-FDMA symbol in the configured subframes. The SRS and DM-RS are located in different SC-FDMA symbols. The PUSCH data transmission is not permitted on the SC-FDMA symbol designated for SRS, resulting in a worst-case sounding signal overhead of around 7% with the SRS symbol in every subframe.

The eNB may either request an individual SRS transmission from a UE, or configure a UE to transmit SRS periodically until it is no longer necessary. A single-bit UE-specific signaling parameter indicates whether the requested SRS transmission is periodic or aperiodic. If periodic SRS transmissions are configured for a UE, the periodicity may be 2, 5, 10, 20, 40, 80, 160, or 320 ms. The SRS periodicity and SRS subframe offset within the period in which the UE should transmit its SRS are configured via a 10-bit UE-specific dedicated signaling

Petitioners' Exhibit 1021
Nokia of America Corp., et al. v. KT Corporation, et al.
Case No. IPR2025-00036; U.S. Patent No. 11,627,631
Page 772 of 1122

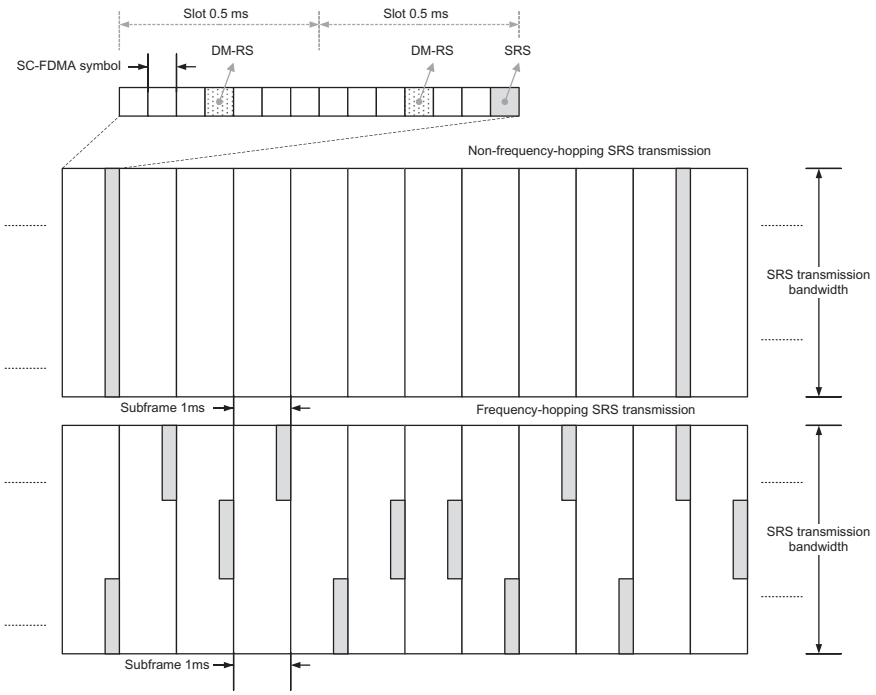


FIGURE 10.23

Non-frequency-hopping (wideband) versus frequency-hopping (sub-band) SRS [16].

parameter. There are differences between cell-specific SRS (signaled via cell-specific broadcast signaling) and UE-specific SRS (signaled via UE-specific dedicated signaling) configuration parameters, and their method of signaling to the UE noted in the forthcoming discussions.

The periodic SRS is based on the extended Zadoff−Chu sequence and is periodically transmitted in the last SC-FDMA symbol of an uplink subframe, as shown in Figure 10.23. As the example in Figure 10.23 shows, the SRS transmitted by the UEs are multiplexed in the time- and frequency-domain through configuring SRS periodicity T_{SRS}, frequency comb pattern, and SRS bandwidth. Similar to DM-RS, up to eight orthogonal SRS transmissions can be code-division multiplexed over a frequency region using different cyclic shifts of the root Zadoff−Chu sequence. The periodic nature of the LTE Rel-8 SRS transmission was not sufficiently flexible to support sounding from an increased number of UE antennas and/or an increased number of UEs, due to use of semi-static RRC signaling for UE configuration. As a result, aperiodic SRS transmission was introduced in LTE Rel-10 to complement periodic SRS transmission, where the eNB dynamically schedules a UE for SRS transmission on demand

Petitioners' Exhibit 1021
Nokia of America Corp., et al. v. KT Corporation, et al.
Case No. IPR2025-00036; U.S. Patent No. 11,627,631
Page 773 of 1122

(see Figure 10.22). Therefore, the SRS resources are not tied to a single UE until RRC (re)configuration by the eNB. This mechanism allows efficient management of a fixed set of time/frequency/code SRS resources for a larger number of UEs.

Periodic and aperiodic SRS transmission share a common set of cell-specific SRS resources (subframe configuration period, subframe offset, and maximum SRS bandwidth). Different sets of UE-specific sounding parameters are independently allocated for periodic and aperiodic SRS transmission including transmission bandwidth, periodicity, frequency comb pattern, and cyclic shift. The UE is configured with a fixed set of subframes in which it may be scheduled for aperiodic SRS transmission. This reduces the eNB scheduling complexity, because in any subframe only a subset of UEs are scheduled for aperiodic SRS transmission. An example of periodic and aperiodic SRS transmission timing is shown in Figure 10.22 for comparison, where periodic and aperiodic SRS have the same subframe offset and $T_{\mathrm{SRS}_{\mathrm{Periodic}}} = 5$ ms. An aperiodic SRS transmission occurs in subframe $n + k$ corresponding to a trigger in subframe n, where $k \geq 4$, corresponding to a 4 ms delay constraint which is meant to maintain the minimum timing response similar to a normal downlink assignment or uplink grant.

To minimize the downlink signaling overhead, a semi-static configuration of aperiodic SRS parameters similar to that of periodic SRS was adopted in LTE Rel-8. Furthermore, the aperiodic SRS-related signaling bits are piggybacked in either a downlink assignment (scheduling downlink data transmission) or an uplink grant (scheduling uplink data transmission), in order to reduce signaling overhead. Since the aperiodic SRS is primarily used to support multi-antenna sounding, further configuration flexibility can be achieved by forming three independent sets of parameters that can be selected via a 2-bit SRS field in the uplink grant, scheduling uplink SU-MIMO data transmission. For an uplink single-antenna transmission, a single-bit aperiodic SRS field in the uplink grant is used [14,16].

There are only a few subframes in which the eNB can send an aperiodic SRS trigger, in order to satisfy the timing constraint ($k \geq 4$) for a specific aperiodic SRS transmission opportunity. The latter scheduling constraint has some impacts on some TDD frame configurations, where only a few uplink subframes are available in a radio frame. Therefore, to increase the scheduling opportunities for aperiodic SRS, LTE Rel-10 specifies a single-bit aperiodic SRS control field in some downlink assignments. Note that the uplink sounding can be used to support downlink beamforming by exploiting channel reciprocity in TDD systems.

To ensure that there is no timing mismatch between CSI estimates from multiple antennas, the UE is configured to simultaneously transmit SRS from all configured antenna ports. The orthogonality of the cyclic shifts falls apart as the frequency selectivity of the channel increases. This degradation is more pronounced as the number of antenna ports increases. Therefore, for both periodic and aperiodic SRS, a combination of the frequency comb (i.e., a multiplexing/interlacing pattern in frequency-domain) and cyclic shift can be used to multiplex the SRS sequences corresponding to four antenna ports in large delay-spread channels, while for low delay-spread channels or when the UE is equipped with

Petitioners' Exhibit 1021
Nokia of America Corp., et al. v. KT Corporation, et al.
Case No. IPR2025-00036; U.S. Patent No. 11,627,631
Page 774 of 1122

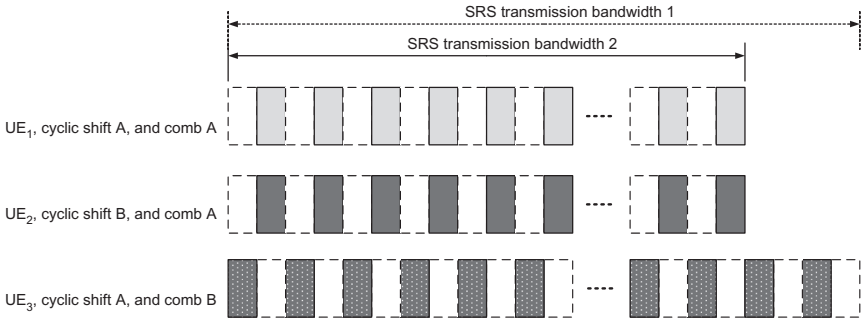


FIGURE 10.24

Multiplexing SRS transmission from different UEs [16].

two antenna ports, only different cyclic shifts are exploited to multiplex the SRS (as shown in Figure 10.24). The cyclic shifts and comb values for all antenna ports are implicitly derived from the values in each of the semi-statically configured parameter sets.

A UE transmits SRS in the serving-cell SRS resources using one of the following (UE-specific) trigger types [5]:

- Trigger type 0 via higher layer signaling.
- Trigger type 1 via DCI format 0/4/1A for FDD and TDD, and DCI format 2B/2C for TDD.

A UE may be configured with SRS parameters for trigger types 0 and 1 in each serving cell. The following SRS parameters are serving-cell specific and semi-statically configurable by higher layers for trigger type 0 and for trigger type 1 [5]:

- Transmission comb for trigger type 0 and each configuration of trigger type 1.
- Starting PRB assignment for trigger type 0 and each configuration of trigger type 1.
- Duration for trigger type 0, i.e., single or indefinite (until disabled).
- SRS configuration index I_{SRS}, SRS periodicity T_{SRS}, and SRS subframe offset $T_{\text{SRS-offset}}$ for trigger type 0 and trigger type 1.
- SRS bandwidth for trigger type 0 and each configuration of trigger type 1.
- Frequency hopping bandwidth for trigger type 0.
- Cyclic shift for trigger type 0 and each configuration of trigger type 1.
- Number of antenna ports for trigger type 0 and each configuration of trigger type 1.

A UE may be configured to transmit SRS on N_p antenna ports of a serving cell where N_p may be configured via higher layer signaling. For PUSCH transmission mode 1, $N_p \in \{0, 1, 2, 4\}$ and for PUSCH transmission mode 2, $N_p \in \{0, 1, 2\}$

when two antenna ports are configured for PUSCH and $N_p \in \{0, 1, 4\}$ when four antenna ports configured for PUSCH.

A UE may be configured for SRS transmission on multiple antenna ports of a serving cell within one SC-FDMA symbol of the same subframe. The SRS transmission bandwidth and starting PRB assignment are the same for all the configured antenna ports of a given serving cell [5]. The UE-specific parameters for SRS trigger type 0 in a serving cell, i.e., periodicity T_{SRS} and subframe offset $T_{\text{SRS-offset}}$ are defined in Table 10.6 for FDD and TDD modes. An example of SRS parameter configuration for an FDD system is shown in Figure 10.25 for better understanding of the effect of each SRS parameter on the SRS transmission. The periodicity of SRS transmission, in number of subframes, is serving-cell specific and is selected from the set $T_{\text{SRS}} \in \{2, 5, 10, 20, 40, 80, 160, 320\}$. For the SRS periodicity value of $T_{\text{SRS}} = 2$ ms in TDD, two SRS resources are configured in half-frame containing uplink subframes. The UE-specific parameters for SRS trigger type 1 in a serving cell, i.e., periodicity T_{SRS} and subframe offset $T_{\text{SRS-offset}}$, are given in Table 10.6 for FDD and TDD modes. The periodicity of the SRS transmission, in number of subframes, is serving-cell specific and is selected from the set $T_{\text{SRS}} \in \{2, 5, 10\}$. For the SRS periodicity value of $T_{\text{SRS}} = 2$ ms in TDD, two SRS resources are configured in a half-frame containing UL subframes in a serving cell [5].

The cell-specific SRS subframe configuration period T_{SFC} and the cell-specific subframe offset Δ_{SFC} for the transmission of SRS are listed in Table 10.7, for frame structure types 1 and 2, where the SRS subframe configuration parameter is provided by the higher layers. The sounding reference signal is transmitted in subframes whose numbers satisfy $\lfloor n_s/2 \rfloor \bmod T_{\text{SFC}} \in \{\Delta_{\text{SFC}}\}$. For frame structure type 2, SRS is transmitted only in configured uplink subframes or UpPTS portion of the special subframe. Note that the cell-specific SRS parameters $(T_{\text{SFC}}, \Delta_{\text{SFC}})$ and UE-specific SRS parameters $(T_{\text{SRS}}, T_{\text{SRS-offset}})$ are not identical.

The SRS sequence is defined by $r_{\text{SRS}}(n, \overline{p}) = r_{\text{uv}}(n, \tau_{\overline{p}})$, where $r_{\text{uv}}(n, \tau_{\overline{p}})$ is a cyclically shifted Zadoff−Chu sequence defined in the previous section, u is the PUCCH sequence-group number, and v is the base sequence number. The antenna-dependent cyclic shift $\tau_{\overline{p}}$ of the SRS is given as $\tau_{\overline{p}} = \frac{\pi}{4}(n_{\text{SRS}} + \frac{8\overline{p}}{N_p}) \bmod 8|_{\overline{p} \in \{0, 1, \ldots, N_p - 1\}}$, where $n_{\text{SRS}} = \{0, 1, 2, 3, 4, 5, 6, 7\}$, is configured separately for periodic and each configuration of aperiodic sounding by the higher-layer signaling for each UE, $\overline{p}$ is sequential numbering of the antenna ports, and N_p is the number of antenna ports used for SRS transmission.

The SRS sequence is scaled with scaling factor β_{SRS} in order to conform to the transmit power P_{SRS} and is then mapped sequentially starting with $r_{\text{SRS}}(0, \overline{p})$ to resource elements (k, l) on antenna port $\overline{p}$ such that $a_{[2k' + k_0(\overline{p})]l} = \frac{1}{\sqrt{N_p}} \beta_{\text{SRS}} r_{\text{SRS}}(k', \overline{p})|_{k' = 0, 1, \ldots, N_{\text{SRS}} - 1}$, where N_p is the number of antenna ports used for SRS transmission and the relation between the index $\overline{p}$ and the antenna port p is described in 3GPP TS 36.211 [3]. The set of antenna ports used for SRS transmission is configured independently for periodic and each configuration of aperiodic sounding. The quantity $k_0(p)$ is the frequency-domain starting position

Table 10.6 UE-Specific SRS Periodicity and Subframe Offset for SRS Trigger Types 0 and 1 [5]

SRS Trigger Type	SRS Configuration Index I_{SRS}	SRS Periodicity T_{SRS} (ms)	SRS Subframe Offset $T_{SRS\text{-}offset}$
	FDD		
0	0–1	2	I_{SRS}
	2–6	5	$I_{SRS} - 2$
	7–16	10	$I_{SRS} - 7$
	17–36	20	$I_{SRS} - 17$
	37–76	40	$I_{SRS} - 37$
	77–156	80	$I_{SRS} - 77$
	157–316	160	$I_{SRS} - 157$
	317–636	320	$I_{SRS} - 317$
	637–1023	Reserved	Reserved
	TDD		
	0	2	0, 1
	1	2	0, 2
	2	2	1, 2
	3	2	0, 3
	4	2	1, 3
	5	2	0, 4
	6	2	1, 4
	7	2	2, 3
	8	2	2, 4
	9	2	3, 4
	10–14	5	$I_{SRS} - 10$
	15–24	10	$I_{SRS} - 15$
	25–44	20	$I_{SRS} - 25$
	45–84	40	$I_{SRS} - 45$
	85–164	80	$I_{SRS} - 85$
	165–324	160	$I_{SRS} - 165$
	325–644	320	$I_{SRS} - 325$
	645–1023	Reserved	Reserved
1	FDD		
	0–1	2	I_{SRS}
	2–6	5	$I_{SRS} - 2$
	7–16	10	$I_{SRS} - 7$
	17–31	Reserved	Reserved
	TDD		
	0	2	0, 1
	1	2	0, 2
	2	2	1, 2

(*Continued*)

Petitioners' Exhibit 1021
Nokia of America Corp., et al. v. KT Corporation, et al.
Case No. IPR2025-00036; U.S. Patent No. 11,627,631
Page 777 of 1122

Table 10.6 (Continued)

SRS Trigger Type	SRS Configuration Index I_{SRS}	SRS Periodicity T_{SRS} (ms)	SRS Subframe Offset $T_{SRS\text{-}offset}$
	FDD		
	3	2	0, 3
	4	2	1, 3
	5	2	0, 4
	6	2	1, 4
	7	2	2, 3
	8	2	2, 4
	9	2	3, 4
	10–14	5	$I_{SRS} - 10$
	15–24	10	$I_{SRS} - 15$
	25–31	Reserved	Reserved

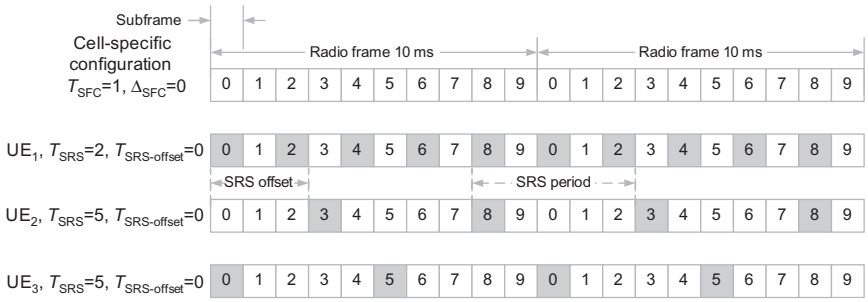


FIGURE 10.25

SRS parameter configuration example (frame structure type 1) [14].

of the SRS, and $N_{SRS}(B_{SRS}) = 6m_{SRS}(B_{SRS})$ is the bandwidth-dependent length of the SRS sequence (see Table 10.8 for the permissible values). The cell-specific SRS bandwidth configuration $C_{SRS} \in \{0, 1, 2, 3, 4, 5, 6, 7\}$ and the UE-specific SRS bandwidth $B_{SRS} \in \{0, 1, 2, 3\}$ are signaled to the UE via higher layers.

10.7 Uplink physical channel processing

The uplink multiple access scheme (SC-FDMA) in LTE employs separate physical channels for transmission of data and control signaling. The structure of the uplink physical channels is designed to make efficient use of the available time–frequency resources, and to effectively support multiplexing between data and control signaling. LTE Rel-8/9 utilizes few uplink multiple antenna techniques,

Petitioners' Exhibit 1021
Nokia of America Corp., et al. v. KT Corporation, et al.
Case No. IPR2025-00036; U.S. Patent No. 11,627,631
Page 778 of 1122

Table 10.7 Cell-Specific SRS Parameters for Frame Structure Type 1 and Type 2 [3]

SRS Subframe Configuration	Frame Structure Type 1		Frame Structure Type 2	
	Configuration Period T_{SFC}(ms)	Transmission Offset Δ_{SFC}(ms)	Configuration Period T_{SFC}(Subframes)	Transmission Offset Δ_{SFC}(ms)
0	1	{0}	5	{1}
1	2	{0}	5	{1,2}
2	2	{1}	5	{1,3}
3	5	{0}	5	{1,4}
4	5	{1}	5	{1,2,3}
5	5	{2}	5	{1,2,4}
6	5	{3}	5	{1,3,4}
7	5	{0,1}	5	{1,2,3,4}
8	5	{2,3}	10	{1,2,6}
9	10	{0}	10	{1,3,6}
10	10	{1}	10	{1,6,7}
11	10	{2}	10	{1,2,6,8}
12	10	{3}	10	{1,3,6,9}
13	10	{0,1,2,3,4,6,8}	10	{1,4,6,7}
14	10	{0,1,2,3,4,5,6,8}	Reserved	Reserved
15	Reserved	Reserved	Reserved	Reserved

Petitioners' Exhibit 1021
Nokia of America Corp., et al. v. KT Corporation, et al.
Case No. IPR2025-00036; U.S. Patent No. 11,627,631
Page 779 of 1122

Table 10.8 SRS Bandwidth Configuration Parameters [3]

SRS Bandwidth Configuration C_{SRS}	Uplink Bandwidth N_{RB}^{UL}	SRS-Bandwidth $B_{SRS}=0$		SRS-Bandwidth $B_{SRS}=1$		SRS-Bandwidth $B_{SRS}=2$		SRS-Bandwidth $B_{SRS}=3$	
		m_0	N_0	m_1	N_1	m_2	N_2	m_3	N_3
0	$6 \le N_{RB}^{UL} \le 40$	36	1	12	3	4	3	4	1
1		32	1	16	2	8	2	4	2
2		24	1	4	6	4	1	4	1
3		20	1	4	5	4	1	4	1
4		16	1	4	4	4	1	4	1
5		12	1	4	3	4	1	4	1
6		8	1	4	2	4	1	4	1
7		4	1	4	1	4	1	4	1
0	$40 < N_{RB}^{UL} \le 60$	48	1	24	2	12	2	4	3
1		48	1	16	3	8	2	4	2
2		40	1	20	2	4	5	4	1
3		36	1	12	3	4	3	4	1
4		32	1	16	2	8	2	4	2
5		24	1	4	6	4	1	4	1
6		20	1	4	5	4	1	4	1
7		16	1	4	4	4	1	4	1
0	$60 < N_{RB}^{UL} \le 80$	72	1	24	3	12	2	4	3
1		64	1	32	2	16	2	4	4
2		60	1	20	3	4	5	4	1
3		48	1	24	2	12	2	4	3
4		48	1	16	3	8	2	4	2
5		40	1	20	2	4	5	4	1
6		36	1	12	3	4	3	4	1
7		32	1	16	2	8	2	4	2
0	$80 < N_{RB}^{UL} \le 110$	96	1	48	2	24	2	4	6
1		96	1	32	3	16	2	4	4
2		80	1	40	2	20	2	4	5
3		72	1	24	3	12	2	4	3
4		64	1	32	2	16	2	4	4
5		60	1	20	3	4	5	4	1
6		48	1	24	2	12	2	4	3
7		48	1	16	3	8	2	4	2

Petitioners' Exhibit 1021
Nokia of America Corp., et al. v. KT Corporation, et al.
Case No. IPR2025-00036; U.S. Patent No. 11,627,631
Page 780 of 1122

including closed-loop antenna selection and a simple form of MU-MIMO. More advanced multi-antenna techniques including closed-loop spatial multiplexing for SU-MIMO and transmit diversity for control signaling were introduced in LTE Rel-10. This section describes the theoretical and implementation aspects of the procedures that are used for processing the uplink physical channels.

Figure 10.26 illustrates different phases of the physical channel processing. For uplink carrier aggregation, different component carriers are associated with separate transport channels with separate physical layer processing. Most of the uplink physical processing steps outlined in Figure 10.26 are similar to the corresponding steps in the downlink physical channel processing. The physical processing of the transport channels can be summarized as follows:

- CRC calculation and insertion per transport block: The CRC is calculated for and appended to each uplink transport block.
- Code block segmentation and code block CRC insertion: Similar to downlink, code block segmentation, including code block CRC insertion, is applied to transport blocks larger than 6144 bits.
- Channel coding: A rate 1/3 turbo code with quadratic permutation polynomial (QPP)-based interleaving is used for the uplink.
- Rate matching and HARQ functions: The physical layer part of the uplink rate-matching and HARQ functionality are essentially the same as downlink, with sub-block interleaving and insertion into a circular buffer, followed by bit selection with four redundancy versions (RVs). Note that there are some important differences between downlink and uplink HARQ protocols, such as asynchronous versus synchronous and adaptive versus non-adaptive HARQ schemes.
- Bit-level scrambling: The goal of the scrambling function in the uplink is to randomize the interference and to ensure that the processing gain provided by the channel coding can be fully utilized.
- Data modulation: QPSK, 16QAM, and 64QAM modulation schemes can be used for the uplink transport channel.
- DFT precoding: The modulation symbols form blocks of N_{DFT} symbols and are fed through a DFT module, where N_{DFT} corresponds to the number of sub-carriers assigned to transmission. The DFT precoding is done to reduce the CM of the transmitted signal. From an implementation point of view, the DFT size should be a power of 2. However, such a constraint would limit the scheduler flexibility in terms of the amount of resources that could be assigned to an uplink transmission. On the other hand, all possible DFT sizes should ideally be allowed for more flexibility. The LTE/LTE-Advanced have chosen to limit the DFT size and the size of the resource allocation to products of the integers 2, 3, and 5.
- Resource element mapping: Mapping of precoded complex-valued symbols to resource elements.
- Antenna mapping and generation of a complex-valued time-domain SC-FDMA signal for each antenna port: In the first release of LTE, only

Petitioners' Exhibit 1021
Nokia of America Corp., et al. v. KT Corporation, et al.
Case No. IPR2025-00036; U.S. Patent No. 11,627,631
Page 781 of 1122

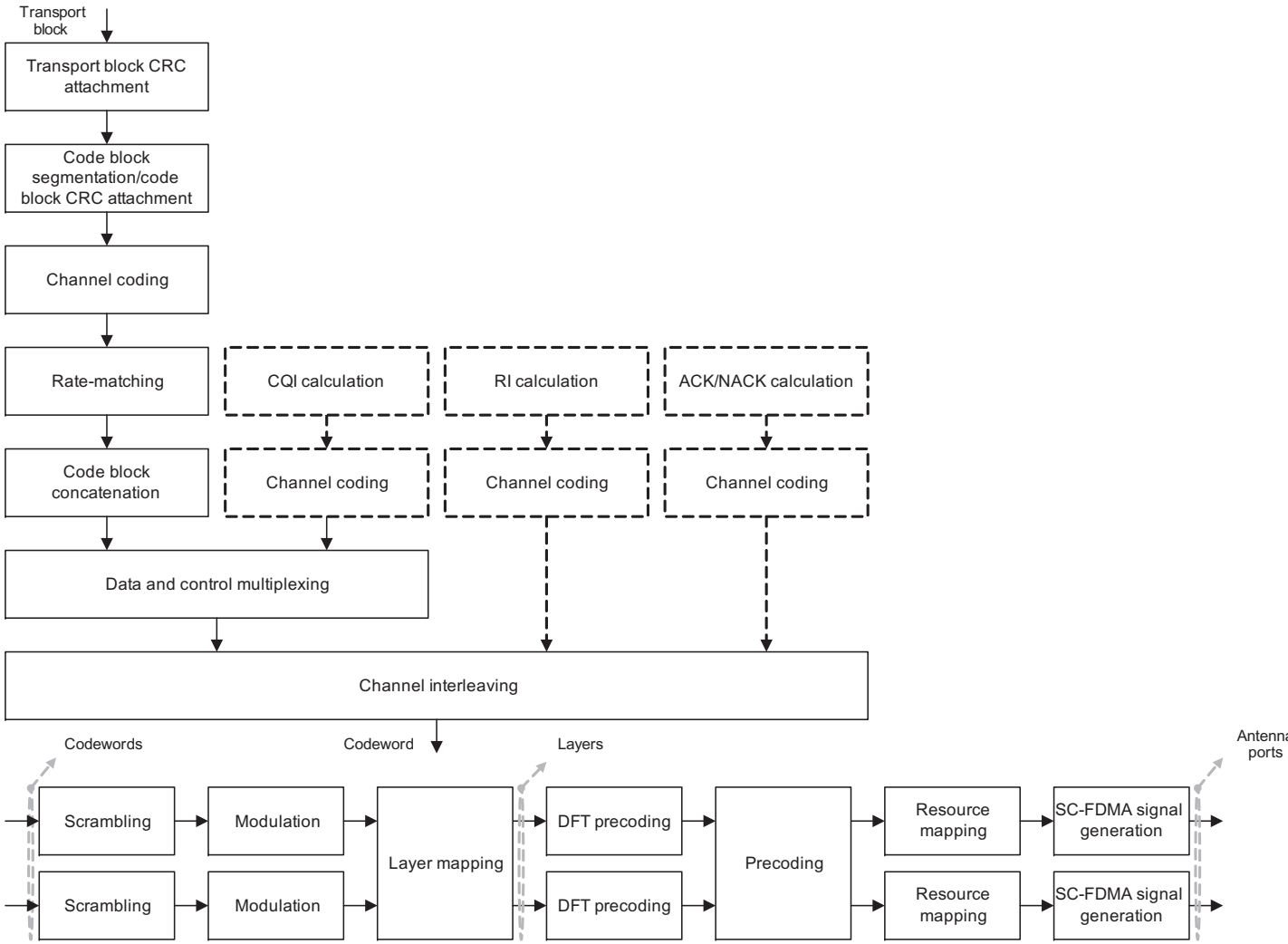


FIGURE 10.26

Uplink physical layer procedures for transport block processing [3].

single-antenna transmission was supported in the uplink. However, as part of LTE Rel-10 improvement of multi-antenna transmission, antenna precoding with up to four antennas ports is now supported in the uplink.

10.7.1 Physical uplink control channel

Uplink control signaling is typically used for the following purposes:

- Control signaling associated with user data, which is always transmitted together with uplink data and is used in the processing of that data. Examples include transport format indications, new data indicators (NDI), and MIMO parameters.
- Control signaling not associated with data is transmitted independent of any uplink data packets. Examples include HARQ ACK/NACK for downlink data packets, CQIs to support link adaptation, and MIMO feedback such as rank indicators and precoding matrix indicators for downlink transmissions, as well as scheduling requests (SRs) for uplink transmissions.

In LTE, the use of an orthogonal uplink multiple access scheme implies that the eNB controls resource allocation and determination of the uplink transmission parameters for the UEs. When simultaneous uplink PUSCH data and control signaling are scheduled, the control signaling is normally multiplexed with data prior to the DFT spreading, in order to preserve the single-carrier low CM property of the uplink transmission (see Figure 10.26). The PUCCH is used by a UE to transmit any necessary control signaling only in subframes in which the UE does not have any allocated resources for PUSCH transmission. In the design of PUCCH, the low PAPR and low CM property has been taken into consideration. The control signaling information on PUCCH is transmitted in a frequency region that is configured at the edges of the uplink system bandwidth. In order to minimize the resources needed for transmission of control signaling, PUCCH in LTE is designed to exploit frequency diversity, i.e., each PUCCH transmission in one subframe comprises a single resource block at or near one edge of the system bandwidth, followed by a second resource block in the second slot of the subframe at or near the opposite edge of the system bandwidth, where the two resource blocks are referred to as a PUCCH region. This design can achieve frequency diversity gain of approximately 2 dB compared to transmission in the same resource block throughout the subframe [16] (Figure 10.27). A snapshot of an uplink slot carrying a single PUCCH is shown in Figure 10.28 [153].

One important aspect of LTE transmitter design is the necessity to minimize unwanted emissions. Because LTE is deployed in the same frequency bands as UMTS and other legacy 3G cellular technologies, the 3GPP specifications [1] regulate the UE emissions to minimize interference and to ensure compatibility between different radio systems. The primary concern is the control of spurious emissions, which can occur at any frequency band. However, new challenges arise at the band edges, where the transmitted signal must comply with rigorous

Petitioners' Exhibit 1021
Nokia of America Corp., et al. v. KT Corporation, et al.
Case No. IPR2025-00036; U.S. Patent No. 11,627,631
Page 783 of 1122

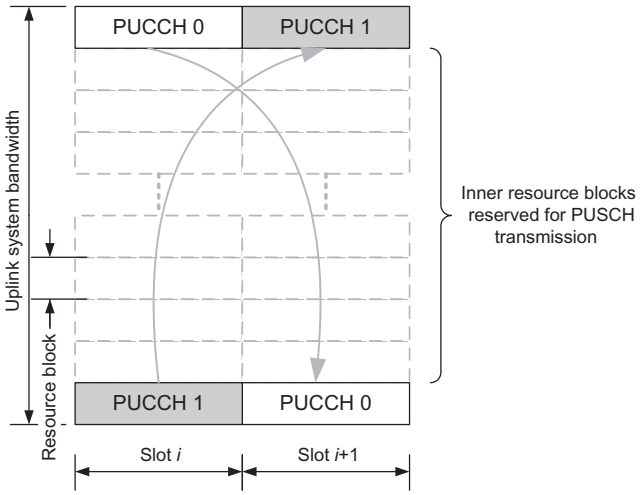


FIGURE 10.27

Example of PUCCH resource-block allocation [3,16].

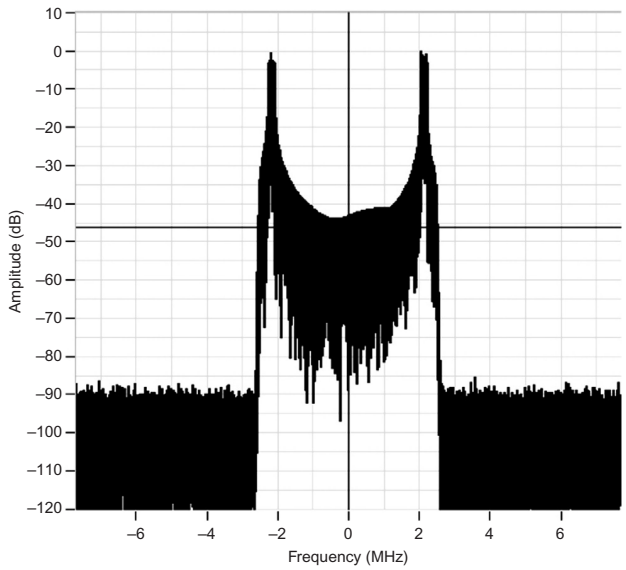


FIGURE 10.28

Snapshot of an uplink slot carrying a single PUCCH [153].

Petitioners' Exhibit 1021
Nokia of America Corp., et al. v. KT Corporation, et al.
Case No. IPR2025-00036; U.S. Patent No. 11,627,631
Page 784 of 1122

power leakage requirements. With LTE supporting channel bandwidths up to 20 MHz, and with many bands too narrow to support more than a few channels, a large proportion of the LTE channels will be at the edge of the band. Controlling transmitter performance at the edge of the band requires a design with filtering to attenuate OOB emissions without affecting in-channel performance. Factors such as cost, power efficiencies, physical size, and location in the transmitter block diagram are also important considerations. Ultimately the LTE transmitter must meet all specified limits for unwanted emissions, including limits on the amount of power that leaks into adjacent channels, as defined by the adjacent-channel leakage power ratio (ACLR).

The uplink control signaling must be transmitted regardless of whether the UE has data to send or whether any uplink resources are allocated for the terminal. As a result, there are two methods for transmission of the uplink control signaling as follows:

- Non-simultaneous transmission of PUCCH and PUSCH: When the terminal does not have any scheduling grant for PUSCH transmission in the current subframe, the uplink control signaling is transmitted on PUCCH. In uplink carrier aggregation scenarios, PUCCH is only transmitted on the primary component carrier. Consequently, data transmissions on multiple component carriers in the downlink can be acknowledged on a single uplink component carrier.
- Simultaneous transmission of PUCCH and PUSCH: When the terminal has a scheduling grant for PUSCH transmission in the current subframe, the uplink control signaling is time-multiplexed with the coded data on the PUSCH prior to DFT precoding and SC-FDMA signal generation (see Figure 10.26). Since the terminal has already been assigned radio resources, there is no need to support transmission of the SR in this case. Instead, scheduling information can be included in the MAC headers. In carrier aggregation scenarios, all control signaling is transmitted on the primary component carrier, i.e., uplink control signaling cannot be distributed across multiple component carriers.

One must differentiate between the above cases in consideration of efficient operation of the uplink PA and maximization of the uplink coverage. However, when there is sufficient power available in the terminal, simultaneous transmission of PUSCH and PUCCH can be used with minimal impact on the uplink coverage. The possibility of simultaneous PUSCH and PUCCH transmission was introduced in LTE Rel-10 which added more flexibility at the expense of slight increase in the CM value. Simultaneous transmission of PUSCH and PUCCH can always be avoided by using the basic mechanism introduced in LTE Rel-8. It should be noted that while PUCCH is only transmitted on the primary component carrier, as the primary component carrier is specified on a per-terminal basis, from a network perspective, PUCCH resources are used on multiple component carriers [16].

Petitioners' Exhibit 1021
Nokia of America Corp., et al. v. KT Corporation, et al.
Case No. IPR2025-00036; U.S. Patent No. 11,627,631
Page 785 of 1122

Since the size of a resource block in any subframe might be too large for control signaling payload transmitted by a single terminal, and in order to efficiently utilize the resources designated for control signaling transmission, multiple terminals can share the same resource block. This can be done by assigning different orthogonal phase rotations (cyclic shifts) of a cell-specific length-12 frequency-domain sequence to the UEs simultaneously using the resource block. Note that a linear phase rotation in the frequency-domain is equivalent to applying a cyclic shift in the time-domain. The resource used by PUCCH is not only specified in the time−frequency-domain by the resource-block pair, but also by the phase rotation applied. There are up to 12 different phase rotations specified, providing up to 12 different orthogonal sequences from each cell-specific sequence. However, in the frequency-selective channels, only some of the 12 phase rotations can be used in order to maintain orthogonality. Typically, up to six rotations are considered usable in a cell from a radio propagation perspective, although inter-cell interference may result in a smaller number of useful phase rotations from an overall system perspective. Higher-layer signaling is used to configure the number of phase rotations used in a cell [16]. There are three formats defined for PUCCH, formats 1, 2, and 3, each capable of carrying a different payload size.

In summary, placing the control regions at the edges of the system bandwidth has a number of advantages, including the following [15]:

- The frequency diversity achieved through frequency hopping is maximized by allowing hopping from one edge of the band to the other.
- OOB emissions[4] are smaller, if a UE only transmits on a single resource block per slot compared to multiple resource blocks. The PUCCH regions can serve as a virtual guard band between the wider-bandwidth PUSCH transmissions of adjacent carriers, and can therefore improve coexistence.
- Using control regions on the band edges maximizes the achievable PUSCH data rate, as the entire central portion of the band can be allocated to a single UE. If the control regions were in the central portion of a carrier, a UE bandwidth allocation would be limited to one side of the control region in order to maintain the single-carrier characteristic of the signal, thus limiting the maximum achievable data rate.
- Control regions on the band edges impose fewer constraints on the uplink data scheduling, both with and without inter-subframe and/or intra-subframe frequency hopping.

[4]Unwanted emissions consist of out-of-band emissions and spurious emissions. Spurious emissions are emissions caused by unwanted transmitter effects such as harmonics emissions, parasitic emissions, intermodulation products, and frequency conversion products. Out-of-band emissions are unwanted emissions outside the channel bandwidth resulting from the modulation process and non-linearity in the transmitter. If unwanted emissions are not sufficiently suppressed, they can considerably impair other intra-band radio services.

Petitioners' Exhibit 1021
Nokia of America Corp., et al. v. KT Corporation, et al.
Case No. IPR2025-00036; U.S. Patent No. 11,627,631
Page 786 of 1122

10.7.2 PUCCH formats

The physical uplink control channel carries uplink control information. The UCI can also be transmitted via PUSCH. The UCI typically consists of (1) SR; (2) HARQ ACK/NACK in response to downlink data packets received on PDSCH (one ACK/NACK bit transmitted in the case of single-codeword downlink transmission, while two ACK/NACK bits are used in the case of two codeword downlink transmission); and (3) CSI, which includes CQI as well as the MIMO-related feedback consisting of RI and PMI (20 bits per subframe are used for the CSI). The amount of UCI that a UE can transmit in a subframe depends on the number of SC-FDMA symbols available for transmission of control signaling excluding the SC-FDMA symbols used for reference signal transmission for coherent detection of PUCCH. For frame structure type 2, PUCCH is not transmitted in the UpPTS field. It must be noted that concurrent transmission of PUCCH and PUSCH in the same subframe by a UE is not allowed in LTE Rel-8/9. Support for simultaneous transmission of PUCCH and PUSCH in the same subframe from the same UE was added in LTE Rel-10, provided that it is configured by the higher layers. The PUCCH supports the multiple formats given in Table 10.9. Formats 2a and 2b are only supported for a normal cyclic prefix. Using the PUCCH formats, the following combinations of UCI on PUCCH are supported [5]:

- Format 1 is used for carrying positive SR.
- Format 1a is used for transmitting 1-bit HARQ ACK/NACK, or in case of FDD for sending 1-bit HARQ ACK/NACK with positive SR.
- Format 1b is used for carrying 2-bit HARQ ACK/NACK, or for transmitting 2-bit HARQ ACK/NACK with positive SR. PUCCH format 1b is further used for sending up to 4-bit HARQ ACK/NACK with channel selection, when the UE is configured with more than one serving cell, or in the case of TDD when the UE is configured with a single serving cell.
- Format 2 is used for sending a CSI report when it is not multiplexed with HARQ ACK/NACK. PUCCH format 2 is also used for transmission of a CSI report multiplexed with HARQ feedback for an extended cyclic prefix.
- Format 2a is used for carrying a CSI report multiplexed with 1-bit HARQ ACK/NACK for a normal cyclic prefix.
- Format 2b is used for sending a CSI report multiplexed with 2-bit HARQ ACK/NACK for a normal cyclic prefix.
- Format 3 is used for transmitting up to 10-bit HARQ ACK/NACK for FDD, and for up to 20-bit HARQ ACK/NACK for TDD. PUCCH format 3 is also used for sending up to 11-bit corresponding to 10-bit HARQ ACK/NACK and 1-bit positive/negative SR for FDD, and for up to 21-bit corresponding to 20-bit HARQ ACK/NACK and 1-bit positive/negative SR for TDD.

All PUCCH formats use a cyclic shift $N_{\mathrm{CS}}(n_{\mathrm{s}}, l)$, which used to be cell-specific until LTE Rel-11, which is a function of the SC-FDMA symbol number l and the slot number n_{s} according to $N_{\mathrm{CS}}(n_{\mathrm{s}}, l) = \sum_{i=0}^{7} c(8N_{\mathrm{s}}^{\mathrm{UL}} n_{\mathrm{s}} + 8l + i)2^i$, where

Table 10.9 PUCCH Formats and Their Usage [3]

PUCCH Format	Modulation Scheme	Number of Bits per Subframe	Usage	Multiplexing Capacity[a] (UE/ Resource Block)
1	N/A	N/A	SR	36, 18[b], 12
1a	BPSK	1	ACK/NACK	36, 18[b], 12
1b	QPSK	2	ACK/NACK	36, 18[b], 12
2	QPSK	20	CQI (20 coded bits)	12, 6[b], 4
2a	QPSK + BPSK	21	CQI (20 coded bits) + ACK/NACK (1 bit)	12, 6[b], 4
2b	QPSK + QPSK	22	CQI (20 coded bits) + ACK/NACK (2 bits)	12, 6[b], 4
3	QPSK	48	Multiple ACK/NACK bits for carrier aggregation (up to 10 ACK/NACK bits in FDD systems with carrier aggregation or up to 20 bits ACK/NACK bits + 1 SR bit in TDD systems with carrier aggregation)	5

[a] *The combination of time-domain cyclic shifts and time-domain orthogonal codes determines the number of UEs which can be multiplexed within a single pair of PUCCH resource blocks. The total number of multiplexing possibilities is defined by the product of the number cyclic shifts and the number of the orthogonal codes.*
[b] *Typical value with six different rotations (choosing every other cyclic shift).*

the pseudo-random sequence $c(i)$ is initialized with $c_{\text{init}} = N_{\text{ID}}^{\text{RS}}$, where $N_{\text{ID}}^{\text{RS}}$ denotes the virtual cell identifier,[5] at the beginning of each radio frame. The definition of the virtual cell identifier $N_{\text{ID}}^{\text{RS}}$ depends on the type of transmission. For transmissions associated with PUSCH $N_{\text{ID}}^{\text{RS}} = N_{\text{ID}}^{\text{cell}}$, if no value for $N_{\text{ID}}^{\text{PUSCH}}$ is configured by higher layers if PUSCH transmission corresponds to a *Random Access Response* or a retransmission of the same transport block as part of the contention-based random access procedure; otherwise $N_{\text{ID}}^{\text{RS}} = N_{\text{ID}}^{\text{PUSCH}}$. For transmissions associated with PUCCH $N_{\text{ID}}^{\text{RS}} = N_{\text{ID}}^{\text{cell}}$, if no value for $N_{\text{ID}}^{\text{PUCCH}}$ is configured by higher layers; otherwise $N_{\text{ID}}^{\text{RS}} = N_{\text{ID}}^{\text{PUCCH}}$. The virtual cell identifier for SRS is defined as $N_{\text{ID}}^{\text{RS}} = N_{\text{ID}}^{\text{cell}}$ [3].

The physical resource allocation for PUCCH depends on two parameters, $N_{\text{RB}}^{(2)}$ and $N_{\text{CS}}^{(1)}$, that are signaled by the higher layers. The variable $N_{\text{RB}}^{(2)} \geq 0$ denotes the

[5] A simple approach is to use the PUCCH resource offset parameter to facilitate frequency-domain separation between inter-cell orthogonal and non-orthogonal resources. A virtual cell identifier may be used in the newly reserved PUCCH resource pool.

Petitioners' Exhibit 1021
Nokia of America Corp., et al. v. KT Corporation, et al.
Case No. IPR2025-00036; U.S. Patent No. 11,627,631
Page 788 of 1122

bandwidth in terms of the number of resource blocks that are available to be used for the PUCCH format 2/2a/2b transmission in each slot. The variable $N_{CS}^{(1)}$ denotes the number of cyclic shifts used for PUCCH format 1/1a/1b in a resource block which is used for a combination of PUCCH formats 1/1a/1b and 2/2a/2b. The value of $N_{CS}^{(1)}$ is an integer multiple of Δ_{shift}^{PUCCH} within the range of $\{0, 1, \ldots, 7\}$, where Δ_{shift}^{PUCCH} is signaled via the higher layers. There is no mixed resource block if $N_{CS}^{(1)} = 0$. There is only one resource block in each slot that can support a mix of PUCCH formats 1/1a/1b and 2/2a/2b. The resources used for transmission of PUCCH formats 1/1a/1b, 2/2a/2b, and 3 are represented by non-negative indices $n_{PUCCH}^{(1,\overline{p})}, n_{PUCCH}^{(2,\overline{p})} < 12N_{RB}^{(2)} + \left\lceil \frac{N_{CS}^{(1)}}{8} \right\rceil (10 - N_{CS}^{(1)})$ and $n_{PUCCH}^{(3,\overline{p})}$, respectively.

The mapping of various PUCCH formats to PUCCH regions is shown in Figure 10.29. The mapping of PUCCH to PRBs follows the steps below:

1. Start from resource blocks in the outer edge of the band toward middle of the band.
2. Allocate PUCCH format 2/2a/2b resources.
3. Allocate PUCCH formats containing mixed ACK/NACK and CQI.
4. Allocate PUCCH format 1/1a/1b resources.

It can be seen in the figure that PUCCH format 2/2a/2b is mapped and transmitted on the outermost band-edge resource blocks followed by a mixed PUCCH resource block of CSI format 2/2a/2b and SR/HARQ ACK/NACK format 1/1a/1b, and then by a PUCCH SR/HARQ ACK/NACK format 1/1a/1b allocation toward the center of the band. The number of PUCCH resource blocks available for use by CSI format 2/2a/2b is signaled to the UEs in the cell through broadcast signaling.

10.7.2.1 PUCCH formats 1, 1a, 1b

The structure of PUCCH format 1 is illustrated in Figure 10.31. PUCCH format 1 is used for transmission of HARQ ACK/NACK (i.e., a single-bit HARQ feedback corresponding to one downlink component carrier is used to generate one BPSK-modulated symbol, and in the case of downlink spatial multiplexing, 2 bits of HARQ feedback are used to generate one QPSK-modulated symbol) and for sending a positive SR, where the same constellation point as for a HARQ NACK is used. The BPSK/QPSK-modulated symbol is then used to generate the signal for transmission in each of the two PUCCH slots. In each of the seven SC-FDMA symbols of a slot assuming a normal cyclic prefix, a length-12 sequence obtained via phase rotation of the cell-specific base sequence is transmitted. Three SC-FDMA symbols are used for reference signals to enable channel estimation and coherent detection by the eNB, and the remaining four SC-FDMA symbols are modulated to generate the BPSK/QPSK-modulated symbols (as shown in Figure 10.31). In principle, the BPSK/QPSK-modulated symbol could directly

Petitioners' Exhibit 1021
Nokia of America Corp., et al. v. KT Corporation, et al.
Case No. IPR2025-00036; U.S. Patent No. 11,627,631
Page 789 of 1122

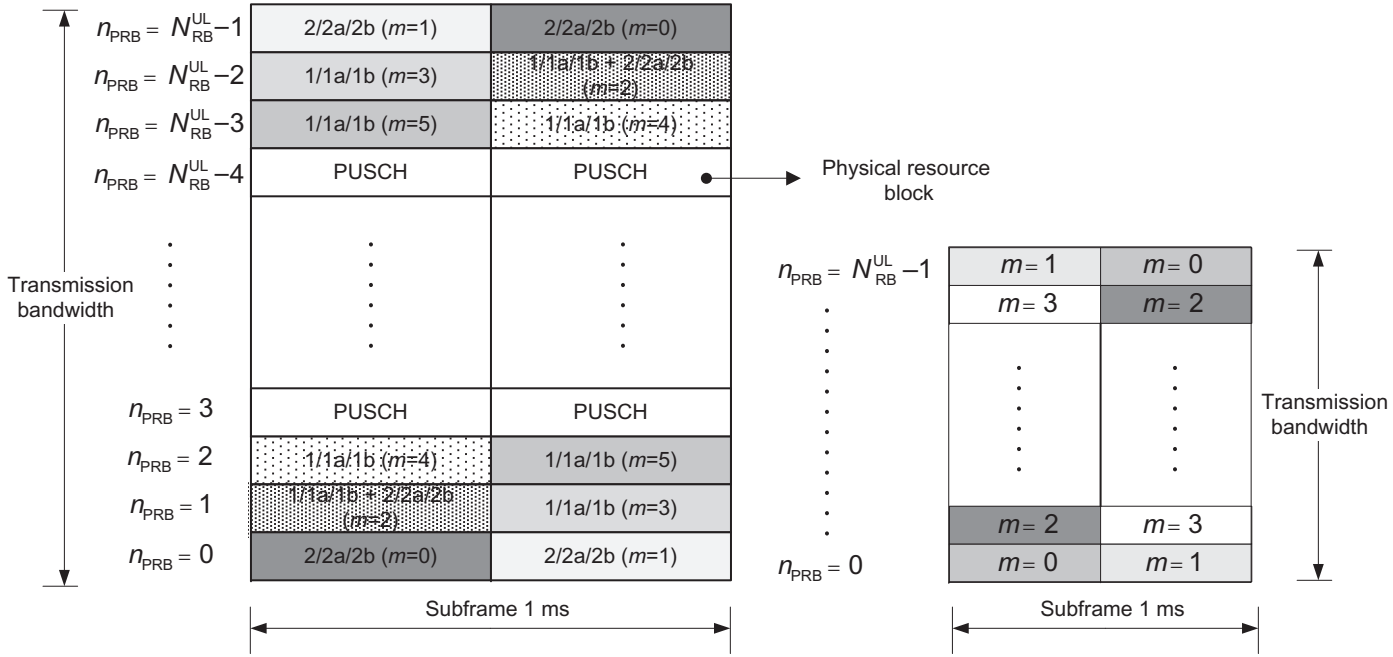


FIGURE 10.29

Example mappings of PUCCH to PRBs in a subframe [3].

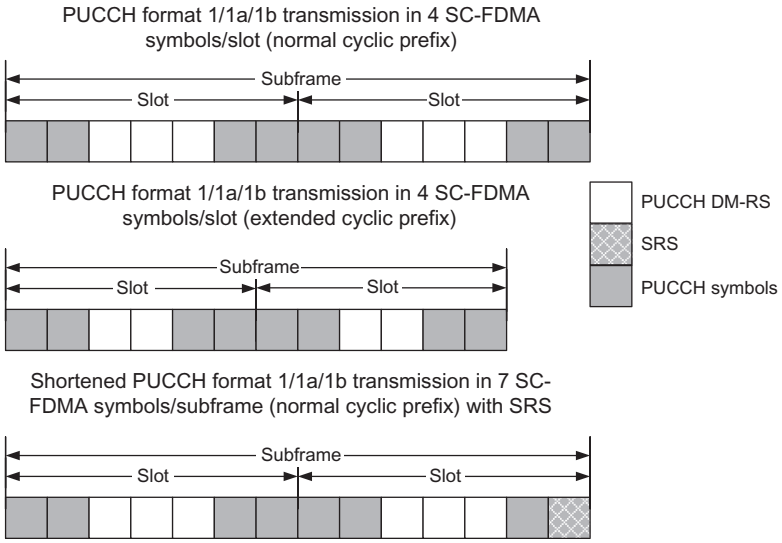


FIGURE 10.30

Relative position of PUCCH, DM-RS, and SRS symbols.

modulate the rotated length-12 sequence used to differentiate terminals transmitting on the same time−frequency resource. However, this would result in unnecessarily lower PUCCH capacity. Therefore, the BPSK/QPSK-modulated symbol is multiplied by a length-4 orthogonal cover code. Multiple terminals may transmit on the same time−frequency resource using the same phase-rotated sequence and can still be separated through different OCCs. In order to estimate the channels for the respective terminals, the reference signals are also scrambled by appropriate orthogonal cover sequences with different length, i.e., three for the case of a normal cyclic prefix and two for an extended cyclic prefix. Each cell-specific sequence can be used for up to 36 different terminals (assuming all 12 phase rotations or cyclic shifts are available, whereas typically 6 of the cyclic shifts are utilized), there is a threefold improvement in the PUCCH capacity compared to the case when no cover sequence is used. The cover sequences are three Walsh sequences of length 4 for the data part and three DFT sequences of length 3 for the reference signals [3,14,16].

A PUCCH format 1 resource, used for either a HARQ feedback or an SR, is represented by a single scalar resource index. From the index, the phase rotation and the orthogonal cover sequence are derived. The use of a phase rotation of a cell-specific sequence, together with orthogonal sequences as described earlier, provides orthogonality between different terminals in the same cell when transmitting PUCCH on the same set of resource blocks. Therefore, there is ideally no intra-cell interference, which helps improve the overall performance. However,

Petitioners' Exhibit 1021
Nokia of America Corp., et al. v. KT Corporation, et al.
Case No. IPR2025-00036; U.S. Patent No. 11,627,631
Page 791 of 1122

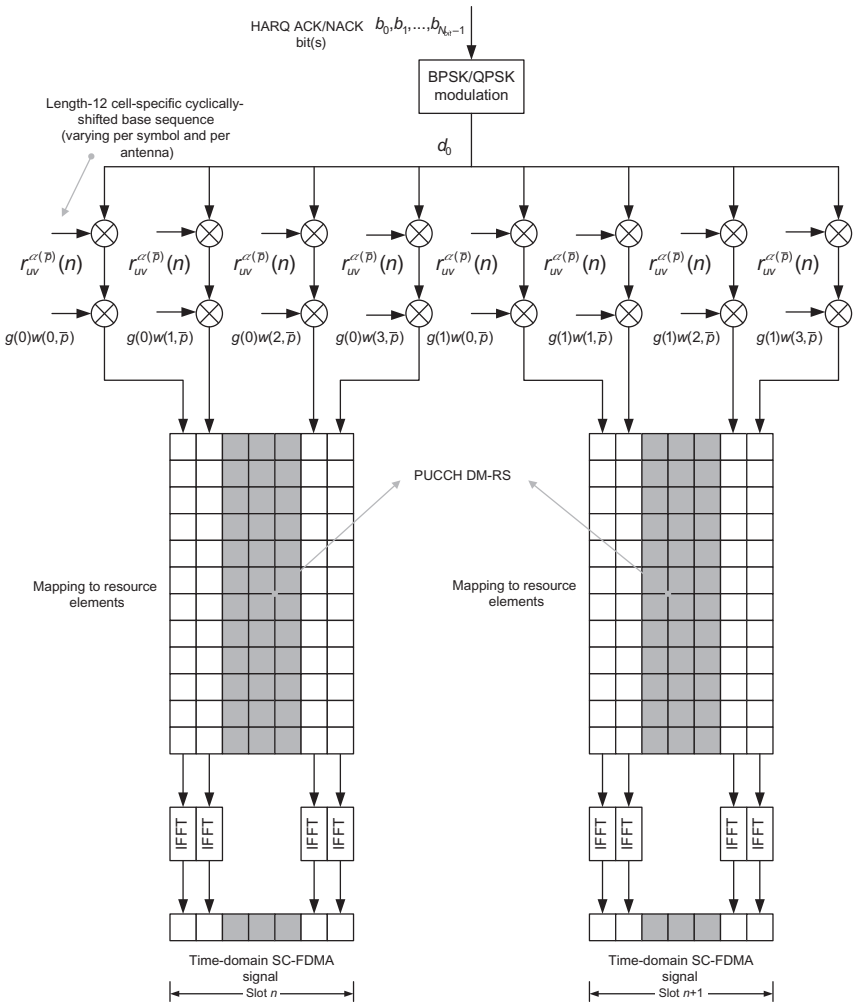


FIGURE 10.31

Physical layer processing for PUCCH format 1/1a/1b (HARQ ACK/NACK and normal cyclic prefix).

PUCCH typically suffers from inter-cell interference since different sequences used in neighboring cells are non-orthogonal. In order to randomize the inter-cell interference, the phase rotation of the sequence used in a cell is changed on a symbol-by-symbol basis in a slot according to a hopping pattern derived from the physical layer cell identity. In addition, slot-level hopping is applied to the orthogonal cover and phase rotation to further randomize the interference.

Petitioners' Exhibit 1021
Nokia of America Corp., et al. v. KT Corporation, et al.
Case No. IPR2025-00036; U.S. Patent No. 11,627,631
Page 792 of 1122

The UE scheduling request is carried by PUCCH format 1 and is signaled by the presence or absence of PUCCH format 1 transmission. For PUCCH formats 1a and 1b, 1 or 2 bits are transmitted depending on the HARQ feedback. The block of bits $b_0, b_1, \ldots, b_{N_{\text{bit}}-1}$ are modulated using BPSK (format 1a) or QPSK (format 1b) modulation, resulting in a complex-valued symbol d_0. Note that the number of bits is $N_{\text{bit}} = 1$ for format 1a and $N_{\text{bit}} = 2$ for format 1b carrying HARQ ACK/NACK. The complex-valued symbol d_0 is multiplied by a cyclically shifted sequence of length $N_{\text{s}}^{\text{PUCCH}} = 12$, $r_{\text{uv}}^{\alpha(\overline{p})}(n)$ for each of the N_p antenna ports used for PUCCH transmission according to the following equation [3]:

$$y^{\overline{p}}(n) = \frac{1}{\sqrt{N_p}} d_0 r_{\text{uv}}^{\alpha(\overline{p})}(n)|_{n=0,1,\ldots,N_{\text{s}}^{\text{PUCCH}}-1} \tag{10.5}$$

where $r_{\text{uv}}^{\alpha(\overline{p})}(n)$ is the cyclically shifted Zadoff−Chu base sequence. The antenna-port-specific cyclic-shift $\alpha(\overline{p})$ varies across symbols and slots. The block of complex-valued symbols $y^{\overline{p}}(0), y^{\overline{p}}(1), \ldots, y^{\overline{p}}(N_{\text{s}}^{\text{PUCCH}} - 1)$ are scrambled by scrambling sequence $g(n_{\text{s}})$ and are block-wise spread with the antenna-port-specific orthogonal sequence $w(i, \overline{p})$ according to the following equation [3]:

$$z^{\overline{p}}(m' N_{\text{SF}}^{\text{PUCCH}} N_{\text{s}}^{\text{PUCCH}} + m N_{\text{s}}^{\text{PUCCH}} + n) = g(n_{\text{s}}) w(m, \overline{p}) y^{\overline{p}}(n) \tag{10.6}$$

where $m = 0, 1, \ldots, N_{\text{SF}}^{\text{PUCCH}} - 1; n = 0, 1, \ldots, N_{\text{s}}^{\text{PUCCH}} - 1; m' = 0, 1$ and $g(n_{\text{s}}) = 1$ if $n'_{\overline{p}}(n_{\text{s}}) \bmod 2 = 0$; otherwise $g(n_{\text{s}}) = e^{j\pi/2}$, $N_{\text{SF}}^{\text{PUCCH}} = 4$ for both slots of normal PUCCH format 1/1a/1b and $N_{\text{SF}}^{\text{PUCCH}} = 4$ for the first slot and $N_{\text{SF}}^{\text{PUCCH}} = 3$ for the second slot of shortened PUCCH format 1/1a/1b (see Figure 10.30).

In addition to dynamic scheduling using PDCCH, a UE can be semi-persistently scheduled according to a specific pattern. In that case, there will be no PDCCH to assign the PUCCH resources in the uplink. The configuration of the semi-persistent scheduling includes information on the PUCCH index to be used for uplink HARQ feedback. Note that a UE can use PUCCH resources only when it has been scheduled in the downlink. The amount of PUCCH resources required for HARQ feedback does not necessarily increase if the number of terminals in the cell increases; rather it is a function of the number of control channel elements (CCEs) in the downlink control signaling.

For downlink carrier aggregation, when there are multiple simultaneous downlink allocations for a single terminal, multiple feedback bits are transmitted in the uplink (i.e., 1 or 2 bits in the case of spatial multiplexing per downlink component carrier). PUCCH format 1b can be used to support more than 2 bits in the uplink by using resource selection. Let us assume that 4 bits are going to be transmitted in the uplink. With resource selection, 2 bits would indicate which PUCCH resource should be used and the remaining 2 bits are transmitted using the normal PUCCH structure, but on the resource addressed by the first 2 bits. One resource is derived from the first CCE using the same rule used in the absence of carrier aggregation, assuming that the scheduling assignment is

Petitioners' Exhibit 1021
Nokia of America Corp., et al. v. KT Corporation, et al.
Case No. IPR2025-00036; U.S. Patent No. 11,627,631
Page 793 of 1122

transmitted on the primary cell. The remaining resources are semi-statically configured by RRC signaling. For more than 4 bits, resource selection is less efficient and PUCCH format 3, which was introduced in LTE Rel-10 for carrier aggregation, is utilized.

Unlike HARQ feedback, whose occurrence is expected and predicable by the eNB, a specific terminal's need for uplink resources is unpredictable, which is why a contention-based mechanism has been provisioned in LTE to allow uplink resource scheduling request. The random-access mechanism is used for SRs. A contention-based mechanism may work well for a small number of UEs; however, by increasing the number of UEs simultaneously requesting resources, the probability of collision increases. Therefore, LTE further provides a contention-free scheduling-request mechanism on PUCCH, where each terminal in the cell is assigned a reserved resource on which it can transmit a request for uplink resources. The contention-free resource is represented by a PUCCH resource index every *n*th subframe. In other words, a request for uplink resources can be made by means of the random-access channel; however, due to the probability of collisions during congestion periods, an alternative method is provided using PUCCH format 1. Each UE in the cell is assigned a specific resource index mapping, a resource which can be used every *n*th subframe in order to transmit a scheduling request. Therefore, if PUCCH energy is detected, the eNB will consider it as an SR from the corresponding UE. Since each UE will have a specific resource allocated, there is no probability of collision. However, as a drawback, the number of available PUCCH resources is reduced.

A single SR is deemed sufficient for the case of carrier aggregation. The discussion earlier has considered transmission of either a HARQ feedback or an SR. However, there are cases where the UE needs to concurrently transmit HARQ feedback and an SR. In such cases, the HARQ ACK/NACK is transmitted on the scheduling-request resource. As we discussed earlier, this is possible because the scheduling request carries no explicit information. By comparing the amount of energy detected on the ACK resource and the scheduling-request resource for a specific terminal, the eNB can determine whether the terminal is requesting resources, as well.

10.7.2.2 PUCCH formats 2, 2a, 2b

The CSI reports are used to provide the eNB with an estimate of the downlink communication channel observed by the UE in order to assist channel-dependent scheduling (Figure 10.32). The CSI report consists of multiple bits transmitted in one subframe and is transmitted using PUCCH format 2. Channel status reports include CQI, RI, and PMI. The HARQ ACK/NACK can also be transmitted with channel status information. There are two forms of channel coding for this purpose, one for the channel quality information (i.e., CQI) only and another one for the combination of CQI and HARQ feedback. The channel quality indicator represents the recommended modulation scheme and coding rate that should be

Petitioners' Exhibit 1021
Nokia of America Corp., et al. v. KT Corporation, et al.
Case No. IPR2025-00036; U.S. Patent No. 11,627,631
Page 794 of 1122

used for the downlink transmission. The RI provides information about the rank of the channel, which is used to determine the optimal number of layers that should be used for the downlink transmission which is only used for spatial multiplexing modes. The PMI provides information about which precoding matrix to use, which is only used in closed-loop spatial multiplexing modes. PUCCH format 2, as shown in Figure 10.32, is generated by phase rotation of a cell-specific base sequence (same as PUCCH format 1), followed by a block coding function using a punctured Reed−Muller code[6] and QPSK modulation of the CSI. There are ten QPSK symbols to be transmitted in a subframe where the first five complex-valued modulation symbols are transmitted in the first slot and the remaining in the next slot. In PUCCH format 2/2a/2b, two SC-FDMA symbols are used as reference signals to allow coherent detection and demodulation at the eNB. In the remaining modulation symbols, each QPSK-modulated symbol is multiplied by a phase-rotated length-12 cell-specific base sequence, inverse Fourier-transformed, and the resulting signal is transmitted over the corresponding SC-FDMA symbol. For an extended cyclic prefix, there are six SC-FDMA symbols per slot; therefore, only one reference symbol per slot is allocated. The transmission of PUCCH format 2 relies on phase rotation of a cell-specific sequence similar to that for PUCCH format 1, which allows the two formats to be transmitted in the same resource block. Note that orthogonal cover sequences are not used for PUCCH format 2. The rotation angles for different symbols carrying PUCCH format 2 are the hopping across symbol and slot boundaries for interference randomization [16].

Resources for transmission of PUCCH format 2 can be represented by an index, which can be interpreted as a channel number that is configurable via higher-layer signaling for each terminal to transmit its CSI report. The CSI reports on PUCCH are periodic. There are also aperiodic reports that are only transmitted on PUSCH. In case of carrier aggregation, multiple periodic reports, one per component carrier, are transmitted that are offset in time such that reports for two different component carriers do not collide (Table 10.10).

---

[6]Reed−Muller codes are a family of linearerror-correcting codes used in communication systems. The special cases of Reed−Muller codes include Hadamard codes, Walsh−Hadamard codes, and Reed−Solomon codes. Reed−Muller codes are denoted by an $RM(d, r)$ notation, where d is the order of the code and r determines the length of code $n = 2^r$. Reed−Muller codes are related to binary functions on field $GF(2^r)$ over the elements $\{0, 1\}$. It can be shown that $RM(0, r)$ codes are repetition codes of length, rate $R = 1/n$ and minimum distance $d_{\min} = n$, $RM(1, r)$ codes are parity check codes of length $n = 2^r$, rate $R = (r + 1)/n$ and minimum distance $d_{\min} = n/2$. Reed−Muller codes have the following properties [ref]:

1. The set of all possible exterior products of up to d of v_i form a basis for $\mathbf{F}_2^n$.
2. The rank of $RM(d, r)$ code is defined as $\sum_{s=0}^{r} \binom{d}{s}$
3. $RM(d, r) = RM(d, r-1)|RM(d-1, r-1)$, where '|'. denotes the bar product of two codes.
4. $RM(d, r)$ has minimum Hamming weight2^{d-r}.

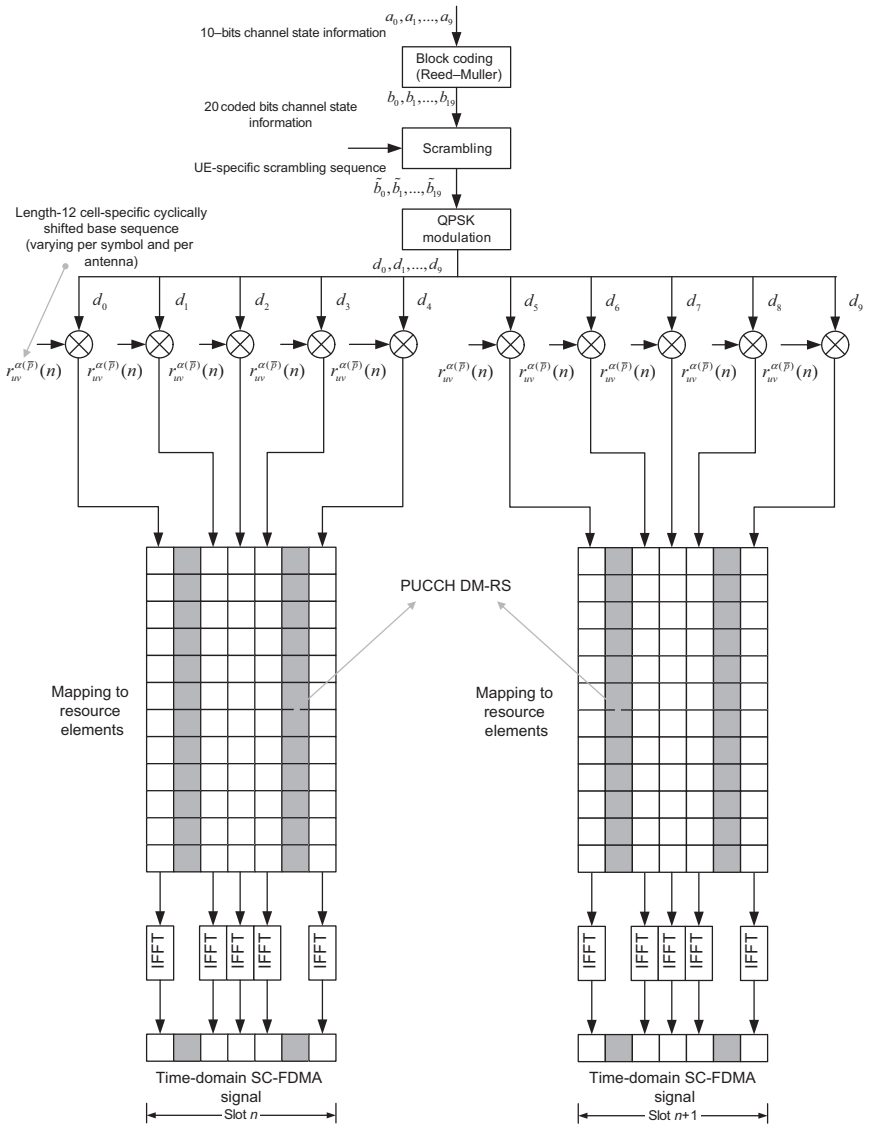


FIGURE 10.32

Physical layer processing for PUCCH format 2/2a/2b (normal cyclic prefix, CQI only) [16].

The structure of PUCCH format 2 in one subframe with normal cyclic prefix is shown in Figure 10.32. The first and the fifth SC-FDMA symbols are used for PUCCH DM-RS transmission with a normal cyclic prefix, whereas in the case of an extended cyclic prefix only one reference symbol is transmitted on the third

Petitioners' Exhibit 1021
Nokia of America Corp., et al. v. KT Corporation, et al.
Case No. IPR2025-00036; U.S. Patent No. 11,627,631
Page 796 of 1122

Table 10.10 Size of the PUCCH Region [15]

System Bandwidth (MHz)	Number of Resource Blocks per Subframe	Number of PUCCH Regions
1.4	2	1
3	4	2
5	8	4
10	16	8
20	32	16

SC-FDMA symbol. The number of reference symbols per slot results from a trade-off between channel estimation accuracy and the sustainable code rate for the UCI bits. For a small number of UCI bits at a low SINR operating point (for a typical 1% target error rate), improving the channel estimation accuracy by using more reference symbols is more desirable than using a lower channel code rate. However, with larger numbers of UCI bits, the required SINR increases and the higher code rate resulting from a larger overhead of reference symbols becomes more critical, thus fewer reference symbols are utilized. In consideration of the above facts, two reference symbols per slot were found to provide the best trade-off in terms of performance and overhead, given the payload sizes required. Therefore, ten CSI bits are channel coded with a rate 1/2 punctured $(20, k)$ Reed−Muller code to generate 20 coded bits, which are then scrambled, similar to PUSCH data, with a length-31 Gold sequence[7] prior to QPSK modulation. One QPSK-modulated symbol (according to Table 10.11) is transmitted on each of the ten SC-FDMA symbols in the subframe by multiplying with a cyclically shifted base sequence of length-12 prior to OFDM modulation. The 12 cyclic shifts allow 12 different UEs to be orthogonally multiplexed on the same PUCCH format 2 resource blocks. The processing of a PUCCH DM-RS reference sequence, i.e., transmitted on the second and sixth SC-FDMA symbols for the normal cyclic prefix and the fourth symbol for the extended cyclic prefix, is similar to the frequency-domain CSI signal sequence without the CSI data modulation. In order to provide inter-cell interference randomization, cell-specific

[7]A Gold sequence is a type of binary sequence that is often used in telecommunication and satellite navigation signal processing. Gold sequences have bounded small cross-correlations within a set. A set of Gold sequences consists of $2^n - 1$ sequences each with a period of $2^n - 1$. A set of Gold sequences can be generated by taking two maximum-length sequences of the same length $2^n - 1$ such that their absolute cross-correlation is less than or equal to $2^{(n+2)/2}$, where n is the size of the linear feedback shift register used to generate the maximum length sequence [165]. The set of $2^n - 1$ logical XOR or of the two sequences in their various phases is a set of Gold codes. The highest absolute cross-correlation in this set of codes is $2^{(n+2)/2} + 1$ for even n and $2^{(n+1)/2} + 1$ for odd n. The logical XOR of two Gold codes from the same set is another Gold code.

Petitioners' Exhibit 1021
Nokia of America Corp., et al. v. KT Corporation, et al.
Case No. IPR2025-00036; U.S. Patent No. 11,627,631
Page 797 of 1122

Table 10.11 Modulation Symbols for PUCCH Format 1a/1b and PUCCH Format 2a/2b [3]

PUCCH Format	$b_0, b_1, \ldots, b_{N_{\text{bit}}-1}$	d_0
1a	0	1
	1	−1
1b	00	1
	01	−j
	10	j
	11	−1
PUCCH Format	$b_{20}, b_{21}, \ldots, b_{N_{\text{bit}}-1}$	d_{10}
2a	0	1
	1	−1
2b	00	1
	01	−j
	10	j
	11	−1

symbol-level cyclic-shift hopping is used. Intra-cell interference randomization is achieved by cyclic-shift re-mapping in the second slot [15].

In mathematical terms, a block of coded bits $b_0, b_1, \ldots, b_{19}$ is scrambled with a UE-specific scrambling sequence, resulting in a block of scrambled coded bits $\tilde{b}_0, \tilde{b}_1, \ldots, \tilde{b}_{19}$ according to $\tilde{b}(i) = [b(i) + c(i)] \bmod 2$, where the scrambling sequence $c(i)$ was defined in Chapter 9 and is initialized with $c_{\text{init}} = \left(\lfloor n_s/2 \rfloor + 1\right)\left(2N_{\text{ID}}^{\text{cell}} + 1\right)2^{16} + n_{\text{RNTI}}$ at the start of each subframe, where n_{RNTI} denotes the 16-bit temporary UE identity in the connected mode.[8] The block of scrambled bits $\tilde{b}_0, \tilde{b}_1, \ldots, \tilde{b}_{19}$ are QPSK modulated, resulting in a block of complex-valued modulation symbols $d_0, d_1, \ldots, d_9$. Each complex-valued symbol $d_0, d_1, \ldots, d_9$ is multiplied by a cyclically shifted length $N_{\text{s}}^{\text{PUCCH}} = 12$ sequence $r_{\text{uv}}^{\alpha(\overline{p})}(n)$ for each of the N_p antenna ports used for PUCCH transmission according to the following equation [3]:

$$z^{(\overline{p})}(N_{\text{s}}^{\text{PUCCH}} n + i) = \frac{1}{\sqrt{N_p}} d(n) r_{\text{uv}}^{\alpha(\overline{p})}(i)|_{n=0,1,\ldots,9; i=0,1,\ldots,11} \tag{10.7}$$

[8]Pseudo-random sequences are defined by a length-31 Gold sequence. The output sequence $c(n), \forall n = 0, 1, \ldots, M-1$ of length M is defined by $c(n) = (x_1(n + N_C) + x_2(n + N_C)) \bmod 2$ in which:
$x_1(n + 31) = (x_1(n + 3) + x_1(n)) \bmod 2$;
$x_2(n + 31) = (x_2(n + 3) + x_2(n + 2) + x_2(n + 1) + x_2(n)) \bmod 2$, and $N_C = 1600$. The first m-sequence is initialized with $x_1(0) = 1, x_1(n) = 0, n = 1, 2, \ldots, 30$. The second m-sequence is initialized by $c_{\text{init}} = \sum_{i=0}^{30} x_2(i)2^i$ with the value depending on the application of the sequence.

Petitioners' Exhibit 1021
Nokia of America Corp., et al. v. KT Corporation, et al.
Case No. IPR2025-00036; U.S. Patent No. 11,627,631
Page 798 of 1122

where $r_{uv}^{\alpha(\overline{p})}(n)$ is an antenna-port-dependent cyclically shifted Zadoff−Chu sequence of length 12. The resources used for transmission of PUCCH format 2/2a/2b are identified by resource index $n_{PUCCH}^{(2,\overline{p})}$ in which the cyclic shift $\alpha_{\overline{p}}(n_s, l)$ is determined according to $\alpha_{\overline{p}}(n_s, l) = \frac{\pi n_{cs}^{\overline{p}}(n_s,l)}{6}$, where $n_{cs}^{\overline{p}}(n_s, l) = [n_{cs}^{cell}(n_s, l) + n'_{\overline{p}}(n_s)]$ mod 12 [3]. A UE is semi-statically configured via higher-layer signaling to periodically report different CQI, PMI, and RI types in PUCCH format 2 using a resource index $n_{PUCCH}^{(2)}$, which indicates both the PUCCH region and the cyclic shift to be used. The allocation index for PUCCH format 2/2a/2b transmission regions is given by $m = \left\lfloor n_{PUCCH}^{(2)}/12 \right\rfloor$ and the assigned cyclic shift is given by $n_{RS}^{PUCCH} = n_{PUCCH}^{(2)} \bmod 12$. The simultaneous transmission of uplink HARQ feedback and CSI on PUCCH can be enabled by UE-specific higher-layer signaling. However, if simultaneous transmission is not enabled or supported and the UE needs to transmit HARQ feedback on PUCCH in the same subframe in which a CSI report has been configured, the CSI is dropped and only HARQ feedback is transmitted. In subframes where the eNB scheduler allows for simultaneous transmission of CSI and HARQ feedback on PUCCH from a UE, the CSI and the 1- or 2-bit HARQ feedback are multiplexed in the same PUCCH resource block without compromising the low cubic-metric property of single-carrier signal.

The time and frequency resources that can be used by the UE to report CSI which consists of CQI, PMI, precoding type indicator (PTI),[9] and/or RI are controlled by the eNB. For spatial multiplexing, the UE determines an RI corresponding to the number of useful transmission layers. A UE is semi-statically configured via higher-layer signaling to periodically send feedback on different CSI metrics (CQI, PMI, PTI, and/or RI) on the PUCCH using the reporting modes given in Table 10.12 [5].

Two periodic CSI reporting modes are supported in LTE/LTE-Advanced as follows:

1. *Wideband reports*, where the average channel quality across the entire cell bandwidth is calculated and represented with a single CQI value. In this case, a single PMI value for the entire bandwidth is further reported, if PMI reporting is enabled.

[9]PTI was introduced in LTE Rel-10 and allows a UE to dynamically switch between different types of PMI reports to the serving eNB. It is applicable to transmission mode 9 which uses a two-stage approach to PMI reporting. The first stage corresponds to reporting wideband and long-term channel characteristics (PMI_1), and the second stage concerns frequency-selective short-term channel properties (PMI_2). A PTI value of "0" indicates that the UE has detected PMI_1 is changing, thus it needs to send an update to the eNB. A PTI value of "1," on the other hand, indicates that PMI_1 is not changing and the report should be on PMI_2, which means that a number of sub-band PMI_2 values as opposed to a single wideband value should be sent to the eNB [14].

Petitioners' Exhibit 1021
Nokia of America Corp., et al. v. KT Corporation, et al.
Case No. IPR2025-00036; U.S. Patent No. 11,627,631
Page 799 of 1122

Table 10.12 CQI and PMI Feedback Types and Corresponding Transmission Modes for PUCCH CSI Reporting [5]

		PMI Feedback Type	
		No PMI	**Single PMI**
PUCCH CQI Feedback Type	Wideband (Wideband CQI)	Mode 1-0 TM1 TM2 TM3 TM7 TM8[a] TM9[b] TM10[c]	Mode 1-1 TM4 TM5 TM6 TM8[a] TM9[b] TM10[c]
	UE selected (sub-band CQI)	Mode 2-0 TM1 TM2 TM3 TM7 TM8[a] TM9[b] TM10[c]	Mode 2-1 TM4 TM5 TM6 TM8[a] TM9[b] TM10[c]

[a]TM 8: Mode 1-1 or 2-1, if the UE is configured with PMI/RI reporting; otherwise, modes 1-0 or 2-0, if the UE is configured without PMI/RI reporting.
[b]TM 9: Mode 1-1 or 2-1, if the UE is configured with PMI/RI reporting and the number of CSI-RS ports is greater than one; otherwise, mode 1-0 or 2-0, if the UE is configured without PMI/RI reporting or the number of CSI-RS ports is equal to one.
[c]TM10: Mode 1-1 or 2-1, if the UE is configured with PMI/RI reporting and the number of CSI-RS ports is greater than one; otherwise modes 1-0 or 2-0, if the UE is configured without PMI/RI reporting or the number of CSI-RS ports is equal to one.

2. *UE-selected reports*, where the total bandwidth of a cell is divided into one to four bandwidth parts, with the number of bandwidth parts derived from the cell bandwidth as given in Table 10.13. For each bandwidth part, the terminal selects the best sub-band within that part. The sub-band size ranges from four to eight resource blocks. Since the supported PUCCH payload size is limited, the reporting cycles through the bandwidth parts and in one subframe reports the wideband CQI and PMI (if enabled) for that bandwidth part, as well as the best sub-band and the CQI for that sub-band. The RI (if enabled) is reported in a separate subframe.

The periodic CSI reporting mode for each serving cell is configured via higher-layer signaling. For wideband periodic CQI reporting, the reporting period can be configured as $\{2, 5, 10, 16, 20, 32, 40, 64, 80, 128, 160\}$ subframes, or it can

Table 10.13 PUCCH Reporting Type Payload Size per PUCCH Reporting Mode and Mode State [5]

PUCCH Reporting Type	Report Contents	Mode State	PUCCH Reporting Modes			
			Mode 1-1 (Bits/ Bandwidth Part)	Mode 2-1 (Bits/ Bandwidth Part)	Mode 1-0 (Bits/ Bandwidth Part)	Mode 2-0 (Bits/ Bandwidth Part)
1	Sub-band CQI	RI = 1	N/A	4 + L	N/A	4 + L
		RI > 1	N/A	7 + L	N/A	4 + L
1a	Sub-band CQI/ PMI_2	$N_p = 8$ RI = 1	N/A	8 + L	N/A	N/A
		$N_p = 8$ 1 < RI < 5	N/A	9 + L	N/A	N/A
		$N_p = 8$ RI > 4	N/A	7 + L	N/A	N/A
2	Wideband CQI/ PMI	$N_p = 2$ RI = 1	6	6	N/A	N/A
		$N_p = 4$ RI = 1	8	8	N/A	N/A
		$N_p = 2$ RI > 1	8	8	N/A	N/A
		$N_p = 4$ RI > 1	11	11	N/A	N/A
2a	Wideband PMI_1	$N_p = 8$ RI < 3	N/A	4	N/A	N/A
		$N_p = 8$ 2 < RI < 8	N/A	2	N/A	N/A
		$N_p = 8$ RI = 8	N/A	0	N/A	N/A
2b	Wideband CQI/ PMI_2	$N_p = 8$ RI = 1	8	8	N/A	N/A
		$N_p = 8$ 1 < RI < 4	11	11	N/A	N/A

Petitioners' Exhibit 1021
Nokia of America Corp., et al. v. KT Corporation, et al.
Case No. IPR2025-00036; U.S. Patent No. 11,627,631
Page 801 of 1122

		$N_p = 8$ RI = 4	10	10	N/A	N/A
		$N_p = 8$ RI > 4	7	7	N/A	N/A
2c	Wideband CQI/ PMI_1/PMI_2	$N_p = 8$ $RI = 1$	8	N/A	N/A	N/A
		$N_p = 8$ $1 < \text{RI} \leq 4$	11	N/A	N/A	N/A
		$N_p = 8$ $4 < \text{RI} \leq 7$	9	N/A	N/A	N/A
		$N_p = 8$ RI = 8	7	N/A	N/A	N/A
3	RI	$N_p = 2, 4$ two-layer spatial multiplexing	1	1	1	1
		$N_p = 8$ two-layer spatial multiplexing	1	N/A	N/A	N/A
		$N_p = 4$ four-layer spatial multiplexing	2	2	2	2
		$N_p = 8$ four-layer spatial multiplexing	2	N/A	N/A	N/A
		Eight-layer spatial multiplexing	3	N/A	N/A	N/A
4	Wideband CQI	$RI = 1, \text{RI} > 1$	N/A	N/A	4	4
5	RI/PMI_1	$N_p = 8$ two-layer spatial multiplexing	4	N/A	N/A	N/A
		$N_p = 4$ and eight-layer spatial multiplexing	5			
6	RI/PTI	$N_p = 8$ two-layer spatial multiplexing	N/A	2	N/A	N/A
		$N_p = 8$ four-layer spatial multiplexing	N/A	3	N/A	N/A
		$N_p = 8$ eight-layer spatial multiplexing	N/A	4	N/A	N/A

Petitioners' Exhibit 1021
Nokia of America Corp., et al. v. KT Corporation, et al.
Case No. IPR2025-00036; U.S. Patent No. 11,627,631
Page 802 of 1122

Table 10.14 Relationship of Sub-band Size and Bandwidth Parts with System Bandwidth [5]

System Bandwidth N_{RB}^{DL} (Resource Blocks)	Sub-band Size L_{SB} (Resource Blocks)	Bandwidth Parts N_{BP}
6–7	N/A	N/A
8–10	4	1
11–26	4	2
27–63	6	3
64–110	8	4

be set to off. For the UE-selected sub-band CQI, a CQI report in a certain subframe of the serving cell describes the channel quality in a particular part or parts of the bandwidth of that serving cell. The bandwidth parts are indexed in order of increasing frequency and decreasing sizes starting at the lowest frequency. The CQI and PMI payload sizes of each PUCCH CSI reporting mode are given in Table 10.14. While the wideband feedback mode is similar to that sent via PUSCH, the UE-selected sub-band CQI transmitted via PUCCH is different. In this case, the total number of sub-bands N_{SB} is divided into fractions called bandwidth parts. The value of the parameters (N_{SB}, L_{SB}, N_{BP}) depends on the system bandwidth as summarized in Table 10.14. In this case, one CQI value is computed and reported for a single selected sub-band from each bandwidth part, along with the corresponding sub-band index. The concept of periodic CQI reporting modes (wideband and sub-band) in time- and frequency-domains is illustrated in Figure 10.33.

For each serving cell, there are a total of N_{SB} equally sized sub-bands corresponding to system bandwidth N_{RB}^{DL} where $N_{SB} = \lfloor N_{RB}^{DL}/L_{SB} \rfloor$ sub-bands of size L_{SB}. A bandwidth part *bp* is frequency-consecutive and consists of N_{bp} sub-bands where N_{BP} bandwidth parts cover the system bandwidth. If the total number of bandwidth parts $N_{BP} = 1$, i.e., the wideband measurement, then $N_{bp} = \lceil N_{RB}^{DL}/L_{SB} \rceil$; otherwise, if $N_{BP} > 1$, then $N_{bp} = \lceil N_{RB}^{DL}/L_{SB}/N_{BP} \rceil$ depending on the values of these parameters, each bandwidth part is scanned in sequential order according to increasing frequency. For UE-selected sub-band feedback, a single sub-band out of N_{bp} sub-bands of a bandwidth part is selected along with the corresponding L bit label indexed in order of increasing frequency, where $L = \lceil \log_2 \lceil N_{RB}^{DL}/L_{SB}/N_{BP} \rceil \rceil$.

For each serving cell, the CQI/PMI reporting period P_{CQI} in number of subframes and relative reporting offset N_{offset}^{CQI} in number of subframes are configured by higher layers. The RI reporting period P_{RI} and relative reporting offset N_{offset}^{RI} are determined based on a parameter provided by higher layers. The relative RI

Petitioners' Exhibit 1021
Nokia of America Corp., et al. v. KT Corporation, et al.
Case No. IPR2025-00036; U.S. Patent No. 11,627,631
Page 803 of 1122

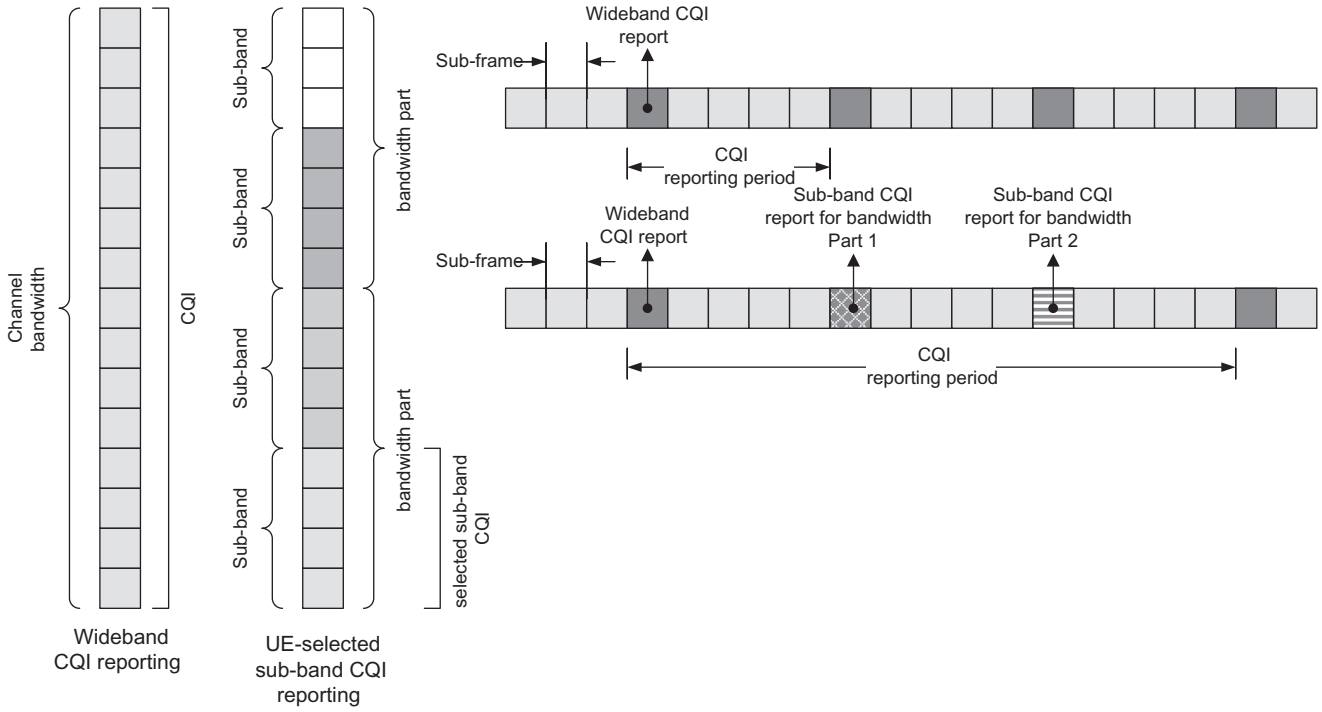


FIGURE 10.33

Illustration of the concept of periodic CQI reporting modes in time and frequency [14].

Petitioners' Exhibit 1021
Nokia of America Corp., et al. v. KT Corporation, et al.
Case No. IPR2025-00036; U.S. Patent No. 11,627,631
Page 804 of 1122

Table 10.15 Reporting Period, Reporting Offset, and Configuration Index of CQI/PMI and RI [5]

CQI/PMI Configuration Index	CQI/PMI Reporting Period P_{CQI}	CQI/PMI Reporting Offset N_{offset}^{CQI}
$0 \le \alpha \le 1$	2	α
$2 \le \alpha \le 6$	5	$\alpha-2$
$7 \le \alpha \le 16$	10	$\alpha-7$
$17 \le \alpha \le 36$	20	$\alpha-17$
$37 \le \alpha \le 76$	40	$\alpha-37$
$77 \le \alpha \le 156$	80	$\alpha-77$
$157 \le \alpha \le 316$	160	$\alpha-157$
$\alpha = 317$	Reserved	
$318 \le \alpha \le 349$	32	$\alpha-318$
$350 \le \alpha \le 413$	64	$\alpha-350$
$414 \le \alpha \le 541$	128	$\alpha-414$
$542 \le \alpha \le 1023$	Reserved	
RI configuration index	RI reporting period P_{RI}	RI reporting offset N_{offset}^{RI}
$0 \le \beta \le 160$	1	$-\beta$
$161 \le \beta \le 321$	2	$-(\beta-161)$
$322 \le \beta \le 482$	4	$-(\beta-322)$
$483 \le \beta \le 643$	8	$-(\beta-483)$
$644 \le \beta \le 804$	16	$-(\beta-644)$
$805 \le \beta \le 965$	32	$-(\beta-805)$
$966 \le \beta \le 1023$	Reserved	

reporting offset values are chosen in the range of $N_{offset}^{RI} \in \{0, -1, \ldots, -(P_{CQI}-1)\}$. If a UE is configured to report more than one CSI subframe set, then different sets of parameters corresponding to different subframe sets will be provided to the UE. When wideband CQI/PMI reporting is configured, the reporting instances satisfy the expression $(10n_f + \lfloor n_s/2 \rfloor - N_{offset}^{CQI}) \bmod P_{CQI} = 0$. When RI reporting is configured, the reporting interval is an integer multiple P_{RI} of period P_{CQI} subframes. The reporting instances for RI are subframes that satisfy the equation $(10n_f + \lfloor n_s/2 \rfloor - N_{offset}^{CQI} - N_{offset}^{RI}) \bmod (P_{CQI}P_{RI}) = 0$. When both wideband CQI/PMI and sub-band CQI reporting are configured, the reporting instances satisfy the equation $(10n_f + \lfloor n_s/2 \rfloor - N_{offset}^{CQI}) \bmod P_{CQI} = 0$. Figure 10.33 illustrates an example of wideband and sub-band CQI reporting. Reporting period, reporting offset, and configuration index of CQI/PMI and RI reports are listed in Table 10.15 [5].

In the case of collision of a CSI report with PUCCH reporting type 3, 5, or 6 of one serving cell with a CSI report with PUCCH reporting type 1, 1a, 2, 2a, 2b, 2c, or 4 of the same serving cell, the CSI report with PUCCH reporting type

Petitioners' Exhibit 1021
Nokia of America Corp., et al. v. KT Corporation, et al.
Case No. IPR2025-00036; U.S. Patent No. 11,627,631
Page 805 of 1122

(1, 1a, 2, 2a, 2b, 2c, or 4) has lower priority and will be dropped. If the UE is configured with more than one serving cell, it transmits a CSI report corresponding to only one serving cell in any given subframe.

10.7.2.3 PUCCH format 3

For downlink carrier aggregation and when there are simultaneous transmissions on multiple downlink component carriers, multiple HARQ feedback bits are generated and sent by the UE. As discussed earlier, PUCCH format 1b in conjunction with resource selection can be used in this case; however, if the number of HARQ feedback bits is greater than four, this method is not going to be an efficient solution from a performance perspective. In order to support efficient transmission of a larger number of HARQ feedback bits, PUCCH format 3, which was introduced in LTE Rel-10, can be used. The main distinction of PUCCH format 3, as illustrated in Figure 10.34, is DFT-precoded OFDM, i.e., the same transmission scheme used for the uplink transmission. The HARQ feedback bits, one or two per downlink component carrier, depending on the transmission mode configured for that particular component carrier, are concatenated with an SR bit into a sequence of bits where the bits corresponding to unscheduled transport blocks are set to zero. The concatenated bits are block coded and scrambled using a cell-specific scrambling sequence to randomize inter-cell interference.

The resulting 48 bits are QPSK-modulated and divided into two groups, one per slot, i.e., 12 QPSK symbols per slot. PUCCH format 3 employs two SC-FDMA symbols in each slot (with normal cyclic prefix) for reference signal transmission. In each slot, the block of 12 DFT-precoded QPSK symbols is transmitted in the remaining SC-FDMA symbols. To further randomize the inter-cell interference, a cyclic shift is applied to the block of 12 QPSK symbols prior to DFT precoding. The cyclic shifts vary from one symbol to another. To increase the multiplexing capacity, an orthogonal sequence of length 5 is multiplied by each of the five SC-FDMA symbols carrying data in a slot. As a result, up to five terminals may share the same resource-block pair for PUCCH format 3. Different orthogonal cover sequences are used in the two slots to improve the performance in high-Doppler scenarios. To enable channel estimation for different transmissions sharing the same resource block, different reference signal sequences are used.

The orthogonal cover sequences are obtained as five DFT sequences. A Walsh sequence of length 4 may be used in the second slot of a subframe in order to make the last SC-FDMA symbol available when SRS is configured in that subframe. Similar to other PUCCH formats, a PUCCH format 3 resource can be represented by a single index from which the orthogonal sequence and the resource-block number can be derived. A terminal can be configured with four different resources for PUCCH format 3. In the scheduling grant for a secondary component carrier, 2 bits are used to inform the terminal of the four resources. In that case, the scheduler can avoid PUCCH collisions between different terminals by assigning different resources to different UEs. Due to significant differences in

Petitioners' Exhibit 1021
Nokia of America Corp., et al. v. KT Corporation, et al.
Case No. IPR2025-00036; U.S. Patent No. 11,627,631
Page 806 of 1122

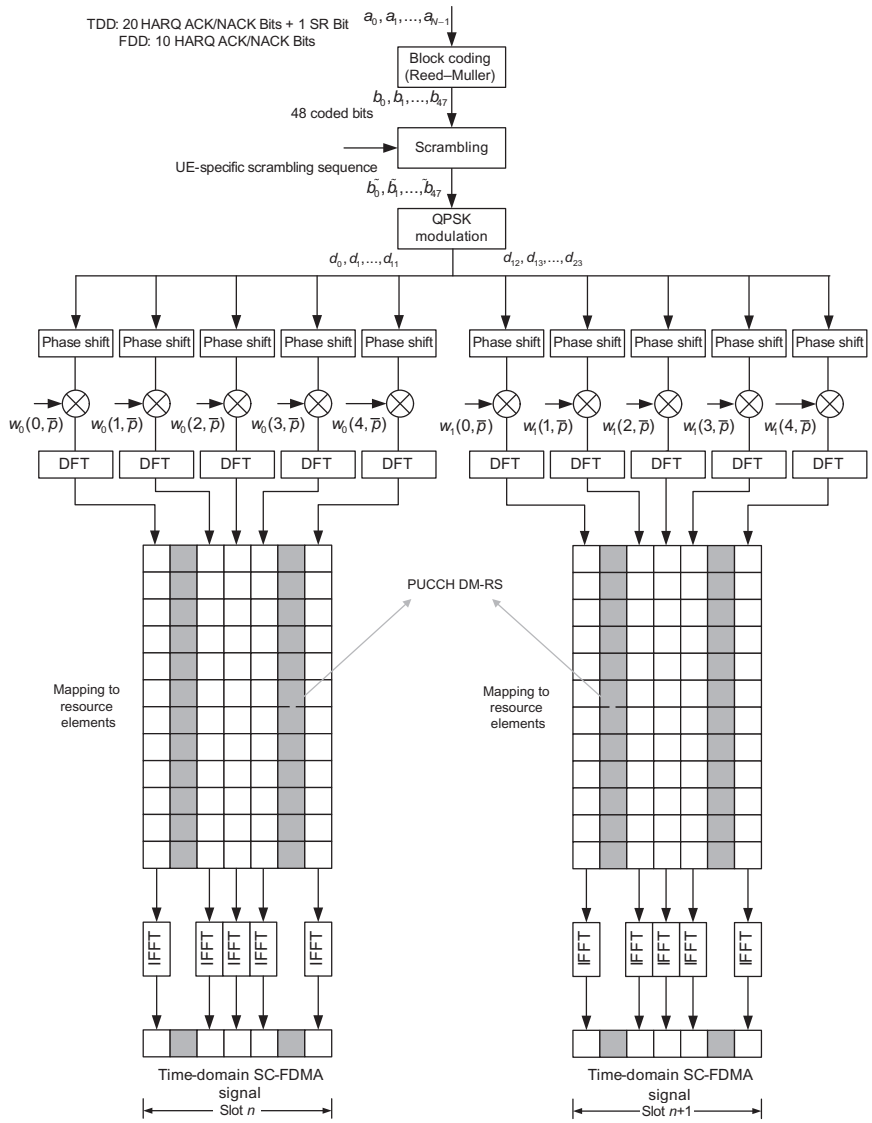


FIGURE 10.34

Illustration of PUCCH format 3 processing [14–16].

the structure of PUCCH format 3 compared to other PUCCH formats, resource blocks cannot be shared between them.

The physical layer processing of PUCCH format 3 can be described as follows. The block of coded bits $b_0, b_1, \ldots, b_{N_{\text{bit}}-1}$ are scrambled with a UE-specific

Petitioners' Exhibit 1021
Nokia of America Corp., et al. v. KT Corporation, et al.
Case No. IPR2025-00036; U.S. Patent No. 11,627,631
Page 807 of 1122

Table 10.16 Values of PUCCH Format 3 Orthogonal-Spreading Sequences [3]

Sequence Index n	Orthogonal Sequence $[w_0(0), w_1(0), \ldots, w_n(N_{SF}^{PUCCH}-1)]$	
	$N_{SF}^{PUCCH}=5$	$N_{SF}^{PUCCH}=4$
0	$[1 \quad 1 \quad 1 \quad 1 \quad 1]$	$[+1 \quad +1 \quad +1 \quad +1]$
1	$[1 \quad e^{j2\pi/5} \quad e^{j4\pi/5} \quad e^{j6\pi/5} \quad e^{j8\pi/5}]$	$[+1 \quad -1 \quad +1 \quad -1]$
2	$[1 \quad e^{j4\pi/5} \quad e^{j8\pi/5} \quad e^{j2\pi/5} \quad e^{j6\pi/5}]$	$[+1 \quad +1 \quad -1 \quad -1]$
3	$[1 \quad e^{j6\pi/5} \quad e^{j2\pi/5} \quad e^{j8\pi/5} \quad e^{j4\pi/5}]$	$[+1 \quad -1 \quad -1 \quad +1]$
4	$[1 \quad e^{j8\pi/5} \quad e^{j6\pi/5} \quad e^{j4\pi/5} \quad e^{j2\pi/5}]$	–

scrambling sequence, resulting in a block of scrambled coded bits $\overline{b}_0, \overline{b}_1, \ldots, \overline{b}_{N_{bit}-1}$ such that $\overline{b}_i = (b_i + c(i)) \bmod 2$, where the scrambling sequence $c(i)$ was defined in Chapter 9 and is initialized with $c_{init} = (\lfloor n_s/2 \rfloor + 1)(2N_{ID}^{cell}+1)2^{16} + n_{RNTI}$ at the start of each subframe where n_{RNTI} denotes the UE temporary identifier C-RNTI. The block of scrambled bits is then QPSK-modulated, resulting in a block of complex-valued modulation symbols $d_0, d_1, \ldots, d_{N_s-1}$ in which $N_s = N_{bit}/2 = 12$. The complex-valued symbols $d_0, d_1, \ldots, d_{N_s-1}$ is block-wise spread with the orthogonal sequences $w_0(i,\overline{p})$ and $w_1(i,\overline{p})$, yielding $N_{SF_0}^{PUCCH} + N_{SF_1}^{PUCCH}$ sets containing 12 values where:

$$y_n^{\overline{p}}(i) = \begin{cases} w_0(\overline{n},\overline{p})\exp\left(j\pi\left\lfloor n_{cs}^{cell}(n_s,l)/64\right\rfloor/2\right)d_i & n < N_{SF_0}^{PUCCH} \\ w_1(\overline{n},\overline{p})\exp\left(j\pi\left\lfloor n_{cs}^{cell}(n_s,l)/64\right\rfloor/2\right)d_{i+12} & n \geq N_{SF_0}^{PUCCH} \end{cases} \tag{10.8}$$

where $\overline{n} = n \bmod N_{SF_0}^{PUCCH}; n = 0, 1, \ldots, N_{SF_0}^{PUCCH} + N_{SF_1}^{PUCCH} - 1; N_{SF_0}^{PUCCH} = N_{SF_1}^{PUCCH} = 5;$ and $i = 0, 1, \ldots, 11$ in both slots in a subframe using normal PUCCH format 3 and $N_{SF_0}^{PUCCH} = 5; N_{SF_1}^{PUCCH} = 4$ in a subframe using shortened PUCCH format 3 to accommodate the SRS placement. The orthogonal sequences $w_0(i,\overline{p})$ and $w_1(i,\overline{p})$ are Walsh sequences whose values are given in Table 10.16.

Each set of the generated complex-valued symbols following the spreading function are cyclically shifted according to $\overline{y}_n^{\overline{p}}(i) = y_n^{\overline{p}}([i + n_{cs}^{cell}(n_s,l)] \bmod 12)$, where $n_{cs}^{cell}(n_s,l)$ is a cell-specific cyclic shift, n_s is the slot number within a radio frame, and l is the SC-FDMA symbol number within a slot. The cyclically shifted sets of complex-valued symbols are DFT-precoded according to:

$$z^{\overline{p}}(12n+k) = \frac{1}{\sqrt{12N_p}}\sum_{i=0}^{11}\overline{y}_n^{\overline{p}}(i)e^{-j\frac{\pi ik}{6}}; k = 0,1,\ldots,11; n = 0,1,\ldots,N_{SF_0}^{PUCCH} + N_{SF_1}^{PUCCH} - 1 \tag{10.9}$$

where N_p is the number of antenna ports used for PUCCH format 3 transmission, resulting in a block of complex-valued symbols $z_0^{\overline{p}}, z_1^{\overline{p}}, \ldots, z_{11\times(N_{SF_0}^{PUCCH}+N_{SF_1}^{PUCCH})}^{\overline{p}}$. The

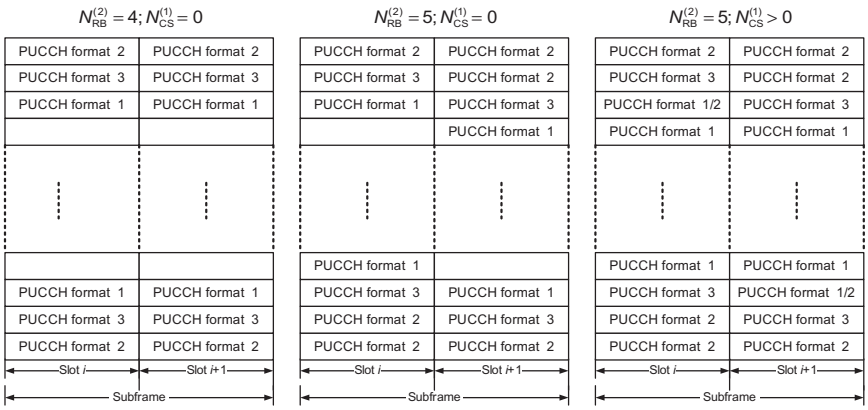


FIGURE 10.35

Example of resource-block allocation for various PUCCH formats [14].

amplitudes of the resulting complex-valued symbols are scaled in order to conform to the PUCCH transmit power, and are mapped in sequence starting with $z_0^{\overline{p}}$ to resource elements. PUCCH uses one resource block in each of the two slots in a subframe. Within the PRB used for PUCCH format 3 transmission, the mapping of complex symbols $z_i^{\overline{p}}|_{0,1,\ldots,11\times(N_{SF_0}^{PUCCH}+N_{SF_1}^{PUCCH})}$ to resource elements (k,l) on antenna port $\overline{p}$ that are not reserved for transmission of reference signals is in increasing order of the first index and then the second index, i.e., frequency first, starting with the first slot in the subframe. The relation between the antenna index $\overline{p}$ and the antenna port number p is given in 3GPP TS 36.211 [3]. In case of simultaneous transmission of SRS and PUCCH format 1, 1a, 1b, or 3 when there is one configured serving cell, a shortened PUCCH format is used where the last SC-FDMA symbol in the second slot of a subframe is skipped. Figure 10.35 shows an example of resource mapping for various PUCCH formats [14].

Precoder-based multi-layer transmission is only applied to uplink data transmission on PUSCH. LTE Rel-10 allows a terminal with multiple transmit antennas to use multi-antenna transmission for uplink control signaling on PUCCH, in order to achieve diversity gain. In that case, two-antenna transmit diversity is used for PUCCH transmission. The scheme is referred to as spatial orthogonal resource transmit diversity (SORTD). The main concept of SORTD is to transmit the uplink control signaling using different resources (time, frequency, and/or code) on different antennas. In principle, the PUCCH transmissions from the two antennas will be identical to PUCCH transmissions from two different terminals using different resources. Thus, SORTD provides additional diversity at the expense of using twice as many PUCCH resources compared to non-SORTD transmission. For four physical antennas at the terminal, implementation-specific antenna virtualization is used, where a transparent scheme is used to map the two-antenna-port signal to four physical antennas [16]. Figure 10.36 illustrates

Petitioners' Exhibit 1021
Nokia of America Corp., et al. v. KT Corporation, et al.
Case No. IPR2025-00036; U.S. Patent No. 11,627,631
Page 809 of 1122

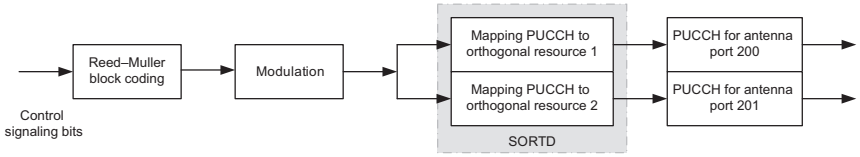


FIGURE 10.36

Illustration of SORTD concept [14,166].

PUCCH transmission using the SORTD concept [14]. SORTD is applicable to PUCCH formats 2/2a/2b and 3. The transmit diversity is not supported in LTE Rel-10 for PUCCH format 1b with channel selection. If the transmit antennas are uncorrelated, the SORTD scheme provides the optimal diversity performance at the expense of consuming extra resources which may reduce the PUCCH multiplexing capacity [15].

As mentioned earlier, PUCCH format 3 supports transmission of 48 coded bits. The actual number of HARQ feedback bits depends on the number of configured cells (active component carriers), the configured transmission modes of each carrier, and the HARQ ACK/NACK bundling window size (i.e., the number of downlink subframes associated with a single uplink subframe applicable to TDD systems). In FDD mode, the maximum payload size of ten HARQ ACK/NACK bits is supported corresponding to five component carriers each configured for MIMO transmission. In TDD mode, PUCCH format 3 supports HARQ feedback payload size of up to 20 bits. If the number of HARQ ACK/NACK bits is greater than 20, spatial bundling (i.e., a logical AND) of the ACK/NACK bits corresponding to the two codewords within a downlink subframe is performed for each of the serving cells. The maximum payload size carried by PUCCH format 3 in LTE Rel-10 is 21 bits, in which 20 bits are associated with HARQ ACK/NACK and 1 bit corresponds to SR. The HARQ feedback bits are concatenated in ascending order of the downlink component-carrier index. For payload sizes less than or equal to 11 bits, Reed−Muller channel codes from LTE Rel-8 are used in conjunction with circular-buffer rate-matching. When the payload size is larger than 11 bits, alternate ACK/NACK bits are input to two separate Reed−Muller encoders [15].

In order to alleviate inter-cell interference effects, cell-specific scrambling per SC-FDMA symbol was introduced. The PUCCH resource to be used for format 3 is signaled explicitly to the UE. A set of four resources is configured by RRC signaling, of which one resource is assigned dynamically for each ACK/NACK occurrence using an indicator transmitted in the transmit power control (TPC) field of the PDCCH corresponding to PDSCH on the secondary component carrier(s) [15]. The PDCCH assignments on the secondary component carriers in a given subframe indicate the same value. If transmit diversity is used for PUCCH format 3, higher-layer signaling is used to configure four pairs of PUCCH resources. The PDCCH assigning resources for the secondary cell PDSCH indicates one of these pairs to be used by the two antenna ports. If no PDCCH

Petitioners' Exhibit 1021
Nokia of America Corp., et al. v. KT Corporation, et al.
Case No. IPR2025-00036; U.S. Patent No. 11,627,631
Page 810 of 1122

corresponding to PDSCH on a secondary cell is received in a given subframe and a single PDSCH is received on the primary cell, a UE that is configured for PUCCH format 3 would instead use the LTE Rel-8 PUCCH format 1a or 1b.

10.7.3 Physical uplink shared channel

The PUSCH is used to transmit the uplink shared channel (UL-SCH) and L1/L2 control information. The UL-SCH is the transport channel used for transmitting uplink data (a transport block). The L1/L2 control signaling carries HARQ acknowledgments for received downlink shared channel (DL-SCH) transport blocks, channel quality reports, and SRs. The physical layer processing stages are shown in Figure 10.37. The information bits are channel coded by a turbo coder with a basic code rate of 1/3, which is adapted to a suitable code rate through a rate-matching process. This is followed by symbol-level channel interleaving which follows a simple time-first mapping where adjacent data symbols are mapped first to the adjacent SC-FDMA symbols in the time-domain and then across the sub-carriers. The coded and interleaved bits are then scrambled by a length-31 Gold code prior to modulation mapping, DFT-spreading, sub-carrier mapping, and OFDM modulation. The signal is frequency-shifted by half a sub-carrier prior to transmission, to avoid the distortion caused by the DC sub-carrier being concentrated in one resource block. The modulation schemes supported in the uplink are QPSK, 16QAM, and 64QAM (optional for lower UE categories). To generate the PUSCH payload, each transport block undergoes transport block coding. The encoding process includes 24-bit CRC calculation, code block segmentation and 24-bit CRC attachment to code segments (if any), turbo encoding, and rate-matching with redundancy and code block concatenation. Furthermore, coding of control signaling information is carried out with the resulting codewords time-multiplexed and interleaved with the UL-SCH data. The control information includes CQI, PMI, RI, and HARQ feedback.

The transport block size for PUSCH data transmission is signaled in the corresponding resource grant in PDCCH, i.e., DCI format 0 or LTE Rel-10 DCI format 4 for SU-MIMO. Combined with the MCS, the transport block size reflects the effective code rate. The permissible transport-block-size indices, MCSs, and RVs for PUSCH are given in Table 10.17. In most cases, a generally linear range of code rates are available for each resource allocation size. However, one exception is an index which allows a transport block size of 328 bits in a single resource-block allocation with QPSK modulation, which corresponds to a code rate greater than unity. This is primarily designed to support cell-edge VoIP transmissions using only one resource block per subframe, allowing the UE's power spectral density to be maximized for improved coverage, as well as using the TTI bundling where the transmission is repeated in four consecutive subframes, together with typically three retransmissions at 16 ms intervals [16].

Following the above summary, let us discuss the physical layer processing of the UL-SCH in more detail. When a transport block $a_0, a_1, \ldots, a_{N_A-1}$ of length N_A

Petitioners' Exhibit 1021
Nokia of America Corp., et al. v. KT Corporation, et al.
Case No. IPR2025-00036; U.S. Patent No. 11,627,631
Page 811 of 1122

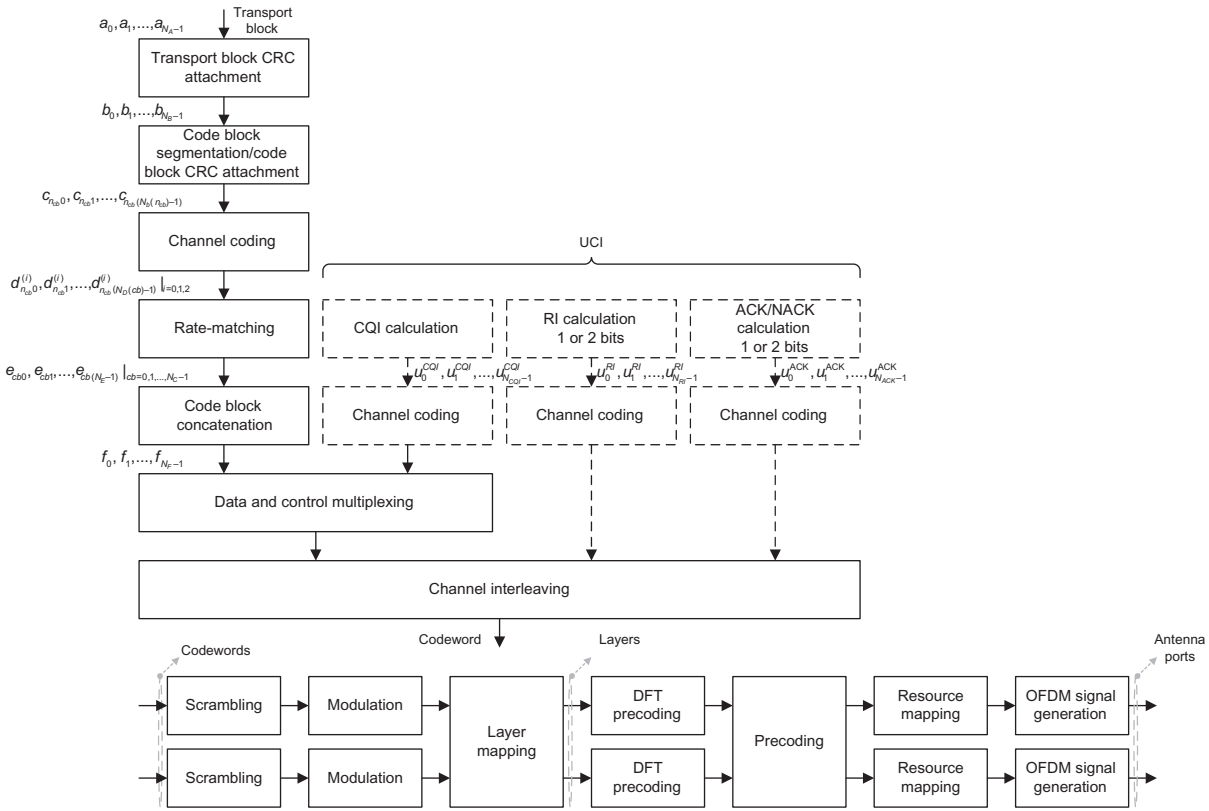


FIGURE 10.37

Physical layer processing for uplink shared channel [15,153].

Table 10.17 Modulation, Transport Block Size Index, and Redundancy Version for PUSCH [5]

MCS Index	Modulation Order	Transport Block Size Index	Redundancy Version
0	2	0	0
1	2	1	0
2	2	2	0
3	2	3	0
4	2	4	0
5	2	5	0
6	2	6	0
7	2	7	0
8	2	8	0
9	2	9	0
10	2	10	0
11	4	10	0
12	4	11	0
13	4	12	0
14	4	13	0
15	4	14	0
16	4	15	0
17	4	16	0
18	4	17	0
19	4	18	0
20	4	19	0
21	6	19	0
22	6	20	0
23	6	21	0
24	6	22	0
25	6	23	0
26	6	24	0
27	6	25	0
28	6	26	0
29		Reserved	1
30			2
31			3

is delivered to the physical layer, it is appended by 24 parity bits $p_0, p_1, \ldots, p_{23}$ where the entire transport block is used to calculate the CRC parity bits. The lowest order information bit a_0 is mapped to the most significant bit of the transport block. The 24 parity bits are calculated using the generator polynomial

Petitioners' Exhibit 1021
Nokia of America Corp., et al. v. KT Corporation, et al.
Case No. IPR2025-00036; U.S. Patent No. 11,627,631
Page 813 of 1122

$G_{\text{CRC-24A}}(D)$.[10] The CRC-attached bits $b_0, b_1, \ldots, b_{N_B-1}$ are fed to the code block segmentation unit, where $N_B = N_A + 24$ is the number of bits in the transport block including CRC (see Figure 10.37).

In LTE/LTE-Advanced, a minimum and maximum code block size is specified so that the block sizes are compatible with the block sizes supported by the turbo interleaver, where the minimum code block size is 40 bits and the maximum code block size is 6144 bits. If the length of the CRC-added input block is greater than the maximum code block size, the input block is segmented. When the input block is segmented, it is segmented into $N_C = \left\lceil N_B/(\underbrace{6144}_{\text{Maximum TB Size}} - \underbrace{24}_{\text{CRC Length}}) \right\rceil$ code blocks. Each code block is appended with 24-bit CRC. Padding bits are appended to the beginning of the segment (if required) so that the code block sizes match a set of valid turbo interleaver block sizes. If no segmentation is needed, then only one code block is produced. If N_B is less than the allowed minimum code block size, then zeros are added to the beginning of the code block in order to attain a total of 40 bits. Figure 10.38 illustrates the code segmentation and second CRC attachment process.

The code block segments, following the code block segmentation function, are denoted by $c_{n_{\text{cb}}0}, c_{n_{\text{cb}}1}, \ldots, c_{n_{\text{cb}}(N_b(n_{\text{cb}})-1)}$, where n_{cb} denotes the code block number and $N_b(n_{\text{cb}})$ is the number of bits in the code block number n_{cb}. The code blocks are appended with 24-bit CRC and are fed to the channel coding block. The total number of code blocks is denoted by N_C and each code block is individually turbo-coded.

The code block segments then go through turbo coding. Turbo coding is a form of forward error correction which improves the transmission reliability and robustness by adding redundancy to the code. The turbo encoder scheme used is a parallel concatenated convolutional code (PCCC)[11] with two recursive convolutional coders and a contention-free QPP interleaver, as shown in Figure 10.39. The encoder generates three output streams $d_k^{(0)}, d_k^{(1)}, d_k^{(2)}$, achieving a code rate of 1/3. Turbo-coded blocks are delivered to the rate-matching block. As shown in Figure 10.39, the input to the first constituent encoder is the input bit stream to the turbo coding block. The input to the second constituent encoder is the output of the QPP interleaver, i.e., a permutated version of the input sequence. The role of the interleaver is to spread the information bits such that in the event of a burst error, the two code streams are affected differently allowing data to be recoverable. There are two output sequences from each encoder: a systematic (x_k, x'_k) output and a parity (z_k, z'_k) output. Only one of the systematic sequences, x_k is used

[10] $G_{\text{CRC}-24A}(D) = D^{24} + D^{23} + D^{18} + D^{17} + D^{14} + D^{11} + D^{10} + D^7 + D^6 + D^5 + D^4 + D^3 + D + 1$.

[11] The first class of turbo code was the PCCC. Since the introduction of the original parallel turbo codes in 1993, many other classes of turbo code have been discovered, including serial versions and repeat-accumulate codes. Iterative turbo decoding methods have also been applied to more conventional FEC systems, including Reed-Solomon corrected convolutional codes [28,54].

Petitioners' Exhibit 1021
Nokia of America Corp., et al. v. KT Corporation, et al.
Case No. IPR2025-00036; U.S. Patent No. 11,627,631
Page 814 of 1122

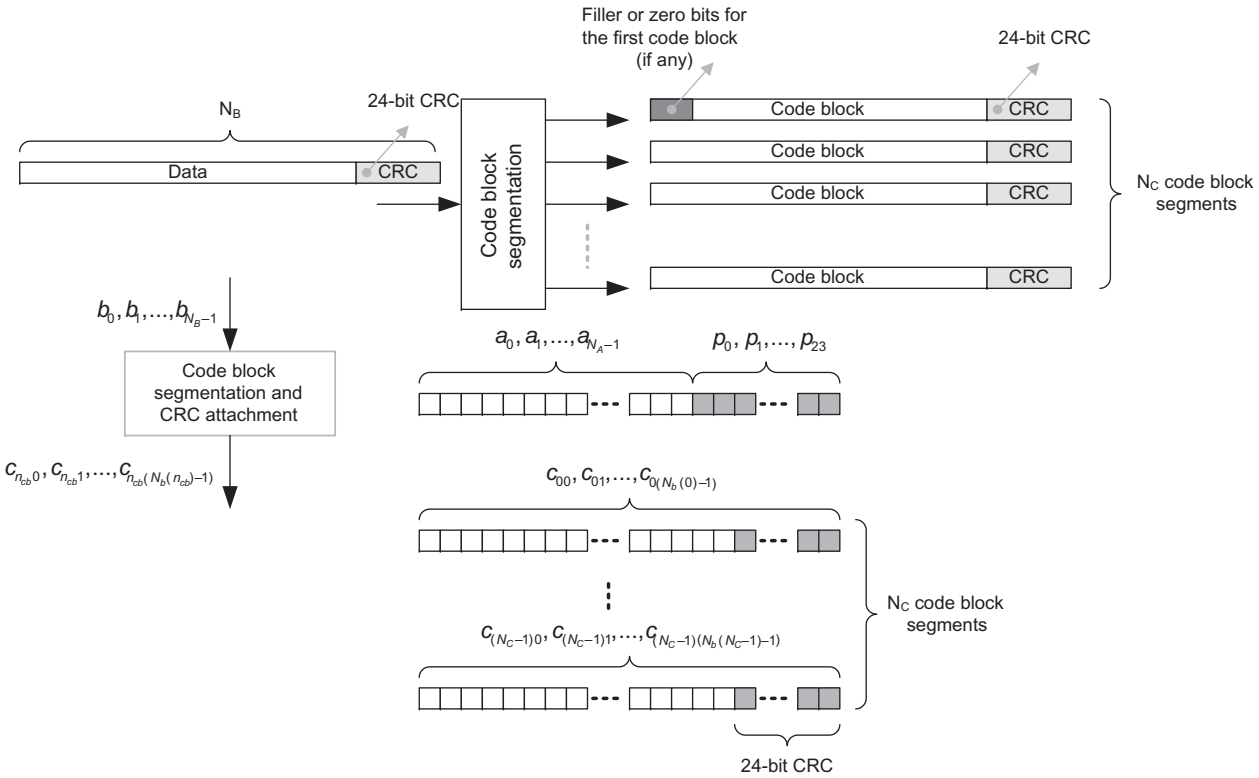


FIGURE 10.38

Code block segmentation and CRC attachment [4,153,155].

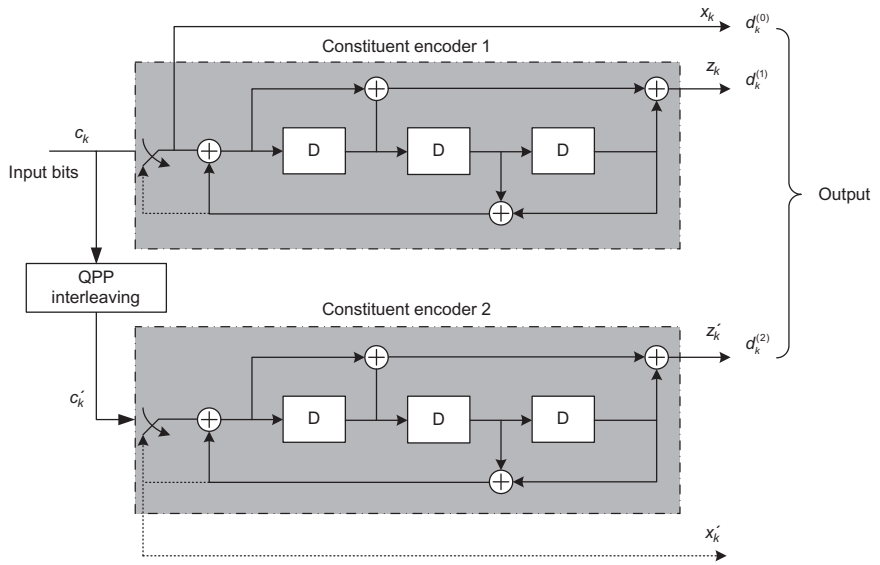


FIGURE 10.39

LTE/LTE-Advanced turbo encoder structure [4].

as an output, as the other x'_k is simply a permutated version of the chosen systematic sequence. After the turbo coding procedure, the output bits are denoted by $d^{(i)}_{n_{\text{cb}}0}, d^{(i)}_{n_{\text{cb}}1}, \ldots, d^{(i)}_{n_{\text{cb}}(N_D-1)}|_{i=0,1,2}$, where $N_D = N_{\text{cb}} + 4$ denotes the number of bits in the ith coded stream for code block number n_{cb}.

Note that a standard convolutional coder initializes its internal registers to an all-zeros state and ensures that the coder finishes in an all-zeros state by padding the end of the input sequence with $L_{\text{constraint-length}}$ zeros. Since the decoder has prior knowledge of the start and end state of the encoder, it can decode the data. Driving a recursive coder to an all-zeros state using this method is not possible. To overcome this problem trellis termination is used. A tail-biting convolutional coder initializes its internal shift registers to the last $L_{\text{constraint-length}}$ bits of the current input block, rather than an all-zeros state. This means that the start and end states are the same without the need to append zeros to the input block, eliminating the unnecessary overhead to terminate the coder by padding the input with zeros. The drawback to this method is that the decoder becomes more complicated since the initial state is unknown. However, it is known that the start and end sequences are the same [28]. Note that the number of output bits N_D following tail-biting convolutional coding with rate 1/3 is $N_D = N_{\text{cb}}$. The tail-biting convolutional coding with different rates is used for coding of control information in the downlink and uplink [4] (Figure 10.40).

Petitioners' Exhibit 1021
Nokia of America Corp., et al. v. KT Corporation, et al.
Case No. IPR2025-00036; U.S. Patent No. 11,627,631
Page 816 of 1122

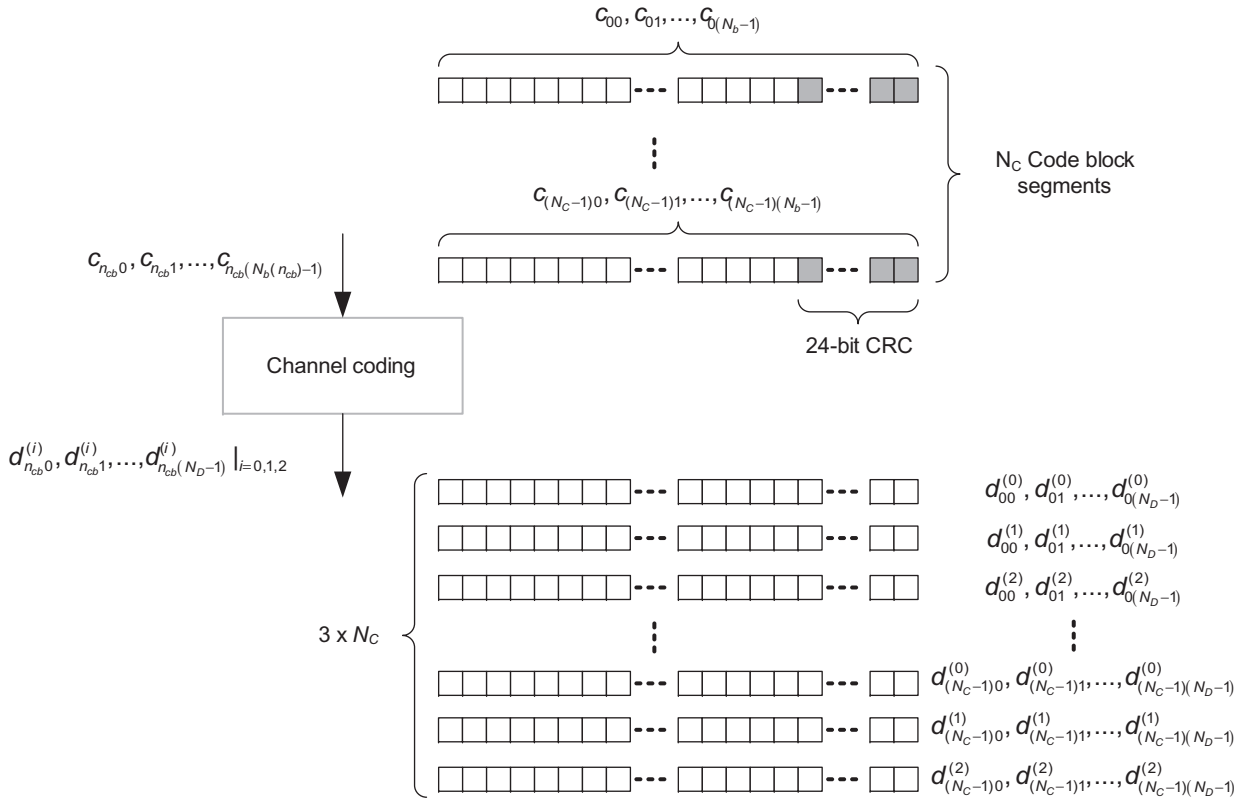


FIGURE 10.40

Demonstration of the channel coding process in LTE/LTE-Advanced [153].

Petitioners' Exhibit 1021
Nokia of America Corp., et al. v. KT Corporation, et al.
Case No. IPR2025-00036; U.S. Patent No. 11,627,631
Page 817 of 1122

The rate-matching block creates an output bit stream with a desired code rate. As the number of bits available for transmission depends on the available resources, the rate-matching algorithm is capable of producing any arbitrary rate. The 3-bit streams from the turbo encoder are interleaved, followed by bit collection to create a circular buffer. Bits are selected and pruned from the buffer to create an output bit stream with the desired code rate. The process is illustrated in Figure 10.41. The three sub-block interleavers used in the rate-matching block are identical. Interleaving is a technique to reduce the impact of burst errors on a signal, as consecutive bits of data will not be corrupted. The sub-block interleaver reshapes the encoded bit sequence in a row-by-row fashion to form a matrix. The bit collection stage creates a virtual circular buffer by combining the three interleaved encoded bit streams. Bits are then selected and pruned from the circular buffer to create an output sequence length which meets the desired code rate.

The HARQ error correction scheme is incorporated into the rate-matching algorithm of LTE/LTE-Advanced. For any desired code rate, the coded bits are output serially from the circular buffer from a starting location, given by the RV, wrapping around to the beginning of the buffer, if the end of the buffer is reached and null bits are discarded. Different redundancy versions and hence starting points allow retransmission of selected data. Being able to select different starting points enables the two main methods of reassembling data at the receiver in the HARQ process. In chase combining, retransmissions contain the same data and parity bits, whereas in incremental redundancy, the retransmissions contain different redundancy information so that the receiver gains knowledge upon each retransmission. The rate-matched code blocks are now concatenated back together. This is done by sequentially concatenating the rate-matched blocks together to create the output of the channel coding.

The output of the rate-matching function $e_{\text{cb0}}, e_{\text{cb1}}, \ldots, e_{\text{cb}(N_E(cb)-1)}$, where cb denotes the code block index and $N_E(\text{cb})$ is the number of rate-matched bits for code block number cb, serves as input to the code block concatenation module, which sequentially concatenates the rate-matched blocks together to create the output of the channel coding $f_0, f_1, \ldots, f_{N_F-1}$, where N_F represents the total number of coded bits for transmission of the given transport block over N_l transmission layers. The latter excludes the bits used for control information when it is multiplexed with UL-SCH data. The control information comprises CQI (and/or PMI), HARQ ACK/NACK, and RI. Different coding rates for the control information are achieved by allocating a different number of coded symbols for its transmission (Figure 10.42).

As shown in Figure 10.37, when control data is transmitted in PUSCH, the channel coding procedures for HARQ feedback $u_0^{\text{ACK}}, u_1^{\text{ACK}}, \ldots, u_{N_{\text{ACK}}-1}^{\text{ACK}}$, RI information $u_0^{\text{RI}}, u_1^{\text{RI}}, \ldots, u_{N_{\text{RI}}-1}^{\text{RI}}$, and CQI information $u_0^{\text{CQI}}, u_1^{\text{CQI}}, \ldots, u_{N_{\text{CQI}}-1}^{\text{CQI}}$ are performed independently.

An important issue related to transmission of control signaling on PUSCH is how to maintain the performance/reliability of control signaling at the desired level. It is noted that power control will set the SINR target of PUSCH according

Petitioners' Exhibit 1021
Nokia of America Corp., et al. v. KT Corporation, et al.
Case No. IPR2025-00036; U.S. Patent No. 11,627,631
Page 818 of 1122

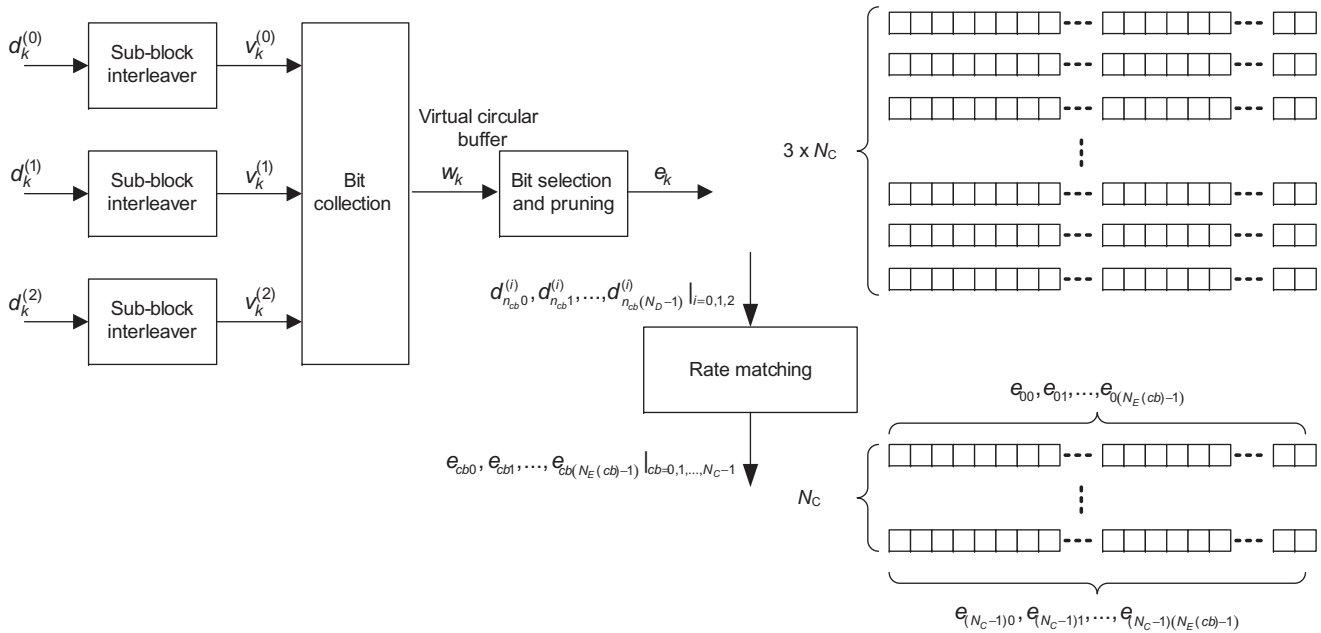


FIGURE 10.41

LTE/LTE-Advanced rate-matching procedures [4].

Petitioners' Exhibit 1021
Nokia of America Corp., et al. v. KT Corporation, et al.
Case No. IPR2025-00036; U.S. Patent No. 11,627,631
Page 819 of 1122

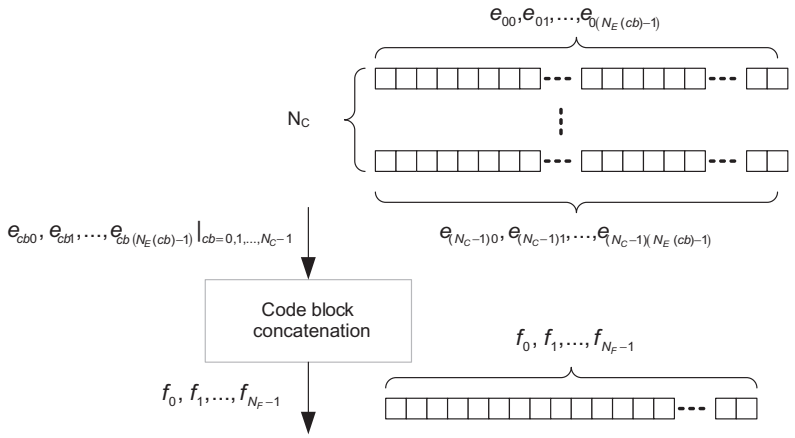


FIGURE 10.42

Illustration of code block concatenation.

to the data channel. Therefore, the control channel has to adapt to the SINR operating point set for data. One way to adjust the available resources would be to apply different power offset values for data and control parts. The problem with the latter power adjustment scheme is that the single-carrier property of the uplink signal is compromised. Therefore, this scheme is not used in the LTE uplink control and data multiplexing. Instead, a scheme based on a variable coding rate for the control information is used. This is achieved by varying the number of coded symbols for control channel transmission. To minimize the overall overhead related to inclusion of the control signaling information, the size of physical resources allocated to control transmission is scaled according to PUSCH quality. Note that the coding rate of control signaling, in this case, is given implicitly by the MCS of PUSCH data.

When the UE transmits HARQ feedback or RI bits, it is required to determine the number of coded modulation symbols per layer N_Q for HARQ ACK/NACK or RI. When only a single transport block is transmitted in PUSCH containing HARQ feedback or RI bits, the number of modulation symbols per layer is determined using the following equation [4]:

$$N_Q = \min\left(\left\lceil \frac{N_x N_{\text{sc}}^{\text{PUSCH-initial}} N_s^{\text{PUSCH-initial}} \beta_{\text{offset}}^{\text{PUSCH}}}{\sum_{\text{cb}=0}^{N_C-1} N_{\text{cb}}} \right\rceil,\ 4\, N_{\text{sc}}^{\text{PUSCH}}\right) \tag{10.10}$$

where $N_x = N_{\text{ACK}}$ or N_{RI} is the number of HARQ ACK/NACK bits or RI bits, $N_{\text{sc}}^{\text{PUSCH}}$ is the number of sub-carriers associated with scheduled PUSCH transmission over one SC-FDMA symbol, and $N_s^{\text{PUSCH-initial}}$ is the number of SC-FDMA symbols per subframe for initial PUSCH transmission for the same transport

Petitioners' Exhibit 1021
Nokia of America Corp., et al. v. KT Corporation, et al.
Case No. IPR2025-00036; U.S. Patent No. 11,627,631
Page 820 of 1122

block, given by $N_s^{\text{PUSCH-initial}} = \left[2(N_s^{\text{UL}} - 1) - N_{\text{SRS}}\right]$, in which $N_{\text{SRS}} = 1$, if the UE transmits PUSCH and SRS in the same subframe for initial transmission, or if the PUSCH resource allocation for initial transmission even partially overlaps with the cell-specific SRS subframe and bandwidth configuration, or if the subframe for initial transmission is a UE-specific type-1 SRS subframe; otherwise $N_{\text{SRS}} = 0$. The parameters $N_{\text{sc}}^{\text{PUSCH-initial}}$, N_C, and N_{cb} are obtained from the initial PDCCH/ePDCCH for the same transport block. For the case where two transport blocks are transmitted in PUSCH containing HARQ feedback or RI bits, the number of modulation symbols per layer is determined by $N_Q = \max[\min(N'_Q, 4N_{\text{sc}}^{\text{PUSCH}}), \min(N_Q)]$ [5].

The offset parameter $\beta_{\text{offset}}^{\text{PUSCH}}$ is used to adjust the quality of control signals for the PUSCH data channel. It is a UE-specific parameter configured by higher layer signaling. Different control channels need their own offset-parameter setting. There are some issues that need to be taken into consideration when configuring the offset parameter as follows [17]:

- BLER operation point for the PUSCH data.
- BLER operation point for the L1/L2 control signaling.
- Difference in coding gain between control and data parts, due to different coding schemes and different coding block sizes (no coding gain with 1-bit ACK/NACK).

Different BLER operating points for data and control parts are due to the fact that HARQ is used for the data channels, whereas the control channels do not benefit from HARQ. The higher the difference in the BLER operating point between data and control channels, the larger is the offset parameter (and vice versa). Similar behavior also relates to the packet size. The highest offset values are needed with ACK/NACK signals due to the lack of coding gain.

The number of coded symbols N_Q used by the UE to transmit the HARQ feedback is determined using the number of HARQ bits (1 or 2 depending on the number of codewords in use), the scheduled PUSCH bandwidth expressed as a number of sub-carriers, the number of SC-FDMA symbols per subframe for the initial PUSCH transmission, and information obtained from the initial PDCCH/ePDCCH for the same transport block. Each positive ACK is encoded as "1", and NACK is encoded as "0." If HARQ feedback consists of a single bit of information u_0^{ACK}, corresponding to a single codeword, then it is encoded depending on the modulation order used for the transport block, e.g., if the transport block is modulated using 16QAM, then encoded HARQ feedback is represented as $\left[u_0^{\text{ACK}} \quad * \quad * \quad *\right]$. If the HARQ feedback consists of 2 bits of information $\left[u_0^{\text{ACK}} \quad u_1^{\text{ACK}}\right]$, where u_0^{ACK} and u_1^{ACK} correspond to the first and second codewords, respectively, and $u_2^{\text{ACK}} = (u_0^{\text{ACK}} + u_1^{\text{ACK}}) \bmod 2$, then they are encoded depending on the number of coded symbols, e.g., if $N_Q = 2$ then the encoded HARQ feedback is represented as $\left[u_0^{\text{ACK}} \quad u_1^{\text{ACK}} \quad u_2^{\text{ACK}} \quad u_0^{\text{ACK}} \; u_1^{\text{ACK}} \; u_2^{\text{ACK}}\right]$. For some values of N_Q, placeholders "*" are used to scramble the HARQ ACK/NACK

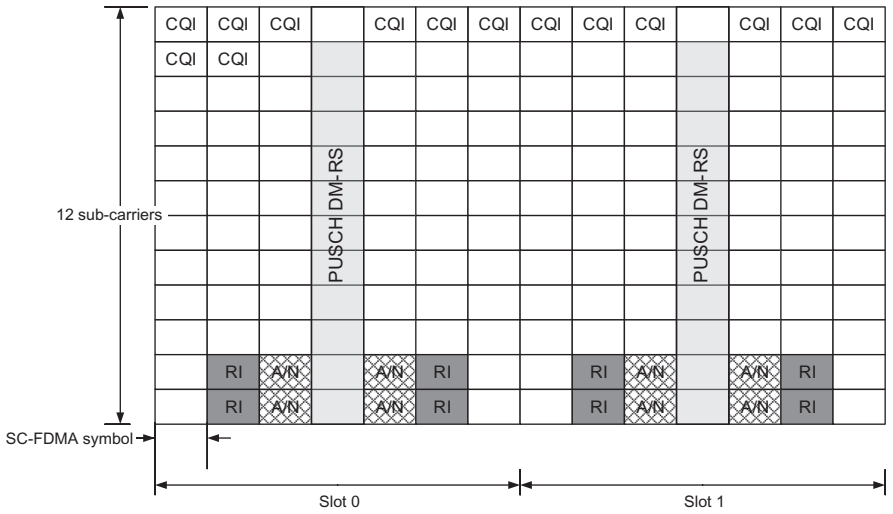


FIGURE 10.43

Multiplexing of control and data bits in PUSCH [15,16].

bits in such a way as to maximize the Euclidean distance of the modulation symbols carrying the HARQ information [4].

Let us further elaborate on the control and data multiplexing scheme on PUSCH. When a UCI is transmitted in a subframe in which the UE has been allocated resources on PUSCH, the UCI is multiplexed with the UL-SCH data prior to DFT operation in order to limit the uplink transmit power. In LTE Rel-8/9, UE is never allocated PUCCH and PUSCH in the same subframe. The number of resource elements reserved for transmission of the control bits in PUSCH is based on the MCS assigned for PUSCH and offset parameters $\beta_{\text{CQI-offset}}$, $\beta_{\text{HARQ-ACK-offset}}$, or $\beta_{\text{RI-offset}}$, which are semi-statically configured by higher layers. This would allow the use of different code rates for different types of UCI. The PUSCH data and UCI are never mapped to the same resource element. The UCI is mapped in such a way that it is present in both slots of the subframe. Since the eNB has prior knowledge of a UCI transmission, it can easily demultiplex the UCI and data. An example of multiplexing of CQI/PMI, HARQ ACK/NACK, and RI with the PUSCH data symbols to uplink resource elements is shown in Figure 10.43. As shown in the figure, the CQI/PMI symbols are mapped first followed by the data symbols. In this example, the RI bits occupy four symbols around DM-RS. The RI symbols are multiplexed with data symbols. The HARQ indicator (HI) ACK/NACK symbols are punctured into data symbols around DM-RS.

Petitioners' Exhibit 1021
Nokia of America Corp., et al. v. KT Corporation, et al.
Case No. IPR2025-00036; U.S. Patent No. 11,627,631
Page 822 of 1122

A modulation order similar to that used for UL-SCH data is applied to CQI/PMI. For small CQI and/or PMI report sizes up to 11 bits, a $(32, k)$ simplex code,[12] similar to the one used for PUCCH, is used, with optional circular repetition of encoded data and no CRC attached. For large CSI reports with greater than 11 bits, an 8-bit CRC is calculated and attached, and channel coding and rate-matching is performed using the tail-biting convolutional code.

The modulated HARQ ACK/NACK symbols are mapped immediately around the DM-RS position and modulated CQI/PMI symbols are time-first mapped across the subframe. The HARQ feedback resources are punctured into data starting from the lowest sub-carrier in the resource block. The maximum number of resources for HARQ ACK/NACK is four SC-FDMA symbols. In the case of 2-bit HARQ ACK/NACK, a $(3, 2)$ simplex coding is performed (see Table 10.18 for the mapping). The CQI resources are placed at the beginning of the data resources. For a CQI payload less than or equal to 11 bits, $(32, k)$ simplex code is used. For a CQI payload larger than 11 bits, tail-biting convolutional code is utilized. The RI bits are positioned next to the HARQ feedback bits in the resource block, irrespective of the presence or absence of HARQ ACK/NACK bits. In case of a 2-bit RI, a $(3, 2)$ simplex coding is employed.

The HARQ ACK/NACK resources are mapped to SC-FDMA symbols by puncturing the UL-SCH data. The positions next to the DM-RS are used in order to improve channel estimation. The maximum amount of resource for HARQ ACK/NACK is four SC-FDMA symbols. The coded RI symbols are placed next to the HARQ ACK/NACK symbol positions regardless of HARQ ACK/NACK presence in a given subframe. The modulation of 1- or 2-bit

Table 10.18 (3,2) Simplex Code for 2-Bit HARQ ACK/NACK and RI [15]

Input Bits	Output Bits
00	000
01	011
10	101
11	110

[12]Simplex codes belong to the family of linear error-correcting or error-detecting block codes that are simply implemented as polynomial codes by means of shift registers. Considered as (n, k) codes, they have a codeword length of $2^k - 1$. The minimum Hamming distance of binary simplex codes is equal to 2^{k-1}. They can be regarded as Reed−Muller codes shortened by one digit and are identical to the m-sequences of length 2^{k-1}, together with the zero word. They are called simplex because their codewords form a simplex, i.e., a finite graph of k points (the vertices) or a geometric figure, in which every vertex is connected to every other vertex, e.g., a triangle, in Hamming space (a Hamming space is the set of all 2^n binary strings of length n) [28].

Petitioners' Exhibit 1021
Nokia of America Corp., et al. v. KT Corporation, et al.
Case No. IPR2025-00036; U.S. Patent No. 11,627,631
Page 823 of 1122

HARQ ACK/NACK or RI is such that the Euclidean distance of the modulation symbols carrying HARQ ACK/NACK and RI is maximized; therefore, the outermost constellation points of the higher-order modulations are used, resulting in increased transmit power for ACK/NACK/ and RI transmission relative to the average PUSCH data power. The coding of the RI and CQI/PMI are performed separately, with the UL-SCH data being rate-matched around the RI resource elements similar to the case of CQI/PMI. The reference CQI/PMI MCS is computed from the CSI payload size and resource allocation. The channel coding and rate-matching of the control signaling without UL-SCH data is the same as that of multiplexing control with UL-SCH data. It is possible for the network to configure a UE to repeat each HARQ ACK/NACK transmission in multiple consecutive subframes in order to improve the reliability of the ACK/NACK transmission from power-limited UEs at the cell-edge, particularly in large cell deployments. The number of subframes over which each ACK/NACK transmission is repeated is signaled to the UE by a UE-specific parameter. Therefore, four different channel coding methods may be applied to control signals that are transmitted on PUSCH as follows:

- Repetition coding when 1-bit ACK/NACK is transmitted.
- $(3, 2)$ simplex coding when 2-bit ACK/NACK or RI are transmitted.
- $(32, k)$ Reed−Muller block codes are used when CQI/PMI information is less than 11 bits.
- Tail-biting convolutional coding with basic code rate of 1/3 is used when CQI/PMI information is greater than 11 bits.

As shown in Figure 10.37, the block of bits $b_0^{\text{cw}}, b_1^{\text{cw}}, \ldots, b_{N_{\text{bit}}(\text{cw})}^{\text{cw}}$, in which $N_{\text{bit}}(\text{cw})$ denotes the number of bits transmitted in codeword cw on PUSCH in one subframe, are scrambled with a UE-specific scrambling sequence prior to modulation, resulting in a block of scrambled bits $\overline{b}_0^{\text{cw}}, \overline{b}_1^{\text{cw}}, \ldots, \overline{b}_{N_{\text{bit}}(\text{cw})}^{\text{cw}}$. Note that each codeword is bit-wise multiplied with an orthogonal sequence and a UE-specific scrambling sequence to create a sequence of symbols for each codeword. The parameter $N_{\text{bit}}(\text{cw})$ is the number of bits transmitted using codeword cw. The scrambling sequence is a pseudo-random sequence based on length-31 Gold sequence which is initialized using the radio network temporary identifier associated with PUSCH transmission n_{RNTI}, the cell identifier $N_{\text{ID}}^{\text{cell}}$, the slot number within the radio frame n_{s}, and the codeword index at the start of each subframe as $c_{\text{init}} = n_{\text{RNTI}} 2^{14} + \ cw 2^{13} + \ \lfloor n_{\text{s}}/2 \rfloor 2^9 + N_{\text{ID}}^{\text{cell}}|_{\text{cw}=0,1}$. Scrambling with a cell-specific sequence serves the purpose of inter-cell interference mitigation. When a base station descrambles a received bit stream with a known cell-specific scrambling sequence, interference from other cells will be descrambled incorrectly and therefore only appear as uncorrelated noise. The scrambled codeword undergoes QPSK, 16QAM, or 64QAM modulation to generate complex-valued symbols, which provides the flexibility to optimize the data transmission depending on the channel conditions.

Petitioners' Exhibit 1021
Nokia of America Corp., et al. v. KT Corporation, et al.
Case No. IPR2025-00036; U.S. Patent No. 11,627,631
Page 824 of 1122

For each codeword cw, the block of scrambled bits $\overline{b}_0^{\text{cw}}, \overline{b}_1^{\text{cw}}, \ldots, \overline{b}_{N_{\text{bit}}(\text{cw})}^{\text{cw}}$ is modulated as described in 3GPP TS 36.211 [3], resulting in a block of complex-valued symbols $d_0^{\text{cw}}, d_1^{\text{cw}}, \ldots, d_{N_s(\text{cw})}^{\text{cw}}$. The complex-valued modulation symbols for each of the codewords to be transmitted are mapped to one or two layers. Complex-valued modulation symbols $d_0^{\text{cw}}, d_1^{\text{cw}}, \ldots, d_{N_s(\text{cw})}^{\text{cw}}$ associated with codeword cw are mapped to spatial layers $\mathbf{x}(i) = [x_0(i), x_1(i), \ldots, x_{N_l-1}(i)]^{\text{T}}|_{i=0,1,\ldots,N_s^l-1}$, where N_l is the number of layers and N_s^l is the number of modulation symbols per layer.

The precoding function in the uplink is not the same as that in the downlink (multi-antenna) precoding in LTE Rel-8/9. The block of complex-valued symbols $d_0^{\text{cw}}, d_1^{\text{cw}}, \ldots, d_{N_s(\text{cw})}^{\text{cw}}$ is divided into $N_s(cw)/N_{\text{sc}}^{\text{PUSCH}}$ sets. Each set of size $N_{\text{sc}}^{\text{PUSCH}} = N_{\text{DFT}}$ corresponds to one SC-FDMA symbol. A DFT is then applied to each set, which is essentially the precoding part of the SC-FDMA modulation. The size of the DFT, i.e., the value of $N_{\text{sc}}^{\text{PUSCH}} = N_{\text{DFT}}$, must be a prime number that is a product of 2, 3, and/or 5 and satisfies the following equation $N_{\text{RB}}^{\text{PUSCH}} = 2^{\alpha_2}3^{\alpha_3}5^{\alpha_5} \leq N_{\text{RB}}^{\text{UL}}$, where $\alpha_2, \alpha_3,$ and α_5 are a set of non-negative integers. The final stage in PUSCH physical layer processing is to map the symbols to the allocated physical resource elements. The allocation sizes are limited to values which are multiples of 2, 3, and 5 as described earlier. The latter limitation is imposed by the precoding stage. The symbols are mapped in increasing order beginning with sub-carriers, then SC-FDMA symbols. The SC-FDMA symbols carrying DM-RS or SRS are avoided during the mapping process. Figure 10.44 illustrates the order of mapping of the output of the precoder to the allocated resource blocks.

The codeword processing structure shown in Figure 10.37 includes enhancements that were added as part of LTE Rel-10, where the complex-valued symbols are mapped to one or more spatial layers following the baseband modulation. The layer mapping function maps the codeword(s) to spatial layer (s). For transmission on a single antenna port, a single layer is used and the antenna mapping is defined by $x_0(i) = d_0(i)|_{i=0,1,\ldots,N_s^l-1}$. For uplink spatial multiplexing, the number of layers N_l is less than or equal to the number of antenna ports N_p used for transmission of the PUSCH. The case of a single codeword mapped to multiple layers is only applicable when there are four antenna ports for PUSCH transmission [3].

As illustrated in Figure 10.37, the modulation symbols in units of $N_{\text{sc}}^{\text{PUSCH}} = 12N_{\text{RB}}^{\text{PUSCH}}$ symbols are fed to $N_{\text{sc}}^{\text{PUSCH}}-$point DFT, where $N_{\text{sc}}^{\text{PUSCH}}$ denotes the number of sub-carriers assigned to the transmission of PUSCH. The reason for the precoding is to reduce the cubic metric of the transmitted signal. For LTE, the DFT size and thus the size of resource allocation is limited to products of integer powers of 2, 3, and 5 ($N_{\text{RB}}^{\text{PUSCH}} = 2^{\alpha_2}3^{\alpha_3}5^{\alpha_5} \leq N_{\text{RB}}^{\text{UL}}$, where $\alpha_2, \alpha_3,$ and α_5 are non-negative integers). For each layer, the block of complex-valued symbols $x^{(l')}(0), x^{(l')}(1), \ldots, x^{(l')}(N_s^l - 1)|_{l'=0,1,\ldots,N_l-1}$ is divided into $N_s^l/N_{\text{sc}}^{\text{PUSCH}}$ sets, each corresponding to one SC-FDMA symbol. The transform

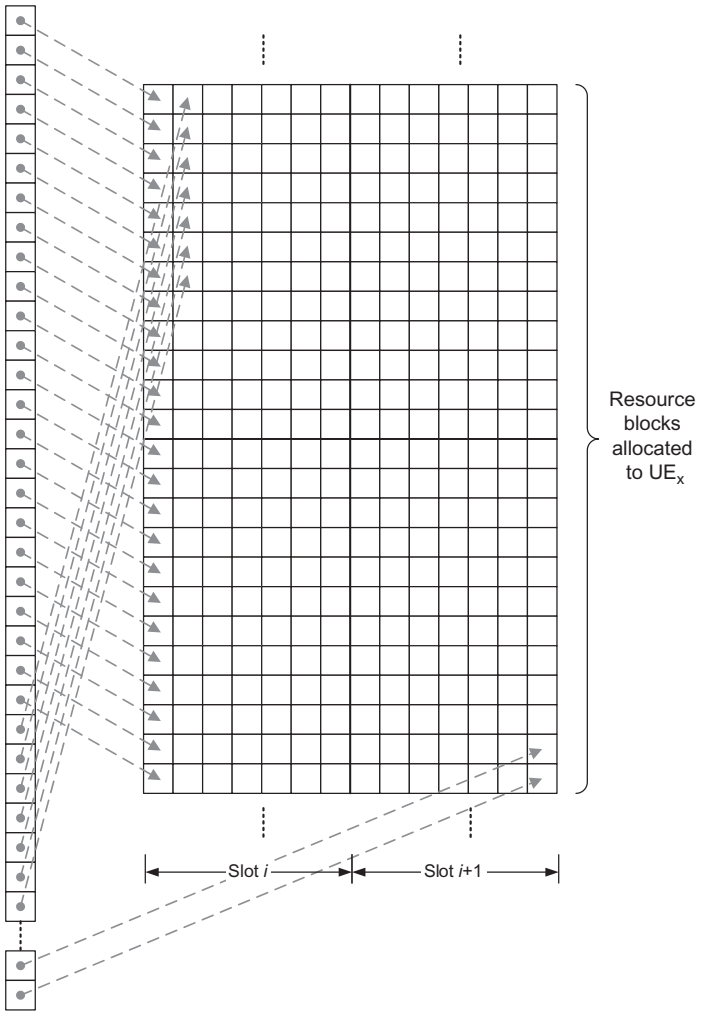


FIGURE 10.44

Example of mapping of the output of the precoder to resource elements in a subframe [155].

precoding is applied to each set, resulting in a block of complex-valued symbols $y^{(l')}(0), y^{(l')}(1), \ldots, y^{(l')}(N_s^l - 1)$ as follows (Table 10.19):

$$y^{(l')}(lN_{\text{sc}}^{\text{PUSCH}} + k) = \frac{1}{\sqrt{N_{\text{sc}}^{\text{PUSCH}}}} \sum_{i=0}^{M_{\text{sc}}^{\text{PUSCH}}-1} x^{(l')}(lN_{\text{sc}}^{\text{PUSCH}} + i)$$
$$\exp\left(-\text{j}\frac{2\pi ik}{N_{\text{sc}}^{\text{PUSCH}}}\right)\Big|_{k=0,1,\ldots,N_{\text{sc}}^{\text{PUSCH}}-1;l=0,1,\ldots,N_s^l/N_{\text{sc}}^{\text{PUSCH}}-1}$$

Petitioners' Exhibit 1021
Nokia of America Corp., et al. v. KT Corporation, et al.
Case No. IPR2025-00036; U.S. Patent No. 11,627,631
Page 826 of 1122

Table 10.19 Codeword-to-Layer Mapping for Uplink Spatial Multiplexing [3]

Number of Layers N_l	Number of Codewords N_{cw}	Layer Mapping $i = 0, 1, \ldots, N_s^l - 1$
1	1	$x_0(i) = d_0(i)$
2	1	$x_0(i) = d_0(2i)$ $x_1(i) = d_0(2i+1)$
2	2	$x_0(i) = d_0(i)$ $x_1(i) = d_1(i)$
3	2	$x_0(i) = d_0(i)$ $x_1(i) = d_1(2i)$ $x_2(i) = d_1(2i+1)$
4	2	$x_0(i) = d_0(2i)$ $x_1(i) = d_0(2i+1)$ $x_2(i) = d_1(2i)$ $x_3(i) = d_1(2i+1)$

The precoder module takes as input a block of vectors $\mathbf{y}(i) = (y^{(0)}(i), y^{(1)}(i), \ldots, y^{(N_l-1)}(i))^{\mathrm{T}}|_{i=0,1,\ldots,N_s^l-1}$ from the transform precoder, and generates a block of vectors $\mathbf{z}(i) = \mathbf{W}\mathbf{y}(i) = (z^{(0)}(i), z^{(1)}(i), \ldots, z^{(N_p-1)}(i))^{\mathrm{T}}|_{i=0,1,\ldots,N_s^p-1}$ that are mapped to resource elements. The precoding matrix $\mathbf{W}$ (codebook) is an $N_p \times N_l$ matrix and is given for $N_p = 2$ in Table 10.20 [3].

For each antenna port $\bar{p}$ that is used for transmission of PUSCH in a subframe, the block of complex-valued symbols $z^{(\bar{p})}(0), z^{(\bar{p})}(1), \ldots, z^{(\bar{p})}(N_s^p - 1)$ are multiplied with an amplitude scaling factor β_{PUSCH} in order to adjust the transmit power P_{PUSCH} and are then mapped sequentially, starting with $z^{(\bar{p})}(0)$, to PRBs on antenna port $\bar{p}$ assigned for transmission of PUSCH. The relation between the index $\bar{p}$ and the antenna port number p is given in 3GPP TS 36.211 [3]. The resource element (k, l) that is assigned to PUSCH information is required to meet certain criteria including the following:

- It is not used for transmission of reference signals.
- It is not part of the last SC-FDMA symbol in a subframe, if the UE transmits SRS in the same subframe.
- It is not part of the last SC-FDMA symbol in a subframe configured with cell-specific SRS, if the PUSCH transmission partly or fully overlaps with the cell-specific SRS bandwidth.
- It is not part of an SC-FDMA symbol reserved for possible SRS transmission in a UE-specific aperiodic SRS subframe.

The mapping to physical resource elements, as shown in Figure 10.44, is in increasing order of first, the sub-carrier (frequency) index k, and then the symbol

Petitioners' Exhibit 1021
Nokia of America Corp., et al. v. KT Corporation, et al.
Case No. IPR2025-00036; U.S. Patent No. 11,627,631
Page 827 of 1122

Table 10.20 Precoding Codebook for Transmission with Two Antenna Ports [3]

	Number of Layers	
Codebook Index	**Single Layer**	**Dual Layer**
0	$\frac{1}{\sqrt{2}}\begin{bmatrix}1\\1\end{bmatrix}$	$\frac{1}{\sqrt{2}}\begin{bmatrix}1 & 0\\0 & 1\end{bmatrix}$
1	$\frac{1}{\sqrt{2}}\begin{bmatrix}1\\-1\end{bmatrix}$	–
2	$\frac{1}{\sqrt{2}}\begin{bmatrix}1\\j\end{bmatrix}$	–
3	$\frac{1}{\sqrt{2}}\begin{bmatrix}1\\-j\end{bmatrix}$	–
4	$\frac{1}{\sqrt{2}}\begin{bmatrix}1\\0\end{bmatrix}$	–
5	$\frac{1}{\sqrt{2}}\begin{bmatrix}0\\1\end{bmatrix}$	–

(time) index l, starting with the first slot in the subframe. If uplink frequency hopping is disabled or the resource blocks allocated to PUSCH transmission are not contiguous in frequency, the set of PRBs to be used for transmission are identified by $n_{\mathrm{PRB}} = n_{\mathrm{VRB}}$, where n_{VRB} is obtained from the uplink scheduling grant. If uplink frequency hopping with a predefined hopping pattern is enabled, the set of PRBs used for PUSCH transmission in slot n_s is identified by the scheduling grant along with a predefined pattern according to the following equation [3]:

$$\underbrace{n'_{\mathrm{PRB}}(n_s)}_{\substack{\text{Allocated PRB with adjusted indexing starting at 0 following PUCCH allocation}}} = \left(\underbrace{n'_{\mathrm{VRB}}}_{\substack{\text{Allocated VRB with adjusted indexing starting at 0 following PUCCH allocation}}} + \underbrace{f_{\mathrm{hopping}}(i)L_{\text{sub-band}}}_{\text{Hopping function}} + \underbrace{\left((L_{\text{sub-band}}-1)-2(n'_{\mathrm{VRB}} \bmod L_{\text{sub-band}})\right)f_{\mathrm{mirror}}(i)}_{\text{Mirroring function}} \right) \bmod (L_{\text{sub-band}}N_{\text{sub-band}}) \tag{10.11}$$

In the above equation $i = \lfloor n_s/2 \rfloor$ for the case of inter-subframe hopping and $i = n_s$ for the case of intra- and inter-subframe hopping, $n_{\mathrm{PRB}}(n_s) = n'_{\mathrm{PRB}}(n_s) + \lceil N_{\mathrm{RB}}^{\mathrm{offset}}/2 \rceil | N_{\text{sub-band}} > 1$, and $n'_{\mathrm{VRB}} = n_{\mathrm{VRB}} - \lceil N_{\mathrm{RB}}^{\mathrm{offset}}/2 \rceil | N_{\text{sub-band}} > 1$. The parameter n_{VRB} is obtained from the scheduling grant and PUSCH hopping offset $N_{\mathrm{RB}}^{\mathrm{offset}}$ is provided by the higher layers. The size of each sub-band is given as $L_{\text{sub-band}} = \lfloor (N_{\mathrm{RB}}^{\mathrm{UL}} - N_{\mathrm{RB}}^{\mathrm{offset}} - N_{\mathrm{RB}}^{\mathrm{offset}} \bmod 2)/N_{\text{sub-band}} \rfloor | N_{\text{sub-band}} > 1$. The number

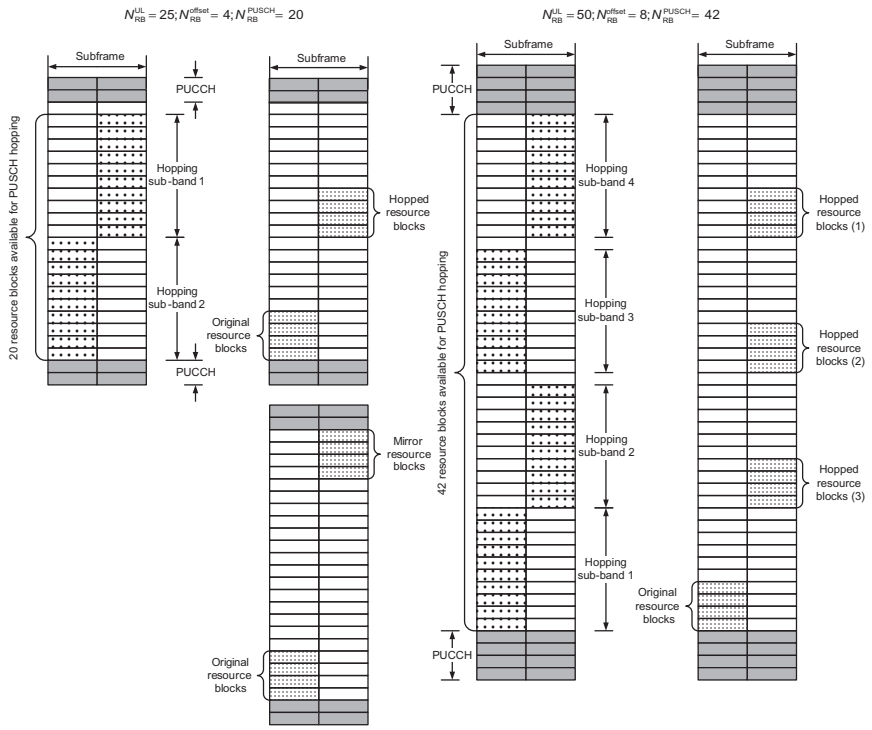


FIGURE 10.45

Example of PUSCH resource hopping/mirroring in 5 and 10 MHz channels [14].

of sub-bands $N_{\text{sub-band}}$ is signaled by the higher layers. The binary function $f_{\text{mirror}}(i) \in \{0, 1\}$ determines if the mirroring function is used.

In the above equation, the component identified as hopping function shifts the VRB allocation by an integer number of sub-bands. The shift is defined using a pseudo-random sequence which can be calculated by the UE and the eNB. In type 1 frame structure, the pseudo-random sequence is initialized using the physical layer cell identity $N_{\text{ID}}^{\text{cell}}$, whereas in type 2 frame structure, the pseudo-random sequence is initialized using a combination of the physical layer cell identity and the radio frame number $(2^9(n_f \bmod 4) + N_{\text{ID}}^{\text{cell}})$. The mirroring component in the above equation mirrors the VRB allocation within the sub-band. Mirroring is applied when the binary pseudo-random function $f_{\text{mirror}}(i) = 1$, which results in reflecting a VRB allocation starting "x" resource blocks from the bottom of the sub-band around the center of the sub-band such that the mirrored VRB allocation starts "x" resource blocks from the top of the sub-band (Figure 10.45). The pseudo-random mirroring component is initialized similar to the hopping component. Modular arithmetic is applied to the result of the hopping pattern function to provide wrap around, which ensures that the resource blocks after hopping remain within the boundaries of the subframe.

Petitioners' Exhibit 1021
Nokia of America Corp., et al. v. KT Corporation, et al.
Case No. IPR2025-00036; U.S. Patent No. 11,627,631
Page 829 of 1122

Note that in addition to the hopping pattern, there is also a cell-specific mirroring pattern defined in a cell. The mirroring pattern controls, on a slot-by-slot basis, whether mirroring within each sub-band should be applied to the assigned resource blocks. In principle, mirroring implies that the resource blocks within each sub-band are numbered in reversed order. Figure 10.45 illustrates an example of PUSCH resource allocations assuming 5 and 10 MHz channel bandwidth. In this example, PUCCH occupies four or eight resource blocks (depending on the bandwidth) in each slot, and the UE is informed through higher-layer signaling that those resource blocks are not available for hopping. The PUSCH hopping offset $N_{\mathrm{RB}}^{\mathrm{offset}}$ is used for this purpose. The value of the hopping offset is rounded up to an even number, if the received value is not even.

As shown in Figure 10.45, there are two hopping modes specified in LTE/LTE-Advanced: (1) inter-subframe hopping where the resource blocks allocated by DCI format 0 are used for even-numbered transmission of uplink transport blocks, while hopped resource blocks are used for odd-numbered transmission of uplink resource blocks; and (2) intra- and inter-subframe hopping where the resource blocks allocated by DCI format 0 are used in the first time slot within the subframe while the hopped resource blocks are used in the second time slot [14].

10.7.4 Physical random-access channel

The physical random access channel is used by non-synchronized UEs during initial system access, handover, and prior to downlink data transmission. The UE transmits a preamble sequence over PRACH, which may be randomly selected from a group of sequences assigned by the eNB. The structure of the sequence is shown in Figure 10.46. The sequences are Zadoff−Chu sequences of length 839 for the FDD mode (139 for TDD mode). There are 64 different cyclic shifts that are generated from each root Zadoff−Chu sequence with zero cross-correlation. Therefore, different cyclic shifts of the base sequence are mutually orthogonal. The PRACH resource consists of six consecutive resource blocks. The location of PRACH is indicated by an offset parameter signaled by higher layers. There is one PRACH region per subframe in the FDD mode. Multiple UEs can access the PRACH region using different preambles. The UEs may select preambles randomly, which may result in a collision. Therefore, contention resolution mechanisms are necessary. The PRACH may not always present in every subframe and every radio frame. The PRACH configuration parameter indicates frame number and subframe numbers in which the PRACH resource is available.

The sub-carrier spacing for PRACH transmission is different from that of other channels in the uplink. The number of sub-carriers is equal to the length of preamble (839 for the FDD mode and 139 for TDD). The sub-carrier spacing is 1.25 kHz, resulting in longer symbol duration of 800 μs for the FDD mode (133 μs for TDD mode). The sub-carrier spacing also results in an effective guard band because the entire 1.08 MHz (six resource blocks) is not used for PRACH transmission.

Petitioners' Exhibit 1021
Nokia of America Corp., et al. v. KT Corporation, et al.
Case No. IPR2025-00036; U.S. Patent No. 11,627,631
Page 830 of 1122

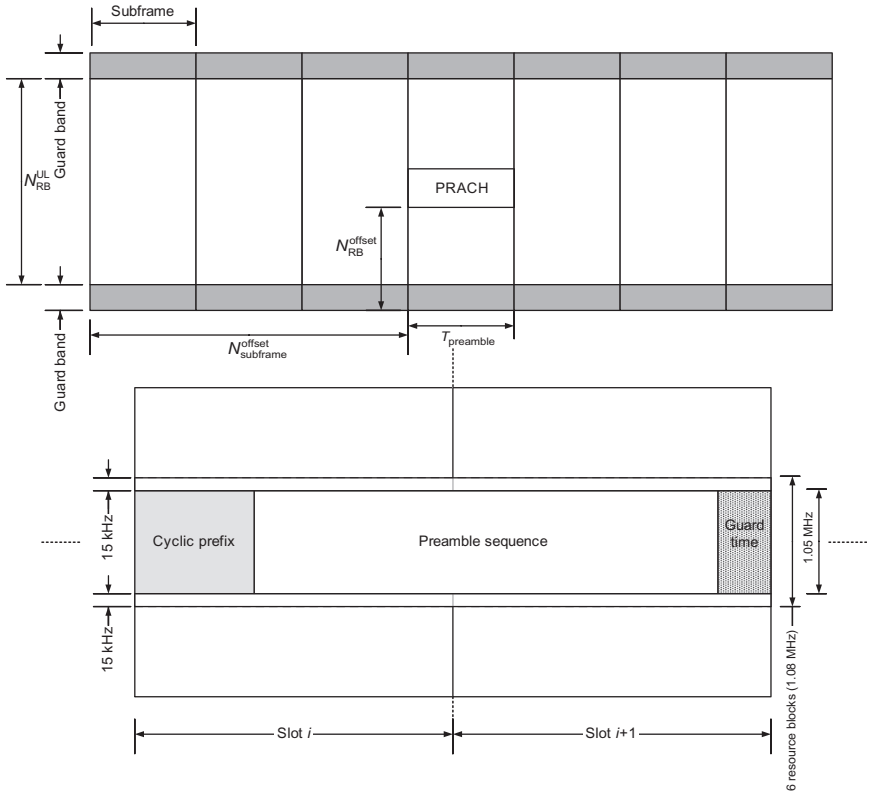


FIGURE 10.46

Structure of PRACH in time- and frequency-domain [14,153].

The PRACH preamble is an OFDM-based signal, but it is generated using a different structure from other uplink transmissions; most notably it uses narrower sub-carrier spacing which is not orthogonal to the PUSCH, PUCCH, and SRS; therefore, those channels will suffer from some interference from the PRACH. However, the sub-carrier spacing used by PRACH is an integer sub-multiple of the sub-carrier spacing used for the other channels, thereby PUSCH, PUCCH, and SRS do not interfere on the PRACH. Prior to initiation of the non-synchronized physical random-access procedure, the physical layer receives random-access channel parameters (i.e., PRACH configuration and time/frequency position), and parameters for determining the root sequences and their cyclic shifts in the preamble sequence set for the primary cell (i.e., index to logical root sequence table, cyclic shift N_{CS}, and whether set type is unrestricted or restricted) from the higher layers.

The PRACH preamble consists of a cyclic prefix, useful part of the sequence, and then a guard period which is simply an unused portion of time up to the end of the last subframe occupied by PRACH. This guard period allows for timing

Petitioners' Exhibit 1021
Nokia of America Corp., et al. v. KT Corporation, et al.
Case No. IPR2025-00036; U.S. Patent No. 11,627,631
Page 831 of 1122

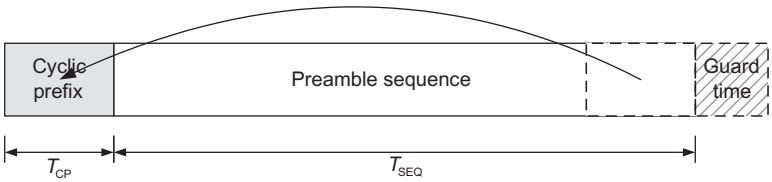


FIGURE 10.47

PRACH preamble structure in time.

uncertainty due to variability of the UE to eNB distance. Therefore, the size of the guard period determines the cell radius, as any propagation delay exceeding the guard time (GT) would cause the random-access preamble to overlap with the following subframe at the eNB receiver. The use of OFDM transmission with a cyclic prefix allows for implementation of an efficient frequency-domain-based receiver in the eNB to perform PRACH detection.

The UE aligns the start of the random-access preamble with the start of the corresponding uplink subframe at the UE, assuming a timing advance of zero. The preamble length is shorter than the PRACH slot in order to accommodate a gap for GT in order to absorb the variable propagation delay. Figure 10.48 shows two preambles received at the eNB with different timings depending on the propagation delay. The PRACH preamble sequence is optimized relative to its periodic autocorrelation property [15]. The random-access preamble, illustrated in Figure 10.47, consists of a cyclic prefix of length T_{CP} and a sequence of length T_{SEQ}. The parameter values are given in Table 10.21 and are configured by higher layers.

The transmission of the random-access preamble is triggered by the MAC sublayer and is restricted to certain time and frequency resources. These resources are identified in increasing order of the subframe number within the radio frame and the PRBs in the frequency-domain such that index 0 corresponds to the lowest numbered PRB and subframe within the radio frame. The PRACH resources within the radio frame are identified by a PRACH resource index. For frame structure type 1 with preamble formats 0−3, there is a maximum of one random-access resource per subframe. The start of the random-access preamble is aligned with the start of the corresponding uplink subframe at the UE assuming $N_{TA} = 0$, where N_{TA} is the length of the timing advance. The first PRB N_{RA} allocated to the PRACH transmission corresponding to preamble formats 0, 1, 2, and 3 is defined as $N_{RA} = N_{RA}^{offset}$, where the PRACH frequency offset parameter $0 \leq N_{RA}^{offset} \leq N_{RB}^{UL} - 6$ is defined as a PRB number configured by the higher layers (see Figure 10.46). For frame structure type 2 supporting PRACH preamble formats 0−4, there is a possibility for multiple random-access resources in an uplink subframe (or UpPTS for preamble format 4) depending on the uplink/downlink ratio. The PRACH sequence duration T_{SEQ} is chosen taking the following considerations into account (Table 10.22):

- There is a trade-off between sequence length and overhead, where on the one hand, the sequence length must be as long as possible to maximize the number

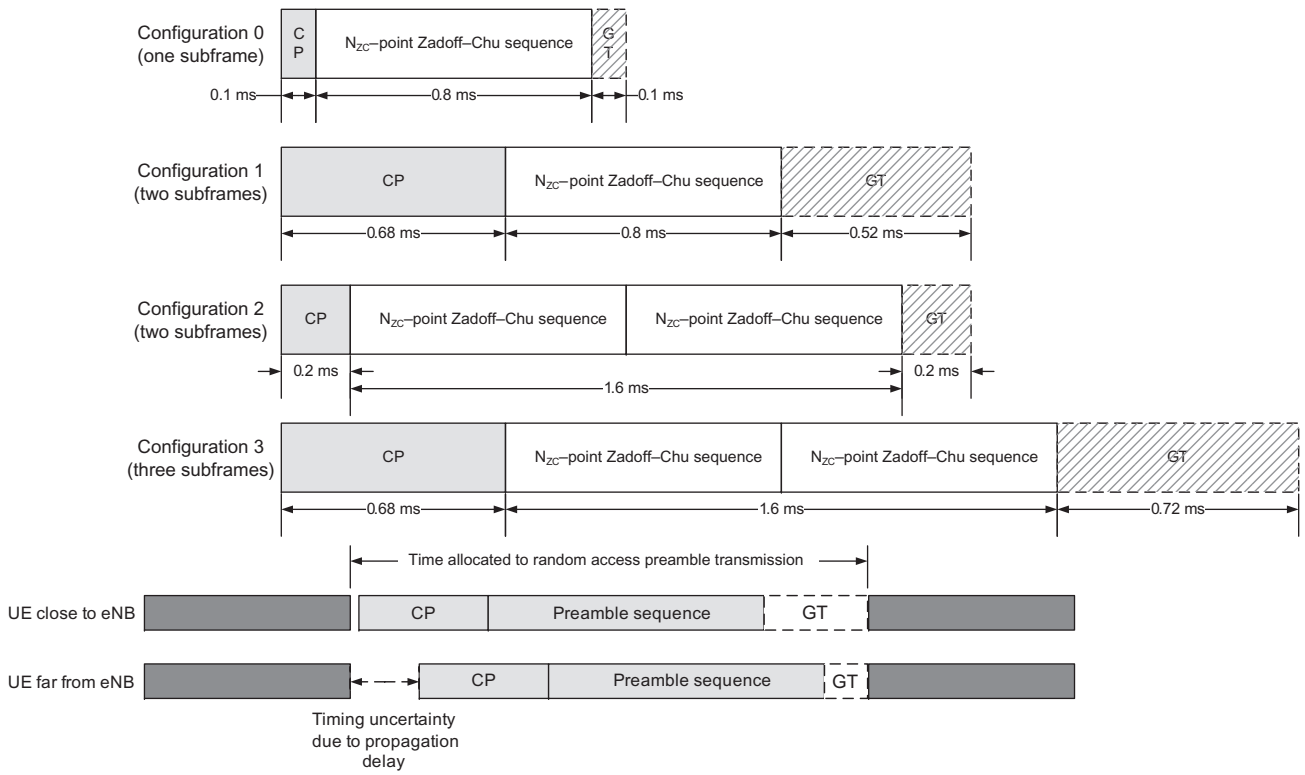


FIGURE 10.48

Illustration of PRACH preamble formats and mitigation of the impact of variable propagation delay on PRACH preamble [16].

Table 10.21 PRACH Preamble Parameters [3,14]

PRACH Preamble Format	Cyclic Prefix T_{CP}(μs)	Sequence Duration T_{SEQ}(μs)	Guard Time (μs)	Preamble Length (ms)	Maximum Supported Cell Range (km)
0	103.13	800	96.88	1	14.5
1	684.38	800	515.53	2	77.3
2	203.13	1600	196.88	2	29.5
3	684.38	1600	715.63	3	100.2
4[†]	14.58	133	9.38	0.16	1.4

[†]*Applicable to frame structure type 2 and special subframe configurations with UpPTS lengths of* 142.71 μs *(2 symbols with normal cyclic prefix) and* 166.67 μs *(2 symbols with extended cyclic prefix).*

of available orthogonal preambles, while on the other hand, the sequence must fit within a subframe in order to minimize the PRACH overhead. The lower bound for T_{SEQ} should support unambiguous round-trip time estimation for a UE located at the edge of the largest expected cell size including the maximum delay spread expected in such large cells.

- The length of the cyclic prefix must encompass the maximum round-trip delay and the maximum delay spread of the channel. Furthermore, for a cell-edge UE, the delay-spread energy at the end of the preamble is replicated at the end of the cyclic prefix, and is therefore within the preamble interval. Consequently, there is no need to include the maximum delay spread in the GT. Therefore, instead of locating the sequence in the center of the PRACH slot, it is shifted later by half of the maximum delay spread, allowing the maximum round-trip delay to be increased by the same amount. Note that, similar to a regular OFDM symbol, the residual delay spread at the end of the preamble from a cell-edge UE leaks into the next subframe, but this is taken care of by the cyclic prefix at the start of the next subframe to avoid any ISI.
- The sub-carrier spacing of PRACH and PUSCH must be numerically proportional. An additional benefit of this property is the possibility to reuse the FFT module from the SC-FDMA signal processing for PUSCH to implement the large DFT block involved in the PRACH transmitter and receiver. It is further desirable to minimize the orthogonality loss in the frequency-domain between the preamble sub-carriers and the sub-carriers of the adjacent uplink data transmissions. This is achieved if the PUSCH data symbol sub-carrier spacing Δf_{PUSCH} is an integer multiple of the PRACH sub-carrier spacing Δf_{RA}.
- Under a noise-limited scenario, which is typical in low density and medium to large suburban or rural cells, coverage performance can be estimated from a link budget calculation. Assuming an Okumura–Hata empirical model of

Petitioners' Exhibit 1021
Nokia of America Corp., et al. v. KT Corporation, et al.
Case No. IPR2025-00036; U.S. Patent No. 11,627,631
Page 834 of 1122

Table 10.22 Frame Structure Type 1 Random-Access Configuration [3]

Configuration Index	Preamble Format	System Frame Number (SFN)	Subframe Number	Configuration Index	Preamble Format	System Frame Number (SFN)	Subframe Number
0	0	Even	1	32	2	Even	1
1	0	Even	4	33	2	Even	4
2	0	Even	7	34	2	Even	7
3	0	Any	1	35	2	Any	1
4	0	Any	4	36	2	Any	4
5	0	Any	7	37	2	Any	7
6	0	Any	1, 6	38	2	Any	1, 6
7	0	Any	2,7	39	2	Any	2,7
8	0	Any	3, 8	40	2	Any	3, 8
9	0	Any	1, 4, 7	41	2	Any	1, 4, 7
10	0	Any	2, 5, 8	42	2	Any	2, 5, 8
11	0	Any	3, 6, 9	43	2	Any	3, 6, 9
12	0	Any	0, 2, 4, 6, 8	44	2	Any	0, 2, 4, 6, 8
13	0	Any	1, 3, 5, 7, 9	45	2	Any	1, 3, 5, 7, 9
14	0	Any	0, 1, 2, 3, 4, 5, 6, 7, 8, 9	46	N/A	N/A	N/A

15	0	Even	9	47	2	Even	9
16	1	Even	1	48	3	Even	1
17	1	Even	4	49	3	Even	4
18	1	Even	7	50	3	Even	7
19	1	Any	1	51	3	Any	1
20	1	Any	4	52	3	Any	4
21	1	Any	7	53	3	Any	7
22	1	Any	1, 6	54	3	Any	1, 6
23	1	Any	2,7	55	3	Any	2,7
24	1	Any	3, 8	56	3	Any	3, 8
25	1	Any	1, 4, 7	57	3	Any	1, 4, 7
26	1	Any	2, 5, 8	58	3	Any	2, 5, 8
27	1	Any	3, 6, 9	59	3	Any	3, 6, 9
28	1	Any	0, 2, 4, 6, 8	60	N/A	N/A	N/A
29	1	Any	1, 3, 5, 7, 9	61	N/A	N/A	N/A
30	N/A	N/A	N/A	62	N/A	N/A	N/A
31	1	Even	9	63	3	Even	9

distance-dependent path loss, the PRACH signal power received at the eNB can be written as follows [15]:[13]

$$\underbrace{P_{\mathrm{RA}}(R)}_{\substack{\text{PRACH signal power}\\ \text{at the eNB}}} = \underbrace{P_{\max}}_{\substack{\text{UE transmitter}\\ \text{EIRP}}} + \underbrace{G_{\mathrm{RX}}}_{\substack{\text{eNB receiver}\\ \text{antenna gain}\\ \text{(including cable loss)}}} - \underbrace{P_{\mathrm{L}}(R)}_{\substack{\text{Distance-dependent}\\ \text{path loss}}} - \underbrace{P_{\mathrm{PL}}}_{\substack{\text{Penetration}\\ \text{loss}}} - \underbrace{P_{\mathrm{FM}}}_{\substack{\text{Log-normal}\\ \text{fade margin}}} \tag{10.12}$$

In the above equation, variable R is the cell radius in kilometers. From the above path-loss estimate, the initial PRACH transmission power is obtained by adding a configurable offset. The random-access mechanism allows power ramping where the actual PRACH transmission power is increased following each unsuccessful random-access attempt. For the first attempt, the PRACH transmission power is set to the initial PRACH power. In most cases, this is sufficient for the random-access attempt to be successful. However, if the random-access attempt fails, the PRACH transmission power for the next attempt is increased by a configurable step size to increase the likelihood of the next attempt being successful. Since the random-access preamble is orthogonal to the user data, the need for power ramping to control intra-cell interference is more relaxed than in other systems with non-orthogonal random-access, and in many cases the transmission power is set such that the first random-access attempt with a high likelihood is successful, which results in lower access latencies.

As mentioned earlier, PRACH uses a narrower sub-carrier spacing than normal uplink transmission, specifically 1250 Hz for random-access preamble formats 0−3, and 7500 Hz for random-access preamble format 4. The ratio of the normal uplink sub-carrier spacing to PRACH sub-carrier spacing is 12 for random-access preamble formats 0−3 and 2 for random-access preamble format 4. The PRACH is designed to fit in the same bandwidth as six resource blocks of normal uplink transmission, i.e., 72 sub-carriers at 15,000 Hz sub-carrier spacing (1.08 MHz). This simplifies scheduling gaps in normal uplink transmission to allow for PRACH transmission opportunities. Therefore, there are 864 sub-carriers for random-access preamble formats 0−3, and 144 sub-carriers for random-access preamble format 4. However, in practice, random-access preamble formats 0−3 use 839 active sub-carriers, and random-access preamble format 4 uses 139 active sub-carriers.

[13]Effective isotropic radiated power (EIRP), also known as equivalent isotropic radiated power, is the measured radiated power in a single direction (i.e., for fixed azimuth and elevation angles). Typically, for antenna radiation pattern measurement, if a single value of EIRP is given, this will be the maximum value of the EIRP over all measured angles. EIRP can also be interpreted as the amount of power that a perfectly isotropic antenna would need to radiate to achieve the same measured value.

Petitioners' Exhibit 1021
Nokia of America Corp., et al. v. KT Corporation, et al.
Case No. IPR2025-00036; U.S. Patent No. 11,627,631
Page 837 of 1122

Similar to normal uplink SC-FDMA transmission, there is a shift equal to half sub-carrier spacing (7500 Hz), which for PRACH is equivalent to six sub-carrier shift. A further sub-carrier offset (seven sub-carriers for random-access preamble formats 0−3 and two sub-carriers for random-access preamble format 4) centers the PRACH transmission within the 1.08 MHz transmission bandwidth. In practice, PRACH sequence is an OFDM-based reconstruction of a Zadoff−Chu sequence in the time-domain. The OFDM modulator is used to position the Zadoff−Chu sequence in the frequency-domain, i.e., to place six resource blocks of PRACH in six consecutive resource blocks starting from a particular PRB denoted as N_{RA}. The output of the OFDM modulator in the time-domain is a Zadoff−Chu sequence, if the input to the OFDM modulator is a Zadoff−Chu sequence in the frequency-domain. Therefore, N_{ZC} active sub-carriers are set to the values of an N_{ZC}-point DFT of an N_{ZC}-sample Zadoff−Chu sequence.

The cyclically shifted Zadoff−Chu sequences have several properties including the following: the amplitude of the sequences is constant, which ensures efficient PA utilization and maintains the low PAPR properties of the single-carrier transmitter; the sequences further have ideal cyclic autocorrelation, which is important for obtaining an accurate timing estimation at the eNB. Finally, the cross-correlation of different preambles based on cyclic shifts of the same Zadoff−Chu root sequence is zero at the receiver as long as the cyclic shift N_{CS} used when generating the preambles is larger than the maximum round-trip propagation time in the cell plus the maximum delay spread of the channel. Therefore, due to the ideal cross-correlation property, there is no intra-cell interference from multiple random-access attempts using preambles derived from the same Zadoff−Chu root sequence. To support different cell sizes, the cyclic shift N_{CS} is broadcast as part of the system information. Therefore, in smaller cells, a small cyclic shift can be configured, resulting in a larger number of cyclically shifted sequences from each root sequence. For cell sizes under 1.5km, all 64 preambles can be generated from a single root sequence. In larger cells, a larger cyclic shift is configured in order to generate 64 preamble sequences, since a greater number of root Zadoff−Chu sequences are in use in the cell. Although the larger number of root sequences is not an issue, the zero cross-correlation property only holds between shifts of the same root sequence and from an interference perspective, it is advantageous to use as few root sequences as possible.

The detection of the random-access preamble, in principle, is based on the cross-correlation of the received signal with the root Zadoff−Chu sequences. One disadvantage of Zadoff−Chu sequences is the difficulty in separating a frequency offset from the distance-dependent delay. A frequency offset results in an additional correlation peak in the time-domain, a correlation peak that corresponds to a spurious terminal-to-base-station distance. In addition, the actual correlation peak is attenuated. At low-frequency offsets, this effect is negligible and the detection performance is hardly affected. However, at high Doppler frequencies,

Petitioners' Exhibit 1021
Nokia of America Corp., et al. v. KT Corporation, et al.
Case No. IPR2025-00036; U.S. Patent No. 11,627,631
Page 838 of 1122

the spurious correlation peak can be larger than the true peak. This results in erroneous detection, i.e., the correct preamble may not be detected or the delay estimate may be incorrect. To avoid the ambiguities resulting from spurious correlation peaks, the set of preamble sequences generated from each root sequence can be restricted. Restrictions imply that only some of the sequences that can be generated from a root sequence are used to define random-access preambles. The location of the spurious correlation peak relative to the actual peak depends on the root sequence; thus different restrictions should be applied for different root sequences. The restrictions are broadcast by the eNB as part of the system information [16].

The transmission opportunities for PRACH are allocated in time first and then in frequency, if time multiplexing is not sufficient to hold all opportunities of a PRACH configuration needed for a certain density value D_{RA} without overlapping in time, for random-access preamble formats 0−3, frequency multiplexing is performed according to the following equation: $N_{\mathrm{RA}} = N_{\mathrm{RA}}^{\mathrm{offset}} + 6\left\lfloor \frac{f_{\mathrm{RA}}}{2} \right\rfloor$ if $f_{\mathrm{RA}} \bmod 2 = 0$; otherwise $N_{\mathrm{RB}}^{\mathrm{UL}} - 6 - N_{\mathrm{RA}}^{\mathrm{offset}} - 6\left\lfloor \frac{f_{\mathrm{RA}}}{2} \right\rfloor$, where $N_{\mathrm{RB}}^{\mathrm{UL}}$ is the total number of uplink resource blocks (uplink bandwidth), f_{RA} is a frequency resource index within the considered time instance, N_{RA} is the first PRB allocated to the PRACH transmission, and PRACH frequency offset parameter $0 \le N_{\mathrm{RA}}^{\mathrm{offset}} \le N_{\mathrm{RB}}^{\mathrm{UL}} - 6$ is the first PRB available for PRACH expressed as a PRB number configured by higher layers (see Figure 10.46). Each random-access preamble occupies a bandwidth corresponding to six consecutive resource blocks for both frame structure types.

The random-access preambles are generated from Zadoff−Chu sequences with a zero-correlation zone. This means that the PRACH sequences are generated from one or several root Zadoff−Chu sequences. The network configures the set of preamble sequences which the UE is allowed to use. There are 64 preambles available in each cell. The set of 64 preamble sequences in a cell is obtained by including, in the order of increasing cyclic shift, all the available cyclic shifts of a root Zadoff−Chu sequence with the logical index *RACH_ROOT_SEQUENCE*, where the parameter *RACH_ROOT_SEQUENCE* is broadcast as part of the system information. Additional preamble sequences, in case 64 preambles cannot be generated from a single root Zadoff−Chu sequence, are obtained from the root sequences with the consecutive logical indices until all 64 sequences are found. The logical root sequence order is cyclic, i.e., the logical index 0 is consecutive to 837. The uth root Zadoff−Chu sequence is defined by:

$$x_u(n) = \exp\left(-\mathrm{j}\frac{\pi u n(n+1)}{N_{\mathrm{ZC}}}\right); 0 \le n \le N_{\mathrm{ZC}} - 1 \tag{10.13}$$

where the length N_{ZC} of the Zadoff−Chu sequence is either 839 for random-access preamble formats 0−3, or 139 for random-access preamble format 4. From the uth root Zadoff−Chu sequence, random-access preambles with zero

correlation zones (ZCZs)[14] of length $N_{CS} - 1$ are defined by cyclic shifts according to $x_{uv}(n) = x_u[(n + C_v) \bmod N_{ZC}]$, in which the value of the cyclic shift depends of the type of the sequence set. The unrestricted set or restricted sets are distinguished based on higher layer signaling.

The parameter N_{CS} is given in 3GPP TS 36.211 [3] for preamble formats 0−3 and 4. The parameter *ZCZ configuration* is provided by the higher layers (Table 10.23). The parameter *high-speed flag* is also provided by higher layers and determines whether unrestricted set or restricted set is used (Table 10.24).

The PRACH preamble sequence duration $T_{SEQ} = 1/\Delta f_{RA}$ is derived from the required PRACH preamble sequence energy to thermal noise power ratio E_s/N_0 in order to meet the target miss detection and false alarm probabilities, as follows: $T_{SEQ} = \frac{N_0 N_F}{P_{RA}(R)} \left(\frac{E_s}{N_0}\right)$, where N_0 is the thermal noise power density (in mW/Hz) and N_F is the noise figure of the eNB receiver. Typical target values for miss detection and false alarm probabilities are 10^{-2} and 10^{-3}, respectively. The 1600 μs preamble sequence of formats 2 and 3 is implemented by repeating the baseline 800 μs preamble sequence. These formats can provide up to 3dB link budget improvement, which is useful in large cells and/or to balance PUSCH/PUCCH and PRACH coverage at low data rates (Figure 10.49).

The PRACH slots shown in Figure 10.50 can be configured to occur in up to 16 different patterns or resource configurations. Depending on the number of UEs attempting to access the system in the same time interval, one or more PRACH resources may be allocated per PRACH slot period. The eNB is required to process the PRACH signal as soon as it is detected so that Msg2 of the RACH procedure can be sent within the required time window. If there is more than one PRACH resource per PRACH period, it is desirable to multiplex the PRACH resources in time rather than in frequency. This helps to avoid excessive processing at the eNB [15]. The available slot configurations are designed to simplify

[14]Definition of ZCZ sequences: let S denote a sequence set with M sequences of period L. Generally, the set of ZCZ sequences are characterized by the period of sequences L, the number of sequences in the set M, the length of the ZCZ L_{ZCZ}, and the number of phases P. It can be shown that the following mathematical upper bound concerning L_{ZCZ} exist $L_{ZCZ} \le L/M - 1$. The set S can be represented as $S = \{S_0, S_1, \ldots, S_p, \ldots, S_{M-1}\}$ and $S_p = \{s_0^p, s_1^p, \ldots, s_q^p, \ldots, s_{L-1}^p\}$, where $0 \le p \le M-1$ and $0 \le q \le L-1$, S_p and s_q^p denote a sequence and a sequence element, respectively. If all of the sequences in the set S satisfy the following autocorrelation and cross-correlation properties, then S is referred to as a set of ZCZ sequences or a ZCZ sequence set $\rho_{S_p}(l) = \sum_{q=0}^{L-1} s_q^p s^{p*}_{(q+l) \bmod L} = \begin{cases} 0 & -L_{ZCZ} \le l \le -1; 1 \le l \le L_{ZCZ} \\ \varepsilon_p & l = 0 \end{cases}$ and $\rho_{S_p S_{p'}}(l) = \sum_{q=0}^{L-1} s_q^p s^{p'*}_{(q+l) \bmod L} = 0$. In the above equation, symbol "*" denotes complex conjugate, $\rho_{S_p}(l)$ represents the periodic autocorrelation function of the sequence S_p, and $\rho_{S_p S_{p'}}(l)$ denotes the periodic cross-correlation function between the sequences S_p and $S_{p'}$, ε_p is the energy of the sequence S_p. If all of the elements of the sequence S_p are normalized complex-valued numbers, then the sequence energy ε_p is equal to L. In general, M, L, and L_{ZCZ} are referred to as the family size of the ZCZ sequence set, the period of the sequences, and the length of the ZCZ, respectively [167].

Petitioners' Exhibit 1021
Nokia of America Corp., et al. v. KT Corporation, et al.
Case No. IPR2025-00036; U.S. Patent No. 11,627,631
Page 840 of 1122

Table 10.23 PRACH Parameters [3,10]

Parameter	Size (bits)	Signaling Method	Description
PRACH time-domain configuration index	6	Broadcast (SIB2)	Provides information about the PRACH time-domain (subframe) configuration
PRACH frequency offset	7	Broadcast (SIB2)	Provides information about the PRACH frequency-domain configuration. Only applicable to TDD mode
Preamble format	2	Broadcast (SIB2)	For TDD there is also a short preamble, i.e., a total of five preamble formats
Root-sequence index	10	Broadcast (SIB2)	Used to generate cyclically shifted Zadoff–Chu sequences
Zero-correlation-zone length	4	Broadcast (SIB2)	Different interpretation depending on high-speed flag
High-speed flag	1	Broadcast (SIB2)	Selects between restricted and unrestricted preamble sets
PRACH transmit power setting	power Ramping Step 2 preamble Initial Received Target Power 4	Broadcast (SIB2)	*powerRampingStep* (0, 2, 4, or 6 dB), *preambleInitialReceivedTargetPower* (–120, –118, –116, –114, –112, –110, –108, –106, –104, –102, –100, –98, –96, –94, –92, or –90 dBm)

Table 10.24 Classification of PRACH Preambles to Restricted and Unrestricted Sets [3]

ZCZ Configuration Parameter	Format 4	Formats 0–3	
		N_{CS}	
	N_{CS}	Unrestricted Set	Restricted Set
0	2	0	15
1	4	13	18
2	6	15	22
3	8	18	26
4	10	22	32
5	12	26	38
6	15	32	46
7	N/A	38	55
8	N/A	46	68
9	N/A	59	82
10	N/A	76	100
11	N/A	93	128
12	N/A	119	158
13	N/A	167	202
14	N/A	279	237
15	N/A	419	–

Petitioners' Exhibit 1021
Nokia of America Corp., et al. v. KT Corporation, et al.
Case No. IPR2025-00036; U.S. Patent No. 11,627,631
Page 841 of 1122

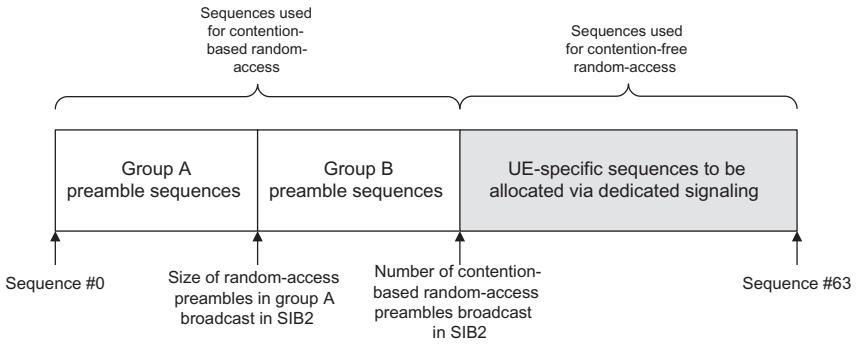


FIGURE 10.49

Classification of random-access preamble sequences [14].

PRACH receiver which may be used for multiple cells of an eNB, assuming a periodic pattern with period 10 or 20 ms.

The random-access preamble sequence can be generated at the system sampling rate by means of a large IDFT unit. The DFT block in Figure 10.51 is optional because the sequence can be directly mapped to the IDFT input in the frequency-domain. The cyclic shift can be implemented either in the time-domain after the IDFT or in the frequency-domain before the IDFT through a phase shift. For all possible system sampling rates, both cyclic prefix and sequence duration correspond to an integer number of samples. The method of Figure 10.51 does not require any time-domain filtering in the baseband, but requires large IDFT sizes (up to 24,576 for a 20 MHz spectrum allocation), which are practically cumbersome. Therefore, another option for generating the preamble consists of using small-size IDFT and shifting the preamble to the required frequency location through time-domain up-sampling and filtering (hybrid frequency/time-domain sequence generation method). Given that the preamble sequence length is 839, the smallest IFFT size that can be used is 1024. The size of the random-access cyclic prefix and preamble sequence duration has been chosen to provide an integer number of samples at the system sampling rate. The cyclic prefix can be inserted before the up-sampling and time-domain frequency shift, in order to minimize the intermediate storage requirements.

Given that the sampling rate for a 20 MHz LTE system is 30.72 MHz, and considering that the random-access preamble spans 0.8 ms, it can be concluded that the number of samples in time is equal to 24,576. Furthermore, it was mentioned that the PRACH sub-carrier spacing is 1.25 kHz, while the sub-carrier spacing for PUSCH and PUCCH is 15 kHz. As shown in Figure 10.51, in order to maintain the same sampling rate, a 12×2048 point DFT operation is needed for the PRACH signal generation at the transmitter side, if the entire processing is done in the frequency-domain. An alternative approach is to use time-domain signal generation and extraction which involves up-sampling and filtering operations at the transmitter. The drawback of

Petitioners' Exhibit 1021
Nokia of America Corp., et al. v. KT Corporation, et al.
Case No. IPR2025-00036; U.S. Patent No. 11,627,631
Page 842 of 1122

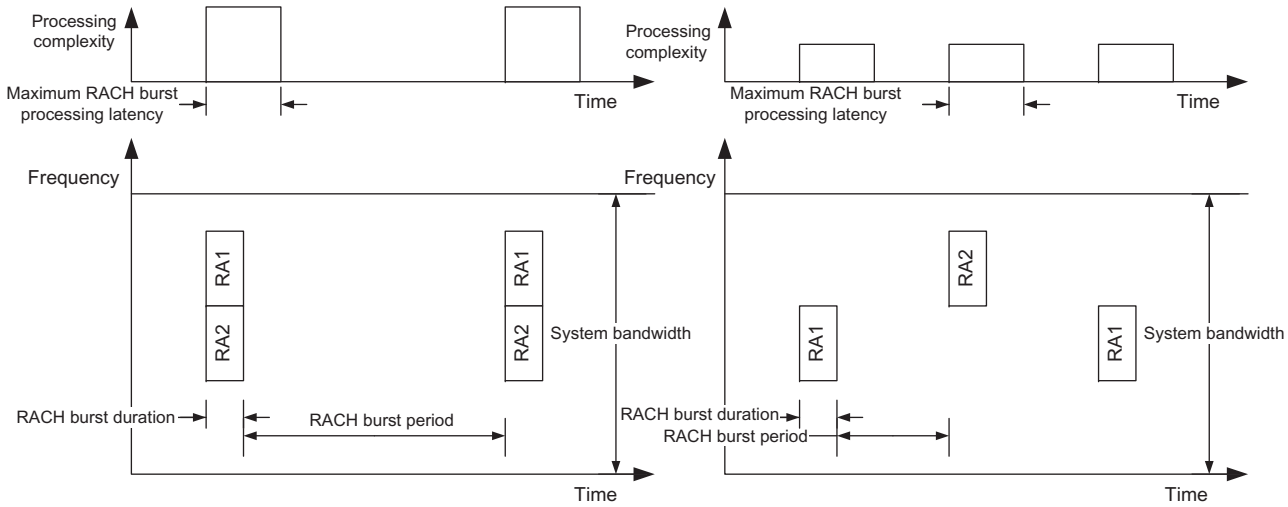


FIGURE 10.50

Example of PRACH resource configuration and processing [15].

Petitioners' Exhibit 1021
Nokia of America Corp., et al. v. KT Corporation, et al.
Case No. IPR2025-00036; U.S. Patent No. 11,627,631
Page 843 of 1122

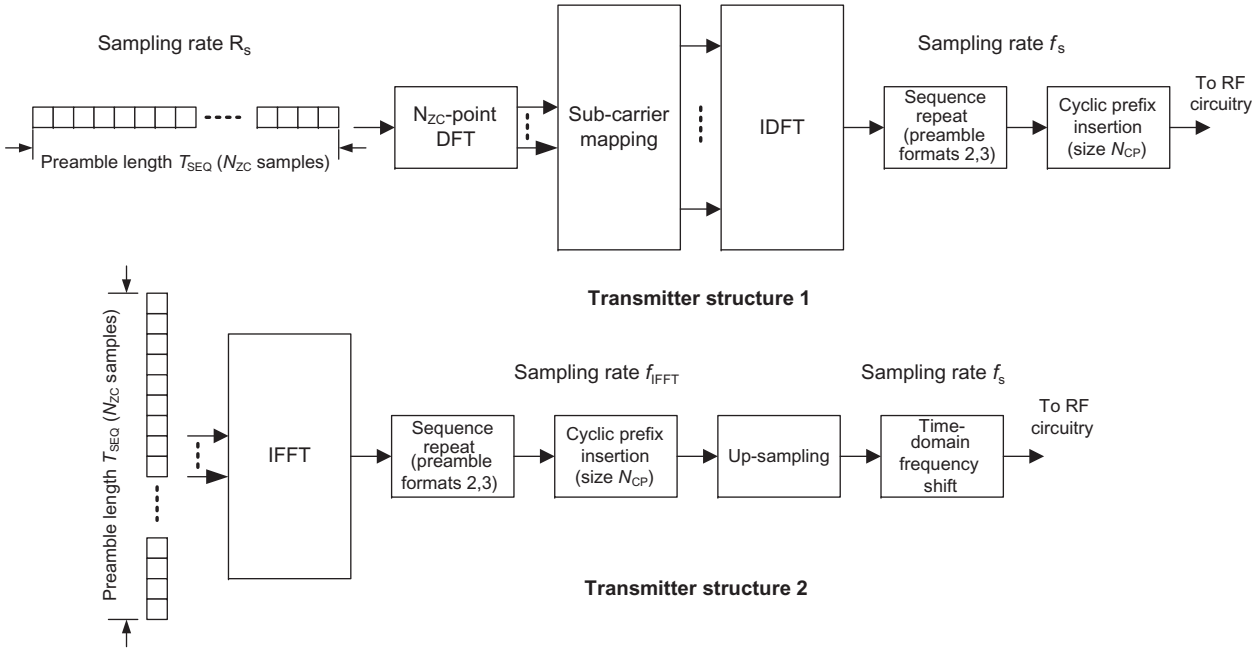


FIGURE 10.51

PRACH transmitter structure options [15,168].

Petitioners' Exhibit 1021
Nokia of America Corp., et al. v. KT Corporation, et al.
Case No. IPR2025-00036; U.S. Patent No. 11,627,631
Page 844 of 1122

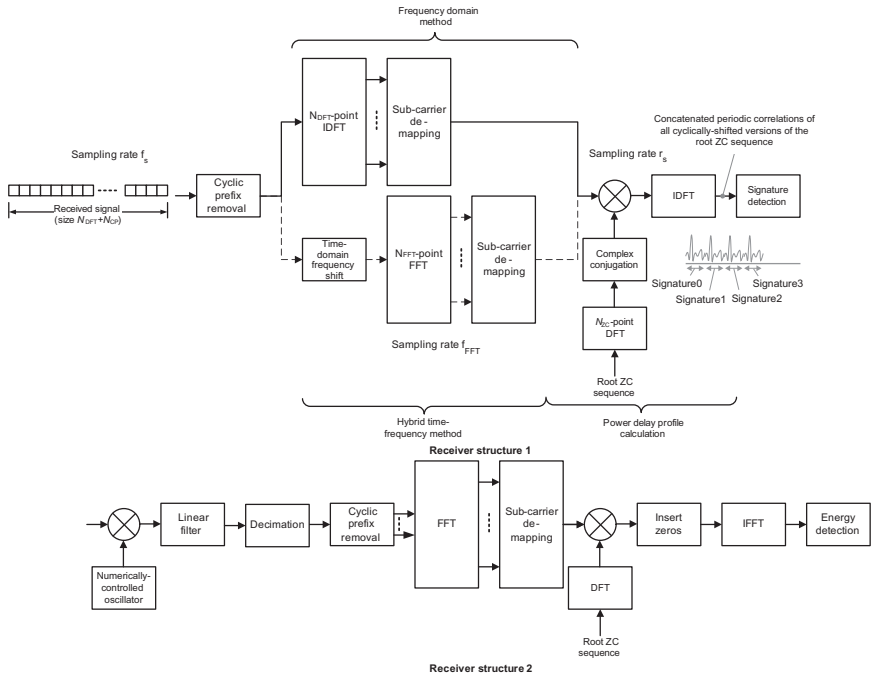


FIGURE 10.52

PRACH receiver structure options [15,168].

time-domain implementation is that the up-sampling from 1.08 MHz to the system sampling rate of 30.72 MHz is difficult to implement.

The implementation of the PRACH signal at the eNB receiver can take a frequency-domain or a hybrid time/frequency-domain approach. As illustrated in Figure 10.52 as an example, the common parts to both approaches are the cyclic prefix removal, which always occurs at the front end at the system sampling rate, the power delay profile calculation, and signature detection. The two approaches differ only in the computation of the sub-carriers carrying the PRACH signal(s). The frequency-domain method computes the full range of sub-carriers used for uplink transmission over the system bandwidth from 800-μs-long received input samples. As a result, the PRACH sub-carriers are directly extracted from the set of uplink sub-carriers, which does not require any frequency shift or time-domain filtering but involves an extremely large DFT computation. Note that even though DFT size $N_{\text{DFT}} = n2^m$, thus allowing fast and efficient DFT computation algorithms, the DFT computation cannot start until the complete sequence is stored in memory, which increases the processing delay.

In order to reduce the implementation complexity, particularly for the number of multiplications in the PRACH detector at the eNB, frequency-domain processing

may be adopted for PRACH preamble detection. As shown in Figure 10.52, the received signal is first processed in the time-domain, is then transformed to the frequency-domain by FFT, and is multiplied by the DFT-transformed RACH sequences (i.e., cross-correlation calculation). The cross-correlation is obtained by transforming back to the time-domain by IFFT, followed by zero insertion. Figure 10.52 further illustrates the main components of another RACH preamble receiver structure using the DFT-based (frequency-domain) method. In the receiver, the down-conversion block uses a numerically controlled oscillator, which shifts the frequency band of PRACH to the lowest frequency band. The down-converted signal is filtered with a linear filter to prevent aliasing effect after decimation.

The hybrid time/frequency-domain method extracts the desired PRACH signal using a time-domain frequency shift along with down-sampling and anti-aliasing filtering. The down-sampling ratio and the corresponding anti-aliasing filter characteristics are chosen to provide a number of PRACH time samples suitable for an FFT or simple DFT computation at a sampling rate which is an integer fraction of the system sampling rate. Unlike the frequency-domain approach, the hybrid time/frequency-domain computation can start as soon as the first samples have been received, reducing the processing latency.

The analog random-access signal $s(t)$ is defined as follows:

$$s(t) = \beta_{\text{PRACH}} \sum_{k=0}^{N_{ZC}-1} \sum_{n=0}^{N_{ZC}-1} x_{uv}(n) e^{-j(2\pi nk/N_{ZC})} \exp[j2\pi(k+\varphi+\gamma(k_0+1/2))\Delta f_{RA}(t-T_{CP})] \tag{10.14}$$

where $0 \le t < T_{SEQ} + T_{CP}$, β_{PRACH} is an amplitude scaling factor in order to ensure conformance to the transmit power P_{PRACH}, and $k_0 = 12N_{RA} - 6N_{RB}^{UL}$. The location of PRACH in the frequency-domain is controlled by the parameter N_{RA}. The factor $\gamma = \Delta f / \Delta f_{RA}$ accounts for the difference in sub-carrier spacing between the random-access preamble and uplink data transmission. The sub-carrier spacing for the random-access preamble $\Delta f_{RA} = 1250$ Hz for random-access preamble formats 0–3, and $\Delta f_{RA} = 7500$ Hz for random-access preamble format 4. The fixed offset determining the frequency-domain location of the random-access preamble within the PRBs $\phi = 7$ for random-access preamble formats 0–3, and $\phi = 2$ for random-access preamble format 4 [3].

10.8 SC-FDMA signal generation

The time-domain analog signal $s_l^p(t)$ for antenna port p over SC-FDMA symbol l in an uplink slot is defined as follows (applicable to all uplink physical signals and physical channels except PRACH):

$$s_l^p(t) = \sum_{k=-\lfloor 6N_{RB}^{UL} \rfloor}^{\lceil 6N_{RB}^{UL} \rceil - 1} \alpha_{k'}^p(l) \exp\{j\pi(2k+1)\Delta f[t - N_{CP}(l)T_s]\}, 0 \le t < (N_{CP}(l) + N_{FFT})T_s \tag{10.15}$$

Petitioners' Exhibit 1021
Nokia of America Corp., et al. v. KT Corporation, et al.
Case No. IPR2025-00036; U.S. Patent No. 11,627,631
Page 846 of 1122

where $k' = k + \lfloor 6N_{\text{RB}}^{\text{UL}} \rfloor$, $N_{\text{FFT}} = 2048$, $\Delta f = 15$ kHz, and α_{kl}^{p} is the complex-valued content of resource element (k, l) on antenna port p. The SC-FDMA symbols in a slot are transmitted in increasing order of symbol index l, starting with $l = 0$, where SC-FDMA symbol $l > 0$ starts at time $\sum_{l'=0}^{l-1}[N_{\text{CP}}(l') + N]T_{\text{s}}$ within the slot [3].

10.9 LTE/LTE-Advanced uplink multi-antenna transmission schemes

Simultaneous transmission from multiple transmit antennas from a single UE was not supported in LTE Rel-8/9. In order to simplify the UE implementation and to reduce power consumption, a single-power amplifier was assumed to be available at the UE. However, LTE Rel-8/9 provided support for open/closed-loop antenna-selection transmit diversity in the uplink from UEs which are equipped with multiple transmit antennas. LTE Rel-8/9 also supported virtual MIMO in the uplink. More advanced multi-antenna techniques, including closed-loop spatial multiplexing for SU-MIMO and transmit diversity for control signaling, were introduced in LTE Rel-10. Uplink closed-loop antenna selection for up to two transmit antennas is supported as an optional UE capability in LTE and is configurable by higher layers. If a UE indicates support for uplink antenna selection, the eNB may configure and schedule the UE based on that capability.

LTE/LTE-Advanced use the concept of antenna ports to differentiate between logical and physical antennas. Logical antennas or antenna ports are mapped to physical antennas based on certain deployment considerations. Prior to LTE Rel-10, there was only one transmit antenna on the UE, thus the notion of antenna ports did not apply. However, LTE Rel-10 extended the multi-antenna capabilities of the uplink and provided support for spatial multiplexing up to four transmit antennas for PUSCH and dual-antenna transmit diversity for PUCCH. Therefore, a new set of logical antennas or antenna ports have been defined that are listed in Table 10.25. As an example, PUSCH transmission, including its DM-RS as well as SRS transmission, is associated with antenna ports $\{10\}, \{20, 21\}$, and $\{40, 41, 42, 43\}$, for one, two, and four transmit antennas, respectively. The virtual antenna port $\overline{p} \in \{0, 1, 2, 3\}$ is used in this book and in 3GPP specifications to refer to the actual uplink antenna ports. Note that each antenna port has its own reference signals, enabling the eNB to estimate the channel from each UE transmit antenna.

Before proceeding to the next sections, recall that a spatial layer is the term used in LTE for one of the different streams generated by spatial multiplexing. A layer can be described as a mapping of complex-valued symbols onto the transmit antenna ports. Each layer is identified by a precoding vector/matrix of size equal to the number of transmit antenna ports, and can be associated with a radiation pattern. The rank of the transmission is the number of layers transmitted. A codeword is an independently encoded data block, corresponding to a single transport block delivered from the MAC sub-layer in the transmitter to the physical layer and protected with a CRC.

Petitioners' Exhibit 1021
Nokia of America Corp., et al. v. KT Corporation, et al.
Case No. IPR2025-00036; U.S. Patent No. 11,627,631
Page 847 of 1122

Table 10.25 Virtual and Physical Antennas in the Uplink [3]

Physical Channel/Signal	Virtual Antenna Port $\bar{p}$	Uplink Antenna Port p — Number of Physical Antennas		
		1	2	4
PUSCH and DM-RS for PUSCH	0	10	20	40
	1	–	21	41
	2	–	–	42
	3	–	–	43
SRS	0	10	20	40
	1	–	21	41
	2	–	–	42
	3	–	–	43
PUCCH and DM-RS for PUCCH	0	100	200	–
	1	–	201	–

10.9.1 Transmit antenna selection

When closed-loop antenna selection is enabled, the eNB indicates which antenna should be used for PUSCH transmission, by implicitly coding this information in the uplink scheduling grant (i.e., DCI format 0 or 4). The 16-bit CRC is scrambled (modulo-2 addition) by one of two antenna selection masks $\langle 0,0,0,0,0,0,0,0,0,0,0,0,0,0,0,0\rangle$ for the UE's first transmit antenna, and/or $\langle 0,0,0,0,0,0,0,0,0,0,0,0,0,0,0,1\rangle$ for the second antenna [4]. The antenna selection mask is applied in addition to the UE identity (RNTI) masking, identifying the UE for which the scheduling grant is intended. This implicit encoding avoids the use of explicit antenna selection bits which would result in an increased overhead for UEs not supporting (or not configured for) transmit antenna selection. The UE identity can be detected directly from the 15 least-significant bits of the decoded mask with no need to use the transmitted antenna selection mask (the 16th bit).

When using the adaptive HARQ, the antenna indicator, using CRC masking, is always sent in the uplink grant to indicate which antenna to use. For example, for a high-Doppler UE with adaptive HARQ, the eNB might instruct the UE to alternate between the transmit antennas or, alternatively, to select the primary antenna. In typical UE implementations, a transmit antenna gain imbalance of 3−6 dB between the secondary and primary antennas is not uncommon. Alternatively, when using non-adaptive HARQ, the UE may choose either antenna; therefore, in low-Doppler scenarios, the UE may use the same antenna

Petitioners' Exhibit 1021
Nokia of America Corp., et al. v. KT Corporation, et al.
Case No. IPR2025-00036; U.S. Patent No. 11,627,631
Page 848 of 1122

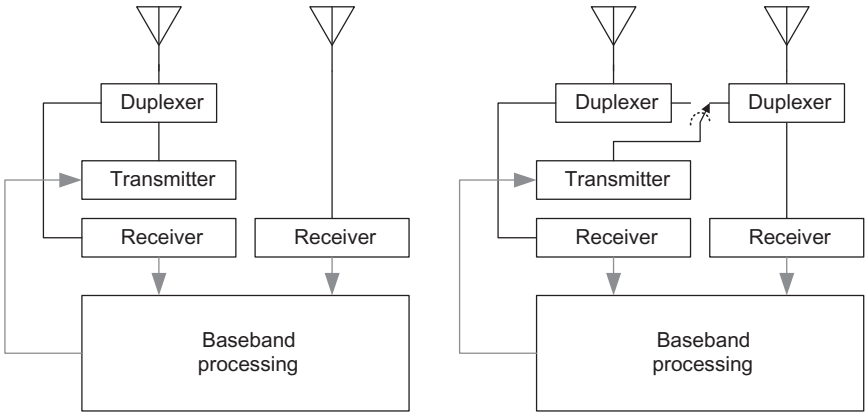


FIGURE 10.53

Illustration of a UE front end with/without transmit antenna selection [14].

signaled in the uplink grant, while in high-Doppler conditions the UE may switch between antennas or select the primary antenna. For a large number of retransmissions with non-adaptive HARQ, the antenna indicated in the uplink grant may not be the best and it is better to let the UE select the antenna. If the eNB instructs the UE to use a specific antenna for the retransmissions, it can use adaptive HARQ. If the eNB enables a UE's closed-loop antenna selection capability, the SRS transmissions alternate between the transmit antennas in successive SRS transmission subframes, irrespective of enablement of the frequency hopping feature [15].

It must be noted that receive diversity is mandatory for all UE categories in LTE, and as such there is more than one antenna on the UE that may be used for transmit antenna selection, as shown in Figure 10.53, with minimal changes to implementation. The transmit antenna selection scheme can be useful, if the UE is held in such a way that one transmit antenna is covered by hand and the other antenna is not covered. Although the inclusion of an RF switch may introduce some insertion loss, this drawback may be overcome by the benefits of the diversity scheme in some practical scenarios. It is not mandatory for the UEs to support transmit antenna selection. The UE capability information message can be used to inform the network of whether the UE supports this feature. The eNB can instruct the UEs supporting this feature to use either open-loop or closed-loop transmit antenna selection.

10.9.2 Virtual MU-MIMO (cooperative MIMO)

Another uplink MIMO mode that was introduced in LTE Rel-8/9 was MU-MIMO. The legacy uplink MU-MIMO is based on transmission from multiple UEs on the same set of resource blocks, each using a single transmit antenna. From the point of view of an individual UE, this is a single-antenna transmission

Petitioners' Exhibit 1021
Nokia of America Corp., et al. v. KT Corporation, et al.
Case No. IPR2025-00036; U.S. Patent No. 11,627,631
Page 849 of 1122

scheme; however, from an eNB perspective, this is a MU-MIMO scheme that requires more sophisticated scheduling and uplink reception. In order to support uplink MU-MIMO, LTE Rel-8/9 provides orthogonal DM-RS using different cyclic shifts to allow the eNB to obtain independent channel estimations for the uplink from each UE. A cell can assign up to eight different cyclic shifts using a 3-bit PUSCH cyclic shift offset in the uplink scheduling grant; therefore, uplink MU-MIMO of up to eight UEs can be theoretically supported in a cell. The inter-cell or cooperative MU-MIMO is supported in LTE by assigning the same base sequence groups and/or reference signal hopping patterns to the different cells.

The main objective of MU-MIMO is to increase the overall system throughput. The uplink MU-MIMO is transparent to the UE and has no effect on the UE implementation. The cooperative or virtual MIMO in the uplink requires the eNB to select and group the spatially uncorrelated UEs that are going to share the same resource blocks, to schedule the UEs within the group for uplink transmission over PDCCH, and to separate and decode uplink transmissions from each UE within the group. Each UE within the group will be assigned a different cyclic shift for the corresponding DM-RS to allow the eNB to estimate the channel from each UE and to decode the corresponding payload. The use of different cyclic shifts provides orthogonality among the UEs within the group, and enables the eNB to separate them as long as the same number of resource blocks is used for the UEs within group. The orthogonality will be lost if each UE is allocated a different number of resource blocks. While LTE Rel-8/9 defined only cyclic shifts to differentiate the UEs in the uplink, LTE Rel-10 introduced an additional level of differentiation using OCCs, as discussed earlier. Therefore, OCC will allow the UEs within the same MU-MIMO group to be allocated a different number of resource blocks.

10.9.3 Closed-loop spatial multiplexing

Closed-loop spatial multiplexing with up to four antennas was introduced as part of the LTE Rel-10 improvements in the uplink. The physical antenna elements required for uplink spatial multiplexing might be already available on the UEs that support spatial multiplexing in the downlink, which can be shared in both directions via an RF switch, e.g., a UE that supports 2×2 spatial multiplexing in the downlink already has two antenna elements. Nevertheless, the uplink spatial multiplexing further requires additional transmission chains and PAs in the uplink that operate simultaneously. The eNB provides the UE with instructions on the number of spatial layers and the codebooks or precoding matrices that must be used. The criterion for selecting the precoding matrix is to maximize the SNR at the eNB receiver [14].

The design principles of spatial multiplexing with precoding for the uplink data transmission are similar to those for the downlink. The precoding operation can mathematically be expressed as multiplication of an $N_{RX} \times 1$ DFT-spread signal vector by an $N_{TX} \times N_{RX}$ precoding matrix, which is chosen from a predefined

Petitioners' Exhibit 1021
Nokia of America Corp., et al. v. KT Corporation, et al.
Case No. IPR2025-00036; U.S. Patent No. 11,627,631
Page 850 of 1122

set of matrices, also known as a codebook. Note that the *i*th column vector of the precoding matrix represents the antenna-spreading weight of the *i*th layer. The main purpose of precoding is to match the precoding matrix with the channel characteristics in order to increase the received signal power and reduce inter-layer interference, thereby improving the SINR of each layer.

Let us assume that the eNB has N_{RX} receive antennas and the eigen-beamforming module precodes each layer with one of $\min(N_{TX}, N_{RX})$ eigenvectors of the channel correlation matrix in order to improve the capacity. In practice, the choice of the precoder must be signaled from the eNB to the UE; therefore, the number of precoding matrices (i.e., codebook size) is limited by the size of the downlink control signaling. The use of a finite codebook results in a reduced precoding gain. If the alphabet for the non-zero elements of the precoding matrix is confined to $(\pm 1, \pm j)$, the matrix calculations involved in the selection of the codebook are significantly simplified. Furthermore, the constant-modulus property of the QPSK alphabet enables all PAs to transmit with equal power level. This balanced power distribution would result in maximization of the PA efficiency, regardless of which precoding matrix is used. A drawback of this alphabet constraint is further reduction of the precoding gain.

The design of a precoding codebook used for downlink MIMO is different from that in the uplink in the sense that the uplink codebook structure should not increase the CM of the transmitted signal relative to single-antenna transmission (measured at each individual antenna port). The Householder codebook of downlink MIMO linearly combines multiple layers and inevitably increases the CM. A design constraint on uplink codebooks is that each row should have at most one non-zero element. In other words, each transmit antenna is not allowed to convey more than one layer; therefore, no linear combination is allowed. This constraint, while it preserves the CM, gives rise to further reduction of the precoding gain. One of the objectives of the uplink precoder design is to optimize the precoding gain under the CM preserving constraint [122].

It is recognized from an information theory perspective that the codebooks with maximum chordal distance are optimal. However, the UE antennas are likely to be practically correlated due to proximity; therefore, the UE antenna configuration and indexing, antenna spacing, and polarization should be carefully considered in selecting the codebook vectors. Since each layer is assigned to a separate group of UE antennas, antenna grouping with lower inter-layer correlation is preferred, leading to lower inter-layer interference. This is also consistent with the eigen-beamforming principle in that eigenvectors of channel correlation tend to have elements with larger amplitude in one antenna group than in the other antenna groups. Under the above constraints, it can be concluded that the full-rank codebooks consist of the identity matrices. For non-full-rank codebooks, it is desirable to maximize the precoding gain while preserving the low CM property.

Since PUSCH DM-RS is precoded with uplink data at the same time, it is impossible to select the precoder (i.e., the rank and precoding matrix) based on DM-RS, since only a subset of the spatial channel dimensions is observed.

Petitioners' Exhibit 1021
Nokia of America Corp., et al. v. KT Corporation, et al.
Case No. IPR2025-00036; U.S. Patent No. 11,627,631
Page 851 of 1122

Table 10.26 Codebook for Uplink Transmission on Two Antenna Ports {20, 21}[3]

	Number of Layers	
Codebook Index	$N_l = 1$	$N_l = 2$
0	$\frac{1}{\sqrt{2}}\begin{bmatrix}1\\1\end{bmatrix}$	$\frac{1}{\sqrt{2}}\begin{bmatrix}1 & 0\\0 & 1\end{bmatrix}$
1	$\frac{1}{\sqrt{2}}\begin{bmatrix}1\\-1\end{bmatrix}$	–
2	$\frac{1}{\sqrt{2}}\begin{bmatrix}1\\j\end{bmatrix}$	–
3	$\frac{1}{\sqrt{2}}\begin{bmatrix}1\\-j\end{bmatrix}$	–
4	$\frac{1}{\sqrt{2}}\begin{bmatrix}1\\0\end{bmatrix}$	–
5	$\frac{1}{\sqrt{2}}\begin{bmatrix}0\\1\end{bmatrix}$	–

Instead, non-precoded SRS transmission is the conventional method for the eNB to efficiently select an appropriate precoder for the uplink data. The SRS is antenna-specific, as opposed to layer-specific in the case of DM-RS; therefore, the required number of orthogonal resources is the same as the number of transmit antennas. There exists a great amount of similarity between DM-RS and SRS. The SRS is derived from the same cell-specific base sequence as DM-RS, and the SRS orthogonality is further provided through different cyclic shifts [122].

In the case of two transmit antennas and rank 1 transmission, the codebook consists of four constant-modulus vectors and two antenna selection vectors (Table 10.26). The inclusion of constant-modulus vectors enables the signals from multiple UE antennas to be combined constructively at the receiving eNB by introducing a relative phase shift of 0°, 90°, 180°, or 270° between UE antennas. In the example shown in Figure 10.54, a phase shift of 270° maximizes the SNR of received signal due to constructive combining, whereas a phase shift of 90° minimizes the SNR due to destructive combining. On the other hand, the inclusion of antenna selection vectors reduces transmit power and is intended for UE power saving. For example, if UE antennas experience significant gain imbalance, one of the antenna selection vectors can be used to switch off the low-gain antenna [122].

The case of four transmit antennas and rank-1 codebook involves 16 constant-modulus vectors for constructive combining and eight antenna-selection vectors for UE power saving. For constant-modulus vectors, four relative phase shifts are considered between the first two antennas. Additional relative phase shifts are applied between the first and third antennas, and between the second and fourth antennas, accounting for imperfect antenna polarization. The rank-2 codebook (given in Table 10.27) covers every possible antenna grouping. For the rank-3

Petitioners' Exhibit 1021
Nokia of America Corp., et al. v. KT Corporation, et al.
Case No. IPR2025-00036; U.S. Patent No. 11,627,631
Page 852 of 1122

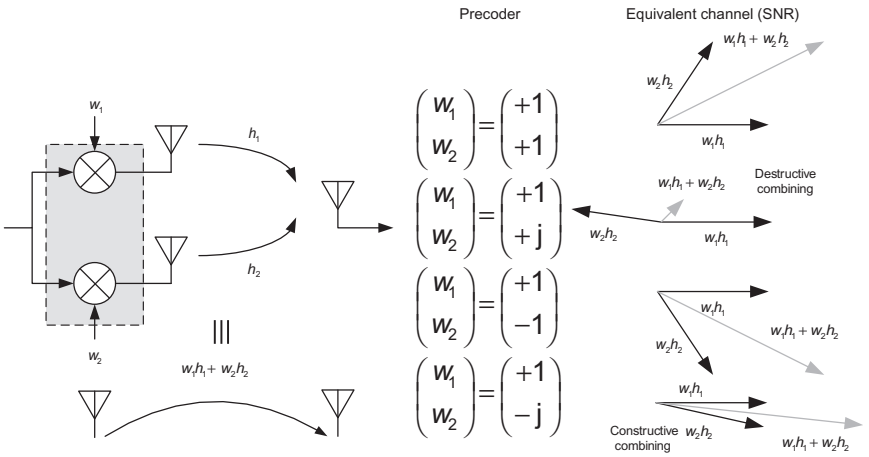


FIGURE 10.54

Illustration of the effect of precoding on SNR (rank 1 transmission) [122].

codebook, the first layer is assigned to two transmit antennas, whereas layers 2 and 3 are each assigned one antenna. Every antenna grouping (six groupings in total) for the first layer is covered, along with an intra-group phase shift of 0° or 180°. It should be noted that no inter-group phase shift is considered in the rank-2 and rank-3 codebooks, since it does not contribute to layer separation. The performance of the system with these codebooks is similar to the Householder codebook used in the downlink MIMO, unless the UE antennas are highly correlated. Note that the Householder codebook has a similar codebook size, while its alphabet is 8PSK and the CM is not concerned. Therefore, it can be concluded that the loss of precoding gain (compared to eigen-beamforming) largely originates from the codebook size constraint, rather than the alphabet restriction and the limitation concerning the CM of the transmitted signal. The precoder is defined by rank and PMI, which are selected by the eNB based on uplink channel measurements and signaled to the UE through the rank indicator and PMI fields in an uplink grant. The rank and PMI may be selected to maximize the throughput.

10.9.4 Transmit diversity

Multi-antenna transmit-diversity techniques are used to provide reliability and to improve coverage for uplink control channels. The transmit diversity scheme introduced for PUCCH in LTE Rel-10 was designed to ensure backward compatibility with the LTE Rel-8 PUCCH design. A dual-antenna transmit diversity scheme for HARQ and SR (PUCCH format 1/1a/1b) is utilized by transmitting the same control information from different UE antennas by using different orthogonal resources, thus providing no multiplexing gain. This is referred to as

Petitioners' Exhibit 1021
Nokia of America Corp., et al. v. KT Corporation, et al.
Case No. IPR2025-00036; U.S. Patent No. 11,627,631
Page 853 of 1122

Table 10.27 Codebook for Transmission on Four Antenna Ports {40, 41, 42, 43} [3]

Codebook Index	Number of Layers $N_l = 2$				Codebook Index	Number of Layers $N_l = 2$			
0–3	$\frac{1}{2}\begin{bmatrix}1 & 0\\1 & 0\\0 & 1\\0 & -j\end{bmatrix}$	$\frac{1}{2}\begin{bmatrix}1 & 0\\1 & 0\\0 & 1\\0 & j\end{bmatrix}$	$\frac{1}{2}\begin{bmatrix}1 & 0\\-j & 0\\0 & 1\\0 & 1\end{bmatrix}$	$\frac{1}{2}\begin{bmatrix}1 & 0\\-j & 0\\0 & 1\\0 & -1\end{bmatrix}$	8–11	$\frac{1}{2}\begin{bmatrix}1 & 0\\0 & 1\\1 & 0\\0 & 1\end{bmatrix}$	$\frac{1}{2}\begin{bmatrix}1 & 0\\0 & 1\\1 & 0\\0 & -1\end{bmatrix}$	$\frac{1}{2}\begin{bmatrix}1 & 0\\0 & 1\\-1 & 0\\0 & 1\end{bmatrix}$	$\frac{1}{2}\begin{bmatrix}1 & 0\\0 & 1\\-1 & 0\\0 & -1\end{bmatrix}$
4–7	$\frac{1}{2}\begin{bmatrix}1 & 0\\-1 & 0\\0 & 1\\0 & -j\end{bmatrix}$	$\frac{1}{2}\begin{bmatrix}1 & 0\\-1 & 0\\0 & 1\\0 & j\end{bmatrix}$	$\frac{1}{2}\begin{bmatrix}1 & 0\\j & 0\\0 & 1\\0 & 1\end{bmatrix}$	$\frac{1}{2}\begin{bmatrix}1 & 0\\j & 0\\0 & 1\\0 & -1\end{bmatrix}$	12–15	$\frac{1}{2}\begin{bmatrix}1 & 0\\0 & 1\\0 & 1\\1 & 0\end{bmatrix}$	$\frac{1}{2}\begin{bmatrix}1 & 0\\0 & 1\\0 & -1\\1 & 0\end{bmatrix}$	$\frac{1}{2}\begin{bmatrix}1 & 0\\0 & 1\\0 & 1\\-1 & 0\end{bmatrix}$	$\frac{1}{2}\begin{bmatrix}1 & 0\\0 & 1\\0 & -1\\-1 & 0\end{bmatrix}$

spatial orthogonal resource transmit diversity and is illustrated in Figure 10.36. In LTE Rel-8/9, the orthogonal resources are available through either various cyclic shifts of length-12 base sequences or OCCs of length-4 for transmission of control information of uplink control channels. The DM-RS for the uplink control channel also uses the orthogonal resources through the cyclic shifts of length-12 base sequences or OCCs of length-3.

In general, there are theoretically 36 orthogonal resources available for the uplink control channel in each subframe. Assuming perfect orthogonality, the signals from multiple transmit antennas are received separately and combined constructively. In the case of four transmit antennas and from the eNB perspective, the UE transmissions use two orthogonal resources, i.e., the cyclic shift and the OCCs, and it is up to the UE implementation if and how the transmission is distributed over the four transmit antennas. One possibility is to allow the third and fourth antennas to use the same orthogonal resources allocated to the first and second antennas, respectively, and transmit the same information. Another possibility is to transmit only on two of the four UE antennas. The same transmit diversity scheme is also applied for the channel quality information report (PUCCH format 2/2a/2b) [122]. If the UE transmit antennas are uncorrelated, SORTD provides the best diversity performance at the expense of consuming multiple orthogonal resources, reducing PUCCH multiplexing capability in general.

10.9.5 Uplink MIMO receivers

The practical constraints against implementing spatial multiplexing particularly in the uplink are the cost of multiple transmit and receive radio chains and the form-factor limitation of multi-antennas for handheld devices. By making use of advanced signal-processing techniques in the baseband processing stage, high-performance MIMO transmission can be achieved. A number of MIMO receiver algorithms can be used, depending on the requirements pertaining to receiver complexity.

In principle, the downlink MIMO channel is a broadcast channel. In this case, the individual data streams transmitted from each antenna are mixed with other transmit data streams at each receive antenna. To separate the mixed data streams at the receiver, designers can multiply the (mixed-stream) received signals with a matrix that is the inverse of the MIMO channel matrix. This is called a zero-forcing receiver. It is a simple MIMO receiver that often suffers performance loss at higher noise and interference levels. To minimize performance loss, the inversion of the MIMO channel matrix operation is adjusted according to the interference or noise level. This is called an MMSE receiver. But both the ZF and MMSE receivers typically have up to 2 dB performance loss compared with maximum likelihood detection (MLD) receivers.

Improved reception of spatial multiplexing MIMO transmission requires an exhaustive search of MIMO signal constellation combinations. The MIMO transmission process is modeled at the receiver in such a way that a specific complex

Petitioners' Exhibit 1021
Nokia of America Corp., et al. v. KT Corporation, et al.
Case No. IPR2025-00036; U.S. Patent No. 11,627,631
Page 855 of 1122

modulation constellation is generated for each transmit antenna stream. The constellations are then applied to the MIMO channel input. At the MIMO channel output, the corresponding received signal is generated for each receive antenna. At this point, the Euclidean distance is computed for the modeled MIMO channel output signal relative to the received signal. In this way, the different modulation constellations at the MIMO channel input constitute different hypothesis tests. If all possible combinations of constellations at the MIMO channel input can be emulated, their associated MIMO channel outputs can be generated, and the Euclidean distance can be computed against the received signal. The minimum Euclidian distance associated with the constellation combination hypothesis provides the most likely decoding. Such an exhaustive constellation search at the MIMO channel input is the optimal MIMO receiver.

Optimal receiver performance, however, comes at the cost of receiver complexity. Performing all the hypothesis tests requires $2^{M \times N_{TX}}$ complex operations, where M is the modulation order and N_{TX} is the number of transmit antennas. As an example, for 64QAM with two transmit antennas, the MLD decoding complexity is $2^{12} = 4096$ complex operations. For 64QAM with four transmit antennas, the MLD decoding complexity is $2^{24} = 16,777,216$ complex operations. On the other hand, the exhaustive constellation-search-based MLD receiver provides a good modular structure. The MLD receiver is suitable for application-specific integrated-circuit implementation. Several fast constellation search algorithms are available such as the sphere decoding algorithm [169]. The MLD-based MIMO receivers have many advantages compared with ZF and MMSE receivers. The MLD receiver performance advantages are significant when the MIMO channels are correlated, i.e., small-form-factor user devices require a compact packaging of multiple antennas, resulting in a high level of antenna correlation as well as a correlated MIMO channel. The ZF and MMSE receivers, conversely, can both suffer sharp performance losses when MIMO channels are correlated.

In addition, because of the limitations of small-form-factor user devices, it is difficult to achieve the same antenna gain for the two receive antennas embedded in the device. In the case of 4 dB antenna gain imbalance, the performance loss for the MLD receiver is negligible. Another advantage is diversity gain. The MLD receiver can not only separate the transmit data streams, but also can achieve the receive diversity gain for multiple receive antennas. Furthermore, the receiver can support a very high-mobility environment including reception at speeds exceeding 120km/h. Reception of the spatial multiplexing MIMO transmissions can be optimized by selecting the best receiver operation, based on the MIMO channel condition and the modulation constellation, to reduce the average processing power required. This reduces the power consumption of the user device and extends its battery life.

Since an MMSE receiver requires fewer computations than the MLD receiver, under certain transmission conditions, the performance difference between the MMSE receiver and the MLD is negligible. We can measure and test the correlation condition of the MIMO channel before we decide which receiver should be

Petitioners' Exhibit 1021
Nokia of America Corp., et al. v. KT Corporation, et al.
Case No. IPR2025-00036; U.S. Patent No. 11,627,631
Page 856 of 1122

used. If the MIMO channel correlation is very low or is orthogonal, the MMSE receiver can be used with no performance loss, while reducing the computational complexity by avoiding the use of the MLD receiver. Similarly, we can use the MMSE receiver when the SNR is high.

The advanced receiver can be further extended by successive interference cancellation (SIC) receiver architecture. The rationale behind the SIC receiver is that the signal quality of the multiple transmit data streams are not the same, because of the fading variations of the MIMO channel. We can successfully demodulate the first data stream, re-modulate it, and then subtract the first data stream from the received input combination in the absence of interference from the first data stream. We can then demodulate the second data stream successfully with a simple maximum ratio combining receiver.

Due to the nature of the MIMO channel, the eigenvalue of the MIMO channel matrix represents the signal strength for the data stream. For the two-transmit and two-receive MIMO configuration, different modulations for the different data streams can be scheduled for transmission at the base station. The user device measures the signal quality (typically one strong data stream and one weak data stream) and uses the feedback channel to request the coding and modulation for each data stream transmitted from the base station. If the user device implements an SIC receiver, the signal-quality measurement can be based on the receiver operation. In this case, the weak data stream's signal quality is measured in the absence of interference from the strong data stream. Therefore, the user device can request the increased coding and modulation transmission level for the second data stream. This can improve the throughput of the second data stream, increasing the overall throughput of the user device.

In the LTE/LTE-Advanced uplink, the use of SC-FDMA for multiple-access introduces ISI in dispersive channels. As a result, the ideal MIMO receiver should address both ISI and spatial multiplexing interference. There are a number of receiver implementation options including linear minimum mean-square error (LMMSE) equalization and SIC that can be used for MIMO detection in the LTE uplink.

In general, the downlink $N_{RX} \times 1$ received-signal vector $\mathbf{y}(k,l)$ at the kth subcarrier and the lth OFDM symbol can be expressed as the sum of the desired signal $\mathbf{H}_1(k,l)\mathbf{s}_1(k,l)$ from the serving eNB and the interference signals $\mathbf{H}_j(k,l)\mathbf{s}_j(k,l)|_{\forall j \neq 1}$ from other base stations and the noise vector $\mathbf{n}(k,l)$ as follows:

$$\mathbf{y}(k,l) = \mathbf{H}_1(k,l)\mathbf{s}_1(k,l) + \sum_{j=2}^{N_{eNB}} \mathbf{H}_j(k,l)\mathbf{s}_j(k,l) + \mathbf{n}(k,l) \tag{10.16}$$

where $\mathbf{s}_j(k,l)|_{j=1,2,\ldots,N_{eNB}}$ and $\mathbf{H}_j(k,l)|_{j=1,2,\ldots,N_{eNB}}$ represent the $N_{TX} \times 1$ transmitted signal vector and the $N_{RX} \times N_{TX}$ channel matrix between the jth cell and the UE including the contribution from both receiver branches. In the above equation $\mathbf{H}_j(k,l) = \begin{pmatrix} \mathbf{H}_j^1(k,l) & \mathbf{H}_j^2(k,l) \end{pmatrix}^T$ in which $\mathbf{H}_j^i(k,l)$ denotes the $N_{TX} \times 1$ channel matrix as seen at the ith receive antenna. The $N_l \times 1$ recovered signal vector at

Petitioners' Exhibit 1021
Nokia of America Corp., et al. v. KT Corporation, et al.
Case No. IPR2025-00036; U.S. Patent No. 11,627,631
Page 857 of 1122

the UE denoted by $\hat{\mathbf{s}}_1(k,l)$ is detected using the $N_l \times N_{\mathrm{RX}}$ receiver weighting matrix $\mathbf{W}_1(k,l)$ as follows:

$$\hat{\mathbf{s}}_1(k,l) = \mathbf{W}_1(k,l)\mathbf{y}_1(k,l) \tag{10.17}$$

The above generic model will be exploited in the receiver algorithms described in the following sections.

10.9.5.1 LMMSE receiver

An LMMSE receiver is a widely used solution which generates an MMSE estimate for each time-domain symbol. The MMSE has been used as a baseline receiver in LTE/LTE-Advanced evaluations due to its simplicity. The detection problem in an LMMSE receiver reduces to finding a weighting matrix such that $\hat{\mathbf{s}}_1(k,l) = \mathbf{W}_1(k,l)\mathbf{y}_1(k,l)$, where the weighting matrix is given as follows [25–27,43,44]:

$$\mathbf{W}_1(k,l) = \hat{\mathbf{H}}_1^H(k,l)\mathbf{R}^{-1}; \quad \mathbf{R} = P_1\hat{\mathbf{H}}_1(k,l)\mathbf{H}_1^H(k,l) + \sigma^2\mathbf{I} \tag{10.18}$$

where $\hat{\mathbf{H}}_j(k,l)$ and σ^2 denote the estimated channel matrix and noise power, respectively, P_1 is the transmission power of the serving cell and is given by $P_1 = E[|\mathbf{s}_1(k,l)|^2]$.

Due to the linearity and unitary properties of DFT, an equivalent equalization method would be to obtain a frequency-domain MMSE estimate for each symbol in the frequency-domain, and then take the IDFT to obtain the time-domain MMSE symbol estimation. The MMSE estimation for each frequency-domain symbol is obtained by linearly combining received signals collected from multiple receive antennas in the frequency-domain, using MMSE combining weights $\mathbf{W}(k) = [\mathbf{H}(k)\mathbf{H}^H(k) + \mathbf{R}(k)]^{-1}\mathbf{H}(k)$, where k is the sub-carrier index, $\mathbf{H}(k)$ is a vector representing the frequency response for the layer signal of interest (one element per receive antenna), and $\mathbf{R}(k)$ is the impairment covariance matrix encompassing the spatial correlation between the impairment components. The performance of this simple MMSE equalizer asymptotically approaches the theoretical capacity in a SIMO channel. However, in a MIMO channel, LMMSE equalizer performance is far from the SIMO capacity due to the presence of spatial multiplexing interference [127].

10.9.5.2 MRC receiver

The weighting matrix in an MRC receiver for rank-1 transmission can be represented as follows [25–27,43,44]:

$$\mathbf{W}_1(k,l) = \hat{\mathbf{H}}_1^H(k,l) \tag{10.19}$$

where $\hat{\mathbf{H}}_1(k,l)$ is the estimated channel matrix.

10.9.5.3 MMSE-IRC receiver

As an enhanced receiver, the MMSE-IRC receiver can suppress not only the inter-stream interference, but also the inter-cell interference when the degrees of

Petitioners' Exhibit 1021
Nokia of America Corp., et al. v. KT Corporation, et al.
Case No. IPR2025-00036; U.S. Patent No. 11,627,631
Page 858 of 1122

freedom at the receiver are sufficient, i.e., the number of receiver antennas is greater than the number of desired data streams. The MMSE-IRC receiver weighting matrix can be expressed as follows:

$$\mathbf{W}_1(k,l) = \hat{\mathbf{H}}_1^H(k,l)\mathbf{R}^{-1} \tag{10.20}$$

where $\hat{\mathbf{H}}_1(k,l)$ and $\mathbf{R}$ denote the estimated channel matrix and channel covariance matrix, respectively. To obtain the MMSE-IRC receiver weighting matrix, the covariance matrix including the sources of inter-cell interference must be estimated. Various schemes can be considered for this purpose, as described below.

In a covariance matrix estimation scheme based on cell-specific reference signals, the covariance matrix is estimated at the location of the CRSs using the following equations:

$$\begin{aligned}\mathbf{R} &= P_1\hat{\mathbf{H}}_1(k,l)\hat{\mathbf{H}}_1^H(k,l) + \frac{1}{N_{\text{sp}}}\sum_{(k,l)\in\{(k_{\text{CRS}},l_{\text{CRS}})\}}\tilde{\mathbf{r}}(k,l)\tilde{\mathbf{r}}^H(k,l)\\ \tilde{\mathbf{r}}(k,l) &= \mathbf{r}(k,l) - \hat{\mathbf{H}}_1(k,l)\mathbf{s}_1(k,l)\end{aligned} \tag{10.21}$$

where P_1 is the transmission power of the serving cell which is given by $P_1 = E[|\mathbf{s}_1(k,l)|^2]$ and N_{sp} is the number of sampling resource elements.

In a DM-RS-based covariance matrix estimation scheme, which is applicable when DM-RS are configured, the covariance matrix is estimated at DM-RS resource elements using the following equations:

$$\begin{aligned}\mathbf{R} &= P_1\hat{\mathbf{H}}_1(k,l)\hat{\mathbf{H}}_1^H(k,l) + \frac{1}{N_{\text{sp}}}\sum_{(k,l)\in\{(k_{\text{DM-RS}},l_{\text{DM-RS}})\}}\tilde{\mathbf{r}}(k,l)\tilde{\mathbf{r}}^H(k,l)\\ \tilde{\mathbf{r}}(k,l) &= \mathbf{r}(k,l) - \hat{\mathbf{H}}_1(k,l)\mathbf{s}_1(k,l)\end{aligned} \tag{10.22}$$

In a data-based covariance matrix estimation scheme, the covariance matrix is estimated at PDSCH resource elements using the following equations:

$$\mathbf{R} = \frac{1}{N_{\text{sp}}}\sum_{(k,l)\in\{(k_{\text{PDSCH/DM-RS}},l_{\text{PDSCH/DM-RS}})\}}\mathbf{r}(k,l)\,\mathbf{r}^H(k,l) \tag{10.23}$$

where $\{(k_{\text{PDSCH/DM-RS}}, l_{\text{PDSCH/DM-RS}})\}$ denotes the set of resource elements assigned to DM-RS or PDSCH data sub-carriers.

10.9.5.4 SIC receiver

An SIC receiver is a good candidate for MIMO reception. It can be shown that SIC receivers with per-layer rate control can achieve MIMO capacity in non-dispersive channels [127]. The operation of an SIC receiver can be described as follows. The receiver first detects the signal sent by the first layer and after successful detection, it cancels the interference contributed by the detected signal before it detects the other layers. The process is repeated until all the layers are detected. Typically, each layer is canceled only when the CRC check is successful. With perfect per-layer rate control, the transmission rate for each layer is

Petitioners' Exhibit 1021
Nokia of America Corp., et al. v. KT Corporation, et al.
Case No. IPR2025-00036; U.S. Patent No. 11,627,631
Page 859 of 1122

chosen to satisfy sufficiently low BLER; consequently, the SIC receiver can cancel interference contributed by previously detected layers. An SIC receiver typically consists of a number of LMMSE equalizers. The role of these MMSE equalizers is to suppress the residual interference. The cancelation of other layers is reflected in the impairment correlation, and thus in the MMSE combining weights. The cancelation of the detected layers allows the MMSE equalizer to use its available degree of freedom to better suppress other dominant interfering signals, resulting in a reduced interference level and a higher SINR.

In practice, there are some limitations pertaining to an SIC receiver operation e.g., an SIC receiver does not address the ISI problem. Although frequency-domain MMSE equalization is effective in suppressing ISI, there is an opportunity to achieve small performance improvement by properly canceling ISI. Moreover, turbo encoding and CRC checking is not necessarily performed on a per-layer basis, rather per-codeword rate control and CRC checking is used for uplink MIMO. For example, for the rank-4 transmission, the first and second layers are mapped to the same codeword and share the same CRC bits. Hence, these two layers need to be decoded jointly rather than individually. As a result, prior to the decoding stage, the second layer receiver cannot cancel the interference contributed by the first layer, resulting in high intra-codeword interference [127].

10.10 Uplink transmission modes

In order to support uplink SU-MIMO, the concept of transmission mode for PUSCH was introduced in the LTE Rel-10 to differentiate between single-antenna and spatial multiplexing transmission. The uplink transmission modes are as follows:

- PUSCH transmission mode 1, in which uplink transmission is from a single antenna port.
- PUSCH transmission mode 2, where uplink transmission is from multiple antenna ports. In this mode, the UE can be configured to transmit from either two or four antenna ports. If a UE is configured in PUSCH transmission mode 2, it can transmit up to two transport blocks per subframe.

The eNB signals the uplink transmission mode to the UE via an RRC connection setup, RRC connection reconfiguration, or RRC connection reestablishment message. Transmission mode 2 allows dynamic switching between single-antenna and spatial multiplexing transmission [14]. The transport blocks are mapped to one or more layers according to the same rules discussed for the downlink in LTE Rel-8. Each transport block is independently acknowledged through PHICH. The PHICH index for the first codeword is the same as that used in LTE Rel-8 for single-codeword PUSCH transmission, i.e., associated with the lowest PRB index of the PUSCH resource allocation. The PHICH index for the second

Petitioners' Exhibit 1021
Nokia of America Corp., et al. v. KT Corporation, et al.
Case No. IPR2025-00036; U.S. Patent No. 11,627,631
Page 860 of 1122

codeword is related to the first by an offset. The PDCCH resource grant for uplink MIMO transmissions includes two independent NDIs to indicate whether a retransmission is anticipated. The closed-loop codebook-based precoding is used for PUSCH in a similar way to the LTE Rel-8 PDSCH in transmission mode 4. The UE is instructed by the eNB to use a specific rank and precoding matrix signaled within the uplink grant [15]. The uplink transmission modes are applicable when UE is addressed by its C-RNTI. The closed-loop spatial multiplexing is not supported when the UE is addressed by an SPS-RNTI [14]. Transmission mode 1 is the default uplink transmission mode for a UE unless the UE is configured for another uplink transmission mode via higher-layer signaling. When a UE configured in transmission mode 2 receives a DCI format 0 (uplink scheduling grant), it assumes that PUSCH transmission is associated with transport block 1 and that transport block 2 is disabled.

10.11 Uplink feedback in LTE/LTE-Advanced

In wireless communications, CSI refers to channel properties of a wireless communication link. This information describes how a signal propagates from the transmitter to the receiver and represents the combined effect of scattering, multipath fading, signal power attenuation with distance, etc. The knowledge of CSI at the transmitter and/or the receiver makes it possible to adapt data transmission to current channel conditions, which is crucial for achieving reliable and robust communication with high data rates in multi-antenna systems. The CSI is often required to be estimated at the receiver, and usually quantized and fed back to the transmitter. The downlink channel can be estimated from uplink reference signals in TDD systems under certain conditions due to reciprocity. In general, the transmitter and receiver can observe different CSI.

There are two types of CSI, i.e., instantaneous CSI and statistical CSI. In instantaneous CSI or short-term CSI, the current channel conditions are known, which can be interpreted as knowing the impulse response of a digital filter. This provides an opportunity to adapt the transmitted signal to the impulse response and thereby to optimize the received signal for spatial multiplexing or to achieve low bit error rates. In statistical CSI or long-term CSI, the statistical characteristics or statistics of the channel are known. The latter information may include the type of fading distribution, the average channel gain, the line-of-sight component, and the spatial correlation. Similar to the instantaneous CSI, this information can be used for optimization of transmission parameters.

The CSI estimation accuracy is practically limited by how fast the channel conditions are varying. In fast-fading channels where the channel conditions may vary rapidly during transmission of a single information symbol, only statistical CSI is reasonable. On the other hand, in slow-fading scenarios, the instantaneous CSI can be estimated with reasonable precision and used for transmission

Petitioners' Exhibit 1021
Nokia of America Corp., et al. v. KT Corporation, et al.
Case No. IPR2025-00036; U.S. Patent No. 11,627,631
Page 861 of 1122

adaptation for a period of time before becoming obsolete. In practical scenarios, the available CSI is often manifested as instantaneous CSI with some estimation/quantization error combined with some statistical information. Recall that in a narrowband flat-fading channel with multiple transmit and receive antennas, the system is modeled as $\mathbf{y} = \mathbf{Hx} + \mathbf{n}$, where $\mathbf{y}$ and $\mathbf{x}$ are the received and transmitted signal vectors, respectively, $\mathbf{H}$ and $\mathbf{n}$ are the channel matrix and the receiver noise vector, respectively. The noise is often modeled as circular symmetric complex normal random variable with statistical distribution $\mathbf{n} \sim Z(\mathbf{0}, \mathbf{R_n})$ where the mean value is zero and the noise covariance matrix $\mathbf{R_n}$ can be estimated. In the case of instantaneous CSI, the channel matrix $\mathbf{H}$ is known; however, due to channel estimation errors, the channel information can be represented as $\hat{\mathbf{H}} = \mathbf{H} + \mathbf{e}$ in which $\text{vec}(\hat{\mathbf{H}}) \sim Z(\text{vec}(\mathbf{H}), \mathbf{R_e})$, where $\hat{\mathbf{H}}$ denotes the estimated channel matrix and $\mathbf{R_e}$ is the estimation error covariance matrix. The vectorization operator[15] $\text{vec}(\cdot)$ is used to obtain the column representation of matrix $\mathbf{H}$. In the case of statistical CSI, the statistics of $\mathbf{H}$ are known. For instance, in a Rayleigh fading channel, this corresponds to $\text{vec}(\mathbf{H}) \sim Z(\mathbf{0}, \mathbf{R_H})$ for a known channel covariance matrix $\mathbf{R_H}$ [170].

The uplink feedback in LTE/LTE-Advanced for support of downlink data transmission consists of RI, PMI, PTI, and CQI. The UE uses the UCI to provide the eNB with feedback that includes CQI, PMI, PTI, RI, scheduling requests, and HARQ acknowledgments. The UE sends the uplink feedback to the eNB using PUCCH or PUSCH. As mentioned earlier, LTE Rel-8/9 does not support simultaneous transmission of PUCCH and PUSCH in the uplink.

Figure 10.55 illustrates the various forms of CSI reporting. The CSI reporting is divided into periodic and aperiodic categories. The periodic CSI reporting uses PUCCH unless data transmission is already scheduled on PUSCH. The aperiodic CSI reporting is always transmitted via PUSCH. The aperiodic reporting can be triggered using a flag within the DCI that is used to allocate PUSCH resources. Since the capacity of PUSCH is greater than that of PUCCH, larger control information payload can be included in aperiodic CSI feedback.

The scheduling request is not explicitly sent on PUSCH, rather the UE includes a buffer status report (BSR) MAC control element in the uplink MAC PDUs. The BSR MAC control element provides the eNB with information regarding the amount of data in the UE's local buffer awaiting transmission. The LTE Rel-10 allows simultaneous transmission of PUCCH and PUSCH in the same uplink subframe. In this case, the UCI and feedback can be sent on PUCCH, whereas aperiodic CSI reports and user data can be transmitted on PUSCH.

[15] In linear algebra and matrix theory, the vectorization of a matrix is a linear transformation which converts the matrix into a column vector. More specifically, the vectorization of an $M \times N$ matrix $\mathbf{H}$, denoted by $\text{vec}(\mathbf{H})$, in which $\text{vec}(\mathbf{H})$ is an $MN \times 1$ column vector is obtained by stacking the columns of the matrix $\mathbf{H}$ on top of each other, as follows: $\text{vec}(\mathbf{H}) = (h_{11}, h_{21}, \ldots, h_{M1}; h_{12}, h_{22}, \ldots, h_{M2}; \ldots; h_{1N}, h_{2N}, \ldots, h_{\text{MN}})^{\text{T}}$ where h_{ij} represents the (i, j) element of matrix $\mathbf{H}$ and the superscript T denotes the transpose operation. The vectorization operation can be interpreted as the isomorphism $\mathbf{H}^{M \times N} := \mathbf{H}^M \otimes \mathbf{H}^N \cong \mathbf{H}^{\text{MN}}$ between these vector spaces (of matrices and vectors) in coordinates [30–33].

Petitioners' Exhibit 1021
Nokia of America Corp., et al. v. KT Corporation, et al.
Case No. IPR2025-00036; U.S. Patent No. 11,627,631
Page 862 of 1122

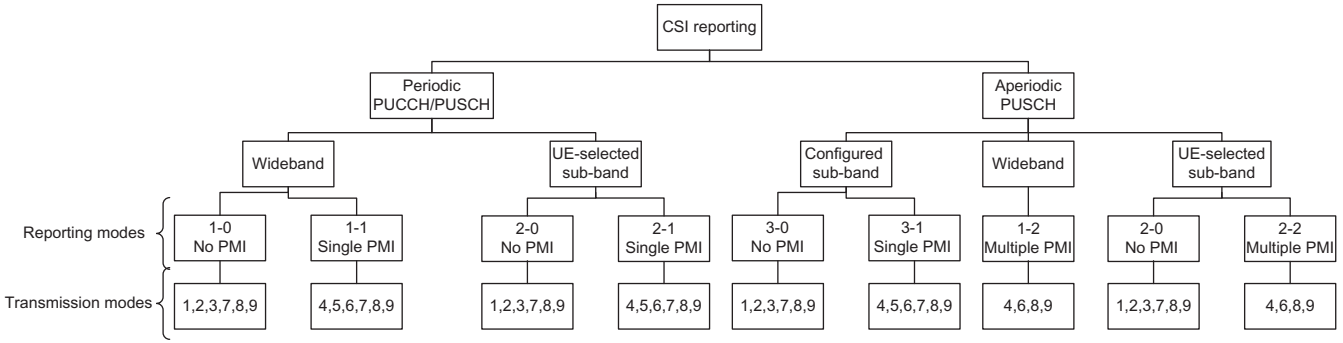


FIGURE 10.55

Classification of CSI reporting modes [14].

Petitioners' Exhibit 1021
Nokia of America Corp., et al. v. KT Corporation, et al.
Case No. IPR2025-00036; U.S. Patent No. 11,627,631
Page 863 of 1122

The RI indicates the number of spatial layers which can be supported by the UE under current channel conditions. It has been observed in the course of LTE evaluation that the frequency-selective RI reporting does not provide significant performance benefit; therefore, only one wideband RI is reported for the entire bandwidth [122]. However, the reporting of PMI and CQI can be in the form of wideband or sub-band (frequency-selective). For RI values equal to one, only one CQI is reported for each reporting unit in frequency, which is either wideband or sub-band in the case of frequency-selective reporting. For RI values greater than one, the CQI for each codeword is reported for the closed-loop spatial multiplexing, as different codewords may be assigned to different layers, while only one CQI is reported for the open-loop spatial multiplexing, as one codeword interacts with all layers. The PMI indicates the preferred precoding candidate for the corresponding frequency unit, e.g., a particular sub-band or the entire system bandwidth, and is selected from the possible precoding candidates depending on the number of transmit antennas and according to the RI value.

The CQI metric indicates a combination of the maximum data rate and the modulation scheme, which can achieve BLER less than 10% at the UE after detection, assuming that the reported rank and PMI are applied to the time−frequency resource (see Figure 10.57). Given this definition of CQI, PMI, and RI, the UE can report the maximum data rate that it can receive and demodulate, taking into account its receiver capability and channel conditions. In the case of the frequency-selective PMI/CQI reporting, the UE reports a PMI/CQI for each sub-band (Figure 10.56). For the non-frequency-selective wideband PMI/CQI reporting, the UE reports a single wideband PMI/CQI corresponding to the entire bandwidth. In the frequency-selective reporting mode, the sub-band CQI is reported as a differential value with respect to the wideband CQI in order to reduce the signaling overhead. The sub-band CQI reports are encoded differentially with respect to the wideband CQI using 2 bits as follows: $\Delta\text{CQI}_{\text{sub-band}} = \text{CQI}_{\text{sub-band(index)}} - \text{CQI}_{\text{wideband}}(\text{index})$, where the permissible sub-band differential CQI offset values are $\{\leq -1, 0, 1, \geq 2\}$. In best-$M$ average reporting, the UE first estimates the channel quality for each sub-band. Then it selects the M best values and reports to the eNB a single average CQI corresponding to the MCS/TBS that the UE can receive correctly, assuming that the eNB schedules the UE on those M sub-bands. The parameter M depends on the system bandwidth and corresponds to approximately 20% of the system bandwidth. Figure 10.56 shows the principle of the best-M average CQI measurement and reporting scheme. The CQI value for the M selected sub-bands for each codeword is encoded differentially using 2 bits relative to the corresponding wideband CQI as follows: $\Delta\text{CQI} = \text{CQI}_{\text{average-bestM-sub-band}}(\text{index}) - \text{CQI}_{\text{wideband}}(\text{index})$, where the possible differential CQI values are $\{\leq 1, 2, 3, \geq 4\}$. It must be noted that the subtraction of the wideband CQI value prior to quantization of sub-band CQI values reduces the dynamic range and thus the quantization error.

When the frequency-selective CQI reporting is configured, sub-band CQIs as well as wideband CQI are reported, and the wideband CQI serves as the baseline

Petitioners' Exhibit 1021
Nokia of America Corp., et al. v. KT Corporation, et al.
Case No. IPR2025-00036; U.S. Patent No. 11,627,631
Page 864 of 1122

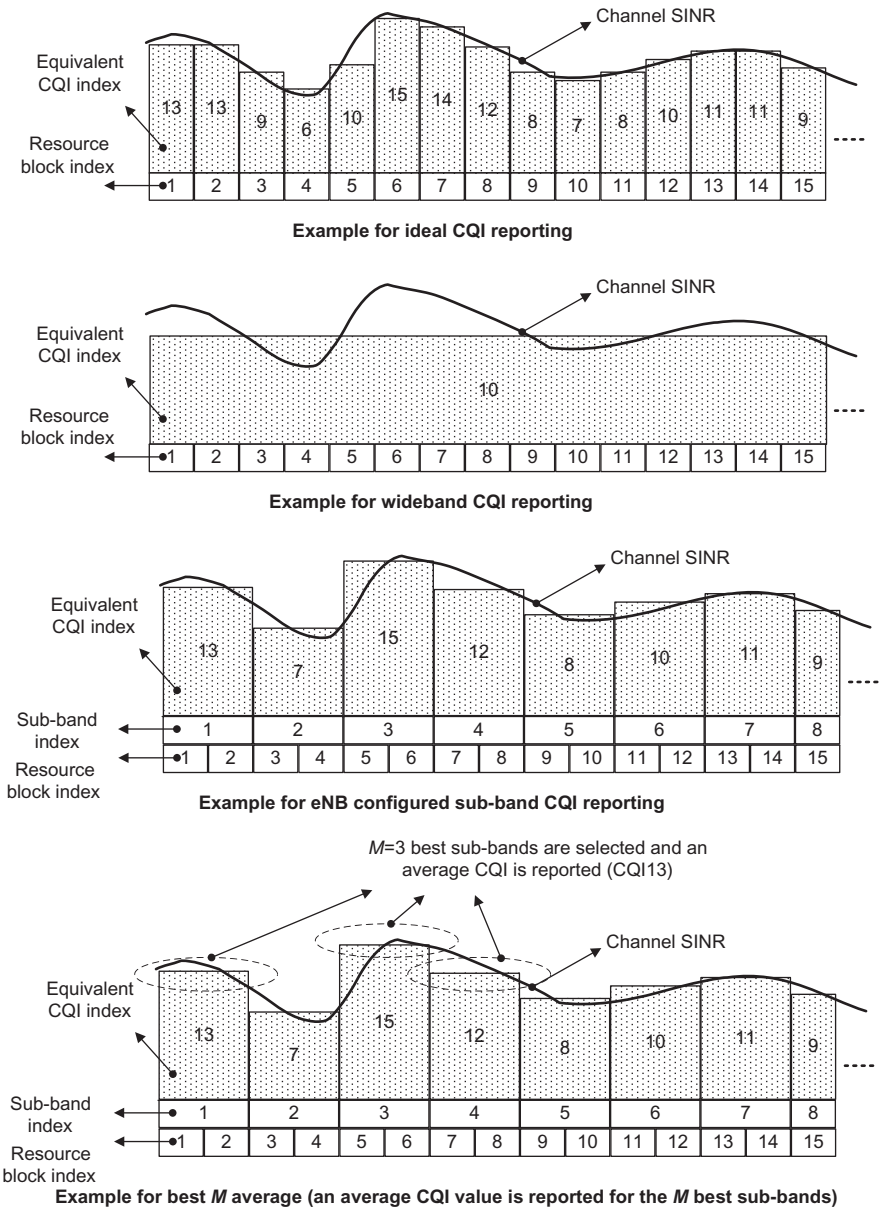


FIGURE 10.56

Graphic comparison of various CQI reporting methods [170].

Petitioners' Exhibit 1021
Nokia of America Corp., et al. v. KT Corporation, et al.
Case No. IPR2025-00036; U.S. Patent No. 11,627,631
Page 865 of 1122

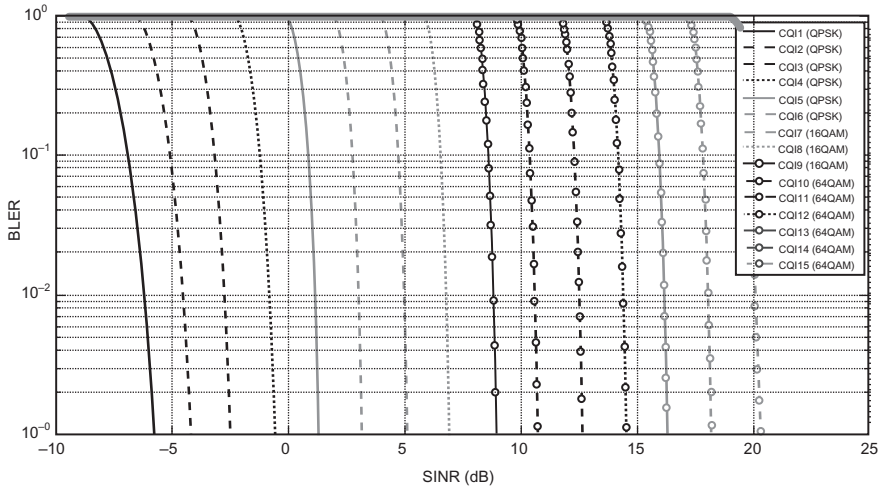


FIGURE 10.57

Link-level variation of BLER versus SINR with CQI as a parameter [137].

for recovering the downlink channel condition over the entire frequency band. The frequency-selective reporting results in a large signaling overhead. In the cases where the uplink overhead is the limiting factor, the eNB can also configure non-frequency-selective CQI/PMI reports, to mitigate various channel conditions and different antenna configurations, while keeping the signaling overhead at an appropriate level. Thus, various feedback modes are specified depending on the frequency selectivity of the CQI and the PMI reports.

The physical channels that can be used for uplink feedback signaling are PUCCH and PUSCH. The uplink feedback via PUSCH is used to accommodate a large amount of feedback information in a single reporting instance. For example, the reporting on PUSCH can include RI, wideband CQI per codeword, and the PMI for each sub-band. Note that the rank indicator is separately encoded from the other fields using 1 bit for the case of two transmit antennas and 2 bits for the case of four transmit antennas. The number of bits for the other information fields is determined according to the rank indicator. Another example is the reporting of the RI, wideband PMI, wideband CQI per codeword, and the sub-band differential CQI for each sub-band per codeword. It is noted that simultaneous reporting of sub-band differential CQI and sub-band PMI is not supported due to excessive signaling overhead.

The physical uplink control channel, on the other hand, is designed for transmission of small amounts of control signaling information. Therefore, for PUCCH reporting modes, separate time instances are used for reporting RI, wideband CQI/PMI, and sub-band CQI of the sub-band selected by the UE. The spatial differential CQI represents the difference between the CQIs of two codewords

Petitioners' Exhibit 1021
Nokia of America Corp., et al. v. KT Corporation, et al.
Case No. IPR2025-00036; U.S. Patent No. 11,627,631
Page 866 of 1122

and is defined for wideband CQI and sub-band CQI. In the case of sub-band CQI feedback, each reporting instance corresponds to a group of sub-bands, from which the UE selects the sub-band with the best CQI. Due to these characteristics, the eNB may configure periodic reporting of a limited amount of feedback information on PUCCH, while triggering the UE to report a large amount of detailed feedback information on PUSCH, if accurate channel information is necessary for transmission of large amounts of data in the downlink.

The set of sub-bands S that the UE is required to conduct measurements for CQI reporting spans the entire downlink system bandwidth. A sub-band is a set of L_{sb} contiguous PRBs, where L_{sb} is dependent on the system bandwidth. Note that the last sub-band in set S may have fewer than k contiguous PRBs depending on N_{RB}^{DL}. The number of sub-bands for system bandwidth N_{RB}^{DL} is defined by $N_{sb} = \lceil N_{RB}^{DL}/L_{sb} \rceil$. The sub-bands are indexed in the order of increasing frequency and non-increasing size starting at the lowest frequency while taking the following rules into consideration [5]:

- For transmission modes 1, 2, 3, and 5 as well as transmission modes 8, 9, and 10 without PMI/RI reporting, transmission mode 4 with RI equal to one, and transmission modes 8, 9, and 10 with PMI/RI reporting and RI equal to one, a single 4-bit wideband CQI is reported.
- For transmission modes 3 and 4 as well as transmission modes 8, 9, and 10 with PMI/RI reporting, CQI is calculated assuming transmission of one codeword for RI equal to one and two codewords for RI greater than one.
- For transmission mode 4 with RI greater than one as well as transmission modes 8, 9, and 10 with PMI/RI reporting, PUSCH-based triggered reporting includes reporting of a wideband CQI which comprises a 4-bit wideband CQI for codeword 0 and a 4-bit wideband CQI for codeword 1.
- For transmission mode 4 with RI greater than one 1 as well as transmission modes 8, 9, and 10 with PMI/RI reporting, PUCCH-based reporting includes reporting a 4-bit wideband CQI for codeword 0 and a wideband spatial differential CQI. The wideband spatial differential CQI value includes a 3-bit wideband spatial differential CQI value for codeword 1 offset level where codeword 1 offset level is the difference between the wideband CQI index for codeword 0 and wideband CQI index for codeword 1.

A UE is semi-statically configured by higher layers to feed back CQI, PMI, and corresponding RI on the same PUSCH using one of the CSI reporting modes provided in Table 10.28. Note that CQI/PMI feedback modes via PUSCH are not supported for a serving cell with bandwidth $N_{RB}^{DL} \leq 7$ [5].

As given in Table 10.28 and shown Figure 10.55, the aperiodic CQI/PMI feedback types reported via PUSCH can be categorized and described as follows [5]:

- *Wideband feedback*
  - Mode 1-2: For each sub-band, a preferred precoding matrix is selected from the codebook subset assuming transmission is scheduled only in that

Petitioners' Exhibit 1021
Nokia of America Corp., et al. v. KT Corporation, et al.
Case No. IPR2025-00036; U.S. Patent No. 11,627,631
Page 867 of 1122

Table 10.28 CQI and PMI Feedback Types for PUSCH/PUCCH CSI Reporting Modes [5]

	PMI Feedback Types via PUSCH			PMI Feedback Types via PUCCH	
	No PMI	Single PMI	Multiple PMI	No PMI	Single PMI
Wideband (wideband CQI)	–	–	Mode 1-2	Mode 1-0	Mode 1-1
UE Selected (sub-band CQI)	Mode 2-0	–	Mode 2-2	Mode 2-0	Mode 2-1
Higher-layer configured sub-band CQI)	Mode 3-0	Mode 3-1	–	–	–

sub-band. The UE reports one wideband CQI value per codeword, which is calculated assuming the use of the corresponding selected precoding matrix in each sub-band and transmission on a set of sub-bands. The UE further reports the selected PMI for a set of sub-bands, except for transmission modes 9 and 10 configured with eight CSI-RS ports where the first PMI is reported for the set of sub-bands, and the second PMI is reported for each sub-band in the set.

- *Higher-layer configured sub-band feedback*
  - Mode 3-0: The UE reports a wideband CQI value which is calculated assuming transmission on a set of sub-bands. The UE also reports one sub-band CQI value for each set of sub-bands. The sub-band CQI value is calculated assuming transmission is scheduled only in that sub-band. Both wideband and sub-band CQI represent channel quality for the first codeword, even if the rank indicator is greater than one.
  - Mode 3-1: A single precoding matrix is selected from the codebook subset assuming transmission on a set of sub-bands. The UE reports one sub-band CQI value per codeword for each set of sub-bands, which are calculated assuming the use of a single precoding matrix in all sub-bands and assuming transmission is scheduled in the corresponding sub-band. The UE reports a wideband CQI value per codeword, which is calculated assuming the use of a single precoding matrix in all sub-bands, and transmission is scheduled on a set of sub-bands. The UE reports the selected single precoding matrix indicator, except for transmission modes 9 and 10 configured with eight CSI-RS ports where two precoding matrix indicators are reported.
- *UE-selected sub-band feedback*
  - Mode 2-0: The UE selects a set of M preferred sub-bands of size L_{sb} (where L_{sb} and M are given in Table 10.29 for each system bandwidth) within the set of sub-bands S. The UE also reports one CQI value

Petitioners' Exhibit 1021
Nokia of America Corp., et al. v. KT Corporation, et al.
Case No. IPR2025-00036; U.S. Patent No. 11,627,631
Page 868 of 1122

Table 10.29 Sub-band Size L_{sb} and Number of Sub-bands M in S as a Function of System Bandwidth [5]

Number of Downlink Resource Blocks N_{RB}^{DL}	Sub-band Size L_{sb} (Resource Blocks)	Number of Sub-bands M
6–7	N/A	N/A
8–10	2	1
11–26	2	3
27–63	3	5
64–110	4	6

reflecting transmission only over the M selected sub-bands determined in the previous step. The CQI represents channel quality for the first codeword, even when RI > 1. Additionally, the UE reports one wideband CQI value which is calculated assuming transmission on a set of sub-bands S. The wideband CQI represents channel quality for the first codeword, even when RI > 1. For transmission mode 3, the reported CQI values are calculated conditioned on the reported RI. For other transmission modes, they are reported conditioned on rank 1.

- Mode 2-2: The UE performs joint selection of the set of M preferred sub-bands of size L_{sb} within the set of sub-bands S and a preferred single precoding matrix selected from the codebook subset that is preferred to be used for transmission over the M selected sub-bands. The UE reports one CQI value per codeword reflecting transmission only over the selected M preferred sub-bands and using the same selected single precoding matrix in each of the M sub-bands. Except for transmission modes 9 and 10 with eight CSI-RS ports configured, the UE also reports the selected single precoding matrix indicator preferred for the M selected sub-bands. A UE further reports the selected single precoding matrix indicator for all sub-bands in the set S. For transmission modes 9 and 10 with eight CSI-RS ports configured, the UE reports the first precoding matrix indicator for all sub-bands in the set S. A UE further reports a second precoding matrix indicator for all sub-bands in the set S and a second precoding matrix indicator for the M selected sub-bands A single precoding matrix is selected from the codebook subset assuming transmission on a set of sub-bands S. A UE provides the wideband CQI value per codeword which is calculated assuming the use of a single precoding matrix in all sub-bands and transmission on a set of S sub-bands S. For transmission modes 4, 8, 9, and 10, the reported PMI and CQI values are calculated conditioned on the reported RI. For other transmission modes, they are reported conditioned on rank 1. For all UE-selected sub-band feedback modes, the UE further provides the positions of the M selected sub-bands using a combinatorial index [5].

Petitioners' Exhibit 1021
Nokia of America Corp., et al. v. KT Corporation, et al.
Case No. IPR2025-00036; U.S. Patent No. 11,627,631
Page 869 of 1122

A UE can be semi-statically configured by higher layers to periodically send different CSI (CQI, PMI, PTI, and/or RI) on PUCCH using the reporting modes given in Table 10.28. The periodic CSI reporting mode for each serving cell is configured by higher-layer signaling. For the UE-selected sub-band CQI, a CQI report in a certain subframe of a certain serving cell describes the channel quality in a particular part or in particular parts of the bandwidth of that serving cell, described subsequently as bandwidth part or parts. The bandwidth parts are indexed in the order of increasing frequency and decreasing sizes starting at the lowest frequency. The following CQI/PMI and RI reporting types with distinct periods and offsets are supported for the PUCCH CSI reporting modes given in Table 10.28 [5]:

- Type 1 report supports CQI feedback for the UE selected sub-bands.
- Type 1a report supports sub-band CQI and second PMI feedback.
- Type 2, 2b, and 2c report supports wideband CQI and PMI feedback.
- Type 2a report supports wideband PMI feedback.
- Type 3 report supports RI feedback.
- Type 4 report supports wideband CQI.
- Type 5 report supports RI and wideband PMI feedback.
- Type 6 report supports RI and PTI feedback.

10.12 Uplink transmitter and receiver chain

An example of a transmitter/receiver chain of an LTE modem is depicted in Figures 10.58 and 10.59 [171–173]. Note that the modem implementation presented in this section only includes the physical layer processing functions assuming higher layer protocols are processed by another processor. The digital front-end unit is the interface between the analog front-end and digital baseband modules in the wireless systems. The function of the digital front end (block of digital filters) is typically to perform gain control, sampling rate conversion, pulse shaping, matched filtering, and phase correction. The digital front end is functionally simple relative to other baseband blocks; however, it consumes a significant portion of the chip area and power. As an OFDM system, LTE is sensitive to carrier frequency offset (CFO) which causes inter-carrier interference. The timing synchronization and fractional CFO estimation/correction can mitigate the effects of CFO and the oscillator phase noise. Integer frequency offset estimation is then applied to remove misalignment, which is an integer multiple of the sub-carrier spacing. Although a large portion of CFO can be compensated, there is still a residual frequency offset due to estimation errors. The residual frequency offset is estimated based on the frequency-domain symbols after the FFT operation in the receiver.

Similar to other OFDM systems, reference signals are inserted during sub-carrier mapping in both time and frequency dimensions. The reference signals

Petitioners' Exhibit 1021
Nokia of America Corp., et al. v. KT Corporation, et al.
Case No. IPR2025-00036; U.S. Patent No. 11,627,631
Page 870 of 1122

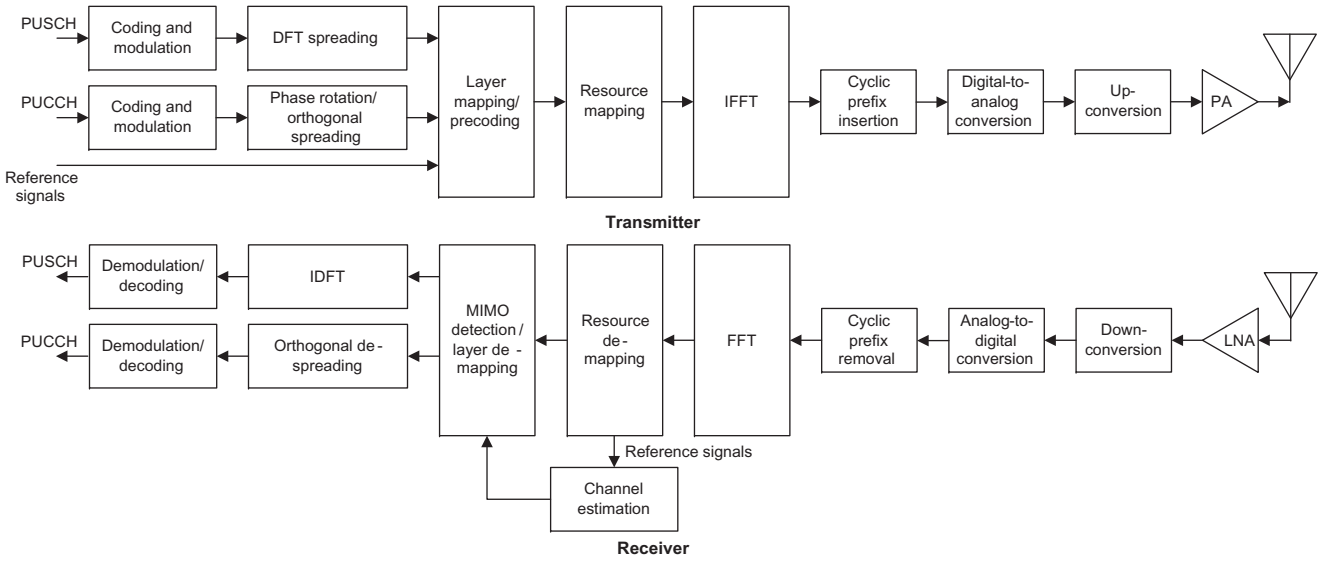


FIGURE 10.58

Example of uplink transmission and reception chains [14].

Petitioners' Exhibit 1021
Nokia of America Corp., et al. v. KT Corporation, et al.
Case No. IPR2025-00036; U.S. Patent No. 11,627,631
Page 871 of 1122

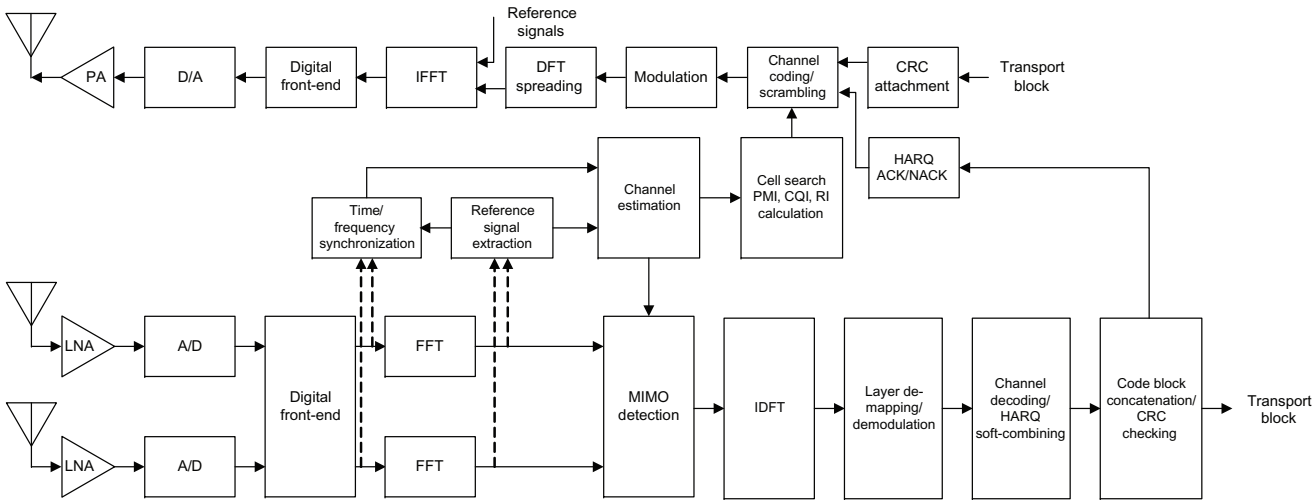


FIGURE 10.59

Block diagram of an example LTE UE modem (physical layer) [173].

transmitted from multiple antennas are mutually orthogonal (provided that the antennas are uncorrelated), which means the channel impulse response between different transmit-receive antenna pairs can be separately estimated. This assumption would reduce high complexity of MIMO channel estimation at the cost of lower spectral efficiency. For MIMO systems, a major challenge is the separation and detection of the transmitted symbols at the receiver given the amount of operations involved (e.g., matrix inversion and multiplication/division). Among different detection algorithms, maximum likelihood detection is an optimum detector that computes the following likelihood function:

$$L(b_i|\mathbf{r}) = \log\left(\frac{\sum_{\mathbf{s}:b_i(\mathbf{s})=1}\exp(-\sigma_0^{-2}||\mathbf{r}-\hat{\mathbf{H}}\mathbf{s}||^2)}{\sum_{\mathbf{s}:b_i(\mathbf{s})=0}\exp(-\sigma_0^{-2}||\mathbf{r}-\hat{\mathbf{H}}\mathbf{s}||^2)}\right) \tag{10.24}$$

In the above equation, $b_i(\mathbf{s})$ denotes the ith bit of the input sequence $\mathbf{s}$, σ_0^2 is the noise variance, and $\mathbf{r} = \mathbf{H}\mathbf{s} + \mathbf{n}$ is the received signal. The functional block diagram in Figure 10.59 shows an example of the internal data flows through an LTE UE with two receive antennas and one transmit antenna. The RF signal is received by the receiver antennas, down-converted, scaled by an automatic gain control, and digitized by an analog-to-digital converter (A/D) within the analog and digital front-end module including a sample rate converter and a numerically controlled oscillator.

The baseband processor receives the digitized signal in the form of complex-valued samples from the A/D and delivers the decoded bit stream to a higher layer protocol and application processor. It first removes the cyclic prefix, transforms the signal into frequency-domain by an FFT operation, performs channel estimation, equalization, log-likelihood ratio (LLR) calculation, HARQ combining, channel decoding, and CRC check for different physical channels. In addition, control information for closed-loop MIMO operation is generated, i.e., CQI, PMI, and RI. In the uplink direction, PUSCH data is channel coded, DFT spread, and mapped to resource elements together with modulated PUCCH and modulated reference signals. Following IFFT and cyclic prefix insertion procedures, the data is sent to transmitter front end and RF circuitry. For random access, the corresponding PRACH is processed. In a typical receiver, synchronization is usually initially conducted to acquire information such as the beginning of frame and the CFO calculation and correction [173].

The solution to Eq. (10.24) requires calculation of the likelihood function over the entire set of possible transmitted vectors, resulting in a significant amount of complexity in practice. However, since maximum likelihood provides the best theoretical performance, it is commonly used as a benchmark when comparing other algorithms. Linear detection algorithms such as MMSE have very low complexity. The MMSE equalizer is defined as follows: $\hat{s}_{\text{MMSE}} = \mathbf{W}_{\text{MMSE}}\mathbf{r} = (\hat{\mathbf{H}}^H\hat{\mathbf{H}} + \sigma_0^2\mathbf{I})^{-1}\hat{\mathbf{H}}^H\mathbf{r}$. The MMSE detection is the most commonly used detection scheme and involves matrix inversion which can be efficiently performed through direct inversion with sufficient numerical stability. Despite the low complexity,

Petitioners' Exhibit 1021
Nokia of America Corp., et al. v. KT Corporation, et al.
Case No. IPR2025-00036; U.S. Patent No. 11,627,631
Page 873 of 1122

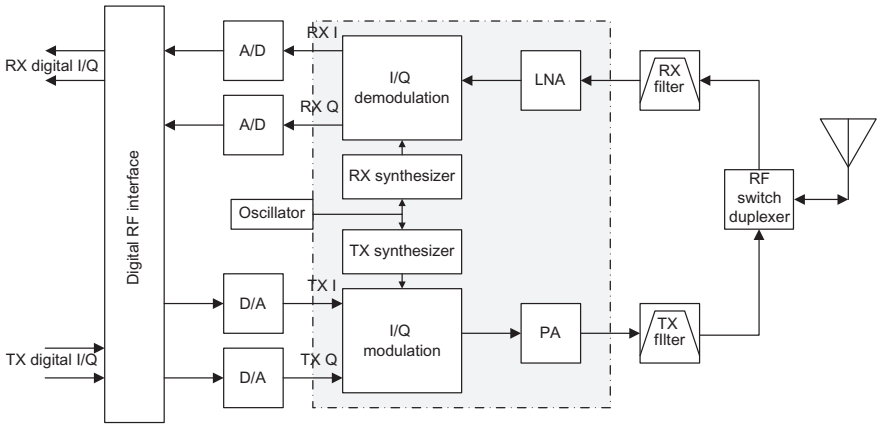


FIGURE 10.60

Simplified block diagram of RF transmitter and receiver in an LTE device [159].

MMSE detection has relatively poor performance, especially in slow fading channels. As a trade-off between detection performance and implementation complexity, soft-output MIMO detectors and sphere decoders can be used [169].

As shown in Figures 10.59 and 10.60, the radio signals received by the RF front end are down-converted to analog baseband signals (using a zero-IF converter), then they are converted to digital baseband signals using A/D converters. The digital front end applies filtering to the baseband signals and FFT is applied to transform the time-domain signal into frequency-domain where channel estimation and symbol detection are performed. In LTE, the channel estimator uses the reference signals to estimate the channel matrix $\mathbf{H}$ for all data sub-carriers. The estimated channel matrix $\hat{\mathbf{H}}$ and the received symbol vector $\mathbf{r}$ belonging to the current user will be extracted for MIMO detection. The above functions are performed by the baseband processor. The estimated channel matrix is conveyed to the MIMO detector together with the received symbols extracted from data sub-carriers. The coefficients are fed to the detector to compute the LLR soft-output $L(b_i^k)$ (i.e., ith bit of the input vector on the kth sub-carrier). For example, in case of MMSE detection, the detector fetches the MMSE weighting matrix $\mathbf{W}_{\text{MMSE}}$ from the local memory and multiplies the MMSE weighting matrix $\mathbf{W}_{\text{MMSE}}$ with the received symbol vectors $\mathbf{r}$ in order to compute $\hat{s}$ and to map $\hat{s}$ to LLR values. The LLR values are then passed to the FEC decoder where it will be de-interleaved and processed by the channel decoder to generate the output bits. The FEC module contains the soft buffer for chase combining in HARQ and a parallel turbo decoder. Although many baseband processing functions can be assigned to a programmable processor, there are still some tasks which need to be implemented in dedicated hardware to meet the performance and power constraints. In that case, hardware accelerators are added to the on-chip system. They are typically

Petitioners' Exhibit 1021
Nokia of America Corp., et al. v. KT Corporation, et al.
Case No. IPR2025-00036; U.S. Patent No. 11,627,631
Page 874 of 1122

controlled by a number of control registers which can be set by the baseband processor.

The RFICs in the UE may include different portions of the schematic block diagram shown in Figure 10.60, with some containing the transmitter or receiver only, and others combining transmitter and receiver in one component. Traditionally RFICs have used analog baseband I/Q inputs and outputs. However, digital I/Q interfaces are becoming more common. The mobile industry processor interface (MIPI) alliance has developed the DigRF standard [174], which describes the high-speed digital baseband to RFIC interface for new generation of cellular radios, which includes embedded control protocols for the RFIC.

References

3GPP Specifications[16]

[1] 3GPP TS 36.101, Evolved Universal Terrestrial Radio Access (E-UTRA); User Equipment (UE) radio transmission and reception (Release 11), December 2012.
[2] 3GPP TS 36.104, Evolved Universal Terrestrial Radio Access (E-UTRA); Base Station (BS) radio transmission and reception (Release 11), December 2012.
[3] 3GPP TS 36.211, Evolved Universal Terrestrial Radio Access (E-UTRA), Physical Channels and Modulation (Release 11), December 2012.
[4] 3GPP TS 36.212, Evolved Universal Terrestrial Radio Access (E-UTRA) Multiplexing and Channel Coding (Release 11), December 2012.
[5] 3GPP TS 36.213, Evolved Universal Terrestrial Radio Access (E-UTRA); Physical layer procedures (Release 11), December 2012.
[6] 3GPP TS 36.214, Evolved Universal Terrestrial Radio Access (E-UTRA); Physical layer – Measurements (Release 11), December 2012.
[7] 3GPP TS 36.300, Evolved Universal Terrestrial Radio Access (E-UTRA) and Evolved Universal Terrestrial Radio Access Network (E-UTRAN) Overall description, Stage 2 (Release 11), December 2012.
[8] 3GPP TS 36.306, Evolved Universal Terrestrial Radio Access (E-UTRA); User Equipment (UE) Radio Access Capabilities (Release 11), December 2012.
[9] 3GPP TS 36.321, Evolved Universal Terrestrial Radio Access (E-UTRA); Medium Access Control (MAC) Protocol specification (Release 11), December 2012.
[10] 3GPP TS 36.331 Evolved Universal Terrestrial Radio Access (E-UTRA); Radio Resource Control (RRC); Protocol specification (Release 11), December 2012.
[11] 3GPP TR 36.912 Feasibility Study for Further Advancements for E-UTRA (LTE-Advanced) (Release 11), September 2012.
[12] 3GPP TR 36.814 Feasibility Study for Further Advancements for E-UTRA (LTE-Advanced) (Release 9), March 2010.
[13] 3GPP TR 36.819 Coordinated Multi-Point Operation for LTE Physical Layer Aspects (Release 11), December 2011.

[16] 3GPP specifications can be found at the following URL: http://www.3gpp.org/ftp/Specs/archive/36_series/.

Books

[14] C. Johnson, Long Term Evolution in Bullets, second ed., Create Space Independent Publishing Platform, 2012.
[15] S. Sesia, I. Toufik, M. Baker, LTE, the UMTS Long Term Evolution, From Theory to Practice, second ed., John Wiley & Sons, 2011.
[16] E. Dahlman, S. Parkvall, J. Skold, 4G, LTE/LTE-Advanced for Mobile Broadband, Academic Press, 2011.
[17] H. Holma, A. Toskala, LTE Advanced, 3GPP Solution for IMT-Advanced, John Wiley & Sons, 2012.
[18] H. Holma, A. Toskala, LTE for UMTS, Evolution to LTE-Advanced, John Wiley & Sons, 2011.
[19] S. Ahmadi, Mobile WiMAX, A Systems Approach to Understanding IEEE 802.16m Radio Access Technology, Academic Press, 2010.
[20] B. Sklar, Digital Communications, Fundamentals and Applications, second ed., Prentice Hall, 2001.
[21] A. Paulraj, et al., Introduction to Space-Time Wireless Communications, Cambridge University Press, 2008.
[22] W.C. Jakes, Microwave Mobile Communications, second ed., Wiley-IEEE Press, 1994.
[23] S.G. Glisic, Advanced Wireless Communications, 4G Cognitive and Cooperative Broadband Technology, second ed., Wiley Inter-science, 2007.
[24] D.E. Dudgeon, R.M. Mersereau, Multidimensional Digital Signal Processing, Prentice Hall, 1984.
[25] D. Tse, P. Viswanath, Fundamentals of Wireless Communication, Cambridge University Press, 2005.
[26] E. Biglieri, et al., MIMO Wireless Communications, Cambridge University Press, 2010.
[27] A. Goldsmith, Wireless Communications, Cambridge University Press, 2005.
[28] S. Lin, D.J. Costello, Error Control Coding, second ed., Prentice Hall, 2004.
[29] S.L. Marple, Digital Spectral Analysis with Applications, Prentice Hall, 1987.
[30] G.H. Golub, C.F. Van Loan, Matrix Computations, third ed., Johns Hopkins University Press, 1996.
[31] A. Papoulis, Probability, Random Variables and Stochastic Processes, fourth ed., McGraw Hill Higher Education, 2002.
[32] L. Rade, Mathematics Handbook for Science and Engineering, Springer, 2010.
[33] G.A. Korn, T.M. Korn, Mathematical Handbook for Scientists and Engineers, Definitions, Theorems, and Formulas for Reference and Review (Revised Edition), Dover Publications, 2000.
[34] C.E. Shannon, W. Weaver, The Mathematical Theory of Communication, University of Illinois Press, 1998.
[35] F. Dowla, Handbook of RF and Wireless Technologies, Newnes, 2003.
[36] G. Arfken, *Bessel Functions*, Mathematical Methods for Physicists, third ed., Academic Press, 1985.
[37] W.G. Bickley, Bessel Functions and Formulae, Cambridge University Press, Cambridge, England, 1957.
[38] F. Bowman, Introduction to Bessel Functions, Dover, 2010.

Petitioners' Exhibit 1021
Nokia of America Corp., et al. v. KT Corporation, et al.
Case No. IPR2025-00036; U.S. Patent No. 11,627,631
Page 876 of 1122

[39] H.G. Myung, D. Goodman, Single Carrier FDMA, A New Air Interface for Long Term Evolution, John Wiley & Sons, 2008.
[40] T.M. Cover, J.A. Thomas, Elements of Information Theory, John Wiley & Sons, 1991.
[41] J.G. Proakis, Digital Communications, fifth ed., McGraw-Hill, 2007.
[42] N. Costa, S. Haykin, Multiple-Input Multiple-Output Channel Models, Theory and Practice, John Wiley & Sons, 2010.
[43] C. Oestges, B. Clerckx, MIMO Wireless Communications, from Real-World Propagation to Space-Time Code Design, Academic Press, 2007.
[44] A. Sibille, C. Oestges, A. Zanella, MIMO, from Theory to Implementation, Academic Press, 2010.
[45] I. Stakgold, M.J. Holst, Green's Functions and Boundary Value Problems, third ed., John Wiley & Sons, 2011.
[46] R.G. Gallager, Principles of Digital Communication, Cambridge University Press, 2008.
[47] K. Fazel, G.P. Fettweis, Multi-Carrier Spread-Spectrum, Kluwer Academic Publishers, 1997.

Articles

[48] G. Bauch, G. Dietl, MIMO for 3GPP LTE-Advanced and beyond, Global Telecommunications Conference (GLOBECOM), 2010.
[49] C. Mehlfuhrer, et al., The Vienna LTE simulators—enabling reproducibility in wireless communication research, EURASIP J. Adv. Signal Process, (1) (2011).
[50] H.G. Myung, J. Lim, D.J. Goodman, Single carrier FDMA for uplink wireless transmission, IEEE Veh. Technol. Mag. 1 (3) (2006).
[51] H. Ekström, et al., Technical solutions for the 3G long-term evolution, IEEE Commun. Mag. 44 (3) (2006).
[52] D. Falconer, et al., Frequency domain equalization for single-carrier broadband wireless systems, IEEE Commun. Mag. 40 (4) (2002).
[53] H. Sari, et al., Transmission techniques for digital terrestrial TV broadcasting, IEEE Commun. Mag. 33 (2) (1995).
[54] C. Berrou, A. Glavieux, P. Thitimajshima, Near Shannon limit error correcting coding and decoding, "turbo codes", in: Proceedings of the IEEE International Conference on Communications, Geneva, Switzerland, May 1993.
[55] 3GPP R1-050397, E-UTRA uplink numerology and frame structure 3GPP TSG RAN WG1, meeting 41, Athens, Greece, 2005.
[56] 3GPP R1-050584, E-UTRA uplink numerology and design, 3GPP TSG RAN WG1, meeting 41bis, Sophia Antipolis, France, 2005.
[57] 3GPP R1-050971, Single carrier uplink options for E-UTRA, 3GPP TSG RAN WG1, meeting 42, London, UK, 2005.
[58] U. Sorger, I. De Broeck M. Schnell, Interleaved FDMA—a new spread-spectrum multiple-access scheme, In: Proceedings of the IEEE International Conference on Communications (ICC), 1998.
[59] K. Bruninghaus, H. Rohling, Multi-carrier Spread Spectrum and its Relationship to Single-Carrier Transmission, In: Proceedings of the IEEE Vehicular Technology Conference (VTC), May 1998.

Petitioners' Exhibit 1021
Nokia of America Corp., et al. v. KT Corporation, et al.
Case No. IPR2025-00036; U.S. Patent No. 11,627,631
Page 877 of 1122

[60] D. Galda, H. Rohling, A Low Complexity Transmitter Structure for OFDM-FDMA Uplink Systems, in: Proceedings of the IEEE Vehicular Technology Conference (VTC), May 2002.
[61] R. Dinis, D. Falconer, C.T. Lam, M. Sabbaghian, A Multiple Access Scheme for the Uplink of Broadband Wireless Systems, in: Proceedings of the IEEE Global Telecommunications Conference, November 2004.
[62] H. Sari, G. Karam I. Jeanclaude, Frequency-Domain Equalization of Mobile Radio and Terrestrial Broadcast Channels, in: Proceedings of the IEEE Global Telecommunications Conference, November 1994.
[63] D. Falconer, S.L. Ariyavisitakul, A. Benyamin-Seeyar, B. Eidson, Frequency domain equalization for single-carrier broadband wireless systems, IEEE Commun. Mag. 40 (2002).
[64] V. Nangia, K.L. Baum, Experimental broadband OFDM system—field results for OFDM and OFDM with frequency domain spreading, in: Proceedings of the IEEE International Conference on Vehicular Technology, Vancouver, BC, Canada, 2002.
[65] 3GPP R1-062061, Uplink DC subcarrier distortion considerations in LTE, 3GPP TSG RAN WG1, meeting 46, Tallinn, Estonia, 2006.
[66] 3GPP R1-050702, DFT-spread OFDM with pulse shaping filter in frequency domain in evolved UTRA uplink, 3GPP TSG RAN WG1, meeting 42, London, UK, 2005.
[67] 3GPP R1-051434, Optimum family of spectrum-shaping functions for PAPR reduction in SC-FDMA, 3GPP TSG RAN WG1, meeting 43, Seoul, Korea, 2005.
[68] D.C. Chu, Poly-phase codes with good periodic correlation properties, IEEE Trans. Inform. Theory (1972).
[69] B.M Popovic, Generalized chirp-like poly-phase sequences with optimal correlation properties, IEEE Trans. Inform. Theory 38 (1992) 1406−1409.
[70] 3GPP R1-060878, E-UTRA SC-FDMA uplink pilot/reference signal design & TP, 3GPP TSG RAN WG1, meeting 44bis, Athens, Greece, 2006.
[71] 3GPP R1-080576, Way forward on the sequence grouping for UL DM-RS, 3GPP TSG RAN WG1, meeting 51bis, Sevilla, Spain, 2008.
[72] 3GPP R1-072584, Way Forward for PUSCH RS, 3GPP TSG RAN WG1, meeting 49, Kobe, Japan, 2007.
[73] 3GPP R1-072585, Way forward for PUCCH RS, 3GPP TSG RAN WG1, meeting 49, Kobe, Japan, 2007.
[74] 3GPP R1-074278, Hopping and planning of sequence groups for uplink RS, 3GPP TSG RAN WG1, meeting 50bis, Shanghai, China, 2007.
[75] 3GPP R1-080719, Hopping patterns for UL RS, 3GPP TSG RAN WG1, meeting 52, Sorrento, Italy, 2008.
[76] 3GPP R1-081133, WF on UL DM-RS hopping pattern generation, 3GPP TSG RAN WG1, meeting52, Sorrento, Italy, 2008.
[77] 3GPP R1-071341, Uplink reference signal planning aspects, 3GPP TSG RAN WG1, meeting 48bis, St. Julian's, Malta, 2007.
[78] 3GPP R1-080983, Way forward on the cyclic shift hopping for PUCCH, 3GPP TSG RAN WG1, meeting 52, Sorrento, Italy, 2008.
[79] 3GPP R1-073756, Benefit of non-persistent UL sounding for frequency hopping PUSCH, 3GPP TSG RAN WG1, meeting 50, Athens, Greece, 2007.
[80] 3GPP R1-082199, Physical-layer parameters to be configured by RRC, 3GPP TSG RAN WG1, meeting 53, Kansas City, MI, 2008.

Petitioners' Exhibit 1021
Nokia of America Corp., et al. v. KT Corporation, et al.
Case No. IPR2025-00036; U.S. Patent No. 11,627,631
Page 878 of 1122

[81] 3GPP R1-072671, Uplink channel interleaving, 3GPP TSG RAN WG1, meeting 49bis, Orlando, FL, 2007.
[82] B. Classon et al., Multi-dimensional adaptation and multi-user scheduling techniques for wireless OFDM systems, in: Proceedings of the IEEE International Conference on Communications, Anchorage, Alaska, 2003.
[83] 3GPP R1-071340, Considerations and recommendations for UL sounding RS, 3GPP TSG RAN WG1, meeting 48bis, St Julian's, Malta, March 2007.
[84] 3GPP R1-073756, Benefit of non-persistent UL sounding for frequency hopping PUSCH, 3GPP TSG RAN WG1, meeting 50, Athens, Greece, 2007.
[85] A. Ghosh et al., Uplink control channel design for 3GPP LTE, in: Proceedings of the IEEE International Symposium on Personal, Indoor and Mobile Radio Communications, Athens, Greece, 2007.
[86] 3GPP R1-070084, Coexistance simulation results for 5 MHz E-UTRA/UTRA FDD uplink with revised simulation assumptions, 3GPP TSG RAN WG4, meeting 42, St. Louis,MI, 2007.
[87] S. Zhou, G.B. Giannakis, C.L. Martret, Chip-interleaved block-spread code division multiple access, IEEE Trans. Commun. 50 (2002).
[88] 3GPP R1-080190, Embedding ACK/NACK in CQI reference signals and receiver structures, 3GPP TSG RAN WG1, meeting 51bis, Sevilla, Spain, 2008.
[89] 3GPP R1-073564, Selection of orthogonal cover and cyclic shift for high speed UL ACK channels, 3GPP TSG RAN WG1, meeting 50, Athens, Greece, 2007.
[90] 3GPP R1-080035, Joint proposal on uplink ACK/NACK channelization, 3GPP TSG RAN WG1, meeting 51bis, Sevilla, Spain, 2008.
[91] 3GPP R1-062072, Uplink reference signal multiplexing structures for E-UTRA, 3GPP TSG RAN WG1, meeting 46, Tallinn, Estonia, 2006.
[92] 3GPP R1-080983, Way forward on the cyclic shift hopping for PUCCH, 3GPP TSG RAN WG1, meeting 52, Sorrento, Italy, 2008.
[93] 3GPP R1-080931, ACK/NACK channelization for PRBs containing both ACK/NACK and CQI, 3GPP TSG RAN WG1, meeting 52, Sorrento, Italy, 2008.
[94] 3GPP R1-104135, Confirmation of UE behavior in case of simultaneously-triggered SR, SRS and CQI, 3GPP TSG RAN WG1, meeting 61bis, Dresden, Germany, 2010.
[95] 3GPP R1-081928, Way forward on indication of UE antenna selection for PUSCH, 3GPP TSG RAN WG1, meeting 53, Kansas City, MI, May 2008.
[96] 3GPP R1-082109, UE transmit antenna selection, 3GPP TSG RAN WG1, meeting 53, Kansas City, MI, May 2008.
[97] 3GPP R1-062175, Random access burst design for E-UTRA, 3GPP TSG RAN WG1, meeting 46, Tallinn, Estonia, 2006.
[98] R.L. Frank, S.A. Zadoff, R. Heimiller, Phase shift pulse codes with good periodic correlation properties, IEEE Trans. Inform. Theory 7 (October 1961).
[99] D.C. Chu, Poly-phase codes with good periodic correlation properties, IEEE Trans. Inform. Theory 18 (1972).
[100] 3GPP R1-072325, Multiple values of cyclic shift increment NCS, 3GPP TSG RAN WG1, meeting 49, Kobe, Japan, 2007.
[101] 3GPP R1-073624, Limitation of RACH sequence allocation for high mobility cell, 3GPP TSG RAN WG1, meeting 50, Athens, Greece, 2007.

Petitioners' Exhibit 1021
Nokia of America Corp., et al. v. KT Corporation, et al.
Case No. IPR2025-00036; U.S. Patent No. 11,627,631
Page 879 of 1122

[102] 3GPP R1-040642, Comparison of PAR and cubic metric for power de-rating, 3GPP TSG RAN WG1, meeting 37, Montreal, Canada, 2004.
[103] 3GPP R1-060023, Cubic metric in 3GPP-LTE, 3GPP TSG RAN WG1, LTE ad-hoc meeting, Helsinki, Finland, 2006.
[104] 3GPP R1-071517, RACH sequence allocation for efficient matched filter implementation, 3GPP TSG RAN WG1, meeting 48bis, St Julian's, Malta, 2007.
[105] 3GPP R1-071409, Efficient matched filters for paired root Zadoff−Chu sequences, 3GPP TSG RAN WG1, meeting 48bis, St Julian's, Malta, 2007.
[106] 3GPP R1-063377, UL timing control accuracy and update rate, 3GPP TSG RAN WG1, meeting 47, Riga, Latvia, 2006.
[107] 3GPP R1-072841, Simulation of uplink timing error impact on PUSCH, 3GPP TSG RAN WGI, meeting 49bis, Orlando, FL, 2007.
[108] M.P.J. Baker, T.J. Moulsley, Power control in UMTS release 99, in: Proceedings of the First IEE International Conference on 3G Communications, 2000.
[109] 3GPP R1-080881, Range and representation of Delta_MCS, 3GPP TSG RAN WG1, meeting 52, Sorrento, Italy, 2008.
[110] J. Lee, J.-K. Han, J. Zhang, MIMO technologies in 3GPP LTE and LTE-advanced, EURASIP J. Wireless Commun. Netw. (2009).
[111] S. Catreux, P.F. Driessen, L.J Greenstein, Attainable throughput of an interference-limited multiple-input multiple-output (MIMO) cellular system, IEEE Trans Commun. 49 (8) (2001).
[112] I. Telatar, Capacity of multi-antenna Gaussian channels, AT&T Tech. Memo. (1995).
[113] G.J. Foschini, M.J. Gans, On limits of wireless communications in a fading environment when using multiple antennas, Wireless Personal Commun. (1998).
[114] M.-S. Alouini, A. Goldsmith, Capacity of Nakagami multipath fading channels, in: Proceedings of the Vehicular Technology Conference, 1997.
[115] D. Chizhik, G.J. Foschini, R.A. Valenzuela, Capacities of multi-element transmit and receive antennas: correlations and keyholes, Electron. Lett. 36 (2000).
[116] D. Gesbert, H. Bölcskei, D. Gore, A. Paulraj, MIMO wireless channels: capacity and performance prediction, Global Telecommunications Conference (GLOBECOM), 2000.
[117] D.A. Gore, R.U. Nabar, A. Paulraj, Selecting an optimal set of transmit antennas for a low rank matrix channel, Proc. ICASSP 2000 49 (8) (2000).
[118] S. Sandhu, R.U. Nabar, D.A. Gore, A. Paulraj, Near-optimal selection of transmit antennas for a MIMO channel based on Shannon capacity, in: Proceedings of the 34th Asilomar Conference on Signals, Systems and Computers, 2000.
[119] A.F. Molisch, M.Z. Win, J.H. Winters, A. Paulraj, Capacity of MIMO systems with antenna selection, in: Proceedings of the IEEE International Conference on Communications (ICC), 2001.
[120] Z. Shen, et al., Overview of 3GPP LTE-advanced carrier aggregation for 4G wireless communications, IEEE Commun. Mag. 50 (2) (2012).
[121] Y.-H. Nam, et al., Evolution of reference signals for LTE-advanced systems, IEEE Commun. Mag. 50 (2) (2012).
[122] L. Liu, et al., Downlink MIMO in LTE-advanced: SU-MIMO vs. MU-MIMO, IEEE Commun. Mag. 50 (2) (2012).

Petitioners' Exhibit 1021
Nokia of America Corp., et al. v. KT Corporation, et al.
Case No. IPR2025-00036; U.S. Patent No. 11,627,631
Page 880 of 1122

[123] D. Lee, et al., Coordinated multipoint transmission and reception in LTE-advanced: deployment scenarios and operational challenges, IEEE Commun. Mag. 50 (2) (2012).
[124] D. Bai, et al., LTE-advanced modem design: challenges and perspectives, IEEE Commun. Mag. 50 (2) (2012).
[125] J. Lee, Kim, et al., Coordinated multipoint transmission and reception in LTE-advanced systems, IEEE Commun. Mag. 50 (2) (2012).
[126] Z. Shen, et al., Dynamic uplink−downlink configuration and interference management in TD-LTE, IEEE Commun. Mag. 50 (2) (2012).
[127] C.S. Park, et al., Evolution of uplink MIMO for LTE-Advanced, IEEE Commun. Mag. 49 (2) (2011).

Miscellaneous

[128] 3G Americas, MIMO and smart antennas for 3G and 4G wireless systems. <http://www.3gamericas.org>, May 2010.
[129] Rohde & Schwarz Application Notes, LTE-Advanced Technology Introduction, March 2010.
[130] 3G Americas, 3GPP Mobile Broadband Innovation Path to 4G: Release 9, Release 10 and Beyond: HSPA + , SAE/LTE and LTE-Advanced, February 2010.
[131] 3G Americas, HSPA to LTE-Advanced: 3GPP Broadband Evolution to IMT-Advanced (4G), September 2009.
[132] 3G Americas, The Mobile Broadband Evolution: 3GPP Release 8 and Beyond HSPA + , SAE/LTE and LTE-Advanced, February 2009.
[133] IEEE 802.16m-07/244r1, Yang Song, Liyu Cai, Keying Wu, and Hongwei Yang, Collaborative MIMO, November 2007.
[134] Agilent Technologies, 3GPP long term evolution: system overview, product development, and test challenges. <http://www.agilent.com>, 2009.
[135] IEEE C802.16m-08/153, Bin-Chul Ihm, Jinsoo Choi and Wookbong Lee, “Pilot Related to DL-MIMO”, March 2008.
[136] MATLAB CENTRAL, An open exchange for the MATLAB and SIMULINK user community. <http://www.mathworks.com/matlabcentral>.
[137] Vienna University of Technology, Institute of Telecommunications, LTE link-level and system-level simulators. <http://www.nt.tuwien.ac.at/about-us/staff/josep-colom-ikuno/lte-simulators>, 2012.
[138] 3GPP R1-060385 Motorola, Cubic Metric in 3GPP-LTE, February 2006.
[139] The Coded Modulation Library (The Iterative Solutions Coded Modulation Library (ISCML) is an open source toolbox for simulating capacity approaching codes in Matlab). <http://www.iterativesolutions.com>.
[140] 4G Americas, 4G Mobile Broadband Evolution: Release 10, Release 11 and Beyond - HSPA, SAE/LTE and LTE-Advanced, October 2012.
[141] 4G Americas, MIMO and Smart Antennas for Mobile Broadband Networks, October 2012.
[142] 4G Americas, Developing & Integrating a High Performance HET-NET, October 2012.
[143] 4G Americas, 4G Mobile Broadband Evolution: 3GPP Release 10 and Beyond - HSPA + , SAE/LTE and LTE-Advanced, February 2011.

Petitioners' Exhibit 1021
Nokia of America Corp., et al. v. KT Corporation, et al.
Case No. IPR2025-00036; U.S. Patent No. 11,627,631
Page 881 of 1122

[144] 3GPP R1-113297, NTT DOCOMO, Enhanced PDCCH for DL MIMO in Rel-11, October 2011.
[145] 3GPP R1-112928, Ericsson, ST-Ericsson, On enhanced PDCCH design, October 2011.
[146] 3GPP R1-113175, Renesas Mobile, Link-level evaluation of E-PDCCH design aspects, October 2011.
[147] 3GPP R1-113194, LG Electronics, Consideration on transmit diversity scheme for enhanced PDCCH transmission, October 2011.
[148] 3GPP R1-113202, Intel Corporation, Performance analysis of enhanced downlink control signaling, October 2011.
[149] 3GPP R1-113238, Research in Motion, E-PDCCH transmission with transmit diversity, October 2011.
[150] 3GPP R1-114302, NTT DOCOMO, DM-RS design for E-PDCCH in Rel-11, November 2011.
[151] Anritsu, Future technologies and testing for fixed mobile convergence, SAE and LTE in Cellular mobile communications. <http://www.anritsu.com/search/en-US/downloadssearch.aspx>, 2008.
[152] Wireless World Initiative New Radio—WINNER + , Enabling techniques for LTE-A and beyond, deliverable D2.2. <http://projects.celtic-initiative.org/winner + /deliverables_winnerplus.html>, 2010.
[153] LTE system description. <http://www.sharetechnote.com>.
[154] DSPLOG signal processing for communication. <http://www.dsplog.com>.
[155] 4G Evolution Lab—LTE and LTE-Advanced Toolbox and Block-set: a simulation library for the 3GPP LTE and LTE Advanced specification for the Mathworks MATLAB and Simulink. <http://www.steepestascent.com>.
[156] Samsung electronics, LTE PHY specification. <http://www.slideshare.net/allabout4g/lte-rel-8-physical-layer>, 2008.
[157] MOTOROLA WHITE PAPER, TD-LTE, exciting alternative global momentum. <www.motorola.com>, 2010.
[158] B. Schulz, LTE Transmission modes and beamforming, Rohde & Schwarz White Paper, 2011.
[159] M. Lew, Real-world stimulus-response testing for LTE transmitter RF components, agilent technologies. <http://www.microwavejournal.com/articles/print/9158-real-world-stimulus-response-testing-for-lte-transmitter-rf-components>, 2010.
[160] Adaptive Multi-Rate (AMR) Feature Descriptions, Agilent Technologies <http://wireless.agilent.com/rfcomms/refdocs/gsm/gprsla_amr_bse_config.html>
[161] Jinbiao Xu, LTE-Advanced Signal Generation and Measurement Using SystemVue, Agilent Technologies, Inc., December 2010.
[162] 3GPP R1-080182, Labelling of UE-selected subbands on PUSCH, Huawei, January 2008.
[163] 3GPP R1-080555, Labelling complexity of UE selected subbands on PUSCH, Huawei, January 2008.
[164] Ben Cooke, Reed-Muller Error Correcting Codes, MIT Undergraduate Journal of Mathematics, Number 1, June 1999 <http://www-math.mit.edu/phase2/UJM/vol1/>.
[165] R. Gold, "Optimal binary sequences for spread spectrum multiplexing", IEEE Transactions on Information Theory, Vol. 13 , Issue 4, February 1967.

Petitioners' Exhibit 1021
Nokia of America Corp., et al. v. KT Corporation, et al.
Case No. IPR2025-00036; U.S. Patent No. 11,627,631
Page 882 of 1122

[166] Hidekazu Taoka et al., "MIMO and CoMP in LTE-Advanced", NTT DoCoMo Tech Journal, September 2010.
[167] Hideyuki Torii et al., "A New Class of Zero-Correlation Zone Sequences", IEEE Transactions on Information Theory, Vol. 50, No. 3, March 2004.
[168] Technical Note, "An Overview of LTE PRACH Detection for the PC20x", picoChip felexible wireless, January 2008.
[169] Ernesto Zimmermann et al., "On the Complexity of Sphere Decoding", in Proceedings International Symposium on Wireless Personal Multimedia Communication, 2004.
[170] Mathew William Churchman Barata, LTE Performance Evaluation with Realistic Channel Quality Indicator Feedback, Universitat Politècnica de Catalunya, April 2011.
[171] J.P.T. Dobbelsteen, Mapping an LTE Baseband Receiver on a Multi-Core Architecture, Eindhoven University of Technology, november 2009.
[172] Di Wu et al., "System Architecture for 3GPP LTE Modem using a Programmable Baseband Processor", International Symposium on System-on-Chip, 2009.
[173] Jens Berkmann et al., "On 3G LTE Terminal Implementation - Standard, Algorithms, Complexities and Challenges", International Wireless Communications and Mobile Computing Conference (IWCMC '08), 2008.
[174] DigRF(SM) Specifications, MIPI Alliance, <http://www.mipi.org/specifications/digrfsm-specifications>.

Petitioners' Exhibit 1021
Nokia of America Corp., et al. v. KT Corporation, et al.
Case No. IPR2025-00036; U.S. Patent No. 11,627,631
Page 883 of 1122

CHAPTER

11 Link-Level and System-Level Performance of LTE-Advanced

CHAPTER CONTENTS

11.1 Definition of the performance metrics 882
11.1.1 Link budget 882
11.1.2 User and sector throughput 883
11.1.3 Outage throughput 885
11.1.4 Packet delay 885
11.1.5 Spectral efficiency 886
11.1.6 Jain fairness index 886
11.1.7 Geometry (wideband SINR distribution) 887
11.1.8 Effective interference over thermal 887
11.1.9 Cell spectral efficiency and cell-edge user spectral efficiency 888
11.2 Calculation of static and dynamic overhead 889
11.3 Traffic models 891
11.3.1 Statistical model for conversational speech 891
11.3.2 Full-buffer traffic model 893
11.4 Link-to-system mapping (PHY abstraction) 893
11.5 IMT-Advanced test environments 902
11.6 Network layout for system-level simulations 902
11.7 IMT-Advanced evaluation methodology and baseline configurations 904
11.8 Link-level and system-level channel models 904
11.9 LTE-Advanced link-level and system-level performance 916
11.9.1 Cell spectral efficiency and cell-edge spectral efficiency 916
11.9.2 VoIP capacity 922
11.9.3 Mobility 923
11.9.4 Peak spectral efficiency 925
11.9.5 User-plane/control-plane latency and handover interruption time 925
11.9.6 Estimation of the L1/L2 overhead 932
11.9.7 Link budget 936
11.9.8 Evaluation of LTE-Advanced against LTE Rel-10 requirements 936
11.10 Miscellaneous evaluations 936
References 947

© 2014 Elsevier Inc. All rights reserved.

Petitioners' Exhibit 1021
Nokia of America Corp., et al. v. KT Corporation, et al.
Case No. IPR2025-00036; U.S. Patent No. 11,627,631
Page 884 of 1122

International telecommunication union-radio telecommunications (ITU-R) was responsible for defining of a global standard for the fourth generation of mobile communication systems known as international mobile telecommunications (IMT)-Advanced. One of the technologies included in this global standard was the LTE-Advanced proposed by 3GPP. The IMT-Advanced systems were required to fulfill a set of requirements specified by ITU-R working party 5D [12–16]. The first set of requirements was verified through inspection of the proposed technologies. Those requirements included the support of scalable bandwidths in the IMT spectrum, a wide range of services and inter-system handover capability with at least with one of systems in the IMT-2000 family. The satisfaction of the second set of requirements was confirmed analytically by conducting numerical calculations of peak spectral efficiency, user-plane and control-plane latency, and handover interruption times. The third set of requirements was required to be evaluated via link-level and system-level simulations initially by the proponent and later by designated external evaluation groups. These requirements were cell spectral efficiency, cell-edge user spectral efficiency, mobility, and VoIP capacity.

In order to reduce the complexity of the process, simulations are often divided into two stages or levels of abstraction known as link-level and system-level. The link-level simulations are used to assess the performance of the physical layer and those higher layer aspects directly related to the radio interface. In link-level simulation, a single-cell radio link is modeled, including some specific features such as synchronization, modulation, channel coding, channel fading, channel estimation, demodulation, multi-antenna processing, etc. On the other hand, a system-level simulator allows evaluation of the performance of a network comprising multiple cells and moving mobile stations. At this level, system modeling encompasses a set of base stations and all their associated mobile terminals. Both the signal level received by each user and other users' interferences are modeled, taking into account the propagation losses and channel fading effects. Signal to interference plus noise ratio (SINR) is calculated for each active user considering the current network configuration and relative random placement of the base stations and mobile stations. These SINR values can be then translated to block error rate (BLER) or effective throughput values using models whose development is based on the results obtained in the link-level simulations. This interaction between link- and system-level simulators is usually referred to as link-to-system mapping or link-level abstraction models.

After developing the simulation platform, a calibration process is performed. The calibration is of paramount importance to ensure the validity of the results obtained with the simulation platform. Calibration is performed through comparison of the outcomes of the developed simulator with the outcomes of the simulation platforms of other sources. The calibration process involves comparison and adjustment of downlink wideband SINR, also known as geometry, and coupling loss distributions under common assumptions. Following the first step, the calibration further includes evaluation and comparison of downlink and uplink

Petitioners' Exhibit 1021
Nokia of America Corp., et al. v. KT Corporation, et al.
Case No. IPR2025-00036; U.S. Patent No. 11,627,631
Page 885 of 1122

spectral efficiencies, user throughput distributions, and SINR distributions for a basic LTE system configuration.

The link-level and system-level simulations are used to evaluate the performance of mobile radio access technologies under various operating conditions and deployment scenarios. While the simulations do not model the entire deployment parameters and propagation conditions that may be involved in a practical scenario due to increased computational complexity of the model, the statistical modeling of the parameters and estimation/measurement errors should be sufficiently accurate such that the simulation results are a faithful representation of the performance in an actual deployment [51]. More specifically:

- *Link-level simulations* would facilitate the study of channel estimation, tracking, and prediction algorithms, as well as synchronization algorithms, MIMO performance, adaptive modulation and coding, and feedback techniques. Furthermore, receiver structures (e.g., MMSE, ZF, MLD, SIC), modeling of channel encoding and decoding, and physical-layer modeling which is crucial for system-level simulations are typically analyzed at the link-level. Although MIMO broadcast channels have been investigated quite extensively over the past decade, there are still many open theoretical and practical questions that need to be resolved. For example, LTE offers the flexibility to adjust many transmission parameters, but it is not clear how to exploit the available degrees of freedom to achieve the optimum performance under different deployment scenarios.
- *System-level simulations* focus more on network-related issues, such as resource allocation and scheduling, multi-user handling, mobility management, admission control, interference management, and network planning optimization. Furthermore, in a multi-user system, such as LTE, it is not directly clear which figure of merits (metrics) should be used to evaluate the performance of the system. The classical measures of (un)coded bit error rate, (un)coded BLER, and throughput may not accurately reflect multi-user properties. More comprehensive measures of the LTE performance include fairness, multi-user diversity, or degree of freedom. However, these theoretical concepts have to be mapped to performance values that can be verified by means of simulations.

As shown in Figure 11.1, an example of an LTE link-level simulation platform comprises three basic building blocks; namely, transmitter, channel model, and receiver. Depending on the type of simulation, one or several instances of these basic building blocks are utilized. The transmitter and receiver blocks are linked by the channel model, which is used to transmit the downlink data, while signaling and uplink feedback are ideally assumed to be error free. Since signaling is more strongly protected than data, by means of lower coding rates and/or lower-order modulations, the assumption of error-free signaling is in fact fairly realistic. Equivalently, errors on the signaling channels will only occur when the data channels are already facing severe performance degradation. In the downlink,

Petitioners' Exhibit 1021
Nokia of America Corp., et al. v. KT Corporation, et al.
Case No. IPR2025-00036; U.S. Patent No. 11,627,631
Page 886 of 1122

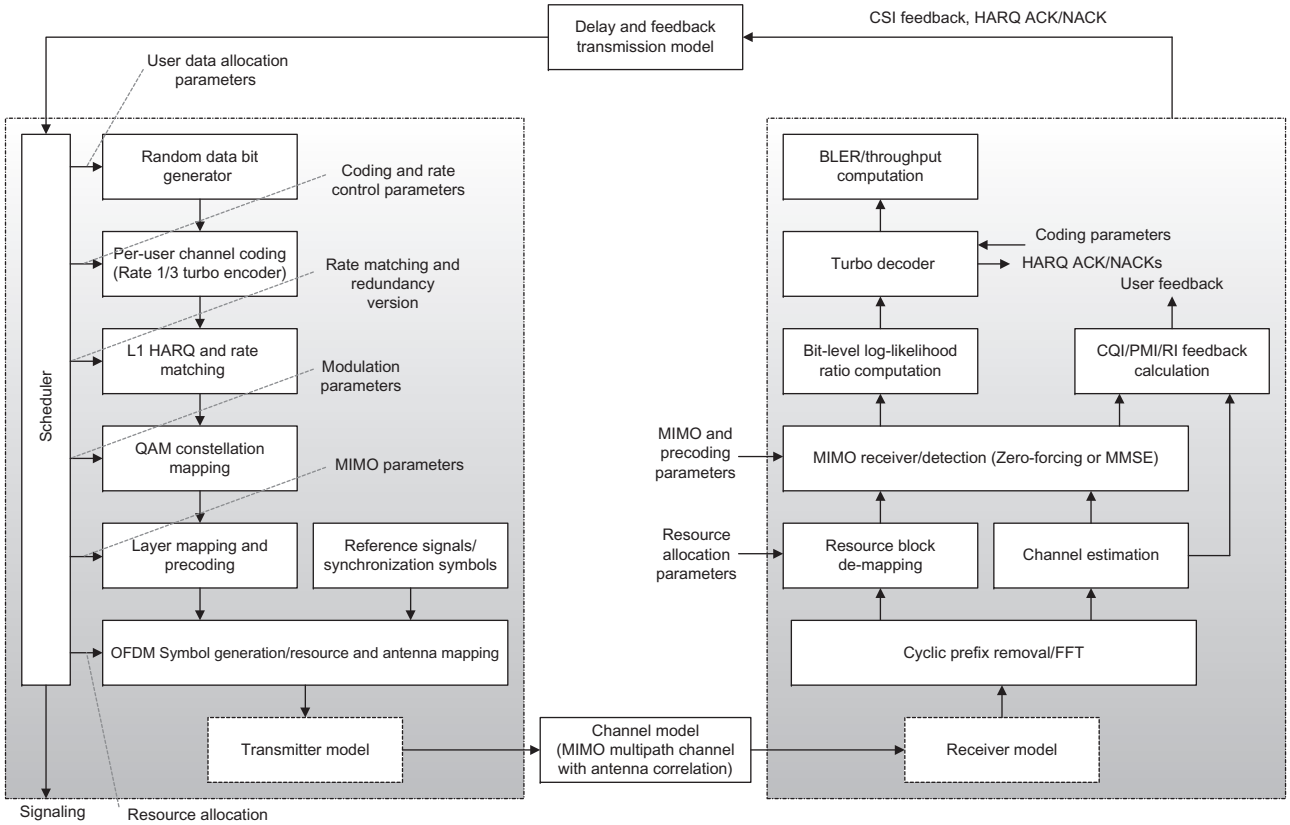


FIGURE 11.1

General structure of an LTE downlink link-level simulation platform [8,9,45].

the signaling information generated by the transmitter to the receiver contains coding, HARQ, scheduling, and precoding parameters. In the uplink, channel quality indicator (CQI), precoding matrix index (PMI), and rank indicator (RI) are signaled, which together form the channel state information (CSI) feedback [45].

In system-level simulations as illustrated in Figure 11.2, the performance of the entire network is evaluated. In an LTE system, such network consists of a number of eNBs that cover a specific geographical area in which several mobile stations are randomly dropped. The system-level simulation platform (shown in Figure 11.2) consists of a link measurement model and a link performance model. The link measurement model measures the link quality, obtained via the UE CSI measurement reports, which is required to perform link adaptation, resource allocation, and MIMO mode selection. An appropriate link quality measure is evaluated per sub-carrier. Based on the SINR metric, the UE calculates the uplink feedback (PMI, RI, and CQI), which is used as input for link adaptation at the eNB. The scheduling algorithm assigns resources to users in order to optimize the performance of the system based on CSI feedback. The scheduling is a key

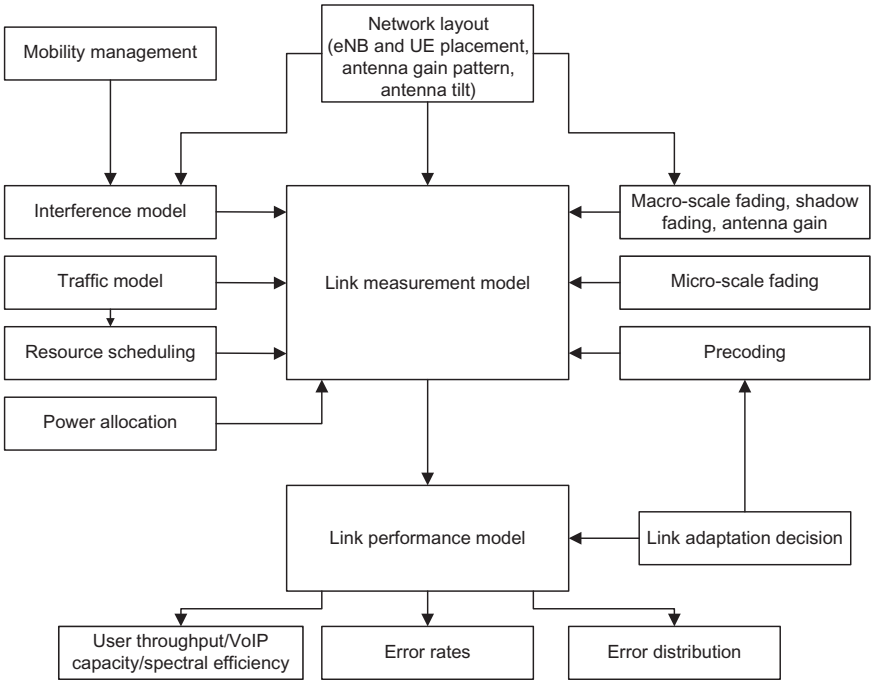


FIGURE 11.2

General structure of an LTE system-level simulation platform [45].

Petitioners' Exhibit 1021
Nokia of America Corp., et al. v. KT Corporation, et al.
Case No. IPR2025-00036; U.S. Patent No. 11,627,631
Page 888 of 1122

component in the proper functioning of the radio interface. Two types of schedulers can be identified: the opportunistic, where the scheduler considers the state of the radio channel to make the best allocation possible; and the non-opportunistic, where the allocation has no knowledge of the radio channel's state.

Based on the link measurement model outputs, the link performance model predicts the BLER of the link according to the receiver SINR and the transmission parameters (e.g., modulation and coding). In order to generate the network topology, transmission sites are generated. The scheduler assigns physical resources, precoding matrices, and selects a suitable modulation and coding scheme for each active UE attached to an eNB. The actual assignment depends on the scheduling algorithm and the UE feedback. At the UE side, the received post-processing SINR is calculated in the link measurement model. The SINR is determined by the signal, interference, and noise power levels, which are dependent on the cell layout that is defined by the eNB relative positions, large-scale (macroscopic, macro-scale) path loss, shadow fading, and the time-variant small-scale (microscopic, micro-scale) fading parameters. The CQI feedback is calculated based on the sub-carrier SINRs and the target transport BLER. The CQI reports are generated by SINR-to-CQI mapping and made available to the eNB via a feedback channel with adjustable delay where the feedback imperfections are modeled. At the transmitter, the appropriate MCS is selected by the CQI value to achieve the targeted BLER during the transmission. In particular, in high mobility scenarios, the feedback delay caused by computation and signaling timings can lead to performance degradation, if the channel state changes rapidly during the delay period. In the link performance model, an additive white Gaussian noise (AWGN)-equivalent SINR γ_{AWGN} is obtained via mutual information effective signal to interference and noise ratio mapping (MIESM). In a second step, γ_{AWGN} is mapped to the BLER via AWGN link performance curves. The BLER value acts as a probability for computing HARQ ACK/NACKs, which are combined with the transport-block size to compute the link throughput. The simulation output consists of traces, containing link throughput and error rates for each user, as well as cell aggregate throughput, from which statistical distributions of throughputs and errors can be extracted [45].

The large-scale path loss and the shadow fading are modeled as position-dependent maps. The large-scale path loss is calculated according to the available models and combined with the antenna gain pattern of the corresponding eNB. An inter-site map correlation for shadow fading is similarly obtained. While the large-scale path loss and the shadow fading are modeled as a position-dependent trace, the small-scale fading is modeled as a time-dependent trace. The calculation of the latter trace is based on the transmitter precoding, the small-scale fading MIMO channel matrix, and the receive filter. The small-scale fading trace consists of the signal power and the interference power after the receive filter.

The link-level and system-level evaluation of the IMT-Advanced candidates was comprehensively performed in strict compliance with the technical

Petitioners' Exhibit 1021
Nokia of America Corp., et al. v. KT Corporation, et al.
Case No. IPR2025-00036; U.S. Patent No. 11,627,631
Page 889 of 1122

parameters and the methodology specified by ITU-R [12–16]. Each requirement was independently evaluated, except for the cell and cell-edge user spectral efficiencies criteria that were jointly assessed using the same system-level simulation; consequently, the candidates were required to simultaneously satisfy the corresponding minimum requirements. Furthermore, the system-level simulation setup used in the assessment of the mobility requirement was the same as that used for the evaluation of cell spectral efficiency and cell-edge user spectral efficiency. In general, the evaluation of the IMT-Advanced candidate technologies followed the following principles [14]:

1. Use of reproducible methods including computer simulation, analytical/theoretical approach, and inspection.
2. Technical evaluation against performance targets that were set for each test environment.
3. Consistency between self-evaluations and technical descriptions provided in technology description templates.
4. Use of unified methodology, software, and common parameter sets by the evaluation groups including channel models, link-level parameters, and link-to-system mapping.
5. Evaluation of multiple proposals using one simulation platform by each evaluation group to ensure comparability of the results.
6. Inclusion of an L1/L2 overhead in the evaluation of cell spectral efficiency, cell-edge user spectral efficiency, and VoIP capacity.
7. Independent drop of the users with uniform distribution over the coverage area where each mobile user corresponds to an active session that runs for the duration of the drop.
8. Random assignment of line-of-sight (LoS) *and* non-line-of-sight (NLoS) path loss models to the users.
9. Cell assignment to a user is based on the air-interface cell selection schemes.
10. Fading signal and fading interference are computed from each mobile station to each cell, and from each cell to each mobile station (in both directions on an aggregated basis).
11. Consideration of the interference over thermal (IoT) constraint in the uplink design such that the average IoT value remains less than or equal to 10 dB.
12. In a full-buffer traffic model, packets are not blocked upon their arrival; that is, buffer sizes are assumed to be infinite.
13. Data and VoIP packets are scheduled with appropriate packet schedulers for full-buffer and VoIP traffic models separately.
14. Modeling of channel quality feedback delay, feedback channel errors, packet errors, and real channel estimation (as opposed to ideal channel estimation) effects and retransmission of erroneous packets.
15. Realistic modeling of the overhead channels, that is, the overhead due to feedback and control channels.

Petitioners' Exhibit 1021
Nokia of America Corp., et al. v. KT Corporation, et al.
Case No. IPR2025-00036; U.S. Patent No. 11,627,631
Page 890 of 1122

For each drop, the system-level simulations were conducted and the process was repeated with the users dropped at new random geographical locations within the network. A large number of drops were simulated to ensure convergence in the system performance metrics, and the width of confidence intervals of the user and system performance metrics was calculated and reported. The confidence interval[1] and the associated confidence level indicate the reliability of the estimated parameter value [23,53]. The confidence level is the probability that the true parameter value is within the confidence interval such that the higher the confidence level, the larger the confidence interval. All cells in the network were simulated assuming dynamic channel models and use of a 19-cell wrap-around scheme to model the inter-cell interference except for the indoor environment.

This chapter describes the link-level and system-level evaluation of 3GPP LTE-Advanced against ITU-R requirements for IMT-Advanced systems using the methodology specified by ITU-R [14]. The theoretical background, including definition of performance metrics, channel models, physical-layer abstraction schemes, and the traffic models are provided to ensure in-depth understanding of the evaluation process and the results.

11.1 Definition of the performance metrics

11.1.1 Link budget

Link budget is a commonly used metric to evaluate the coverage of a cellular system in the downlink or uplink. In order to calculate the link budget, one must account for all gains and losses from the transmitter to the receiver over the air-interface. It accounts for the attenuation of the transmitted signal due to propagation as well as the antenna gains, cable and implementation loss, and other miscellaneous losses. The time-varying channel gains such as fading are taken into account by adding some margin depending on the anticipated severity of its effects. The amount of

[1]A confidence interval provides an estimated range of values which is likely to include an unknown population parameter, the estimated range being calculated from a given set of sample data. If independent samples are taken repeatedly from the same population and a confidence interval is calculated for each sample, then a certain percentage (confidence level) of the intervals will include the unknown population parameter. Confidence intervals are more informative than the simple results of hypothesis tests since they provide a range of plausible values for the unknown parameter.
In mathematical terms, let X denote a random sample from a probability distribution with statistical parameters α, which is a quantity to be estimated, and β, representing quantities that are not of immediate interest. A *confidence interval* for the parameter α, with confidence level or confidence coefficient γ, is an interval with random endpoints $(f_1(X),f_2(X))$, determined by the pair of random variables $f_1(X)$ and $f_2(X)$, with the property $\Pr_{\alpha,\beta}(f_1(X) < \alpha < f_2(X)) = \gamma \forall \alpha, \beta$. The number γ, with typical values close to but not greater than one, is sometimes given in the form $1 - \gamma'$, where γ' is a small non-negative number close to zero. In the latter expression, $\Pr_{\alpha,\beta}(x)$ indicates the probability distribution of X characterized by (α, β). An important part of this definition is that the random interval $(f_1(X),f_2(X))$ covers the unknown value α with a high probability no matter what the true value of α actually is [23,53].

Petitioners' Exhibit 1021
Nokia of America Corp., et al. v. KT Corporation, et al.
Case No. IPR2025-00036; U.S. Patent No. 11,627,631
Page 891 of 1122

margin required can be reduced by the use of mitigating techniques, such as antenna diversity or frequency hopping. An abstract description of the link budget in any direction (downlink/uplink) has the following form [14,26]:

$$\text{Received power (dBm)} = \text{Transmitted power (dBm)} + \text{Gains (dB)} - \text{Losses (dB)} \tag{11.1}$$

Link budget evaluation is a well-known method for initial cell planning that needs to be carried out separately for the downlink and uplink. Although the link budget can be calculated separately for each link, it is the combination of the links that determines the performance of the system. Using the margins in the link budget, the expected signal-to-noise ratio can be evaluated at given distances. Using these results, the noise-limited range can be evaluated for the system. The typical link budget parameters are summarized in Table 11.1.

11.1.2 User and sector throughput

Although a user may be sufficiently covered within certain areas of a cell for a given service, when multiple users are in a cell, the radio resources (time, frequency, space, and power) must be shared among the active users. It can be expected that a user's average data rate may be reduced by a factor of N_{user} when

Table 11.1 Typical Link Budget Parameters [14,26]

Link Budget Parameters	Link Budget Parameters
Carrier frequency/channel bandwidth	Number of receive antennas
BS/MS antenna heights (m)	Receive antenna gain (dBi)
Area coverage (km)	Receiver cable, connector, or body losses (dB)
Type of service (VoIP, full-buffer data, etc.)	Receiver noise figure (dB)
MCS	Thermal noise density (dBm/Hz)
Multipath channel model	Receiver interference density (dBm/Hz)
Mobile speed (km/h)	Required SNR (dB)
Number of transmit antennas	Receiver implementation margin (dB)
Maximum transmitter power per antenna (dBm)	Fast fading margin including scheduler gain (dB)
Transmitter power amplifier back-off (dB)	HARQ combining gain (dB)
Transmit antenna gain (dBi)	Handover gain (dB)
Transmit array gain (dB)	BS/MS diversity gain (dB)
Control channel power boosting gain (dB)	Lognormal shadow fading standard deviation (dB)
Data carrier power loss due to pilot/control boosting (dB)	Shadow fading margin (dB)
Transmitter cable, connector, combiner, body losses (dB)	Penetration loss (dB)

Petitioners' Exhibit 1021
Nokia of America Corp., et al. v. KT Corporation, et al.
Case No. IPR2025-00036; U.S. Patent No. 11,627,631
Page 892 of 1122

there are N_{user} active users, assuming resources are equally shared among active users and there is no multi-user diversity gain, relative to that of a single user. Therefore, any coverage assessment for any particular service must be coupled with the number of active users in the cell and their associated quality of service requirements. If the users with poor channel conditions are provided with more radio resources, it would adversely impact the total cell throughput. Thus, there is a trade-off between coverage and capacity. The performance metric that is typically used is the number of admissible users, parameterized by the service minimum bit rate, maximum tolerable latency, permissible outage probability, etc. It is assumed that simulation statistics are collected from sectors belonging to the test cells of a 19-cell deployment scenario in order to model the effects of inter-cell interference. In the following, downlink and uplink throughputs are separately evaluated and the corresponding metrics are differentiated by superscripts "DL" and "UL," respectively.

The user throughput is defined as the ratio of the number of information bits that the user successfully received divided by the total simulation time. If user k has $p_k^{\text{DL(UL)}}$ downlink (uplink) packet transmissions during the simulation period T_{sim}, if there are $q_{ik}^{\text{DL(UL)}}$ packets in the ith transmission, and if b_k^{ij} denotes the number of the correctly received bits in the jth packet; then the average user throughput for user k is given as follows:

$$R_k^{\text{DL(UL)}} = \frac{\sum_{i=1}^{p_k^{\text{DL(UL)}}} \sum_{j=1}^{q_{ik}^{\text{DL(UL)}}} b_k^{ij}}{T_{\text{sim}}} \tag{11.2}$$

The average user throughput is defined as the sum of the user throughput of each user in the cell divided by the total number of users in the cell. Let N_{user} denote the number of users in the sector/cell and user $k = 1, 2, \ldots, N_{\text{user}}$ has throughput $R_k^{\text{DL(UL)}}$, then DL (or UL) sector throughput is defined as:

$$R^{\text{DL(UL)}} = \sum_{k=1}^{N_{\text{user}}} R_k^{\text{DL(UL)}} \tag{11.3}$$

The user throughput per transmission is the number of correctly received bits per packet divided by the duration of the transmission. If user k has $p_k^{\text{DL(UL)}}$ downlink (uplink) transmissions, if there are $q_{ik}^{\text{DL(UL)}}$ packets in the ith transmission, and if there are b_k^{ij} correctly received bits in the jth packet, then the average transmission throughput can be defined as follows:

$$R_k^{\text{DL(UL)}} = \frac{1}{p_k^{\text{DL(UL)}}} \left(\sum_{i=1}^{p_k^{\text{DL(UL)}}} \frac{\sum_{j=1}^{q_{ki}^{\text{DL(UL)}}} b_k^{ij}}{\Delta T_{ki}^{\text{DL(UL)}}} \right) \tag{11.4}$$

where $\Delta T_{ki}^{\text{DL(UL)}}$ denotes the duration of the ith transmission to user k. The average user throughput per transmission is defined as the sum of the user throughputs per transmission divided by the number of users in the cell.

Petitioners' Exhibit 1021
Nokia of America Corp., et al. v. KT Corporation, et al.
Case No. IPR2025-00036; U.S. Patent No. 11,627,631
Page 893 of 1122

11.1.3 Outage throughput

The outage throughput $\eta_{\text{outage}}(R_{\min})$ is defined as the percentage of users with data rate R_k^{DL} less than a predefined minimum data rate $R_{\min}$. The cell-edge user throughput is defined as the fifth percentile point of the cumulative distribution function (CDF) of users' average throughput per transmission assuming that 95% of the users are expected to achieve a certain throughput per transmission regardless of their geographical location in the cell.

11.1.4 Packet delay

If the jth packet of the ith transmission belongs to user k, if the packet arrives at the BS (or MS) MAC at time instant T_{arrival}^{kij} and is delivered to the MS (or BS) MAC sublayer at time instant $T_{\text{departure}}^{kij}$, then the packet delay can be calculated as follows:

$$D_{kij}^{\text{DL(UL)}} = T_{\text{arrival}}^{kij} - T_{\text{departure}}^{kij} \tag{11.5}$$

The downlink and uplink delays are denoted by superscript "DL" or "UL," respectively. The packets that are dropped or erased may not be included in the analysis of packet delays depending on the traffic model. For example, in the modeling of traffic for delay sensitive applications, packets may be dropped, if packet transmissions are not completed within a specified delay bound. The impact of the dropped packets is included in the packet loss rate. The CDF of the packet delay per user provides a basis in which maximum latency, second percentile, and average latency as well as jitter can be derived. The second percentile point of the CDF of packet delay denotes the packet delay value for which 98% of packets have a delay less than that value. As an example, the VoIP capacity is defined such that the percentage of users in outage is less than 2% where a user is assumed to have experienced a service outage, if less than 98% of the VoIP packets have been delivered successfully to the user within a one-way radio access delay bound of 50 ms.

The average packet delay is defined as the average interval between packets originated at the source (either MS or BS) and received at the destination (either BS or MS) in a system for a given duration of transmission. The average packet delay for user k, $\overline{D}_k^{\text{DL(UL)}}$ is given by:

$$\overline{D}_k^{\text{DL(UL)}} = \frac{\sum_{i=1}^{p_k} \sum_{j=1}^{q_{ki}} (T_{\text{departure}}^{kij} - T_{\text{arrival}}^{kij})}{\sum_{i=1}^{p_k} q_{ki}} \tag{11.6}$$

The CDF of users' average packet delay is the cumulative distribution of the average packet delay observed by all users in the cell. The packet loss ratio per user is defined as:

$$\text{Packet loss ratio} = 1 - \frac{\text{Total number of successfully delivered packets}}{\text{Total number of packets}} \tag{11.7}$$

Petitioners' Exhibit 1021
Nokia of America Corp., et al. v. KT Corporation, et al.
Case No. IPR2025-00036; U.S. Patent No. 11,627,631
Page 894 of 1122

where the total number of packets includes packets that were transmitted over the air-interface and packets that were dropped prior to transmission. The data throughput of a BS is defined as the number of information bits per second that a cell can successfully deliver or receive via the air-interface using appropriate scheduling algorithms.

11.1.5 Spectral efficiency

We consider both physical-layer spectral efficiency and MAC sublayer spectral efficiency as important performance indicators for a cellular system. The physical-layer spectral efficiency is the system throughput measured at the interface of the physical layer and the MAC sublayer, thus including physical-layer overhead but excluding MAC and upper layer protocol overheads. The MAC sublayer spectral efficiency represents the system throughput measured at the interface of the MAC sublayer and the upper layers, thus including both the physical layer and MAC protocol overheads. The MAC efficiency of the system is evaluated by dividing the MAC sublayer spectral efficiency by the physical-layer spectral efficiency. The average cell spectral efficiency is defined as:

$$\mathrm{SE}_{\mathrm{cell}} = \frac{R_{\mathrm{aggregate}}}{\mathrm{BW}_{\mathrm{effective}}} \tag{11.8}$$

where $R_{\mathrm{aggregate}}$ denotes the aggregate cell throughput and $\mathrm{BW}_{\mathrm{effective}}$ is the effective channel bandwidth. The effective channel bandwidth is defined as $\mathrm{BW}_{\mathrm{effective}} = \alpha_{\mathrm{DL-UL}}\mathrm{BW}_{\mathrm{transmission}}$ where $\mathrm{BW}_{\mathrm{transmission}}$ denotes the channel bandwidth, and $\alpha_{\mathrm{DL-UL}}$ is the downlink/uplink ratio in the TDD systems. Note that for FDD systems $\alpha_{\mathrm{DL-UL}} = 1$ and for TDD systems with DL:UL ratio of 2:1; $\alpha_{\mathrm{DL-UL}} = 2/3$ for the downlink and 1/3 for the uplink, respectively.

The CDF of SINR is defined as the CDF for the signal to interference plus noise ratio measured at the BS for each MS on the uplink, or at the MS for the BS in the downlink. This metric would allow comparison between different reuse scenarios, network loading conditions, multi-antenna algorithms, resource allocation, power control schemes, etc.

11.1.6 Jain fairness index

Fairness measures or metrics are used in network engineering to determine whether users or applications are receiving a fair share of system resources. There are several mathematical and conceptual definitions of fairness among which the Jain index is a commonly used metric defined as follows [44]:

$$J(x_1, x_2, \ldots, x_n) = \frac{\left(\sum_{i=1}^{n} x_i\right)^2}{n\sum_{i=0}^{n} x_i^2} \tag{11.9}$$

Petitioners' Exhibit 1021
Nokia of America Corp., et al. v. KT Corporation, et al.
Case No. IPR2025-00036; U.S. Patent No. 11,627,631
Page 895 of 1122

The Jain index rates the fairness of a set of values where there are n users and x_i is the throughput for the ith connection. The result ranges from $J = 1/n$ (worst case) to $J = 1$ (best case), and it is maximum when all users receive the same allocation. This index is $J = k/n$ when k users equally share the resources, and the other $n - k$ users receive zero allocation. This metric identifies under-utilized channels and is not excessively sensitive to atypical network flow patterns. Alternatively, the Jain index can be defined as:

$$J = \frac{\overline{R}^2_{\text{throughput}}}{\overline{R}^2_{\text{throughput}} + \sigma_{R_{\text{throughput}}}} \tag{11.10}$$

where $\overline{R}_{\text{throughput}}$ and $R_{\text{throughput}}$ denote the average throughput and throughput values, respectively.

11.1.7 Geometry (wideband SINR distribution)

In the calibration of the large-scale parameters of the channel model, all the multipath effects are not considered. Simulations are conducted to obtain for each user a path gain and a wideband SINR value. The path gain is defined as the average signal gain between an MS and its serving BS. It includes distance attenuation, shadowing, and antenna gains. The wideband SINR is the ratio of the average power received from the serving cell and the average interference power received from other cells plus noise. Sometimes this measure is called the geometry factor, since it presents a great dependency with the position of the user in relation to the position of the base stations. Then, the calibration of this measure ensures not only the calibration of the channel model, but also the calibration of the network layout. In addition, it involves the calibration of the physical layer considered in the simulation platform functional description, since the SINR is calculated in this layer.

11.1.8 Effective interference over thermal

In code division multiple access (CDMA) systems, the rise over thermal (RoT) indicates the ratio between the total power received from wireless sources at a base station and the thermal noise. In order to decode the data at the base station, a minimum SINR at the receiver must be guaranteed. The RoT metric is a measure of the uplink loading. By increasing the number of transmitting UEs and their transmit power, the level of interference in the uplink increases. This interference is perceived by the base station as noise adversely affecting the SINR. The base station controls the interference level by adjusting the UE uplink assignments and transmit power [25]. Similarly, IoT reflects the effective interference received by the base station. The definition of effective IoT measure takes the interference suppression capabilities of the base station receiver into consideration.

Petitioners' Exhibit 1021
Nokia of America Corp., et al. v. KT Corporation, et al.
Case No. IPR2025-00036; U.S. Patent No. 11,627,631
Page 896 of 1122

In order to formulate a mathematical expression for effective IoT, we consider a single-input multiple-output (SIMO) system and further assume that the base station has a linear receiver, such as maximal ratio combining (MRC) or MMSE with N_{RX} antennas. The received signal at the mth receive antenna can be expressed as $r_m = h_m x + e_m + n_m$ where h_m is the channel between the single transmit antenna and the mth receive antenna, x is the transmitted symbol, e_m is the sum of the interfering signals, and n_m is the thermal noise at the mth receive antenna. The receiver processing consists of estimating the transmitted symbol x by appropriately weighting the received signal at each antenna with a complex-valued weight w_m^H, and then summing the weighted signals. The sum-weighted output signal is given by $y = \sum_{m=1}^{N_{\mathrm{RX}}} w_m^H r_m = \sum_{m=1}^{N_{\mathrm{RX}}} w_m^H (h_m x + e_m + n_m)$. Alternatively, using vector notations, one can write the latter equation as $\mathbf{y} = \mathbf{w}^H(\mathbf{h}x + \mathbf{e} + \mathbf{n})$.

The effective SINR at the receiver output is given by the ratio of the power of the desired part of the filtered received signal $\mathbf{w}^H\mathbf{h}x$ to the power of the undesired part of the weighted received signal $\mathbf{w}^H(\mathbf{e} + \mathbf{n})$ which under the assumption that noise and interference are independent can be written as:

$$\mathrm{SINR}_{\mathrm{effective}} = \frac{\mathbf{w}^H\mathbf{h}\mathbf{h}^H\mathbf{w}}{\mathbf{w}^H(\mathbf{Q} + \mathbf{N})\mathbf{w}} \tag{11.11}$$

where $\mathbf{Q} = \varepsilon\{\mathbf{e}\mathbf{e}^H\}$ is the covariance matrix of the interference, and $\mathbf{N} = \varepsilon\{\mathbf{n}\mathbf{n}^H\}$ is the covariance matrix of the thermal noise. Note that typically $\mathbf{N} = \sigma^2\mathbf{I}$ where σ^2 is the noise variance per antenna and $\mathbf{I}$ is the $N_{\mathrm{RX}} \times N_{\mathrm{RX}}$ identity matrix. The denominator in Eq. (11.11) is defined as the power of the interference and thermal noise. $P_{I+N_{\mathrm{effective}}} = \mathbf{w}^H(\mathbf{Q} + \mathbf{N})\mathbf{w}$. The effective IoT can now be defined as the ratio between the total effective noise and interference power to the effective thermal noise power:

$$IoT_{\mathrm{effective}} = \frac{P_{I+N_{\mathrm{effective}}}}{P_{N_{\mathrm{effective}}}} = \frac{\mathbf{w}^H(\mathbf{Q} + \mathbf{N})\mathbf{w}}{\mathbf{w}^H\mathbf{N}\mathbf{w}} \tag{11.12}$$

Since receiver weights typically vary over frequency and time, the effective IoT should be calculated per frequency and time instant, and then averaged. The average is taken over allocated resources and unused resources are excluded.

11.1.9 Cell spectral efficiency and cell-edge user spectral efficiency

Cell spectral efficiency $\mathrm{SE}_{\mathrm{cell}}$ is defined as the aggregate throughput of all users, that is, the number of correctly received bits delivered to the upper layers at the MAC service access point over a certain period of time, divided by the channel bandwidth divided by the number of cells. The channel bandwidth is defined as the effective bandwidth multiplied by the frequency reuse factor, where the effective bandwidth is the operating bandwidth that is appropriately scaled by the uplink/downlink ratio. The cell spectral efficiency is measured in bits/s/Hz/cell.

Petitioners' Exhibit 1021
Nokia of America Corp., et al. v. KT Corporation, et al.
Case No. IPR2025-00036; U.S. Patent No. 11,627,631
Page 897 of 1122

If d_i denotes the number of correctly received bits by user i (in the downlink) or from user i (in the uplink) in a system comprising N_{user} active users and N_{cell} cells, and if B denotes the channel bandwidth and T the time over which the data bits are received. The cell spectral efficiency can be expressed as follows:

$$\text{SE}_{\text{cell}} = \frac{\sum_{i=1}^{N_{\text{user}}} d_i}{TBN_{\text{cell}}} \tag{11.13}$$

The (normalized) user throughput is defined as the average user throughput, that is, the number of correctly received bits by users delivered to upper layers at the MAC service access point over a certain period of time, divided by the channel bandwidth, and is measured in bits/s/Hz. The cell-edge user spectral efficiency is defined as the 5% point of the CDF of the normalized user throughput. Let $d_i, T_i,$ and B denote the number of correctly received bits by user i, the active session duration for user i, and the channel bandwidth, respectively. The (normalized) user throughput of user i is defined as:

$$R^{(i)}_{\text{user-throughput}} = \frac{d_i}{T_i B} \tag{11.14}$$

11.2 Calculation of static and dynamic overhead

The calculation and analysis of the signaling and control channels' overhead, as well as the physical-layer overhead associated with synchronization and broadcast channels, guard times and guard bands, reference signals, and that of the cyclic prefix are important in determining the actual performance of a cellular system. In general, the overhead channels are essential for proper operation of a cellular system and statically (independent of the number of the users in the cell) or dynamically (depending on the number of the users in the cell) consume some radio resources and make them permanently or temporarily unavailable for data transmission. There are two types of overhead channels: static and dynamic. A static overhead channel requires fixed base station power, time slot, and/or bandwidth. On the other hand, a dynamic overhead channel requires base station power, time, and/or bandwidth which dynamically change over time as a function of the number of active users.

The layer 1 (L1) and layer 2 (L2) overhead are accounted for in time, frequency, or space for calculation of system performance metrics, such as spectral efficiency, user throughput, VoIP capacity, etc. Examples of L1 overhead include synchronization signals, guard sub-carriers and DC sub-carrier, guard time (in TDD systems), reference signals, and cyclic prefix. Examples of L2 overheads include common and dedicated control channels, HARQ ACK/NACK feedback, channel quality feedback, random access channel, packet headers and sub-headers, as well as cyclic redundancy check (CRC). The power allocation/boosting should

Petitioners' Exhibit 1021
Nokia of America Corp., et al. v. KT Corporation, et al.
Case No. IPR2025-00036; U.S. Patent No. 11,627,631
Page 898 of 1122

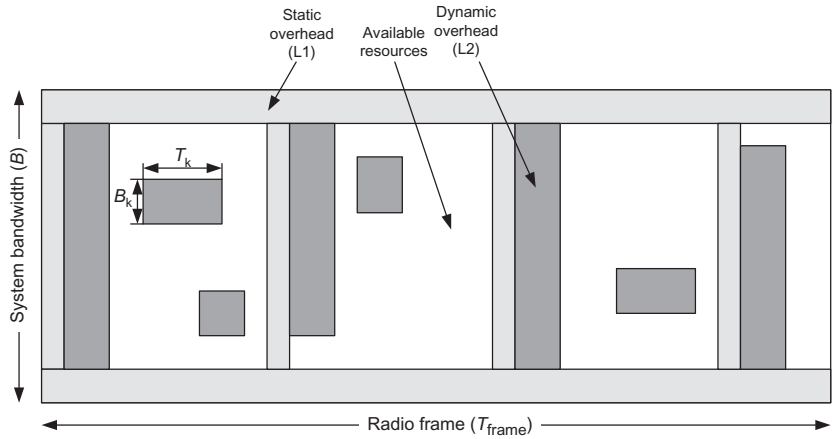


FIGURE 11.3

Illustration of the static and dynamic overhead.

also be accounted for in modeling resource allocation for control channels. Based on the example two-dimensional time-frequency model shown in Figure 11.3, the L1 and L2 overhead can be calculated as:

$$O_{\mathrm{L1+L2}} = \lim_{T_{\mathrm{frame}} \to \infty} \frac{\sum_{k \in S(\mathrm{L1}) \cup S(\mathrm{L2})} B_k T_k}{B T_{\mathrm{frame}}}, \quad 0 \le O_{\mathrm{L1+L2}} < 1 \tag{11.15}$$

where B denotes the system bandwidth and T_{frame} is the radio frame size, B_k is the resource occupied by the kth L1 (or L2) overhead channel across frequency dimension, and T_k denotes the required time resource for transmission of the kth L1 (or L2) overhead channel in time.

Using this model, the total resources consumed by the L1 overhead over a relatively long period of time is given as:

$$O_{\mathrm{L1}} = \lim_{T_{\mathrm{frame}} \to \infty} \frac{1}{B T_{\mathrm{frame}}} \sum_{k \in S(\mathrm{L1})} B_k T_k, \quad 0 \le O_{\mathrm{L1}} < 1 \tag{11.16}$$

where S(L1) denotes the set of resources used for static L1 overhead channels. The total resources consumed by the L2 overhead over a relatively long period of time is given as:

$$O_{\mathrm{L2}} = \lim_{T_{\mathrm{frame}} \to \infty} \frac{1}{B T_{\mathrm{frame}}(1 - O_{\mathrm{L1}})} \sum_{k \in S(L2)} B_k T_k, \quad 0 \le O_{\mathrm{L2}} < 1 \tag{11.17}$$

Note that the amount of resources that have already been used by the L1 overhead must not be recounted in calculation of O_{L2} and that $O_{\mathrm{L1+L2}} \neq O_{\mathrm{L1}} + O_{\mathrm{L2}}$. Furthermore, S(L2) denotes the set of resources used for L2 overhead channels

Petitioners' Exhibit 1021
Nokia of America Corp., et al. v. KT Corporation, et al.
Case No. IPR2025-00036; U.S. Patent No. 11,627,631
Page 899 of 1122

The average spectral efficiency inclusive of the effect of the L1/L2 overhead can be obtained as $SE_{average}(1 - O_{L1+L2})$ where $SE_{average}$ denotes the average spectral efficiency that has been obtained via system-level simulation excluding the L1/L2 overhead.

11.3 Traffic models

11.3.1 Statistical model for conversational speech

VoIP refers to real-time delivery of coded voice packets across a network using the Internet protocols. Several robust voice codecs for encoding conversational speech have been developed and discussed in the literature, including ITU-T G.729 (8 kbps) [17] and adaptive multi-rate (AMR) codec (4.75−12.2 kbps) [5,27]. In the following discussion, a VoIP session is defined as the entire user call time, and a typical conversation is characterized by periods of active speech or talk spurts followed by silence periods. Figure 11.4 illustrates a two-state Markov model[2] for conversational speech [23,24,54].

The steady-state condition of the model requires that $P_0 = a/(a + c)$ and $P_1 = c/(a + c)$ where P_0 and P_1 are the probabilities of being in state 0 and state 1, respectively. As shown in Figure 11.4, the probability of a transition from state 1 (the active speech state) to state 0 (the inactive state) while in state 1 is equal to a, whereas the probability of a transition from state 0 to state 1 while in state 0 is c. The model is updated at the speech encoder frame rate $R = 1/T$, where T is the

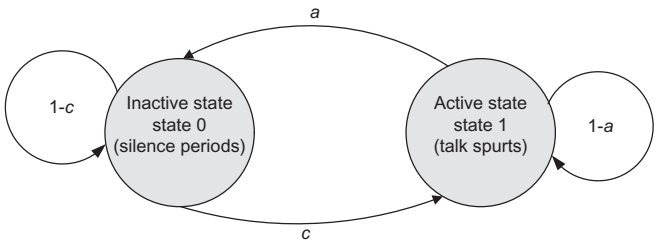


FIGURE 11.4

Two-state Markov model for speech [23,24].

[2]A sequence $X_1, X_2, \ldots, X_{n-1}, X_n$ of random variables is called a Markov sequence, if for any n, the conditional probability of X_n satisfies the following condition $F(X_n|X_{n-1}, X_{n-2}, \ldots, X_1) = F(X_n|X_{n-1})$, that is, the conditional distribution of X_n given $X_{n-1}, X_{n-2}, \ldots, X_1$ have been observed is equal to the conditional distribution X_n assuming only X_{n-1} has been observed. The transitional densities of a Markov sequence satisfy the Chapman−Kolmogorov equation. A random process whose future probabilities are determined by its most recent values is called a Markov process. A stochastic process $x(t)$ is called Markov, if for any n and $t_1 < t_2 < \ldots < t_n$ we have $P(x(t_n) \leq x_n|x(t_{n-1}), x(t_{n-2}), \ldots, x(t_1)) = P(x(t_n) \leq x_n|x(t_{n-1}))$[23,24,54].

Petitioners' Exhibit 1021
Nokia of America Corp., et al. v. KT Corporation, et al.
Case No. IPR2025-00036; U.S. Patent No. 11,627,631
Page 900 of 1122

encoder frame duration which is typically 20 ms for most speech encoders. Packets are generated at time intervals $iT + \tau$ where τ is the packet arrival delay, and i denotes the encoder frame index. During the active state, packets of fixed sizes are generated at these time intervals, while the model is updated at regular frame intervals. The size of the packets and the rate at which the packets are sent depend on the corresponding voice codecs and compression schemes. The voice activity factor (VAF) λ is defined as $\lambda = P_1 = c/(a+c)$. A talk-spurt is defined as the time period τ_{TS} between entering the active state and leaving the active state. The probability that a talk spurt has duration nT is given by $P(\tau_{TS} = nT) = a(1-a)^{n-1}, n = 1, 2, \ldots$ whereas the probability that a silence period has duration mT is given as $P(\tau_{SP} = mT) = c(1-c)^{m-1}, m = 1, 2, \ldots$. The average talk spurt duration μ_{TS} (in number of speech frames) is defined as $\mu_{TS} = \varepsilon[\tau_{TS}] = 1/a$. The mean silence period duration μ_{SP} (in number of speech frames) is given by $\mu_{SP} = \varepsilon[\tau_{SP}] = 1/c$. The distribution of the time period τ_{AE} (in number of speech frames) between successive active state entries is defined as the convolution of the distributions of τ_{SP} and $\tau_{TS:}$

$$P(\tau_{AE} = nT) = \frac{c}{c-a}a(1-a)^{n-1} + \frac{a}{a-c}c(1-c)^{n-1}, \quad n = 1, 2, \ldots \tag{11.18}$$

It must be noted that τ_{AE} can be further considered as the time between MAC layer resource reservations, provided that a single reservation is made per user per talk-spurt. Note that in practice, very small values of τ_{AE} may not result in separate reservation requests. Since the transitions from state 1 to state 0 and vice versa are independent, the mean time μ_{AE} between active state entries is the sum of the mean time in each state, that is, $\mu_{AE} = \mu_{TS} + \mu_{SP}$. Therefore, the mean rate of arrival $\overline{R}_{AE}$ of transitions into the active state can be expressed as $\overline{R}_{AE} = 1/\mu_{AE}$.

The voice capacity calculation assumes the use of 12.2 kbps mode of 3GPP AMR codec with a 50% VAF provided that the percentage of users in outage is less than 2%, where a user is defined to have experienced outage if more than 2% of the VoIP packets are dropped, erased, or otherwise not delivered successfully to the user within the delay bound of 50 ms. The packet delay is defined based on the 98th percentile of the CDF of all individual users' 98th percentiles of packet delay (i.e., the 98th percentile of the packet delay CDF is first determined for each user and then the 98th percentile of the CDF that describes the 98th percentiles of the individual user delay is obtained). The VoIP capacity is measured in terms of the number of active users/MHz/cell. It is the minimum of the capacity calculated for either downlink or uplink divided by the effective bandwidth in the respective direction. In other words, the effective bandwidth is the operating bandwidth normalized appropriately considering the uplink/downlink ratio (in TDD systems).

During each VoIP session, a user will be in the active or inactive state. The duration of time that the user stays in each state is exponentially distributed. In the active or inactive state, voice packets of fixed sizes will be generated at

Petitioners' Exhibit 1021
Nokia of America Corp., et al. v. KT Corporation, et al.
Case No. IPR2025-00036; U.S. Patent No. 11,627,631
Page 901 of 1122

Table 11.2 VoIP Traffic Model Parameters [4,26]

VoIP Model Attribute	Statistical Distribution	Parameters	Probabilistic Distribution
Active/inactive state duration	Exponential	$\mu = 1.25$ s	$f_x = \lambda e^{-\lambda x}, x \geq 0$ $\lambda = 1/\mu$
Probability of state transition	N/A	$c = 0.01$, $d = 0.99$	N/A
Packet arrival delay jitter (downlink only)	Laplacian	$\beta = 5.11$ ms	$f_x = \frac{1}{2\beta} e^{\frac{-\lvert x \rvert}{\beta}}$ $-80 \text{ ms} \leq \tau \leq 80 \text{ ms}$

intervals of $iT + \tau$ seconds, where T is the voice-codec frame size which is typically 20 ms, τ is the network delay jitter (delay variations) in the downlink, and i is the VoIP frame number. In the uplink direction, τ is equal to zero. Given that the range of the delay jitter is limited to 120 ms, the model may be implemented by generating packets at times $iT + \tau'$ seconds where $\tau' = \tau + 80$ (ms) denotes a positive delay value (Table 11.2). The air-interface delay is measured as the time interval between the packet arrival time $iT + \tau'$ to successful reception and decoding of the packet at the receiver. Statistical distribution and parameters associated with the VoIP traffic model are summarized in Table 11.2. The assumptions that were used for VoIP capacity calculation are shown in Table 11.3.

11.3.2 Full-buffer traffic model

In the full-buffer user traffic model, all users in the system are assumed to have data to send or receive at any given time. In other words, there is always a constant amount of data that needs to be transferred, as opposed to bursts of data with probabilistic arrival time distribution. This model allows the assessment of the spectral efficiency of the system independent of the actual user traffic distribution model. A user is in outage if the residual packet error rate after HARQ retransmissions exceeds 1%.

11.4 Link-to-system mapping (PHY abstraction)

The objective of physical-layer abstraction is to model link-level performance and to reduce the amount of computations and complexity in system-level simulations. The motivation for abstraction of the physical layer is that simulating the physical layer across multiple base stations and mobile stations in a cellular network simulation platform can be computationally cumbersome and practically impossible [46,50]. The abstraction must be reasonably accurate, computationally simple,

Petitioners' Exhibit 1021
Nokia of America Corp., et al. v. KT Corporation, et al.
Case No. IPR2025-00036; U.S. Patent No. 11,627,631
Page 902 of 1122

Table 11.3 EESM/MIESM Parameters and MSE for all CQIs in a Bandwidth of Four PRBs [50]

CQI	Code Block Size	Approximate Code Rate	EESM					MIESM		
			β	MSE	α_1	α_2	MSE	α_1	α_2	MSE
1	72	0.072	0.372	0.003	0.363	0.360	0.003	0.278	0.276	0.002
2	112	0.113	0.531	0.004	0.519	0.515	0.004	0.389	0.385	0.003
3	192	0.185	0.865	0.004	0.858	0.855	0.003	0.633	0.629	0.002
4	312	0.297	1.403	0.014	1.439	1.460	0.012	1.056	1.067	0.008
5	456	0.435	1.636	0.076	1.647	1.675	0.073	1.111	1.112	0.045
6	608	0.585	1.646	0.023	1.636	1.621	0.022	1.035	1.019	0.013
7	768	0.368	3.418	0.159	3.748	4.123	0.057	1.065	1.121	0.002
8	1008	0.477	5.042	0.182	5.160	5.491	0.121	1.034	1.065	0.008
9	1248	0.600	6.122	0.106	6.307	6.649	0.066	0.937	0.980	0.013
10	1440	0.455	1.010	0.553	9.790	12.262	0.064	0.942	1.150	0.008
11	1728	0.553	0.399	0.713	11.489	14.827	0.024	0.556	0.727	0.010
12	2048	0.650	0.621	0.658	17.669	23.625	0.051	0.700	0.935	0.017
13	2368	0.753	0.962	0.825	24.081	32.971	0.069	0.760	1.017	0.038
14	2688	0.852	7.933	0.382	22.622	28.049	0.007	0.657	0.821	0.006
15	2880	0.925	15.859	0.077	25.245	28.103	0.034	0.840	0.985	0.024

Petitioners' Exhibit 1021
Nokia of America Corp., et al. v. KT Corporation, et al.
Case No. IPR2025-00036; U.S. Patent No. 11,627,631
Page 903 of 1122

Table 11.4 Baseline Configuration Parameters for IMT-Advanced Evaluations [14]

Simulation Parameters	Indoor Hotspot (InH)	Urban Micro-Cellular (UMi)	Urban Macro-Cellular (UMa)	Rural Macro-Cellular (RMa)
Baseline Parameters				
Base station antenna height (m)	6 (on the ceiling)	10 (below rooftop)	25 (above rooftop)	35 (above rooftop)
Number of BS antennas (receive/transmit)	Up to 8/up to 8	Up to 8/up to 8	Up to 8/up to 8	Up to 8/up to 8
Base station transmit power (dBm)	24 (40 MHz) 21 (20 MHz)	41 (10 MHz) 44 (20 MHz)	46 (10 MHz) 49 (20 MHz)	46 (10 MHz) 49 (20 MHz)
Mobile station transmit power (dBm)	21	24	24	24
Number of MS antennas (receive/transmit)	Up to 2/up to 2	Up to 2/up to 2	Up to 2/up to 2	Up to 2/up to 2
Minimum distance between MS and BS (m)	≥ 3	≥ 10	≥ 25	≥ 35
RF carrier frequency (GHz)	3.4	2.5	2	0.8
Outdoor-to-indoor penetration loss	N/A	See Annex 1, Table A1-2 of [14]	N/A	N/A
Outdoor to in-car penetration loss	N/A	N/A	9 dB (lognormal, $\sigma = 5$ dB)	9 dB (lognormal, $\sigma = 5$ dB)
Parameters for Analytical Assessment of Peak Spectral Efficiency				
Number of BS antennas (receive/transmit)	Up to 4/up to 4	Up to 4/up to 4	Up to 4/up to 4	Up to 4/up to 4
Number of MS antennas (receive/transmit)	Up to 4/up to 2	Up to 4/up to 2	Up to 4/up to 2	Up to 4/up to 2

(*Continued*)

Petitioners' Exhibit 1021
Nokia of America Corp., et al. v. KT Corporation, et al.
Case No. IPR2025-00036; U.S. Patent No. 11,627,631
Page 904 of 1122

Table 11.4 (Continued)

Simulation Parameters	Indoor Hotspot (InH)	Urban Micro-Cellular (UMi)	Urban Macro-Cellular (UMa)	Rural Macro-Cellular (RMa)
Parameters for System-Level Simulations				
Network layout	Indoor floor	Hexagonal grid	Hexagonal grid	Hexagonal grid
Inter-site distance (m)	60	200	500	1732
Channel model	Indoor hotspot channel model	Urban micro-cellular channel model	Urban macro-cellular channel model	Rural macro-cellular channel model
User distribution	Randomly and uniformly distributed over area	Randomly and uniformly distributed over area 50% pedestrian users and 50% users indoor	Randomly and uniformly distributed over area 100% vehicular users	Randomly and uniformly distributed over area 100% high-speed vehicular users
User mobility	All mobile stations have fixed and identical speed with randomly and uniformly distributed direction	All mobile stations have fixed and identical speed with randomly and uniformly distributed direction	All mobile stations have fixed and identical speed with randomly and uniformly distributed direction	All mobile stations have fixed and identical speed with randomly and uniformly distributed direction
MS speed (km/h)	3	3	30	120
Inter-site interference	Explicitly modeled	Explicitly modeled	Explicitly modeled	Explicitly modeled
BS noise figure (dB)	5	5	5	5
MS noise figure (dB)	7	7	7	7
BS antenna gain (bore-sight) (dBi)	0	17	17	17
MS antenna gain (dBi)	0	0	0	0
Thermal noise level (dBm/Hz)	−174	−174	−174	−174

Petitioners' Exhibit 1021
Nokia of America Corp., et al. v. KT Corporation, et al.
Case No. IPR2025-00036; U.S. Patent No. 11,627,631
Page 905 of 1122

Parameters for Assessment of Cell Spectral Efficiency and Cell-Edge User Spectral Efficiency				
Traffic model	Full buffer	Full buffer	Full buffer	Full buffer
System bandwidth	2 × 20 MHz (FDD) 40 MHz (TDD)	2 × 10 MHz (FDD) 20 MHz (TDD)	2 × 10 MHz (FDD) 20 MHz (TDD)	2 × 10 MHz (FDD) 20 MHz (TDD)
Number of users/cell	10	10	10	10
Parameters for Evaluation of VoIP Capacity				
Traffic model	VoIP	VoIP	VoIP	VoIP
System bandwidth	2 × 5 MHz (FDD) 10 MHz (TDD)	2 × 5 MHz (FDD) 10 MHz (TDD)	2 × 5 MHz (FDD) 10 MHz (TDD)	2 × 5 MHz (FDD) 10 MHz (TDD)
Simulation duration for a single drop(s)	20	20	20	20
Parameters for Link-Level Simulation (Mobility Requirement)				
Traffic model	Full buffer	Full buffer	Full buffer	Full buffer
Channel model	Indoor hotspot channel model	Urban micro-cellular channel model	Urban macro-cellular channel model	Rural macro-cellular channel model
System bandwidth (MHz)	10	10	10	10
Number of users/cell	1	1	1	1

Petitioners' Exhibit 1021
Nokia of America Corp., et al. v. KT Corporation, et al.
Case No. IPR2025-00036; U.S. Patent No. 11,627,631
Page 906 of 1122

relatively independent of channel models, and extensible to interference models and multi-antenna processing methods. The system-level simulations are used to characterize the average user/system performance, which may be useful in providing insights for deployment of the system in terms of cell and frequency planning. For such simulations, the average performance of a system is quantified using the topology and macro channel characteristics to calculate a wideband SINR distribution across the cell (alternatively known as geometry). Each subscriber's SINR distribution is then mapped to the highest MCS that could be supported, based on link-level SINR tables which include fast fading characteristics of the channel. The link-level SINR-BLER look-up tables serve as the PHY abstraction for predicting average link-level performance. The instantaneous channel conditions are used to improve the performance of the cellular systems. Channel-dependent scheduling and adaptive coding and modulation are examples of channel-adaptive schemes employed to improve system performance. Therefore, properly designed system-level simulation methodologies do explicitly model the dynamic behavior of the system [28,37,50,51].

In system-level simulations, an encoded data/control packet may be transmitted over a time-frequency selective channel. In OFDM-based systems, the encoded block is transmitted over several sub-carriers, the post-processing SINR values of the pre-decoded streams are thus non-uniform, and the channel gains of sub-carriers can be time-varying. As a result, in the transmission of a large encoded packet, the encoded symbols with unequal SINR ratios at the input of the decoder are considered due to the time or frequency selectivity of the channel impulse or frequency response over the duration of packet transmission.

The goal of a PHY abstraction or a link-to-system mapping is to predict the encoded BLER for a given received channel realization across the OFDM subcarriers that are used to transmit the channel-coded blocks. In order to predict the performance, the post-processing SINR values at the input to the forward error correction (FEC) decoder are considered as input to the PHY abstraction. As the link-level curves are generated assuming a frequency flat channel response at a given SINR, an effective SINR is defined to accurately map the system-level SINR to the link-level curves in order to determine the resulting BLER. The latter mapping is known as effective SINR mapping (ESM) in the literature. The ESM PHY abstraction compresses the vector of received SINR values to a single effective SINR value, which can then be further mapped to a BLER value. Several ESM approaches to predict the instantaneous link-level performance have been studied in the literature. Examples include mean instantaneous capacity, exponential effective SINR mapping (EESM), and mutual information (MI) ESM. Each of these PHY abstractions uses a different function to map the vector of SINR values to a single number. Given the instantaneous EESM SINR, mean capacity or mutual information effective SINR, the BLER for each MCS is calculated using a suitable mapping function. The general process of link-to-system mapping is illustrated in Figure 11.5.

Petitioners' Exhibit 1021
Nokia of America Corp., et al. v. KT Corporation, et al.
Case No. IPR2025-00036; U.S. Patent No. 11,627,631
Page 907 of 1122

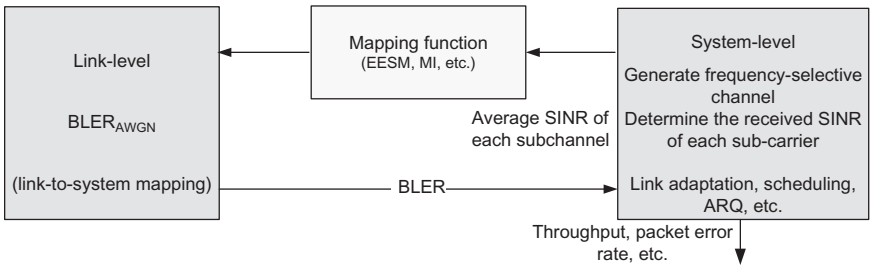


FIGURE 11.5

Link-to-system mapping process [26].

Given an experimental BLER measured in a multi-state channel with a specific MCS, the effective SINR of that channel is defined as the SINR that would produce the same BLER, with the same MCS, in AWGN conditions. In general, for a given multi-state channel with N_{FFT} different SINR measurements $\{\text{SINR}_1, \text{SINR}_2, \text{SINR}_3, \ldots, \text{SINR}_{NFFT}\}$, the effective SINR can be described as follows:

$$\text{SINR}_{\text{effective}} = \alpha_1 \Phi^{-1}\left(\frac{1}{N_{\text{FFT}}}\sum_{n=1}^{N_{\text{FFT}}} \Phi\left(\frac{\text{SINR}_n}{\alpha_2}\right)\right) \tag{11.19}$$

where $\text{SINR}_{\text{effective}}$ denotes the effective SINR, SINR_n is the SINR measured at the nth sub-carrier, N_{FFT} is the number of symbols in a coded block, or the number of sub-carriers used in an OFDM system, and $\Phi(.)$ is an invertible function. In the case of the mutual information-based ESM the function $\Phi(.)$ is derived from the constrained capacity, whereas in the case of EESM, the function $\Phi(.)$ is derived from the Chernoff bound[3] on the probability of error [55]. The EESM model uses the mapping function $\Phi(x) = 1 - \exp(-x)$ for all modulation schemes and in many cases, the constants α_1 and α_2 are assumed to be equal $\alpha_1 = \alpha_2 = \beta$. The parameter β can be interpreted as a shift in $\Phi(.)$ function to adapt the model to different MCSs. If a MIMO scheme is utilized assuming use of linear processing (ZF or MMSE) in the receiver, one still can use the effective SINR concept

[3]In the theory of probability and stochastic processes, the Chernoff bound provides exponentially decreasing bounds (asymptotic) on tail distributions of sums of independent random variables compared to the first or second moment based tail bounds such as Markov's inequality or Chebyshev inequality, which only yield power-law bounds on tail decay. Let $\mathbf{x}_1, \mathbf{x}_2, \ldots, \mathbf{x}_n$ denote discrete and independent random variables with probability $p > 1/2$. Then, the probability of simultaneous occurrence of more than $n/2$ of the events x_k has an exact value P, where $P = \sum_{i=\lfloor n/2 \rfloor}^{n} \binom{n}{i} p^i (1-p)^{n-i}$. The Chernoff bound provides a lower bound for P given by $P \geq 1 - \exp[-2n(p-1/2)^2]$. The Chernoff bound applies to a class of random variables and provides exponential falloff of probability with distance from the mean. The critical condition that is needed for a Chernoff bound is that the random variable must be a sum of independent indicator random variables [55].

Petitioners' Exhibit 1021
Nokia of America Corp., et al. v. KT Corporation, et al.
Case No. IPR2025-00036; U.S. Patent No. 11,627,631
Page 908 of 1122

by taking the MIMO post-processing SINR as the set of measurements $\{SINR_1, SINR_2, SINR_3, \ldots, SINR_{NFFT}\}$ of the multi-state channel. Assuming that the receiver has a good estimation of the MIMO channel matrix, it can calculate the post-processing SINR based on well-known expressions. In spatial multiplexing mode, the antenna correlation is translated into degradation of the post-processing SINR, thus assuming that the channel is known, the effective SINR model may also capture the effect of antenna correlation. The parameters α_1 and α_2 depend on the modulation scheme, the code block size, and the code rate, but should be valid for SISO and MIMO with linear equalization regardless of the MIMO antenna correlation. Based on the above discussion, in the case of EESM, the effective SINR in snapshot i can be written as follows:

$$\mathrm{SINR}^{i}_{\mathrm{effective}}(\beta) = \beta \ln\left(\frac{1}{N_{\mathrm{FFT}}}\sum_{n=1}^{N_{\mathrm{FFT}}}\exp\left(\frac{\mathrm{SINR}^{i}_{n}}{\beta}\right)\right) \tag{11.20}$$

If M denotes the number of simulated snapshots, the value of β can be obtained as follows:

$$\hat{\beta} = \arg\min_{\beta}\left\{\sum_{i=1}^{N_{\mathrm{snapshots}}}\left[\log(\mathrm{BLER}_i) - \log(\mathrm{BLER}_R(\mathrm{SINR}^{i}_{\mathrm{effective}}(\beta)))\right]^2\right\} \tag{11.21}$$

where $\mathrm{BLER}_R(.)$ is the reference BLER curve in the AWGN channel for the current MCS and code block size. That is, to obtain β, we minimize the mean squared error between the estimated BLER and the simulated BLER for the set of simulated snapshots using numerical methods. By using the logarithmic BLER error in Eq. (11.21), the minimization algorithm tries to obtain minimal error at low BLER, which is the region of interest. For MIESM Eq. (11.19) is rewritten as follows:

$$\mathrm{SINR}^{i}_{\mathrm{effective}}(\alpha_1, \alpha_2) = \alpha_1 \ln\left(\frac{1}{N_{\mathrm{FFT}}}\sum_{n=1}^{N_{\mathrm{FFT}}}\exp\left(\frac{\mathrm{SINR}^{i}_{n}}{\alpha_2}\right)\right) \tag{11.22}$$

In which, the calculation of α_1 and α_2 involves a two-dimensional minimization of the mean square error (MSE) as follows:

$$(\hat{\alpha}_1, \hat{\alpha}_2) = \arg\min_{\alpha_1,\alpha_2}\left\{\sum_{i=1}^{N_{\mathrm{snapshots}}}\left[\log(\mathrm{BLER}_i) - \log(\mathrm{BLER}_R(\mathrm{SINR}^{i}_{\mathrm{effective}}(\alpha_1, \alpha_2)))\right]^2\right\} \tag{11.23}$$

In the case of MIESM, there is an additional challenge that the mutual-information function $\Phi(.)$ must be inverted numerically. Table 11.3 lists the obtained EESM/MIESM parameters as well as the MSE for each CQI. The values of the parameters in each case are in good agreement with those previously

Petitioners' Exhibit 1021
Nokia of America Corp., et al. v. KT Corporation, et al.
Case No. IPR2025-00036; U.S. Patent No. 11,627,631
Page 909 of 1122

published in the literature [50,51]. The main advantage of EESM over MIESM is that the nonlinear weighting function $\Phi(.)$ and its inverse function used to calculate the effective SINR are closed-form and easy to compute. The performance of EESM to predict the BLER in the MIMO high-correlation scenarios can be tested in two ways, that is, using a single parameter (one-dimension minimization) or using two different parameters. The advantage of using a single parameter is that minimization effort is simple and there is a single minimum. This is the reason that there are two sets of parameters for EESM shown in Table 11.3. The values of the EESM parameters in Table 11.3 are in good agreement with those published in the literature for QPSK and 16QAM and deviate for 64QAM [28,34,50,51]. Comparing the MSEs corresponding to MIESM and EESM in the table suggests that MIESM outperforms EESM and provides more accurate link-abstraction relative to reference link-level curves at the expense of more complexity.

The accuracy of a mutual information-based metric depends on the equivalent channel over which this metric is defined. The capacity is defined as the mutual information based on a Gaussian channel with Gaussian distributed inputs. The modulation constrained capacity is the mutual information of a symbol channel, that is, constrained by the input symbols drawn from a complex set. The computation of the mutual information per coded bit can be derived from the received symbol-level mutual information which is regarded as received bit mutual information rate (RBIR) link-to-system mapping. An alternative approach directly arrives at the bit-level mutual information and is known as the mean mutual information per bit (MMIB) PHY abstraction method. The procedure of the MIESM approach is illustrated in Figure 11.6. Given a set of N received encoder symbol SINRs from the system-level simulation, denoted as $\{\text{SINR}_1, \text{SINR}_2, \text{SINR}_3, \ldots, \text{SINR}_N\}$; a mutual-information metric is calculated. Based on the computed MI metric, an equivalent SINR is obtained and used to look-up the BLER value [34,50,51].

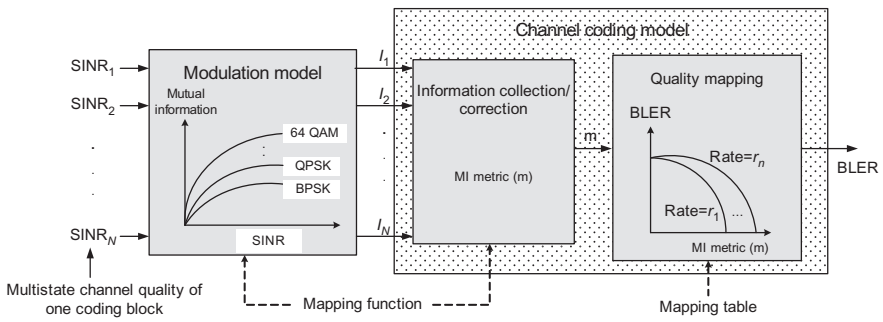


FIGURE 11.6

Procedure for MIESM link-to-system mapping method [26].

11.5 IMT-Advanced test environments

For evaluation of the IMT-Advanced candidates, the ITU-R WP 5D defined several test environments where each test environment is characterized with certain user mobility, path loss and channel models, and system configuration parameters. The evaluation of candidate radio access technologies was performed in selected scenarios of the following test environments [12–14]:

- Indoor test environment models isolated cells at offices and/or in hotspots comprising stationary and pedestrian users. In this model, the emphasis is on very small cells, very high user throughputs, and high user density inside buildings.
- Urban micro-cellular test environment with higher user density was defined to model pedestrian and slow vehicular users. The micro-cellular test environment's focus is on small cells and high user densities which demonstrates typical traffic load in city centers and dense urban areas. The key characteristic of this test environment is high traffic loads as well as outdoor and outdoor-to-indoor coverage. This scenario is interference-limited. A continuous cellular layout and the associated interference are assumed and radio access points are located below rooftop level.
- Urban macro-cellular environment (base coverage urban) was defined to model coverage for pedestrian users up to fast-moving vehicular users. The base coverage urban test environment focuses on large cells and continuous coverage. The main characteristics of this test environment are continuous and ubiquitous coverage in urban areas. This scenario is interference-limited, using macro-cells with radio access points above rooftop level. In an urban macro-cell test environment, mobile stations are located outdoor at street level and fixed base station antennas are located clearly above surrounding building heights. Therefore, NLoS or obstructed sight can be considered in this scenario.
- High-speed or rural test environment models high-speed vehicular and trains. The high-speed test environment focuses on larger cells and continuous coverage. The key characteristics of this test environment are continuous wide area coverage supporting high-speed vehicles. This scenario will therefore be noise-limited and/or interference-limited and uses macro-sized cells.

11.6 Network layout for system-level simulations

In the rural or high-speed, macro- and micro-cellular environments, no specific topographical details are taken into consideration. Base stations are placed in regular grids conforming to a hexagonal layout. A basic hexagonal layout with three cells/sectors per site is shown in Figure 11.7 where antenna bore-sight, cell range, and inter-site distance are also illustrated. The system-level simulations use a wrap-around model with 19 sites each comprising 3 cells. The users are dropped

Petitioners' Exhibit 1021
Nokia of America Corp., et al. v. KT Corporation, et al.
Case No. IPR2025-00036; U.S. Patent No. 11,627,631
Page 911 of 1122

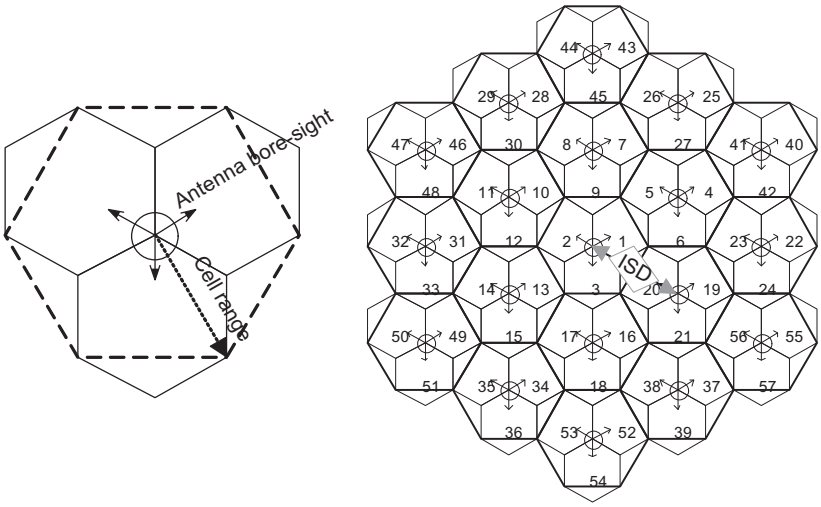


FIGURE 11.7

Illustration of a hexagonal cellular network layout [14].

uniformly over the entire coverage area (Monte Carlo method[4]) in order to model the inter-cell interference. Depending on the configuration being simulated and required output, the effect of the surrounding outer cells may be disregarded. In such cases, only 19 cells of the center cluster may be modeled. For the cases where modeling of the interfering outer cells is necessary for accuracy of the results, the wrap-around structure with the seven cluster network can be used. A cluster is defined as six displacements of the center hexagon. In the wrap-around inter-cell interference model, the network is extended to a cluster of networks consisting of seven replicas of the original hexagonal network, with the original hexagonal network in the middle while the other six copies are attached to it symmetrically on six sides. The number of mobile stations is predetermined for each sector/cell, where each MS location is randomly distributed with uniform distribution (see Figure 11.7).

The serving cell of each MS is determined in two steps due to the wrap-around nature of the cell layout. The first step is to determine the 19 shortest-distanced cells for each MS from all seven logical cell clusters, and the second step is to determine the serving cell/sector among the nearest 19 cells for each MS based on the strongest link according to the path loss and shadowing. To determine the shortest-distanced cell for each MS, the distances between the MS

[4]Monte Carlo methods are a class of computational algorithms that rely on repeated random sampling to compute their results. Monte Carlo methods are often used in simulating physical and mathematical systems. Because of their reliance on repeated computation of random or pseudorandom quantities, these methods are most suited to calculation by a computer and tend to be used when it is unfeasible or impossible to find a closed-form result with a deterministic algorithm [56].

Petitioners' Exhibit 1021
Nokia of America Corp., et al. v. KT Corporation, et al.
Case No. IPR2025-00036; U.S. Patent No. 11,627,631
Page 912 of 1122

and all logical cell clusters are calculated and the 19 cells with a shortest distance in all seven cell clusters are selected. The serving cell for each MS provides the strongest link with a strongest received long-term signal power. It should be noted that the shadowing experienced on the link between MS and cells located in different clusters is the same.

11.7 IMT-Advanced evaluation methodology and baseline configurations

The IMT-Advanced candidate technologies were required to be evaluated under at least three test environments. ITU-R WP 5D specified a common evaluation methodology based on which the candidates were required to be configured and assessed against the IMT-Advanced minimum system requirements. Table 11.4 provides the common parameters for evaluation of radio access technologies as specified by ITU-R recommendations [6,12–14].

The BS antennas in each sector are assumed to have antenna patterns in azimuth and elevation directions that are given by:

$$\begin{aligned} A_e(\phi) &= -\min\left[12\left(\frac{\phi-\phi_{\text{tilt}}}{\phi_{3\text{dB}}}\right)^2, A_m\right] \text{ Elevation direction} \\ A(\theta) &= -\min\left[12\left(\frac{\theta}{\theta_{3\text{dB}}}\right)^2, A_m\right] \text{ Azimuth direction} \end{aligned} \tag{11.24}$$

where $A(\theta)$ is the relative antenna gain (in dB) in the direction of $-180^\circ \le \theta \le 180^\circ$, $\theta_{3\ \text{dB}}$ is the 3 dB beam-width ($\theta_{3\text{dB}} = 70^\circ$),$A_m = 20$ dB is the maximum attenuation, $A_e(\phi)$ is the relative antenna gain (in dB) in the elevation direction $-90^\circ \le \phi \le 90^\circ$, $\phi_{3\text{dB}}$ is the elevation 3 dB beam-width ($\phi_{3\text{dB}} = 15^\circ$), and ϕ_{tilt} is the tilt angle. The value of the antenna tilt angle is assumed to be $\phi_{\text{tilt}} = 0^\circ$ for InH, $\phi_{\text{tilt}} = 12^\circ$ for UMi, $\phi_{\text{tilt}} = 12^\circ$ for UMa, and $\phi_{\text{tilt}} = 6^\circ$ for RMa test environments.

The combined antenna pattern at angles off the cardinal axes is computed as $-\min[-(A(\theta) + A_e(\phi)), A_m]$. The antenna bearing is defined as the angle between the main antenna lobe center and a line directed due east given in degrees. The bearing angle increases in a clockwise direction. The center directions of the main antenna lobe in each sector point to the corresponding side of the hexagon. For an indoor test environment, the BS is assumed to have an omni-directional antenna pattern. The mobile station is assumed to have omni-directional antennas.

11.8 Link-level and system-level channel models

The channel behavior is described by its long- and short-term fading characteristics where the former often depends on the geometrical location of a user in a wireless network and the latter defines the time-variant spatial channels.

Petitioners' Exhibit 1021
Nokia of America Corp., et al. v. KT Corporation, et al.
Case No. IPR2025-00036; U.S. Patent No. 11,627,631
Page 913 of 1122

In general, there are two ways of modeling a channel, deterministic and stochastic. The deterministic category encompasses all models that describe the propagation channel for a specific transmitter location, receiver location, and environment. Deterministic channel models are site-specific, as they clearly depend on the location of transmitter, receiver, and the properties of the environment. They are therefore most suitable for network planning and deployment. In many cases, it is not possible or desirable to model the propagation channel in a specific environment. Especially for system testing and evaluation, it is more appropriate to consider channels that reflect "typical," "best case," and "worst case" propagation scenarios. A stochastic channel model thus reflects the statistics of the channel impulse responses and during the actual simulation; impulse responses are generated as realizations according to those statistics[18–22,29–33,35–43].

Essential to the evaluation of multiple-antenna techniques, which are the key enabling technology for IMT-Advanced systems, is the modeling of MIMO channels that can be represented as double-directional channels or as vector (or matrix) channels. The former representation is more related to the physical propagation effects, while the latter is more focused on the mathematical effect of the channel on the system. The double-directional model is a physical model in which the channel is constructed from summing over multiple waves or rays. Thus, it can also be referred to as a "ray-based model." The vector or matrix channel is a mathematical or analytical model in which the space-time channel as seen by the receiver is constructed mathematically, assuming certain system and antenna parameters. In this approach, the channel coefficients are correlated random processes in both space and time, where the correlation is defined mathematically.

The ITU-R WP 5D specified channel models for the evaluation of IMT-Advanced candidate technologies which consisted of primary and extension modules. The framework of the primary module is based on the WINNER II channel model,[5] which applies the same approach as the 3GPP/3GPP2 spatial channel model (SCM).[6] The extension module extends the capabilities of the IMT-Advanced channel model to cover additional deployment scenarios beyond that of IMT-Advanced candidate technology evaluations, allowing the use of modified parameters to generate large-scale parameters. The ITU-R WP 5D specified channel model is a geometric stochastic model. It does not explicitly specify the locations of the scatterers, rather the directions of the rays generated as a result of scattering objects. The geometric modeling of the radio channel enables separation of propagation parameters and antennas. The channel parameters for individual snapshots are determined stochastically based on statistical distributions extracted from channel measurements. Antenna geometries and radiation patterns

[5]Information on WINNER II channel models can be found at http://www.ist-winner.org/deliverables.html.

[6]Information on the 3GPP/3GPP2 spatial channel model can be found in 3GPP TR 25.996 *spatial channel model for multiple input multiple output* (MIMO), September 2003.

Petitioners' Exhibit 1021
Nokia of America Corp., et al. v. KT Corporation, et al.
Case No. IPR2025-00036; U.S. Patent No. 11,627,631
Page 914 of 1122

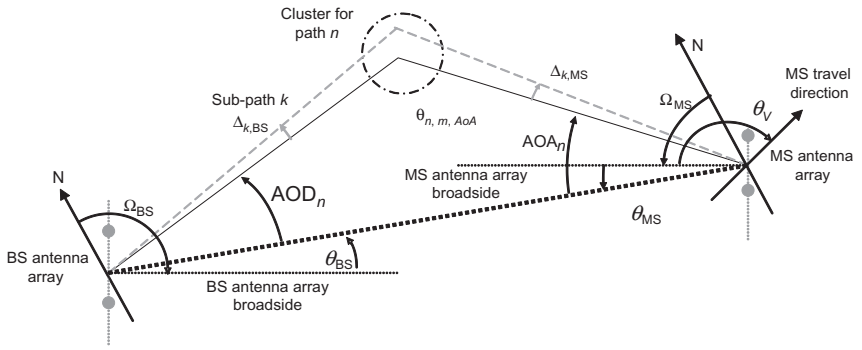


FIGURE 11.8

Illustration of angular parameters in the MIMO channels [1,14].

can be defined properly by the user of the model. As shown in Figure 11.8, channel realizations are generated through the application of the geometrical principle by summing the rays (plane waves) with specific small-scale parameters, such as delay, power, angle-of-arrival (AoA), and angle-of-departure (AoD). The superposition results in correlation between antenna elements and temporal fading with geometry-dependent Doppler spectrum. A number of rays constitute a cluster. A cluster and a propagation path diffused in space are equivalent in delay and angle domains. A generic MIMO channel model is applied to all test scenarios. The time-variant impulse response matrix of the MIMO channel can be written as (assuming N_{TX} transmit antennas at the BS and N_{RX} receive antennas at the MS) $\mathbf{H}(t;\tau) = \sum_{n=1}^{N} \mathbf{H}_n(t;\tau)$ where τ denotes the delay and $N = N_{\mathrm{RX}} \times N_{\mathrm{TX}}$ is the number of multipaths. The channel impulse response is composed of the antenna array response matrices $\mathbf{F}_{\mathrm{TX}}$ and $\mathbf{F}_{\mathrm{RX}}$ for the transmitter and the receiver, respectively, as well as the dual-polarized propagation channel response matrix $\mathbf{h}_n$ for the nth cluster, hence:

$$\mathbf{H}_n(t;\tau) = \iint \mathbf{F}_{\mathrm{RX}}(\phi)\, \mathbf{h}_n(t;\tau,\varphi,\phi)\, \mathbf{F}_{\mathrm{TX}}^{T}(\varphi)\, \mathrm{d}\varphi\, \mathrm{d}\phi \tag{11.25}$$

The channel from transmit antenna element s to receive antenna element u for cluster n can be expressed as follows:

$$H_{u,s,n}(t;\tau) = \sum_{m=1}^{M} \begin{bmatrix} \mathbf{F}_{\mathrm{RX},u,V}(\phi_{n,m}) \\ \mathbf{F}_{\mathrm{RX},u,H}(\phi_{n,m}) \end{bmatrix}^{T} \begin{bmatrix} \alpha_{n,m,VV} & \alpha_{n,m,VH} \\ \alpha_{n,m,HV} & \alpha_{n,m,HH} \end{bmatrix} \begin{bmatrix} \mathbf{F}_{\mathrm{TX},s,V}(\varphi_{n,m}) \\ \mathbf{F}_{\mathrm{TX},s,H}(\varphi_{n,m}) \end{bmatrix} \times \exp\left(j2\pi\upsilon_{n,m}t\right)\delta\left(\tau - \tau_{n,m}\right) \times \exp\left(j2\pi\lambda_0^{-1}(\overline{\phi}_{n,m}\cdot\overline{r}_{RX,u})\right)\exp\left(j2\pi\lambda_0^{-1}(\overline{\varphi}_{n,m}\cdot\overline{r}_{TX,s})\right) \tag{11.26}$$

where $\mathbf{F}_{\mathrm{RX},u,V}$ and $\mathbf{F}_{\mathrm{RX},u,H}$ denote the antenna element u field patterns for vertical and horizontal polarizations, respectively, $\alpha_{n,m,VV}$ and $\alpha_{n,m,VH}$ are the

Petitioners' Exhibit 1021
Nokia of America Corp., et al. v. KT Corporation, et al.
Case No. IPR2025-00036; U.S. Patent No. 11,627,631
Page 915 of 1122

complex-valued gains of vertical-to-vertical and horizontal-to-vertical polarizations of ray n, m, respectively, λ_0 represents the wave length of the RF carrier, $\overline{\varphi}_{n.m}$ AoD unit vector, $\overline{\phi}_{n.m}$ is the AoA unit vector, $\overline{r}_{\mathrm{TX},s}$ and $\overline{r}_{rx,u}$ are the location vectors of element s and u, respectively, and $\upsilon_{n,m}$ denotes the Doppler frequency component of ray n, m [1,14,26]. If the radio channel is dynamically modeled, the above-mentioned small-scale parameters are going to be time-variant.

In Figure 11.8, the placement of the MS with respect to each BS is to be determined according to the cell layout. From this placement, the distance between the MS and the BS d and the LoS directions with respect to the BS and MS, θ_{BS} and θ_{MS} can be determined. Note that θ_{BS} and θ_{MS} are defined relative to the broadside directions. The MS antenna array orientations Ω_{MS} are independent and identically distributed and are obtained from a uniform $0-360^{\circ}$ distribution.

The generic MIMO channel model is a stochastic model with two levels of unpredictability: large-scale parameters, such as shadow fading, delay, and angular spreads that are drawn randomly from tabulated distribution functions; and small-scale parameters, such as delay, power, and direction of arrival and departure that are selected randomly according to tabulated distribution functions and large-scale parameters. An infinite number of different realizations of the channel model can be generated randomly selecting different initial phases for the scattering objects.

The general approach in the SCM is based on the geometry of a network layout. The large-scale parameters, such as path loss and shadowing factor, are generated according to the geometric positions of the BS and MS. Then the statistical channel behavior is defined using distribution functions of delay and angle, and also by the power delay and angular profiles. Typically, an exponential power delay profile and Laplacian power angular profile are assumed with the function completely defined once the root mean-square (RMS) delay spread and angular spread are specified. The RMS delay and angular spread parameters can be random variables with a mean and standard deviation. The RMS delay and angular spread can be mutually correlated, together with other large-scale parameters, such as shadowing factors. According to the exact profile and distribution functions defined by the particular RMS delay and angular spread values, a finite number of channel taps are randomly generated with a per-tap delay, mean power, mean AoA and AoD, and RMS angular spread. They are defined in a way such that the overall power profile and distribution function are satisfied. Each tap is the contribution of a number of rays (plane waves) arriving at the same time, with each ray having its own amplitude, AoA, and AoD. The number of taps and their delay and angles may be randomly defined, but a reduced-complexity model can specify the delays, mean powers, and angles of the channel taps in a predetermined manner when typical values are often chosen. Similar to the well-known tapped-delay-line version of the wide-sense stationary uncorrelated scattering model, where the power delay profile is fixed, a spatial tapped-delay-line reduced-complexity model additionally defines the spatial information, such as per-tap mean AoA, AoD, and per-tap angular spread, and the power angular

Petitioners' Exhibit 1021
Nokia of America Corp., et al. v. KT Corporation, et al.
Case No. IPR2025-00036; U.S. Patent No. 11,627,631
Page 916 of 1122

profile. Spatial tapped-delay-line models are also referred to as cluster-delay-line models as each tap is modeled as the effect of a cluster of rays arriving at the same time. Each tap suffers from fading in space and over time. The spatial fading process will satisfy a predetermined power angular profile.

The realization of a time-varying spatial channel can be performed in two ways:

- Ray-based: The channel coefficient between each transmit and receive antenna pair is the summation of all rays at each tap and at each time instant, according to the antenna configuration, gain pattern, AoA, AoD of each ray. The temporal channel variation depends on the traveling speed and direction relative to the AoA/AoD of each ray.
- Correlation-based: The antenna correlation for each tap is computed first according the per-tap mean AoA/AoD, per-tap power angular profile, and antenna configuration parameters (e.g., spacing and polarization). The per-tap Doppler spectrum depends on the traveling speed and direction relative to the mean per-tap AoA/AoD, as well as the per-tap power angular profile. The MIMO channel coefficients at each tap can then be generated mathematically by transforming typically the independent and identically distributed Gaussian random variables according to the antenna correlation and the temporal correlation (correspondingly the particular Doppler spectrum).

The generic channel model is based on the drop concept. The system-level simulation is performed in a sequence of "drops," where a "drop" is defined as one simulation run over a certain time period when using the generic model. A drop (or snapshot of a channel segment) is a simulation instance where the random properties of the channel remain constant except for the fast fading caused by the changing phases of the rays. The constant properties during a single drop are the power, delay, and direction of the rays. In a simulation, the number and the length of drops are selected based on the evaluation requirements and the deployment scenario. The generic channel model allows simulation of several statistically independent drops in order to obtain a statistical representation of system performance. The channel model parameters for evaluation of IMT-Advanced technologies in various test environments are shown in Table 11.5. In Table 11.5, DS is the RMS delay spread, ASD is the RMS azimuth spread of departure angles, ASA denotes the RMS azimuth spread of arrival angles, SF represents the shadow fading, and parameter K denotes the Rician K-factor. IMT-Advanced primary module path loss model parameters for a hexagonal cell layout are summarized in Table 11.6.

The break point distance in the above table is defined as $d'_{BP} = 4h'_{BS}h'_{MS}f_c/c$ where f_c is the center frequency (Hz), $c = 3.0 \times 10^8$ m/s is the propagation velocity in free space, h'_{BS} and h'_{MS} are the effective antenna heights at the BS and the MS, respectively. The effective antenna heights h'_{BS} and h'_{MS} are computed as follows: $h'_{BS} = h_{BS} - 1$ and $h'_{MS} = h_{MS} - 1$ where h_{BS} and h_{MS} are the actual antenna heights. The effective height in urban environments is assumed to be equal to 1.0m. In the above table, PL_b denotes basic path loss, PL_{B1} is loss of UMi

Table 11.5 Channel Model Parameters for IMT-Advanced Test Environments [4,14]

Channel Model Parameters		InH		UMi			UMa		RMa	
		LoS	NLoS	LoS	NLoS	Outdoor-to-Indoor	LoS	NLoS	LoS	NLoS
Delay spread (DS) $\log_{10}$(s)	μ	−7.70	−7.41	−7.19	−6.89	−6.62	−7.03	−6.44	−7.49	−7.43
	σ	0.18	0.14	0.40	0.54	0.32	0.66	0.39	0.55	0.48
AoD spread (ASD) $\log_{10}$(degrees)	μ	1.60	1.62	1.20	1.41	1.25	1.15	1.41	0.90	0.95
	σ	0.18	0.25	0.43	0.17	0.42	0.28	0.28	0.38	0.45
AoA spread (ASA) $\log_{10}$(degrees)	μ	1.62	1.77	1.75	1.84	1.76	1.81	1.87	1.52	1.52
	σ	0.22	0.16	0.19	0.15	0.16	0.20	0.11	0.24	0.13
Shadow fading (SF) (dB)	σ	3	4	3	4	7	4	6	4	8
K-factor (*K*) (dB)	μ	7	N/A	9	N/A	N/A	9	N/A	7	N/A
	σ	4	N/A	5	N/A	N/A	3.5	N/A	4	N/A
Cross-correlations	ASD vs. DS	0.6	0.4	0.5	0	0.4	0.4	0.4	0	−0.4
	ASA vs. DS	0.8	0	0.8	0.4	0.4	0.8	0.6	0	0
	ASA vs. SF	−0.5	−0.4	−0.4	−0.4	0	−0.5	0	0	0
	ASD vs. SF	−0.4	0	−0.5	0	0.2	−0.5	−0.6	0	0.6
	DS vs. SF	−0.8	−0.5	−0.4	−0.7	−0.5	−0.4	−0.4	−0.5	−0.5
	ASD vs. ASA	0.4	0	0.4	0	0	0	0.4	0	0
	ASD vs. *K*	0	N/A	−0.2	N/A	N/A	0	N/A	0	N/A
	ASA vs. *K*	0	N/A	−0.3	N/A	N/A	−0.2	N/A	0	N/A
	DS vs. *K*	−0.5	N/A	−0.7	N/A	N/A	−0.4	N/A	0	N/A
	SF vs. *K*	0.5	N/A	0.5	N/A	N/A	0	N/A	0	N/A

(*Continued*)

Petitioners' Exhibit 1021
Nokia of America Corp., et al. v. KT Corporation, et al.
Case No. IPR2025-00036; U.S. Patent No. 11,627,631
Page 918 of 1122

Table 11.5 (Continued)

Channel Model Parameters		InH		UMi			UMa		RMa	
		LoS	NLoS	LoS	NLoS	Outdoor-to-Indoor	LoS	NLoS	LoS	NLoS
Delay distribution		Exponential	Exponential	Exponential	Exponential	Exponential	Exponential	Exponential	Exponential	Exponential
AoD and AoA distribution		Laplacian		Wrapped Gaussian			Wrapped Gaussian		Wrapped Gaussian	
Delay scaling parameter r_τ		3.6	3	3.2	3	2.2	2.5	2.3	3.8	1.7
Cross-polarization ratio (dB)	μ	11	10	9	8.0	9	8	7	12	7
Number of clusters		15	19	12	19	12	12	20	11	10
Number of rays per cluster		20	20	20	20	20	20	20	20	20
Cluster ASD		5	5	3	10	5	5	2	2	2
Cluster ASA		8	11	17	22	8	11	15	3	3
Per cluster shadowing standard deviation ζ (dB)		6	3	3	3	4	3	3	3	3
Correlation distance (m)	DS	8	5	7	10	10	30	40	50	36
	ASD	7	3	8	10	11	18	50	25	30
	ASA	5	3	8	9	17	15	50	35	40
	SF	10	6	10	13	7	37	50	37	120
	K	4	N/A	15	N/A	N/A	12	N/A	40	N/A

Petitioners' Exhibit 1021
Nokia of America Corp., et al. v. KT Corporation, et al.
Case No. IPR2025-00036; U.S. Patent No. 11,627,631
Page 919 of 1122

Table 11.6 IMT-Advanced Primary Module Path Loss Models (f_c Is in GHz, All Distances Are in Meters, and a Hexagonal Cell Layout Is Assumed) [14]

Scenario		Path Loss PL (dB)	Shadow Fading Standard Deviation (dB)	Applicability Range (m)/Antenna Height (m)
InH	LoS	$16.9\ \log_{10}(d) + 32.8 + 20\ \log_{10}(f_c)$	$\sigma = 3$	$3 < d < 100$ $h_{BS} = 3 - 6$ $h_{MS} = 1 - 2.5$
	NLoS	$43.3\ \log_{10}(d) + 11.5 + 20\ \log_{10}(f_c)$	$\sigma = 4$	$10 < d < 150$ $h_{BS} = 3 - 6$ $h_{MS} = 1 - 2.5$
UMi	LoS	$22.0\ \log_{10}(d) + 28.0 + 20\ \log_{10}(f_c)$ $40\ \log_{10}(d_1) + 7.8 - 18\ \log_{10}(h'_{BS}) -$ $18\ \log_{10}(h'_{MS}) + 2\ \log_{10}(f_c)$	$\sigma = 3$	$10 < d_1 < d'_{BP}$ $d'_{BP} < d_1 < 5000$ $h_{BS} = 10; h_{MS} = 1.5$
	NLoS	$36.7\ \log_{10}(d) + 22.7 + 26\ \log_{10}(f_c)$	$\sigma = 4$	$10 < d < 2000$ $h_{BS} = 3$ $h_{MS} = 1 - 2.5$
	Outdoor-to-indoor	$PL_b + PL_{tw} + PL_{in}$ $PL_b = PL_{B1}(d_{out} + d_{in})$; $PL_{tw} = 20$; $PL_{in} = 0.5 d_{in}$	$\sigma = 7$	$10 < d_{out} + d_{in} < 1000$ $0 < d_{in} < 25$
UMa	LoS	$22.0\ \log_{10}(d) + 28.0 + 20\ \log_{10}(f_c)$ $40.0\ \log_{10}(d_1) + 7.8 - 18.0\ \log_{10}(h'_{BS})$ $- 18.0\ \log_{10}(h'_{MS}) + 2.0\ \log_{10}(f_c)$	$\sigma = 4$	$10 < d_1 < d'_{BP}$ $d'_{BP} < d_1 < 5000$ $h_{BS} = 25; h_{MS} = 1.5$
	NLoS	$161.04 - 7.1\ \log_{10}(W) + 7.5\ \log_{10}(h)$ $-(24.37 - 3.7(h/h_{BS})^2)\ \log_{10}(h_{BS})$ $+ (43.42 - 3.1\ \log_{10}(h_{BS}))\ (\log_{10}(d) - 3)$ $+ 20\ \log_{10}(f_c) - (3.2\ (\log_{10}(11.75 h_{MS}))^2 - 4.97$	$\sigma = 6$	$10 < d < 5000\ h_{BS} = 25;\ h_{MS} = 1.5;$ $W = 20; h = 205 < h < 50;$ $5 < W < 50\ 10 < h_{BS} < 150;$ $1 < h_{MS} < 10$

(*Continued*)

Petitioners' Exhibit 1021
Nokia of America Corp., et al. v. KT Corporation, et al.
Case No. IPR2025-00036; U.S. Patent No. 11,627,631
Page 920 of 1122

Table 11.6 (Continued)

Scenario		Path Loss PL (dB)	Shadow Fading Standard Deviation (dB)	Applicability Range (m)/Antenna Height (m)
RMa	LoS	$PL_1 = 20\ \log_{10}(40\pi d f_c/3) + \min(0.03h^{1.72}, 10)$ $\log_{10}(d) - \min(0.044h^{1.72}, 14.77) + 0.002\log_{10}(h)d$ $PL_2 = PL_1(d_{BP}) + 40\ \log_{10}(d/d_{BP})$	$\sigma = 4$ $\sigma = 6$	$10 < d < d_{BP}\ d_{BP} < d < 10000$ $h_{BS} = 35; h_{MS} = 1.5\ W = 20; h = 5$
	NLoS	$161.04 - 7.1\ \log_{10}(W) + 7.5\ \log_{10}(h)$ $-(24.37 - 3.7(h/h_{BS})^2)\log_{10}(h_{BS})$ $+ (43.42 - 3.1\ \log_{10}(h_{BS}))(\log_{10}(d) - 3)$ $+ 20\ \log_{10}(f_c) - (3.2\ (\log_{10}(11.75\ h_{MS}))^2 - 4.97)$	$\sigma = 8$	$10 < d < 5000\ h_{BS} = 35;$ $h_{MS} = 1.5W = 20; h = 5$

Petitioners' Exhibit 1021
Nokia of America Corp., et al. v. KT Corporation, et al.
Case No. IPR2025-00036; U.S. Patent No. 11,627,631
Page 921 of 1122

outdoor scenario, PL_{tw} is penetration loss through the wall, PL_{in} denotes the loss inside, d_{out} is the distance from the BS to the wall next to the MS location, d_{in} denotes the perpendicular distance from the wall to the MS which is evenly distributed between 0 and 25 m, and the break point distance is defined as $d_{BP} = 2\pi h_{BS} h_{MS} f_c / c$.

Spatial correlation is often said to degrade the performance of multi-antenna systems and impose a limit on the number of antennas that can effectively fit in a small mobile device. This seems intuitive as the spatial correlation decreases the number of independent channels that can be created by precoding. When modeling spatial correlation, it is useful to employ the Kronecker model, where the correlation between transmit and receive antennas are assumed independent and separable. This model is reasonable when the main scattering appears close to the antenna arrays and has been validated by outdoor and indoor measurements. Assuming Rayleigh fading, the Kronecker model means that the channel matrix can be represented as $\mathbf{H} = \mathbf{R}_{RX}^{1/2} \mathbf{H}_{channel} (\mathbf{R}_{TX}^{1/2})^T$ where the elements of $\mathbf{H}_{channel}$ are independent and identically distributed as circular symmetric complex Gaussian with zero-mean and unit variance. The important part of the model is that $\mathbf{H}_{channel}$ is pre-multiplied by the receive-side spatial correlation matrix $\mathbf{R}_{RX}$ and post-multiplied by the transmit-side spatial correlation matrix $\mathbf{R}_{TX}$. Equivalently, the channel matrix can be expressed as $\mathbf{H} \sim Z(0, \mathbf{R}_{TX} \otimes \mathbf{R}_{RX})$ where $\otimes$ denotes the Kronecker product.

Using the Kronecker model, the spatial correlation depends directly on the eigenvalue distributions of the correlation matrices $\mathbf{R}_{RX}$ and $\mathbf{R}_{TX}$. Each eigenvector represents a spatial direction of the channel and its corresponding eigenvalue describes the average channel/signal gain in this direction. For the transmit-side, the correlation matrix $\mathbf{R}_{TX}$ describes the average gain in a spatial transmit direction, while the receive-side correlation matrix $\mathbf{R}_{RX}$ describes a spatial receive direction. High spatial correlation is represented by a large eigenvalue spread in $\mathbf{R}_{TX}$ or $\mathbf{R}_{RX}$, implying that some spatial directions are statistically stronger than the others. On the other hand, low spatial correlation is represented by a small eigenvalue spread in $\mathbf{R}_{TX}$ or $\mathbf{R}_{RX}$, which implies that almost the same signal gain can be expected from all spatial directions [57].

Let us now focus on a specific case of downlink transmission from a base station to a mobile station. Denoting the nth snapshot of the spatial correlation matrices at the BS and the MS by $\mathbf{R}_{BS,n}$ and $\mathbf{R}_{MS,n}$, the per-tap spatial correlation is determined as the Kronecker product[7] of the BS and MS's antenna correlation matrices:

[7]Given an $m \times n$ matrix $\mathbf{A}$ and a $p \times q$ matrix $\mathbf{B}$, the Kronecker product $\mathbf{C} = \mathbf{A} \otimes \mathbf{B}$, also called the matrix direct product, is an $mp \times nq$ matrix with elements defined by $c_{\alpha\beta} = a_{ij} b_{kl}$, where $\alpha \equiv p(i-1) + k$ and $\beta \equiv q(j-1) + l$. The matrix direct product provides the matrix of the linear transformation induced by the vector space tensor product of the original vector spaces. More precisely, suppose that operators $S: V_1 \to W_1$ and $T: V_2 \to W_2$ are given by $S(x) = Ax$ and $T(y) = By$. Then $S \otimes T: V_1 \otimes V_2 \to W_1 \otimes W_2$ is determined by $S \otimes T(x \otimes y) = (Ax) \otimes (By) = (A \otimes B)(x \otimes y)$[57].

Petitioners' Exhibit 1021
Nokia of America Corp., et al. v. KT Corporation, et al.
Case No. IPR2025-00036; U.S. Patent No. 11,627,631
Page 922 of 1122

$$\mathbf{R}_n = \mathbf{R}_{\mathrm{BS},n} \otimes \mathbf{R}_{\mathrm{MS},n} \tag{11.27}$$

We denote the number of receive antennas by N_{RX} and the number of transmit antennas by the N_{TX}. If cross-polarized antennas are present at the receiver, it is assumed that $N_{\mathrm{RX}}/2$ receive antennas have the same polarization, while the remaining $N_{\mathrm{RX}}/2$ receive antennas have orthogonal polarization. Likewise, if cross-polarized antennas are present at the transmitter, it is assumed that the $N_{\mathrm{TX}}/2$ transmit antennas have the same polarization; while the remaining $N_{\mathrm{TX}}/2$ transmit antennas have orthogonal polarization. It is further assumed that the antenna arrays are composed of pairs of collocated antennas with orthogonal polarization. With these assumptions, the per-tap channel correlation is determined as follows:

$$\mathbf{R}_n = \mathbf{R}_{\mathrm{BS},n} \otimes \mathbf{\Gamma} \otimes \mathbf{R}_{\mathrm{MS},n} \tag{11.28}$$

Where $\mathbf{R}_{\mathrm{MS},n}$ is an $N_{\mathrm{RX}} \times N_{\mathrm{RX}}$ matrix if all receive antennas have the same polarization, or an $N_{\mathrm{RX}}/2 \times N_{\mathrm{RX}}/2$ matrix if the receive antennas are cross-polarized. Likewise, $\mathbf{R}_{\mathrm{BS},n}$ is an $N_{\mathrm{TX}} \times N_{\mathrm{TX}}$ matrix if all the transmit antennas have the same polarization, or an $N_{\mathrm{TX}}/2 \times N_{\mathrm{TX}}/2$ matrix if the transmit antennas are cross-polarized. Matrix $\mathbf{\Gamma}$ is a cross-polarization matrix based on the cross-polarization defined in the cluster-delay-line models. Matrix $\mathbf{\Gamma}$ is a 2×2 matrix if cross-polarized antennas are used at the transmitter or at the receiver. It is a 4×4 matrix if cross-polarized antennas are used at both the transmitter and the receiver.

Table 11.7 defines the correlation matrices for the eNB and UE in E-UTRA with a different number of transmit/receive antennas at each entity [4].

For the scenarios with more antennas at either eNB, UE, or both, the channel spatial correlation matrix can be expressed as the Kronecker product of $\mathbf{R}_{\mathrm{eNB}}$ and $\mathbf{R}_{\mathrm{UE}}$ according to $\mathbf{R}_{\mathrm{spatial}} = \mathbf{R}_{\mathrm{eNB}} \otimes \mathbf{R}_{\mathrm{UE}}$. The parameters α and β for different antenna correlation types are given in Table 11.8.

Table 11.7 eNB/UE Correlation Matrix [4,58]

	Number of Antennas		
Entity	**1**	**2**	**4**
eNB	$\mathbf{R}_{\mathrm{eNB}} = 1$	$\mathbf{R}_{\mathrm{eNB}} = \begin{pmatrix} 1 & \alpha \\ \alpha^* & 1 \end{pmatrix}$	$\mathbf{R}_{\mathrm{eNB}} = \begin{pmatrix} 1 & \alpha^{1/9} & \alpha^{4/9} & \alpha \\ \alpha^{1/9*} & 1 & \alpha^{1/9} & \alpha^{4/9} \\ \alpha^{4/9*} & \alpha^{1/9*} & 1 & \alpha^{1/9} \\ \alpha^* & \alpha^{4/9*} & \alpha^{1/9*} & 1 \end{pmatrix}$
UE	$\mathbf{R}_{\mathrm{UE}} = 1$	$\mathbf{R}_{\mathrm{UE}} = \begin{pmatrix} 1 & \beta \\ \beta^* & 1 \end{pmatrix}$	$\mathbf{R}_{\mathrm{UE}} = \begin{pmatrix} 1 & \beta^{1/9} & \beta^{4/9} & \beta \\ \beta^{1/9*} & 1 & \beta^{1/9} & \beta^{4/9} \\ \beta^{4/9*} & \beta^{1/9*} & 1 & \beta^{1/9} \\ \beta^* & \beta^{4/9*} & \beta^{1/9*} & 1 \end{pmatrix}$

Petitioners' Exhibit 1021
Nokia of America Corp., et al. v. KT Corporation, et al.
Case No. IPR2025-00036; U.S. Patent No. 11,627,631
Page 923 of 1122

Table 11.8 Values of α and β for Different Antenna Correlations [4]

Low Correlation		Medium Correlation		High Correlation	
α	β	α	β	α	β
0	0	0.3	0.9	0.9	0.9

Table 11.9 EPA/EVA/ETA Multipath Power Delay Profiles [4,58]

Tap Excess Delay (ns)	Relative Power (dB)	Tap Excess Delay (ns)	Relative Power (dB)	Tap Excess Delay (ns)	Relative Power (dB)
EPA		EVA		ETU	
0	0.0	0	0.0	0	−1.0
30	−1.0	30	−1.5	50	−1.0
70	−2.0	150	−1.4	120	−1.0
90	−3.0	310	−3.6	200	0.0
110	−8.0	370	−0.6	230	0.0
190	−17.2	710	−9.1	500	0.0
410	−20.8	1090	−7.0	1600	−3.0
–	–	1730	−12.0	2300	−5.0
–	–	2510	−16.9	5000	−7.0

Table 11.10 Delay Profiles of LTE Channel Models [4,58]

Model	Number of Channel Taps	RMS Delay Spread (ns)	Maximum Tap Excess Delay (ns)
EPA	7	45	410
EVA	9	357	2510
ETU	9	991	5000

The multipath fading channel model specifies three different delay profiles which are representative of low, medium, and high delay spread environments, that is, extended pedestrian A (EPA) model, extended vehicular A (EVA) model, and extended typical urban (ETU) model [52]. The multipath delay profiles for these channels are shown in Table 11.9 and the associated number of channel taps, RMS delay spread, and maximum tap excess delays are provided in Table 11.10. In addition to a multipath delay profile, a maximum Doppler frequency is specified for each multipath fading propagation condition as follows: EPA 5 Hz ($\nu_{\max} = 5$ Hz), EVA 70 Hz ($\nu_{\max} = 70$ Hz), and ETU 300 Hz ($\nu_{\max} = 300$ Hz).

Petitioners' Exhibit 1021
Nokia of America Corp., et al. v. KT Corporation, et al.
Case No. IPR2025-00036; U.S. Patent No. 11,627,631
Page 924 of 1122

11.9 LTE-Advanced link-level and system-level performance

The 3GPP LTE-Advanced was a candidate for IMT-Advanced whose performance was fully characterized based on the ITU-R defined evaluation methodology. The following sections summarize the performance characterization of the 3GPP LTE-Advanced as part of the IMT-Advanced submission.

11.9.1 Cell spectral efficiency and cell-edge spectral efficiency

Cell spectral and cell-edge spectral efficiencies were evaluated through extensive simulations conducted by a number of 3GPP member companies. The simulation results were reported based on specific 3GPP LTE-Advanced configurations, that is, downlink and uplink MU-MIMO, downlink and uplink CoMP, and uplink SU-MIMO, for both FDD and TDD duplex schemes in various test scenarios. It must be noted that during LTE Rel-10 development and prior to IMT-Advanced submission, CoMP was an incomplete study item in 3GPP and no standard technique was specified for CoMP at that time; therefore, CoMP simulation results presented in this chapter, which were provided by a number of 3GPP member companies, did not use standard techniques and may not agree with each other in various conditions. Nevertheless, the CoMP study item was later completed and CoMP was specified as a feature in LTE Rel-11 specifications that will be discussed in the next chapter [11].

The performance differences among contributing sources can be explained by implementation-specific functionalities at the transmitter and the receiver that are not explicitly specified by the standard, such as receiver type, scheduling algorithms, and error modeling. In the results reported for the downlink, the size of the control channel (L OFDM symbols) and the number of the MBSFN subframes are the factors that affect the overhead. Note that in 3GPP submission, the control channel overhead is statically modeled, that is, the downlink control channels occupy a fixed number of OFDM symbols irrespective of the number of users, although it is expected that the size of the physical downlink control channel dynamically varies with the number of active users in the cell. In the MBSFN subframes and in the MBSFN region, there are no cell-specific reference signals (CRS), which effectively reduces the overhead.

Channel estimation and receiver types are the factors that affect the demodulation performance. Availability of CSI at the eNB is the assumption that impacts the transmit signal processing at the eNB for MU-MIMO and CoMP schemes. In the tables for the uplink, physical uplink control channel bandwidth is the factor that affects the overhead. Each value in Tables 11.11 and 11.12 is obtained as an average of all samples provided by different companies. The results suggest that the requirements are fulfilled with $L = 3$ corresponding to the largest overhead except for the system bandwidth of 1.4 MHz where the requirements cannot be met. If the control overhead

Petitioners' Exhibit 1021
Nokia of America Corp., et al. v. KT Corporation, et al.
Case No. IPR2025-00036; U.S. Patent No. 11,627,631
Page 925 of 1122

Table 11.11 LTE-Advanced Downlink Cell Spectral and Cell-Edge Spectral Efficiencies [2,6]

Scheme and Antenna Configuration	Test Environment	Duplex Scheme	ITU-R Requirement Cell Spectral Efficiency/Cell-Edge Spectral Efficiency	Cell Spectral Efficiency (bits/s/Hz/cell)			Cell-Edge Spectral Efficiency (bits/s/Hz)		
				$L = 1$	$L = 2$	$L = 3$	$L = 1$	$L = 2$	$L = 3$
Rel-8 SU-MIMO 4 × 2(A)	InH	FDD	3/0.1	4.8	4.5	4.1	0.23	0.21	0.19
MU-MIMO 4 × 2 (C)			3/0.1	6.6	6.1	5.5	0.26	0.24	0.22
Rel-8 SU-MIMO 4 × 2 (A)		TDD	3/0.1	4.7	4.4	4.1	0.22	0.20	0.19
MU-MIMO 4 × 2 (C)			3/0.1	6.7	6.1	5.6	0.24	0.22	0.20
MU-MIMO 4 × 2 (C)	UMi	FDD	2.6/0.075	3.5	3.2	2.9	0.10	0.096	0.087
MU-MIMO 4 × 2 (A)			2.6/0.075	3.4	3.1	2.8	0.12	0.11	0.099
CS/CB-CoMP 4 × 2 (C)			2.6/0.075	3.6	3.3	3.0	0.11	0.099	0.089
JP-CoMP 4 × 2 (C)			2.6/0.075	4.5	4.1	3.7	0.14	0.13	0.12
MU-MIMO 8 × 2 (C/E)			2.6/0.075	4.2	3.8	3.5	0.15	0.14	0.13
MU-MIMO 4 × 2 (C)		TDD	2.6/0.075	3.5	3.2	3.0	0.11	0.096	0.089
MU-MIMO 4 × 2 (A)			2.6/0.075	3.2	2.9	2.7	0.11	0.10	0.095

(*Continued*)

Petitioners' Exhibit 1021
Nokia of America Corp., et al. v. KT Corporation, et al.
Case No. IPR2025-00036; U.S. Patent No. 11,627,631
Page 926 of 1122

Table 11.11 (Continued)

Scheme and Antenna Configuration	Test Environment	Duplex Scheme	ITU-R Requirement Cell Spectral Efficiency/Cell-Edge Spectral Efficiency	Cell Spectral Efficiency (bits/s/Hz/cell)			Cell-Edge Spectral Efficiency (bits/s/Hz)		
				$L = 1$	$L = 2$	$L = 3$	$L = 1$	$L = 2$	$L = 3$
CS/CB-CoMP 4 × 2 (C)			2.6/0.075	3.6	3.3	3.1	0.10	0.092	0.086
JP-CoMP 4 × 2 (C)			2.6/0.075	4.6	4.2	3.9	0.10	0.092	0.085
MU-MIMO 8 × 2 (C/E)			2.6/0.075	4.2	3.9	3.6	0.12	0.11	0.099
MU-MIMO 4 × 2 (C)	UMa	FDD	2.2/0.06	2.8	2.6	2.4	0.079	0.073	0.066
CS/CB-CoMP 4 × 2 (C)			2.2/0.06	2.9	2.6	2.4	0.081	0.074	0.067
JP-CoMP 4 × 2 (A)			2.2/0.06	3.0	2.7	2.5	0.080	0.073	0.066
CS/CB-CoMP 8 × 2 (C)			2.2/0.06	3.8	3.5	3.2	0.10	0.093	0.084
MU-MIMO 4 × 2 (C)		TDD	2.2/0.06	2.9	2.6	2.4	0.079	0.071	0.067
CS/CB-CoMP 4 × 2 (C)			2.2/0.06	2.9	2.6	2.4	0.083	0.075	0.070
JP-CoMP 4 × 2 (C)			2.2/0.06	3.6	3.3	3.1	0.090	0.082	0.076
CS/CB-CoMP 8 × 2 (C/E)			2.2/0.06	3.7	3.3	3.1	0.10	0.093	0.087

Petitioners' Exhibit 1021
Nokia of America Corp., et al. v. KT Corporation, et al.
Case No. IPR2025-00036; U.S. Patent No. 11,627,631
Page 927 of 1122

Rel-8 SU-MIMO 4 × 2 (C)	RMa	FDD	1.1/0.04	2.3	2.1	1.9	0.081	0.076	0.069
Rel-8 SU-MIMO 4 × 2 (A)			1.1/0.04	2.1	2.0	1.8	0.067	0.063	0.057
MU-MIMO 4 × 2 (C)			1.1/0.04	3.9	3.5	3.2	0.11	0.099	0.090
MU-MIMO 8 × 2 (C)			1.1/0.04	4.1	3.7	3.4	0.13	0.12	0.11
Rel-8 SU-MIMO 4 × 2 (C)		TDD	1.1/0.04	2.0	1.9	1.8	0.072	0.067	0.063
Rel-8 SU-MIMO 4 × 2 (A)			1.1/0.04	1.9	1.7	1.6	0.057	0.053	0.049
MU-MIMO 4 × 2 (C)			1.1/0.04	3.5	3.2	3.0	0.098	0.089	0.083
MU-MIMO 8 × 2 (C/E)			1.1/0.04	4.0	3.6	3.4	0.12	0.11	0.10
Rel-8 Single-Layer BF 8 × 2 (E)			1.1/0.04	2.5	2.3	2.1	0.11	0.10	0.093

Table 11.12 3GPP LTE-Advanced Uplink Cell Spectral and Cell-Edge Spectral Efficiencies [2,6]

Scheme and Antenna Configuration	Test Environment	Duplex Scheme	ITU-R Requirement Cell Spectral Efficiency/Cell-Edge Spectral Efficiency	Cell Spectral Efficiency (bits/s/Hz/cell)	Cell-edge Spectral Efficiency (bits/s/Hz)
Rel-8 SIMO 1 × 4 (A)	InH	FDD	2.25/0.07	3.3	0.23
Rel-8 SIMO 1 × 4 (C)			2.25/0.07	3.3	0.24
Rel-8 MU-MIMO 1 × 4 (A)			2.25/0.07	5.8	0.42
SU-MIMO 2 × 4 (A)			2.25/0.07	4.3	0.25
Rel-8 SIMO 1 × 4 (A)		TDD	2.25/0.07	3.1	0.22
Rel-8 SIMO 1 × 4 (C)			2.25/0.07	3.1	0.23
Rel-8 MU-MIMO 1 × 4 (A)			2.25/0.07	5.5	0.39
SU-MIMO 2 × 4 (A)			2.25/0.07	3.9	0.25
Rel-8 SIMO 1 × 4 (C)	UMi	FDD	1.8/0.05	1.9	0.073
Rel-8 MU-MIMO 1 × 4 (A)			1.8/0.05	2.5	0.077
MU-MIMO 2 × 4 (A)			1.8/0.05	2.5	0.086
Rel-8 SIMO 1 × 4 (C)		TDD	1.8/0.05	1.9	0.070
Rel-8 MU-MIMO 1 × 4 (A)			1.8/0.05	2.3	0.071
MU-MIMO 2 × 4 (A)			1.8/0.05	2.8	0.068
MU-MIMO 1 × 8 (E)			1.8/0.05	3.0	0.079

Petitioners' Exhibit 1021
Nokia of America Corp., et al. v. KT Corporation, et al.
Case No. IPR2025-00036; U.S. Patent No. 11,627,631
Page 929 of 1122

Rel-8 SIMO 1 × 4 (C)	UMa	FDD	1.4/0.03	1.5	0.062
CoMP 1 × 4 (A)			1.4/0.03	1.7	0.086
CoMP 2 × 4 (C)			1.4/0.03	2.1	0.099
Rel-8 SIMO 1 × 4 (C)		TDD	1.4/0.03	1.5	0.062
CoMP 1 × 4 (C)			1.4/0.03	1.9	0.090
CoMP 2 × 4 (C)			1.4/0.03	2.0	0.097
MU-MIMO 1 × 8 (E)			1.4/0.03	2.7	0.076
Rel-8 SIMO 1 × 4 (C)	RMa	FDD	0.7/0.015	1.8	0.082
Rel-8 MU-MIMO 1 × 4 (A)			0.7/0.015	2.2	0.097
CoMP 2 × 4 (A)			0.7/0.015	2.3	0.13
Rel-8 SIMO 1 × 4 (C)		TDD	0.7/0.015	1.8	0.080
Rel-8 MU-MIMO 1 × 4 (A)			0.7/0.015	2.1	0.093
CoMP 2 × 4 (A)			0.7/0.015	2.5	0.15
MU-MIMO 1 × 8 (E)			0.7/0.015	2.6	0.10

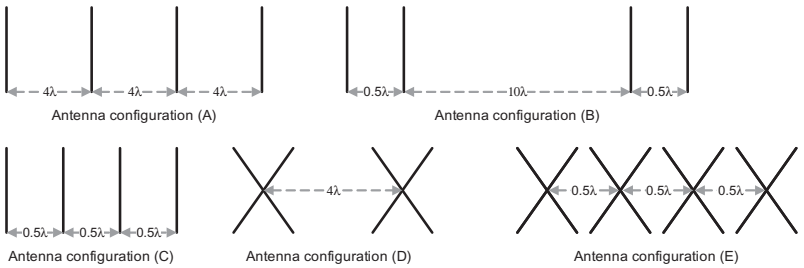


FIGURE 11.9

Illustration of antenna configurations used in LTE evaluations.

assumption is relaxed, that is the number of active users decreases, $L = 1, 2$ can be considered and thereby the performance can be further improved. The tables show that LTE Rel-8 with SU-MIMO 4×2 configuration can already fulfill the ITU-R requirements. The tables also show that further performance improvements can be achieved using additional technical features.

In the following tables, various antenna configurations have been utilized. There are four or eight transmit antennas with the following configurations: (A) uncorrelated co-polarized, that is, co-polarized antennas are four-wavelength apart; (B) grouped co-polarized, that is, two groups of co-polarized antennas where there is a 10-wavelength distance between the center of each group and 0.5-wavelength separation between antennas within each group; (C) correlated and co-polarized, that is, 0.5-wavelength between antennas; (D) uncorrelated and cross-polarized, that is, columns with $\pm 45^{\circ}$ linearly polarized antennas and separated by four wavelengths; and (E) correlated and cross-polarized, that is, columns with $\pm 45^{\circ}$ linearly polarized antennas and separated by 0.5-wavelengths. These configurations are illustrated in Figure 11.9.

The downlink and uplink cell spectral and cell-edge spectral efficiencies in various test environments for the TDD and FDD duplex schemes are shown in Tables 11.11 and 11.12, respectively. In these tables, the acronyms "JP-CoMP," "CS-CoMP," and "CB-CoMP" refer to joint processing, coordinated scheduling, and coordinated beamforming multi-point transmission schemes, respectively. The joint processing refers to a CoMP scheme where data is available at each of the geographically separated transmission points and physical downlink shared channel (PDSCH) transmission occurs from multiple points, whereas coordinated scheduling/beamforming is an alternative CoMP technique where data is only available at serving cell and data transmission is from that point, but user scheduling/beamforming decisions are made with coordination among different cells.

11.9.2 VoIP capacity

While most of the modern packet-switched air-interfaces do not specify voice codecs, calculation of the VoIP capacity requires explicit assumptions about a particular voice codec and its parameters, such as the frame rate, real-time

Petitioners' Exhibit 1021
Nokia of America Corp., et al. v. KT Corporation, et al.
Case No. IPR2025-00036; U.S. Patent No. 11,627,631
Page 931 of 1122

transport protocol (RTP) payload size, and discontinuous transmission (DTX) capability. The VoIP capacity of LTE-Advanced was calculated assuming use of AMR 12.2 kbps codec with a 50% speech activity factor. It was further assumed that the percentage of users in outage is less than 2% where a user is defined to have experienced outage if less than 98% of the VoIP packets have been delivered successfully to the user within a one-way radio access delay bound of 50 ms. The assumptions and the configuration parameters used in the system-level simulations for VoIP are as described in Table 11.13. The number of active VoIP users was calculated through extensive system-level simulations that were conducted by a number of 3GPP member companies. Table 11.14 shows the VoIP capacity results in the indoor, micro-cellular, macro-cellular, and high-speed test environments for FDD and TDD duplex schemes. The results suggest that LTE-Advanced satisfies the ITU-R requirements in various deployment scenarios. The antenna configurations are illustrated in Figure 11.9.

11.9.3 Mobility

IMT-Advanced specified four mobility classes based on UE speeds as follows: Stationary (0 km/h); Pedestrian (0 to 10 km/h); Vehicular (10 to 120 km/h); and High-speed vehicular (120 to 350 km/h). In order to evaluate LTE-Advanced against mobility requirement, the methodology that is set forth in Report ITU-R M.2135-1 [14] is followed, where in the first step the system-level simulation is performed for each test environment in the uplink to obtain the uplink SINR distribution (see Figure 11.10). From the uplink SINR distribution the 50% point of CDF is obtained for each test environment. In the second step, link-level simulation is conducted to generate the spectral efficiency versus SINR curves for each test environment. The spectral efficiency values include the effect of control channel overhead from the uplink system-level simulations for each test scenario. The mobility requirement in each mobility class is satisfied, if the uplink traffic channel

Table 11.13 Assumptions for VoIP Capacity Calculation [14,26]

Parameter	Value
Codec	AMR12.2 kbps mode
Encoder frame length	20 ms
VAF	50%
Payload	Active: 33 bytes (octet-aligned mode) Inactive: 7 bytes SID packet is sent every 160 ms during silence intervals
Protocol overhead with compressed header	10 bits + padding (RTP-pre-header) 4 bytes (RTP/UDP/IP) 2 bytes (radio link control (RLC)/ security) 16 bits (CRC)

Petitioners' Exhibit 1021
Nokia of America Corp., et al. v. KT Corporation, et al.
Case No. IPR2025-00036; U.S. Patent No. 11,627,631
Page 932 of 1122

Table 11.14 LTE-Advanced VoIP Capacity [6]

Antenna Configuration	Duplex Scheme	Test Environment	ITU-R Requirement	VoIP Capacity (Active Users/MHz/Cell)
Antenna configuration (A)	FDD	InH	50	140
		UMi	40	80
		UMa	40	68
		RMa	30	91
Antenna configuration (C)		InH	50	131
		UMi	40	75
		UMa	40	69
		RMa	30	94
Antenna configuration (A)	TDD	InH	50	137
		UMi	40	74
		UMa	40	65
		RMa	30	86
Antenna configuration (C)		InH	50	130
		UMi	40	74
		UMa	40	67
		RMa	30	92

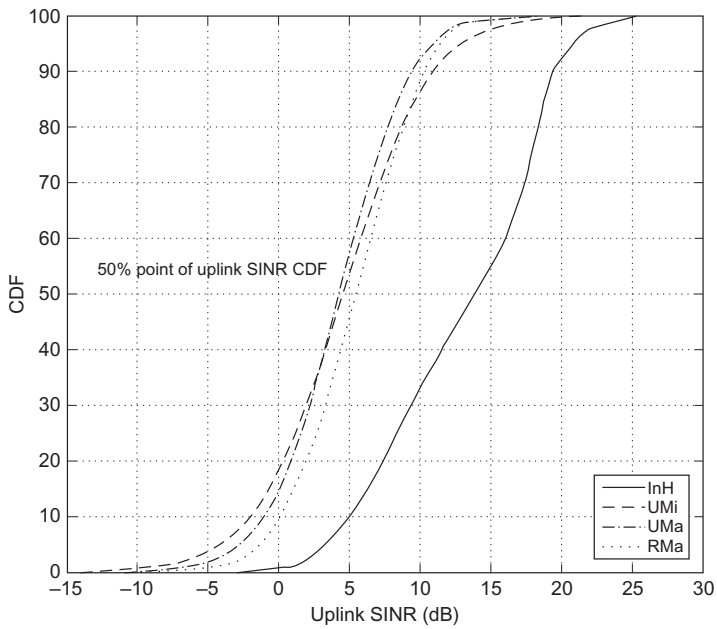


FIGURE 11.10

Statistical distribution of the uplink SINR in various test environments [6].

Petitioners' Exhibit 1021
Nokia of America Corp., et al. v. KT Corporation, et al.
Case No. IPR2025-00036; U.S. Patent No. 11,627,631
Page 933 of 1122

link-level data rate, normalized by bandwidth, is greater than the minimum requirements shown in Table 11.15, when the user is moving at the maximum speed in that mobility class in each of the test environments [14].

It can be concluded from Table 11.15 that the evaluated LTE-Advanced configurations can fulfill the ITU-R requirements concerning the mobility in all test environments.

11.9.4 Peak spectral efficiency

The peak spectral efficiency of LTE-Advanced is calculated based on the following assumptions: 20 MHz bandwidth; one OFDM symbol for downlink control signaling; CRS corresponding to one and four antenna ports; UE-specific reference signals corresponding to 24 and zero resource elements per resource-block pair. It was further assumed that physical broadcast channel and synchronization sequences occupy a total of 564 (Rel-10 MU-MIMO/CoMP with six MBSFN subframes per 10 ms) and 528 (Rel-8 downlink SU-MIMO) resource elements per radio frame for downlink eight- and four-layer spatial multiplexing, respectively. In addition, DL/UL configuration 1 (2 DL subframes, 1 special subframe, 2 uplink subframes) and special-subframe configuration 4 (12 DwPTS, 1 GP, 1 UpPTS, UpPTS is used for sounding reference signal transmission) are assumed for the TDD mode. The results shown in Table 11.16 suggest that LTE Rel-8 already fulfills the ITU-R requirements for downlink peak spectral efficiency. The table also shows the additional performance improvement that can be achieved using advanced features, for example, downlink eight-layer spatial multiplexing.

The uplink peak spectral efficiency is calculated assuming 20 MHz bandwidth, PUCCH occupying two pairs of resource blocks per subframe, and physical random access channel consuming six resource-block pairs per radio frame. The same TDDDL/UL and special-subframe configurations are assumed as for the downlink peak spectral efficiency calculation. Table 11.16 shows that the extension of LTE Rel-8 with two-layer spatial multiplexing can fulfill the ITU-R requirement in the uplink.

11.9.5 User-plane/control-plane latency and handover interruption time

The LTE user-plane one-way access latency for a scheduled UE consists of fixed node-processing delays, which include radio frame alignment and 1 ms transmission time interval (TTI) duration. Using the latency calculation model shown in Figure 11.11, and assuming that the number of HARQ processes is 8 for the FDD mode, the one-way latency is given as $T_{\text{USER-PLANE}} = 4 + 8p$ where p is the probability of HARQ retransmissions or the error probability of the first HARQ retransmission. While the minimum latency of $T_{\text{USER-PLANE}} = 4$ ms is achieved for $p = 0$, a more realistic value of $T_{\text{USER-PLANE}} = 4.8$ ms is obtained for $p = 0.1$.

Petitioners' Exhibit 1021
Nokia of America Corp., et al. v. KT Corporation, et al.
Case No. IPR2025-00036; U.S. Patent No. 11,627,631
Page 934 of 1122

Table 11.15 3GPP LTE Uplink Link-Level Simulation Results for the Mobility Requirements [2,6,14]

Path Loss Model (LoS/NLoS)	Duplex Scheme	Test Environment	ITU-R Requirements	Median SINR (dB)	Uplink Spectral Efficiency (bits/s/Hz)
Antenna configuration 1 × 4 (NLoS)	FDD	InH	1.0	13.89	2.56
		UMi	0.75	4.54	1.21
		UMa	0.55	4.30	1.08
		RMa	0.25	5.42	1.22
Antenna configuration 1 × 4 (LoS)		InH	1.0	13.89	3.15
		UMi	0.75	4.54	1.42
		UMa	0.55	4.30	1.36
		RMa	0.25	5.42	1.45
Antenna configuration 1 × 4 (NLoS)	TDD	InH	1.0	13.89	2.63
		UMi	0.75	4.54	1.14
		UMa	0.55	4.30	0.95
		RMa	0.25	5.42	1.03
Antenna configuration 1 × 4 (LoS)		InH	1.0	13.89	3.11
		UMi	0.75	4.54	1.48
		UMa	0.55	4.30	1.36
		RMa	0.25	5.42	1.38

Table 11.16 3GPP LTE-Advanced Peak Spectral Efficiency [2]

Scheme	Duplex Scheme	Direction	Spectral Efficiency (bits/s/Hz)
ITU-R requirement	FDD	Downlink	15
Rel-8 four-layer spatial multiplexing			16.3
Eight-layer spatial multiplexing			30.6
ITU-R requirement		Uplink	6.75
Two-Layer spatial multiplexing			8.4
Four-Layer spatial multiplexing			16.8
ITU-R requirement	TDD	Downlink	15
Rel-8 four-layer spatial multiplexing			16.0
Eight-Layer spatial multiplexing			30.0
ITU-R requirement		Uplink	6.75
Two-Layer spatial multiplexing			8.1
Four-Layer spatial multiplexing			16.1

The user-plane one-way latency for a scheduled UE in the TDD mode consists of fixed node-processing delays, radio frame alignment, and TTI duration. The latency component can be seen in Figure 11.11 for the downlink and uplink. Using the latency model shown in Figure 11.11, the total one-way processing time is 2.5 ms, T_{FA} is the radio frame alignment which depends on various configurations of the TDD frame structure, and the TTI duration is 1 ms, hence, the user-plane latency of the TDD mode can be written as $T_{USER\text{-}PLANE} = 3.5 + T_{FA} + pT_{RTT}$ where T_{RTT} is the average HARQ round-trip time and p is the error probability of the first HARQ transmission.

Table 11.17 shows the user-plane latency component breakdown in downlink and uplink for different TDD DL/UL configurations when $p = 0.1$ is assumed. It is shown that in all cases, LTE can meet the ITU-R requirements for user-plane latency.

The above analysis further shows that the 5 ms user-plane latency requirement can be satisfied in the TDD mode in uplink and downlink using the DL/UL configuration 6 only when $p = 0$ is assumed.

In order to calculate the control-plane latency, the model shown in Figure 11.12 is used. The transition from the RRC_IDLE to the RRC_CONNECTED state in LTE comprises several steps that are shown in sequential order in Table 11.18.

While the results of the analysis suggest that LTE Rel-8 satisfies the ITU-R requirements, using the improved features and protocols introduced in later releases would allow reduction of the control-plane latency to 50 ms. Note that since the non-access stratum (NAS) setup process can be executed in parallel with the RRC connection setup, it does not appear in the total latency calculation.

Petitioners' Exhibit 1021
Nokia of America Corp., et al. v. KT Corporation, et al.
Case No. IPR2025-00036; U.S. Patent No. 11,627,631
Page 936 of 1122

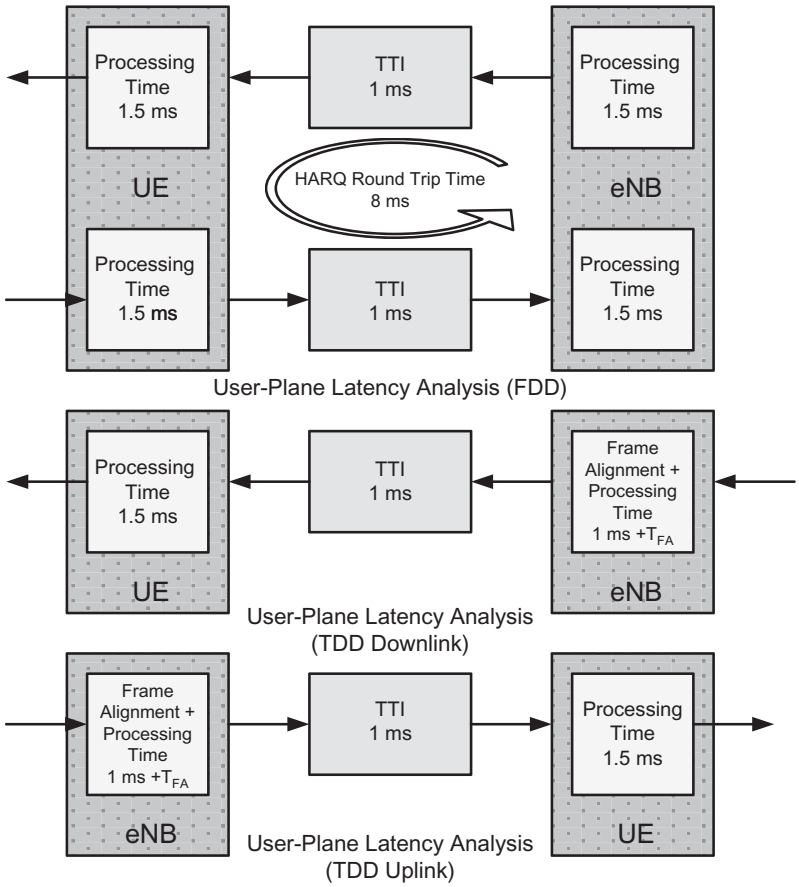


FIGURE 11.11

LTE user-plane latency calculation model [2].

The analysis shown in Table 11.18 shows that any of the LTE configurations can fulfill the ITU-R requirements related to control-plane latency.

The calculation of the user-plane latency was carried out for synchronized (or prescheduled) UEs. In the case where the UE is not prescheduled or when the UE is required to synchronize in order to be allocated uplink resources, reduced RACH scheduling period, shorter PUCCH cycle, and reduced processing delays can be applied to satisfy the control-plane latency requirements.

The LTE-Advanced general handover procedure is based on that of LTE Rel-8, which was described in Chapter 4, and is illustrated in Figure 11.13. The model shown in the figure has been used for calculation of the handover interruption time. As shown in the figure, once the handover command has been processed by

Petitioners' Exhibit 1021
Nokia of America Corp., et al. v. KT Corporation, et al.
Case No. IPR2025-00036; U.S. Patent No. 11,627,631
Page 937 of 1122

Table 11.17 TDD Mode User-Plane Latency Analysis with 10% HARQ Retransmission Probability [2]

Step	Procedure	Direction	DL/UL Configuration						
			0	**1**	**2**	**3**	**4**	**5**	**6**
1	eNB processing delay (ms)	Downlink	1	1	1	1	1	1	1
2	Frame alignment (ms)		1.7	1.1	0.7	1.1	0.8	0.6	1.4
3	TTI duration (ms)		1	1	1	1	1	1	1
4	UE processing delay (ms)		1.5	1.5	1.5	1.5	1.5	1.5	1.5
5	HARQ retransmission (ms)		0.1×10	0.1×10.2	0.1×9.8	0.1×10.5	0.1×11.6	0.1×12.4	0.1×11.2
	Total one-way delay (ms)		6.2	5.62	5.18	5.65	5.46	5.34	6.02
1	UE processing delay (ms)	Uplink	1	1	1	1	1	1	1
2	Frame alignment (ms)		1.1	1.7	2.5	3.3	4.1	5	1.4
3	TTI duration (ms)		1	1	1	1	1	1	1
4	eNB processing delay (ms)		1.5	1.5	1.5	1.5	1.5	1.5	1.5
5	HARQ retransmission (ms)		0.1×11.6	0.1×10	0.1×10	0.1×10	0.1×10	0.1×10	0.1×11.5
	Total one-way delay (ms)		5.76	6.2	7	7.8	8.6	9.5	6.05

Petitioners' Exhibit 1021
Nokia of America Corp., et al. v. KT Corporation, et al.
Case No. IPR2025-00036; U.S. Patent No. 11,627,631
Page 938 of 1122

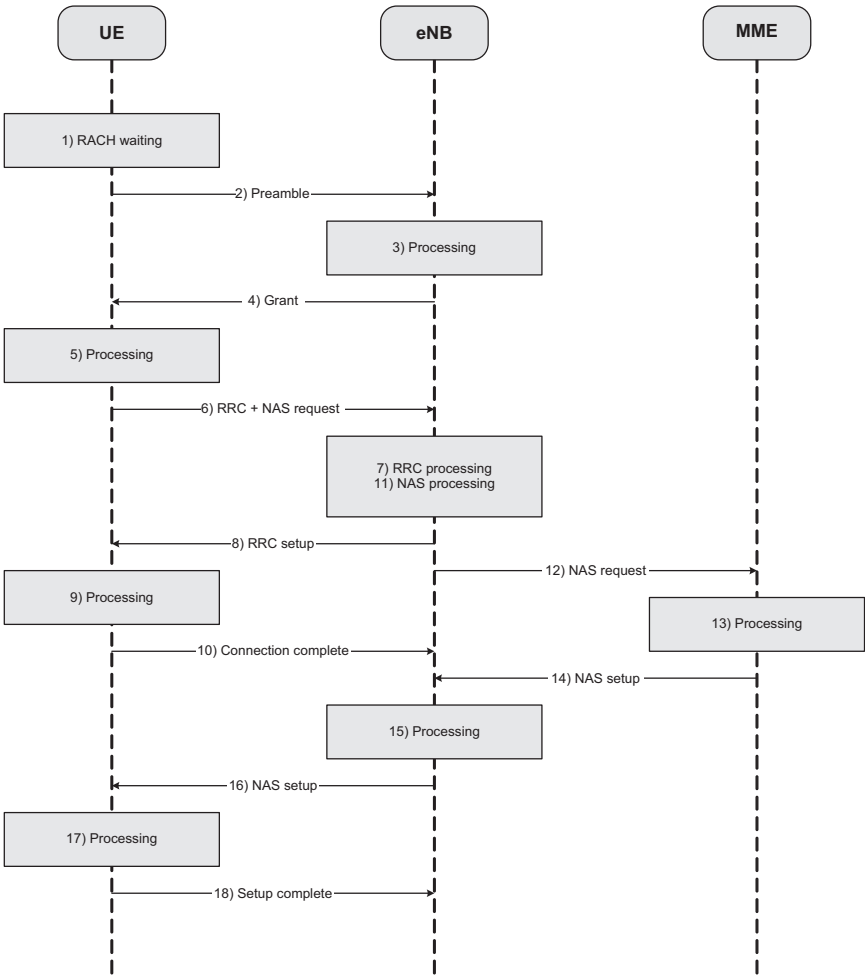


FIGURE 11.12

Analysis of RRC_IDLE to RRC_CONNECTED state transition in 3GPP LTE [2].

the UE, the UE detaches from the source eNB and stops receiving data. This marks a point in time where the user-plane connectivity is interrupted. The UE then performs frequency synchronization with the target eNB depending on whether the target cell is operating on the same carrier frequency as the current serving cell. Since the UE has already identified and measured the target cell, the corresponding delay will be negligible. The UE then performs downlink synchronization. Although baseband and RF timing alignments are part of the delay budget, since the UE has already acquired downlink synchronization with the target

Petitioners' Exhibit 1021
Nokia of America Corp., et al. v. KT Corporation, et al.
Case No. IPR2025-00036; U.S. Patent No. 11,627,631
Page 939 of 1122

Table 11.18 Analysis of Control-Plane Latency Components [2]

Step	Procedure	Processing Time (ms)
1	Average delay due to RACH scheduling period (1 ms RACH cycle)	0.5
2	RACH preamble	1
3–4	Preamble detection and transmission of random access response (time between the end RACH transmission and UE's reception of scheduling grant and timing adjustment)	3
5	UE processing delay (decoding of scheduling grant, timing alignment, and C-RNTI assignment + L1 encoding of RRC connection request)	5
6	Transmission of RRC and NAS request	1
7	Processing delay in eNB (L2 and RRC)	4
8	Transmission of RRC connection setup and UL grant	1
9	Processing delay in the UE (L2 and RRC)	12
10	Transmission of RRC connection setup complete	1
11	Processing delay in eNB (Uu→S1-C)	–
12	S1-C transfer delay	–
13	MME Processing Delay (including UE context retrieval of 10 ms)	–
14	S1-C transfer delay	–
15	Processing delay in eNB (S1-C→Uu)	4
16	Transmission of RRC security mode command and connection reconfiguration + TTI alignment	1.5
17	Processing delay in UE (L2 and RRC)	16
	Control-plane delay	50

cell in conjunction with previous measurements and can relate the target cell downlink timing to the source cell downlink timing with a time offset, the corresponding delay is going to be less than 1 ms. The data forwarding between the two eNBs is initiated before the UE moves and establishes connection to the target cell, and because the backhaul is faster than the radio interface, forwarded data is already awaiting transmission in the target cell when the user-plane with the target cell is reestablished. The latter delay component thereby does not affect the overall delay.

Based on the analysis shown in Table 11.19, the minimum handover interruption time is 10.5 ms for the FDD mode and 12.5 ms for the TDD mode. Note that this delay does not depend on the frequency of the target cell as long as the cell frequency has already been measured by the UE during the measurement gap.

As explained earlier, the minimum handover interruption time is 10.5 ms for FDD and 12.5 ms for TDD regardless of the frequency of the target cell and

Petitioners' Exhibit 1021
Nokia of America Corp., et al. v. KT Corporation, et al.
Case No. IPR2025-00036; U.S. Patent No. 11,627,631
Page 940 of 1122

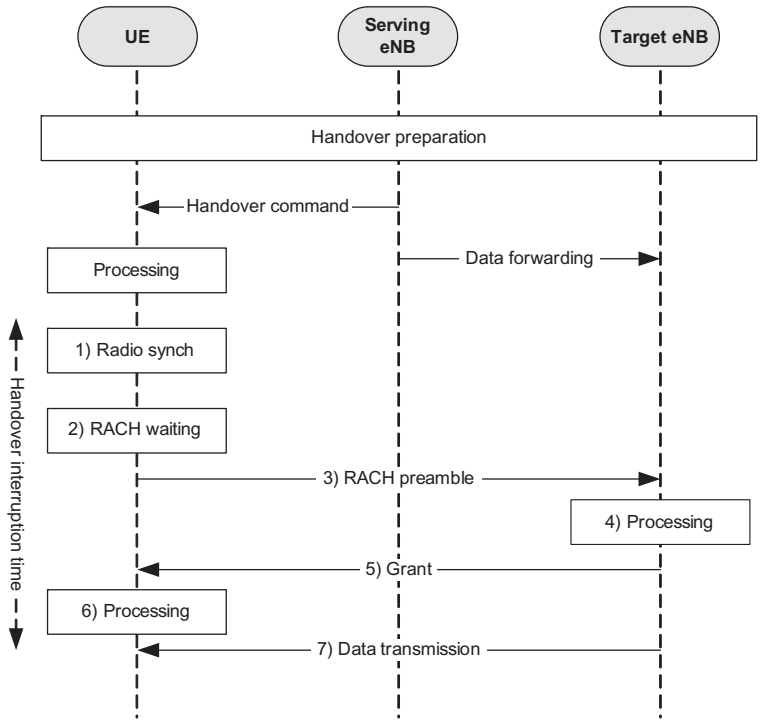


FIGURE 11.13

Model for calculation of handover interruption time [2,10].

measurements. Note that in the FDD mode, the average delay due to RACH scheduling is 0.5 ms assuming 1 ms RACH periodicity, whereas in the TDD mode, the minimum delay is obtained with configuration 0 (i.e., six normal uplink subframes); however, when taking into account the average waiting time for a downlink subframe to receive the random access response and to initiate transmission of downlink data, TDD configuration 1 (with random access preambles in special subframes) offers the shortest handover interruption time.

11.9.6 Estimation of the L1/L2 overhead

The downlink L1/L2 overhead of the LTE-Advanced includes different types of reference signals, that is, CRS transmitted within each resource block, UE-specific demodulation reference signals (DM-RS), and the reference signals that are specifically utilized in the estimation of CSI (CSI-RS). The overhead channels further include control signaling channels that are transmitted in the first L OFDM symbols ($L = 1$, 2, or 3) of each subframe ($L = 4$ in the case of 1.4 MHz bandwidth system bandwidth) and the synchronization signals, as

Petitioners' Exhibit 1021
Nokia of America Corp., et al. v. KT Corporation, et al.
Case No. IPR2025-00036; U.S. Patent No. 11,627,631
Page 941 of 1122

Table 11.19 Breakdown of Handover Interruption Time [2]

Step	Procedure	FDD Mode Processing Time (ms)	TDD Mode Processing Time (ms)
1	Radio synchronization to the target cell	1	1
2	Average delay due to RACH scheduling period assuming 1 ms periodicity	0.5	2.5
3	RACH preamble	1	1
4–5	Preamble detection and transmission of random access response (time between the end RACH transmission and UE's reception of scheduling grant and timing adjustment)	5	5
6	Decoding of scheduling grant and timing alignment	2	2
7	Transmission of downlink data	1	1
	Handover interruption time	10.5	12.5

well as physical broadcast control channel. The protocol headers corresponding to layer-2 sub-layers (MAC/RLC/PDCP) were also included in the self-evaluation results. The overhead due to CRS and L1/L2 control signaling depend on the number of antenna ports and the number of OFDM symbols used for the control region. The number of overhead resource elements per resource-block pair (168 resource elements in total) and the corresponding relative overhead is shown in Table 11.20 for non-MBSFN and MBSFN subframes. The overhead (due to L1/L2 control signaling and CRS) in Table 11.20 is shown in terms of the number of resource elements per resource-block pair and in percentages.

In the case of MBSFN subframes, the overhead is reduced. All subframes in a radio frame are assumed to be either regular or MBSFN type in overhead estimation. The total overhead depends on the fraction of MBSFN subframes. In the self-evaluation results, a fraction of 0% and 60% was assumed. The overhead due to UE-specific reference signals depends on the number of UE-specific antenna-ports and is 12 resource elements (7.1%) for one and two antenna ports, and 24 resource elements (14.3%) for three to eight antenna ports. Note that the overhead due to UE-specific reference signals is only present in resource blocks in which UE-specific reference signals are transmitted.

The relative overhead due to synchronization signals and physical broadcast channel depends on the operation bandwidth. A total of 528 resource elements per 10 ms radio frame are used for the synchronization signals and physical broadcast channel for four CRS antenna ports, corresponding to approximately 0.6% and 0.3% overhead for 10 and 20 MHz operating bandwidth, respectively.

Petitioners' Exhibit 1021
Nokia of America Corp., et al. v. KT Corporation, et al.
Case No. IPR2025-00036; U.S. Patent No. 11,627,631
Page 942 of 1122

Table 11.20 LTE-Advanced L1/L2 Overhead [2,6]

Control-Region Size	Subframe Type	FDD Duplex Scheme Number of Cell-Specific Antenna Ports			TDD Duplex Scheme Number of Cell-Specific Antenna Ports		
		1	2	4	1	2	4
$L = 1$	Regular subframes	18 (10.7%)	24 (14.3%)	32 (19.0%)	18 (10.7%)	24 (14.3%)	32 (19.0%)
$L = 2$		30 (17.9%)	36 (21.4%)	40 (23.9%)	30 (17.9%)	36 (21.4%)	40 (23.9%)
$L = 3$		42 (25%)	48 (28.6%)	52 (31.0%)	42 (25%)	48 (28.6%)	52 (31.0%)
$L = 1$	MBSFN subframes	12 (7.1%)	12 (7.1%)	12 (7.1%)	12 (7.1%)	12 (7.1%)	12 (7.1%)
$L = 2$		24 (14.2%)	24 (14.2%)	24 (14.2%)	24 (14.2%)	24 (14.2%)	24 (14.2%)
$L = 3$		36 (21.4%)	36 (21.4%)	36 (21.4%)	36 (21.4%)	36 (21.4%)	36 (21.4%)

Petitioners' Exhibit 1021
Nokia of America Corp., et al. v. KT Corporation, et al.
Case No. IPR2025-00036; U.S. Patent No. 11,627,631
Page 943 of 1122

The overhead due to protocol headers is proportional to data packet size and is approximately 2.7%, 0.51%, and 0.32% for physical-layer data rates of 1, 10, and 100 Mbps, respectively. This overhead was not included in the self-evaluation results. The relative overhead due to CSI-RS depends on the number of antennas and periodicity. In a typical case, it is about 0.12% per antenna port (0.48% for four antenna ports and 0.96% for eight antenna ports). The relative overhead due to UE-specific reference signals is estimated at approximately 7% in case of rank 1 and rank 2 transmission, and 14% for rank 3 to rank 8 transmission.

In the uplink, the L1/L2 overhead includes the demodulation reference symbols that are used in uplink channel estimation for coherent demodulation and are transmitted once every 0.5 ms. It further includes the sounding reference signal used for uplink channel state estimation at the eNB and the L1/L2 control signaling transmitted on configurable amount of resource blocks, as well as L2 control overhead due to random access, uplink time-alignment control, power headroom reports, and buffer-status reports. The L2 overhead associated with the PDU headers (MAC/RLC/PDCP) is further taken into consideration in the total overhead calculation. The amount of overhead due to DM-RS is approximately 14%, corresponding to one SC-FDMA symbol in each slot. The relative overhead is estimated independent of the rank of the transmission. The amount of SRS overhead depends on the sounding reference signal transmission interval and the bandwidth. Using a 10 ms SRS transmission interval and full-band SRS, the relative overhead is approximately 0.7%. The amount of uplink resources reserved for random access depends on the PRACH configuration, for example, a typical case with PRACH preamble format 0 is six resource blocks per radio frame, resulting in a relative overhead of 0.6%, 1.2%, and 2.4% for a channel bandwidth of 20, 10, and 5 MHz, respectively.

The relative overhead due to uplink timing-alignment control depends on the configuration and the number of active UEs within a cell. The absolute overhead is typically less than 32 bits/s per UE. The amount of overhead for buffer-status reports depends on the configuration; assuming a continuous data and reporting interval of 10−20 ms, the absolute overhead is 0.8−3.2 kbps. The amount of overhead due to protocol headers depends on the data packet size and is approximately 2.7%, 0.51%, and 0.32% for L1 data rates of 1, 10, and 100 Mbps, respectively. The above overhead calculations are based on a normal cyclic prefix length. In the case of MBSFN subframes in the TDD mode, all the subframes are assumed to be of MBSFN type in the overhead estimation. The total overhead depends on the fraction of MBSFN subframes. In self-evaluation results, a fraction of 0% and 33% has been assumed for a TDDDL:UL ratio of 3:2 (i.e., TDDDL/UL configuration 1).

In the TDD mode, the relative overhead due to synchronization signals and physical broadcast channel depends on the operation bandwidth and DL/UL configuration. A total of 528 resource elements per 10 ms radio frame are used for the synchronization signals and the broadcast channel when using four CRS antenna ports. For a DL:UL ratio of 3:2, the latter overhead translates into

Petitioners' Exhibit 1021
Nokia of America Corp., et al. v. KT Corporation, et al.
Case No. IPR2025-00036; U.S. Patent No. 11,627,631
Page 944 of 1122

approximately 1.0% and 0.5%, for 10 and 20 MHz operation bandwidth, respectively. The amount of SRS overhead depends on the SRS transmission interval and bandwidth as well as the usage of UpPTS in the special subframe. For a DL:UL ratio of 3:2 with four DL/UL switching points per 10 ms radio frame, the SRS transmission interval of 5 ms and full-band SRS within UpPTS, the relative overhead is approximately 3.45%. The amount of uplink resources reserved for random access depends on the configuration of the random access channel. In a typical case with a DL:UL ratio of 3:2 and PRACH preamble format 0, i.e., six resource blocks per radio frame are used for the PRACH, resulting in a relative overhead of 1.4%, 2.8%, and 5.6% for channel bandwidth of 20, 10, and 5 MHz, respectively.

11.9.7 Link budget

The LTE-Advanced link budget under various deployment scenarios specified by ITU-R was evaluated as part of the IMT-Advanced submission (Table 11.21). Table 11.21 summarizes the link budget of the TDD mode. It is shown that LTE-Advanced control and data channel coverage meets the IMT-Advanced link budget requirements.

11.9.8 Evaluation of LTE-Advanced against LTE Rel-10 requirements

This section provides the self-evaluation results of LTE-Advanced against LTE Rel-10 requirements [3], where the target values for cell spectral efficiency and cell-edge spectral efficiency are specified for 3GPP case 1 channel model [4] with 2×2, 4×2, and 4×4 antenna configurations in the downlink, and 1×2 and 2×4 antenna configurations in the uplink. Table 11.22 shows the downlink/uplink cell and cell-edge spectral efficiency results under 3GPP Case 1 configuration for the FDD and TDD modes. The results suggest that, if LTE Rel-8 is extended with MU-MIMO 4×2 in the downlink, the LTE Rel-10 performance targets can be fulfilled. The table also includes the advanced features by which the performance can be further improved. The uplink performance results indicate that LTE Rel-8 SIMO and LTE-Advanced CoMP, SU-MIMO, and MU-MIMO schemes can fulfill the LTE Rel-10 requirements. In 3GPP case 1 scenario, the center frequency is 2.0 GHz, the transmission bandwidth is 2×10 MHz for the FDD mode and 20 MHz for the TDD mode, inter-site distance is 500 m, the penetration loss is 20 dB, and all users are assumed moving at 3 km/h.

11.10 Miscellaneous evaluations

In order to investigate the usage and advantages of various LTE downlink MIMO schemes in realistic deployment scenarios, link-level and system-level simulations were performed under certain assumptions [47–49]. In order to

Table 11.21 LTE-Advanced Link Budget in Various Deployment Scenarios for the TDD Mode [2,6,15]

Parameter	InH		UMi		UMa		RMa	
	Downlink	Uplink	Downlink	Uplink	Downlink	Uplink	Downlink	Uplink
System Configuration								
Carrier frequency (GHz)	3.4	3.4	2.5	2.5	2.0	2.0	0.8	0.8
BS antenna heights (m)	6	6	10	10	25	25	35	35
MS antenna heights (m)	1.5	1.5	1.5	1.5	1.5	1.5	1.5	1.5
Cell area reliability for control channels	95%	95%	95%	95%	95%	95%	95%	95%
Cell area reliability for control channels	90%	90%	90%	90%	90%	90%	90%	90%
Transmission bit rate for control channel (kbps)	46.93	1.60	44.80	1.60	44.80	1.60	44.80	1.60
Transmission bit rate for data channel (Mbps)	4.65	0.37	2.25	0.074	2.25	0.074	2.25	0.074
Target packet error rate for control channels	1%	1%	1%	1%	1%	1%	1%	1%
Target packet error rate for data channels	10%	10%	10%	10%	10%	10%	10%	10%
Spectral efficiency (bits/s/Hz) for data	0.23	0.52	0.22	0.21	0.22	0.21	0.22	0.21
Path loss model	NLoS	NLoS	NLoS	NLoS	NLoS	NLoS	NLoS	NLoS
Mobile speed (km/h)	3	3	3	3	30	30	120	120
Feeder loss (dB)	2	2	2	2	2	2	2	2
Transmitter								
Number of transmit antennas	2	1	2	1	2	1	2	1
Maximum transmit power per antenna (dBm)	21	21	41	24	46	24	46	24
Total transmit power (dBm)	24	21	44	24	49	24	49	24
Transmitter antenna gain (dBi)	0	0	17	0	17	0	17	0

(*Continued*)

Petitioners' Exhibit 1021
Nokia of America Corp., et al. v. KT Corporation, et al.
Case No. IPR2025-00036; U.S. Patent No. 11,627,631
Page 946 of 1122

Table 11.21 (Continued)

Parameter	InH		UMi		UMa		RMa	
	Downlink	**Uplink**	**Downlink**	**Uplink**	**Downlink**	**Uplink**	**Downlink**	**Uplink**
Transmitter array gain (dB)	0	0	0	0	0	0	0	0
Control channel power boosting gain (dB)	0	0	0	0	0	0	0	0
Data channel power loss due to pilot/control boosting (dB)	0	0	0	0	0	0	0	0
Cable, connector, combiner, body losses, etc. (dB)	3	1	3	1	3	1	3	1
Control channel EIRP (dBm)	21	20	58	23	63	23	63	23
Data channel EIRP (dBm)	21	20	58	23	63	23	63	23
Receiver								
Number of receive antennas	2	4	2	4	2	4	2	4
Receiver antenna gain (dBi)	0	0	0	17	0	17	0	17
Cable, connector, combiner, body losses, etc. (dB)	1	3	1	3	1	3	1	3
Receiver noise figure (dB)	7	5	7	5	7	5	7	5
Thermal noise density (dBm/Hz)	− 174	− 174	− 174	− 174	− 174	− 174	− 174	− 174
Receiver interference density for control channels (dBm/Hz)	− 174	− 174.9	− 169.3	− 161.7	− 169.3	− 161.7	− 169.3	− 161.7
Receiver interference density for data channels (dBm/Hz)	− 174	− 174.9	− 169.3	− 165.7	− 169.3	− 165.7	− 169.3	− 165.7
Total noise plus interference density for control channels (dBm/Hz)	− 167	− 168	− 165	− 161	− 165	− 161	− 165	− 161
Total noise plus interference density for data channels (dBm/Hz)	− 167	− 168	− 165	− 164	− 165	− 164	− 165	− 164

Occupied channel bandwidth for control channels (MHz)	36	0.18	18	0.18	18	0.18	18	0.18
Occupied channel bandwidth for data channels (MHz)	36	1.8	18	0.90	18	0.9	18	0.90
Effective noise power for control channels (dBm)	− 91	− 115	− 92	− 108	− 92	− 108	− 92	− 108
Effective noise power for control channels (dBm)	− 91	− 105	− 92	− 104	− 92	− 104	− 92	− 104
Required SNR for the control channel (dB)	− 4.2	− 10.6	− 4.2	− 10.5	− 4.2	− 10.1	− 4.2	− 9.9
Required SNR for the data channel (dB)	− 1.6	− 2.3	− 1.7	− 5.5	− 1.7	− 5.1	− 1.7	− 4.8
Receiver implementation margin (dB)	2	2	2	2	2	2	2	2
HARQ gain for control channel (dB)	0	0	0	0	0	0	0	0
HARQ gain for data channel (dB)	0.5	0.5	0.5	0.5	0.5	0.5	0.5	0.5
Receiver sensitivity for control channel (dBm)	− 94	− 124	− 95	− 117	− 95	− 117	− 95	− 116
Receiver sensitivity for data channel (dBm)	− 91	− 106	− 93	− 108	− 93	− 108	− 93	− 108
Hardware link budget for control channel (dB)	115	144	153	157	158	157	158	156
Hardware link budget for data channel (dB)	113	126	151	148	156	148	156	148
Calculation of Available Path Loss								
Lognormal shadow fading standard deviation (dB)	4	4	4	4	6	6	8	8
Shadow fading margin for control channels (dB)	2.8	2.8	3.1	3.1	5	5	5	5
Shadow fading margin for data channels (dB)	0.9	0.9	1.3	1.3	8.1	8.1	10.5	10.5
BS selection/macro-diversity gain (dB)	0	0	0	0	4.9	4.9	6.7	6.7

(*Continued*)

Table 11.21 (Continued)

Parameter	InH		UMi		UMa		RMa	
	Downlink	Uplink	Downlink	Uplink	Downlink	Uplink	Downlink	Uplink
Penetration loss (dB)	0	0	0	0	0	0	0	0
Other gains (dB)	0	0	0	0	9	9	9	9
Available path loss for control channel (dB)	111	138	149	151	0	0	0	0
Available path loss for data channel (dB)	111	122	148	144	140	136	137	134
Range/Coverage Efficiency Calculation								
Maximum range for control channel (m)	100.0	100.0	1405.2	1621.2	1175.6	978.0	3210.9	2634.3
Maximum range for data channel (m)	100.0	100.0	1383.9	1062.7	1258.4	714.4	3565.5	1975.1
Coverage area for control channel (km^2/site)	0.031	0.031	6.20	8.26	4.34	3.01	32.4	21.8
Coverage area for data channel (km^2/site)	0.031	0.031	6.02	3.55	4.97	1.60	39.9	12.3

Table 11.22 Self-Evaluation of LTE-Advanced Against LTE Rel-10 Requirements [4]

Scheme and Antenna Configuration	Direction	Duplex Scheme	Rel-10 Requirements (Cell Spectral Efficiency/Cell-Edge Spectral Efficiency)	Cell Spectral Efficiency (bits/s/Hz/cell) $L = 3$	Cell-Edge Spectral Efficiency (bits/s/Hz) $L = 3$
MU-MIMO 2 × 2 (C)	Downlink	FDD	2.4/0.07	2.69	0.090
JP-CoMP 2 × 2 (C)			2.4/0.07	2.70	0.104
MU-MIMO 4 × 2 (C)			2.6/0.09	3.43	0.118
CS/CB-CoMP 4 × 2 (C)			2.6/0.09	3.34	0.129
JP-CoMP 4 × 2 (C)			2.6/0.09	3.87	0.162
MU-MIMO 4 × 4 (C)			3.7/0.12	4.69	0.203
CS/CB-CoMP 4 × 4 (C)			3.7/0.12	4.66	0.205
JP-CoMP 4 × 4 (C)			3.7/0.12	5.19	0.269
MU-MIMO 2 × 2 (C)		TDD	2.4/0.07	2.88	0.113
JP-CoMP 2 × 2 (C)			2.4/0.07	3.15	0.130
MU-MIMO 4 × 2 (C)			2.6/0.09	3.76	0.151
JP-CoMP 4 × 2 (C)			2.6/0.09	4.64	0.199
MU-MIMO 4 × 4 (C)			3.7/0.12	4.97	0.209

(*Continued*)

Petitioners' Exhibit 1021
Nokia of America Corp., et al. v. KT Corporation, et al.
Case No. IPR2025-00036; U.S. Patent No. 11,627,631
Page 950 of 1122

Table 11.22 (Continued)

Scheme and Antenna Configuration	Direction	Duplex Scheme	Rel-10 Requirements (Cell Spectral Efficiency/Cell-Edge Spectral Efficiency)	Cell Spectral Efficiency (bits/s/Hz/cell) $L = 3$	Cell-Edge Spectral Efficiency (bits/s/Hz) $L = 3$
CS/CB-CoMP 4 × 4 (C)			3.7/0.12	5.06	0.244
JP-CoMP 4 × 4 (C)			3.7/0.12	6.61	0.330
Rel-8 SIMO 1 × 2 (C)	Uplink	FDD	1.2/0.04	1.33	0.047
CoMP 1 × 2 (C)			1.2/0.04	1.40	0.051
SU-MIMO 2 × 4 (C)			2.0/0.07	2.27	0.091
Rel-8 SIMO 1 × 2 (C)		TDD	1.2/0.04	1.24	0.045
CoMP 1 × 2 (C)			1.2/0.04	1.51	0.051
SU-MIMO 2 × 4 (C)			2.0/0.07	2.15	0.090
MU-MIMO 2 × 4 (C)			2.0/0.07	2.59	0.079

Petitioners' Exhibit 1021
Nokia of America Corp., et al. v. KT Corporation, et al.
Case No. IPR2025-00036; U.S. Patent No. 11,627,631
Page 951 of 1122

Table 11.23 System-Level Simulation Parameters (Other Parameters Same as [4] Case 1 Scenario)

Parameter/Feature	Value/Configuration
Bandwidth	1.4 MHz
Frequency	2.1 GHz
Network layout	19-cell wrap-around (tri-sector with 3D antenna models)
Scheduler algorithm	Proportional fair
Channel model	WINNER +
Receiver type	Zero-forcing
Simulation length	5000 subframes
Number of UEs/Cell	10
Path loss model	$PL = 128.1 + 37.6 \log_{10} R$
Feedback delay	Modeled

reduce the simulation run time, a 1.4 MHz system bandwidth was assumed. Figures 11.14–11.19 show snapshots of the simulation results. Table 11.23 provides the assumptions that were made in addition to baseline configuration for 3GPP case 1 that is included in 3GPP TR 36.814 [4]. The UEs are randomly dropped in the cell, but all UEs are assumed to be in the outdoor area. MIESM link-to-system mapping scheme is used in the simulations.

Figure 11.14 shows the LTE-Advanced downlink throughput versus SNR, as well as downlink spectral efficiency CDF for SISO and closed-loop spatial multiplexing (CLSM) transmission mode 4 with various antenna configurations.

The CDF of wideband SINR (geometry) with macroscopic path loss with and without additional lognormal-distributed space-correlated shadow fading is illustrated in Figure 11.15. The downlink spectral efficiency (bits/s/Hz) for various MIMO configurations with lognormal-distributed space-correlated shadow fading effect is shown in Figure 11.16. This figure shows how spectral efficiency is distributed geographically across the cells and the network. In particular, the cell-edges and the effect of MIMO to improve cell-edge performance must be noted. Figure 11.17 illustrates the sector SINR calculated with distance-dependent macroscopic path loss and additional lognormal-distributed space-correlated shadow fading. In this case we assume a SISO configuration. Figure 11.18 depicts downlink spectral efficiency (bits/s/Hz) without the effect of shadow fading. The geographical distribution of sector SINR calculated with distance-dependent macroscale path loss is shown in Figure 11.19. Figure 11.19 further shows CQI mapping across the cell. As expected, the lower modulation order and coding rates are used near cell-edges, and as we move toward the eNB, higher CQI values are reported by the UEs. The results closely correlate with the expectations of the system behavior as well as those published in the literature under given assumptions.

Petitioners' Exhibit 1021
Nokia of America Corp., et al. v. KT Corporation, et al.
Case No. IPR2025-00036; U.S. Patent No. 11,627,631
Page 952 of 1122

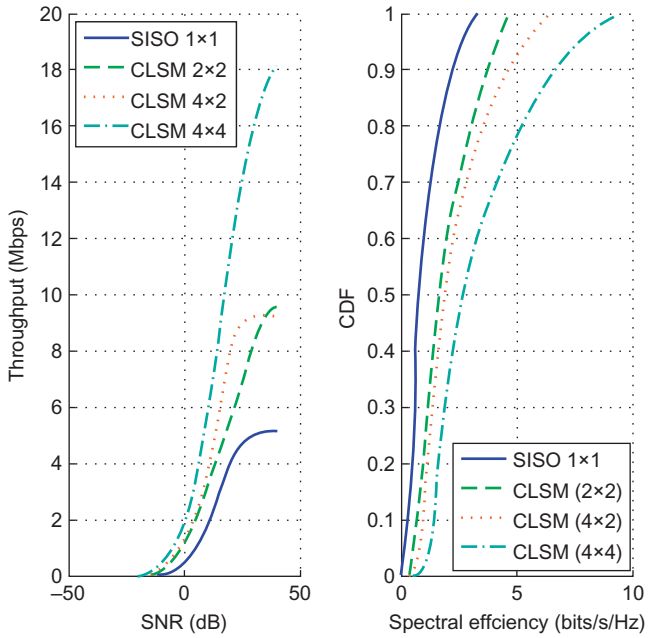


FIGURE 11.14

LTE-Advanced downlink throughput versus SNR and spectral efficiency CDF for various MIMO modes (1.4 MHz bandwidth) [45].

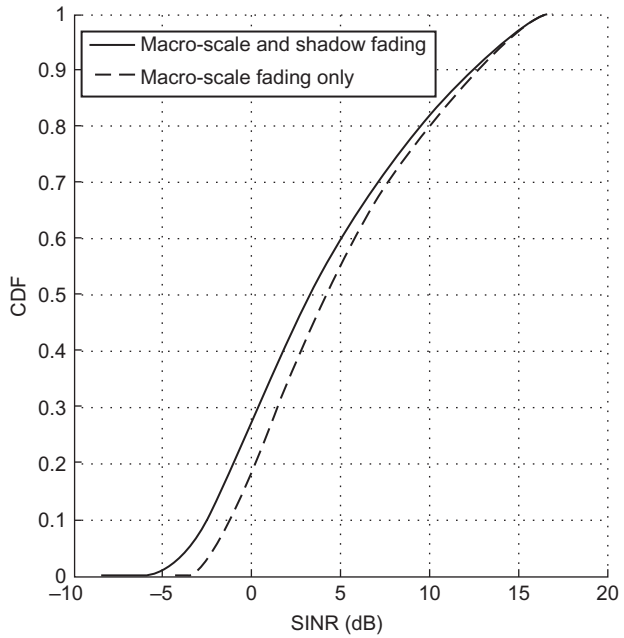


FIGURE 11.15

Distribution of downlink wideband SINR [45].

Petitioners' Exhibit 1021
Nokia of America Corp., et al. v. KT Corporation, et al.
Case No. IPR2025-00036; U.S. Patent No. 11,627,631
Page 953 of 1122

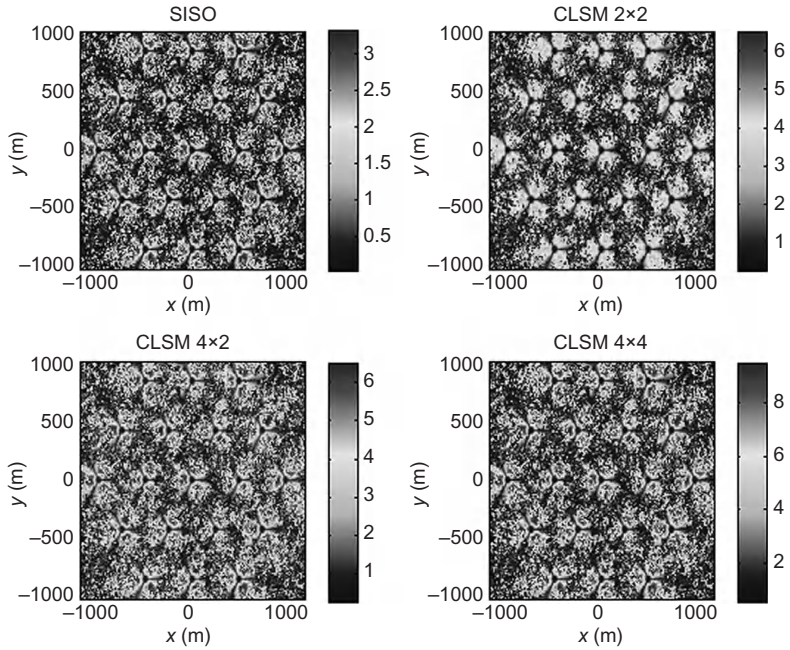


FIGURE 11.16

Spectral efficiency (bits/s/Hz) for various MIMO configurations (1.4 MHz bandwidth, with shadow fading) [45]

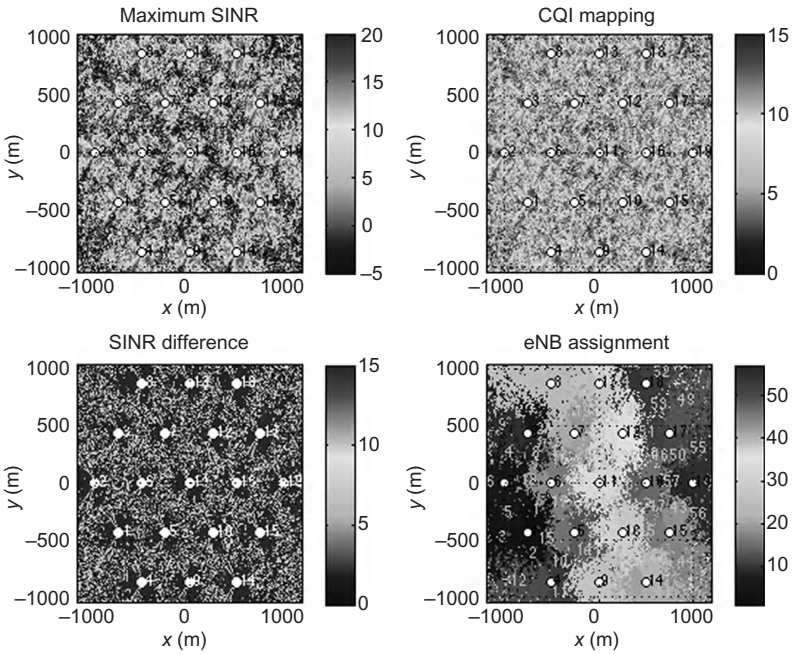


FIGURE 11.17

Sector SINR calculated with distance-dependent macroscopic path loss and additional lognormal-distributed space-correlated shadow fading (1.4 MHz bandwidth, SISO) [45]

Petitioners' Exhibit 1021
Nokia of America Corp., et al. v. KT Corporation, et al.
Case No. IPR2025-00036; U.S. Patent No. 11,627,631

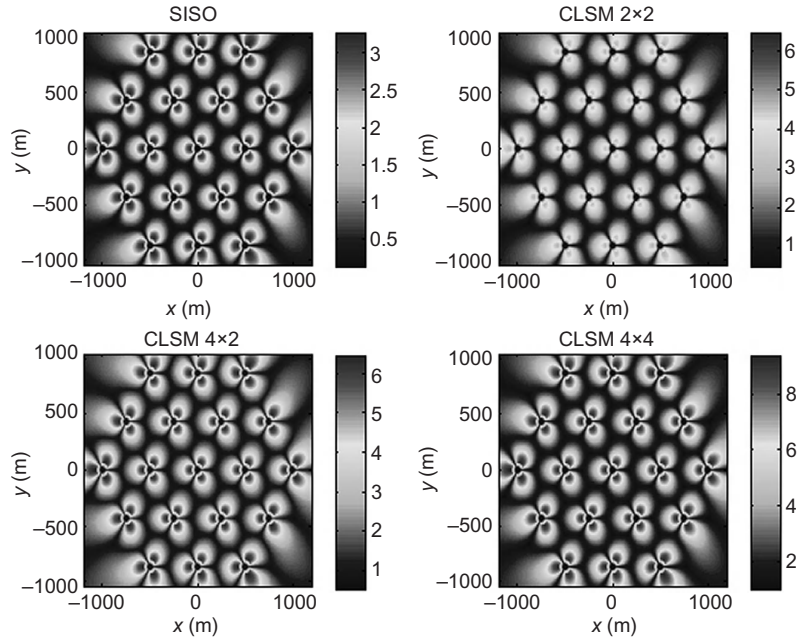


FIGURE 11.18

Spectral efficiency (bits/s/Hz) (1.4 MHz bandwidth and no shadow fading) [45]

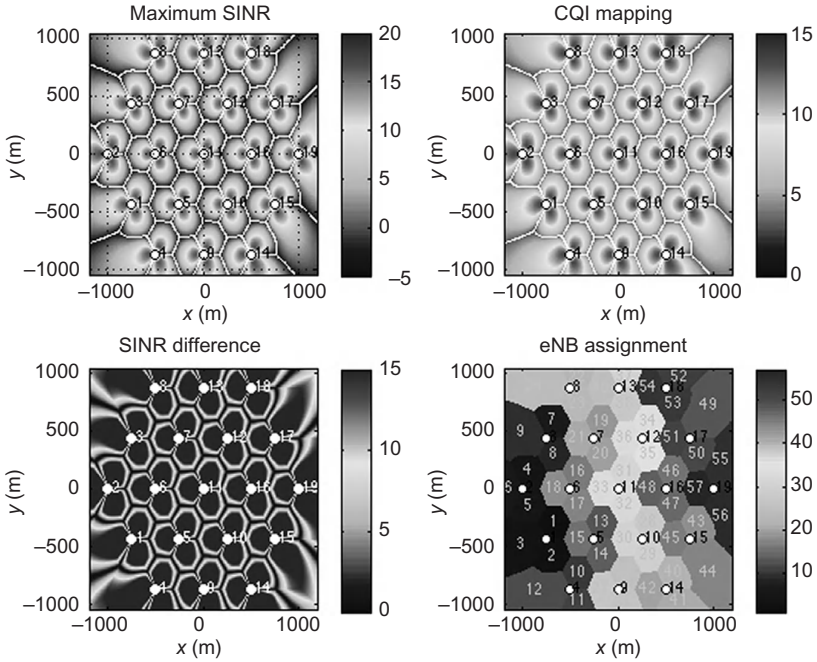


FIGURE 11.19

Sector SINR calculated with distance-dependent macro-scale path loss and CQI mapping (1.4 MHz bandwidth, SISO) [45]

Petitioners' Exhibit 1021
Nokia of America Corp., et al. v. KT Corporation, et al.
Case No. IPR2025-00036; U.S. Patent No. 11,627,631

References

3GPP Specifications

[1] 3GPP TR 25.996, Spatial Channel Model for Multiple Input Multiple Output (MIMO) Simulations (Release 11), September 2012.
[2] 3GPP TR 36.912, Feasibility Study for Further Advancements for E-UTRA (LTE-Advanced) (Release 11), September 2012.
[3] 3GPP TR 36.913, Requirements for further advancements for Evolved Universal Terrestrial Radio Access (E-UTRA) (LTE-Advanced) (Release 11), September 2012.
[4] 3GPP TR 36.814, Further Advancements for E-UTRA Physical Layer Aspects, March 2010.
[5] 3GPP TS 26.101, AMR Speech Codec Frame Structure (Release 11), September 2012.
[6] 3GPP RP-090738, TR 36.912 Annex A3: Self-Evaluation Results, September 2009.
[7] ETSI Technical Report 101 112 v3.2.0, Universal Mobile Telecommunications System (UMTS); Selection procedures for the choice of radio transmission technologies of the UMTS (UMTS 30.03 version 3.2.0), April 1998.
[8] 3GPP TS 36.211, Evolved Universal Terrestrial Radio Access (E-UTRA), Physical Channels and Modulation (Release 11), December 2012.
[9] 3GPP TS 36.212, Evolved Universal Terrestrial Radio Access (E-UTRA) Multiplexing and Channel Coding (Release 11), December 2012.
[10] 3GPP TS 36.331 Evolved Universal Terrestrial Radio Access (E-UTRA); Radio Resource Control (RRC); Protocol specification (Release 11), December 2012.
[11] 3GPP TR 36.819 Coordinated Multi-Point Operation for LTE Physical Layer Aspects (Release 11), December 2011.

ITU Specifications

[12] Report ITU-R M.2133, Requirements, evaluation criteria and submission templates for the development of IMT-Advanced, November 2008.
[13] Report ITU-R M.2134, Requirements related to technical performance for IMT-Advanced radio interface(s), November 2008.
[14] Report ITU-R M.2135-1, Guidelines for evaluation of radio interface technologies for IMT-Advanced, December 2009.
[15] Report ITU-R M.2012, Detailed specifications of the terrestrial radio interfaces of International Mobile Telecommunications Advanced (IMT-Advanced), January 2012.
[16] Recommendation ITU-R M.1225, Guidelines for evaluation of radio transmission technologies for IMT-2000, 1997.
[17] Recommendation ITU-T G.729: Coding of Speech at 8 kbit/s Using Conjugate-Structure Algebraic-Code-Excited Linear Prediction (CS-ACELP), January 2007.

Books

[18] L. Rade, Mathematics Handbook for Science and Engineering, Springer, Berlin Heidelberg, 2010.
[19] W.H. Tranter, et al., Principles of Communication Systems Simulation with Wireless Applications, Prentice Hall, 2004.
[20] J.D. Parsons, The Mobile Radio Propagation Channel, John Wiley and Sons, 2000.
[21] W.C. Jakes, Microwave Mobile Communications, John Wiley & Sons, New York, NY, 1974.
[22] M. Patzold, Mobile Fading Channels, John Wiley & Sons, 2002.
[23] A. Papoulis, Probability, Random Variables, and Stochastic Processes, fourth ed., McGraw Hill, 2002.

Petitioners' Exhibit 1021
Nokia of America Corp., et al. v. KT Corporation, et al.
Case No. IPR2025-00036; U.S. Patent No. 11,627,631
Page 956 of 1122

[24] A.T. Bharucha-Reid, Elements of the Theory of Markov Processes and Their Applications, McGraw-Hill, 1960.
[25] S. Sesia, I. Toufik, M. Baker, LTE, the UMTS Long Term Evolution: From Theory to Practice, second ed., John Willey & Sons, 2011.

Articles

[26] IEEE 802.16m-08/004r5, IEEE 802.16m Evaluation Methodology Document (EMD), March 2009.
[27] IETF RFC 3267, Real-Time Transport Protocol (RTP) Payload Format and File Storage Format for the Adaptive Multi-Rate (AMR) and Adaptive Multi-Rate Wideband (AMR-WB) Audio Codecs, J. Sjoberg, et al., June 2002.
[28] Rodriguez-Herrera, et al., Link-To-System mapping techniques using a spatial channel model, IEEE 62nd Vehicular Technology Conference 2005, vol. 3, 2005.
[29] 3GPP-3GPP2 Spatial Channel Ad-hoc Group, Spatial Channel Model Text Description, v7.0, August 2003.
[30] WINNER Project IST-4-027756, WINNER D1.1.2 v1.2, WINNER II Channel Models. <https://www.ist-winner.org>, September 2007.
[31] WINNER Project IST-2003-507581, WINNER D5.4 v. 1.4, Final Report on Link Level and System Level Channel Models. <https://www.ist-winner.org>, November 2005.
[32] WINNER Project, IST-2003-507581, WINNER D1.3 version 1.0, Final usage scenarios, June 2005.
[33] 3GPP2 TSG-C30-20061204-062A, cdma2000 Evaluation Methodology (v6), December 2006.
[34] S. Tsai, A. Soong, Effective-SNR Mapping for Modeling Frame Error Rates in Multiple-State Channels, 3GPP2-C30-20030429-010, April 2003.
[35] Digital mobile radio towards future generation systems, COST Action 231 Final Report, EUR 18957, 1999.
[36] Y. Oda, K. Tsunekawa, M. Hata, Advanced LoS path-loss model in microcellular mobile communications, IEEE Trans. Antennas Propag. 51 (2003).
[37] 3GPP R1-061001, Ericsson, LTE Channel Models and Link Simulations, March 2006.
[38] Source Code for a MATLAB/ANSI-C Implementation of the WINNER Phase I Channel Model. <https://www.ist-winner.org/phase_model.html>, August 2006.
[39] WINNER Project IST-WINNER II Deliverable D1.1.1 v1.0, WINNER II Interim Channel Models, December 2006.
[40] M. Steinbauer, A.F. Molisch, E. Bonek, The double-directional radio channel, IEEE Antennas Propag. Mag. (2001).
[41] G.J. Foschini, M.J. Gans, On limits of wireless communications in a fading environment when using multiple antennas, Wirel. Pers. Commun. 6 (1998).
[42] P. Almers, et al., Survey of channel and radio propagation models for wireless MIMO systems, EURASIP J. Wirel. Commun. Networking (2007).
[43] W. Dong, et al., Cluster Identification and Properties of Outdoor Wideband MIMO Channel, IEEE 66th Vehicular Technology Conference, VTC-2007, September 2007.
[44] R. Jain, D.M. Chiu, W. Hawe, A Quantitative Measure of Fairness and Discrimination for Resource Allocation in Shared Computer Systems, DEC Research Report TR-301, 1984.

Petitioners' Exhibit 1021
Nokia of America Corp., et al. v. KT Corporation, et al.
Case No. IPR2025-00036; U.S. Patent No. 11,627,631
Page 957 of 1122

[45] Technical University of Vienna LTE Simulators available at <http://www.nt.tuwien.ac.at/ltesimulator/>.
[46] J.C. Ikuno, M. Wrulich, M. Rupp, System level simulation of LTE networks, in: Proceedings of the 71st IEEE Vehicular Technology Conference, Taipei, Taiwan, May 2010.
[47] H. Claussen, Efficient modeling of channel maps with correlated shadow fading in mobile radio systems, September 2005.
[48] L. Hentila, et al., MATLAB implementation of the WINNER Phase II Channel Model ver1.1. <https://www.ist-winner.org/phase2model.html>, December 2007.
[49] L. Thiele, et al., Modeling of 3D Field Patterns of Down-tilted Antennas and Their Impact on Cellular Systems, in: International ITG Workshop on Smart Antennas, Berlin, Germany, February 2009.
[50] J. Olmos, et al., Link Abstraction Models Based on Mutual Information for LTE Downlink, Universitat Politècnica de Catalunya and Universidad Politécnica de Valencia, 2010.
[51] D. Martín-Sacristán, et al., LTE-Advanced System Level Simulation Platform for IMT-Advanced Evaluation, Universitat Politècnica de València, 2011.
[52] R. Jain, Channel models: a tutorial, WiMAX Forum AATG, February 2007.
[53] Confidence interval, Wikipedia, <http://en.wikipedia.org/wiki/Confidence_interval>.
[54] Markov Sequence, Wolfram MathWorld, <http://mathworld.wolfram.com/MarkovSequence.html>.
[55] H. Chernoff, A measure of asymptotic efficiency for tests of a hypothesis based on the sum of observations, Ann. Math. Stat. 23 (4) (1952).
[56] Monte Carlo method, Wikipedia, <http://en.wikipedia.org/wiki/Monte_Carlo_method>.
[57] Kronecker Product, Wolfram MathWorld, <http://mathworld.wolfram.com/KroneckerProduct.html>.
[58] Propagation Channel Models, Steepest Ascent Ltd, <http://www.steepestascent.com/content/mediaassets/html/LTE/Help/PropagationConditions.html>.

Petitioners' Exhibit 1021
Nokia of America Corp., et al. v. KT Corporation, et al.
Case No. IPR2025-00036; U.S. Patent No. 11,627,631
Page 958 of 1122

CHAPTER

Coordinated Multipoint Transmission and Reception (CoMP)

12

CHAPTER CONTENTS

12.1 Interference cancellation in cellular networks 952
12.2 Distributed antenna systems 955
12.3 Theory of CoMP operation 959
12.4 CoMP architectures 964
12.4.1 Air-interface and network support for CoMP schemes 968
12.4.2 Downlink CoMP 969
12.4.3 Uplink CoMP 971
12.4.4 CSI measurement and feedback in CoMP-enabled networks 974
12.5 Effects of X2 latency on CoMP performance 977
12.6 Performance of CoMP scenarios 978
References 981

The MIMO or network MIMO techniques are used for improving sector throughput and cell-edge throughput through multi-cell collaborative precoding, network coordinated beamforming, or inter-cell interference nulling. When a mobile station is at the cell-edge, it may be able to receive signals from multiple cell sites, and the mobile station's transmission may also be received at multiple cell sites. If the data transmission and signaling from multiple cell sites can be coordinated, the downlink performance can be significantly improved. This coordination can be similar to the interference avoidance techniques or the case where the same data is transmitted from multiple cell sites. In the uplink, since the signal can be received by multiple cell sites, the system can take advantage of coordinated multi-point reception to significantly improve the link performance. The coordinated multi-point (CoMP) transmission/reception specified in long-term evolution (LTE) Rel-11 is a method of MIMO transmission for interference reduction, which enables features such as network synchronization, cell- and user-specific reference signals, feedback of

© 2014 Elsevier Inc. All rights reserved.

Petitioners' Exhibit 1021
Nokia of America Corp., et al. v. KT Corporation, et al.
Case No. IPR2025-00036; U.S. Patent No. 11,627,631
Page 959 of 1122

multi-cell channel state information (CSI), and synchronous data transfer between the base stations that can be used for interference mitigation and to achieve macro-diversity gain [23–26].

The LTE Rel-11 specifications provide support for coordinated transmission in the downlink and coordinated reception in the uplink. The use cases include homogeneous configurations, where the points are different cells, as well as heterogeneous configurations, where a set of low-power nodes (e.g., remote radio heads (RRH) or pico-cells) are located in the geographical area served by a macro-cell. For coordinated transmission in the downlink, the signals transmitted from multiple transmission points are coordinated to improve the received strength of the desired signal at the UE or to reduce the co-channel interference. The main advantage of coordinated reception in the uplink is to ensure that the uplink signal from the UE is reliably received by the network while limiting uplink interference, taking into account the existence of multiple reception points. Note that the mechanisms discussed in this chapter apply to both FDD and TDD modes of operation [5].

In this chapter, we will discuss the theoretical and practical aspects of coordinated multipoint transmission/reception not only from the radio access network perspective, but also from the core network and backhaul point of view and will investigate whether some of the proposed schemes would realistically offer any gains when their backhaul implications and cost of implementation and operation are considered.

12.1 Interference cancellation in cellular networks

In the downlink of an LTE system, the UE often suffers from different types of interference. In the case of single-user MIMO (SU-MIMO), the signal received by the UE includes a linear combination of multiple streams, which causes inter-stream interference. On the other hand, in a multi-user MIMO (MU-MIMO) scenario, where a single cell communicates with many UEs simultaneously using the same time–frequency resources, the signal received by each UE suffers from interference caused by the signals intended for other UEs served by the same cell. This interference is known as inter-user interference. A UE at the cell-edge suffers from inter-cell interference, i.e., interference caused by the signals sent from a neighbor cell to its UEs. The neighbor cell might belong to the same site as the serving cell (intra-site) or to a different site (inter-site). Different interference cancellation schemes are applied at the receiver to mitigate the interference in the above cases. While the inter-stream interference cancellation can be performed at the UE without requiring any additional information, inter-user interference cancellation may require knowledge of the precoding matrices of the other UEs that one wishes to cancel. Moreover, the inter-cell interference cancellation needs an estimate of the channels seen between the neighbor interfering cells and the UE. The above interference models are illustrated in Figure 12.1 [26].

Petitioners' Exhibit 1021
Nokia of America Corp., et al. v. KT Corporation, et al.
Case No. IPR2025-00036; U.S. Patent No. 11,627,631
Page 960 of 1122

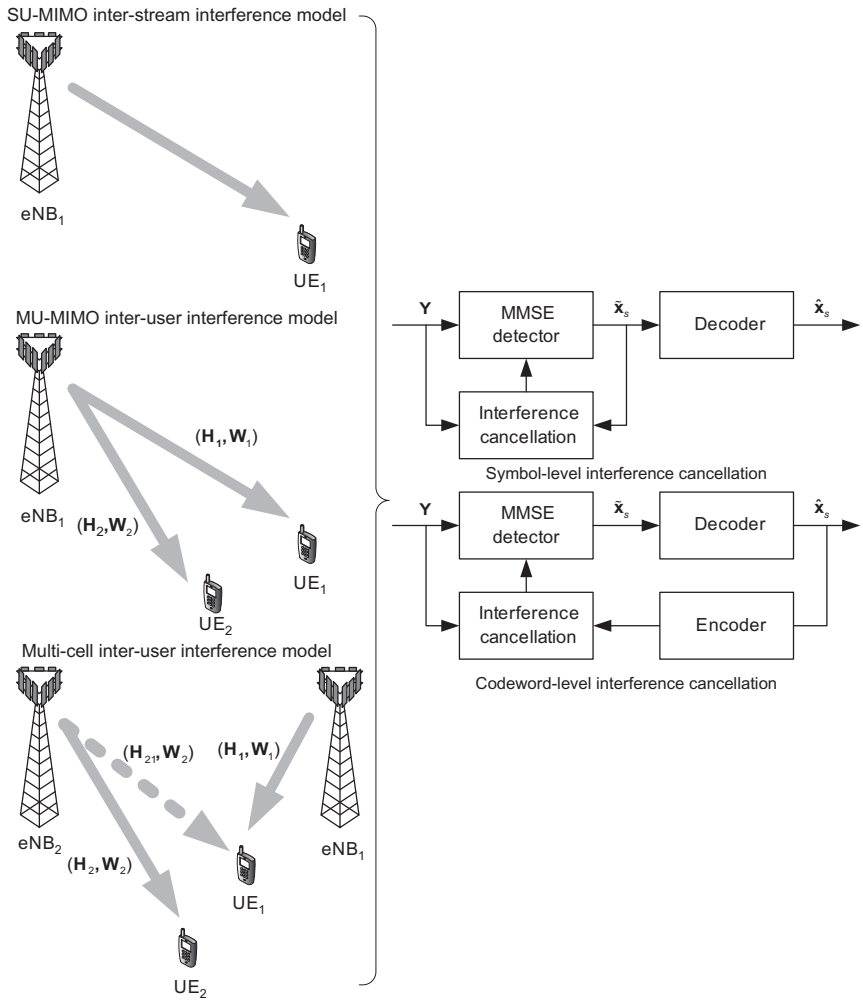


FIGURE 12.1

Illustration of interference models and cancelation at symbol and codeword level [26]. MMSE, minimum mean square error.

Let us consider a scenario where eNBs and UEs have multiple transmit/receive antennas (i.e., a MIMO channel). As shown in Figure 12.1 and in the case of a SU-MIMO inter-stream interference model, the signal received at the UE includes, in addition to noise, a linear combination of multiple streams. The beam is generated by using a non-identity precoding matrix. For simplicity, we assume that the channel is flat. In order to mitigate the inter-stream interference at the

Petitioners' Exhibit 1021
Nokia of America Corp., et al. v. KT Corporation, et al.
Case No. IPR2025-00036; U.S. Patent No. 11,627,631
Page 961 of 1122

UE, interference cancellation can be applied either at the modulated symbol level, where we cancel the estimated interfering stream before decoding, or at the codeword level where we cancel the interfering decoded codeword (see Figure 12.1).

Interference cancellation techniques have been widely studied in the literature [23–26]. While successive interference cancellation scheme processes each stream successively by canceling the previously decoded streams, parallel interference cancellation scheme processes all stream in parallel and cancel their interference after they have all been decoded independently. In order to avoid the propagation of interference cancellation error, each stream can be canceled only if it was correctly decoded by checking the corresponding decoded packet cyclic redundancy check (CRC). Successive interference cancellation can also be done iteratively, i.e., after the first iteration over all streams; we can further improve the quality of the decoded streams by canceling the residual errors estimated in the first iteration, and so on. There are methods proposed in the literature for reducing the complexity of iterative interference cancellation algorithms. In Figure 12.1, and in the case of the MU-MIMO inter-user interference model, the cell serves both UEs simultaneously using the same time–frequency resources. The first user UE_1 receives, in addition to its own data, interference due to data intended for the second user UE_2, i.e., inter-user interference. In order to cancel the inter-user interference, UE_1 needs to know the precoding matrix $\mathbf{W_2}$ that was used for UE_2. In general, $\mathbf{W_2}$ is not known by UE_1, and some additional signaling would be required in order to make $\mathbf{W_2}$ available at UE_1.

In Figure 12.1 and in the case of the multi-cell MU-MIMO interference model, UE_1 at the cell-edge is served by the eNB_1 through channel $\mathbf{H_1}$ and with the precoding matrix $\mathbf{W_1}$, and suffers from inter-cell interference, i.e., interference from the neighbor cell which serves another user UE_2 with the precoding matrix $\mathbf{W_2}$. In order to cancel the inter-cell interference, UE_1 needs an estimate of the channel $\mathbf{H}_{21}$ and the precoding matrix $\mathbf{W_2}$ intended for UE_2. The channel $\mathbf{H}_{21}$ can be estimated by UE_1 based on some reference signals sent from the neighbor cell. The precoding matrix $\mathbf{W_2}$ is in general not known by UE_1 and would require some additional signaling from eNB_2.

Let us consider the case of multi-cell inter-user interference shown in Figure 12.1. It can be shown that the signal to interference plus noise ratio (SINR) at UE_1 can be formulated as follows:

$$\mathrm{SINR}_1(\mathbf{W}_1, \mathbf{W}_2) = \frac{|\mathbf{H}_1\mathbf{W}_1|^2}{\sigma_n^2 + \sigma_I^2 + |\mathbf{H}_{21}\mathbf{W}_2|^2} \tag{12.1}$$

In Eq. (12.1), $\mathbf{W}_1$ and $\mathbf{W}_2$ represent the beamforming optimization matrices/vectors at the eNBs; $\mathbf{H}_1$ and $\mathbf{H}_{21}$ denote information that is not typically available at the CoMP scheduling unit, but measurable at the UEs; σ_n^2 denotes the receiver noise variance; and σ_I^2 indicates the interference from eNBs outside the coordinated set. Thus, the inter-cell interference propagated through channels $\mathbf{H}_{21}$ and $\mathbf{H}_{12}$ results in degradation of SINR measured at UE_1 and UE_2, respectively.

Petitioners' Exhibit 1021
Nokia of America Corp., et al. v. KT Corporation, et al.
Case No. IPR2025-00036; U.S. Patent No. 11,627,631
Page 962 of 1122

As mentioned above, the UE in the downlink of an LTE system can suffer from inter-stream, inter-user, and/or intra-site/inter-cell interference. While the UE is able to perform inter-stream interference cancellation without any additional information, it needs the precoding matrices of other UEs served by the same cell in an MU-MIMO system in order to cancel the interuser interference, and it additionally requires an estimate of the channels of the interfering neighboring cells in order to be able to cancel the inter-cell interference. An important use case for successive interference cancellation is MU-MIMO, but the principles can also be generalized to CoMP schemes. Multi-user MIMO is well known to improve the spectral efficiency by allowing a group of users to simultaneously share the same radio resources. In addition, MIMO provides antenna gain that improves the overall performance. The capacity region of the multi-user channel can be theoretically increased by MIMO through the so-called multiplexing gain. For the spatially separated (uncorrelated) users, the multiplexing gain can be achieved if CSI is available at the base station.

12.2 Distributed antenna systems

A distributed antenna system (DAS) is a network of spatially separated antennas connected to a common source via a transport medium that provides wireless service within a geographic area (cell) or a structure (indoor coverage). The basic notion of DAS was to split the transmit power among several antenna elements which are geographically separated, in order to provide coverage over the same area as a centralized antenna system, but with reduced total power and improved reliability. Thus, a set of centralized antennas radiating at high power are replaced by a group of low-power antenna elements to cover the same area. This concept was initially described in a paper by Saleh et al. [9]. Different variants of DAS have recently been deployed by selected network operators worldwide [10,16]. Examples include systems comprising RRH which consist of multiple outdoor units in which only the radio frequency (RF) front-end functionalities are implemented. The RRHs are connected to the baseband processing part of the base station through a bi-directional high-capacity/low-latency link. The DAS scheme can be implemented as a multi-airlink/multi-frequency/multi-wireless network, or a fiber-optic-based network. While the basic DAS concept is very similar to RRH, it can be differentiated with the latter features based on its greater flexibility and capacity that can be dynamically adapted to and optimized for varying traffic and user mobility conditions. The DAS enables independent operation of multiple frequency bands and multiple protocols across a single access network; consequently, multiple operator network sharing can be supported by a DAS [8,10–14,18]. Recent studies have shown that in addition to coverage improvements, a DAS can also provide other advantages such as reduced power and increased system capacity in a single-cell environment. Each distributed antenna module is connected to a home base station (or central unit) via dedicated wires,

Petitioners' Exhibit 1021
Nokia of America Corp., et al. v. KT Corporation, et al.
Case No. IPR2025-00036; U.S. Patent No. 11,627,631
Page 963 of 1122

fiber optics, or an exclusive RF link. Although the connections via the same RF link used in a cell are possible, the connections with the same RF link construct information-theoretic relay channels are categorized as another research area called cooperative communications. Since the distributed antenna modules and the home base station together construct a macroscopic multiple-input single-output (MISO) vector channel, the DAS can be also interpreted as a macroscopic multiple-antenna system [19].

The advantage of the DAS scheme is that less power is consumed in overcoming penetration and shadowing losses, since a line-of-sight channel is often present, leading to reduced fading depths and reduced delay spread. A DAS can be implemented using passive splitters and feeders, and active repeater amplifiers can be included to overcome the feeder loss. If a given area is covered by N distributed antenna elements rather than a single antenna, then the total radiated power is reduced by approximately a factor of $N^{1-n/2}$, and the power per antenna is reduced by a factor of $N^{n/2}$, where a path loss model with path loss exponent n[1] is assumed. As an alternative, the total area covered could be extended for a given limit of effective radiated power, which may be important to ensure compliance with regulatory limits. In other words, for a given target radiated power, an N-element antenna system will have increased coverage area over a single-antenna system by a factor of $N^{1-2/n}$. Given the same coverage area, the maximum path loss for an N-element distributed antenna system is reduced by a factor of $N^{n/2}$. The transmit power of user devices can then be reduced by a factor of $N^{n/2}$, resulting in a more energy-efficient uplink and lower battery consumption. The use of distributed antenna systems is expected to reduce inter-cell interference and to improve SINR especially for users near cell boundaries, which are often performance limiting users, compared to conventional cellular systems in an interference-limited multi-cell environment. As a result, distributed antenna systems achieve lower symbol error probability and higher capacity than conventional cellular systems. Recent studies suggest that distributed antenna architectures could be an effective solution for reducing inter-cell interference in an interference-limited cellular environment.

Let us look at a distributed antenna system from mathematical point of view. As shown in Figure 12.2, in a distributed antenna system the main baseband processing modules such as channel cards are centralized at a location (central processing unit), and are connected with distributed antenna modules. Each distributed antenna module is physically connected with a home base station via a dedicated link. The general architecture of a DAS in a multi-cell environment is illustrated in Figure 12.2, where a cell is covered by a small base station and six

[1]In the study of wireless communications, path loss can be represented by the path loss exponent, whose value is normally in the range of 2−4, where 2 is for propagation in free space and 4 is for a relatively lossy environment and for the case of full specular reflection from the earth's surface. In some environments, such as buildings, stadiums, and other indoor environments, the path loss exponent can reach values in the range of 4−6. On the other hand, a tunnel may act as a waveguide, resulting in a path loss exponent of less than 2.

Petitioners' Exhibit 1021
Nokia of America Corp., et al. v. KT Corporation, et al.
Case No. IPR2025-00036; U.S. Patent No. 11,627,631
Page 964 of 1122

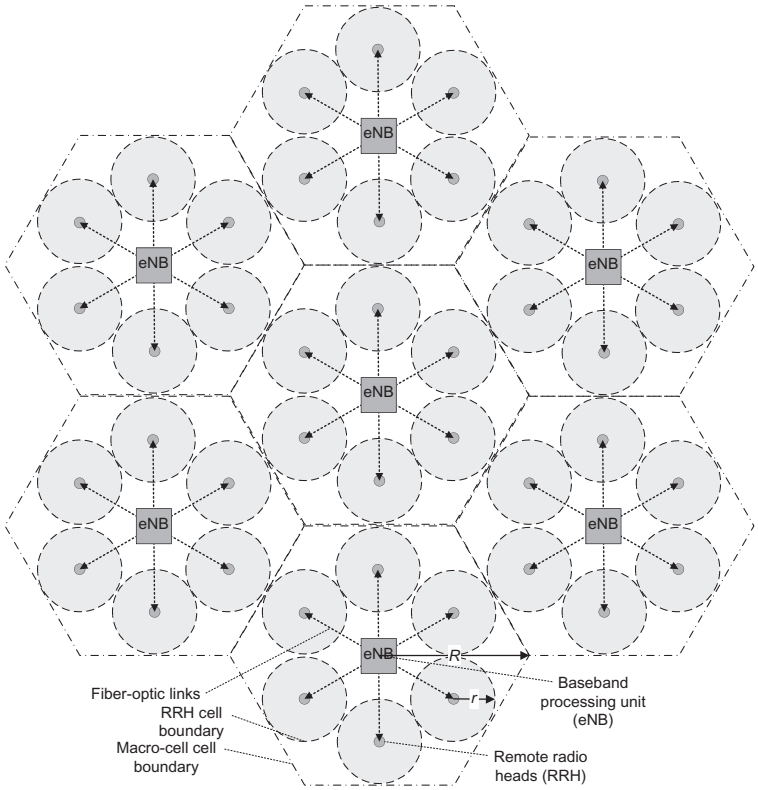


FIGURE 12.2

Example of the architecture of a distributed antenna system with one-tier interference model.

distributed antenna modules. In contrast, the same area is covered by only a single high-power base station in traditional cellular systems. The actual number of distributed antenna modules would be determined by coverage, user densities, and other deployment/economic/environmental factors. Let $P_i^{(j)}$ denote the total transmit power of the ith distributed antenna module of the jth cell, where the small base station of each cell and home cell are indexed by $i = 0$ and $j = 0$, respectively. Let us further assume that $\sum_{i=1}^{N_{\text{unit}}} P_i^{(j)} = P \ \forall j$, where P is the total transmit power of the conventional base station for a fair comparison. The radius of a cell is R, and the coverage radius of a distributed antenna module is r. We further assume a seven cell cellular structure with universal frequency reuse, where a given cell is surrounded by one continuous tier of six cells, as shown in Figure 12.2.

Let us assume (without loss of generality) that there are six RRHs in each cell, and further in each site, downlink signals are transmitted through all the

Petitioners' Exhibit 1021
Nokia of America Corp., et al. v. KT Corporation, et al.
Case No. IPR2025-00036; U.S. Patent No. 11,627,631
Page 965 of 1122

distributed antenna modules and the home base station. In this case, the multiple distributed antenna modules and the home base station together construct a macroscopic MISO vector channel given by [19]:

$$\mathbf{h} = \left(\sqrt{PL_0^{(0)}} h_0^{(0)} \quad \sqrt{\mathrm{PL}_1^{(0)}} h_1^{(0)} \quad \sqrt{\mathrm{PL}_2^{(0)}} h_2^{(0)} \quad \sqrt{\mathrm{PL}_3^{(0)}} h_3^{(0)} \right.$$
$$\left. \sqrt{\mathrm{PL}_4^{(0)}} h_4^{(0)} \quad \sqrt{\mathrm{PL}_5^{(0)}} h_5^{(0)} \quad \sqrt{\mathrm{PL}_6^{(0)}} h_6^{(0)} \right) \tag{12.2}$$

In Eq. (12.2), $h_i^{(j)}$ denotes short-term fading channel from the ith distributed antenna module in the jth cell which is an independent and identically distributed complex Gaussian random variable $h_i^{(j)} \sim \mathbb{C}(0, 1)$. The fading channel is assumed to be static during orthogonal frequency division multiplexing (OFDM) symbol duration. The coefficient $\mathrm{PL}_i^{(j)}$ denotes path loss and shadow fading from the ith distributed antenna module in the jth cell. The transmitted signal vector is represented as $\mathbf{x} = (x_0^{(0)}, x_1^{(0)}, \ldots, x_6^{(0)})^{\mathrm{T}}$, where each entry $x_i^{(j)}$ represents the transmitted signal from the ith distributed antenna module in the jth cell with $\mathscr{E}\{|x_i^{(j)}|^2\} = P_i^{(j)}$. Under these conditions, the received signal at a mobile station in a given OFDM symbol duration is given by [19]:

$$y = \underbrace{\mathbf{hx}}_{\text{Desired signal}} + \underbrace{\sum_{j=1}^{6} \sum_{i=0}^{6} h_i^{(j)} \sqrt{\mathrm{PL}_i^{(j)}} x_i^{(j)}}_{\text{Inter-cell interference}} + \underbrace{n}_{\text{Receiver noise}} \tag{12.3}$$

where n is an additive white Gaussian noise with normal distribution $n \sim \mathcal{N}(0, \sigma_n^2)$. Since the number of interfering sources is sufficiently large and the interfering sources are independent of each other, the interference plus noise can be assumed to be a complex Gaussian random variable z with variance $\sigma_z^2 = \sum_{j=1}^{6} \sum_{i=0}^{6} \mathrm{PL}_i^{(j)} P_i^{(j)} + \sigma_n^2$ according to the central limit theorem[2], whereas the interference plus noise power of the conventional cellular system is given by $\sigma_c^2 = \sum_{j=1}^{6} \mathrm{PL}_0^{(j)} P_0^{(j)} + \sigma_n^2$. When only a single distributed antenna module or the

[2]In probability theory, the central limit theorem states that, given certain conditions, the mean of a sufficiently large number of independent random variables, each with finite mean and variance, will be approximately normally distributed. Let $X_1, X_2, \ldots, X_n$ be a set of n independent random variables and let each X_i have an arbitrary probability distribution $p(x_1, x_2, \ldots, x_N)$ with mean μ_i and a finite variance σ_i^2. Then, the normal form variable $X_{\text{normal}} = \left(\sum_{i=1}^{N} (x_i - \mu_i) \right) / \sqrt{\sum_{i=1}^{N} \sigma_i^2}$ has a limiting cumulative distribution function which approaches a normal distribution. Under additional conditions on the distribution of the addend, the probability density itself is also normal with mean $\mu = 0$ and variance $\sigma^2 = 1$. If conversion to normal form is not performed, then the random variable $X = \left(\sum_{i=1}^{N} x_i \right) / N$ is normally distributed with $\mu_X = \mu_x$ and $\sigma_X = \sigma_x / \sqrt{N}$ [28].

Petitioners' Exhibit 1021
Nokia of America Corp., et al. v. KT Corporation, et al.
Case No. IPR2025-00036; U.S. Patent No. 11,627,631
Page 966 of 1122

home base station is selected for transmission (based on the criterion of minimizing propagation path loss), the received signal is given by [19]:

$$y = \underbrace{h_m^{(0)}\sqrt{\mathrm{PL}_m^{(0)}}x_m^{(0)}}_{\text{Desired signal}} + \underbrace{\sum_{j=1}^{6} h_i^{(j)}\sqrt{PL_i^{(j)}}x_i^{(j)}}_{\text{Inter-cell interference}} + \underbrace{n}_{\text{Receiver noise}} \tag{12.4}$$

where $m = \arg\min_{k=0,1\ldots6}(\mathrm{PL}_0^{(j)}, \mathrm{PL}_1^{(j)}, \ldots, \mathrm{PL}_6^{(j)})$ and qj is randomly selected from the set $\{0, 1, \ldots, 6\}$. The interference plus noise can be shown to be a complex Gaussian random variable u with variance $\sigma_u^2 = \sum_{j=1}^{6} \mathrm{PL}_{qj}^{(j)} P_{qj}^{(j)} + \sigma_n^2$. Since other cells adopt the same transmission scheme as the home cell, only one of the interfering sources in the other cells can be randomly selected in a dynamic point switching scheme. If the CSI is known only at the receiver and the channel is ergodic, the ergodic capacity at a given location of the mobile station under study can be written as follows:

$$C_{\text{ergodic}} = \mathscr{E}_{\mathbf{h}}\left\{\log_2\left(1 + \frac{1}{\sigma_z^2}\mathbf{h}\boldsymbol{\Phi}\mathbf{h}^H\right)\right\} \tag{12.5}$$

where $\boldsymbol{\Phi}$ is the covariance matrix of the transmitted signal vector $\mathbf{x}$ given by $\boldsymbol{\Phi} = \mathrm{diag}(P_0^{(0)}, P_1^{(0)}, \ldots, P_6^{(0)})$. When the channel is known in the transmitter side, the ergodic capacity at a given location of the mobile station is given by:

$$C_{\text{ergodic}} = \mathscr{E}_{\mathbf{h}}\left\{\max_{\varphi_{ii} \le P_i^{(0)} \forall i} \log_2\left(1 + \frac{1}{\sigma_z^2}\mathbf{h}\boldsymbol{\Phi}\mathbf{h}^H\right)\right\} \tag{12.6}$$

where φ_{ii} is the ith diagonal element of matrix $\boldsymbol{\Phi}$. The maximum capacity is achieved by proper design of the transmit power spectrum matrix $\boldsymbol{\Phi}$ under individual power constraints of the distributed antenna modules and the home base station. If power cooperation among the distributed antenna modules and the home base station is allowed, this problem reduces to a standard water-filling problem in a macroscopic MISO vector channel [19].

The above study suggests that the distributed antenna systems effectively reduce inter-cell interference and improve SINR especially for the cell-edge users, which are typically performance limiting users, compared to conventional cellular systems in an interference-limited multi-cell environment. As a result, distributed antenna systems achieve lower symbol error probability and higher capacity than conventional cellular systems; thus, distributed antenna architectures appear to be an effective solution for reducing inter-cell interference in an interference-limited cellular environment.

12.3 Theory of CoMP operation

Future cellular networks are required to provide high-data-rate services to a large number of users, which necessitates high spectral efficiency over the entire cell

Petitioners' Exhibit 1021
Nokia of America Corp., et al. v. KT Corporation, et al.
Case No. IPR2025-00036; U.S. Patent No. 11,627,631
Page 967 of 1122

coverage area. In order to address this problem, it is important to ensure robustness of the radio interface to interference, in particular inter-cell interference, which appears when the same radio resources are reused in different cells in an uncoordinated manner. The inter-cell interference particularly degrades the performance of users located in the cell-edge areas, which causes an inconsistent level of performance among cell-edge and inner-cell users. One possible solution to alleviate this performance discrepancy is to employ coordinated multi-point transmission and reception, which refers to a system where the transmission or reception at multiple, geographically separated antenna sites is dynamically coordinated in order to improve system performance. The coordination can be distributed either by means of direct communication between different sites, or by means of a central coordinating node [34–47].

The notion of clustering (grouping of the cooperating cells) is essential to coordinated beamforming and relaxed coherent joint processing. Indeed, the term CoMP suggests that a number of base stations share some knowledge about users. However, as the number of users and eNBs increases, the signaling overhead required for the inter-eNB information exchange and the amount of feedback needed from the users dramatically increase. Therefore, cooperation should be limited to a small number of cells/sites. To achieve this goal, the network is divided into clusters of cooperating cells. Cluster selection is important to the performance of cooperation strategies. Cluster formation may be static, if the clusters remain fixed in time, or dynamic (see Figures 12.7 and 12.8). Selection may be performed in a network-centric or in a user-centric manner. The network-centric clustering typically divides the network into a set of disjoint clusters of eNBs such that one eNB can belong only to one cluster. In contrast, in the user-centric clustering approach, one eNB may belong to more than one cluster, depending on the parameter under consideration. From the user point of view, this means that, in a given cell, each user may have a different set of cooperating eNBs. The concept of clustering is similar to cooperative sets and/or measurement sets, which will be defined later.

CoMP architectures may include centrally located or distributed processing among the collaborating nodes. The use of geographically distributed antennas in CoMP and the introduction of multiple transmission nodes is conceptually similar to the distributed antenna systems. In particular, in a CoMP scheme exploiting DAS principles, there are several possible transmission strategies including the power-weighted transmission scheme and the single transmit-selection scheme.

Assuming linear transceiver processing, a CoMP system with N antennas is ideally able to accommodate up to N streams without becoming interference limited. The inter-stream interference can be controlled or even completely eliminated by proper precoder selection. This is especially true in the coherent joint processing case, where user data is conveyed from multiple base station antenna nodes over a large virtual MIMO channel. The coherent multi-user multi-cell precoding techniques have strict requirements in terms of signaling and measurements. In addition to the complete channel knowledge of all jointly processed links, a stringent

Petitioners' Exhibit 1021
Nokia of America Corp., et al. v. KT Corporation, et al.
Case No. IPR2025-00036; U.S. Patent No. 11,627,631
Page 968 of 1122

synchronization across the transmitting nodes and centralized entities performing scheduling and computation of joint precoding weights is required in order to avoid carrier phase drifting at different transmit nodes. A large amount of data needs to be exchanged between the network nodes. Therefore, broadband links, such as optical fibers or dedicated radio links, are needed.

Another form of coordinated transmission is dynamic multi-cell scheduling and interference avoidance, where the network nodes coordinate their transmissions (precoder design, scheduling) in order to minimize the inter-cell interference. Carrier phase coherence between the transmit nodes is not required, since each data stream is transmitted from a single transmission point. As a result, the non-coherent coordinated multi-cell transmission approaches have somewhat looser requirements on the coordination and the backhaul, but could potentially need centralized resource management mechanisms.

In order to understand how the above coordinated transmission schemes are mathematically formulated, consider an example of a centralized non-codebook-based coordinated beamforming scenario with static cooperating clusters. Let us assume a general downlink system model for the network consisting of N_{cell} cells and N_{user} single-antenna UEs per cell. This scenario can be considered a traditional cellular network, in which only one transmitter per cell is used, or a CoMP network, in which more than one transmitter per cell is used. We refer to this model as a CoMP system made of N_{unit} single-antenna remote units per cell. In general, the downlink system model of a CoMP cellular network can be expressed as $\mathbf{y} = \mathbf{HWx} + \mathbf{n}$, where $\mathbf{H} \in \mathbb{C}^{N_{\text{user}} \times N_{\text{cell}} N_{\text{unit}}}$, and $\mathbf{W} \in \mathbb{C}^{N_{\text{cell}} N_{\text{unit}} \times N_{\text{user}}}$ are the CoMP processing matrices, which depend on the particular CoMP configuration, $\mathbf{x} = (x_1, x_2, \ldots, x_{N_{user}})^T \in \mathbb{C}^{N_{\text{user}} \times 1}$ is a complex vector that contains the transmitted signal, $\mathbf{y} = (y_1, y_2, \ldots, y_{N_{\text{user}}})^{\text{T}} \in \mathbb{C}^{N_{\text{user}} \times 1}$ is a complex vector containing N_{user} signals received by N_{user} UEs, and $\mathbf{n} \in \mathbb{C}^{N_{\text{user}} \times 1}$ is the noise vector. The ijth entry $\{h_{ij}^{(k)}\}$ of matrix $\mathbf{H}$ represents the complex-valued channel gain between the ith UE ($1 \le i \le N_{\text{user}}$) and the jth remote unit ($1 \le j \le N_{\text{unit}}$) belonging to the kth cell ($1 \le k \le N_{\text{cell}}$). The jith element $\{w_{ji}^{(k)}\}$ of the matrix $\mathbf{W}$ is the square root of the transmission power applied at the jth remote unit ($1 \le j \le N_{\text{unit}}$), transmitting toward the ith UE ($1 \le i \le N_{\text{user}}$), belonging to the kth cell ($1 \le k \le N_{\text{cell}}$). In this model, we assume a flat fading channel as typically observed at each subcarrier in an OFDM system. The above model can be extended to the case of remote units and mobile terminals equipped with multiple antennas. In the following, we assume that there are two cells in the network, and there are three remote units per cell, and further there are two users in each cell, thus $N_{\text{cell}} = 2$, $N_{\text{unit}} = 3$, and $N_{\text{user}} = 2$. Using the above hypotheses, one can rewrite the received signal equation as follows [24]:

$$\begin{pmatrix} y_1 \\ y_2 \end{pmatrix} = \begin{pmatrix} \mathbf{H}^{(1)} & \mathbf{H}^{(2)} \end{pmatrix} \begin{pmatrix} \mathbf{W}^{(1)} \\ \mathbf{W}^{(2)} \end{pmatrix} \begin{pmatrix} x_1 \\ x_2 \end{pmatrix} + \begin{pmatrix} n_1 \\ n_2 \end{pmatrix} \tag{12.7}$$

Petitioners' Exhibit 1021
Nokia of America Corp., et al. v. KT Corporation, et al.
Case No. IPR2025-00036; U.S. Patent No. 11,627,631
Page 969 of 1122

which can be further expanded as follows:

$$\begin{pmatrix} y_1 \\ y_2 \end{pmatrix} = \begin{pmatrix} h_{11}^{(1)} & h_{12}^{(1)} & h_{13}^{(1)} & h_{11}^{(2)} & h_{12}^{(2)} & h_{13}^{(2)} \\ h_{21}^{(1)} & h_{22}^{(1)} & h_{23}^{(1)} & h_{21}^{(2)} & h_{22}^{(2)} & h_{23}^{(2)} \end{pmatrix} \begin{pmatrix} w_{11}^{(1)} & w_{12}^{(1)} \\ w_{21}^{(1)} & w_{22}^{(1)} \\ w_{31}^{(1)} & w_{32}^{(1)} \\ w_{11}^{(2)} & w_{12}^{(2)} \\ w_{21}^{(2)} & w_{22}^{(2)} \\ w_{31}^{(2)} & w_{32}^{(2)} \end{pmatrix} \begin{pmatrix} x_1 \\ x_2 \end{pmatrix} + \begin{pmatrix} n_1 \\ n_2 \end{pmatrix} \tag{12.8}$$

where y_i is the signal received by the ith UE and x_j denotes the signal transmitted by the jth remote unit. The particular expressions of $\mathbf{W} \in \mathbb{C}^{N_{\text{cell}}N_{\text{unit}} \times N_{\text{user}}}$ for CoMP transmit-selection and power-weighted schemes when only one user per cell is considered are as follows:

$$\mathbf{W}_{\text{transmit-selection}} = \begin{pmatrix} 0 & 0 \\ w_{\text{ji}}^{(1)} & 0 \\ 0 & 0 \\ 0 & 0 \\ 0 & w_{\text{ji}}^{(2)} \\ 0 & 0 \end{pmatrix} \mathbf{W}_{\text{weighted-power}} = \begin{pmatrix} w_{11}^{(1)} & 0 \\ w_{21}^{(1)} & 0 \\ w_{31}^{(1)} & 0 \\ 0 & w_{12}^{(2)} \\ 0 & w_{22}^{(2)} \\ 0 & w_{32}^{(2)} \end{pmatrix} \tag{12.9}$$

In the above expressions, and for the CoMP transmit-selection scheme, the only non-zero term $w_{\text{ji}}^{(k)}$ for $k = 1, 2$ is selected by a certain criterion such as minimizing the path loss between any of the remote units transmitting toward the mobile user which is being served, i.e., $w_{\text{ji}}^{(k)} = \min_j \{PL(j, i)\}|_{k=1,2}$ for the ith mobile user. In the CoMP power-weighted scheme $\sum_{j=1}^{N_{\text{unit}}} w_{\text{ji}}^{(k)} = P_{\text{total}}$ for $k = 1, 2$ where P_{total} is the total transmit power of the conventional base station, for the ith mobile user.

Consider a coordination cluster with N_{TP} transmission points, each equipped with an antenna array comprising N_{TX} antenna elements, and N_{user} UEs equipped with N_{RX} receive antennas. Assuming an OFDM transmission, the baseband signal received by the ith UE at the kth subcarrier in the downlink is given by:

$$\mathbf{y}_i(k) = \mathbf{H}_i(k)\mathbf{x}(k) + \mathbf{n}_i(k) \tag{12.10}$$

where the $N_{\text{RX}} \times N_{\text{unit}}N_{\text{TX}}$ matrix $\mathbf{H}_i(k)$ is the composite channel between all transmission points and the ith UE; $\mathbf{n}_i(k)$ represents thermal noise vector including inter-cluster interference which is assumed to be white Gaussian distributed with

Petitioners' Exhibit 1021
Nokia of America Corp., et al. v. KT Corporation, et al.
Case No. IPR2025-00036; U.S. Patent No. 11,627,631
Page 970 of 1122

covariance matrix $\mathscr{E}\{\mathbf{n}_i(k)\mathbf{n}_i^H(k)\} = \sigma_i^2\mathbf{I}$; $\mathbf{x}$ is an $N_{\text{unit}}N_{\text{TX}} \times 1$ vector representing the sum signal transmitted from all transmission points, given by:

$$\mathbf{x}(k) = \sum_{i=1}^{N_{\text{user}}} \mathbf{x}_i(k) = \sum_{i=1}^{N_{\text{user}}} \sqrt{p_i}\mathbf{u}_i s_i(k) \tag{12.11}$$

where $s_i(k)$ is a modulation symbol drawn from a unit-variance symbol alphabet, which is transmitted to the ith UE using the transmit power p_i and beamforming vector $\mathbf{u}_i$, respectively. The beamforming vectors are normalized to have unit power $\mathscr{E}(\mathbf{u}_i^H\mathbf{u}_i) = 1$ for $i = 1, 2, \ldots, N_{\text{user}}$. The average SINR for the ith UE, assuming an MRC receiver type, is given by [24]:

$$\text{SINR}_i(\mathbf{U},\mathbf{p}) = \frac{\mathbf{p}_i\mathbf{u}_i^H\mathbf{R}_i\mathbf{u}_i}{\sum_{j\neq i}\mathbf{p}_j\mathbf{u}_j^H\mathbf{R}_i\mathbf{u}_j + \sigma_i^2} \tag{12.12}$$

where $\mathbf{U}$ is the transmit beamforming matrix given by $\mathbf{U} = (\mathbf{u}_1 \quad \mathbf{u}_2 \quad \ldots \quad \mathbf{u}_{N_{\text{user}}})$, $\mathbf{p}_i$ is the vector of transmit powers, and $\mathbf{R}_i$ is the transmit correlation matrix for the ith UE, given by $\mathbf{R}_i = \mathscr{E}\{\mathbf{H}_i^H(k)\mathbf{H}_i(k)\} = \text{diag}(R_{i1}, R_{i2}, \ldots, R_{iN_{\text{unit}}})$. Since the transmission points are separated by large distances, their antennas are mutually uncorrelated. The considered coordinated beamforming scheme is a modified form of the multiuser beamforming algorithm, in which the beamforming vectors and power allocations are obtained by maximizing the jointly achievable SINR margin as follows [24]:

$$C = \max_{\mathbf{U},\mathbf{p}} \min_{i\in\{1,2,\ldots,N_{\text{user}}\}} \frac{\text{SINR}_i(\mathbf{U},\mathbf{p}_i)}{\gamma_i} \tag{12.13}$$

The above optimization is performed under per-transmitter power constraint:

$$\sum_{i\in S_n} p_i \leq P_{\max} \quad n\in\{1, 2, \ldots, N_{\text{unit}}\} \tag{12.14}$$

where γ_i is the target SINR for the ith UE, S_n is the set of UEs connected to the nth transmission point, and $P_{\max}$ is the maximum transmission point transmit power. The beamforming vectors and downlink power allocations are found iteratively using the uplink−downlink duality theorem, which states that the downlink broadcast channel has a virtual dual uplink multiple access channel which has the same SINR achievable regions as the downlink, and the same beamforming vectors to achieve the SINRs in both links [24].

It can be expected that the most appropriate scenarios for coordinated beamforming have low angular spreads which are found in the urban, suburban, and rural environments with above-rooftop antenna deployment. Due to low feedback requirements, coordinated beamforming is especially of interest in the FDD mode. The joint processing might be difficult to realize in a practical system due to the stringent feedback requirements. It can also be expected that coordinated beamforming is robust to user mobility, hence making it an attractive alternative

Petitioners' Exhibit 1021
Nokia of America Corp., et al. v. KT Corporation, et al.
Case No. IPR2025-00036; U.S. Patent No. 11,627,631
Page 971 of 1122

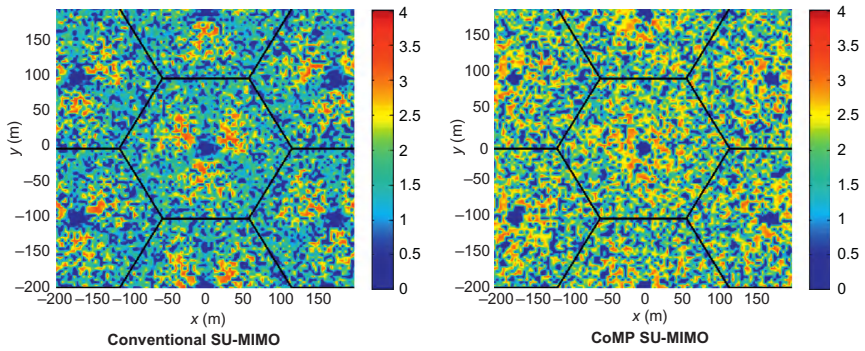


FIGURE 12.3

Performance of intra-eNB CoMP with SU-MIMO and implicit feedback relative to conventional SU-MIMO.

both in low and high mobility scenarios [24]. The performance (cell spectral efficiency) of an intra-eNB CoMP with SU-MIMO and implicit feedback relative to a conventional SU-MIMO scheme have been simulated and are shown in Figure 12.3. The improvement of cell spectral efficiency due to use of CoMP in different areas of the cell and in particular the cell-edge areas can be seen in Figure 12.3. The simulation assumptions are consistent with those recommended in 3GPP TR 36.814 [4].

12.4 CoMP architectures

In LTE Rel-8, MIMO transmission in each cell is controlled independent of that of the neighbor cells. Inter-cell interference coordination (ICIC) was supported by means of coordination message exchanges between base stations via a standardized inter-eNB interface known as X2 [6,7]. The goal of ICIC is to provide the scheduler at one cell with information about the current or prospective interference condition at its neighbors. However, in reality, the transfer latency of these coordination messages depends on the backhaul technology and is not negligible. While ICIC techniques are primarily designed for semi-static coordination, CoMP techniques target more dynamic coordination and may require much lower latency. The macro-cells constitute the basis of a mobile network's coverage; the deployment of low-power nodes (e.g., pico- or femto-cells or relay nodes) within the macro-cell is expected to be an effective solution in the future to address ever-increasing mobile traffic demands. Such networks, referred to as heterogeneous networks, are characterized by severe inter-cell interference between the macro and the low-power nodes due to their proximity and different transmit power classes. The inter-cell interference effect is even more detrimental when the effective cell size of the low-power node is expanded to balance the traffic

Petitioners' Exhibit 1021
Nokia of America Corp., et al. v. KT Corporation, et al.
Case No. IPR2025-00036; U.S. Patent No. 11,627,631
Page 972 of 1122

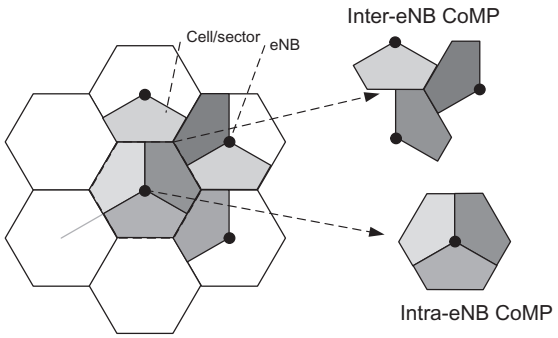


FIGURE 12.4

Illustration of inter-eNB and intra-eNB CoMP scenarios.

load between the macro-cell and the low-power node cell; thus, the UE may be associated with a cell that does not provide the strongest received signal power.

In general, and as shown in Figure 12.4, CoMP transmission/reception techniques can be classified into the following two major categories:

1. Inter-eNB CoMP, wherein coordination amongst eNBs is done via the X2 interface with typical feedback delay of 5−30 ms. This method requires standardization of the feedback channel with consideration for overhead and delay reduction.
2. Intra-eNB CoMP, wherein transmission points are usually connected via wideband/low-delay optical fibers with typical feedback delay of 5 ms and with minimal impact on the X2 interface.

LTE Rel-11 has focused on the intra-eNB CoMP scenarios in order to limit the scope of specification impacts on lower protocol layers.

One recent deployment trend that is foreseen to be widely applied to LTE networks consists of splitting the base station functionalities into a baseband unit, which performs in particular the scheduling and the baseband processing functions, and a number of RRHs responsible for all RF transmission/reception aspects. The baseband processing unit is typically located at the center of the cell and is connected via optical fiber to the RRHs. In addition to suppressing the feeder loss (since the power amplifier is immediately close to the antenna), this approach allows the baseband processing unit to manage different radio sites in a central manner. Furthermore, having geographically separated RRHs controlled from the same location enables either centralized baseband processing units jointly managing the operation of several radio sites, or the exchange of very low-latency coordination messages among individual baseband processing units. The RRH deployments facilitate the tight coordination between transmission/reception points that is required for some CoMP schemes. The applicability and benefits of CoMP techniques depend to a great extent on the backhaul characteristics (latency and capacity), which determine the type of CoMP processing and the corresponding

Petitioners' Exhibit 1021
Nokia of America Corp., et al. v. KT Corporation, et al.
Case No. IPR2025-00036; U.S. Patent No. 11,627,631
Page 973 of 1122

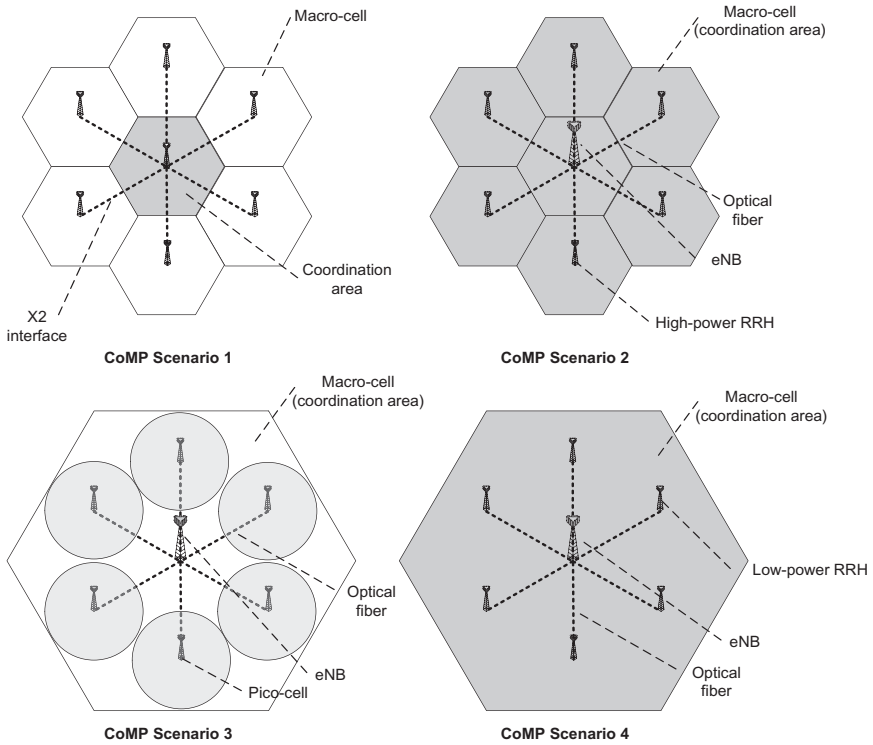


FIGURE 12.5

Illustration of CoMP scenarios [5].

performance. In order to account for the various possible network topologies and backhaul characteristics, the study of CoMP in 3GPP focused on the following scenarios (Figure 12.5) [5,27]:

- CoMP scenario 1 (homogeneous macro network with intra-site CoMP): Coordination among the cells (sectors) controlled by the same macro base station (where no backhaul connection is needed).
- CoMP scenario 2 (homogeneous macro network with inter-site CoMP): Coordination between cells belonging to different radio sites from a macro network.
- CoMP scenario 3 (heterogeneous network with low-power pico-cells within the macro-cell coverage area): Coordination between a macro-cell and low-power transmit/receive points within its coverage, each point controlling its own cell (with its own cell identity).
- CoMP scenario 4 (heterogeneous network with low-power RRH): Coordination between a macro-cell and low-power transmit/receive points

Petitioners' Exhibit 1021
Nokia of America Corp., et al. v. KT Corporation, et al.
Case No. IPR2025-00036; U.S. Patent No. 11,627,631
Page 974 of 1122

within its coverage, each point controlling its own cell, except that the low-power transmit/receive points constitute geographically distributed antennas of the macro-cell, and are thus all associated with the macro-cell identity.

CoMP scenario 1 is defined for homogeneous networks where the coordination area is restricted to the cells of a single site controlled by an eNB. Although the extent of coordination is limited to the cells of the same site, CoMP scenario 1 has the advantage of requiring no inter-eNB interface among different sites. Such an advantage would make CoMP scenario 1 attractive to the network operators.

CoMP scenario 2 is for homogeneous networks where the coordination area is expanded from the CoMP scenario 1 to include the cells of different sites. CoMP scenario 2 may be realized by having a single eNB control the RRHs at different sites, or by having multiple eNBs at different sites to coordinate with each other. CoMP scenario 2 is depicted in Figure 12.5 with high-power RRHs at different sites controlled by a single eNB. Depending on the number of cells involved and the latency of connections between the sites, which are both dependent on network implementation, different levels of performance gain over CoMP scenario 1 may be obtained.

CoMP scenario 3 relies on a heterogeneous network model where macro-cells with high transmission power and pico-cells with low transmission power are connected. In practice, this scenario may be realized by a single eNB controlling the high-power RRH of the macro-cell and the low-power RRHs of pico-cells within the macro-cell coverage area. Another possible network implementation is that the eNBs of the macro-cell and the pico-cells are different and coordinate with each other. Figure 12.5 illustrates CoMP scenario 3 with low-power RRHs at different sites controlled by a single eNB.

CoMP scenario 4 is defined for heterogeneous networks where low-power RRHs are distributed throughout the coverage area of a macro-cell. The difference between this scenario and the other intra-eNB scenarios is that all low-power RRHs in this case share the same physical cell identity with the macro-cell. Therefore, it can be construed that the low-power RRHs form a set of distributed antennas in the macro-cell area. Since the coordination is done among distributed antennas within the same cell, depending on the size of macro-cell, there may not be a need for conventional mobility support such as handover procedures among the RRHs. Furthermore, since each RRH is not an independent cell, a low-delay and high-capacity backhaul connection such as optical fiber can provide the radio connection between the macro-eNB and the RRHs. CoMP scenarios 3 and 4 are expected to find applications in metropolitan areas where network deployment is dense and RRHs with different transmission power levels can be deployed to improve control/data coverage and capacity [17].

A set of geographically collocated antennas that correspond to a particular sectorization scheme are traditionally configured as a cell. A UE attempts to connect to a single cell at any given time, if the measured received reference signal strength from that cell is higher relative to that from other cells. This cell then

Petitioners' Exhibit 1021
Nokia of America Corp., et al. v. KT Corporation, et al.
Case No. IPR2025-00036; U.S. Patent No. 11,627,631
Page 975 of 1122

becomes its serving cell. Given the new definition of CoMP scenarios as introduced earlier, the antennas configured as a cell may not be geographically collocated. The term transmission point can then be used to refer to a set of collocated antennas, and a cell can correspond to one or more such transmission points. Note that a single geographical site may contain multiple transmission points in the case of sectorization, with one transmission point corresponding to one sector. CoMP techniques can also be defined in a more straightforward manner as the coordination between transmission points.

A mobile station is said to be connected to a cooperating set/cluster if its serving cell belongs to the cluster. We assume no coordination between clusters, which also means that a cell belongs to one, and only one, cluster. The serving cell selection in LTE Rel-8 is based on the long-term average reference signal received power (RSRP) measurements. The cell with the strongest RSRP acts as the serving cell. The serving cell also defines the cluster to which the mobile is connected. Since each cell uniquely belongs to one cluster, the serving cluster is determined once the serving cell is selected. It is assumed that the measurement set of a UE is a subset of the cluster.

12.4.1 Air-interface and network support for CoMP schemes

In order to enable CoMP operation, the network architecture must be able to provide sufficient coordination and synchronization among different transmission points and/or cells/sites. If inter-eNB coordination is enabled, user data and/or CSI will be exchanged and shared between eNBs; thus, low-latency and high-capacity backhaul would be required to support inter-eNB CoMP deployment scenarios. The impacts on the radio interface mainly depend on type of CoMP scheme that is utilized, which may include, but is not limited to, the following [5]:

- CSI measurement and feedback mechanisms at the UE, which may include reporting dynamic channel conditions between transmission points in the CoMP measurement set and the UE. Depending on the duplex scheme, channel reciprocity may be exploited to facilitate channel estimation at the transmission points.
- Low-latency and configurable reporting mechanisms to facilitate the decision-making process concerning the set of participating transmission points.
- Static and dynamic coordination and tight synchronization are required prior to transmission of the signal over multiple transmission points.
- Reference signals with unique signatures are required to enable inter-cell/intra-cell interference and channel measurements. Depending on the CoMP scheme, the LTE Rel-10 CSI reference signal (CSI-RS) structures were found to be suitable to provide support for certain interference measurement and characterization [33].
- Improved control signaling design may be required to support signaling and feedback for certain CoMP algorithms. LTE Rel-11 provided the enhanced physical downlink control channel (ePDCCH) and other downlink control

Petitioners' Exhibit 1021
Nokia of America Corp., et al. v. KT Corporation, et al.
Case No. IPR2025-00036; U.S. Patent No. 11,627,631
Page 976 of 1122

signaling improvements, as well as transmission mode 10 to accommodate the CoMP design and operation.

Different impacts on the network architecture are foreseen depending on the CoMP scenario being deployed, including coordination among base stations, use of radio over fiber links to connect different transmission/reception points, or coordinated relaying, affecting both data-plane and control-plane protocols. The optical fiber links have a small impact on the current network architecture since the interface between base station control unit and the associated RRH can be either proprietary or based on an open standard interface such as the Common Public Radio Interface (CPRI)[3] standard which defines the interface between entities known as RECs and local or RRH referred to as radio equipment (RE) [29]. It is necessary to further study the transfer of data and control information over optical fiber interfaces. Cooperation among distributed base stations has a higher impact on the network. A central control/scheduling/processing unit may be necessary depending on the required coordination scheme.

Other important aspects to be considered when deploying CoMP in a network include centralized/decentralized management of UEs connected to multiple transmit/receive points. Most proposals addressing multi-antenna schemes often assume power constraints on the sum of power transmitted by different antennas. This assumption may not hold when each antenna in a multi-antenna base station is powered by its own power amplifier and is limited by the linearity of that amplifier, or when the system uses distributed antennas belonging to the same or coordinated base stations, and each one is subject to its own power limits and emission constraints [23].

12.4.2 Downlink CoMP

A set of geographically separated points directly and/or indirectly involved in downlink data transmission to a UE over a time−frequency resource is defined as a CoMP cooperating set. Note that this set may be transparent to the UE. The transmission points in a cooperating set are either directly participating in transmission of data in the time−frequency resource, or indirectly participating in transmission,

[3]The CPRI is an initiative to define a publicly available specification that standardizes the protocol interface between the radio equipment control (REC) and the radio equipment (RE) in wireless base stations. This allows interoperability of equipment from different vendors and preserves the software investment made by wireless service providers. Conventional base stations are located adjacent to the antenna in a small building at the base of the antenna tower. Finding suitable sites can be a challenge because of the footprint required for the building, the need for structural reinforcement of rooftops, and the availability of both primary and backup power sources. CPRI allows the use of a distributed architecture where base stations, containing the REC, are connected to remote radio heads via low-loss fiber links that carry the CPRI data. This architecture reduces costs for service providers because only the remote radio heads containing the REs need to be situated in environmentally challenging locations. The base stations can be centrally located in less challenging locations where footprint, climate, and availability of power are more easily managed [29].

Petitioners' Exhibit 1021
Nokia of America Corp., et al. v. KT Corporation, et al.
Case No. IPR2025-00036; U.S. Patent No. 11,627,631
Page 977 of 1122

which make them candidate points for data transmission that do not transmit data but contribute in making decisions on the user scheduling/beamforming in the time−frequency resource. The CoMP transmission points (TPs) are defined as a set of points transmitting data to a UE. It is understood that CoMP TPs are a subset of the CoMP cooperating set. In general, the downlink CoMP schemes may be classified into one of the following categories (see Figure 12.6) [5]:

- Joint processing (JP) where data for a UE is available at more than one transmission point in the CoMP cooperating set for a time−frequency resource. A subcategory of JP CoMP is the joint transmission (JT) in which data is simultaneously transmitted from multiple points (part of or an entire CoMP cooperating set) to a single UE or multiple UEs in a time−frequency resource. Alternatively, the data to a UE can be simultaneously transmitted from multiple points, e.g., to (coherently or noncoherently) improve the received signal quality and/or data throughput. Another subgroup of JP CoMP is known as dynamic point selection (DPS)/muting where data is transmitted from one point (within the CoMP cooperating set) in a time−frequency resource. The transmitting/muting point may change from one subframe to another, including varying over the resource block pairs within a subframe. The data is available simultaneously at multiple points. This includes dynamic cell selection (DCS). The DPS may be combined with JT, in which case, multiple points can be selected for data transmission in the time−frequency resource.
- Coordinated scheduling/beamforming (CS/CB) in which data for a UE is only available and is transmitted from one point in the CoMP cooperating set, i.e., downlink data is transmitted from that point for a time−frequency resource but user scheduling/beamforming decisions are made with coordination among points corresponding to the CoMP cooperating set. In this case, the transmission points are selected semi-statically. Semi-static point selection (SSPS) is a method where data is transmitted to a specific UE from one point at a time. The transmitting point may only change in a semi-static manner. Muting may be applied in a dynamic and semi-static manner to the above transmission schemes (Figure 12.6).

The CS/CB scheme reduces the interference level experienced by a UE terminal by appropriately selecting the beamforming weights of interfering points to steer the interference toward the null space of the interfered UE. The JT scheme allows one or more neighboring points to transmit the desired signal rather than interfering signals from the point of view of the selected UE. The transmission point selection scheme enables the UE to be dynamically scheduled via the most appropriate transmission point by exploiting changes in the channel slow/fast fading conditions. Hybrid methods may also be implemented in a network to cope with different types of interference. A combination of JP and CS/CB schemes is possible in the downlink. Data for a UE may be available only in a subset of points in the CoMP cooperating set for a particular time−frequency resource, but user scheduling/beamforming decisions are made with coordination among points

Petitioners' Exhibit 1021
Nokia of America Corp., et al. v. KT Corporation, et al.
Case No. IPR2025-00036; U.S. Patent No. 11,627,631
Page 978 of 1122

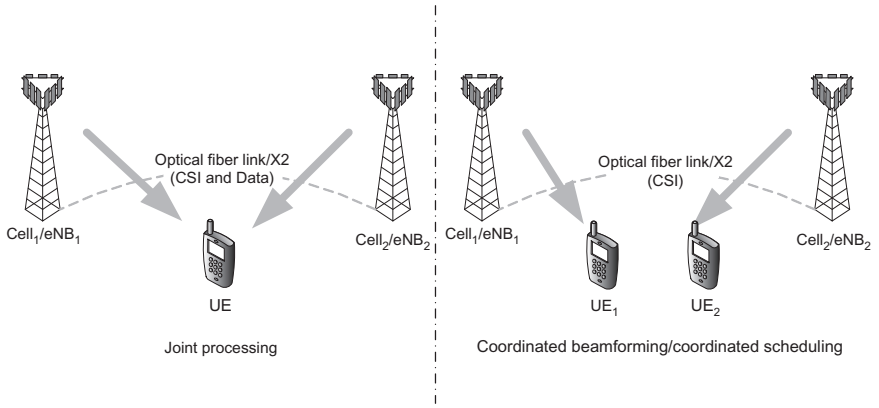


FIGURE 12.6

Illustration of downlink CB/CS and JT CoMP concepts.

corresponding to the CoMP cooperating set. For example, some points in the cooperating set may transmit data to the target UE according to a JP scheme, while other transmission points in the cooperating set may perform one form of CS/CB scheme. For the JT scheme, CoMP transmission points may include multiple points in the CoMP cooperating set at each subframe for a certain time−frequency resource, whereas in the case of CS/CB, DPS, SSPS, a single point in the CoMP cooperating set is the CoMP transmission point at each subframe for a certain time−frequency resource. For SSPS, this CoMP transmission point can change semi-statically within the CoMP cooperating set. Examples of static and dynamic formation of CoMP clusters (cooperating sets) are shown in Figures 12.7 and 12.8.

12.4.3 Uplink CoMP

The uplink CoMP schemes may be divided into one of the following categories:

- Joint reception (JR) in which physical uplink shared channel (PUSCH) transmitted by the UE is received jointly at multiple points which are part of or the entire CoMP cooperating set at a certain time, e.g., to improve the received signal quality.
- CS/CB where user scheduling and precoding decisions are made with coordination among points within the CoMP cooperating set. The user data is only intended for one recipient point in the set.

Similar to the downlink, the uplink CoMP cooperating set is a set of geographically separated points that may be designated for data reception from a UE. The uplink CoMP reception points are a set of points for receiving data from a UE. The CoMP reception points are a subset of the CoMP cooperating set in the uplink. For the JR scheme, CoMP reception points may include multiple points in

Petitioners' Exhibit 1021
Nokia of America Corp., et al. v. KT Corporation, et al.
Case No. IPR2025-00036; U.S. Patent No. 11,627,631
Page 979 of 1122

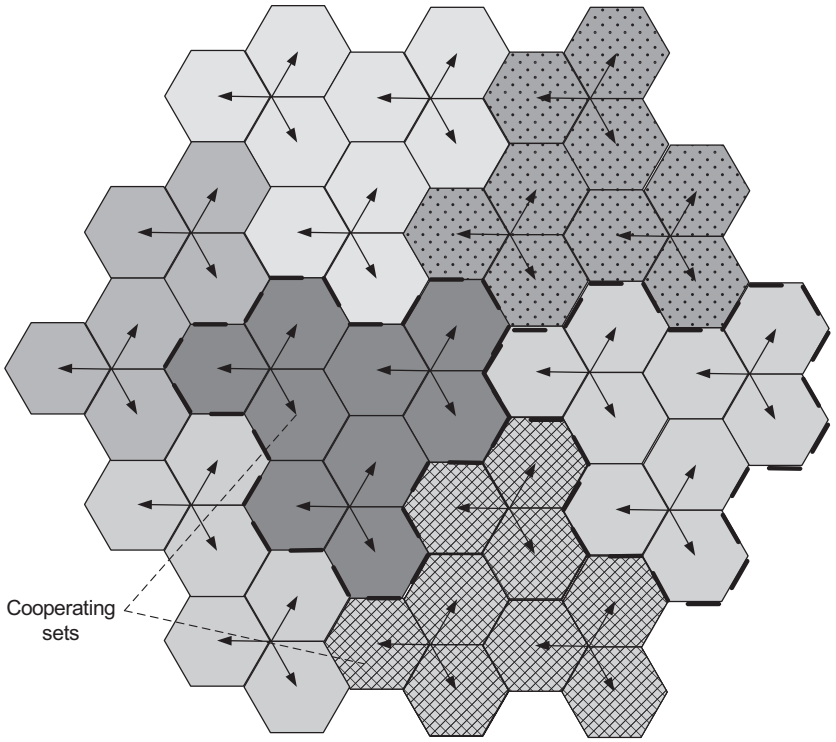


FIGURE 12.7

Illustration of static CoMP clusters (Scenario 2, 9 cells per cooperating set) [5].

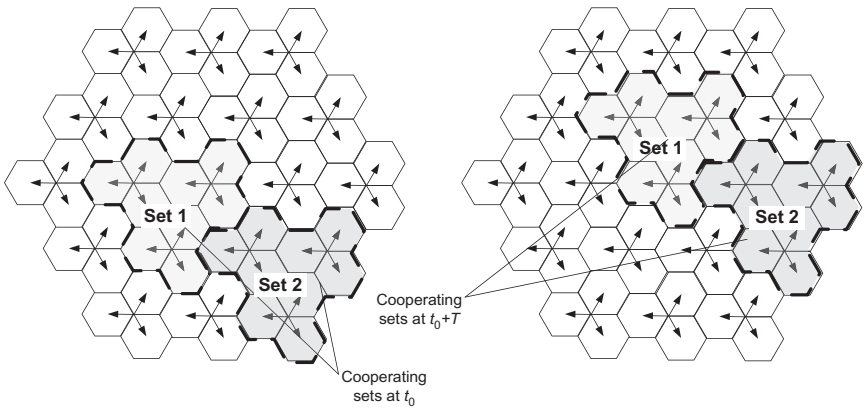


FIGURE 12.8

Dynamic clustering of CoMP (change of cooperating CoMP sets across time).

Petitioners' Exhibit 1021
Nokia of America Corp., et al. v. KT Corporation, et al.
Case No. IPR2025-00036; U.S. Patent No. 11,627,631
Page 980 of 1122

the CoMP cooperating set at each subframe for a certain time−frequency resource, whereas for uplink CS/CB, a single point in the CoMP cooperating set is the CoMP reception point at each subframe for a certain time−frequency resource [5].

In other words, uplink CoMP schemes can be divided into two major groups. The first group uses dynamic selection of the best reception point according to short-term channel quality. The second category uses joint reception, where several reception points act as a joint receiver with a larger number of antennas. Joint reception is more complex to implement, but it offers larger gains relative to DPS. One of the most important aspects of coordinated uplink reception is the decoupling of the points that transmit downlink control from those that receive uplink data. Important aspects of the implementation pertain to coordination and exchange of information among reception points in terms of selection of reception points, computation of the receive combiner, coordinated scheduling, and exchange of received signal samples (e.g., quantized received signals, locally combined signals, or log-likelihood ratios). These functions are typically centralized in the baseband processing unit connected to the coordinated eNBs via optical fiber links [17].

In uplink coordinated multi-point reception, the UE signals which were previously treated as interference at a reception points, other than the serving node, would become desired signals. Uplink reference signals that are used for channel estimation in the demodulation process of PUSCH are very sensitive to interference. In LTE Rel-8/9/10, the assignment of the pseudo-random base sequences for scrambling the reference signals of a UE was made by a single serving cell. It was possible to assign orthogonal sequences to the UE, whose reference signals were received by the same receiving point, via either different cyclic shifts of the same base sequence or orthogonal cover codes. At the same time, several interference randomization techniques improved the inter-cell interference generated by uncoordinated uplink scheduling assignments across multiple neighboring cells. These randomization techniques include sequence-group hopping, sequence hopping, and different cyclic shifts [1−3]. The opportunity offered by CoMP to receive the UE's signals at one cell when the UE's transmission is intended for another cell created new constraints for assigning orthogonal sequences to the users allocated in overlapping time−frequency resources [17].

LTE Rel-11 introduced new capabilities for configuring reference signal initialization parameters. In particular, the initialization of the pseudo-random sequences is no longer associated with the physical cell identity, but rather is explicitly signaled as a UE-specific virtual cell identity [1]. This enables the assignment of the same base sequence with different cyclic shifts to the UE which is connected to different cells, allowing virtual cells to be created within the coverage area of a macro-cell deployed with RRHs, as in CoMP scenario 4. Furthermore, it is possible to configure the initialization of the cyclic shift hopping in a dedicated manner for each UE, which enables grouping of UEs by orthogonal cover codes across different cells even when these UEs are assigned different base sequences [17].

Petitioners' Exhibit 1021
Nokia of America Corp., et al. v. KT Corporation, et al.
Case No. IPR2025-00036; U.S. Patent No. 11,627,631
Page 981 of 1122

12.4.4 CSI measurement and feedback in CoMP-enabled networks

A downlink CoMP measurement set is defined as a group of transmission points relative to which the UE measures and reports the CSI. The UE reports may select points for which actual feedback is transmitted. The measurement set typically encompasses cells for which the mobility-management-related measurements are conducted for the purpose of cell selection/reselection and handover. The proper operation of any CoMP scenario depends on the accuracy and timeliness of the CSI measurement and feedback in the network. Some CoMP schemes are more affected by CSI inaccuracy and feedback delays. LTE Rel-11 has specified a general control signaling framework that enables all CoMP schemes to properly operate by enhancing and extending the features that existed in the previous releases. The CoMP measurement set is alternatively defined as a set of CSI-RS resources on which the UE is required to measure and report the CSI that may include rank indicator, precoding matrix index, and channel quality indicator. There is typically a unique correspondence between a CSI-RS resource and a transmission point. As shown in Figure 12.9, the CoMP measurement set is a subset of the CoMP cluster/cooperating set ($S_{\text{measurement}-\text{set}} \subset S_{\text{cooperating}-\text{set}}$). The size of a CoMP measurement set that can be configured for a UE is limited to three CSI-RS resources in order to reduce the uplink signaling overhead. The UE at different locations may observe different sets of strong-signal transmission points; thus, the configuration of a CoMP measurement set is UE-specific. Due to UE mobility, CoMP measurement sets dynamically change and need to be reconfigured when necessary to ensure optimal CoMP performance. To assist the network in managing the CoMP measurement set of each UE, a CoMP resource management procedure based on CSI-RS measurement has been defined in LTE Rel-11. While the CoMP resource management concept can be applied to all CoMP scenarios, it is particularly useful for CoMP scenario 4 where the transmission points are not identifiable from their transmitted cell-specific reference signals, making it impossible to compare the received signal strengths based on cell-specific reference signals.

The CoMP resource management procedure requires the UE to perform CSI-RS-based received signal quality measurements on a set of CSI-RS resources that are candidates for inclusion in the CoMP measurement set. The set of CSI-RS resources explicitly configured by the network for CoMP resource management is called the CoMP resource management set. The latter set can be configured independently of the CoMP measurement set [17]. The measurement of CSI-RS received power is similar to that defined for RSRP measurement on cell-specific reference signals. Nevertheless, there are some differences between the two types of measurements. The UE is only required to conduct measurement on CSI-RS resources in the CoMP resource management set. Therefore, the UE does not autonomously detect CSI-RS resources, resulting in reduced UE operational complexity. The CoMP resource management measurement/reporting is event-driven and the triggers can be either absolute, i.e., a measurement report is triggered

Petitioners' Exhibit 1021
Nokia of America Corp., et al. v. KT Corporation, et al.
Case No. IPR2025-00036; U.S. Patent No. 11,627,631
Page 982 of 1122

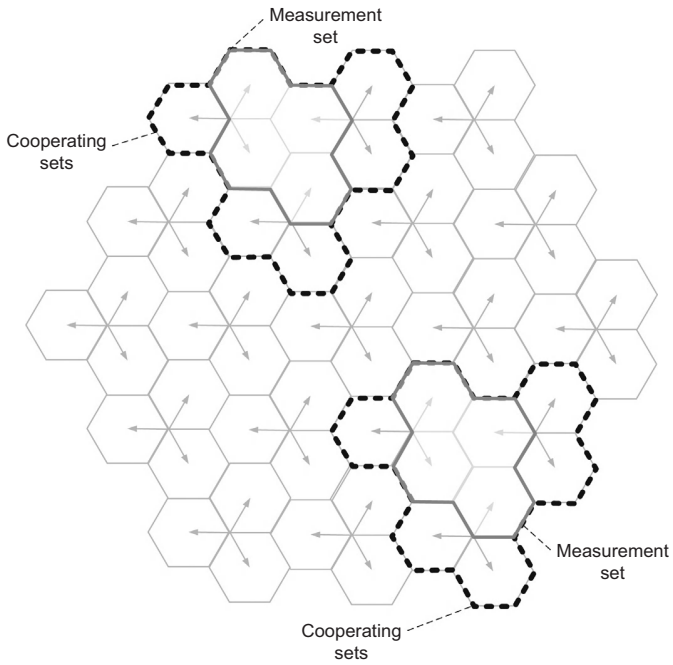


FIGURE 12.9

Example illustration of cooperating and measurement sets.

when the received signal power goes beyond an absolute threshold, or relative, i.e., the received signal power is compared to that of another CSI-RS resource.

To ensure the CSI-RS received power measurement is immune to interference and to ensure the accuracy of the measurement, the network can mute the transmissions on the resource elements from the neighboring TPs that correspond to the CSI-RS resource elements of the transmission point being measured. When performing CSI-RS received power measurements, the UE may assume that the timing of the received CSI-RS is the same as that derived from the primary and secondary synchronization signals of the serving cell. This allows the UE to use a single timing derived from the synchronization signals of the serving cell to receive CSI-RS that might be transmitted from a different TP. While this simplifies UE implementation, the impact on the accuracy of CSI-RS received power depends on the extent of the timing error. Studies suggest that there is no significant impact on CSI-RS measurement provided that a timing error is limited to ± 3 ms [17,21,27].

Since a UE needs to measure CSI-RS to generate CSI feedback and receive UE-specific reference signals to coherently demodulate PDSCH, it is imperative that the CSI-RS and DM-RS are transmitted such that the interference among the reference signals of multiple TPs is sufficiently randomized. LTE Rel-10

Petitioners' Exhibit 1021
Nokia of America Corp., et al. v. KT Corporation, et al.
Case No. IPR2025-00036; U.S. Patent No. 11,627,631
Page 983 of 1122

addresses this requirement by defining unique initialization seeds for generating the scrambling sequences of each transmission point/cell's reference signals based on the physical cell identity. This approach may not work for CoMP scenario 4 since multiple TPs share the same cell identity. In order to provide sufficient interference randomization, LTE Rel-11 replaced the use of the physical cell identifier for initialization of the scrambling sequences with a virtual cell identifier, which is signaled to the UE using higher layer signaling, allowing flexible deployment of transmission points in CoMP scenario 4, and providing sufficient interference randomization for DM-RS and CSI-RS. In the case of CSI-RS, the interference among CSI-RSs of different TPs is further reduced by allocating different time or frequency resources for CSI-RS transmissions. The use of a virtual cell identifier provides interference randomization when the same time and frequency resources are used across different cells for CSI-RS transmissions [1].

The feedback scheme for CoMP in LTE Rel-11 is defined per CSI-RS resource, where the UE reports the CSI individually for multiple CSI-RS resources. Note that each CSI-RS resource is transmitted from one transmission point. As a result, when the UE is configured with multiple CSI-RS resources and performs per CSI-RS resource feedback, it reports individual CSIs for each of the TPs transmitting the configured CSI-RS resources. There is at least one feedback process associated with each CSI-RS resource within the CoMP measurement set. Each feedback process provides the eNB with the measured CSI (measured on a particular CSI-RS resource). The CSI feedback can be configured to be periodically reported, or scheduled for aperiodic reporting. For CS/CB, separate CSI feedback for at least two TPs can be configured where one of the processes would be used for reporting the CSI for the serving TP, and the other(s) can be used for reporting the CSI associated with the interfering TP(s). Similarly, for a dynamic point switching scheme, multiple CSI feedback processes can be configured, allowing the network to dynamically switch the transmitting TPs. The above feedback mechanism can also support other CoMP schemes including non-coherent JT, where precoding is applied individually to the transmit antennas belonging to each TP, and coherent JT in a non-standardized form by aggregating multiple TPs under a single CSI-RS resource.

The reader's attention is drawn to the fact that there are two types of feedback in general to support CoMP operation, as follows:

1. Explicit feedback which is characterized by having a channel part and a noise-and-interference part. The channel part includes reports for each point in the UE's measurement set that is reported in a given subframe that contains one or several channel properties. The channel properties include instantaneous channel matrix either in the form of full matrix or main eigen component(s) of the channel matrix; and transmit channel covariance either in the form of full covariance matrix or main eigen component(s) of the channel covariance matrix. Inter-point channel properties may also be reported including a noise-and-interference part, total interference received power, total received signal covariance matrix, and covariance matrix of the noise and interference.

Petitioners' Exhibit 1021
Nokia of America Corp., et al. v. KT Corporation, et al.
Case No. IPR2025-00036; U.S. Patent No. 11,627,631
Page 984 of 1122

2. Implicit feedback is based on certain hypotheses at the UE, and the feedback is generated depending on the operation scheme, e.g., SU-MIMO/MU-MIMO, single cell/point or coordinated transmission, and single-point CS/CB or multi-point (JP) transmission. Under this category, other forms of feedback may be considered such as precoding matrix index (PMI) with fine quantization granularity, wideband/subband PMI, and channel quality indicator (CQI). Note that CQI only accounts for interference outside the CoMP measurement set or relative received power between CoMP transmission points.

LTE Rel-11 does not specify any standardized support for coherent JT. Another important feature that has been included in LTE Rel-11 to support CoMP is the interference measurement resource (IMR), which is a set of resource elements where a UE can be configured to measure interference. Prior to LTE Rel-11, interference measurement was mainly implementation-specific and based on cell-specific reference signals. Such interference measurement schemes may not be applicable to CoMP because in CoMP scenario 4, multiple TPs may share a common cell identity. In that case, TPs within a cell are not distinguishable since they are transmitting the same cell-specific reference signals. Moreover, the interference measured using cell-specific reference signals does not allow the network to adaptively control the interference measured by the UE. As an example, if the effect of a particular TP shutdown is desired, the network can configure two separate IMRs for two feedback processes. One of the IMRs would capture the interference with the TP turned off, while the other the IMR would capture the interference with the TP turned on. The configuration of the IMR is done on a per-UE basis via higher layer signaling. Depending on the measurement reports from the UE, the network can determine which transmission points should be added to, removed from, or replaced in the CoMP measurement set in order to select the set of transmission points with the strongest signal measured at the UE [3].

12.5 Effects of X2 latency on CoMP performance

The X2 latency is defined as the accumulation of the time needed to send a message across the X2 interface, as well as the required time to process the X2 message in the eNB [20,30]. The non-zero X2-latency affects HARQ ACK/NACK round trip time and the CSI feedback delay. The HARQ ACK/NACK round trip time is defined as the time interval between the first transmission of PDSCH using a HARQ process identifier and the earliest retransmission/fresh transmission using the same HARQ process identifier. The CSI feedback delay is the time interval between the CQI measurement period at the UE and the next downlink data transmission from the eNB that is based on the knowledge of this CQI. Since both CQI as well as HARQ information need to be transmitted from the serving cells to the master cell of a cluster across the X2 interface, the X2 delay impacts

Petitioners' Exhibit 1021
Nokia of America Corp., et al. v. KT Corporation, et al.
Case No. IPR2025-00036; U.S. Patent No. 11,627,631
Page 985 of 1122

both HARQ delay as well as CQI delay. The ACK/NACK delay determines the number of HARQ processes that are needed to guarantee continuous transmission (efficient channel utilization), if the mobile station is scheduled all the time. Therefore, the impact of long HARQ ACK/NACK delays is important for low to medium cell loads. In highly loaded cells, the number of required HARQ processes decreases, since each mobile station attains less access to the channel. This impact is therefore dependent on the cell load. Due to the increased CQI delay, the CQI contains less information about the channel at the time when it is accessed. This means that it becomes more difficult to adapt the MCS and other transmission parameters to the instantaneous channel conditions.

In order to investigate the effect of X2 latency on the inter-eNB JT CoMP operation, let us assume that a sufficient number of HARQ processes are available such that the impact of the X2 delay on the HARQ ACK/NACK delay can be neglected. This is ensured by setting the number of available HARQ processes to infinity. To investigate the impact of X2 latency on CQI delay, X2 delays of 0, 1, 3, 5, 10, 15, and 20 ms were simulated. Figure 12.10 shows the loss in average user throughput for various X2 delays relative to an ideal interface with zero delay. The losses are given for the 5th, 50th, and 95th percentile of the cumulative distribution function (CDF) of average user throughput without X2 delay. It can be seen that the losses become larger with increasing values of X2 delay. This indicates that inter-eNB JT CoMP is very sensitive to X2 delay.

12.6 Performance of CoMP scenarios

The performance of intra-eNB CoMP techniques has been extensively studied and evaluated in 3GPP and documented in Ref. [5] as part of the CoMP feasibility studies. The detailed simulation assumptions and simulation models used in this evaluation are described in 3GPP TR 36.814 and TR 36.819 [4,5]. The evaluations were conducted by various sources in the following deployment scenarios [31,32]:

1. Scenario 1: Homogeneous network with intra-site CoMP.
2. Scenario 2: Homogeneous network with high transmit-power RRHs.
3. Scenario 3: Heterogeneous network with low-power RRHs within the macro-cell coverage, where transmission/reception points are identified by different cell IDs.
4. Scenario 4: Heterogeneous network with low-power RRHs within the macro-cell coverage where the transmission/reception points created by the RRHs have the same cell IDs as the macro-cell.

Despite the fact that there was a detailed evaluation methodology that was used by all companies participating in the evaluations, there were discrepancies in the reported results among sources because they used different assumptions concerning (unspecified parameters) channel estimation error modeling, channel reciprocity modeling, the feedback/SRS mechanisms, scheduling algorithm, and the

Petitioners' Exhibit 1021
Nokia of America Corp., et al. v. KT Corporation, et al.
Case No. IPR2025-00036; U.S. Patent No. 11,627,631
Page 986 of 1122

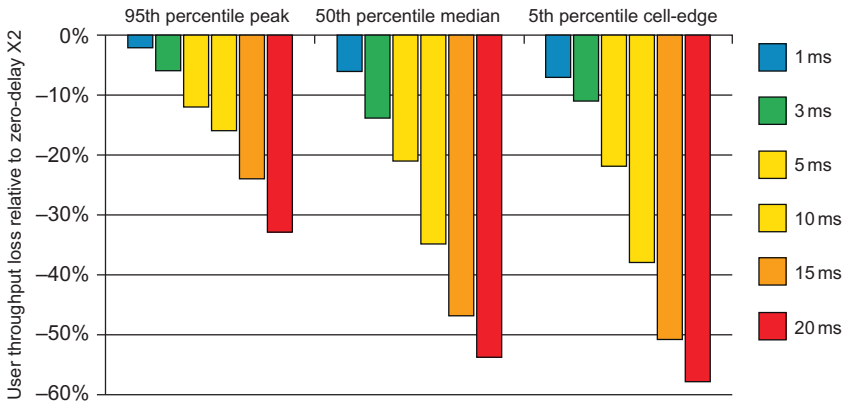


FIGURE 12.10

Impact of X2 latency on user throughput using inter-eNB JT CoMP scheme [15,22].

receiver architecture. In the full-buffer/non-full-buffer evaluations, cell average spectral efficiency in bits/s/Hz/cell and 5% user spectral efficiency in bits/s/Hz/user were evaluated and reported. The user spectral efficiency is defined as the amount of data (file size) per time needed to download data per occupied bandwidth. The time needed to download the data starts when the packet is received in the transmit buffer, and ends when the last bit of the packet is correctly delivered to the receiver. The serving cell spectral efficiency represents the total amount of data for all users during the entire observation time per the number of cells and per occupied bandwidth.

It was observed from the evaluation results for scenarios 1 and 2 that in the downlink, CoMP schemes offer performance gains in homogeneous networks. In the uplink, considerable gain is achievable with a CoMP JR scheme in scenarios 1 and 2. The results were obtained based on ideal and realistic assumptions. It was concluded from the evaluation results in scenarios 3 and 4 that CoMP can provide performance benefits in heterogeneous networks both with full-buffer and FTP traffic models. Based on the evaluation results on the impact of backhaul constraints (capacity/latency), it was concluded that the performance of CoMP schemes relying on spatial information exchange is sensitive to the delay between two transmission points; however, the level of sensitivity depends on the CoMP scheme.

The macro-cell area average spectral efficiency in Figure 12.11 is defined as the sum of cell throughputs in the macro-cell area, which also includes pico-cells/RRHs deployed in the macro-cell area. The results of evaluations show that performance gains can be achieved using CoMP compared to the traditional single-cell schemes in both homogeneous and heterogeneous networks. CoMP performance gains are noted for UEs severely affected by interference. These UEs are typically found at the cell-edges in homogeneous networks. In general, JT CoMP

Petitioners' Exhibit 1021
Nokia of America Corp., et al. v. KT Corporation, et al.
Case No. IPR2025-00036; U.S. Patent No. 11,627,631
Page 987 of 1122

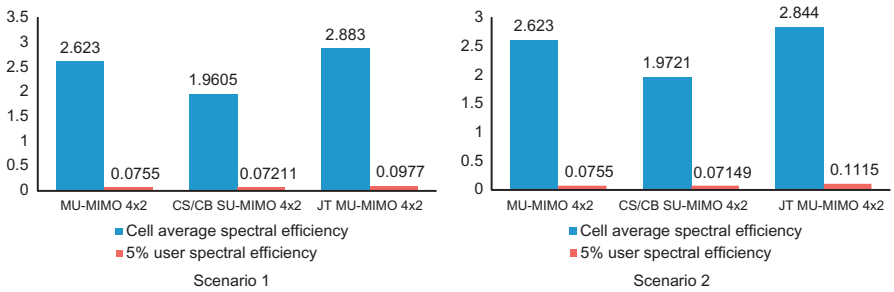


FIGURE 12.11

Comparison of the absolute performance downlink MU-MIMO, CS/CB SU-MIMO, and JT MU-MIMO (FDD, full-buffer, 3GPP spatial channel model, cross-polarized antennas) [4,5].

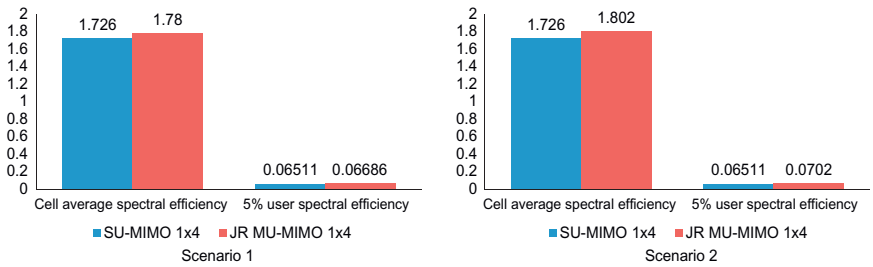


FIGURE 12.12

Comparison of the absolute performance uplink SU-MIMO and JR MU-MIMO (FDD, full-buffer, 3GPP spatial channel model, cross-polarized antennas) [4,5].

techniques provide larger performance gains relative to CS/CB CoMP schemes, but at the expense of larger backhaul overheads and more stringent requirements on backhaul capacity and latency (see Figure 12.11). These observations suggest that CoMP techniques are a promising trend for LTE-Advanced networks. CoMP will thereby contribute to providing the end users with a more consistent experience of mobile broadband across the network coverage areas (Figure 12.12).

The relative performance gains of CoMP scenarios 3 and 4 over HetNet with and without enhanced ICIC (eICIC) were evaluated and are shown in Figure 12.13.

The impact of lower capacity/higher latency links connecting the transmission points was also investigated. The evaluation results were obtained for CoMP in a homogeneous network [5]. Figure 12.14 shows the evaluation results for SU-MIMO CS/CB and MU-MIMO JT CoMP schemes with varying levels of backhaul delay. The CSI feedback delay is assumed to be 5 ms. The results suggest that the JT CoMP scheme demonstrates larger performance variation, and is more sensitive to backhaul delays compared to the CS/CB CoMP scheme.

Petitioners' Exhibit 1021
Nokia of America Corp., et al. v. KT Corporation, et al.
Case No. IPR2025-00036; U.S. Patent No. 11,627,631
Page 988 of 1122

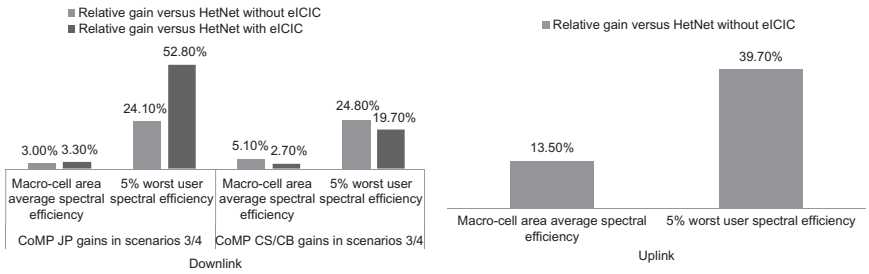


FIGURE 12.13

Relative performance gain of downlink/uplink CoMP in scenarios 3/4 (FDD, full-buffer, configuration 1) [4,5].

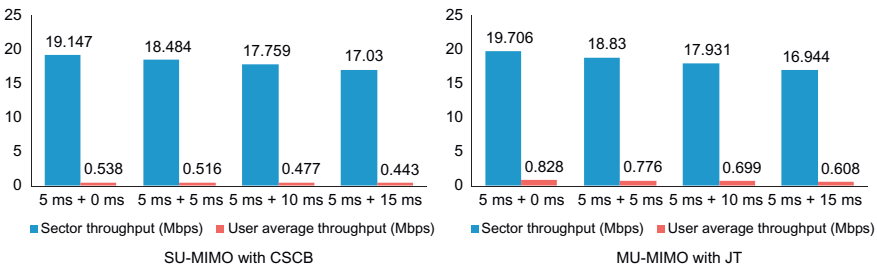


FIGURE 12.14

Effect of CSI feedback delay + backhaul delay on sector and user average throughput [4,5].

References

3GPP Specifications

[1] 3GPP TS 36.211, Evolved Universal Terrestrial Radio Access (E-UTRA); Physical Channels and Modulation (Release 11), December 2012.
[2] 3GPP TS 36.212, Evolved Universal Terrestrial Radio Access (E-UTRA); Multiplexing and Channel Coding (Release 11), December 2012.
[3] 3GPP TS 36.213, Evolved Universal Terrestrial Radio Access (E-UTRA); Physical Layer Procedures (Release 11), December 2012.
[4] 3GPP TR 36.814, Further Advancements for E-UTRA; Physical Layer Aspects (Release 9), March 2010.
[5] 3GPP TR 36.819, Coordinated Multi-point Operation for LTE Physical Layer Aspects (Release 11), December 2011.
[6] 3GPP TS 36.420, X2 General Aspects and Principles (Release 11), September 2012.
[7] 3GPP TS 36.423, X2 Application Protocol (X2AP) (Release 11), December 2012.

Petitioners' Exhibit 1021
Nokia of America Corp., et al. v. KT Corporation, et al.
Case No. IPR2025-00036; U.S. Patent No. 11,627,631
Page 989 of 1122

Books

[8] Y. Zhang, H. Hu, J. Luo, Distributed Antenna Systems: Open Architecture for Future Wireless Communications, Auerbach Publications, June 2007.

Articles

[9] A.M. Saleh, A.J. Rustako, R.S. Roman, Distributed antennas for indoor radio communications, IEEE Trans. Commun. 35 (December 1987).

[10] The distributed antenna systems forum. <http://thedasforum.org>.

[11] B. Chow, et al., Radio-over-fiber distributed antenna system for WiMAX bullet train field trial, IEEE Mobile WiMAX Symposium, California, USA, July 2009.

[12] Distributed antenna systems. <http://www.alino.com/Info/DistributedAntennaSystems/das.htm>.

[13] Jiwon Kang, Bin-Chul Ihm, Wookbong Lee, Distributed antenna system for future 802.16, LG Electronics, IEEE C802.16-10/0018, March 2010.

[14] Distributed antenna systems. <http://en.wikipedia.org/wiki/Distributed_Antenna_System>.

[15] S. Brueck, et al., Centralized scheduling for joint transmission coordinated multipoint in LTE-Advanced, International ITG Workshop on Smart Antennas (WSA 2010), 2010.

[16] O. Simeone, Distributed Antenna Systems: Open Architecture for Future Wireless Communications, New Jersey Institute of Technology, August 2006.

[17] J. Lee, et al., Coordinated multipoint transmission and reception in LTE-Advanced systems, IEEE Commun. Mag. (November 2012).

[18] S. Firouzabadi, A. Goldsmith, Downlink Performance and Capacity of Distributed Antenna Systems, Stanford University, September 2011.

[19] W. Choi, et al., Downlink performance and capacity of distributed antenna systems in a multi-cell environment, IEEE Trans. Wireless Commun. 6 (1) (January 2007).

[20] J. Robson, Guidelines for LTE backhaul traffic estimation, NGMN White Paper, NGMN Alliance, July 2011.

[21] R. Irmer, et al., Coordinated multipoint: concepts, performance, and field trial results, IEEE Commun. Mag. (February 2011).

[22] White Paper, Backhauling X2, Cambridge Broadband Networks Limited.

[23] P. Komulainen, M. Boldi, D1.4 initial report on advanced multiple antenna systems, wireless world initiative new radio—WINNER+. <http://projects.celtic-initiative.org/winner+/deliverables_winnerplus.html>, January 2009.

[24] S. Mayrargue, D1.8 intermediate report on CoMP (Coordinated Multi-Point) and relaying in the framework of CoMP, wireless world initiative new radio—WINNER+. <http://projects.celtic-initiative.org/winner+/deliverables_winnerplus.html>, January 2010.

[25] A. Osseiran, D2.2 enabling techniques for LTE-A and beyond, wireless world initiative new radio—WINNER+. <http://projects.celtic-initiative.org/winner+/deliverables_winnerplus.html>, July 2010.

[26] A. Tyrrell, H. Schöneich, Definitions and architecture requirements for supporting interference exploitation techniques, advanced radio interface technologies for 4G systems ARTIST4G. <https://ict-artist4g.eu/projet/deliverables>, August 2010.

[27] D. Lee, et al., Coordinated multipoint transmission and reception in lte-advanced: deployment scenarios and operational challenges, IEEE Commun. Mag. (February 2012).

Petitioners' Exhibit 1021
Nokia of America Corp., et al. v. KT Corporation, et al.
Case No. IPR2025-00036; U.S. Patent No. 11,627,631
Page 990 of 1122

[28] Wolfram MathWorld, Central limit theorem. <http://mathworld.wolfram.com/CentralLimitTheorem.html>.
[29] Common public radio interface (CPRI). <http://www.cpri.info/>.
[30] 3GPP R1-111174, Backhaul Modeling for CoMP, Orange, Telefónica, February 2011.
[31] 3GPP R1-111944, Phase 1 CoMP simulation evaluation results and analysis for full buffer, LG Electronics, May 2011.
[32] 3GPP R1-111944, Phase 1 CoMP results, Samsung, May 2011.
[33] Y.H. Nam, et al., Evolution of reference signals for LTE-advanced systems, IEEE Commun. Mag. 50 (2) (February 2012).
[34] S. Brueck, Backhaul Requirements for Centralized and Distributed Cooperation Techniques, ITG Heidelberg, July 2010. <http://www.ikr.uni-stuttgart.de/Content/itg/fg524/Meetings/2010-07-08-Heidelberg/index.html>.
[35] P. Marsch, S. Khattak, G. Fettweis, A framework for determining realistic capacity bounds for distributed antenna systems, Proceedings of the IEEE Information Theory Workshop, Chengdu, China, October 2006.
[36] K.M. Karakayli, G.J. Foschini, R.A. Valenzuela., Network coordination for spectrally efficient communications in cellular systems, IEEE Wireless Commun. 13 (4) (August 2006).
[37] P. Marsch, G. Fettweis, On multi-cell cooperative transmission in backhaul-constrained cellular systems, Ann. Télécomm. 63 (5–6) (May 2008).
[38] V. Jungnickel, et al., Interference aware scheduling in the multiuser MIMO-OFDM downlink, IEEE Commun. Mag. 47 (6) (June 2009).
[39] V. Jungnickel, et al., Field trials using coordinated multi-point transmission in the downlink, Third IEEE International Workshop on Wireless Distributed Networks, IEEE PIMRC, September 2010.
[40] P. Marsch, Coordinated Multi-Point Under a Constrained Backhaul and Imperfect Channel Knowledge, PhD thesis, Technische Universitat Dresden, March 2010.
[41] A. Müller, P. Frank, Cooperative interference prediction for enhanced link adaptation in the 3GPP LTE uplink, IEEE VTC, Spring 2010.
[42] A.Müller, P.Frank, Performance of the LTE uplink with intra-site joint detection and joint link adaptation, IEEE VTC, Spring 2010.
[43] M. Grieger, et al., Field trial results for a coordinated multi-point (CoMP) uplink in cellular systems, Proceedings of the ITG/IEEE Workshop on Smart Antennas, Bremen, Germany, February 2010.
[44] V. Kotzsch, G. Fettweis, Interference analysis in time and frequency asynchronous network MIMO OFDM systems, IEEE WCNC 2010, Sydney, Australia, April 2010.
[45] J. Giese, M.A. Awais, Performance upper bounds for coordinated beam selection in LTE-advanced, Proceedings of the ITG/IEEE Workshop on Smart Antennas, Bremen, Germany, February 2010.
[46] G. Fettweis et al., Field trial results for LTE-advanced concepts, Proceedings of the IEEE ICASSP, Dallas, TX, March 2010.
[47] L. Thiele, V. Jungnickel, T. Haustein, Interference management for future cellular OFDMA systems using coordinated multi-point transmission, IEICE Trans. Commun. (December 2010) Special issue on wireless distributed networks.

Petitioners' Exhibit 1021
Nokia of America Corp., et al. v. KT Corporation, et al.
Case No. IPR2025-00036; U.S. Patent No. 11,627,631
Page 991 of 1122

CHAPTER

Carrier Aggregation 13

CHAPTER CONTENTS

13.1 Principles of carrier aggregation 986
13.2 Deployment scenarios 990
13.3 Physical and MAC layer aspects of carrier aggregation 992
13.3.1 Physical layer aspects 992
13.3.2 MAC layer aspects 999
13.4 Protocol and signaling aspects of carrier aggregation 1002
13.5 Radio resource management aspects of carrier aggregation 1005
13.6 RF and implementation aspects of carrier aggregation 1006
13.6.1 Temporal/spectral masks and unwanted emissions 1008
13.6.2 Operating bands for carrier aggregation 1010
13.6.3 Transmitter characteristics for carrier aggregation 1016
13.6.4 Receiver characteristics for carrier aggregation 1022
References 1027

LTE Rel-8/9 specified system bandwidths of 1.4, 3, 5, 10, 15, and 20 MHz to meet different spectrum and deployment requirements. Support of wider bandwidths up to 100 MHz was one of the distinctive features of IMT-Advanced systems. The IMT-Advanced systems targeted peak data rates in excess of 1 Gbps for low mobility and 100 Mbps for high mobility scenarios [32,33]. In order to support wider transmission bandwidths, LTE Rel-10 introduced the carrier aggregation concept, where two or more component carriers with arbitrary bandwidths belonging to the same or different frequency bands could be aggregated. The support of system bandwidths up to 100 MHz would allow a substantial increase in link-level peak data rate, as well as in the system capacity and user throughput. Another advantage of carrier aggregation is to allow efficient use of fragmented spectrum in the form of a virtually wideband spectrum. The fragmented spectrum may belong to the same or different frequency bands and may be of different bandwidths. LTE Rel-11 further extended the advantages of carrier

© 2014 Elsevier Inc. All rights reserved.

Petitioners' Exhibit 1021
Nokia of America Corp., et al. v. KT Corporation, et al.
Case No. IPR2025-00036; U.S. Patent No. 11,627,631
Page 992 of 1122

aggregation by configuring extended carriers and carrier segments. Furthermore, carrier aggregation can be used to mitigate inter-cell interference in heterogeneous networks [30,31].

Using the carrier aggregation scheme, it would be possible to simultaneously schedule a user on multiple component carriers for downlink or uplink data transmission, resulting in some challenges in resource scheduling and load balancing across the network. In a non-contiguous inter-band carrier aggregation scenario, where the aggregated carriers belong to different frequency bands, the fading characteristics might be different between component carriers; as a result, the coverage may vary significantly from one carrier to another. At different locations in the cell, some users may only be scheduled on fewer carriers, while other users may have access to the entire carrier set, which may have a negative impact on sustained user throughput within the coverage area of an eNB.

To allow smooth network migration and upgrades to new releases, it was essential to ensure backward compatibility of LTE-Advanced with LTE Rel-8/9, as well as to support mixed operation of the legacy LTE systems and LTE Rel-10 on the same carrier in an operator's network. LTE Rel-10 carrier aggregation satisfied this requirement by configuring each component carrier in a backward compatible manner with LTE Rel-8/9, and by further supporting at least one of the bandwidths compatible with LTE Rel-8/9. The backward compatibility implies that the complete set of LTE Rel-8/9 downlink physical channels and signals are transmitted on each component carrier using LTE Rel-8/9 signaling procedures, including broadcast channel, synchronization signals, reference signals, and control channels. This would also allow reuse of the LTE Rel-8/9 RF designs and implementations at the eNB and the UE. Although we will primarily focus on carrier aggregation for FDD systems, carrier aggregation is fully supported in the TDD systems, as well.

In this chapter, we will take a pragmatic and systematic approach to describe carrier aggregation principles and its impact on different protocol layers. Various aspects of carrier aggregation including deployment scenarios, physical and MAC layer support, as well as higher-layer signaling and RF transceiver design challenges, will be discussed and examples will be provided.

13.1 Principles of carrier aggregation

In LTE-Advanced carrier aggregation terminology, a component carrier is often referred to as a serving cell, is assigned its own cell identifier, and is managed as a serving cell by the higher layers. Each individual RF carrier is known as a component carrier. A component carrier can be downlink and uplink or downlink only, but it cannot be an uplink-only RF carrier for obvious reasons. The number of downlink component carriers may be different than that of the

Petitioners' Exhibit 1021
Nokia of America Corp., et al. v. KT Corporation, et al.
Case No. IPR2025-00036; U.S. Patent No. 11,627,631
Page 993 of 1122

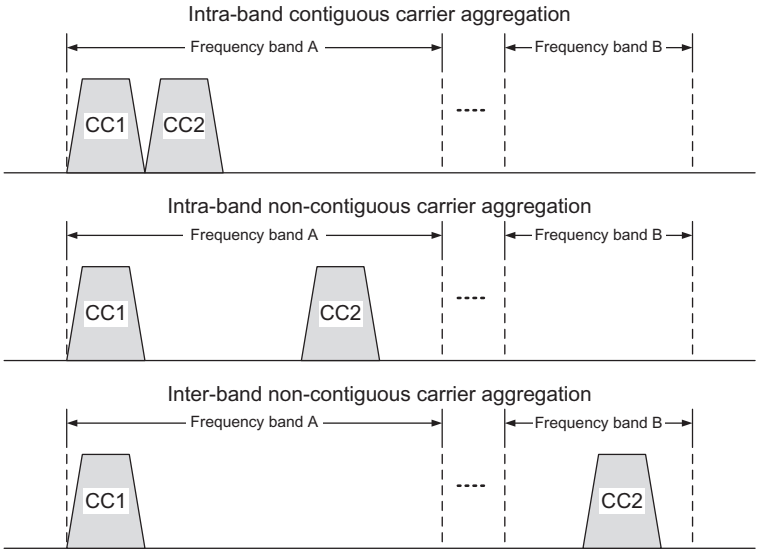


FIGURE 13.1

Carrier aggregation scenarios [16,18,20].

uplink. In general, a different number of component carriers can be aggregated for the downlink and uplink. The UE may support carrier aggregation only in the downlink or in both directions. Up to five component carriers, possibly each with different bandwidth can be aggregated, allowing transmission bandwidths of up to 100 MHz [12,14]. In FDD systems, a serving cell comprises a pair of different carrier frequencies for downlink and uplink transmissions, whereas for TDD, a serving cell is defined as a single-carrier frequency where downlink and uplink transmissions occur in different transmission time intervals. Given that component carriers do not have to be contiguous in frequency which enables utilization of fragmented spectrum, operators with a fragmented spectrum can provide high data-rate services based on the availability of a virtually wide bandwidth even though they do not own a single wideband spectrum allocation.

Each UE has a single serving cell that provides all necessary control information and functions, such as non-access stratum mobility information, security establishment, RRC connection establishment/reconfiguration, etc. This serving cell is referred to as the primary cell (PCell). Other auxiliary cells or component carriers are referred to as secondary cells (SCells).

As shown in Figure 13.1, there are three different carrier aggregation scenarios, as follows [11]:

1. Intra-band contiguous carrier aggregation: This type of carrier aggregation uses a single frequency band. It is the simplest form of carrier aggregation from an implementation point of view. In this scenario, the

Petitioners' Exhibit 1021
Nokia of America Corp., et al. v. KT Corporation, et al.
Case No. IPR2025-00036; U.S. Patent No. 11,627,631
Page 994 of 1122

carriers are contiguous and the frequency spacing between center frequencies of contiguously aggregated RF carriers is a multiple of 300 kHz in order to be compatible with the 100 kHz frequency raster of LTE Rel-8/9 and preserve orthogonality of the subcarriers with 15 kHz spacing.

2. Intra-band non-contiguous carrier aggregation: In this scenario, the aggregated carriers are not adjacent and the multi-carrier signal cannot be treated as a single signal; therefore, two transceivers may be required. This adds significant complexity particularly to the UE where form-factor, power consumption, and cost are the major concerns.
3. Inter-band non-contiguous: This type of carrier aggregation uses different frequency bands which might be appealing to network operators due to the possibility of using fragmented frequency bands. In this scenario, the UE may have to use multiple transceivers, having unavoidable impact on cost, performance, and power consumption. In addition, there are also further complexities resulting from the requirements to reduce intermodulation and cross-modulation impairments created by the transceivers. This type of carrier aggregation may improve mobility by exploiting radio propagation characteristics of different bands.

An enhanced carrier aggregation work item was approved for LTE Rel-11, where as part of that work item, new non-backward-compatible partially configured carrier types could be defined for LTE Rel-11 and beyond to address the ever-increasing demand for higher capacity and higher data rates in cellular networks [19]. The new carrier types are going to be useful in practical deployments where the size of the available frequency block does not match the provisioned bandwidths of 1.4, 3, 5, 10, 15, and 20 MHz in LTE Rel-8/9. If the size of the frequency block is smaller than 5 MHz (corresponding to 25 resource blocks), the number of resources on the carrier segment or extension carrier may not be adequate to efficiently transmit user data and synchronization signals, broadcast and control channels. Although it is desirable to reduce the overhead of the new carrier types (i.e., extension carrier and carrier segment), in practical deployment scenarios, if the frequency gap between the reference carrier and the extension/segment carrier is excessively large, the time and frequency synchronization and slot/subframe alignment of the carriers in a carrier set may not be maintained without including synchronization signals on the extension carrier/carrier segments.

Any fully configured backward compatible carrier in a carrier set may be extended by an extension carrier or appended by segment carriers. The design of the new carrier types has been required to support the operation in the following scenarios, but not necessarily equally optimized for both cases:

- Synchronized carriers: The base carrier and the new carrier types are synchronized in time and frequency to the extent that no separate synchronization is needed in the receiver.

Petitioners' Exhibit 1021
Nokia of America Corp., et al. v. KT Corporation, et al.
Case No. IPR2025-00036; U.S. Patent No. 11,627,631
Page 995 of 1122

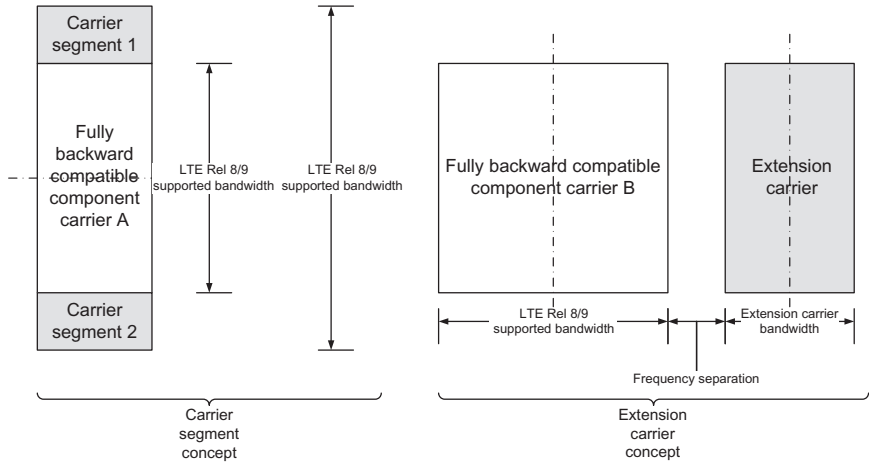


FIGURE 13.2

Illustration of the carrier segments and extension carriers [15].

- Unsynchronized carriers: The base carrier and the new carrier types are not synchronized with the same degree of accuracy as the synchronized carriers.

Note that synchronization is considered from the perspective of the UE receiver. Energy efficiency, flexible spectrum usage, heterogeneous network deployments, and machine type communications were identified as key objectives for the enhanced carrier aggregation project in 3GPP [19]. The considerations for the design of the additional carrier types that could assist in addressing the above goals mainly focused on operation with no cell-specific reference signals, enhanced control signaling with self-contained reference signals, and configurability of synchronization and other reference signal types when needed.

The new carrier types are defined as follows [15]:

- Carrier segment: The carrier segments are defined as the bandwidth extensions of an LTE Rel-8 compatible component carrier, provided that the total number of resource blocks is limited to 110. The combined RF carrier (i.e., LTE Rel-8 RF carrier + carrier segments as shown in Figure 13.2) utilizes the same backward compatible mechanisms of accessing the additional resources on the carrier segments as well as the base RF carrier. As an example, if two 2.5 MHz carrier segments are combined with a 5 MHz LTE Rel-8 RF carrier, the resulting 10 MHz RF carrier is going to be utilized as a 10 MHz LTE Rel-8 RF carrier. The use of carrier segments in the above manner would allow more efficient utilization of small fragments of spectrum without having to transmit additional overhead due to synchronization, broadcast, and control channels on the carrier

Petitioners' Exhibit 1021
Nokia of America Corp., et al. v. KT Corporation, et al.
Case No. IPR2025-00036; U.S. Patent No. 11,627,631
Page 996 of 1122

segments. The notion of carrier segment allows for aggregation of additional resource blocks to a component carrier, while still retaining the backward compatibility of the original carrier, Note that carrier segments are always adjacent and linked to one component carrier and cannot be used as stand-alone. They do not provide synchronization signals, system information, or paging, and therefore cannot be used for random access or camping. They support the same HARQ process and transmission mode as the component carrier to which they are linked.

- Extension carrier: The extension carrier is a carrier that cannot be operated as a single stand-alone RF carrier and must be part of a component carrier set where at least one of the carriers in the set is a stand-alone backward compatible component carrier. Depending on whether the extension carriers are adjacent or non-adjacent to a component carrier carrying synchronization signals, the extension carrier may or may not be required to carry synchronization signals. If the extension carrier does not carry the synchronization signals, then it must be located close to a component carrier with synchronization signals for reliable synchronization. No legacy control channel PDCCH, PHICH, PCFICH, and no cell-specific reference signals is another possible configuration for the extension carriers which allows reduced overhead and more efficient use of radio resources on that carrier. The extension carrier supports a separate HARQ process, PDCCH, and transmission mode, which is configured from its linked component carrier.

13.2 Deployment scenarios

Carrier aggregation enables various network deployments. In general, carrier aggregation is used to improve data rates for users within overlapped areas of the cells (cell boundaries). However, carrier aggregation can also be used to mitigate inter-cell interference in heterogeneous networks (see Chapter 14). The following network deployment scenarios were considered during the development of LTE-Advanced. Although exemplified with two component carriers at frequencies f_{c_1} and f_{c_2} as shown in Figure 13.3, the concept can be generalized to any number of component carriers [7,22,23,29]:

- Deployment Scenario 1: In this case, cells with carrier frequencies f_{c_1} and f_{c_2} are (geographically) collocated, and their coverage is overlaid with f_{c_1} and f_{c_2} in the same frequency band. They provide approximately the same coverage due to similar path loss characteristics within the same band. This carrier aggregation scenario achieves higher data rates throughout the cell where both layers provide sufficient coverage and mobility. An example scenario is the case where $f_{c_1} = 2000$ MHz and $f_{c_2} = 800$ MHz are of the same band where aggregation is possible between the overlaid cells.

Petitioners' Exhibit 1021
Nokia of America Corp., et al. v. KT Corporation, et al.
Case No. IPR2025-00036; U.S. Patent No. 11,627,631
Page 997 of 1122

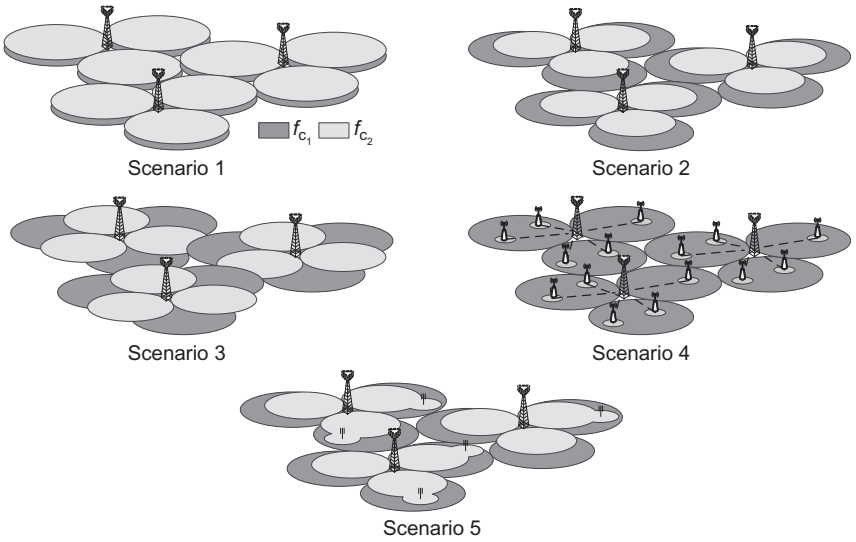


FIGURE 13.3

Carrier aggregation deployment scenarios [7].

- Deployment Scenario 2: In this case, the cells with carrier frequencies f_{c_1} and f_{c_2} are collocated and overlaid with f_{c_1} and f_{c_2} in different frequency bands. Different coverage is provided on different carriers due to the larger path loss in the higher frequency band. Mobility is typically supported on the carrier in the lower frequency band which further provides sufficient coverage. The carrier in the higher frequency band is used to improve data rates and throughput. The cells f_{c_1} and f_{c_2} are collocated and overlaid, but f_{c_2} has smaller coverage due to larger path loss. In other words, only f_{c_1} provides sufficient coverage and f_{c_2} is used to improve throughput. An example scenario would be the case where $f_{c_1} = \{800\ \text{MHz}, 2000\ \text{MHz}\}$ and $f_{c_2} = \{3500\ \text{MHz}\}$ where aggregation is possible between the overlaid cells.
- Deployment Scenario 3: In this case, the cells comprising carrier frequencies f_{c_1} and f_{c_2} are collocated with f_{c_1} and f_{c_2} in different frequency bands. The antennas for cells of f_{c_2} are directed to the cell boundaries of f_{c_1} to improve the cell-edge data rates and user throughput. Due to the larger path loss, coverage holes exist for cells in the higher frequency band on which mobility management is typically not performed. The carrier aggregation is supported in areas with overlapping coverage and the mobility is based on f_{c_1} coverage. An example would be the case where $f_{c_1} = \{800\ \text{MHz}, 2000\ \text{MHz}\}$ and $f_{c_2} = \{3500\ \text{MHz}\}$ in which aggregation is possible between the overlaid cells.

Petitioners' Exhibit 1021
Nokia of America Corp., et al. v. KT Corporation, et al.
Case No. IPR2025-00036; U.S. Patent No. 11,627,631
Page 998 of 1122

- Deployment Scenario 4: In this case the cells associated with carrier frequency f_{c_1} provide macro coverage and remote radio heads (RRHs) corresponding to carrier frequency f_{c_2} are used to improve throughput at hot spots. The mobility is performed based on the cell coverage of frequency f_{c_1}. In this deployment scenario, the carrier frequencies f_{c_1} and f_{c_2} are usually of different bands. The carrier aggregation is applicable to users within the coverage of RRHs and the underlying macro-cells. An example would be the case where $f_{c_1} = \{800\ \text{MHz}, 2000\ \text{MHz}\}$ corresponds to a larger cell and $f_{c_2} = \{3500\ \text{MHz}\}$ corresponds to smaller cell, in which aggregation is possible between the overlaid cells.
- Deployment Scenario 5: This case is similar to the second scenario where frequency-selective repeaters or distributed antenna systems are additionally deployed to extend the coverage for one of the carrier frequencies. It is expected that f_{c_1} and f_{c_2} cells of the same eNB can be aggregated where coverage overlaps.

13.3 Physical and MAC layer aspects of carrier aggregation

In this section, we discuss the physical and MAC layer aspects of carrier aggregation, and we will particularly focus on the impacts of carrier aggregation on the system operation at the lower protocol layers. Note that scheduling and use of the RF carriers are related to physical and MAC layers, and to a great extent are transparent to the upper layers.

13.3.1 Physical layer aspects

The physical layer is in charge of processing and transmission of data and control signaling between the radio access network and the user device. The LTE-Advanced carrier aggregation feature enables concurrent data transmission on multiple component carriers (up to five), where the transmission schemes are largely inherited from LTE Rel-8/9 data transmission procedures per component carrier, including the multiple access scheme; modulation and coding; and multi-antenna processing. Some additional UE functionalities beyond those of LTE Rel-8/9 are supported in LTE Rel-10, including data transmissions over two clusters of contiguous bandwidth on the same carrier where the data is precoded by a single DFT unit (see Chapter 10 for a description of clustered SC-FDMA), simultaneous transmission of a control channel and a data channel in the PCell (see Chapter 10 for simultaneous PUCCH and PUSCH transmission), and data transmissions from multiple antennas with spatial multiplexing [3–6]. Nevertheless, improving the downlink and uplink control signaling to efficiently support data transmission was the main challenge in the design of LTE-Advanced carrier aggregation [29].

Petitioners' Exhibit 1021
Nokia of America Corp., et al. v. KT Corporation, et al.
Case No. IPR2025-00036; U.S. Patent No. 11,627,631
Page 999 of 1122

The PDCCH provides information on resource allocation; modulation and coding scheme HARQ; and other parameters for downlink and uplink data transmission on the physical downlink/uplink shared channel. It is possible to configure each component carrier to transmit the PDCCH for scheduling PDSCH/PUSCH on the same carrier frequency and associated linked uplink carrier, where the linkage of the downlink and uplink carriers is conveyed in SIB2 [10]. In addition, the PDCCH on a component carrier can be configured to schedule PDSCH and PUSCH transmissions on other component carriers through a cross-carrier scheduling feature. Cross-carrier scheduling was primarily developed to support heterogeneous networks comprising a combination of macro-eNBs and low-power nodes (e.g., pico-cell, femto-cell, and RRHs) where significant intercell interference may arise when those networks are deployed on the same carrier [30,31]. Since the PDCCH is transmitted across the entire bandwidth of the respective carrier, interference coordination methods based on fractional frequency reuse may not be adequate in reducing the inter-cell interference on the PDCCH. Carrier aggregation can address this issue by configuring the UE connected to different network nodes to receive the PDCCH on different carriers, thereby reducing or even eliminating inter-cell interference on the PDCCH. With cross-carrier scheduling, only one component carrier needs to be protected for the PDCCH transmission, which can be used to allocate resources on other component carriers.

Cross-carrier scheduling enables a PDCCH on a component carrier to be configured in order to schedule PDSCH and PUSCH transmissions on another component carrier using a 3-bit carrier indicator field (CIF) which is inserted at the beginning of the downlink control information (DCI) messages. The carrier aggregation can reduce or even eliminate inter-cell interference on the PDCCH using cross-carrier scheduling. Figure 13.4 shows a hypothetical heterogeneous network scenario where a component carrier at f_1 is used by the macro-cell at full power and by the pico-cells at reduced power; whereas component carrier f_2 is used by the macro-cell at reduced power and by the pico-cells at nominally low power. In this case, cross-carrier scheduling from component carrier f_2 allows inter-cell interference mitigation among the macro- and pico-cells.

Cross-carrier scheduling is also an effective mechanism to schedule data transmissions on carriers of small bandwidth from a carrier with a larger bandwidth, considering that the PDCCH reliability targets are more challenging to achieve on carriers with small bandwidth due to limited frequency diversity gain. The PDCCH search space consists of a set of PDCCH candidates over which the UE performs blind decoding operations to determine whether there is any PDCCH addressed to it in a subframe. A common PDCCH search space is monitored by all UEs only in their respective PCells for receiving system information, paging, power control, and random access-related control information. Each UE also monitors a UE-specific PDCCH search space primarily carrying scheduling grants for downlink and uplink data transmissions. The start of the UE-specific PDCCH search space is a function of the UE's radio network temporary identifier (RNTI).

Petitioners' Exhibit 1021
Nokia of America Corp., et al. v. KT Corporation, et al.
Case No. IPR2025-00036; U.S. Patent No. 11,627,631
Page 1000 of 1122

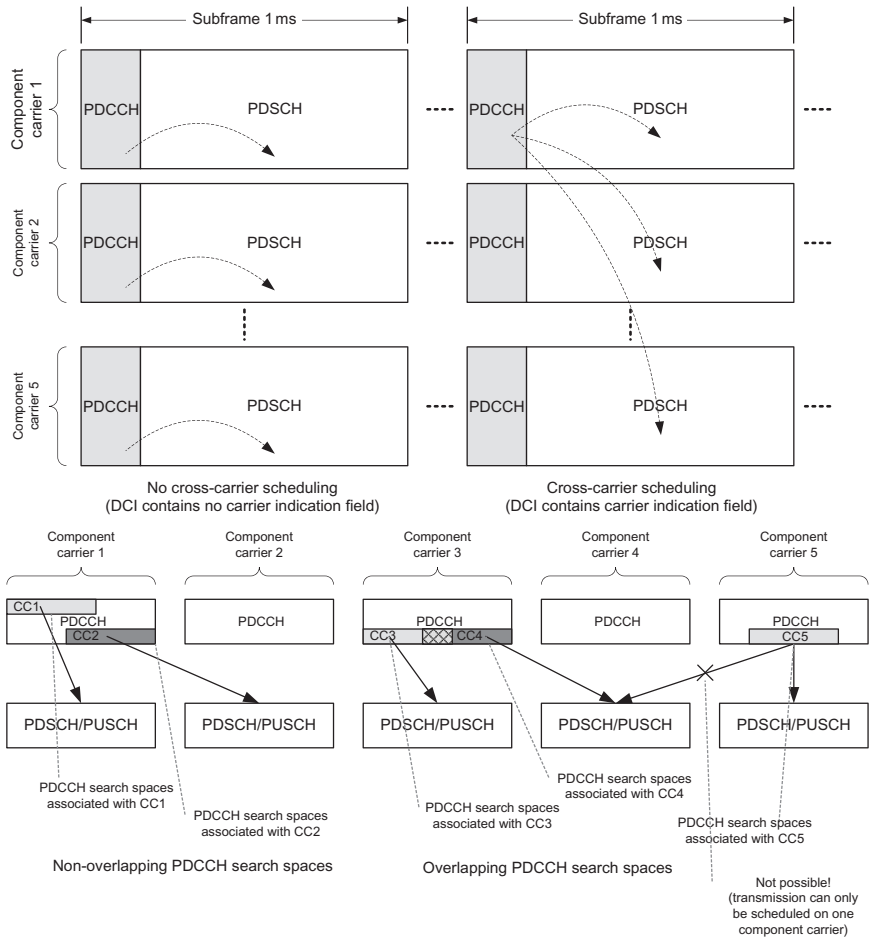


FIGURE 13.4

Illustration of the cross-carrier scheduling concept in carrier aggregation [13,14].

Since the same set of resources for PDCCH transmission is shared by all UEs, a PDCCH for a UE may not be transmitted due to partial overlapping with another PDCCH belonging to a different UE; this condition is referred to as PDCCH blocking. To maintain the PDCCH blocking probability at LTE Rel-8/9 level, an LTE Rel-10/11 UE monitors one UE-specific PDCCH search space for each activated component carrier. For a UE that is not configured with cross-carrier scheduling, the UE-specific PDCCH search space on each component carrier is the same as that in LTE Rel-8/9, whereas for a UE that is configured with cross-carrier scheduling, the UE-specific PDCCH search space is defined by a

Petitioners' Exhibit 1021
Nokia of America Corp., et al. v. KT Corporation, et al.
Case No. IPR2025-00036; U.S. Patent No. 11,627,631
Page 1001 of 1122

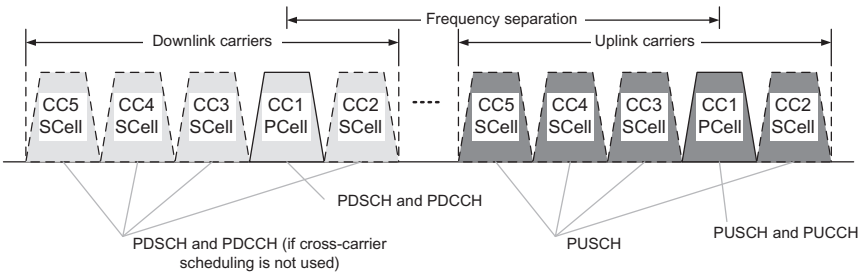


FIGURE 13.5

Symmetric carrier aggregation in the downlink and uplink (example) [16].

combination of the UE's RNTI and the serving cell index. The number of PDCCH blind decoding operations performed by a UE scales (approximately) linearly with the number of its activated component carriers [29]. If carrier aggregation is configured, the maximum number of blind decoding operations that a UE performs is 44 for the PCell plus 32 for each active downlink SCell. An additional 16 blind decodings are needed for each uplink component carrier that is configured for uplink MIMO operation. When cross-carrier scheduling is configured, CIF is only present in the PDCCH messages in the UE-specific search space and not in the common search space [13].

The PDSCH/PUSCH on a component carrier can only be scheduled from one component carrier. Therefore, for each PDSCH/PUSCH component carrier, there is an associated component carrier, configured via UE-specific RRC signaling, where the corresponding DCI can be transmitted. Figure 13.4 illustrates an example, where PDSCH/PUSCH transmissions on component carrier 1 are scheduled using PDCCHs transmitted on component carrier 1. In this case, since cross-carrier scheduling is not used, there is no carrier indicator in the corresponding DCI formats. The PDSCH/PUSCH transmissions on component carrier 2 are cross-carrier scheduled from PDCCHs transmitted on component carrier 1. Therefore, the DCI formats in the UE-specific search space for component carrier 2 include the CIF. Note that the transmissions on a component carrier can be scheduled by the PDCCHs on one component carrier; thus, component carrier 4 cannot be scheduled by PDCCHs on component carrier 5, given that there is a semi-static association between component carriers 3 and 4 for PDCCH transmission in this example [14].

As mentioned earlier, there is one UE-specific search space per aggregation level and component carrier used for PDSCH/PUSCH. This is illustrated in Figure 13.4, where PDSCH/PUSCH transmissions on component carrier 1 are scheduled using PDCCHs transmitted on component carrier 1. There is no CIF in the UE-specific search space for component carrier 1 since cross-carrier scheduling is not used. For component carrier 2, on the other hand, a carrier indicator field exists in the UE-specific search space, given that component carrier 2 is

Petitioners' Exhibit 1021
Nokia of America Corp., et al. v. KT Corporation, et al.
Case No. IPR2025-00036; U.S. Patent No. 11,627,631
Page 1002 of 1122

cross-carrier scheduled from the PDCCHs transmitted on component carrier 1. Search spaces for different component carriers may overlap in some subframes. In Figure 13.4, this happens for the UE-specific search spaces for component carriers 3 and 4. The terminal can identify the two search spaces independently, assuming that a CIF is used for component carrier 4, but is not used for component carrier 3. If the UE-specific and common search spaces corresponding to different component carriers happen to overlap for some aggregation levels when cross-carrier scheduling is configured, the terminal only needs to monitor the common search space. The reason for this is to avoid ambiguities arising from this condition; if the component carriers have different bandwidths, a DCI format in the common search space may have the same payload size as another DCI format in the UE-specific search space corresponding to another component carrier [14].

The PCFICH is transmitted in each subframe and conveys a control format indicator (CFI) field, which indicates the number of OFDM symbols carrying control information in each subframe (up to three OFDM symbols per subframe). The UE derives the starting OFDM symbol used for the PDSCH transmission based on the decoded CFI value. For the PDSCH scheduled by PDCCH on the same component carrier, the UE is required to decode the PCFICH in order to determine the starting OFDM symbol used for the PDSCH. When cross-carrier scheduling is utilized, the starting OFDM symbol for the PDSCH transmission is configured by the network through higher layers, and the UE is not required to decode PCFICH on that component carrier.

The physical HARQ indicator channel carries HARQ feedback (ACK/NACK) information associated with a PUSCH transmission. The PHICH structure in LTE Rel-10/11 carrier aggregation is the same as that for LTE Rel-8/9. The PHICH corresponding to a PUSCH transmission is always transmitted on the component carrier where the PDCCH schedules the PUSCH transmission.

The uplink control information (UCI) includes HARQ feedback corresponding to one or more PDSCHs, channel state information, and scheduling request. Similar to LTE Rel-8/9, the UCI can be transmitted on the PUCCH, if there is no transmission on PUSCH in a subframe, or transmitted on PUSCH, if there is a scheduled transmission on PUSCH. LTE-Advanced further supports simultaneous PUCCH and PUSCH transmissions in a subframe (see Figure 13.6). This allows the eNB to flexibly control the performance of the PUCCH and PUSCH independently and to avoid the UCI overhead on PUSCH by utilizing existing PUCCH resources. The PUCCH can only be transmitted on the PCell, since it typically has more reliable link quality and coverage relative to the SCells (see Figure 13.5). When applicable, UCI is always transmitted on a single PUSCH.

HARQ feedback indicates whether a transport block is correctly received and decoded. LTE Rel-8/9 supports transmitting a maximum of two and four ACK/NACKs in an uplink subframe for FDD and TDD, respectively. Given independent HARQ processes per component carrier, the maximum number of HARQ feedback bits in a subframe in response to PDSCH transmissions can be 10 bits

Petitioners' Exhibit 1021
Nokia of America Corp., et al. v. KT Corporation, et al.
Case No. IPR2025-00036; U.S. Patent No. 11,627,631
Page 1003 of 1122

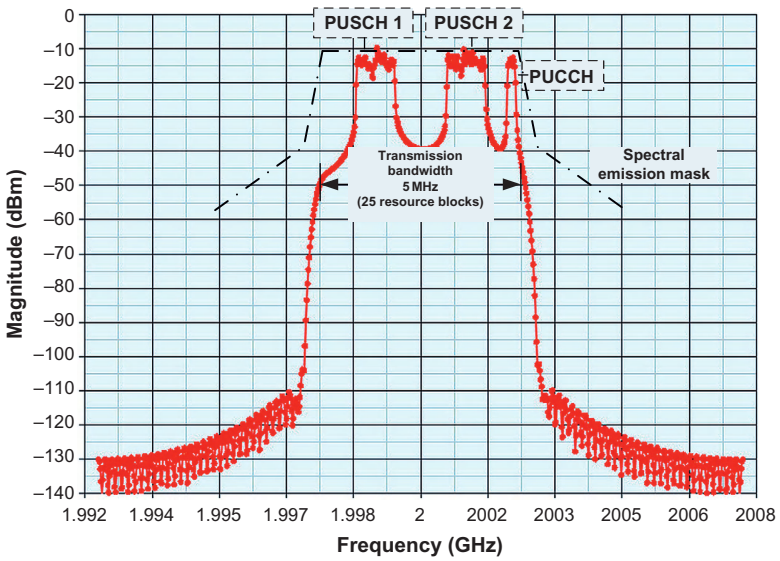


FIGURE 13.6

Snapshot of clustered SC-FDMA (simultaneous PUSCH and PUCCH transmission) in the uplink [17,18].

for FDD and up to 90 bits for TDD (assuming five component carriers with MIMO transmission modes per component carrier and TDD subframe configuration 5). Reliable transmission of large number of HARQ ACK/NACK bits in an uplink subframe requires a substantial amount of resources and sufficiently high signal to interference plus noise ratio. Therefore, HARQ feedback bundling/multiplexing schemes are designed for TDD systems to limit the maximum number of ACK/NACK bits in an uplink subframe to 20. Multiple HARQ feedback bits are bundled by a logical AND operation to produce one HARQ feedback bit per component carrier and per subframe for certain TDD subframe configurations. The PUCCH format 3 was introduced in LTE Rel-10 to support HARQ feedback for a UE configured with downlink carrier aggregation. The PUCCH format 3 uses a SC-FDMA waveform with five SC-FDMA symbols per slot carrying HARQ feedback information and one or two SC-FDMA symbols per slot (depending on the size of the cyclic prefix) for transmission of demodulation reference signals, to enable coherent demodulation of HARQ feedback (see Chapter 10 for more information on PUCCH format 3). An orthogonal cover code of length 5 is applied to the encoded HARQ feedback bits in the corresponding SC-FDMA symbols, allowing multiplexing of up to five UEs in one resource block. Assuming QPSK modulation, k HARQ feedback bits are encoded using the $(32, k)$ Reed−Muller code with circular rate matching into 48 encoded HARQ acknowledgment bits, which are transmitted in a subframe comprising two slots.

Petitioners' Exhibit 1021
Nokia of America Corp., et al. v. KT Corporation, et al.
Case No. IPR2025-00036; U.S. Patent No. 11,627,631
Page 1004 of 1122

LTE-Advanced further supports the HARQ feedback multiplexing scheme for TDD, where two HARQ feedback bits are generated per component carrier, representing the number of consecutively correctly received PDSCHs on the component carrier. PUCCH format 1b can be used to carry four acknowledgments when channel selection is used, i.e., the PUCCH payload carries two acknowledgments and the selection of PUCCH resources carries the other two acknowledgments. The use of bundled acknowledgments in a single uplink subframe is not limited to the TDD duplex mode. The carrier aggregation in FDD with a different number of uplink and downlink component carriers encounters the same problem. In LTE Rel-10, there is only one PUCCH that is always transmitted on the primary component carrier. Hence, even in asymmetric carrier aggregation scenarios, the possibility to transmit more than two HARQ acknowledgment bits in the uplink must be supported. This is performed via resource selection or by using PUCCH format 3. The acknowledgments in response to PUSCH transmissions are transmitted using multiple PHICHs, where the PHICH is transmitted on the same downlink component carrier as the uplink scheduling grant which initiated the uplink transmission.

The channel-state information feedback enables the eNB to perform PDSCH scheduling including resource allocation, MCS selection, transmission rank adaptation, and the choice of precoding matrix. To accommodate different channel conditions and interference levels among different component carriers, CSI is fed back for each component carrier. Both periodic and aperiodic CSI feedbacks are supported in LTE Rel-10/11, where periodic CSI is transmitted on a set of semi-statically configured subframes, and aperiodic CSI is dynamically scheduled by the eNB via the PDCCH. Periodic CSI feedback is independently configured for each component carrier and transmitted on the PUCCH using PUCCH format 2. Since the payload size of PUCCH format 2 is limited, the periodic CSI for only one component carrier can be unconditionally transmitted in a subframe. A priority based on the periodic CSI reporting type determines the component carrier for which periodic CSI is reported in the event that periodic CSI feedback of multiple carriers collide in a subframe. If the collisions involve the same periodic CSI reporting type, the priority is according to ascending cell index. Aperiodic CSI feedback is transmitted on PUSCH and typically carries more CSI bits than periodic CSI feedback. LTE Rel-10/11 supports aperiodic CSI feedback for a single or multiple component carriers in a subframe so that the eNB can balance the CSI accuracy and feedback overhead [29].

Uplink power control is a mechanism to instruct the UEs to determine the PUSCH/PUCCH transmission power with the objective of ensuring that the target reception reliability of that channel is met. The uplink power control supported in LTE Rel-8/9/10 consists of an open-loop component adjusting for the path loss between the UE and its serving eNB, and of a closed-loop component based on transmission power control commands in the PDCCH. The uplink power control processes are independent among the respective activated cells and each process is the same as LTE Rel-8/9. The resulting transmission power for PUSCH or

Petitioners' Exhibit 1021
Nokia of America Corp., et al. v. KT Corporation, et al.
Case No. IPR2025-00036; U.S. Patent No. 11,627,631
Page 1005 of 1122

PUCCH is referred to as nominal transmission power. The key differentiation with respect to the LTE Rel-8/9 uplink power control operation occurs when the sum of the nominal transmission powers from the UE exceeds the total maximum output power for which the UE is configured in a specific subframe. Depending on whether the UE is configured for simultaneous PUCCH and PUSCH transmissions, on the UCI types for transmission, and on the existence of any PUSCH transmission, the UE may transmit in a subframe one PUCCH, one PUSCH with UCI, one or more PUSCH transmissions without UCI, or any other combination. As control information is more important than data information and does not benefit from the use of HARQ, the UE transmission power is distributed by descending priority to the PUCCH, PUSCH with UCI, and PUSCH without UCI, where the nominal transmission power for a channel with higher priority is first guaranteed until the UE total maximum output power is reached. For one or more PUSCH transmissions without UCI, the UE scales each respective nominal PUSCH transmission power by the same factor, considering that the same quality of service for data transmission is required on all component carriers [29].

The eNB may not know the exact UE transmission power due to the possibility of missing power control commands, UE-specific implementation of maximum power reduction (MPR),[1] and additional maximum power reduction (A-MPR)[2] in order to meet regulatory requirements. To provide the eNB with more accurate information on the UEs transmission power, power headroom reporting was supported in LTE Rel-8/9. The UE may report type 1 and/or type 2 power headroom for an activated cell. The type 1 and type 2 power headroom reports indicate the amount of remaining the UEs transmission power beyond those already used for PUSCH, or PUSCH and PUCCH transmission in a subframe, respectively [29].

13.3.2 MAC layer aspects

From the MAC perspective, the carrier aggregation simply provides additional conduits, thus the MAC sublayer plays the role of a multiplexing entity for the aggregated component carriers. Figure 13.7 shows an overview of the downlink

[1]The purpose of MPR is to allow the UE, in some configurations, to lower its maximum output power in order to meet the general requirements on signal quality and out-of-band (OOB) emissions. Note that MPR is an allowance and the UE is not required to use it [13].

[2]The eNB may inform the UE of the possibility of further lowering its maximum power by signaling an additional MPR (A-MPR). The need for an A-MPR occurs with certain combinations of E-UTRA bands, channel bandwidths, and transmission bandwidths for which the UE must meet additional (more stringent) requirements for spectrum emission mask and spurious emissions. As with MPR, the A-MPR is an allowance, not a requirement, and it applies in addition to MPR. Regardless of whether the UE makes use of the allowed MPR and A-MPR, the additional requirements for spectrum emission mask and spurious emissions that are signaled by the network always apply. The reason for the complex set of conditions for the relaxation is the expected intermodulation products which may fall into adjacent bands which have different levels of sensitivity (e.g., public safety bands) [13].

Petitioners' Exhibit 1021
Nokia of America Corp., et al. v. KT Corporation, et al.
Case No. IPR2025-00036; U.S. Patent No. 11,627,631
Page 1006 of 1122